UNCLASSIFIED

AD NUMBER

AD864990

LIMITATION CHANGES

TO:

Approved for public release; distribution is unlimited.

FROM:

Distribution authorized to U.S. Gov't. agencies and their contractors; Critical Technology; JAN 1970. Other requests shall be referred to Army Research Office-Duram, Duram, NC. This document contains export-controlled technical data.

AUTHORITY

USARO ltr, 15 Mar 1971

THIS PAGE IS UNCLASSIFIED

ARO-D Report 70-1

TRANSACTIONS OF THE FIFTEENTH CONFERENCE OF ARMY MATHEMATICIANS

AD 864990



DDC
RECEIVED
FEB 13
A

This document is subject to special export controls and each transmittal to foreign governments or foreign nationals may be made only with prior approval of the U. S. Army Research Office—Durham, Durham, North Carolina.

The findings in this report are not to be construed as an official Department of the Army position, unless so designated by other authorized documents.

Reproduced by the
CLEARINGHOUSE
for Federal Scientific & Technical
Information Springfield Va. 22151

Sponsored by

The Army Mathematics Steering Committee

on Behalf of

THE OFFICE OF THE CHIEF OF RESEARCH AND DEVELOPMENT

639

U. S. ARMY RESEARCH OFFICE-DURHAM

Report No. 70-1
January 1970

TRANSACTIONS OF THE FIFTEENTH CONFERENCE OF ARMY MATHEMATICIANS

Sponsored by the Army Mathematics Steering Committee

Host

U. S. Army Aviation Systems Command
St. Louis, Missouri

11-12 June 1969

This document is subject to special export controls and each transmittal to foreign governments or foreign nationals may be made only with prior approval of the U. S. Army Research Office-Durham, Durham, North Carolina.

The findings in this report are not to be construed as an official Department of the Army position, unless so designated by other authorized documents.

U. S. Army Research Office-Durham
Box CM, Duke Station
Durham, North Carolina

FOREWORD

At the Fourteenth Conference of Army Mathematicians, two members of the Army Mathematics Steering Committee, Fred Frishman and Joseph Weinstein, discussed with John Mundy of the U. S. Army Aviation Systems Command, St. Louis, Missouri, the possibility of his installation serving as host to the next conference in this series. Mr. Mundy thought that the best way to approach this matter would be to write to Colonel Edward Chryster, Chief of the Research, Development and Engineering Directorate. On 15 July 1968 Mr. Weinstein sent the suggested letter. Colonel Harry L. Buck, Deputy Commander for Research, Engineering and Data answered his letter as follows:

> Thank you for your letter of 15 July inviting USAAVCOM to act as host for the 15th Conference of Army Mathematicians. I have discussed the matter with Major General John Norton, the Commanding General of AVCOM, and am happy to convey to you his keen interest in hosting the next conference.
>
> I have appointed Mr. Havard M. Bauer, Systems Analysis Division, to coordinate the AVCOM planning. Please contact him on 698-2687/3271 (AUTOVON) in regard to the proposed site and exact dates.

Mr. Bauer, serving as Chairman on Local Arrangements, set the dates for the conference as 11-12 June 1969, and it was held at the Sheraton-Jefferson Hotel in St. Louis. Those in attendance at this symposium would like to thank Mr. Bauer and members of his staff for their many efforts in so ably handling the various problems associated with the conduction of such an affair.

On behalf of the Office of the Chief of Research and Development, the Army Mathematics Steering Committee sponsors this series of conferences. Members of this Committee were pleased to see such a large turn-out for this meeting. There were 98 persons in attendance. Of these, 24 were from the host installation, and one was a visitor from Canada. There were 31 contributed papers on the agenda, together with two invited addresses. Professor Norman N. Royall, Jr., of the University of Missouri at Kansas City, gave his invited talk following the banquet. The title of his informative address was, "Facts and Fantasy in the Space Age." The other invited address had the short title, "Surf," and was given by Professor R. E. Meyer of the University of Wisconsin. Scientific discoveries made about properties of ocean waves by Professor Meyer and his colleagues formed the basis for this interesting closing address of the conference.

The AMSC wishes to thank all the speakers and the chairmen for the important parts they played in the conduction of the Fifteenth Conference of Army Mathematicians. Members of this group have asked that the transactions of this conference be published in order that those unable to attend this meeting would have access to the presented scientific papers.

TABLE OF CONTENTS

Title	Page
Foreword	iii
Table of Contents	v
Program	viii
A Note on an Elastic Sphere Indenting an Elastic Spherical Cavity by M. A. Hussain and S. L. Pu	1
Torsional Dynamics of Joined Concentric Cylindrical Shells by E. J. Brunelle	25
Feedback in Information Systems (The Effect of Feedback on System Entropy) by Erwin Biser and M. Z. v. Krzywoblocki	47
Tensor Concepts Applied to Projective Geometry by Shunsuke Takagi	123
A General Theory of Stresses and Displacements in Elastic and Viscoelastic Layered Systems by Y. T. Chou	141
Adaptation of Valanis' Method to the Kinetics of Viscoelastic Plate by Struan R. Robertson	169
Third Order Positive Cyclic Systems of Linear Differential Equations by Leon Kotin and Garrett Birkhoff	187
Perturbations of Functional Differential Systems by Gerald A. Shanholt	203
Stress Wave Propagation in a Class of Nonhomogeneous Elastic Media by Shun-Chin Chou	213
Free Extensional Vibrations in Plate Strips by Gary Anderson	241
Forced Oscillation of a Mass with a Bilinear Spring by Royce Beckett and K. C. Pan	269
On Eigenvalues and Structure of the Hurwitz Matrix by Siegfried Lehnigk	283

Matrix Square Root Formulation of the Kalman Filter Covariance Equations
by William Agee. 291

Solution of the Fourier Equation and Associated Boundary Equations Using Analog and Digital Algorithms
by Darrel M. Thomsen 299

A General Solution to the Axisymmetric Thermoelasticity Problem in Cylindrical Coordinates
by John G. Avery 315

Elasto-Plastic Plane Strain Analysis for a Circular Hole in a Uniaxial Tensile Field*
by O. L. Bowie and C. E. Freese

Approximate Analysis of a Flat Circular Parachute in Steady Descent
by Edward W. Ross 343

Bond Stretch in Diatomic Molecular and the Fues Potential
by Romas Shatas and John D. Stettler 387

Numerical Study of a Best Interval Approximation of the Square Root of a Positive Number
by Fred Frishman and William Shepherd. 395

A Dynamic Model of Vehicle System Availability
by Martin Wachs and Russel Purvis. 403

Fact and Fantasy in the Space Age*
by Norman N. Royall, Jr.

Wave Propagation in a Transversely Isotropic Half-Space*
by R. L. Ryan

The Characteristics of a Fluidic Vortex Rate Sensor in the Range of Fully Developed Flow*
by Arthur J. Ostdiek

Analog/Hybrid Solutions to Algebraic Equations and Boundary-Value Problems
by Arthur Hausner. 427

Mathematical Techniques for Concept Formulation and Contrast Definition in the Design of Major End-Items*
by John Mundy

*This paper was presented at the conference. It does not appear in these Transactions.

A Rapidly Converging Iterative Technique for Computing Wind Compensation Launcher Settings for Unguided Rockets
by Louis D. Duncan and Bernard F. Engebos 455

A Dimensional Analysis of the Errors of Atmospheric Sound Ranging*
by Robert P. Lee

On the Vortex Solution for the Turbine Blade-Flow-Field and Correlation with Observed Performance
by Jacqueline A. Benton and F. Edward McDonald 477

Forced Oscillations in Second Order Systems with Unbounded Nonlinearities
Jagdish Chandra and B. A. Fleishman. 521

An Evaluation of the Constants in the Integral of Schwarz-Christoffel Transformation by an Iterative Technique
by Kanu Gandhi 535

A Numerical Technique for the Generation of Contours
by Merle J. Biggin 553

The Stresses Produced in a Semi-Infinite Linear Cosserat Continuum by a Moving Surface Force
by George Eason. 559

Surf
by R. E. Meyer 587

Attendance List 627

*This paper was presented at the conference. It does not appear in these Transactions.

FIFTEENTH CONFERENCE OF ARMY MATHEMATICIANS
11-12 June 1969
The U. S. Army Aviation Systems Command, St. Louis, Missouri

Wednesday, 11 June 1969

0800-0830 REGISTRATION - Centennial Room

0830-0850 CALLING OF CONFERENCE TO ORDER - Centennial Room

Havard M. Bauer, Chairman on Local Arrangements

ADDRESS OF WELCOME

BG John P. Traylor, Deputy Commanding General, AVSCOM

0850-1010 TECHNICAL SESSION 1 - Centennial Room

Chairman: Edward Ross, Jr., U. S. Army Natick Laboratories, Natick, Massachusetts

A NOTE ON AN ELASTIC SPHERE INDENTING AN ELASTIC SPHERICAL CAVITY
M. A. Hussain and S. L. Pu, Maggs Research Center, U. S. Army Watervliet Arsenal, Watervliet, New York

THE FREE AND FORCED TORSIONAL MOTION OF JOINED CONCENTRIC CYLINDRICAL SHELLS
E. J. Brunelle, Maggs Research Center, Watervliet Arsenal, Watervliet, New York

0850-1010 TECHNICAL SESSION 2 - Arch Room

Chairman: Badrig Kurkjian, U. S. Army Materiel Command, Washington, D. C.

FEEDBACK IN INFORMATION SYSTEMS (The Effect of Feedback on System Entropy)
Erwin Biser, Avionics Laboratory, U. S. Army Electronics Command, Fort Monmouth, New Jersey

TENSOR CONCEPTS APPLIED TO PROJECTIVE GEOMETRY
Shunsuke Takagi, U. S. Army Terrestrial Sciences Center, Hanover, New Hampshire

1010-1040 BREAK

1040-1200 TECHNICAL SESSION 3 - Centennial Room

Chairman: O. L. Bowie, Army Materials & Mechanics Research Center, Watertown, Massachusetts

THE GENERAL THEORY OF STRESSES AND DISPLACEMENTS IN ELASTIC AND VISCOELASTIC LAYERED SYSTEMS
Yu-Tang Chou, Waterways Experiment Station, Corps of Engineers, Vicksburg, Mississippi

ADAPTATION OF VALANIS' METHOD TO KINETICS OF VISCOELASTIC PLATES
Struan Robertson, Maggs Research Center, U. S. Army Watervliet Arsenal, Watervliet, New York

1040-1200 TECHNICAL SESSION 4 - Arch Room

Chairman:

THIRD-ORDER POSITIVE CYCLIC SYSTEMS OF LINEAR DIFFERENTIAL EQUATIONS
Leon Kotin, Institute for Exploratory Research, U. S. Army Electronics Command, Fort Monmouth, New Jersey; and, Garrett Birkhoff, Harvard University, Cambridge, Mass.

PERTURBATIONS OF FUNCTIONAL DIFFERENTIAL SYSTEMS
Gerald A. Shanholt, U. S. Army Engineer Topographic Laboratories, Fort Belvoir, Virginia

1200-1315 LUNCH

1315-1445 TECHNICAL SESSION 5 - Centennial Room

Chairman: L. C. Young, University of Wisconsin, Mathematics Research Center, Madison, Wisconsin

STRESS WAVE PROPAGATION IN A CLASS OF NONHOMOGENEOUS ELASTIC MEDIA
Shun-Chin Chou, Army Materials & Mechanics Research Center, Watertown, Massachusetts

HIGH FREQUENCY EXTENSIONAL VIBRATIONS IN PLATE STRIPS
Gary Anderson, Research Laboratory, U. S. Army Watervliet Arsenal, Watervliet, New York

FORCED OSCILLATION OF A MASS WITH A BILINEAR SPRING
Royce Beckett, HQ, U. S. Army Weapons Command, Rock Island Arsenal, Rock Island, Illinois

1315-1445 TECHNICAL SESSION 6 - Arch Room

Chairman: Catherine F. Robinder, Research and Development Division, Rock Island Arsenal, Rock Island, Illinois

PRELIMINARY RESULTS ON EIGENVALUES AND STRUCTURE OF HURWITZ AND HERMITE MATRICES
Siegfried Lehnigk, Physical Sciences Laboratory, HQ, U. S. Army Missile Command, Redstone Arsenal, Alabama

MATRIX SQUARE ROOT FORMULATION OF THE KALMAN FILTER COVARIANCE EQUATIONS
William Agee, National Range Operations, White Sands Missile Range, White Sands, New Mexico

SOLUTION OF THE FOURIER EQUATION AND ASSOCIATED BOUNDARY EQUATIONS USING ANALOG AND DIGITAL ALGORITHMS
Darrel M. Thomsen, Science and Technology Laboratory, Research and Engineering Directorate, U. S. Army Weapons Command, Rock Island, Illinois

1445-1515 BREAK

1515-1645 TECHNICAL SESSION 7 - Centennial Room

Chairman: Julian Davis, U. S. Army Munitions Command, Picatinny Arsenal, Dover, New Jersey

THE STATE OF STRESS IN A LONG, HOLLOW CYLINDER DUE TO GENERAL RADIAL AND LOGITUDINAL TEMPERATURE VARIATION
John G. Avery, Solid Mechanics Branch, Physical Sciences Laboratory, U. S. Army Missile Command, Redstone Arsenal, Alabama

ELASTO-PLASTIC PLANE STRAIN ANALYSIS FOR A CIRCULAR HOLE IN A UNIAXIAL TENSILE FIELD
O. L. Bowie and C. E. Freese, Army Materials & Mechanics Research Center, Watertown, Massachusetts

APPROXIMATE ANALYSIS OF A FLAT, CIRCULAR PARACHUTE IN STEADY DESCENT
Edward W. Ross, Jr., U. S. Army Natick Laboratories, Natick, Massachusetts

1515-1645 TECHNICAL SESSION 8 - Arch Room

Chairman: Siegfried Lehnigk, Physical Sciences Laboratory, HQ, U. S. Army Missile Command, Redstone Arsenal, Alabama

VARIATIONAL METHODS IN EXPECTATION VALUE CALCULATIONS
Romas Shatas and John D. Stettler, Solid State Physics Branch, Physical Sciences Laboratory, U. S. Army Missile Command, Redstone Arsenal, Alabama

EXTENSIONS AND NUMERICAL STUDIES OF BEST INTERVAL APPROXIMATIONS TO ROOTS OF POSITIVE NUMBERS
Fred Frishman, Office, Chief of Research & Development, Department of the Army, Washington, D. C.; and, William Shepherd, Instrumentation Development Directorate, National Range Engineering, White Sands Missile Range, White Sands, New Mexico

A DYNAMIC MODEL OF VEHICLE SYSTEM AVAILABILITY
Martin Wachs and Russell Purvis, Army Materiel Systems Analysis Agency, U. S. Army Aberdeen Research and Development Center, Aberdeen Proving Ground, Maryland

1900 BANQUET - Boulevard Room

FACT AND FANTASY IN THE SPACE AGE
Professor Norman N. Royall, Jr., University of Missouri at Kansas City, Kansas City, Missouri

Thursday, 12 June 1969

0820-0950 TECHNICAL SESSION 9 - Arch Room

Chairman: Gary Anderson, Research Laboratory, U. S. Army Watervliet Arsenal, Watervliet, New York

WAVE PROPAGATION IN A TRANSVERSELY ISOTROPIC HALF-SPACE
R. L. Ryan, Maggs Research Center, U. S. Army Watervliet Arsenal, Watervliet, New York

THE CHARACTERISTICS OF A FLEURIC VORTEX RATE SENSOR IN THE RANGE OF FULLY DEVELOPED FLOW
Arthur J. Ostdiek, Harry Diamond Laboratories, Washington, D. C.

0820-0950 TECHNICAL SESSION 10 - Mirror Room

Chairman: Jagdish Chandra, Maggs Research Center, U. S. Army Watervliet Arsenal, Watervliet, New York

ANALOG/HYBRID SOLUTIONS TO ALGEBRAIC EQUATIONS AND BOUNDARY-VALUE PROBLEMS
Arthur Hausner, Harry Diamond Laboratories, Washington, D. C.

MATHEMATICAL TECHNIQUES FOR CONCEPT FORMULATION AND CONTRACT DEFINITION IN THE DESIGN OF MAJOR END-ITEMS
John Mundy, U. S. Army Aviation Systems Command, St. Louis, Missouri

0950-1020 BREAK

1020-1150 TECHNICAL SESSION 11 - Arch Room

Chairman: Ceslovas Masaitis, Aberdeen Research and Development Center, Aberdeen Proving Ground, Maryland

A RAPIDLY CONVERGING ITERATIVE TECHNIQUE FOR COMPUTING WIND COMPENSATION LAUNCHER SETTINGS FOR UNGUIDED ROCKETS
Louis Duncan and Bernard F. Engebos, U. S. Army Electronics Command, White Sands Missile Range, White Sands, New Mexico

A DIMENSIONAL ANALYSIS OF THE ERRORS OF ATMOSPHERIC SOUND RANGING
Robert P. Lee, Atmospheric Sciences Laboratory, U. S. Army Electronics Command, White Sands Missile Range, White Sands, New Mexico

ON THE VORTEX SOLUTION FOR THE TURBINE BLADE-FLOW-FIELD, AND CORRELATION WITH OBSERVED PERFORMANCE
Jacqueline A. Benton, and F. Edward McDonald, U. S. Army Mobility Equipment Research & Development Center, Fort Belvoir, Virginia

1020-1150 TECHNICAL SESSION 12 - Mirror Room

Chairman: Louis Rall, University of Wisconsin, Mathematics Research Center, Madison, Wisconsin

FORCED OSCILLATIONS IN SECOND ORDER SYSTEMS WITH UNBOUNDED NONLINEARITIES
Jagdish Chandra, Maggs Research Center, U. S. Army Watervliet Arsenal, Watervliet, New York; and,
B. A. Fleishman, Rensselaer Polytechnic Institute, Troy, New York

1020-1150 TECHNICAL SESSION 12 (Continued)

AN EVALUATION OF THE CONSTANTS IN THE INTEGRAL OF SCHWARZ-CHRISTOFFEL TRANSFORMATION BY AN ITERATIVE TECHNIQUE
Kanu Gandhi, Army Materials & Mechanics Research Center, Watertown, Massachusetts

A NUMERICAL TECHNIQUE FOR THE GENERATION OF CONTOURS
Merle J. Biggin, U. S. Army Topographic Command, Corps of Engineers, Washington, D. C.

1150-1310 LUNCH

1310-1510 GENERAL SESSION - Mirror Room

Chairman: Dr. Alan S. Galbraith, Mathematics Division, U. S. Army Research Office-Durham, Durham, North Carolina

THE STRESSES PRODUCED IN A SEMI-INFINITE LINEAR COSSERAT CONTINUUM BY A MOVING SURFACE FORCE
Dr. George Eason, Mathematics Research Center, U. S. Army, The University of Wisconsin, Madison, Wisconsin

SURF
Professor R. E. Meyer, Department of Mathematics, The University of Wisconsin, Madison, Wisconsin

A NOTE ON AN ELASTIC SPHERE INDENTING AN ELASTIC SPHERICAL CAVITY

M. A. Hussain

and

S. L. Pu

Research Mathematicians
Mem. ASME
Maggs Research Center
U. S. Army Watervliet Arsenal
Watervliet, N. Y.

ABSTRACT

The indentation of a smooth elastic sphere upon the infinite medium exterior to the sphere is considered. In the absence of a bond between the spherical indentor and the spherical cavity there appear a region of separation and a region of contact. The region where the sphere remains in contact with the external body is a spherical cap. Our primary objective is to determine the colatitude, η , of the boundary circle of this spherical cap in contact.

By means of Boussinesq potentials of the linear three-dimensional theory of elasticity the mixed boundary value problem is reduced to dual series involving spherical harmonics. The dual series are replaced by an equivalent Fredholm integral equation with unknown η at the upper limit of integration.

This article has been reproduced photographically from the author's manuscript.

This integral equation is solved by a variational technique which leads to a transcendental equation for the approximate determination of η .

INTRODUCTION

In this note we consider the problem of an infinite medium indented by a smooth spherical inclusion to which a concentrated force has been applied. In the absence of a bond at the interface the region of contact between the sphere and the outer body appears to be a spherical cap, Fig. 1. The primary objective of this note is to determine the region of contact.

The problem is essentially non-Hertzian in the sense that the area of contact cannot be considered small. In the classical Hertz problem of two spherical bodies in contact there are two basic results. Firstly, the radius of the circular region of contact is proportional to $P^{1/3}$ [1] where P is the load applied between two bodies in contact. Secondly, the relative approach due to the application of P, i.e., the relative normal displacement of any two points, one in each of the two bodies, which are far away from the contact surface, is proportional to $P^{2/3}$. We propose to investigate these two statements for the present non-Hertzian problem and to compare the results.

The spherical indentation problem is a mixed boundary value

problem in which the region of contact is not known apriori. The displacements over the contact region, which is not small as mentioned before, cannot be determined solely from the geometric considerations as done in the Hertz problem or in reference [2].

We use Boussinesq potentials in spherical coordinates. The mixed conditions lead to dual series involving Legendre functions which are further reduced to a Fredholm integral equation of the first kind for the contact stress. In the integral equation not only the contact stress but also the range of integration (corresponding to the region of contact) is unknown. An approximate solution is obtained by applying a variational method. The reader is referred to [3] for details of the method and its applications.

An approximate solution of the problem for an elastic sphere indenting an elastic cavity is given in [2]. However, the solution is not applicable to the case in which the radii of the sphere and the cavity are equal or nearly equal by virtue of the geometric considerations used in obtaining the displacements, equation (4) of [2].

For the analogous two-dimensional indentation problem, an approximate solution is given by Sheremetév [4] while the exact

solution is obtained in [5].

STATEMENT OF THE PROBLEM

Consider a smooth sphere inside an infinite, homogeneous and isotropic body. The elastic constants of the sphere are G′ and ν', those of the external medium are G and ν . We assume that there no bonds and no friction exist between the sphere and the outer body. The sphere is perfectly fitted in the spherical cavity in a state free from stresses and strains. The region of contact becomes a spherical cap as soon as a concentrated force F_z is applied at the center of the sphere in the direction of the positive z-axis, Fig. 1. With reference to the spherical coordinates (r , θ, γ), the problem is independent of γ and the boundary surface of the sphere is r = a. Our objective is to determine the value of θ , say η , for the point A and the relation between the coefficient ($\delta / 2G'$), defined later, and the force F_z. The approximate normal stress distribution in the contact surface will also be obtained.

Using the usual notation, the boundary conditions at the interface r = a are as follows:

$$\tau_{r\theta}(a,\theta) = \tau_{r\theta}'(a,\theta) = 0 \quad , \quad 0 \le \theta \le \pi \qquad (1)$$

$$\sigma_r(a,\theta) = \sigma_r'(a,\theta) = 0 \quad , \quad \eta \le \theta \le \pi \qquad (2)$$

$$u_r(a,\theta) = u'_r(a,\theta) \quad , \quad 0 \le \theta \le \eta \tag{3}$$

$$\sigma_r(a,\theta) = \sigma'_r(a,\theta) \le 0 \quad , \quad 0 \le \theta \le \eta \tag{4}$$

Unprimed and primed quantities refer to $r \ge a$ and $r \le a$, respectively.

REDUCTION TO DUAL SERIES

The general axisymmetric solutions of the equations of elasticity in spherical coordinates are given in terms of Boussinesq potentials in [6]. Retaining the notations used in [6], the internal and external solutions for the present problem are expressed in the forms

$$[S'] = \delta[A_{-2}] - \frac{F_z}{8\pi(1-\nu)}[B'_0] + \sum_{2,3,\cdots}^{\infty} g_n[A_{-n-1}] + \sum_{0,1,\cdots}^{\infty} h_n[B_{-n-2}] \tag{5}$$

$$[S] = \frac{-F_z}{8\pi(1-\nu)}[B_0] + \sum_{0,1,\cdots}^{\infty} e_n[A_n] + \sum_{2,3,\cdots}^{\infty} f_n[B_{n-1}] \tag{6}$$

where sol. $[A_{-2}]$ corresponds to the rigid body displacements and $(\delta / 2G')$ is the relative rigid displacement of the center of the sphere with respect to the center of the cavity in the positive z-axis. Solutions $[B'_0]$ and $[B_0]$ represent a concentrated force of magnitude $8\pi(1-\nu)$ acting at $r = o$ in an infinite body in the direction of the negative z-axis for $r \le a$

and $r \geq a$, respectively, see [6]. Superposition coefficients e_n, f_n, g_n, h_n and δ are to be determined from (1) through (4).

The components of displacement and stress for solutions $[An]$ and $[Bn]$, n = $\pm$ integer, are given by equations (12), (13) and (17), (18) in [6]. To satisfy the boundary conditions (1) we have

$$\left.\begin{aligned} h_1 &= -\frac{(1-2\nu')}{16\pi(1-\nu'^2)a^3}F_z \\ e_1 &= -\frac{(1-2\nu)a^2}{24\pi(1-\nu)}F_z \\ g_n &= \frac{(n^2+2n-1+2\nu')}{n-1}a^2 h_n \quad , \quad n \geq 2 \\ f_n &= -\frac{n+2}{(n^2-2+2\nu)a^2}e_n \quad , \quad n \geq 2 \end{aligned}\right\} \tag{7}$$

Substituting (7) into (5) and (6), we sum all the radial components of the stress and displacement respectively to obtain boundary values for $[S']$ and $[S]$. The results read

$$\begin{aligned} \sigma_r'(a,\theta) &= 2(1+\nu')h_0 - \frac{3F_z}{4\pi a^2}\cos\theta \\ &\quad + \sum_{2,3,\cdots}^{\infty} 2(n^2+n+1+2n\nu'+\nu')a^n h_n P_n \end{aligned} \tag{8}$$

$$2G'u_r'(a,\theta) = \delta\cos\theta + 2a\,h_0(1-2\nu') + \frac{3(1+2\nu'-4\nu'^2)F_z}{8\pi a(1-\nu'^2)}\cos\theta + \sum_{2,3,\cdots}^{\infty} \frac{2(2n^2-2n^2\nu'+n\nu'-1+2\nu')}{n-1} a^{n+1} h_n P_n \tag{9}$$

$$\sigma_r(a,\theta) = \frac{2e_0}{a^3} - \frac{3F_z}{4\pi a^2}\cos\theta + \sum_{2,3,\cdots}^{\infty} \frac{-2(n+2)(n^2+n+1-2n\nu-\nu)}{(n^2-2+2\nu)a^{n+3}} e_n P_n \tag{10}$$

$$2Gu_r(a,\theta) = -\frac{e_0}{a^2} + \frac{(7-8\nu)F_z}{12\pi(1-\nu)a}\cos\theta + \sum_{2,3,\cdots}^{\infty} \frac{2(2n^2-2n^2\nu+4n-5n\nu+1-\nu)}{(n^2-2+2\nu)a^{n+2}} e_n P_n \tag{11}$$

where $P_n = P_n(\cos\theta)$ denotes the Legendre polynomial of degree n. To meet the boundary conditions given by (2), we first define new coefficients Fn as follows

$$\left.\begin{aligned} \frac{2e_0}{a^3} &= 2(1+\nu')h_0 = F_0 \\ -\frac{3F_z}{4\pi a^2} &= 3F_1 \\ 2(n^2+n+1+2n\nu'+\nu')a^n h_n &= \frac{-2(n+2)(n^2+n+1-2n\nu-\nu)}{(n^2-2+2\nu)a^{n+3}} e_n \\ &= (2n+1)F_n \qquad \text{for } n = 2, 3, 4 \ldots \end{aligned}\right\} \tag{12}$$

so that both (8) and (10) are reduced to

$$\sigma_r(a,\theta) = \sigma_r'(a,\theta) = \sum_{0,1,2,\cdots}^{\infty} (2n+1)F_n P_n \tag{13}$$

Equations (9) and (11) become, with the relations of (12),

$$\frac{2G'u_r'(a,\theta)}{a} = \frac{\delta}{a}\cos\theta + \frac{(1-2\nu')}{(1+\nu')}F_0 -$$

$$-\frac{3(1+2\nu'-4\nu'^2)}{2(1-\nu'^2)}F_1\cos\theta + \sum_{2,3,\cdots}^{\infty}\gamma_n F_n P_n \qquad (14)$$

$$\frac{2Gu_r(a,\theta)}{a} = -\frac{F_0}{2} - \frac{7-8\nu}{3(1-\nu)}F_1\cos\theta + \sum_{2,3,\cdots}^{\infty}\beta_n F_n P_n \qquad (15)$$

where γ_n and β_n are abbreviations denoting

$$\gamma_n = \frac{(2n+1)(2n^2-2n^2\nu'+n\nu'-1+2\nu')}{(n-1)(n^2+n+1+2n\nu'+\nu')} \qquad (16)$$

$$\beta_n = -\frac{(2n+1)(2n^2-2n^2\nu+4n-5n\nu+1-\nu)}{(n+2)(n^2+n+1-2n\nu-\nu)} \qquad (17)$$

Applying boundary conditions (2) and (3), we obtain the dual series

$$\sum_{0,1,2,\cdots}^{\infty}(2n+1)F_n P_n(\cos\theta) = 0 \quad , \quad \eta \le \theta \le \pi \qquad (18)$$

$$\sum_{0,1,2,\cdots}^{\infty}\psi_n F_n P_n(\cos\theta) = -\frac{\alpha\delta\cos\theta}{a} \quad , \quad 0 \le \theta \le \eta \qquad (19)$$

where

$$\alpha = \frac{G}{G'} \qquad (20)$$

$$\left.\begin{aligned} \psi_0 &= \frac{1}{2} + \frac{\alpha(1-2\nu')}{1+\nu'} \\ \psi_1 &= \frac{7-8\nu}{3(1-\nu)} - \frac{3\alpha(1+2\nu'-4\nu'^2)}{2(1-\nu'^2)} \\ \psi_n &= -\beta_n + \alpha\gamma_n \quad , \quad n = 2, 3, \ldots \end{aligned}\right\} \tag{21}$$

INTEGRAL EQUATION AND AN APPROXIMATE SOLUTION

Let $\sigma(\theta)$ be the unknown radial stress $\sigma_r(a, \theta)$ at the interface r = a. It is obvious that $\sigma(\theta)$ is a continuous function over the entire region $0 \le \theta \le \pi$ and is even in θ. Using Fourier-Legendre analysis, $\sigma(\theta)$ is represented by

$$\sigma(\theta) = \sum_{0,1,2,\cdots}^{\infty} (2n+1) F_n P_n(\cos\theta) \quad , \quad 0 \le \theta \le \pi \tag{22}$$

with $\sigma(\theta)$ vanishing over the region $\eta \le \theta \le \pi$. The coefficients F_n are then given by

$$F_n = \frac{1}{2}\int_0^{\eta} \sigma(t) P_n(\cos t) \sin t \, dt \tag{23}$$

Putting (23) into (19) and interchanging the order of integration and summation, the set of two infinite series (18) and (19) is reduced to a single integral equation for σ

$$\int_0^{\eta} \sigma(t) K(\theta, t) \sin t \, dt = R(\theta) \quad , \quad 0 \le \theta \le \eta \tag{24}$$

where η is unknown, the kernel $K(\theta, t)$ and the right-hand member $R(\theta)$ are known functions given by

$$K(\theta, t) = \sum_{0,1,2,\cdots}^{\infty} \psi_n P_n(\cos\theta) P_n(\cos t) \tag{25}$$

$$R(\theta) = -\frac{2\alpha\delta}{a} \cos\theta \tag{26}$$

Since no closed form solution could be obtained for the Fredholm integral equation (24), we followed an approximate method [3] which has been established in particular for such types of integral equations. To apply the variational method, the kernel has to be symmetric, i.e. $K(t, \theta) = K(\theta, t)$ and the kernel may have at most a logarithmic singularity at $\theta = t$. Equation (25) shows that the kernel is symmetric. The principal part of the kernel can be shown to have a logarithmic singularity at $\theta = t$ by employing the technique introduced in [7] in which a perturbation scheme was established. Hence the variational method is applicable to our problem.

According to the method we must choose a trial function for $\sigma(\theta)$ and construct the functional

$$I(\sigma) = \int_0^{\eta} \sigma(t) \sin t \left\{ \int_0^{\eta} \sigma(\theta) \sin\theta K(\theta, t) d\theta - 2R(t) \right\} dt \tag{27}$$

If the function $\sigma(\theta)$ is chosen in the form

$$\sigma(\theta) = B(\cos\theta - \cos\eta)^{-1/2} + A(\cos\theta - \cos\eta)^{1/2} \quad , \quad 0 \le \theta \le \eta \tag{28}$$

where A and B are unknown coefficients their values depend upon the value of η . Substituting (28) into (27) we obtain

$$I = A^2 I_1 + 2AB I_2 + B^2 I_3 - 2A I_4 - 2B I_5 \tag{29}$$

where

$$\begin{matrix} I_1 \\ I_2 \end{matrix} = \int_0^\eta \int_0^\eta K(\theta,t)\sin\theta\sin t(\cos\theta - \cos\eta)^{1/2}(\cos t - \cos\eta)^{\pm 1/2} d\theta\, dt \tag{30}$$

$$\begin{matrix} I_4 \\ I_5 \end{matrix} = \int_0^\eta R(t)\sin t(\cos t - \cos\eta)^{\pm 1/2} dt \tag{31}$$

the positive signs go with I_1, I_4 while the negative signs go with I_2 and I_5. Based on the variational principle the functional is stationary when the trial function varies around the exact σ and the approximate value of η varies around the exact η , provided $B(\eta) = 0$. Hence the values of A and B are formally determined by

$$\frac{\partial I}{\partial A} = \frac{\partial I}{\partial B} = 0 \tag{32}$$

Equations (32) give us

$$A = \frac{I_4 I_3 - I_2 I_5}{I_1 I_3 - I_2^2} \quad , \qquad B = \frac{I_1 I_5 - I_2 I_4}{I_1 I_3 - I_2^2} \tag{33}$$

From the boundary conditions (4) there must exist a value of η such that $B(\eta) = 0$ and then the singular term in (28) is dropped out. This gives the equation for the determination of η

$$I_1 I_5 - I_2 I_4 = 0 \tag{34}$$

The expression for A is reduced from (33) to

$$A = I_4 / I_1 \tag{35}$$

which becomes known after η is found from (34). The approximate contact radial stress $\sigma_r(a,\theta)$ is given by (28) with B = o and A obtained in (35).

Now following the steps outlined in the preceding paragraph, we are required to carry out the integrals (30) and (31). With the results, which are derived in the appendix of this paper,

$$\begin{aligned} I_n'(\cos\eta) &= \int_0^{\eta} (\cos\theta - \cos\eta)^{1/2} \sin\theta \, P_n(\cos\theta)\, d\theta \\ &= \frac{\sqrt{2}}{2n+1}\left\{ \frac{\sin(n-\frac{1}{2})\eta}{2n-1} - \frac{\sin(n+\frac{3}{2})\eta}{2n+3} \right\} \end{aligned} \tag{36}$$

and

$$I_n^{-1}(\cos\eta) = 2\sqrt{2}\,\frac{\sin(n+\frac{1}{2})\eta}{2n+1} \tag{37}$$

integrals I_1, I_2, I_4 and I_5 become, with the necessary change of order of integration and summation,

$$\left.\begin{aligned} I_1 &= \sum_{0,1,\cdots}^{\infty} \Psi_n \left[I_n'(\cos\eta)\right]^2 \\ I_2 &= \sum_{0,1,\cdots}^{\infty} \Psi_n \left[I_n^{-1}(\cos\eta)\right]\left[I_n'(\cos\eta)\right] \\ I_4 &= -\frac{2\alpha\delta}{a} I_1'(\cos\eta) \\ I_5 &= -\frac{2\alpha\delta}{a} I_1^{-1}(\cos\eta) \end{aligned}\right\} \tag{38}$$

where I_1' and I_1^{-1} are given respectively by (36) and (37) with n = 1. Substituting (36) and (37) into (38) then (38) into (34) the equation for η becomes

$$\sum_{0,1,\cdots}^{\infty} \frac{\Psi_n}{(2n+1)^2}\left\{\frac{\sin(n-\frac{1}{2})\eta}{2n-1} - \frac{\sin(n+\frac{3}{2})\eta}{2n+3}\right\}\cdot$$

$$\cdot\left[\sin(n+\tfrac{1}{2})\eta\left(\sin\frac{\eta}{2} - \frac{1}{5}\sin\frac{5\eta}{2}\right) - \sin\frac{3}{2}\eta\left\{\frac{\sin(n-\frac{1}{2})\eta}{2n-1} - \frac{\sin(n+\frac{3}{2})\eta}{2n+3}\right\}\right] = 0 \tag{39}$$

This equation is of course independent of δ .

RELATION BETWEEN THE CONCENTRATED FORCE F_z AND THE COEFFICIENT $\delta/(2G')$

The ratio $\delta/(2G')$ is the coefficient of rigid body motion or "relative approach" of the inclusion. In the limit, when the inclusion becomes rigid, the force applied to the outer body is due to a rigid body motion of the inclusion only, i.e. $\lim_{G'\to\infty} \delta/(2G')$ is finite. In general there is a definite relation between the force F_z and this rigid body motion of the inclusion. This relation can be obtained as follows.

From the fact that the applied force F_z must be balanced by the net traction on any spherical surface of arbitrary radius centered at the point of application of F_z we have

$$F_z = -2\pi \int_0^{\pi} (\sigma_r \cos\theta - \tau_{r\theta} \sin\theta) r^2 \sin^2\theta \, d\theta \quad , \quad r \geq a \qquad (40)$$

and a similar relation for $r \leq a$. At the interface $r = a$, the shearing stress vanishes and the above equation is reduced to

$$F_z = -2\pi a^2 \int_0^{\eta} \sigma(\theta) \cos\theta \sin\theta \, d\theta \qquad (41)$$

From equation (28) with $B = o$, the approximate contact stress is expressed by

$$\sigma(\theta) = A (\cos\theta - \cos\eta)^{1/2} \quad , \quad 0 \leq \theta \leq \eta \qquad (42)$$

where A is, from (35) and (38)

$$A = -\frac{\sqrt{2}\,a\,\delta}{3a}\;\frac{\sin\frac{\eta}{2} - \frac{1}{5}\sin\frac{5}{2}\eta}{\sum_{0,1,\cdots}^{\infty} \Psi_n (2n+1)^{-2}\left\{\frac{\sin(n-\frac{1}{2})\eta}{2n-1} - \frac{\sin(n+\frac{3}{2})\eta}{2n+3}\right\}^2} \tag{43}$$

Substituting (43) and (42) into (41) and carrying out the integrals with the help of the formulae derived in the appendix we obtain the following relation

$$\frac{F_z}{Ga(\delta/G')} = \frac{4\pi}{9}\;\frac{\left(\sin\frac{\eta}{2} - \frac{1}{5}\sin\frac{5}{2}\eta\right)^2}{\sum_{0,1,\cdots}^{\infty} \Psi_n (2n+1)^{-2}\left\{\frac{\sin(n-\frac{1}{2})\eta}{2n-1} - \frac{\sin(n+\frac{3}{2})\eta}{2n+3}\right\}^2} \tag{44}$$

NUMERICAL RESULTS AND CONCLUSIONS

The quantities of interest in this problem are the angle η of the contact cap, the contact stress σ_r at the interface r = a and the relation between the force F_z and the coefficient $(\delta/2G')$. Among them η is the most fundamental. It depends only upon the material constants but not upon the size of the sphere nor upon the magnitude of the force or the relative approach $(\delta/2G')$. Hence we concentrated our efforts in the computation of η for various values of α, ν and ν'. To limit the use of computer time it is further assumed that $\nu = \nu'$. The single real non-trivial root of equation (39) has been obtained for $\nu = \nu' = 0$, 0.1, ..., 0.5 and for α from 0 to 10. The results are shown in (a) and (b) of Figure 2. In Figure 2(a) the angle η is

plotted versus the ratio α for $\nu = \nu' = 0$, 0.1, 0.2 and 0.3 while figure 2(b) gives the similar graph for $\nu = \nu' = 0.3$ and 0.5 in different scales. For large values of α , i.e. the indenting sphere is rather soft in comparison with the material being indented, the variation in η depends greatly upon the Poisson ratios. The angle η increases from $\eta \approx 80^{\circ}$ for $\nu = \nu' = 0$ to $\eta \approx 104^{\circ}$ for $\nu = \nu' = 0.5$ for $\alpha = 10$. The dependence on ν becomes weak for small values of α . In the case of a rigid sphere, i.e. $\alpha = 0$, the graph of η versus ν $(= \nu')$ is shown in Figure 3. The angle decreases from $\eta \approx 82.2^{\circ}$ for $\nu = \nu' = 0$ to $\eta \approx 77.5^{\circ}$ for $\nu = \nu' = 0.5$. Note that η is in general less than 90°. It becomes greater than 90° only when the sphere is softer ($\alpha > 1$) and the materials are nearly incompressible.

Contrary to the classical Hertz results, it may be concluded i) that the region of contact is independent of the force F_z applied and ii) that the relation between the relative approach and F_z is linear. This is in agreement with the results of the analogous two-dimensional problem given in [5].

APPENDIX

Let us denote

$$I_n^m(\cos\eta) = \int_0^\eta (\cos\theta - \cos\eta)^{\frac{m}{2}} P_n(\cos\theta)\sin\theta\, d\theta \tag{45}$$

The integral representation of legendre functions [8] is given by

$$P_\nu^\mu(\cos\theta) = \sqrt{\frac{2}{\pi}}\frac{(\sin\theta)^\mu}{\Gamma(-\mu+\frac{1}{2})}\int_0^\theta \frac{\cos(\nu+\frac{1}{2})\varphi\, d\varphi}{(\cos\varphi - \cos\theta)^{\mu+\frac{1}{2}}} \tag{46}$$

Substituting (46) with ν = n and μ = o into (45) and interchanging the order of integration, we have

$$I_n^m(\cos\eta) = \frac{\sqrt{2}}{\pi}\int_0^\eta \cos(n+\tfrac{1}{2})\varphi\left\{\int_\varphi^\eta \frac{(\cos\theta - \cos\eta)^{m/2}}{(\cos\varphi - \cos\theta)^{1/2}}\sin\theta\, d\theta\right\} d\varphi \tag{47}$$

Introducing a new variable $t = (\cos\varphi - \cos\theta)/(\cos\varphi - \cos\eta)$, we obtain

$$\int_\varphi^\eta \frac{(\cos\theta - \cos\eta)^{m/2}}{(\cos\varphi - \cos\theta)^{1/2}}\sin\theta\, d\theta = \frac{\Gamma(\frac{1}{2})\Gamma(\frac{m}{2}+1)}{\Gamma(\frac{m+3}{2})}(\cos\varphi - \cos\eta)^{\frac{m+1}{2}} \tag{48}$$

in which $\Gamma(x)$ is the Gamma function. Substituting (48) into (47) gives

$$I_n^m(\cos\eta) = \sqrt{\frac{2}{\pi}}\,\frac{m\Gamma(\frac{m}{2})}{2\Gamma(\frac{m+3}{2})}\int_0^\eta (\cos\varphi - \cos\eta)^{\frac{m+1}{2}}\cos(n+\tfrac{1}{2})\varphi\, d\varphi \tag{49}$$

Using the expression (46), equation (49) becomes

$$I_n^m(\cos\eta) = \frac{m}{2}\Gamma\left(\frac{m}{2}\right)(\sin\eta)^{\frac{m+2}{2}} P_n^{-\frac{m+2}{2}}(\cos\eta) \qquad (50)$$

For $m = \pm 1$ we immediately obtain equations (36) and (37) which were given previously in the text.

REFERENCES

1. Timoshenko, S. and Goodier, J. N., Theory of Elasticity, 2nd Edition, McGraw-Hill, 1951, p. 375.

2. Goodman, L. E. and Keer, L. M., "The Contact Stress Problem for an Elastic Sphere Indentry an Elastic Cavity" International Journal of Solids and Structures, Vol. 1, 1965, pp. 407-415.

3. Noble, B., and Hussain, M., "A Variational Method for Inclusion and Indentation Problems," Journal of the Institute of Mathematics and Its Application, England (to be published).

4. Sheremetév, M. P., "The Solution of the Equations of Certain Contact Problems of the Theory of Elasticity (Equation of the Prandtle type)." Problems of Continuum Mechanics, SIAM, 1961, pp. 419-439.

5. Noble, B. and Hussain, M., "Exact Solution of Certain Dual Series for Indentation and Inclusion Problems" International Journal of Engineering Science (to be published).

6. Sternberg, E., Eubanks, R. A., and Sadowski, M. A., "On the Axisymmetric Problem of Elasticity Theory for a Region Bounded by Two Concentric Spheres," Proc. 1st U. S. National Congress of Applied Mechanics, 1951, pp. 209-215.

7. Noble, B. and Hussain, M., "Angle of Contact for Smooth Elastic Inclusions," Developments in Mechanics, Vol. 4, Proceedings of the Tenth Midwestern Mechanics Conference, 1967, pp. 459-476.

8. Magnus, W., and Oberhettinger, F., Formulas and Theorems for the Special Functions of Mathematical Physics, Chelsea Publishing Co., New York, N.Y., 1949, p. 66 and p. 4.

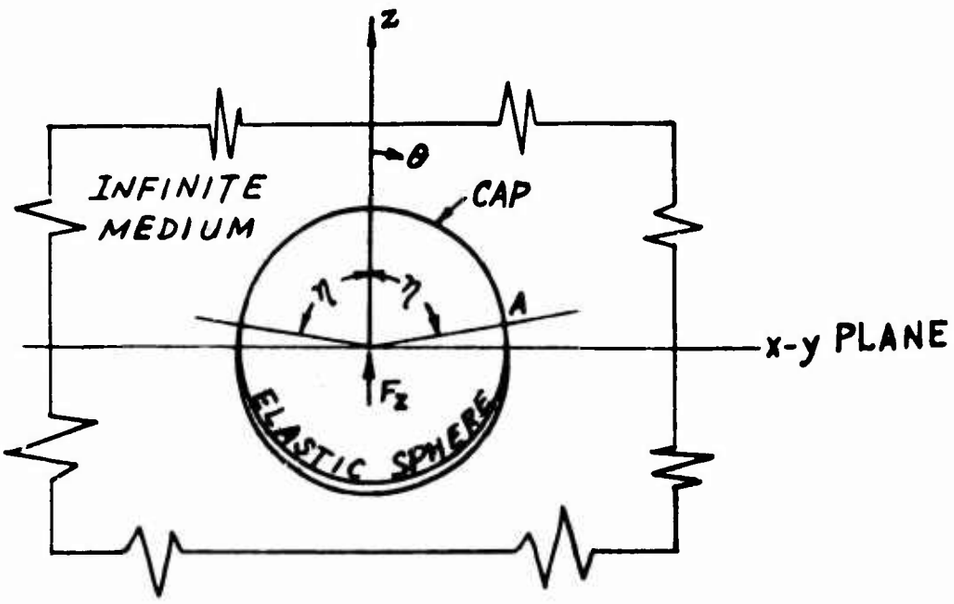


Fig. 1 A Sphere Indenting a Spherical Cavity.

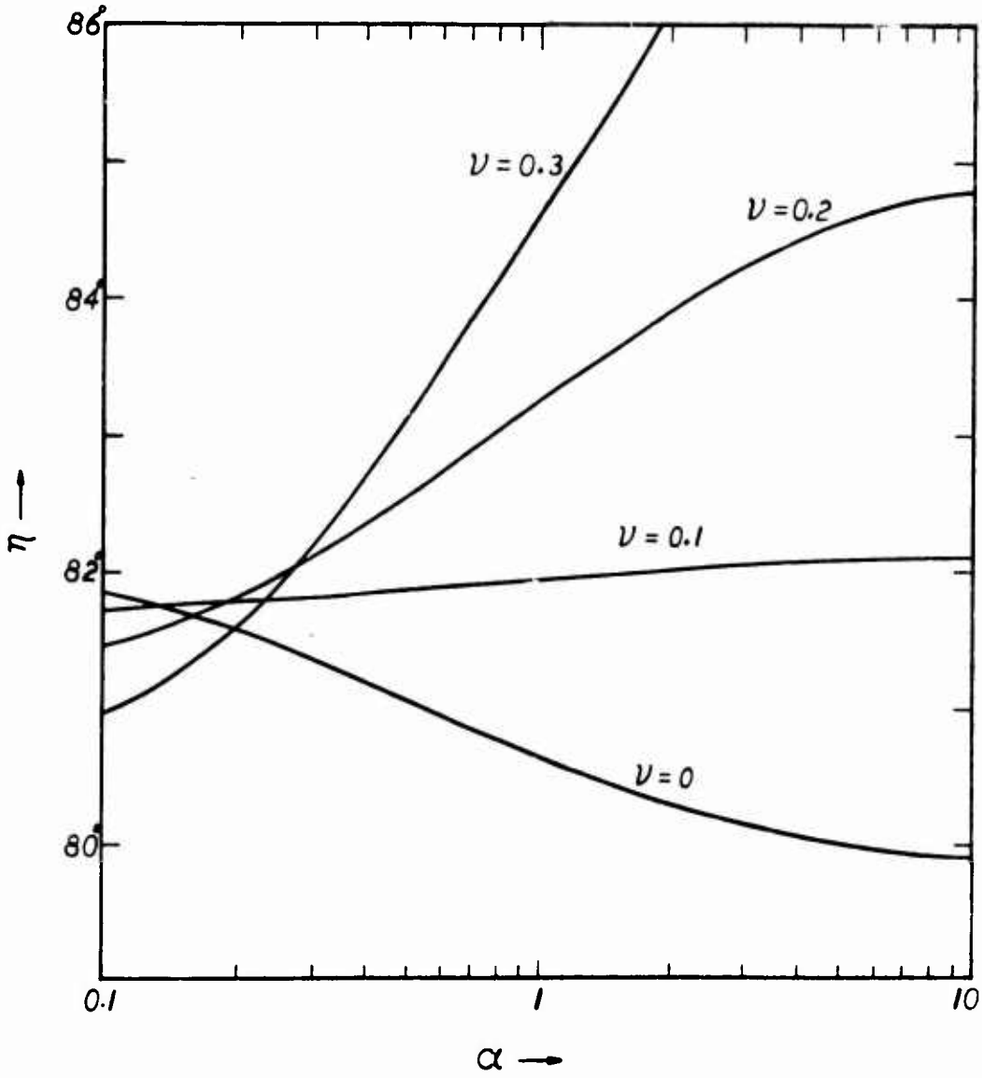
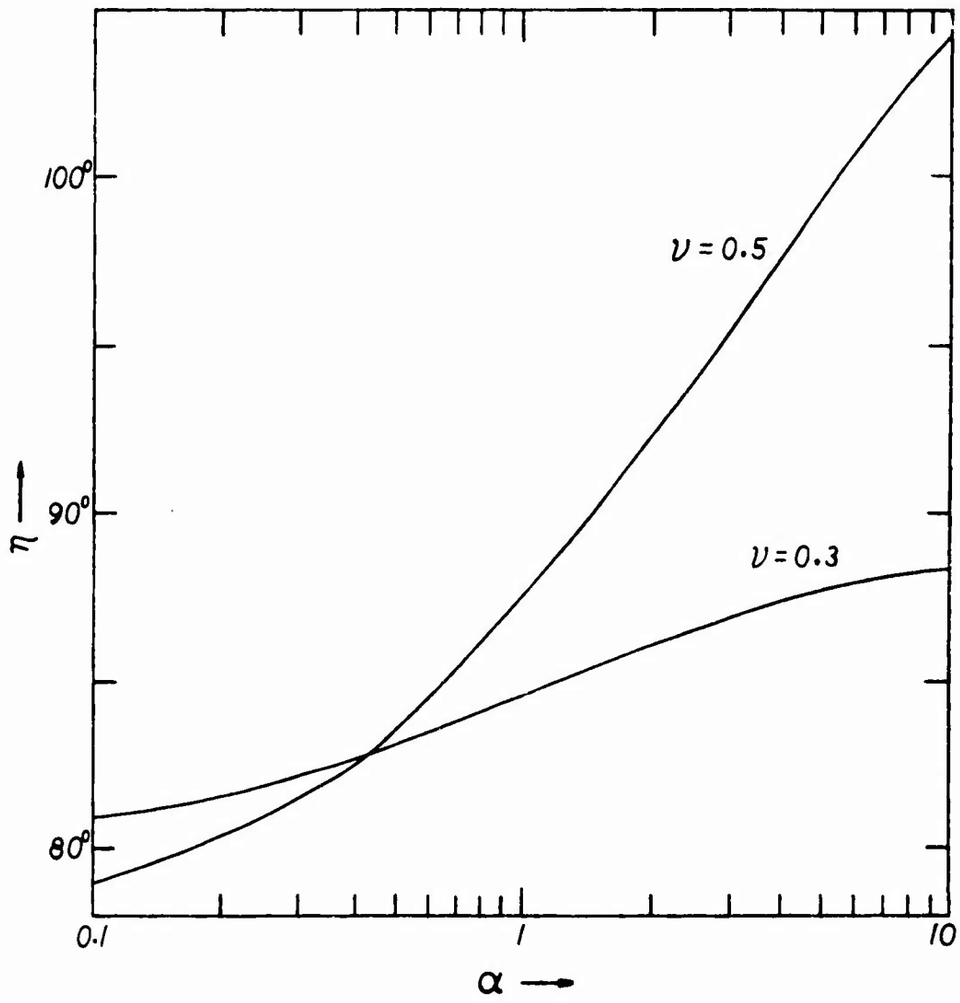


Fig. 2 The Colatitude η of the Spherical Cap in Contact vs. the Ratio α of Elastic Constants

(a) For $\nu = \nu' =$ 0, 0.1, 0.2 and 0.3



(b) For $\nu = \nu' =$ 0.3 and 0.5

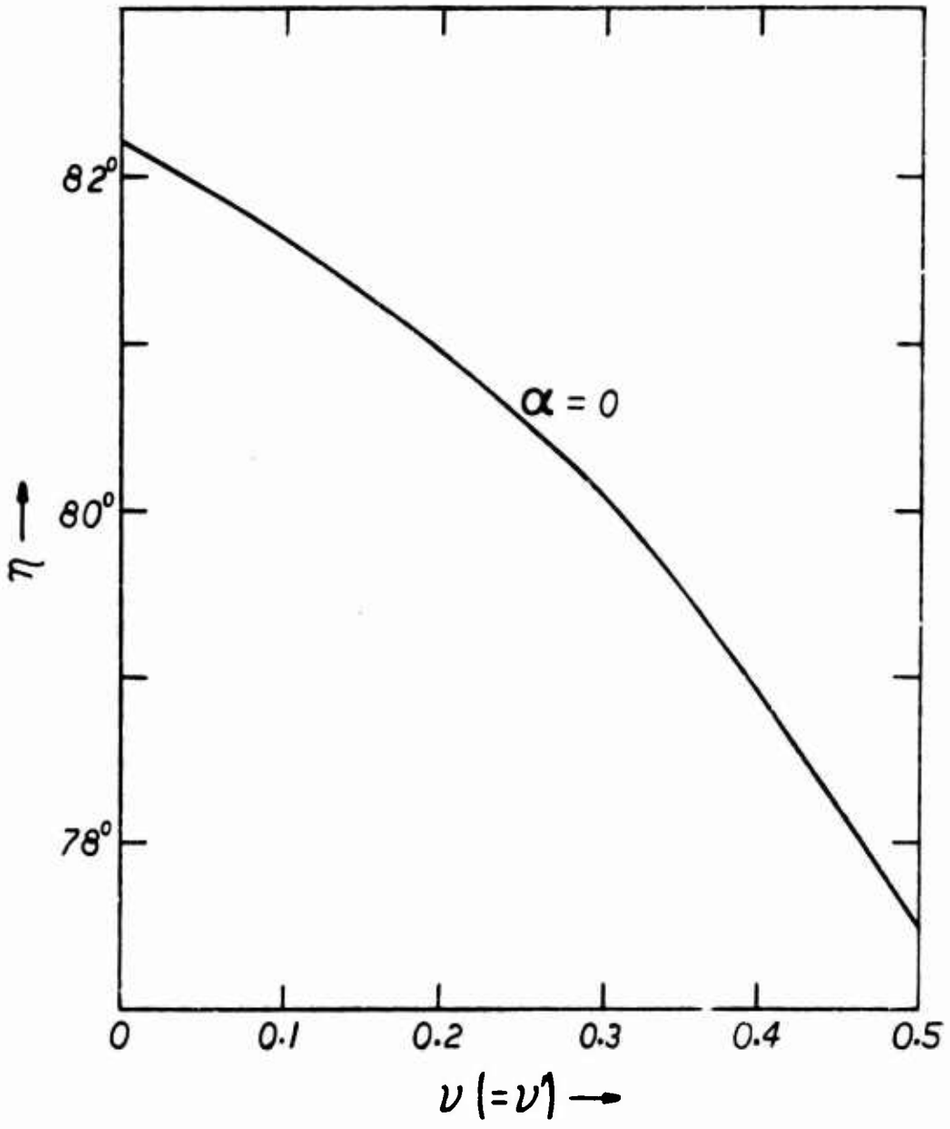


Fig. 3 The Colatitude η of the Spherical Cap vs. the Poisson Ratio for the Case of a Rigid Inclusion

TORSIONAL DYNAMICS OF JOINED CONCENTRIC CYLINDRICAL SHELLS

E. J. Brunelle*
Watervliet Arsenal
Watervliet, New York

ABSTRACT. This paper describes the free and forced motion of two, thin, concentric, circular cylindrical shells joined at their ends by rigid diaphragms with inertial properties. Mathematically, the problem is described by two special Sturm-Liouville systems with common eigenvalues coupled only through the boundary conditions. The systems possess a modified orthogonality principle and give rise to a modified expansion principle for the associated non-homogeneous systems. These principles are derived in detail and several free motion problems are presented to illustrate the theory.**

*Also, Associate Professor, Rensselaer Polytechnic Institute, Troy, New York.

**The remainder of this article has been reproduced photographically from the author's manuscript.

I. Introduction

Much has been written concerning the free and forced motion of various types of shells subjected to a variety of boundary conditions. However there appears to be no counterpart work involving shells that are concentrically nested and joined to one another in various ways. (Such shells are hereafter called joined shells). In order to understand clearly the modified principles and procedures that arise in the analysis of joined shells we now investigate the simplest type of a joined shell executing its simplest motion, i.e., two joined circular cylindrical shells executing torsional motion subjected to various boundary conditions. Referring to Fig. 1, the non-dimensionalized equation of motion for the $i^{\underline{th}}$ shell [1],[2][2] is given by (1) and the associated effective tangential shear resultant is given by (2) where,

$\bar{v}_i$ = twist angle of the $i^{\underline{th}}$ cylinder ($\equiv \frac{u_i}{a_i}$)

$\bar{u}_i$ = circumferential displacement of the $i^{\underline{th}}$ cylinder

a_i = radius of the $i^{\underline{th}}$ cylinder middle surface

x_i = ξ_i / L = non-dimensional coordinate of $i^{\underline{th}}$ cylinder

L = length of all cylinders[3]

Λ_i = $[\rho_i/G_i]^{\frac{1}{2}}$ = inverse of shear wave speed in the $i^{\underline{th}}$ infinite medium

h_i = thickness of the $i^{\underline{th}}$ shell

λ_i^2 = $\Omega_i^2 L^2/[1+h_i^2/12a_i^2]$

p_i = tangential force per unit area of the $i^{\underline{th}}$ middle surface

ρ_i = mass density of the $i^{\underline{th}}$ shell

F_i = $p_i/a_i\rho_i h_i$

Numbers in square brackets refer to references at the end of the text.

This is assumed for convenience; problems with different L_i are easily formulated and solved with some increases in algebraic manipulation.

$$\partial^2\bar{v}_i(x_i,t)/\partial x_i^2 + \lambda_i^2[F_i(x_i,t) - \partial^2\bar{v}_i(x_i,t)/\partial t^2] = 0 \; ; \quad i = 1,2 \quad (1)$$

$$\bar{T}_i(x_i,t) = h_i a_i G_i L^{-1}[1 + h_i^2/12a_i^2]\partial\bar{v}_i(x_i,t)/\partial x_i \; ; \quad i = 1,2 \quad (2)$$

The various boundary conditions associated with this set of equations are (3) clamped end, (4) end joined by weightless rigid diaphragm, and (5) end joined by rigid disk with inertial properties,

$$\bar{v}_1(\tilde{x}_1,t) = \bar{v}_2(\tilde{x}_2,t) = 0 \quad (3)$$

$$\left.\begin{aligned} &\bar{v}_1(\tilde{x}_1,t) = \bar{v}_2(\tilde{x}_2,t) \\ &2\pi a_1^2\bar{T}_1(\tilde{x}_1,t) + 2\pi a_2^2\bar{T}_2(\tilde{x}_2,t) = 0 \end{aligned}\right\} \quad (4)$$

$$\left.\begin{aligned} &\bar{v}_1(\tilde{x}_1,t) = \bar{v}_2(\tilde{x}_2,t) \\ &2\pi a_1^2\bar{T}_1(\tilde{x}_1,t) + 2\pi a_2^2\bar{T}_2(\tilde{x}_2,t) \mp I_{\tilde{x}}\partial^2\bar{v}_i(\tilde{x}_1,t)/\partial t^2 = 0 \end{aligned}\right\} \quad (5)$$

where the minus sign is used (in (5)) if $\tilde{x}_1$ is zero and the plus sign is used if $\tilde{x}_1$ is unity; and where

$\tilde{x}_i$ = either 0 or 1 ; $i = 1,2$

$I_{\tilde{x}}$ = angular moment of inertia of the disk at the end $\tilde{x}$

II. The Orthogonality Principle

The homogeneous counterparts of (1) and (2) and the boundary conditions corresponding to (5) are now used to derive the orthogonality principle associated with this type of joined shell. It will be seen that the orthogonality principles using (3) and (4) will be special cases of the orthogonality principle to be derived in this section. Hence the system to be investigated is (6) and (7), with the boundary conditions (8) through (11) where,

$v_i(x_i) = e^{-i\omega t}\bar{v}_i(x_i,t)$

ω = frequency of oscillation

$\mu = \rho_1 h_1 a_1^3 (\rho_2 h_2 a_2^3)^{-1}$

$\lambda = \lambda_2/\lambda_1$

$\Omega = \lambda_1\omega$

$\mathcal{Q}_0 = I_0/2\pi\rho_1 h_1 L a_1^3$

$\mathcal{Q}_1 = I_1/2\pi\rho_1 h_1 L a_1^3$

I_0 = angular moment of inertia of disk at $x_1 = x_2 = 0$

I_1 = angular moment of inertia of disk at $x_1 = x_2 = 1$

$$v_1''(x_1) + \lambda_1^2\omega^2 v_1(x_1) = 0 \tag{6}$$

$$v_2''(x_2) + \lambda_2^2\omega^2 v_2(x_2) = 0 \tag{7}$$

$$v_1(0) = v_2(0) \tag{8}$$

$$v_1(1) = v_2(1) \tag{9}$$

$$\mu\lambda^2[v_1'(0) + \mathcal{Q}_0\Omega^2 v_1(0)] + v_2'(0) = 0 \tag{10}$$

$$\mu\lambda^2[v_1'(1) - \mathcal{Q}_1\Omega^2 v_1(1)] + v_2'(1) = 0 \tag{11}$$

Notice that primes have been used to denote differentiation <u>with respect to the argument</u> so that, for example, $v_1'(0) = \partial v_1(0)/\partial x_1$ and $v_2'(0) = \partial v_2(0)/\partial x_2$ etc.

Since (6) and (7) are valid for the $m^{\underline{th}}$ and $n^{\underline{th}}$ modes of vibration, the standard orthogonality derivation procedures yield (12) and (13).

$$[v_{1n}(x_1)v_{1m}'(x_1) - v_{1m}(x_1)v_{1n}'(x_1)]_0^1 + (\Omega_m^2 - \Omega_n^2)\int_0^1 v_{1n}(x_1)v_{1m}(x_1)dx_1 = 0 \tag{12}$$

$$[v_{2n}(x_2)v_{2m}'(x_2) - v_{2m}(x_2)v_{2n}'(x_2)]_0^1 + \lambda^2(\Omega_m^2 - \Omega_n^2)\int_0^1 v_{2n}(x_2)v_{2m}(x_2)dx_2 = 0 \tag{13}$$

Using (8) through (11) we find that

$$[v_{2n}(x_2)v'_{2m}(x_2)-v_{2m}(x_2)v'_{2n}(x_2)]_0^1 = v_{1n}(1)[\mathfrak{Q}_1\Omega_m^2 v_{1m}(1)-v'_{1m}(1)]\mu\lambda^2$$
$$-v_{1m}(1)[\mathfrak{Q}_1\Omega_n^2 v_{1n}(1)-v'_{1n}(1)]\mu\lambda^2 + v_{1n}(0)[v'_{1m}(0)+\mathfrak{Q}_0\Omega_m^2 v_{1m}(0)]\mu\lambda^2 \qquad (14)$$
$$-v_{1m}(0)[v'_{1n}(0)+\mathfrak{Q}_0\Omega_n^2 v_{1n}(0)]\mu\lambda^2$$

Multiplying (12) by $\mu\lambda^2$, adding the result to (13) and using (14), yields (15).

$$[\Omega_m^2-\Omega_n^2][\mathfrak{Q}_1 v_{1n}(1)v_{1m}(1) + \mathfrak{Q}_0 v_{1n}(0)v_{1m}(0)$$
$$+ \int_0^1 v_{1n}(x_1)v_{1m}(x_1)dx_1 + \mu^{-1}\int_0^1 v_{2n}(x_2)v_{2m}(x_2)dx_2] = 0 \qquad (15)$$

Therefore if $\Omega_m^2 \neq \Omega_n^2$ the desired orthogonality principle is given by (16) for the elastic shell modes

$$\mathfrak{Q}_1 v_{1n}(1)v_{1m}(1) + \mathfrak{Q}_0 v_{1n}(0)v_{1m}(0)$$
$$+ \int_0^1 v_{1n}(x_1)v_{1m}(x_1)dx_1 + \mu^{-1}\int_0^1 v_{2n}(x_2)v_{2m}(x_2)dx_2 = 0 \qquad (16)$$

The rigid shell mode is found by letting ω be zero in (6) and (7) so that

$$v''_{10}(x_1) = v''_{20}(x_2) = 0 \qquad (17)$$

where we have put the mode index (m or n) equal to zero. Applying (8) through (11) to (17) we find the result (18) where A is a constant.

$$v_{10}(x_1) = v_{20}(x_2) \equiv A \qquad (18)$$

The orthogonality principle for mixed elastic and rigid shell modes is found by observing that the sum of the angular inertial moments for a freely vibrating joined shell must be zero. Therefore,

$$\mathcal{Q}_0 \partial^2 \bar{v}_1(0,t)/\partial t^2 + \mathcal{Q}_1 \partial^2 \bar{v}_1(1,t)/\partial t^2 + \int_0^1 (\partial^2 \bar{v}_1(x_1,t)/\partial t^2)dx_1 + \mu^{-1}\int_0^1 (\partial^2 \bar{v}_2(x_2,t)/\partial t^2)dx_2 = 0. \tag{19}$$

But since $\bar{v}_{in}(x_i,t) = e^{i\omega_n t} v_{in}(x_i)$, $v_{10}(x_1) = v_{20}(x_2) \equiv A$, and since $-\omega_n^2 e^{i\omega_n t} \neq 0$, (19) becomes (20) which is the desired mixed orthogonality principle; note that formal replacement of either m or n by zero in (16) yields the same result as (20).

$$\mathcal{Q}_0 v_{1n}(0)v_{10}(0) + \mathcal{Q}_1 v_{1n}(1)v_{10}(1) + \int_0^1 v_{1n}(x_1)v_{10}(x_1)dx_1 + \mu^{-1}\int_0^1 v_{2n}(x_2)v_{20}(x_2)dx_2 = 0 \tag{20}$$

If the end $x_i = 0$ is joined by an inertia-less disk (or is clamped) then the orthogonality principle reduces to (21).

$$\mathcal{Q}_1 v_{1n}(1)v_{1m}(1) + \int_0^1 v_{1n}(x_1)v_{1m}(x_1)dx_1 + \mu^{-1}\int_0^1 v_{2n}(x_2)v_{2m}(x_2)dx_2 = 0 \tag{21}$$

Finally, if both ends are joined by inertia-less disks (or one end clamped) the orthogonality principle further reduces to (22).

$$\int_0^1 v_{1n}(x_1)v_{1m}(x_1)dx_1 + \mu^{-1}\int_0^1 v_{2n}(x_2)v_{2m}(x_2)dx_2 = 0 \tag{22}$$

III. The Forced Motion Expansion Principle

We now seek solutions of (1) and (5) in the form

$$\bar{v}_i(x_i,t) = \sum_{n=0}^{\infty} \xi_n(t) v_{in}(x_i) \; ; \quad i = 1,2 \tag{23}$$

where the $v_{in}(x_i)$ are the mode shapes of the homogeneous equations associated with (1). Inserting (23) in (1) yields

$$\sum_{n=1}^{\infty} \xi_n(t) v''_{in}(x_i) + \lambda_i^2 F_i(x_i,t) - \lambda_i^2 \sum_{n=0}^{\infty} \ddot{\xi}_n(t) v_{in}(x_i) = 0; \; i = 1,2 \tag{24}$$

where dots are now used to denote differentiations with respect to time.

Multiplying (24) by $v_{im}(x_i)dx_i$ and integrating over the x_i interval 0 to 1 yields (25)

$$\sum_{n=1}^{\infty} \xi_n(t)\int_0^1 v_{im}v_{in}''dx_i + \lambda_i^2\int_0^1 F_i(x_i,t)v_{im}dx_i - \lambda_i^2 \sum_{n=0}^{\infty} \ddot{\xi}_n(t)\int_0^1 v_{im}v_{in}dx_i = 0 \; ; \quad i = 1,2 \tag{25}$$

Inserting (26), which may be obtained by suitably integrating the homogeneous form of (1), into (25) yields (27) where we note that in the sequel $\omega_0^2 \equiv 0$.

$$\int_0^1 v_{in}''v_{im}dx_i = -\lambda_i^2\omega_n^2\int_0^1 v_{in}v_{im}dx_i \; ; \quad i = 1,2 \tag{26}$$

$$\sum_{n=0}^{\infty} [\ddot{\xi}_n(t) + \omega_n^2\xi_n(t)]\int_0^1 v_{im}v_{in}dx_i = \int_0^1 F_i(x_i,t)v_{im}dx_i \; ; \quad i = 1,2 \tag{27}$$

Multiplying the second relation of (27) by μ^{-1} and adding this to the first relation of (27) yields (28).

$$\sum_{n=0}^{\infty} [\ddot{\xi}_n(t)+\omega_n^2\xi_n(t)][\int_0^1 v_{1m}v_{1n}dx_1+\mu^{-1}\int_0^1 v_{2m}v_{2n}dx_2] = \int_0^1 F_1(x_1,t)v_{1m}dx_1 + \mu^{-1}\int_0^1 F_2(x_2,t)v_{2m}dx_2 \tag{28}$$

Adding (29) to both sides of (28) and using the orthogonality relations (16) and (20) yields (30), where M_m is given by (31).

$$\sum_{n=0}^{\infty} [\ddot{\xi}_n(t) + \omega_n^2\xi_n(t)][\mathcal{Q}_1v_{1n}(1)v_{1m}(1) + \mathcal{Q}_0v_{1n}(0)v_{1m}(0)] \tag{29}$$

$$[\ddot{\xi}_m(t) + \omega_m^2\xi_m(t)]M_m = \int_0^1 F_1(x_1,t)v_{1m}dx_1 + \mu^{-1}\int_0^1 F_2(x_2,t)v_{2m}dx_2 + \sum_{n=0}^{\infty} [\ddot{\xi}_n(t) + \omega_n^2\xi_n(t)][\mathcal{Q}_1v_{1n}(1)v_{1m}(1) + \mathcal{Q}_0v_{1n}(0)v_{1m}(0)] \tag{30}$$

$$M_m = \mathcal{Q}_1 v_{1m}^2(1) + \mathcal{Q}_0 v_{1m}^2(0) + \int_0^1 v_{1m}^2 dx_1 + \mu^{-1}\int_0^1 v_{2m} dx_2 \tag{31}$$

Using (23) we easily determine (32), and using both (23) and the homogeneous form of (1) yields (33). These relations when inserted in the summation term on the right-hand side of (30), and use made of (1), yield equations for the ξ_n as given by (34), where Ξ_n and M_n are given by (35) and (36) respectively.

$$\partial^2 \overline{v}_1(x_1,t)/\partial t^2 = \sum_{n=0}^{\infty} \ddot{\xi}_n(t) v_{1n} \tag{32}$$

$$-\lambda_1^{-2} \overline{v}_1''(x_1,t) = \sum_{n=1}^{\infty} \omega_n^2 \xi_n(t) v_{1n} \tag{33}$$

$$\ddot{\xi}_n(t) + \omega_n^2 \xi_n(t) = M_n^{-1} \Xi_n(t) \; ; \quad n = 0,1,2, \ldots \tag{34}$$

$$\begin{aligned} \Xi_n(t) = {} & \mathcal{Q}_1 v_{1n}(1) F_1(1,t) + \mathcal{Q}_0 v_{1n}(0) F_1(0,t) \\ & + \int_0^1 F_1(x_1,t) v_{1n} dx_1 + \mu^{-1} \int_0^1 F_2(x_2,t) v_{2n} dx_2 \end{aligned} \tag{35}$$

$$M_n = \mathcal{Q}_1 v_{1n}^2(1) + \mathcal{Q}_0 v_{1n}^2(0) + \int_0^1 v_{1n}^2 dx_1 + \mu^{-1} \int_0^1 v_{2n}^2 dx_2 \tag{36}$$

However, in order for (23) to satisfy (5), it can be shown that $F_1(0,t) = F_1(1,t) = 0$ (see Appendix 1) so that the final form for the $\Xi_n(t)$ is given by

$$\Xi_n(t) = \int_0^1 F_1(x_1,t) v_{1n} dx_1 + \mu^{-1} \int_0^1 F_2(x_2,t) v_{2n} dx_2 \tag{35a}$$

From a physical standpoint the actual response is affected by a negligible amount because of the $F_1(0,t) = F_1(1,t) = 0$ condition, since $F_1(x_1,t)$ may take on the desired values in the interval $0+\varepsilon_1 \leq x_1 \leq 1-\varepsilon_2$ where ε_1 and ε_2 may be as small as desired.

Finally, once the initial conditions have been specified on $\bar{v}_i(x_i,t)$, all integration constants may be determined, and hence the forced motion expansion principle has been established.

IV. Free Vibrations

This section presents free vibration results (i.e., frequency equations and mode shape ratios) for cylindrical shells joined by rigid diaphram(s). Of particular interest are the interpretations of the frequency equations as $\mu \to 0$ and as $\mu \to \infty$, which quickly permit one to map out regions on the frequency plot in which solutions exist. This procedure saves substantial amounts of computer time when completing the solution details.

(A) Cylinders Clamped at $x_i = 0$ and Joined with a Rigid Inertia-less Diaphragm at $x_i = 1$.

The equations of free vibrations, (37) and (38), subject to the boundary conditions (39) thru (41) yield the mode shapes (42), the amplitude ratio (43), and the frequency relation (44).

$$v_1''(x_1) + \Omega^2 v_1(x_1) = 0 \tag{37}$$

$$v_2''(x_2) + \lambda^2\Omega^2 v_2(x_2) = 0 \tag{38}$$

$$v_1(0) = v_2(0) = 0 \tag{39}$$

$$v_1(1) = v_2(1) \tag{40}$$

$$\mu\lambda^2 v_1'(1) + v_2'(1) = 0 \tag{41}$$

$$v_{1n}(x_1) = A_{1n}\sin\Omega_n x_1 \quad \text{and} \quad v_{2n}(x_2) = A_{2n}\sin\lambda\Omega_n x_2 \tag{42}$$

$$A_{1n}/A_{2n} = \sin\lambda\Omega_n/\sin\Omega_n \tag{43}$$

$$\sin\Omega_n \cos\lambda\Omega_n + \mu\lambda\sin\lambda\Omega_n \cos\Omega_n = 0 \tag{44}$$

Since μ is not in the arguments of (44) it is convenient to think in terms of a λ versus Ω_n plot with μ as a parameter.

Solutions independent of μ are given by (45) and (46) which are obtained by demanding that $\sin\Omega_n = \sin\lambda\Omega_n = 0$ and $\cos\Omega_n = \cos\lambda\Omega_n = 0$ respectively.

$$\Omega_n = n\pi \text{ and } \lambda = m/n \quad ; \quad m,n = 1,2,3, \ldots \tag{45}$$

$$\Omega_n = (2n-1)\frac{\pi}{2} \text{ and } \lambda = (2m-1)/(2n-1) \quad ; \quad m,n = 1,2,3,\ldots \tag{46}$$

Furthermore, the limiting solutions as $\mu \to 0$ and as $\mu \to \infty$ are given by (47) and (48) respectively.

$$\Omega_n = n\pi \text{ and } \Omega_n = (2n-1)\frac{\pi}{2\lambda} \quad ; \quad n = 1,2,3,\ldots \tag{47}$$

$$\Omega_n = n\pi/\lambda \text{ and } \Omega_n = (2n-1)\frac{\pi}{2} \quad ; \quad n = 1,2,3,\ldots \tag{48}$$

Finally, since only positive values of μ are physically possible, just the positive solutions of (49) are sought.

$$\mu = -\tan\Omega/\lambda\tan\lambda\Omega \tag{49}$$

Using (45) thru (48), the solution regions for the first five modes on the λ versus Ω_n plot are easily sketched as shown by the shaded portions of Fig. 2. The solution details are then obtained by numerical procedures and Fig. 3 shows the completed λ versus Ω_n plot (for the first four modes) for three values of the parameter μ.

(B) Free-Free Cylinders Joined at Both Ends by Rigid Inertia-Less Diaphragms

The equations of free vibration, (37) and (38), subject to the boundary conditions (50) thru (53) yield the mode shapes (54), the amplitude ratio (55),

and the frequency relation (56).

$$v_1(0) = v_2(0) \tag{50}$$

$$v_1(1) = v_2(1) \tag{51}$$

$$\mu\lambda^2 v_1'(0) + v_2'(0) = 0 \tag{52}$$

$$\mu\lambda^2 v_1'(1) + v_2'(1) = 0 \tag{53}$$

$$\left.\begin{aligned} v_{1n}(x_1) &= A_{1n}\sin\Omega_n x_1 + B_{1n}\cos\Omega_n x_1 \\ \text{and}\quad v_{2n}(x_2) &= -\mu\lambda A_{1n}\sin\lambda\Omega_n x_2 + B_{1n}\cos\lambda\Omega_n x_2 \end{aligned}\right\} \tag{54}$$

$$A_{1n}/B_{1n} = (\cos\lambda\Omega_n - \cos\Omega_n)/(\sin\Omega_n + \mu\lambda\sin\lambda\Omega_n) \tag{55}$$

$$2\mu\lambda[1-\cos\Omega_n\cos\lambda\Omega_n] + [1+(\mu\lambda)^2]\sin\Omega_n\sin\lambda\Omega_n = 0 \tag{56}$$

The solutions of (56) independent of μ are given by (57) and (58) and the limiting solution of (56), as both $\mu \to 0$ and $\mu \to \infty$, is given by (59).

$$\Omega_n = 2n\pi \quad \text{and} \quad \lambda = m/n \; ; \begin{cases} m = 0,1,2,\ldots \\ n = 1,2,\ldots \end{cases} \tag{57}$$

$$\Omega_n = (2n-1)\pi \quad \text{and} \quad \lambda = (2m-1)/(2n-1) \; ; \quad m,n = 1,2,\ldots \tag{58}$$

$$\Omega_n = n\pi \quad \text{and} \quad \Omega_n = n\pi/\lambda \; ; \quad n = 1,2,\ldots \tag{59}$$

Dividing (56) by λ and taking the limit as $\lambda \to 0$ yields

$$\lim_{\lambda\to 0} \mu = \Omega_n \sin\Omega_n/[2(\cos\Omega_n - 1)] \tag{60}$$

Additionally, solving (56) for μ results in (61), from which only the positive values of μ are sought.

$$\mu = -[1-\cos\Omega_n\cos\lambda\Omega_n \pm |\cos\lambda\Omega_n - \cos\Omega_n|]/(\lambda\sin\Omega_n\sin\lambda\Omega_n) \tag{61}$$

Furthermore (61) has a double root when $\cos\lambda\Omega_k = \cos\Omega_k$, so that the frequencies at which the double roots occur are given by (62), and the value of the double roots are given by (63). Eqn. (63) is obtained by noting that when $\Omega = \Omega_k$, (61) yields $\mu = (1-\cos\Omega_k\cos\lambda\Omega_k)/(-\lambda\sin\Omega_k\sin\lambda\Omega_k)$ and then substituting this result into (56) yields (63) directly.

$$\Omega_k = 2\pi k/(\lambda\pm 1) \; ; \quad k = 0,1,2,... \tag{62}$$

$$\mu = \pm\lambda^{-1} \tag{63}$$

When $\mu = \lambda^{-1}$ and (62) is satisfied, two successive modes will have the same frequency and since $\Omega_m^2 = \Omega_n^2$, the orthogonality relation (16) is not valid. Thus these modes must be chosen such that they are orthogonal so that the forced expansion principle may be used correctly. The worst example of this behavior is when $\lambda = 1$ (i.e., cylinders made of the same material) for then all values of μ will produce an infinity of paired equal frequencies.

Furthermore, in regions close to frequency pairs, the successive modes will have nearly equal frequencies which will make experimental results very difficult to interpret; thus theory will play a decisive part in interpreting some of the experimental data obtained for joined shell vibrations.

Using (57) thru (59), the solution regions for the first four modes on the λ versus Ω_n plot are easily sketched and Fig. 4 shows the completed solution details for three values of the parameter μ.

Problems (A) and (B) adequately represent the free torsional motion of actual joined cylinders when (i) the inertial properties of the joining

disk(s) is(are) negligible and (ii) the joining disk(s) is(are) so stiff that it(they) may be considered rigid. The present theory, as given in Section II, permits the relaxing of assumption (i) but relaxing the second assumption requires a straight-forward but laborious modification of the equations of motion and hence of the orthogonality principle and the expansion principle. As an example of relaxing assumption (i), problem (A) is now partially re-worked, letting the diaphragm have non-zero angular inertial properties.

(C) Cylinders Clamped at $x_i = 0$ and Joined with a Rigid Inertial Diaphragm at $x_i = 1$.

This problem is basically the same as that problem stated by (37) through (41) except that (41) is replaced by (64).

$$\mu\lambda^2[v_1'(1) - \alpha_1\Omega^2 v_1(1)] + v_2'(1) = 0 \tag{64}$$

Therefore using (37)-(40) and (64) yields the mode shapes (65), the amplitude ratio (66), and the frequency relation (67).

$$v_{1n}(x_1) = A_{1n}\sin\Omega_n x_1 \quad \text{and} \quad v_{2n}(x_2) = A_{2n}\sin\lambda\Omega_n x_2 \tag{65}$$

$$A_{1n}/A_{2n} = \sin\lambda\Omega_n/\sin\Omega_n \tag{66}$$

$$\sin\Omega_n\cos\lambda\Omega_n + \mu\lambda(\cos\Omega_n - \alpha_{1n}\Omega_n\sin\Omega_n)\sin\lambda\Omega_n = 0 \tag{67}$$

Solving (67) for μ, and since only positive values of μ are physically possible, just the positive solutions of (68) are sought.

$$\mu = \sin\Omega_n\cos\lambda\Omega_n/(\alpha_{1n}\Omega_n\sin\Omega_n - \cos\Omega_n)\lambda\sin\lambda\Omega_n \tag{68}$$

Letting Ω_n^* be the solutions of $(\cos\Omega_n - \alpha_{1n}\Omega_n\sin\Omega_n) = 0$, the solutions of (67) independent of μ are given by (69) and (70).

$$\Omega_n = n\pi \quad \text{and} \quad \lambda = m/n \qquad ; \quad m,n = 1,2,... \tag{69}$$

$$\Omega_n = \Omega_n^* \quad \text{and} \quad \lambda = (2m-1)\pi/2\Omega_n^* \; ; \quad m,n = 1,2,... \tag{70}$$

Furthermore, the limiting solutions as $\mu \to 0$ and as $\mu \to \infty$ are given by (71) and (72) respectively.

$$\Omega_n = n\pi \quad \text{and} \quad \Omega_n = (2n-1)\pi/2\lambda \quad ; \quad n = 1,2,... \tag{71}$$

$$\Omega_n = n\pi/\lambda \quad \text{and} \quad \Omega_n = \Omega_n^* \quad ; \quad n = 1,2,... \tag{72}$$

Notice that only one limiting boundary is different than the limiting boundaries obtained for problem (A); that is, (48) has been replaced by (72). Thus it is easy to visualize how the limiting solution boundaries shift with increasing $\mathfrak{Q}_1$ as is shown in Figure 5. The main feature to be noticed is the increasingly abrupt change of λ versus Ω (for increasing $\mathfrak{Q}_1$) in the regions near $\Omega = n\pi$. These abrupt changes appear to be similar to those observed by Mindlin for certain plate vibration problems governed by transcendental equations [3].

Finally, although the Ω_n^* values may be found via the computer, it is useful to have approximate solutions for the Ω_n^* for both large and small values of $\mathfrak{Q}_1$. These approximate solutions are now presented for the roots Ω_n^* of (73),

$$\cos\Omega_n - \mathfrak{Q}_1\Omega_n\sin\Omega_n = 0 \tag{73}$$

which may be re-written as

$$\cot\Omega_n = \mathfrak{Q}_1\Omega_n \tag{74}$$

For large Ω_1 we may assume $\Omega_n^* = n\pi + \varepsilon$ for $n = 0,1,2,\cdots$. Thus $\cot\Omega_n^* = \cot(n\pi + \varepsilon) \cong \varepsilon^{-1}$ and hence (74) becomes

$$\varepsilon^{-1} \cong \Omega_1(n\pi + \varepsilon) \tag{75}$$

Solving (75) for ε yields

$$\varepsilon \cong -(n\pi/2) + [(n\pi/2)^2 + (\Omega_1)^{-1}]^{1/2} \tag{76}$$

Thus, for large values of Ω_1, Ω_n^* is given by

$$\Omega_n^* \cong \begin{cases} (\Omega_1)^{-1/2} & ; \quad n = 0 \\ n\pi[1 + (n\pi)^{-2}(\Omega_1)^{-1}] & ; \quad n = 1,2, \end{cases} \tag{77}$$

It should be noted that this approximation improves as n increases.

For small Ω_1 we may assume $\Omega_n^* = (2n-1)(\pi/2) - \varepsilon$ for $n = 1,2,\cdots$.

Thus $\cot\Omega_n^* \cong \varepsilon$ and hence (74) becomes

$$\varepsilon \cong \Omega_1[(2n-1)(\pi/2) + \varepsilon] \tag{78}$$

Solving (78) for ε yields

$$\varepsilon \cong \Omega_1(\pi/2)(2n-1)/(1-\Omega_1) \tag{79}$$

Thus, for small values of Ω_1, Ω_n^* is given by

$$\Omega_n^* \cong (2n-1)(\pi/2)[1-\Omega_1(1-\Omega_1)^{-1}] \; ; \quad n = 1,2,\cdots \tag{80}$$

It should be noted that this approximation gets worse as n increases.

Appendix 1

We now demonstrate the conditions under which the assumed forced solution (23) satisfies the second expression in (5). When (5) is written in expanded form for $\tilde{x} = 1$ it becomes

$$\mu\lambda^2\partial\bar{v}_1(1,t)/\partial x_1 + \partial\bar{v}_2(1,t)/\partial x_2 + \Omega_1\mu\lambda^2\lambda_1^2\partial^2\bar{v}_1(1,t)/\partial t^2 = 0 \qquad (1\text{-}1)$$

Inserting (23) in (1-1) yields

$$\mu\lambda^2 \sum_{n=0}^{\infty} \xi_n(t)v'_{1n}(1) + \sum_{n=0}^{\infty} \xi_n(t)v'_{2n}(1) + \Omega_1\mu\lambda^2\lambda_1^2\partial^2\bar{v}_1(1,t)\partial t^2 \stackrel{?}{=} 0 \qquad (1\text{-}2)$$

but from (11), and using $\Omega_n = \lambda_1\omega_n$, we have

$$\mu\lambda^2 v'_{1n}(1) + v'_{2n}(1) = \mu\lambda^2\lambda_1^2\Omega_1 v_{1n}(1)\omega_n^2$$

so that (1-2) becomes

$$\mu\lambda^2\lambda_1^2\Omega_1 \left\{ \sum_{n=0}^{\infty} (\xi_n(t)v_{1n}(1)\omega_n^2) + \partial^2\bar{v}_{1n}(1,t)/\partial t^2 \right\} \stackrel{?}{=} 0 \qquad (1\text{-}3)$$

Now using (6), (1-3) becomes

$$\mu\lambda^2\Omega_1 \left\{ - \sum_{n=0}^{\infty} \xi_n(t)v''_{1n}(1) + \lambda_1^2\partial^2\bar{v}_{1n}(1,t)/\partial t^2 \right\} \stackrel{?}{=} 0 \qquad (1\text{-}4)$$

and noting that

$$\bar{v}''_1(1,t) = \sum_{n=0}^{\infty} \xi_n(t)v''_{1n}(1)$$

and using (1), (1-4) becomes

$$\mu\lambda^2\Omega_1[\lambda_1^2 F_1(1,t)] \stackrel{?}{=} 0 \qquad (1\text{-}5)$$

Therefore (1-5) and hence (5) is satisfied when $F_1(1,t) = 0$, and in a like fashion we can show that $F_1(0,t)$ must be zero for (5) to be satisfied when $\tilde{x} = 0$.

References

[1]Garnet, H.; Goldberg, M. A. and Salerno, V. L., "Torsional Vibrations of Shells of Revolution", Journal of Applied Mechanics, Vol. 28, No. 4, Dec. 1969, pp. 571-573.

[2]Brunelle, E. J., "Torsional Vibrations of Thin Shells of Revolution", Proceedings of the Eleventh Midwestern Mechanics Conference, 1969 (to be published).

[3]Mindlin, R. D., Schacknow, A. and Deresiewicz, H., "Flexural Vibrations of Rectangular Plates", Journal of Applied Mechanics, Vol. 23, No. 3, Sept. 1956, pp. 430-436.

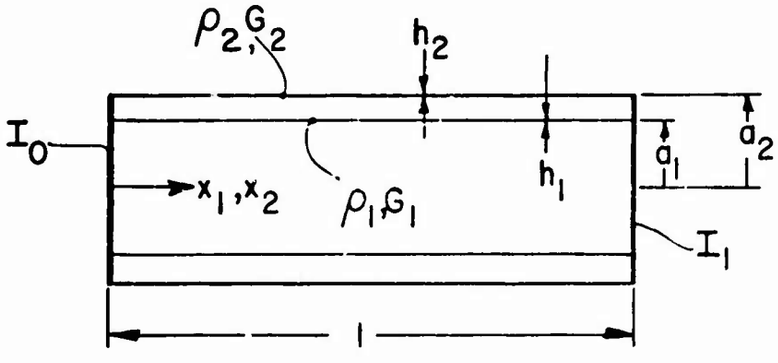


Figure 1

Two Joined Circular Cylindrical Shells

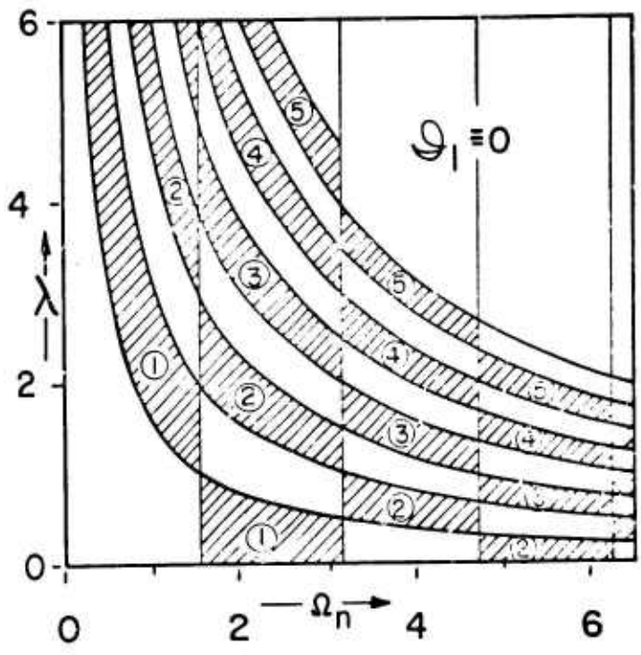


Figure 2

Case A: λ versus Ω_n Solution Regions

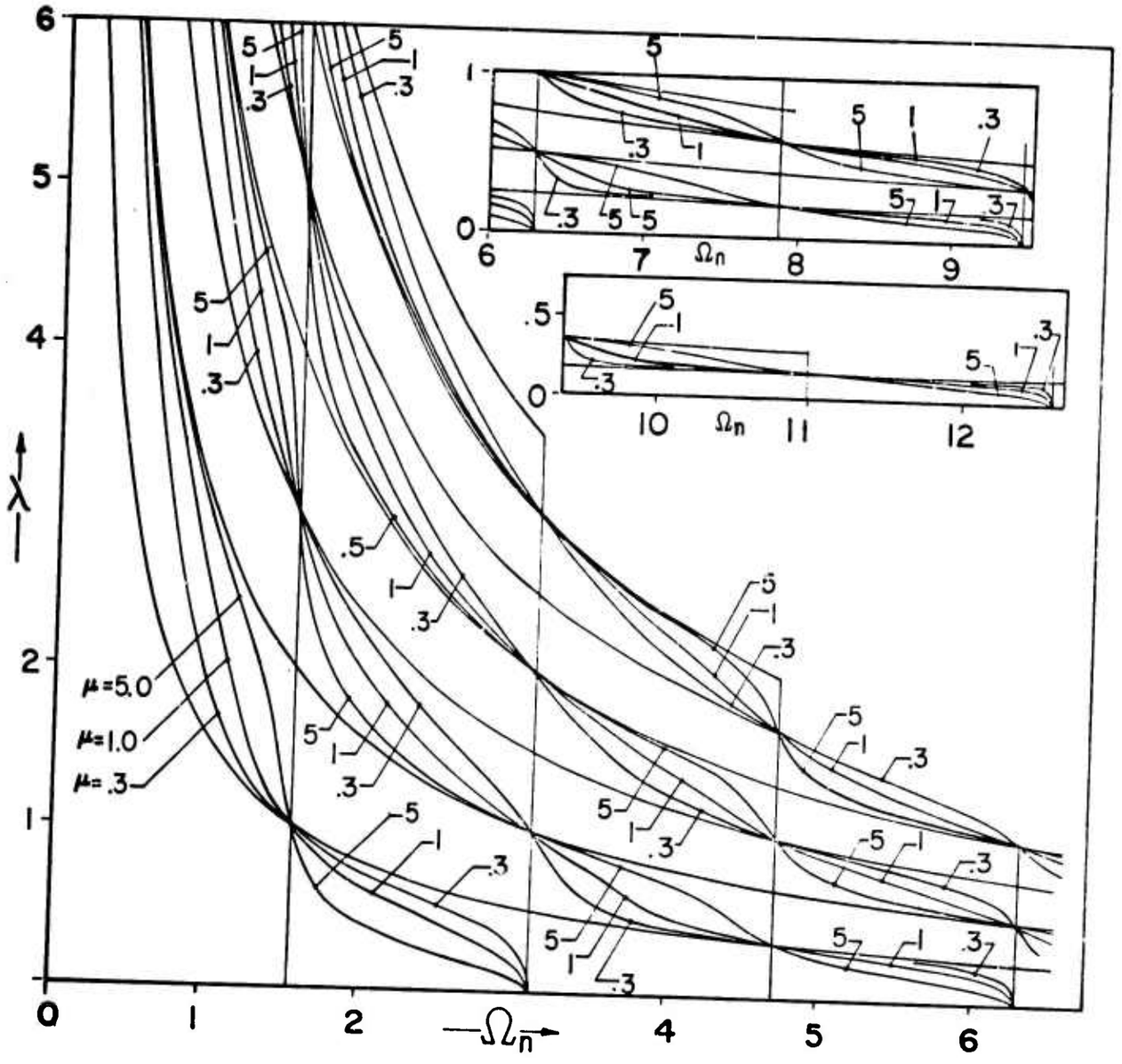


Figure 3

Case A: λ versus Ω_n Curves (n = 1,2,3,4) for μ = .3,1.0, and 5.0

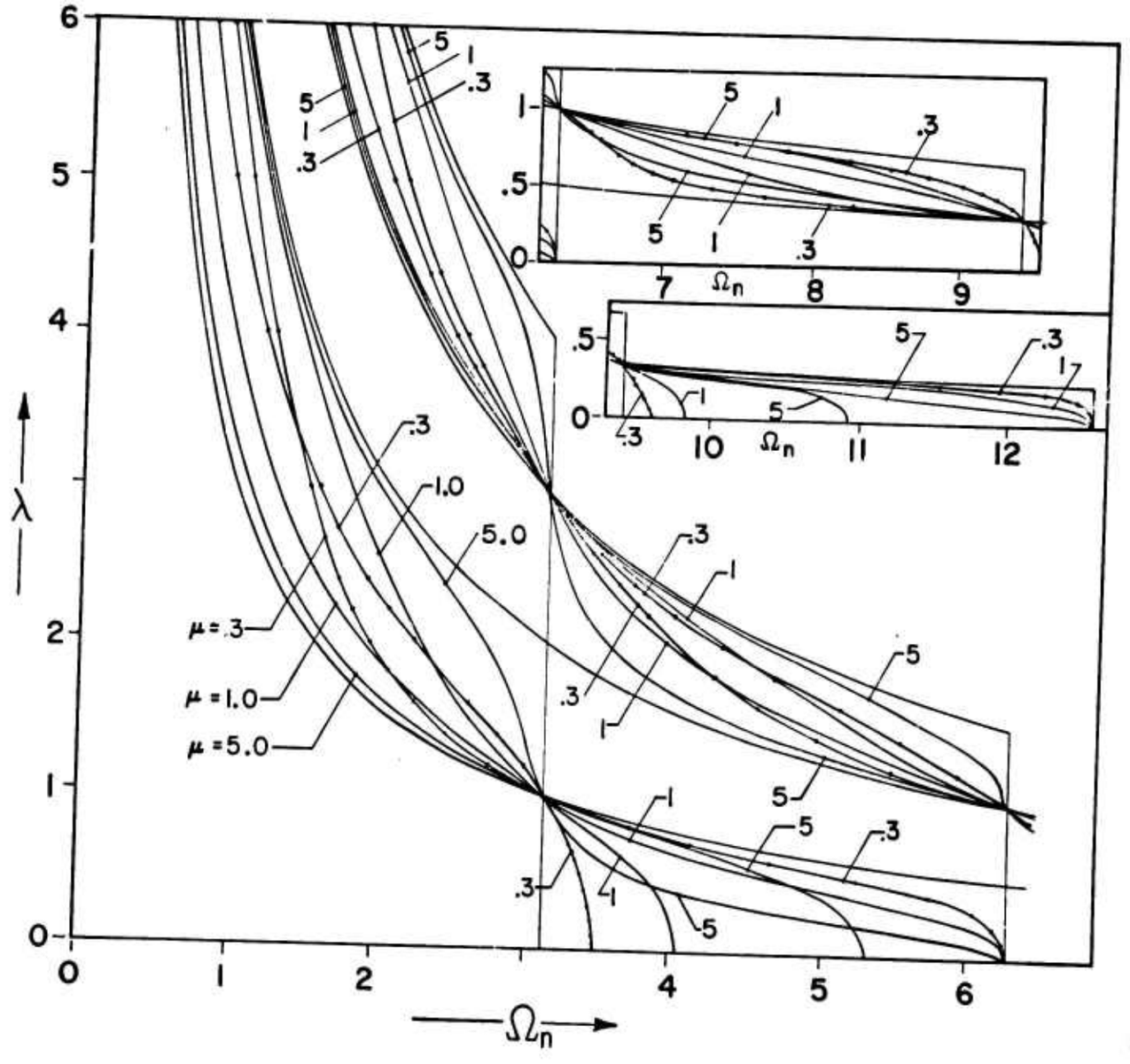


Figure 4

Case B: λ versus Ω_n Curves (n = 1,2,3,4) for μ = .3,1.0, and 5.0

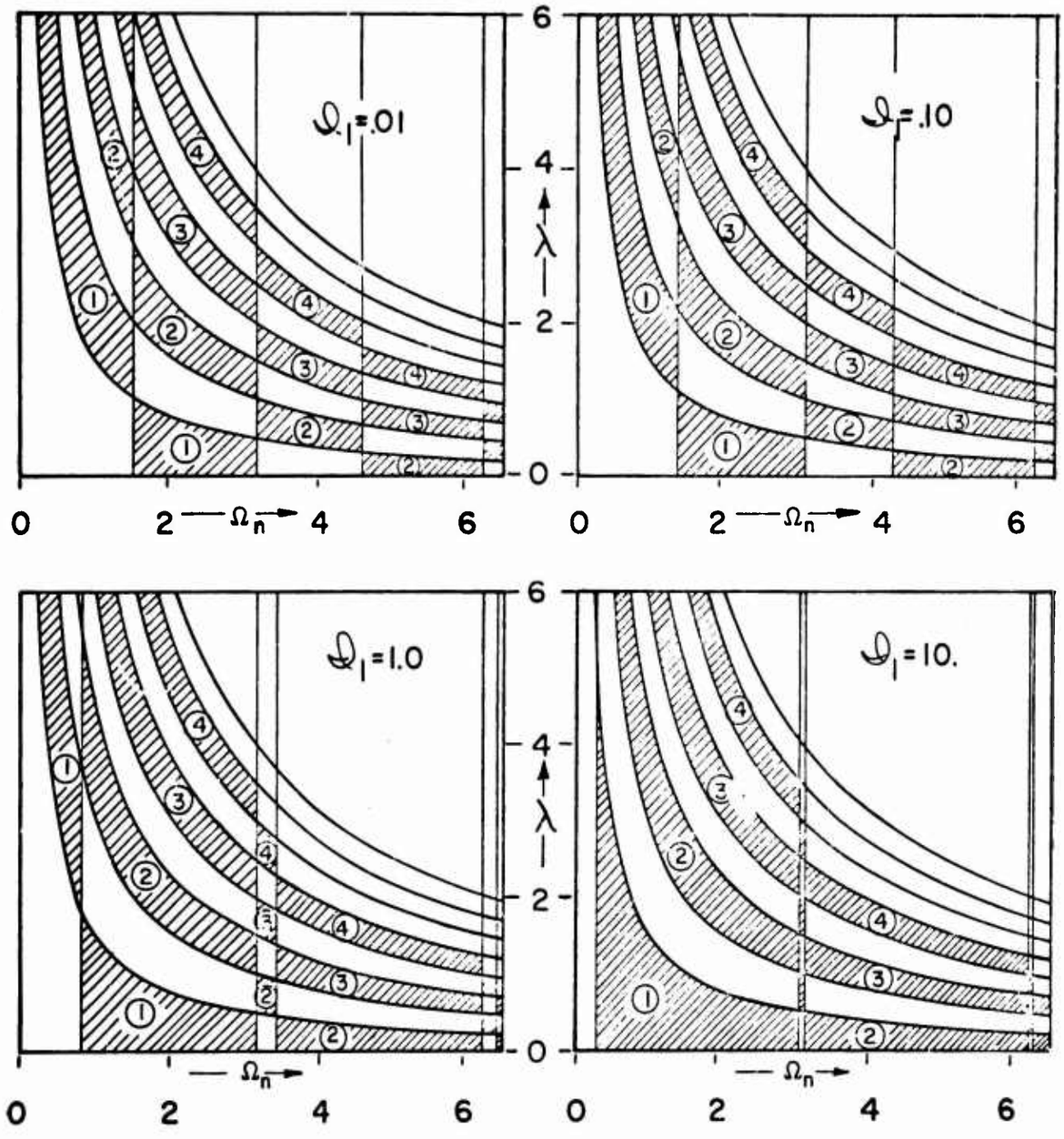


Figure 5

Case C: λ versus Ω_n Solution Regions for $\mathcal{J}_1$ = .01, .10, 1.0 and 10

FEEDBACK INFORMATION SYSTEMS
(The Effect of Feedback on System Entropy)

Erwin Biser
Avionics Laboratory, USAECOM
Fort Monmouth, New Jersey

and

M. Z. v. Krzywoblocki
Michigan State University
East Lansing, Michigan

SUMMARY. The paper deals primarily with transfer of information among subsystems. This is done within the context of the concepts of entropy applied to probabilistic systems defined as sets of elements termed parameters that are the carriers of probabilities.

The analysis of entropy exchange considers the effect of subsystem information feedback on the entropy of the whole system when all the subsystems are statistically independent. Feedback is determined by transporting parameters from one subsystem to another. Sensitivity coefficients of the entropy exchange within the information system are developed and computed.

The entire information system is partitioned, for the sake of simplicity, into four subsystems. Each subsystem consists of a finite number of parameters and the probabilities associated with these parameters. The probabilities associated with each parameter are normalized to unity. The entire information system is subjected to a discrete sequence of corrective transformations of its subsystems.

We start with the 0-State of the system partitioned into four subsystems:

$$S^{(0)} = \left\{ S^{(0)}_{1n_1}, S^{(0)}_{2n_2}, S^{(0)}_{3n_3}, S^{(0)}_{4n_4} \right\}$$

Assuming the subsystems to be statistically independent, one obtains the entropy of each subsystem as well as the entropy of the entire system.

After the operations are performed for the initial state 0, the total system is transformed from state 0 to state 1, etc., by changing either the total number of subsystems and/or changing the numer of parameters. The sum of the probabilities associated with each parameter after the transformation must be renormalized to unity.

For each transformed subsystem one computes the sensitivity index:

$$S_{e_{ln_1}}^{(0,1)} = \frac{H(S_{ln_1}^{(0)}) - H(S_{ln_1}^{(1)})}{H(S_{ln_1}^{(0)})}$$

One may also obtain sensitivity indices for particular parameters.

In a similar manner one computes the sensitivity index between two arbitrary states of the system:

$$S_e^{(1,\ p)} = \frac{H(S^{(1)}) - H(S^{(b)})}{H(S^{(1)})}$$

If the index is positive, the system is losing some of its randomness; i.e., it is assuming deterministic characteristics.

PREFACE. A few years ago, the first named author of this paper suggested and initiated the concepts of Information System Analysis by considering the phenomenon of transporting information from one subsystem to another. What is significant in this analysis is that it measured the effect of this phenomenon upon the distribution of the entropy in the entire system. The system is assumed to be discrete; hence, the distribution of entropy is to be considered as a point-wise concentration at a finite number of points.

In the early stages of the study, Dr. E. Biser devised an information model to obtain the information content (entropy) of a system by partitioning a system into mutually exclusive subsystems (sets). The information content of each subsystem is correlated with the information content of the entire system.

In the first approach, consideration was given to the following salient topics:

a. The consistency of information spaces and of their underlying probability spaces.

b. The grouping of system parameters into disjoing subsystems.

c. The derivation of information correlators to measure the degree of independence and mutual connectedness of the subsystems under investigation.

d. The extent to which entropy correlators have a bearing on the analysis and synthesis of systems.

The earlier paper essentially laid the structural foundations for the Information Systems Analysis. In this paper, we aim to extend these contexts and to construct the fundamentals of information exchange and feedback between subsystems. The efficacy of the concept of feedback is facilitated by means of the transformation of the states of the subsystems (as well as of the entire system). The quantitative effect of the feedback phenomenon is partially measured by means of the sensitivity coefficients (indices) of the subsystems as well as by the sensitivity coefficients of the total system.

In addition to the problem of constructing an information theoretical model enabling us to understand the exchange of entropy, there arise practical problems of a physical nature. For example, the probability of receiving a signal sent from one of the subsystems is not of constant magnitude but varies depending on such factors as noise, terrain configurations and weather conditions, etc. Thus, the probabilities associated with the parameters of a system (or subsystem) are to be regarded as variable parameters.

As for the problem of entropy exchange, the central concept is that of information feedback. It is for this reason that sensitivity indices are developed to study:

a. The effects of information feedback, to and from subsystems, on the entropy of the whole system.

b. The differential gain (or loss) of information as a result of the entropy exchange.

Expressions are derived for the entropy and sensitivity indices (coefficients) for the subsystems and the whole system before and after the feedback process.

I. INTRODUCTION: CYBERNETICS AND SYSTEMS ANALYSIS. In an earlier paper, Dr. E. Biser attempted to extend (and to apply) the concept of entropy to probabilistic systems, or to put it poignantly, to systems characterized by stochastic coupling.*

The great importance of stochastic coupling was attributed to conditional probabilities. It is stochastic coupling that establishes

*"Partitions of Discrete Information Spaces with Some Systems Applications," Transactions of the Tenth Conference of Army Mathematicians, AROD 65-2, pp. 305-359.

the possibility of mutual information flow and cybernetic interaction among the subsystems of a system. It redounds to the great merit of information theory that the concept of entropy can be extended from the field of physics (statistical mechanics) and the domain of telecommunications systems. The concept of entropy is too general in scope to be restricted to communications systems. It can be extended to probabilistic systems with known probability laws.

Norbert Wiener defined cybernetics as the "science of control and communications, in the animal and the machine." It is the art of steermanship (the Greek word "kybernao:" I control). It connotes organization, coordination, regulation and control. It is the science of controlling processes and systems of all kinds: physical, biological, as well as economic systems.

The amount of information, or information content, is a cybernetic concept, especially so since it is closely liked, via cybernetic correlators (see referenced paper) with organization and stochastic coupling among the subsystems of a larger system. The correlators measure the degree of connectedness, organization among the subsystems (or parameters), and the dependence of subsystems on each other, of a probabilistic system under investigation. It was shown that a completely deterministic (causal) connectedness is analogous to a "noiseless" channel in information theory. It bears emphasizing that the entropy concept need not be restricted solely to the transmission of signals. It can be fruitfully applied to the cybernetics of systems as well as to systems analysis and synthesis. We still retain the concept of "amount of information" or "information content" as a measure. Within the context of systems, however, it is extended and generalized into a measure of organization, connectedness, dependence of subsystems on each other, the interrelatedness of subsystems to a subsystem as a whole. Cybernetic correlators were derived to measure the effects of stochastic coupling between a subsystem and the "rest of the entire system."

Like information theory, cybernetics is based on the probability laws of a system; it is empirical, pragmatic, and practical.

In this paper, steps were taken to unify three concepts: the concept of entropy as used in information theory, the cybernetic category of organization, and the statistical concept of correlation. These three primal concepts were brought to bear on some of the problems of systems synthesis and analysis. These three concepts are fundamental in that they jointly enable the ascertaining and measuring the degrees of causal or stochastic dependence of subsystems in terms of entropy and correlation.

II. SYSTEMS. A system in this paper is defined by a finite number of parameters that are purported to characterize its state description and its behavior. The parameters may stand for operations, activities, functions

of subsystems and their associated finite set of probabilities; e.g., detection, pattern recognition, target location, operator response, etc. Each parameter is restricted to a finite set of values.

A system is represented by:

$$S = \{u_1, u_2, \ldots, u_n\}$$

Thus, $u_1, u_2, \ldots, u_n$ are the distinct parameters characterizing system S. The domain of u_k are x_k: $\{x_{k1}, x_{k2}, \ldots x_{k,n_k}\}$; and the set of probabilities associated with parameter u_k are (say, $u_k = u_3$):

$$\{p(u_3 = x_{31}),\ p(u_3 = x_{32}), \ldots p(u_3 = x_{3,n_3})\}$$

where n_3 is the number of discrete values u_3 may assume.

$$\sum_{n_3=1}^{m_1} p_{n_3} (u_3 = x_{3,n_3}) = 1$$

e.g., if $n_3 = 4$, then $\sum_{n_3=1}^{4} p_{n_3} (u_3 = x_{3,n_3}) = 1.$

In general: $\sum_{n_k=1}^{m_1} p_{n_k} (u_k = x_{k,n_k}) = 1$

III. PARTITIONS OF A SYSTEM. From the definition of a system as a set of paramters with their associated probability schemes, it is evident that subsystems can be generated by constructing a set of non-empty subsets of the original set of parameters constituting the system.

We know from elementary set theory that the set of such subsystems is the power set of the given set. In our discussions the empty set will not be included in the set of subsystems, since we are dealing with non-empty subsystems.

The set of all subsets of a given set is called the power set of the set. If A is any set, $\Pi(A)$, the power set, is defined as the set of all subsets of A:

$$\Pi(A) = \{B \mid B \subseteq A\}$$

The empty set (the null set, symbolized by ϕ) as well as the original set A itself, are elements of the power set. Thus, if A = {3, 1, c}, then $\Pi(A)$ = {{3}, {1}, {c}, {1,3}, {3,c},{1,c},{3,1,c,} ϕ}

If S is a system: $S = \{u_1, u_2, \ldots u_n\}$. Then a one-partition of S is: $\Pi^{(1)}(S) = \{\{u_1, u_2, \ldots u_n\}\} = \{S\}$. This is, in effect, the original system S unpartitioned.

A two-partition of S is:

$$\Pi^{(2)}(S) = \left\{S_{n_1}, S_{n_2}\right\}$$

$$\Pi^{(3)}(S) = \left\{S_{n_1}, S_{n_2}, S_{n_3}\right\}$$

$$\vdots$$

$$\Pi^{(k)}(S) = \left\{S_{n_1}, S_{n_2}, \ldots S_{n_k}\right\}$$

where $n_1, n_2, \ldots, n_k \neq 0$ and $n_1 + n_2 + \ldots + n_k = n$.

n_1 = number of parameters (u's) in S_{n_1}.

$\vdots$

n_k = number of parameters in S_{n_k}.

$$S = S_{n_1} \cup S_{n_2} \cup \ldots \cup S_{n_k} \equiv \bigcup_{i=1}^{k} S_{n_i}$$

$$\bigcap_{i=1}^{k} S_{n_i} \equiv S_{n_1} \bigcap S_{n_2} \bigcap \cdots \bigcap S_{n_k} = \phi \text{ (the null set).}$$

Thus, $\Pi(S)$ is a partition of S if and only if:

(a) If S_{n_1} is an element of $\Pi(S)$, then $S_{n_1} \neq \phi$; i.e., S_{n_1} is not an empty set.

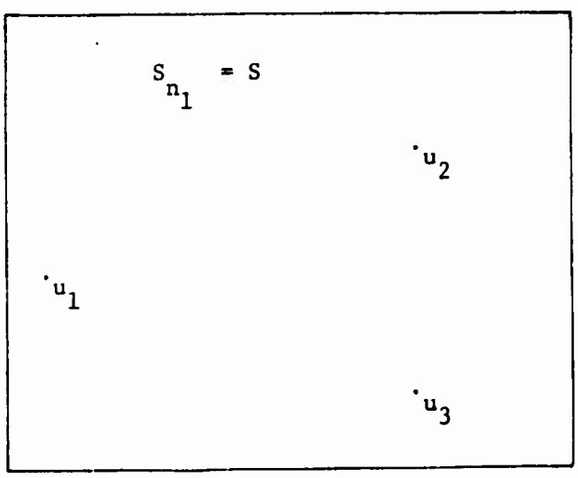
(b) If S_{n_i} and S_{n_j} are elements of $\Pi(S)$, then $S_{n_i} \bigcap S_{n_j} = \phi$ for $n_i \neq n_j$.

(c) $S = \bigcup_{i=1}^{n} S_{n_i}$.

IV. SET-THEORETICAL REPRESENTATION OF PARTITIONS OF SYSTEMS.

$$S = S_{n_1} = \{u_1, u_2, u_3\} : n_1 = 3$$

$$\Pi^{(1)}(S) = \{ \{u_1, u_2, u_3\} \} = \{ \{S_{n_1}\} \}$$



$S_{n_1} = S$

$\Pi^{(1)}(S)$: 1 - partition of S (unique).

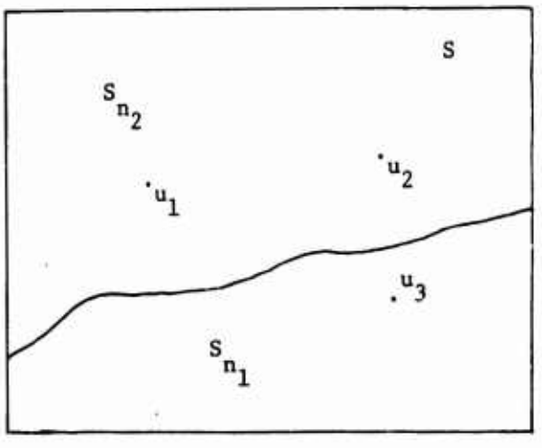
$\Pi^{(2)}(S)$: a two-partition of S:

$$\{S_{n_1}, S_{n_2}\} = \{\{u_3\}, \{u_1, u_2\}\}$$

$$S_{n_1} = \{u_3\}, \quad S_{n_2} = \{u_1, u_2\}$$

here $n_1 = 1$; $n_2 = 2$; $n_1 + n_2 = 3$

$\{u_1\ u_2\} \bigcup \{u_3\} = S_{n_2} \bigcup S_{n_1} = S$ and $S_{n_1} \bigcap S_{n_2} = \phi$(null set).



$$\Pi^{(2)}(S) = \{S_{n_1}, S_{n_2}\}$$

To summarize: The practical application of partitioning is that it is advisable, nay, at times, almost necessary, to divide (partition) a whole system into functionally non-overlapping subsystems. In fact, this is the way most systems are designed, costed, built, field tested, maintained, serviced, and operated.

V. ENTROPY RELATIONS IN SYSTEMS. If a system S is partitioned into two subsystems S_{n_1} and S_{n_2}, then

$$H(S) \leq H(S_{n_1}) + H(S_{n_2}) \qquad (1)$$

where $\{S_{n_1}, S_{n_2}\}$ is a two-partition of S; $S = \{u_1, u_2, \ldots, u_n\}$.

Likewise: $$H(S) \leq H(S_{n_1}) + H(S_{n_2}) + \ldots + H(S_{n_k}) \qquad (2)$$

where $\{S_{n_1}, S_{n_2}, \ldots S_{n_k}\}$ is a k-partition of S. The inequality (2) constitutes the necessary and sufficient condition for the consistency of the information space induced by the partition of the system S. Note that $S_{n_1}, S_{n_2}, \ldots, S_{n_k}$ are each product spaces.

The inequality (2) states that the entropy of a system cannot decrease upon its being partitioned. It states that the information conveyed by a system as a whole, when all its parameters are observed simultaneously, is at most equal to the sum of the entropies conveyed by its subsystems; i.e., when each subsystem is observed as a separate entity.

An information space is said to be consistent if its subspaces satisfy theorem (2). It merits repetition to state that entropy is the amount of uncertainty (the mean uncertainty) associated with a probability space. In this paper, we are dealing with discrete probability spaces. The quantity measures the extent to which the mean uncertainty of a probability space is being eliminated as a result of an experiment involving a set of observations.

Let A = a probability space such that:

$$\begin{bmatrix} A \\ P \end{bmatrix} = \begin{bmatrix} A_1, A_2, \ldots, A_n \\ p_1, p_2, \ldots, p_n \end{bmatrix};$$

$$p(A_1) = p_1, \ldots, p(A_n) = p_n$$

$$\sum_{i=1}^{n} p_i = 1; \quad A = \bigcup_{i=1}^{n} A_1$$

$$A_i \cap A_j = \phi \text{ for } i \neq j$$

$$= A_i \text{ for } i = j$$

$$H(A) = -\sum p_i \log_2 p_i \equiv -\sum_{x \in A} p(A) \log p(A)$$

Entropy, uncertainty and information are taken to be equivalent to each other: Uncertainty ≡ Information ≡ Entropy.

Uncertainty is associated with an event before we observe it; and the amount of information is obtained after the observation. The degree or amount of uncertainty before the observation is equal to the amount of information after the observation. We can speak of the amount of information as the elimination of the uncertainty after the message is received.

It was shown that:

$$H(S_{n_1} \mid S_{n_2}) = H(S) - H(S_{n_2}) \geq 0$$

$$H(S_{n_2} \mid S_{n_1}) = H(S) - H(S_{n_1}) \geq 0 \qquad (3)$$

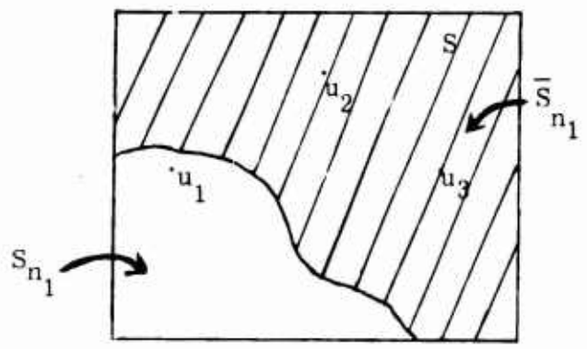
where $H(S_{n_1} \mid S_{n_2})$ is the amount of information provided by the subsystem S_{n_2} about subsystem S_{n_1}. It is the a posteriori (observational) information about S_{n_1}.

$$H(S_{n_1} \mid \overline{S}_{n_1}) = H(S) - H(\overline{S}_{n_1}) \qquad (4)$$

where $H(S_{n_1} \mid \overline{S}_{n_1})$ is the information provided about subsystem S_{n_1} by the "rest of the system." $\overline{S}_{n_1}$ is the relative complement of S_{n_1} in the system S. $H(S_{n_1} \mid \overline{S}_{n_1})$ is a conditional entropy. This is illustrated in the following example: (loc. cit, p. 325)

Let $S = \{u_1, u_2, u_3\}$ and $S_{n_1} = \{u_1\}$; $\overline{S}_{n_1} = \{u_2, u_3\}$.

$\{ \{S_{n_1}\}, \{\overline{S}_{n_1}\} \}$ is a two-partition of the system S.



$\bar{S}_{n_1} = S - S_{n_1}$: /////

VI. CYBERNETIC (INFORMATION) CORRELATORS.

$$R_2(S) = 1 - \frac{H(S)}{H(S_{n_1}) + H(S_{n_2})} \qquad (1)$$

$$0 \leq R_2(S) \leq 1$$

$R_2(S)$ is an information correlator. The subscript "2" designates the fact that the correlator is associated with a two-partition of S.

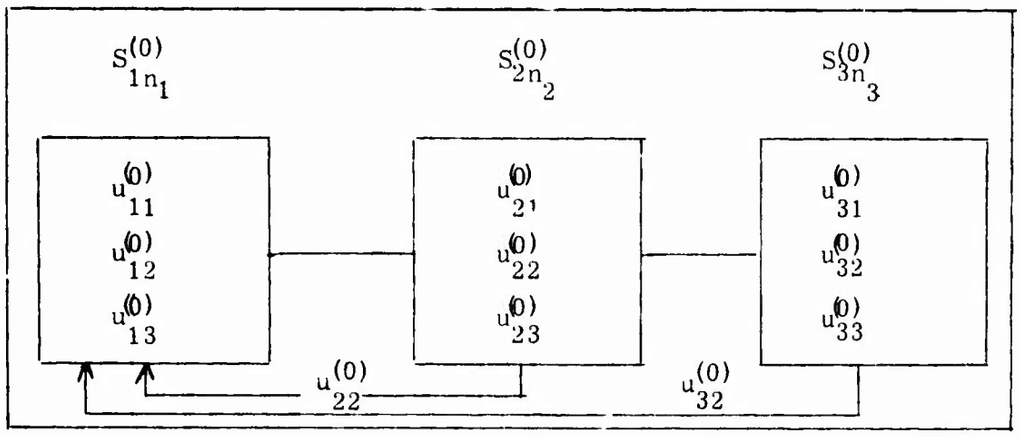
$$R_{(3)}(S) = 1 - \frac{H(S)}{H(S_{n_1}) + H(S_{n_2}) + H(S_{n_3})} \qquad (2)$$

$$0 \leq R_{(3)}(S) \leq 1$$

$$R_{(3)}(S) = \frac{\text{amount of organization}}{\text{maximum possible organization}}$$

VII. INFORMATION FEEDBACK. In the ensuing discussion, we shall assume that a system has been partitioned into several mutually disjoint subsystems. Since feedback, whether positive (regenerative) or negative (degenerative) may be of overriding importance in systems of all types, information feedback in terms of entropy is to be defined in meaningful and operational terms.

Let us consider the following system:



SYSTEM $S^{(0)}$

$$S^{(0)} = \{\{S^{(0)}_{n_1}\}, \{S^{(0)}_{n_2}\}, \{S^{(0)}_{n_3}\}\}$$

$H(S^{(0)}_{1n_1}) - H(S^{(1)}_{1n_1})$ is the entropy differential feedback of subsystem S_{n_1} as a result of a change in the number of parameters of the subsystem.

Likewise, $H^{(0)}(S) - H^{(1)}(S)$ is the entropy differential of the entire system.

The entropy differentials measure the information feedback of subsystems and of the entire system.

The entropy sensitivity of a subsystem, say, S_{1n_1} is defined as:

$$\frac{H(S_{1n_1}^{(0)}) - H(S_{1n_1}^{(1)})}{H(S_{1n_1}^{(0)})}$$

Likewise for the entropy sensitivity of the system S:

$$\frac{H(S^{(0)}) - H(S^{(1)})}{H(S^{(0)})}$$

The symbolism adopted facilitates the recording of the history of each parameter and of the transformation of subsystems. The superscripts (0), (1), (2), etc., designate the initial state, the 0-state, the subsequent states of the subsystems as well as of the system.

In general, each of the subsystems at each state is characterized by a certain number of distinct parameters:

$$\left\{ \begin{array}{lcl} S_{1n_1}^{(0)} & = & \left\{ u_{11}^{(0)} , u_{12}^{(0)} , \ldots , u_{1n_1}^{(0)} \right\} \\ S_{2n_2}^{(0)} & = & \left\{ u_{21}^{(0)} , u_{22}^{(0)} , \ldots , u_{2n_2}^{(0)} \right\} \\ \vdots & & \\ S_{kn_k}^{(0)} & = & \left\{ u_{k1}^{(0)} , u_{k2}^{(0)} , \ldots , u_{kn_k}^{(0)} \right\} \end{array} \right\}$$

The remainder of this paper has been reproduced photographically from the author's manuscript.

VIII. TRANSFORMATION OF SYSTEMS

The entire information system, S, is partitioned into a few subsystems. "Information signals" are sent from one subsystem to another; this is equivalent to a transformation of states of the entire system, S, from state 0, to state 1, from state 1 to state 2, etc.

After each transformation, the parameters are regrouped and reordered among various subsystems. The sets of values assigned to each parameter are regrouped; and the probabilities associated with each parameter are renormalized, since the sum of the probabilities associated with each parameter must be equal to unity.

The information chain developed in this paper is independent of any special location of the source of the transmitted signals or of a receiving subsystem (e.g., an antenna). The transformations of the entire system are accomplished in discrete state-wise steps. The regrouping, reordering, and renormalization take place after the subsystems are in the new state. The subsystem entropies, the sensitivity indices, are computed. Finally the entropy and sensitivity index for the entire system S is computed as the S passes from, say, ... state 1 to state 2 .

What follows is an explicit delineation of such transformations:

Initial State 0 : We begin with the 0 state of the system and assume that the system in this state consists of four subsystems. $S^{(0)}$ denotes that the entire system is in state 0 . Each of the subsystems, $S_{in_i}^{(0)}$ has a certain number of parameters. i = 1 to 4 . .

S_{1n_1}, for example, denotes subsystem 1 and n_1 denotes the number of parameters that make up subsystem 1 . Similarly for

$$S_{2n_2}^{(0)}, \quad S_{3n_3}^{(0)}, \quad \text{and for} \quad S_{4n_4}^{(0)} .$$

Thus: $S_{1n_1}^{(0)} = \left\{ u_{11}^{(0)}, \; u_{12}^{(0)}, \; \ldots \; u_{1n_1}^{(0)} \right\}$; similarly for other subsystems.

The other subsystems are shown in Figure 1.

Parameters $u_{n_1}^{(0)}$ of Subsystem $S_{1n_1}^{(0)}$

The probabilities associated with parameters are normalized to unity:

$$\sum_{a_1=1}^{m_1} p_{a_1}(u_{11}^{(0)} = x_{11,a_1}^{(0)}) = 1, \quad 0 \leq p_{a_1} \leq 1$$

$$\sum_{a_2=1}^{m_2} p_{a_2}(u_{12}^{(0)} = x_{12,a_2}^{(0)}) = 1, \quad 0 \leq p_{a_2} \leq 1$$

$$\vdots$$

$$\sum_{a_{n_1}=1}^{m_{n_1}} p_{a_{n_1}}(u_{1n_1}^{(0)} = x_{1n,a_{n_1}}^{(0)}) = 1, \quad 0 \leq p_{a_{n_1}} \leq 1$$

Parameters u_{2n_2} of subsystem $S_{2n_2}^{(0)}$:

$$\sum_{a_1=1}^{\ell_1} p_{a_1}(u_{21}^{(0)} = x_{21,a_1}^{(0)}) = 1, \quad 0 \leq p_{a_1} \leq 1$$

$$\sum_{a_2=1}^{\ell_2} p_{a_2}(u_{22}^{(0)} = x_{22,a_2}^{(0)}) = 1, \quad 0 \leq p_{a_2} \leq 1$$

$$\vdots$$

$$\sum_{a_n=1}^{\ell_{n_2}} p_{a_{n2}}(u_{2n_2} = x_{2n_2,a_{n2}}) = 1, \quad 0 \leq p_{a_{n_2}} \leq 1$$

Parameters u_{4n_4} of the subsystem $S^{(0)}_{4n_4}$:

$$\sum_{a_1=1}^{S_1} p_{a_1}(u^{(0)}_{41} = x_{41,\,a_1}) = 1, \quad 0 \le p_{a_1} \le 1$$

$$\sum_{a_2=1}^{S_2} p_{a_2}(u^{(0)}_{42} = x_{42,\,a_2}) = 1, \quad 0 \le p_{a_2} \le 1$$

.
.
.

$$\sum_{a_{n4}=1}^{S_{n4}} p_{an_4}(u^{(0)}_{n_4} = x_{4n_4},\ a_{n_4}) = 1, \quad 0 \le p_{a_{n4}} \le 1$$

Thus all the probabilities in the state 0 are normalized.

We then compute the entropy of each subsystem, assuming that they are statistically independent of each other.

Since A is a finite probability space, we have:

$$H(A) = -\sum_{x \in A} p(A) \log p(A)$$

$$H(S^{(0)}_{1n_1}) = -\sum_{a_1=1,\, a_2=2,\, \ldots a_{n_1}=1}^{m_1, \ldots m_{n_1}} p_{a_j}(u^{(0)}_{1j} = x_{1j,\,aj}) \log p_{a_j} \quad ; \quad j=1, 2, 3, \ldots n_1$$

where $-\sum$ is given by: $H(S^{(0)}_{1n_1}) = -\left\{ \sum_{a_1=1}^{m_1} p_{a_1}(u^{(0)}_{11} = x^{(0)}_{11,\,a_1}) \log p_{a_1} + \right.$

$$\left. \sum_{a_2=1}^{m_2} p_{a_2}(u^{(0)}_{12} = x^{(0)}_{12,\,a_2}) \log p_{a_2} + \ldots\ldots + \sum_{a_{n_1}=1}^{m_{n_1}} p_{an_1}(u^{(0)}_{1n_1} = x^{(0)}_{1n_1,\,an_1}) \log p_{an_1} \right\}$$

Similarly:

$$H(S^{(0)}_{2n_2}) = -\sum_{a_1=1,\, a_2=1,\, \ldots\, a_{n_1}=1}^{\ell_1,\, \ell_2,\, \ldots,\, \ell_{n_2}} p_{a_j}(u^{(0)}_{2_j} = x^{(0)}_{2_j}, a_j) \log p_{a_j}$$

$$j = 1, 2, 3, \ldots, a_{n_2}$$

$$H(S^{(0)}_{4n_4}) = -\sum_{a_1=1,\, a_2=1,\, \ldots\, a_{n_4}=1}^{s_1,\, s_2,\, \ldots,\, s_{n_4}} p_{a_j}(u^{(0)}_{4_j} = x^{(0)}_{4_j}, a_j) \log p_{a_j}$$

The foregoing formalism describes all the operations to be performed on the system in the initial state 0 .

State 1 :

With the 0 state closed, the entire information system undergoes a transformation of states. The signals and the associated probabilities are sent from $S^{(0)}$ to what will eventuate as $S^{(1)}$. The description and analysis of $S^{(1)}$ will be discussed. It is pertinent to make the following statements concerning the structure of and operations to be performed on $S^{(1)}$:

a. The number of subsystems of $S^{(1)}$ need not be equal to the number of subsystems of $S^{(0)}$. It may happen that some subsystems in $S^{(0)}$ have disappeared as a result of the transformation: $S^{(0)} \xrightarrow{T} S^{(1)}$ New subsystems may be introduced into $S^{(1)}$ that did not exist in $S^{(0)}$.

b. Similarly for the number of parameters in any of the subsystems after the transformation from $S^{(0)}$ to $S^{(1)}$. The numbers of parameters in any subsystem of S need not be preserved as a result of the transformation.

c. The probabilities associated with each parameter in any of the subsystems of S need not be preserved in the transformation. These may decrease or increase depending on the contingencies of the situation.

In the algorithm used in this paper the place of any parameter (in a subsystem) that disappears from S as $S^{(0)}$ is transformed into $S^{(1)}$ is marked by a dash (or by some other computerized mark).

The number of subsystems in this paper is set as four; and this number is not changed during the transformations:

$$S^{(0)} \longrightarrow S^{(1)} \longrightarrow S^{(2)} \longrightarrow S^{(3)} \longrightarrow S^{(4)} .$$

The number of parameters and the number of probabilities associated with each of these parameters are changed. The following operations are performed after each transformation:

d. Restructuring the subsystems in $S^{(1)}$, some may disappear, others may be added to $S^{(1)}$.

e. Regrouping the parameters in each subsystem, some parameters may be transmitted from one subsystem to another. The number of parameters in each subsystem may change during the transformation (see b. of previous section). In order to devise a consistent algorithm, we adopt the following convention: if the probability associated with a specific parameter is set equal to zero, its location is marked by a dash.

f. Renormalizing the probabilities associated with each parameter: This is an important operation, since it may happen that the sum of the probabilities (associated with each parameter) after the transformation of state may not be equal to one. A few words about renormalization are relevant at this juncture. We know that the sum of the probabilities associated with each parameter must be equal to unity. This is what is meant by normalization. It may happen, however, that after the system changes from state p, ($p \geq 0$), to its succeeding state $p+1$, the sum of the probabilities associated with one or more of the regrouped parameters is no longer equal to one. We then renormalize these probabilities, which is either to reduce or increase the values of all the probabilities associated with each parameter.

It may happen that, $x^{(0)}_{11, m_1}$, the values assigned to parameter $u^{(0)}_1$ may be numerically equal to the set of values $x^{(1)}_{11, m_1}$ assigned to the parameter $u^{(1)}_{11}$ after the system changes from state 0 to state 1. Although the sum of probabilities associated with $x^{(0)}_{11, m_1}$ is equal to unity, the sum of the probabilities corresponding to $x^{(1)}_{11, m_1}$ may add up to, say, 1.6, by upgrading some of the probabilities associated with $u^{(1)}_1$. Under such circumstances we smooth the increase in probability by distributing this rise above unity among all the probabilities, as shown below:

$$\sum_{a_1=1}^{m_1} p_{a_1}(u^{(1)}_{11} = x^{(1)}_{11, m_1}) = 1.6 \text{ (before renormalization).}$$

To renormalize we divide <u>each</u> of the probabilities p_{a_1} by 1.6 (the sum of the probabilities before renormalization):

(Each) $p_{a_1}(u_{11}^{(1)} = x_{11,a_1}^{(1)})$ (after renormalization)

$$= \frac{p_{a_1}(u_{11}^{(1)} = x_{11,a_1}^{(1)}) \quad \text{(before renormalization)}}{\text{the sum of } p_{a_1}\text{'s} \quad \text{(after renormalization)}}$$

$$= \frac{p_{a_1}(u_{11}^{(1)} = x_{11,a_1}^{(1)})}{\sum_{a_1=1}^{m} p_{a_1} = i.6}$$

Thus $\sum_{a_1=1}^{m_1} p_{a_1}(u_{11}^{(1)} = x_{11,a_1}^{(1)}) = 1$ (after renormalization)

g. The history of each parameter is recorded. The system S is shown in Figures 11 and 12 after the transformation to $S^{(1)}$ is closed.

Figure 11 exhibits the final structure of $S^{(1)}$. $S^{(1)}$ consists of four subsystems:

$$S_{1n_1}^{(1)}, S_{2n_2}^{(1)}, S_{3n_3}^{(1)}, S_{4n_4}^{(1)}.$$

Each subsystem S_{in_i} contains a certain number of parameters. But the number of parameters in each $S_{in_i}^{(1)}$, $i=1, 2, 3, 4$ is not equal to the number of parameters in the subsystems $S_{in_i}^{(0)}$, $i=1, 2, 3, 4$. Some parameters have been eliminated, some are added.

In Figure 12 the dashes denote parameters that disappear during the transformation from the state 0 to state 1. Their locations are preserved; and they are considered in the count. It is possible that some of these, or all of these, may re-enter into the system during one of the consecutive transformations.

The numerical values of the indices $m_1, m_2, \ldots m_n$; $\ell_1, \ell_2, \ldots \ell_{n_2}$; $s_1, s_2, \ldots, s_{n_4}$ need not be the same in the subsystems:

$$S_{1n_1}^{(0)}; \; S_{2n_2}^{(0)}; \; S_{3n_3}^{(0)}; \; S_{4n_4}^{(0)},$$

as those in the subsystems: $S^{(0)}_{1n_1+1}$; $S^{(0)}_{2n_2+2}$; $S^{(0)}_{3n_3+2}$; $S^{(0)}_{4n_4}$. These indices only represent symbols; the numerical values must always be supplied.

It is seen from Figure 12 that the number of parameters in subsystem $S^{(1)}_{1n_1+1}$ equals to (n_1+1); the number of parameters in $S^{(0)}_{1n_1}$ is equal to n_1.

In Figures 11 and 12 the numbers $1, 2, 3, \ldots, n_i, n_i+1, n_i+2$ in the first column (on the left-hand side) denote the consecutive numbers (of parameters) in each subsystem.

Figure 12 exhibits only those parameters in the system $S^{(1)}$ that were either transmitted from the system $S^{(1)}$ to another system, or were transmitted from another system to $S^{(1)}$. A transmission from the system $S^{(1)}$ to another system $S^{(n)}$, $n>1$, is called the output from the system $S^{(1)}$. A transmission from a system $S^{(n)}$, $n\neq 1$, to the system $S^{(1)}$ is called the input into the system $S^{(1)}$.

The symbolic notation: $u^{(1)}_{12} \rightarrow u^{(1)}_{2n_2+1}$ denotes that the parameter $u^{(1)}_{12}$, missing in Figure 12 is transmitted from the subsystem $S^{(1)}_{1n_1+1}$ to $S^{(1)}_{2n_2+2}$; and changes its identification from $u^{(1)}_{12}$ to $u^{(1)}_{2n_2+1}$.

The same explanation holds for the symbolic transmission of parameters:

$u^{(1)}_{24} \rightarrow u^{(1)}_{n1}+1$; $\quad u^{(1)}_{42} \rightarrow u^{(1)}_{2n_2+2}$; $\quad u^{(1)}_{43} \rightarrow u^{(1)}_{3n_3+1}$.

The parameter representation of the four subsystems is given as follows:

$S^{(1)}_{1n_1+1} = \{ u^{(1)}_{11}, -, u^{(1)}_{13}, u^{(1)}_{14} \ldots, u^{(1)}_{1n_1}, u^{(1)}_{1n_1+1} \}$

$S^{(1)}_{2n_2+2} = \{ u^{(1)}_{21}, u^{(1)}_{22}, u^{(1)}_{23}, -, u^{(1)}_{25}, \ldots, u^{(1)}_{2n_2}, u^{(1)}_{2n_2+1}, u^{(1)}_{2n_2+2} \}$

$S^{(1)}_{3n_3+1} = \{ u^{(1)}_{31}, -, u^{(1)}_{33}, -, u^{(1)}_{35} \ldots, u^{(1)}_{3n_3}, u^{(1)}_{3n_3+1} \}$

$S^{(1)}_{4n_4} = \{ u^{(1)}_{41}, -, -, u^{(1)}_{44}, u^{(1)}_{45} \ldots, u^{(1)}_{4n_4} \}$

Figure 12 illustrates how the history of each parameter can be recorded, yielding the complete transmission pattern (history) of each parameter as the system undergoes changes from $S^{(i)}$ to $S^{(p)}$ $(p>i)$; $p = 1, 2, \ldots, r$.

Probabilities and Transformation of System S

A set of probabilities is associated with each parameter. It is assumed that the probabilities associated with each parameter in all subsystems are renormalized. When a parameter is transmitted from one subsystem to another, its associated probability is carried along with it. (This is adopted as a procedural convention in this paper.)

The probabilities associated with each parameter are normalized to unity.

Parameters $u^{(1)}_{1n_1+1}$ of Subsystem $S^{(1)}_{1n_1+1}$:

$$\sum_{a_1=1}^{m_1} p_{a_1} (u^{(1)}_{11} = x^{(1)}_{11, a1}) = 1 ; \qquad 0 \le p_{a_1} \le 1$$

$$\sum_{a_3}^{m_3} p_{a_3} (u^{(1)}_{13} = x^{(1)}_{13, a3}) = 1 ; \qquad 0 \le p_{a_3} \le 1$$

$$\sum_{a_{n_1+1}}^{m_{n+1}} p_{an_1+1} (u^{(1)}_{1n_1+1} = x^{(1)}_{1n_1+1}, a_{n_1+1}) = 1 ; \qquad 0 \le p_{a_{n_1+1}} \le 1$$

Parameters $u^{(1)}_{2n_2+2}$ of Subsystem $S^{(1)}_{2n_2+2}$:

$$\sum_{a_1=1}^{\ell_1} p_a(u^{(1)}_{21} = x^{(1)}_{21, a_1}) = 1 ; \qquad 0 \le p_{a_1} \le 1$$

$$\sum_{a_2=1}^{\ell_2} p_{a_2} (u^{(1)}_{22} = x^{(1)}_{22, a_2}) = 1 ; \qquad 0 \le p_{a_2} \le 1$$

$$\sum_{a_{n_2+2}}^{\ell_{n_2+2}} p_{a_{n_2+2}} (u^{(1)}_{2n_2+2} = x^{(1)}_{2n_2+2}, a_{n_2+2}) = 1 ; \qquad 0 \le p_{a_{n_2+2}} \le 1$$

Parameters $u^{(1)}_{4n_4}$ of Subsystem $S^{(1)}_{4n_4}$:

$$\sum_{a_1=1}^{s_1} p_{a_1}(u^{(1)}_{41} = x^{(1)}_{41, a_1}) = 1 \quad ; \qquad 0 \le p_{a_1} \le 1$$

$$\sum_{a_2=1}^{s_2} p_{a_2}(u^{(1)}_{42} = x^{(1)}_{42, a_2}) = 1 \quad ; \qquad 0 \le p_{a_2} \le 1$$

$$\sum_{a_{n_4}=1}^{s_{n_4}} p_{a_{n_4}}(u^{(1)}_{4n_4} = = x^{(1)}_{4n_4, a_{n_4}}) = 1 \quad ; \qquad 0 \le p_{a_{n_4}} \le 1$$

With this symbolism separate records have to be kept of all the transformations of the subsystems of the paramaters, and of the associated probability values during the transitions of the entire system from any state N to the consecutive state N+1 .

The entropies of the respective subsystems are computed:

$$H(S^{(1)}_{1n_1+1}) = - \sum_{a_1=1, a_3=1, \ldots, a_{n_1+1}=1}^{m_1, m_3, \ldots, m_{n_1+1}} p_{a_j}(u^{(1)}_{1_j} = x^{(1)}_{1_j, a_j}) \cdot \log p_{a_j}$$

where $j = 1, 2, 3, \ldots, n_1+1$

$$H(S^{(1)}_{2n_2+2}) = - \sum_{a_1=1, a_2=1, \ldots, a_{n_2+2}=1}^{l_1, l_2, \ldots, l_{n_2+2}} p_{a_j}(u^{(1)}_{2_j} = x^{(1)}_{2_j, a_j}) \cdot \log p_{a_j}$$

where $j=1, 2, 3, \ldots, n_2+2$

$$H(S^{(1)}_{4_{n_4}}) = -\sum_{a_1=1,\, a_2=1,\, \ldots,\, a_{n_4}=1}^{s_1,\, s_2,\, \ldots,\, sn_4} p_{a_j}(u^{(1)}_{4_j} = x^{(1)}_{4_j, a_j}) \cdot \log p_{a_j}$$

where $j = 1, 2, 3, \ldots, n_4$

IX SENSITIVITY INDICES FOR SUBSYSTEMS AND PARAMETERS

There is an additional operation to be performed on $S^{(1)}$, namely the calculation of the sensitivity indices. Some of these are given below:

$S^{(0)}_{1_{n_1}} \rightarrow S^{(0)}_{1_{n_1+1}}$:

$$S_{e^{(0,1)}_{1_{n_1}}} = \frac{H(S^{(0)}_{1_{n_1}}) - H(S^{(1)}_{1_{n_1+1}})}{H(S^{(0)}_{1_{n_1}})}$$

Subsystem $S_{2_{n_2}}$:

$$S_{e^{(0,1)}_{2_{n_2}}} = \frac{H(S^{(0)}_{2_{n_2}}) - H(S^{(1)}_{2_{n_2+2}})}{H(S^{(0)}_{2_{n_2}})}$$

Subsystem $S_{4_{n_4}}$:

$$S_{e^{(0,1)}_{4_{n_4}}} = \frac{H(S^{(0)}_{4_{n_4}}) - H(S^{(1)}_{4_{n_4}})}{H(S^{(0)}_{4_{n_4}})}$$

We can also compute the sensitivity indices of a particular parameter, as shown below:

Transformation, Subsystems $S^{(0)}_{1_{n_1}} \rightarrow S^{(1)}_{1_{n_1+1}}$

Parameter Change: $u^{(0)}_{11} \rightarrow u^{(1)}_{11}$

Sensitivity Index: $S_{e^{(0,1)}_{11}}$:

$$S_{e_{11}}^{(0,1)} = \frac{\sum_{a_1=1}^{m_1} p_{a_1}(u_{11}^{(0)} = x_{11,a_1}^{(0)}) \log p_{a_1} - \sum_{a_1=1}^{m_1} p_{a_1}(u_{11}^{(1)} = x_{11,a_1}^{(1)}) \log p_{a_1}}{\sum_{a_1=1}^{m_1} p_{a_1}(u_{11}^{(0)} = x_{11,a_1}^{(0)}) \log p_{a_1}}$$

where the superscript $(0,1)$ denotes the transformation: $u_{11}^{(0)} \rightarrow u_{11}^{(1)}$, i.e. from state 0 to state 1 .

Transformation, Subsystems: $S_{1n_1}^{(0)} \rightarrow S_{1n_1+1}^{(1)}$

Parameter Change: $u_{1n_1}^{(0)} \rightarrow u_{1n_1}^{(1)}$

$$S_{e_{1n_1}}^{(0,1)} = \frac{\sum_{a_{n_1}=1}^{m_{n_1}} p_{a_{n_1}}(u_{1n_1}^{(0)} = x_{1n_1,a_{n_1}}^{(0)}) \log p_{a_{n_1}} - \sum_{a_{n_1}=1}^{m_{n_1}} p_{a_{n_1}}(u_{1n_1}^{(1)} = x_{1,a_{n_1}}) \log p_{a_{n_1}}}{\sum_{a_{n_1}}^{m_{n_1}} p_{a_{n_1}}(u_{1n_1}^{(0)} = x_{1_{n_1},a_{n_1}}) \log p_{a_{n_1}}}$$

Sinilar expressions can be given $S_{e_{22}}^{(0)}$ for: $u_{22}^{(0)} \rightarrow u_{22}^{(1)}$, in the transformation:

$$S_{2n_2}^{(0)} \rightarrow S_{2n_2+2}^{(1)}$$

and for: $u_{4_n}^{(0)} \rightarrow u_{4_n}^{(1)}$ in the transformation: $S_{4n_4}^{(0)} \rightarrow S_{4n_4}^{(1)}$.

There may be instances in which the sensitivity index cannot be meaningfully defined. A new parameter may be introduced, say, parameter $u_{24}^{(1)}$ in the transformation: $S_{2n_2}^{(0)} \rightarrow S_{n_2+1}^{(1)}$. This parameter does not exist in any of the subsystems of $S^{(0)}$; but it makes its first appearance in the system at state 1.

We shall adopt the convention that under such circumstances the sensitivity index of such a parameter shall be set equal to zero.

There may be instances in which the parameter whose sensitivity index is sought does not change probabilities, for example:

$$\sum_{a_1=1}^{m_1} p_{a_1}(u_{11}^{(0)} = x_{11,a_1}^{(0)}) \log p_{a_1} = \sum_{a_1=1}^{m_1} p_{a_1}(u_{11}^{(1)} = x_{11,a_1}^{(1)}) \log p_{a_1}$$

$$S_{e_{11}}^{(0,1)} = \frac{\sum_{a_1=1}^{m_1} p_{a_1}(u_{11}^{(0)} = x_{11,a_1}^{(0)}) \log p_{a_1} - \sum_{a_1=1}^{m_1} p_{a_1}(u_{11}^{(1)} = x_{11,a_1}^{(1)}) \log p_{a_1}}{\sum_{a_1=1}^{m_1} p_{a_1}(u_{11}^{(0)} = x_{11,a_1}^{(0)}) \log p_{a_1}} \equiv 0,$$

i.e., $S_{e_{11}}^{(0,1)}$ is identically equal to zero.

X. TRANSFORMATIONS: $S^{(1)}$, $S^{(2)}$, $S^{(2)}$, $S^{(3)}$ $S^{(3)}$, $S^{(4)}$.

The transformations from $S^{(i)}$ to $S^{(p)}$ $(i > 1)$ are governed by the same operations as in $S^{(0)} \rightarrow S^{(1)}$, i.e.:

a. The probabilities associated with each parameter are normalized to unity.

b. The values of the subsystem entropies are then calculated.

c. The sensitivity indices are calculated.

d. We may calculate sensitivity indices of particular parameters.

e. The entropy of the total system is computed. Since all the subsystems are assumed to be statistically independent, the calculation of the total entropy reduces to adding the entropies of the particular subsystems into which the system had been partitioned.

The system $S^{(2)}$; its input and output is shown in Figures 22 and 23.

The expressions of some subsystem entropies are given below:

$$H(S_{2n_1}^{(2)}) = - \sum_{a_1=1, a_2=1, \ldots, a_{n_i}=1}^{m_1, m_2, \ldots, m_{n_1}} p_{a_j}(u_j^{(2)} = x_{1_j, a_j}^{(2)}) \cdot \log p_{a_j}$$

$$j=1, 2, \ldots, n_1$$

$$H(S_{2n_2+1}^{(2)}) = - \sum_{a_1=1, a_2=1, \ldots, a_{n_2+1}=1}^{\ell_1, \ell_2, \ldots, \ell_{n_2+1}} p_{a_j}(u_{2_j}^{(2)} = x_{2_j, a_j}^{(2)}) \cdot \log p_{a_j}$$

$$j=1, 2, \ldots, n_2+1$$

$$H(S_{4n_4}^{(2)}) = - \sum_{a_1=1, a_2=1, \ldots, a_{n_4}=1}^{s_1, s_2, \ldots, s_{n_4}} p_{a_j}(u_{4_j}^{(2)} = x_{4_j, a_j}^{(2)}) \cdot \log p_{a_j}$$

$$j=1, 2, \ldots, n_4.$$

The expressions for subsystem sensitivity indices of $S^{(1)}$, $S^{(2)}$ are shown in Figure 27.

The entropy of the total system after state transformation 1, 1, 2 are given in Figure 28.

Values of subsystem and system efficiency indices are shown in Figures 25 and 26.

XI THE ENTROPY OF THE ENTIRE SYSTEM

With the assumption that the systems, subsystems and parameters are statistically independent, the calculation of the total entropy reduce simply to the operation of addition of the entropies of the separate subsystems. Hence, we obtain:

The 0-State: $$H(S^{(0)}) = H(S_{1_{n_1}}^{(0)}) + H(S_{2_{n_2}}^{(0)}) + H(S_{3_{n_3}}^{(0)}) + H(S_{4_{n_4}}^{(0)})$$

The 1-State: $$H(S^{(1)}) = H(S_{1_{n_1+1}}^{(1)}) + H(S_{2_{n_2+2}}^{(1)}) + \ldots + H(S_{4_{n_4}}^{(1)})$$

The 2-State: $$H(S^{(2)}) = H(S_{1_{n_1}}^{(2)}) + H(S_{2_{n_2+1}}^{(2)}) + \ldots + H(S_{4_{n_4}}^{(2)}); \text{ etc.}$$

The sensitivity indices can be calculated in the usual manner:

Transformation from 0-State to 1-State: $$S_e^{(0,1)}(S) = \frac{H(S^{(0)}) - H(S^{(1)})}{H(S^{(0)})}$$

Transformation from 1-State to 2-State: $$S_e^{(1,2)}(S) = \frac{H(S^{(1)}) - H(S^{(2)})}{H(S^{(1)})}$$

The sensitivity index can be calculated for the transformations of any two arbitrary states in the sequence. For example:

$$S_e^{(1,4)}(S) = \frac{H(S^{(1)}) - H(S^{(4)})}{H(S^{(1)})} \quad \text{or} \quad S_e^{(0,3)}(S) = \frac{H(S^{(0)}) - H(S^{(3)})}{H(S^{(0)})}$$

From the definition of the sensitivity index, it is seen that if the index is positive, say, $S_e^{(1,4)}(S)$, then the system in State 4 has lost randomness (entropy) relative to the system in State 1. However, if the value of this (sensitivity) index is negative, then $S^{(4)}$ has gained randomness relative to $S^{(1)}$.

If the number of transformations of the system S is equal to n, a finite number, then the sensitivity index between $S^{(0)}$ and $S^{(n)}$ may under certain circumstances give quantitative overviews of all the total entropy changes of the system in question.

XII THE APPLICATION OF THE INFORMATION FEEDBACK MODEL TO (ENVIRONMENTAL SETTINGS OF) DETECTION SYSTEMS. (COMPUTER SIMULATION)

The concepts, structure and formal expressions presented in the preceding pages were applied by means of computer simulation to environmental parameters that might affect the performance and operation of target detection systems such as radar, infrared, and optical systems.

The computer simulation consisted of three very similar programs; each of which having six to eight parameters. The numerical calculations were performed on the CDC 3600 computer at Michigan State University.

The probability of target detection by a radar system depends upon two prime factors (a) the technical design of the system and (b) the operating environment in which target detection occurs.

For a radar system the design is fixed with the choice of pulse shape, pulse duration repetition rate, peak power, speed of antenna rotation, antenna beam width and frequency. A major radar limitation is the inability to recognize the characteristics of objects. Radar systems see too much and the picture is confused by unwanted echoes, or clutter.

The maximum performance is therefore fixed by the design of the radar. The operational environment degrades operating performance, which is always less than design performance.

Infrared Target Detection: The environmental paremeters for this system are as follows:

PARAMETERS:

U_1 : Camouflage; U_2 : Weather; U_3 : Altitude
U_4 : Emission and Reflection from Target
U_5 : Time of day
U_6 : Time of appearance near Target
U_7 : Condition of Infrared detector
U_8 : Electromagnetic noise in atmosphere

Sixty-two missions were simulated for the infrared detection system; two of those are given below:

MISSION NUMBER 1:

U_1 : Camouflage -

$P(U_{11} = X_{11}) = 0.000$: Heavy
$P(U_{12} = X_{12}) = 0.050$: Moderate
$P(U_{13} = X_{13}) = 0.100$: Light
$P(U_{14} = X_{14}) = 0.850$: None

U_2 : Weather

$P(U_{21} = X_{21}) = 0.800$: Very dry
$P(U_{22} = X_{22}) = 0.100$: Very low humidity
$P(U_{23} = X_{23}) = 0.045$: Low humidity
$P(U_{24} = X_{24}) = 0.035$: Low humidity of light clouds or fog
$P(U_{25} = X_{25}) = 0.015$: Moderate humidity or heavy clouds or fog
$P(U_{26} = X_{26}) = 0.005$: Heavy humidity or heavy clouds or fog
$P(U_{27} = X_{27}) = 0.000$: Very high humidity

U_3 : Altitude

$P(U_{31} = X_{31}) = 0.650$: 0 to 1000 ft.
$P(U_{32} = X_{32}) = 0.250$: above 1000 up to 5000 ft.
$P(U_{33} = X_{33}) = 0.080$: above 5000 ft. up to 10, 000 ft.
$P(U_{34} = X_{34}) = 0.010$: above 10, 000 up to 20, 000 ft.
$P(U_{35} = X_{35}) = 0.008$: above 20, 000 up to 40, 000 ft.
$P(U_{36} = X_{36}) = 0.002$: above 40, 000 up to 50, 000 ft.
$P(U_{37} = X_{37}) = 0.000$: above 50, 000 ft.

U_4 : Emission and Reflection from Target

$P(U_{41} = X_{41}) = 0.850$: Excellent
$P(U_{42} = X_{42}) = 0.100$: Very good
$P(U_{43} = X_{43}) = 0.040$: Good
$P(U_{44} = X_{44}) = 0.010$: Medium
$P(U_{45} = X_{45}) = 0.00$: Weak

U_5 : Time of day

$P(U_{51} = X_{51}) = 0.050$: early morning
$P(U_{52} = X_{52}) = 0.400$: midmorning
$P(U_{53} = X_{53}) = 0.100$: noon
$P(U_{54} = X_{54}) = 0.400$: afternoon
$P(U_{55} = X_{55}) = 0.050$: evening
$P(U_{56} = X_{56}) = 0.000$: night

U_6 : Time of Appearance near target

$P(U_{61} = X_{61}) = 0.900$: exact
$P(U_{62} = X_{62}) = 0.050$: a little early
$P(U_{63} = X_{63}) = 0.000$: very late
$P(U_{64} = X_{64}) = 0.050$: a little late
$P(U_{65} = X_{65}) = 0.000$: very late
$P(U_{66} = X_{66}) = 0.000$: no appearance

U_7 : Condition of infrared detector

$P(U_{71} = X_{71}) = 0.850$: excellent
$P(U_{72} = X_{72}) = 0.100$: very good
$P(U_{73} = X_{73}) = 0.050$: good
$P(U_{74} = X_{74}) = 0.000$: fair
$P(U_{75} = X_{75}) = 0.000$: poor

U_8 : Electromagnetic Noise in Atmosphere

$P(U_{81} = X_{81}) = 0.070$: very strong
$P(U_{82} = X_{82}) = 0.100$: strong
$P(U_{83} = X_{83}) = 0.800$: moderate
$P(U_{84} = X_{84}) = 0.030$: weak
$P(U_{85} = X_{85}) = 0.000$: very weak

Total Entropy for Mission 1 = 8.105 bits

Mission Number 4 :

U_1 : Camouflage

$P(U_{11} = X_{11}) = 0.050$: heavy
$P(U_{12} = X_{12}) = 0.150$: moderate
$P(U_{13} = X_{13}) = 0.700$: light
$P(U_{14} = X_{14}) = 0.100$: None

U_2 : Weather

$P(U_{21} = X_{21}) = 0.005$: very dry
$P(U_{22} = X_{22}) = 0.050$: dry
$P(U_{23} = X_{23}) = 0.255$: very low humidity
$P(U_{24} = X_{24}) = 0.455$: low humidity or fog
$P(U_{25} = X_{25}) = 0.140$: moderate humidity
$P(U_{26} = X_{26}) = 0.040$: heavy humidity (or heavy clouds)
$P(U_{27} = X_{27}) = 0.005$: very high humidity

U_3 : Altitude

$P(U_{31} = X_{31}) = 0.650$: 0 to 1000 ft.
$P(U_{32} = X_{32}) = 0.250$: above 1,000 ft up to 5,000 ft.
$P(U_{33} = X_{33}) = 0.080$: above 5,000 ft. up to 10,000 ft.
$P(U_{34} = X_{34}) = 0.010$: above 10,000 ft. up to 20,000 ft.
$P(U_{35} = X_{35}) = 0.008$: above 20,000 ft. up to 40,000 ft.
$P(U_{36} = X_{36}) = 0.002$: above 40,000 ft. up to 60,000 ft.
$P(U_{37} = X_{37}) = 0.000$: above 60,000 ft. up to 80,000 ft.

U_4 : Emission and Reflection From Target

$P(U_{41} = X_{41}) = 0.850$: excellent
$P(U_{42} = X_{42}) = 0.100$: very good
$P(U_{43} = X_{43}) = 0.040$: good
$P(U_{44} = X_{44}) = 0.010$: medium
$P(U_{45} = X_{45}) = 0.000$: weak
$P(U_{46} = X_{46}) = 0.000$: poor
$P(U_{47} = X_{47}) = 0.000$: very poor

U_5 : Time of day

$P(U_{51} = X_{51}) = 0.050$: early morning
$P(U_{52} = X_{52}) = 0.400$: midmorning
$P(U_{53} = X_{53}) = 0.100$: noon
$P(U_{54} = X_{54}) = 0.400$: afternoon
$P(U_{55} = X_{55}) = 0.050$: evening
$P(U_{56} = X_{56}) = 0.000$: night

U_6 : Time of Appearance near Target

$P(U_{61} = X_{61}) = 0.900$: exact
$P(U_{62} = X_{62}) = 0.050$: a little early
$P(U_{63} = X_{63}) = 0.000$: very early
$P(U_{64} = X_{64}) = 0.050$: a little late
$P(U_{65} = X_{65}) = 0.000$: very late
$P(U_{66} = X_{66}) = 0.000$: no appearance

U U_7 : Condition of Infrared Detector

$P(U_{71} = X_{71}) = 0.850$
$P(U_{72} = X_{72}) = 0.100$
$P(U_{73} = X_{73}) = 0.050$
$P(U_{74} = X_{74}) = 0.000$
$P(U_{75} = X_{75}) = 0.000$
$P(U_{76} = X_{76}) = 0.000$

U_8 : Electromagnetic Noise in Atmosphere

$P(U_{81} = X_{81}) = 0.070$: very strong
$P(U_{82} = X_{82}) = 0.100$: strong
$P(U_{83} = X_{83}) = 0.030$: moderate
$P(U_{84} = X_{84}) = 0.000$: weak
$P(U_{85} = X_{85}) = 0.000$: very weak

Total Entropy for Mission 4 = 9.482 bits

Operational environmental parameters for a Radar Detection System : Forty-seven missions were computed for this set of parameters to be considered:

PARAMETERS:

U_1 : Time of appearance near target
U_2 : Weather

U_3 : Time of day
U_4 : Defense
U_5 : Pilot's Condition
U_6 : Visibility
U_7 : Reflection from target
U_8 : Electromagnetic noise

Mission Number 3 :

U_1 :

$P(U_{11} = X_{11}) = 0.800$: exact
$P(U_{12} = X_{12}) = 0.050$: exact
$P(U_{13} = X_{13}) = 0.030$: a little early
$P(U_{14} = X_{14}) = 0.050$: a little late
$P(U_{15} = X_{15}) = 0.030$: very late
$P(U_{16} = X_{16}) = 0.040$: no appearance

U_2 :

$P(U_{21} = X_{21}) = 0.800$: perfect sun
$P(U_{22} = X_{22}) = 0.100$: some clouds
$P(U_{23} = X_{23}) = 0.080$: clouds moderately
$P(U_{24} = X_{24}) = 0.020$: heavy clouds
$P(U_{25} = X_{25}) = 0.000$: very dark clouds

U_3 :

$P(U_{31} = X_{31}) = 0.000$; daylight, early morning
$P(U_{32} = X_{32}) = 0.000$: daylight, midmorning
$P(U_{33} = X_{33}) = 0.100$: daylight, noon
$P(U_{34} = X_{34}) = 0.800$: daylight, afternoon; 0.100 : twilight
$P(U_{35} = X_{35}) = 0.000$: evening
$P(U_{36} = X_{36}) = 0.000$: night stars and moon

U_4 :

$P(U_{41} = X_{41}) = 0,850$: heavy flak artillery fire
$P(U_{42} = X_{42}) = 0.050$: light flak artillery fire
$P(U_{43} = X_{43}) = 0.040$: light anti-aircraft missile fire
$P(U_{44} = X_{44}) = 0.010$: heavy anti-aircraft missle fire
$P(U_{45} = X_{45}) = 0.050$: ground fire
$P(U_{46} = X_{46}) = 0.000$: no fire

U_5 :

$P(U_{51} = X_{51}) = 0.850$: excellent
$P(U_{52} = X_{52}) = 0.100$: very good

$P(U_{53} = X_{53}) = 0.030$: good
$P(U_{54} = X_{54}) = 0.020$: fair
$P(U_{55} = X_{55}) = 0.000$: poor
$P(U_{56} = X_{56}) = 0.000$: dead

U_6 :

$P(U_{61} = X_{61}) = 0.850$: excellent
$P(U_{62} = X_{62}) = 0.100$: good
$P(U_{63} = X_{63}) = 0.050$: fair
$P(U_{64} = X_{64}) = 0.000$: poor
$P(U_{65} = X_{65}) = 0.000$

U_7 :

$P(U_{71} = X_{71}) = 0.850$: excellent
$P(U_{72} = X_{72}) = 0.100$: very good
$P(U_{73} = X_{73}) = 0.050$: good
$P(U_{74} = X_{74}) = 0.000$: medium
$P(U_{75} = X_{75}) = 0.000$: weak

U_8 :

$P(U_{81} = X_{81}) = 0.030$: very strong
$P(U_{82} = X_{82}) = 0.050$: strong
$P(U_{83} = X_{83}) = 0.850$: moderate
$P(U_{84} = X_{84}) = 0.050$: weak
$P(U_{85} = X_{85}) = 0.020$: very weak

Mission 8 :

U_1 :

$P(U_{11} = X_{11}) = 0.800$: exact
$P(U_{12} = X_{12}) = 0.050$: a little early
$P(U_{13} = X_{13}) = 0.030$: very early
$P(U_{14} = X_{14}) = 0.050$: a little late
$P(U_{15} = X_{15}) = 0.030$: very late
$P(U_{16} = X_{16}) = 0.040$: no appearance

VISUAL TARGET DETECTION :

Fifty-two missions were computed for this set of parameters. The environmental parameters for this system are as follows:

U_1 : Camouflage :

$P(U_1 = X_{11}) = 0.100$: heavy
$P(U_1 = X_{12}) = 0.750$: moderate
$P(U_1 = X_{13}) = 0.100$: light
$P(U_1 = X_{14}) = 0.050$: none

U_2 : Weather :

$P(U_2 = X_{21}) = 0.100$: perfect sun
$P(U_2 = X_{22}) = 0.800$: some clouds
$P(U_3 = X_{23}) = 0.070$: moderate clouds
$P(U_4 = X_{24}) = 0.030$: heavy clouds
$P(U_5 = X_{25}) = 0.000$: very dark clouds

U_3 : Time of day :

$P(U_3 = X_{31}) = 0.040$: early morning
$P(U_3 = X_{32}) = 0.750$: morning - noon
$P(U_3 = X_{33}) = 0.100$: noon
$P(U_3 = X_{34}) = 0.050$: afternoon
$P(U_3 = X_{35}) = 0.040$: evening
$P(U_3 = X_{36}) = 0.020$: night (moon and stars)
$P(U_3 = X_{37}) = 0.000$: night (no moon, stars)
$P(U_3 = X_{38}) = 0.000$: night dark

U_4 : Distance :

$P(U_4 = X_{41}) = 0.800$: 0 to .5 miles
$P(U_4 = X_{42}) = 0.100$: above .5 up to 1 miles
$P(U_4 = X_{43}) = 0.060$: above 1 up to 3 miles
$P(U_4 = X_{44}) = 0.030$: above 3 up to 8 miles
$P(U_4 = X_{45}) = 0.010$: above 8 up to 15 miles
$P(U_4 = X_{46}) = 0.000$: above 15 miles

U_5 : Pilots Condition :

$P(U_5 = X_{51}) = 0.850$: excellent
$P(U_5 = X_{52}) = 0.100$: very good
$P(U_5 = X_{53}) = 0.030$: good
$P(U_5 = X_{54}) = 0.020$: fair
$P(U_5 = X_{55}) = 0.000$: poor
$P(U_5 = X_{56}) = 0.000$: dead

U_6	: Time of Appearance near Target	:
$P(U_6 = X_{61})$	= 0.960	: exact
$P(U_6 = X_{62})$	= 0.020	: a little early
$P(U_6 = X_{63})$	= 0.000	: very early
$P(U_6 = X_{64})$	= 0.020	: a little late
$P(U_6 = X_{65})$	= 0.000	: very late
$P(U_6 = X_{66})$	= 0.000	: no appearance

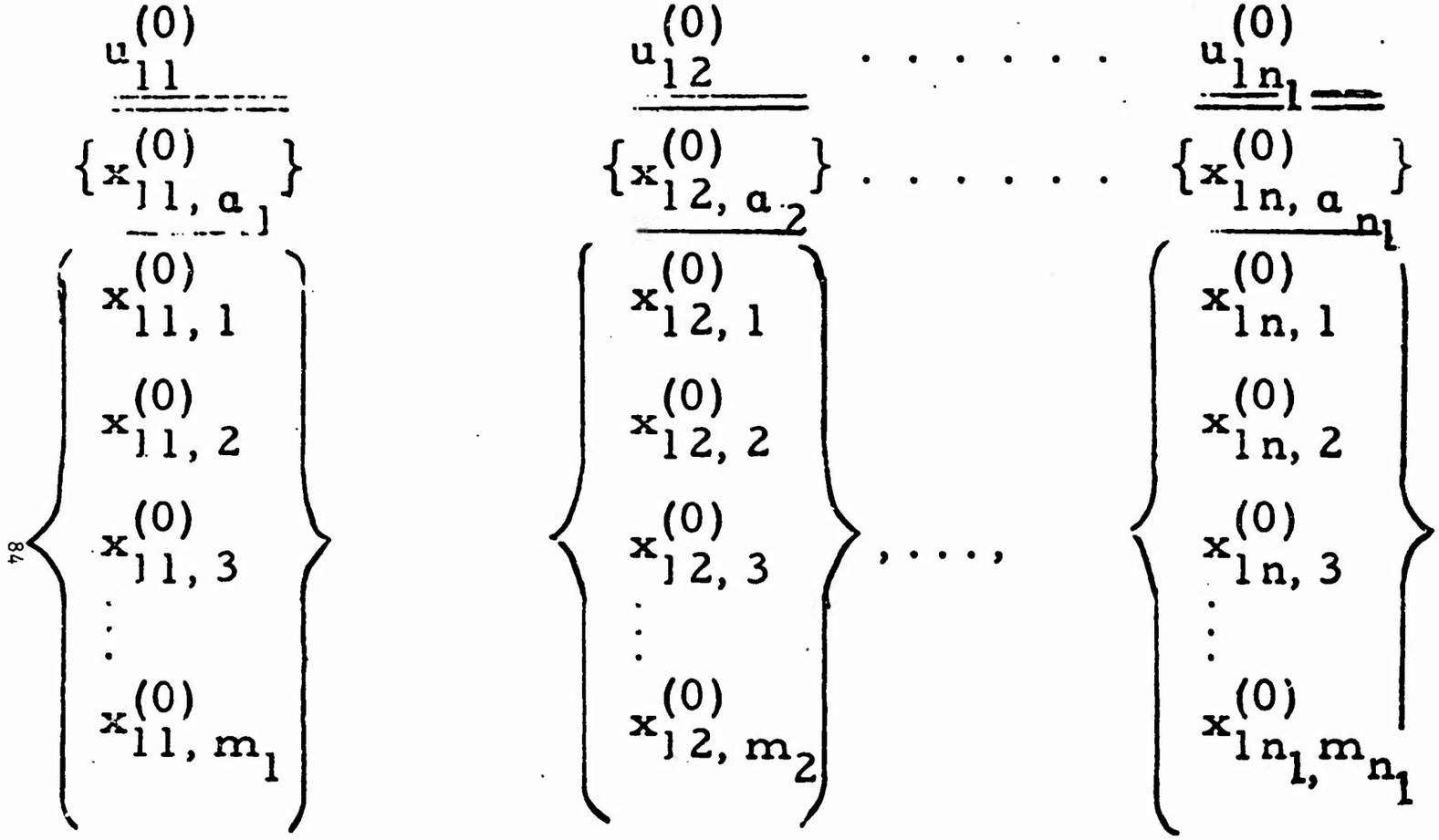
Total Entropy = 5.676 bits

PARAMETERS, SYSTEMS, SUBSYSTEMS

$S^{(0)}_{1n_1}$	$S^{(0)}_{2n_2}$	$S^{(0)}_{3n_3}$	$S^{(0)}_{4n_4}$
$u^{(0)}_{11}$	$u^{(0)}_{21}$	$u^{(0)}_{31}$	$u^{(0)}_{41}$
$u^{(0)}_{12}$	$u^{(0)}_{22}$	$u^{(0)}_{32}$	$u^{(0)}_{42}$
$u^{(0)}_{13}$	$u^{(0)}_{23}$	$u^{(0)}_{33}$	$u^{(0)}_{43}$
$u^{(0)}_{14}$	$u^{(0)}_{24}$	$u^{(0)}_{34}$	$u^{(0)}_{44}$
$\vdots$	$\vdots$	$\vdots$	$\vdots$
$u_{1_{n1}}$	$u_{2_{n2}}$	$u_{3_{n3}}$	$u_{4_{n4}}$

The System $S^{(0)}$

FIGURE 1



Sets of Values Assigned to Each Parameter of Subsystem $S_{1n_1}^{(0)}$

FIGURE 2

$$\sum_{a_1=1}^{m_1} p_{a_1}(u_{11}^{(0)} = x_{11,a_1}^{(0)}) = 1, \qquad 0 \le p_{a_1} \le 1,$$

$$\sum_{a_2=1}^{m_2} p_{a_2}(u_{12}^{(0)} = x_{12,a_2}^{(0)}) = 1, \qquad 0 \le p_{a_2} \le 1,$$

$$\sum_{a_{n_1}=1}^{m_{n_1}} p_{a_{n_1}}(u_{1n_1}^{(0)} = x_{1n,a_{n_1}}^{(0)}) = 1, \qquad 0 \le p_{a_{n_1}} \le 1;$$

Probabilities Associated with Each Parameter of Subsystem $S_{1n_1}^{(0)}$

FIGURE 3

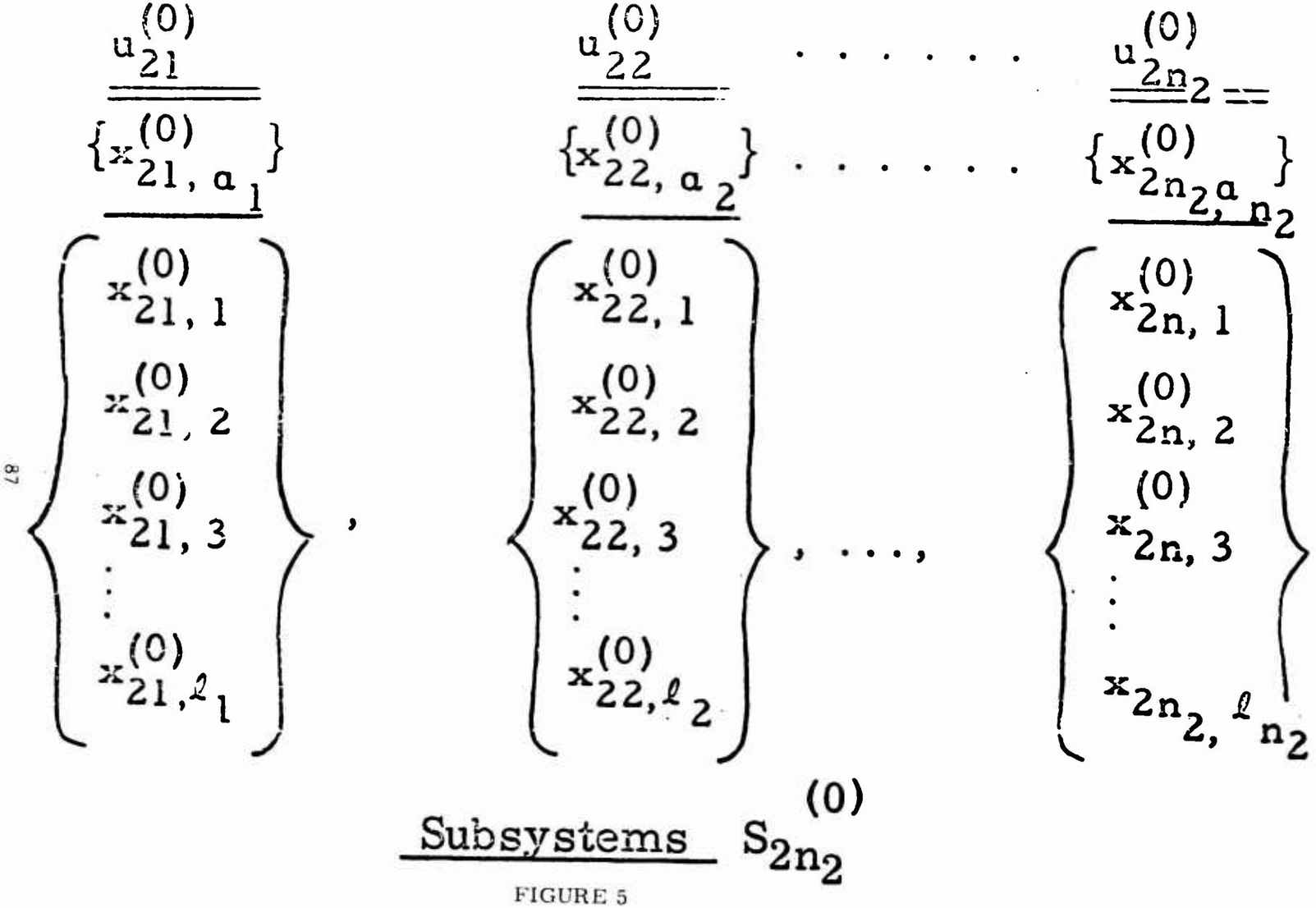
$$H(S_{1n_1}^{(0)}) = -\left\{\sum_{a_1=1}^{m_1} p_{a_1}(u_{11}^{(0)} = x_{11,a_1}^{(0)}) \log p_{a_1} + \right.$$

$$+ \sum_{a_2=1}^{m_2} p_{a_2}(u_{12}^{(0)} = x_{12,a_2}^{(0)}) \log p_{a_2} + \ldots \ldots$$

$$\ldots \ldots + \left. \sum_{a_{n_1}=1}^{m_{n_1}} p_{a_{n_1}}(u_{1n_1}^{(0)} = x_{1n_1,a_{n_1}}^{(0)}) \log p_{a_{n_1}} \right\}$$

The Entropy of Subsystem $S_{1n_1}^{(0)}$

FIGURE 4



Subsystems $S_{2n_2}^{(0)}$

FIGURE 5

$$\sum_{a_1=1}^{\ell_1} p_{a_1}(u_{21}^{(0)} = x_{21,a_1}^{(0)}) = 1, \qquad 0 \le p_{a_1} \le 1,$$

$$\sum_{a_2=1}^{\ell_2} p_{a_2}(u_{22}^{(0)} = x_{22,a_2}^{(0)}) = 1, \qquad 0 \le p_{a_2} \le 1,$$

$$\vdots$$

$$\sum_{a_n=1}^{\ell_{n_2}} p_{a_{n_2}}(u_{2n_2}^{(0)} = x_{2n_2,a_{n_2}}^{(0)}) = 1, \qquad 0 \le p_{a_{n_2}} \le 1;$$

Probabilities Associated with Parameters of Subsystem $S_{2n_2}^{(0)}$

FIGURE 6

$$\sum_{a_1=1}^{s_1} p_{a_1}(u_{41}^{(0)} = x_{41,a_1}^{(0)}) = 1, \qquad 0 \le p_{a_1} \le 1,$$

$$\sum_{a_2=1}^{s_2} p_{a_2}(u_{42}^{(0)} = x_{42,a_2}^{(0)}) = 1, \qquad 0 \le p_{a_2} \le 1,$$

.

.

.

$$\sum_{a_{n_4}=1}^{s_{n_4}} p_{a_{n_4}}(u_{4n_4}^{(0)} = x_{4n_4,a_{n_4}}^{(0)}) = 1, \qquad 0 \le p_{a_{n_4}} \le 1 .$$

Probabilities Associated with Parameters $u_{4n_4}^{(0)}$

FIGURE 7

$$H(S^{(0)}_{1n_1}) = -\sum_{a_1=1,\, a_2=1,\, \ldots,\, a_{n_1}=1}^{m_1,\, m_2,\, \ldots,\, m_{n_1}} p_{a_j}(u^{(0)}_{ij} = x^{(0)}_{ij,\, a_j}) \log p_{a_j},$$

$$j = 1, 2, 3, \ldots, n_1;$$

$$H(S^{(0)}_{2n_2}) = -\sum_{a_1=1,\, a_2=1,\, \ldots,\, a_{n_2}=1}^{\ell_1,\, \ell_2,\, \ldots,\, \ell_{n_2}} p_{a_j}(u^{(0)}_{2j} = x^{(0)}_{2j,\, a_j}) \log p_{a_j},$$

$$j = 1, 2, 3, \ldots, n_2;$$

. . . . . .

$$H(S^{(0)}_{4n_4}) = -\sum_{a_1=1,\, a_2=1,\, a_{n_4}=1}^{s_1,\, s_2,\, \ldots,\, s_{n_4}} p_{a_j}(u^{(0)}_{4j} = x^{(0)}_{4j,\, a_j}) \log p_{a_j},$$

$$j = 1, 2, 3, \ldots, n_4.$$

The Entropy of the Entire System $S^{(0)}$

FIGURE 8

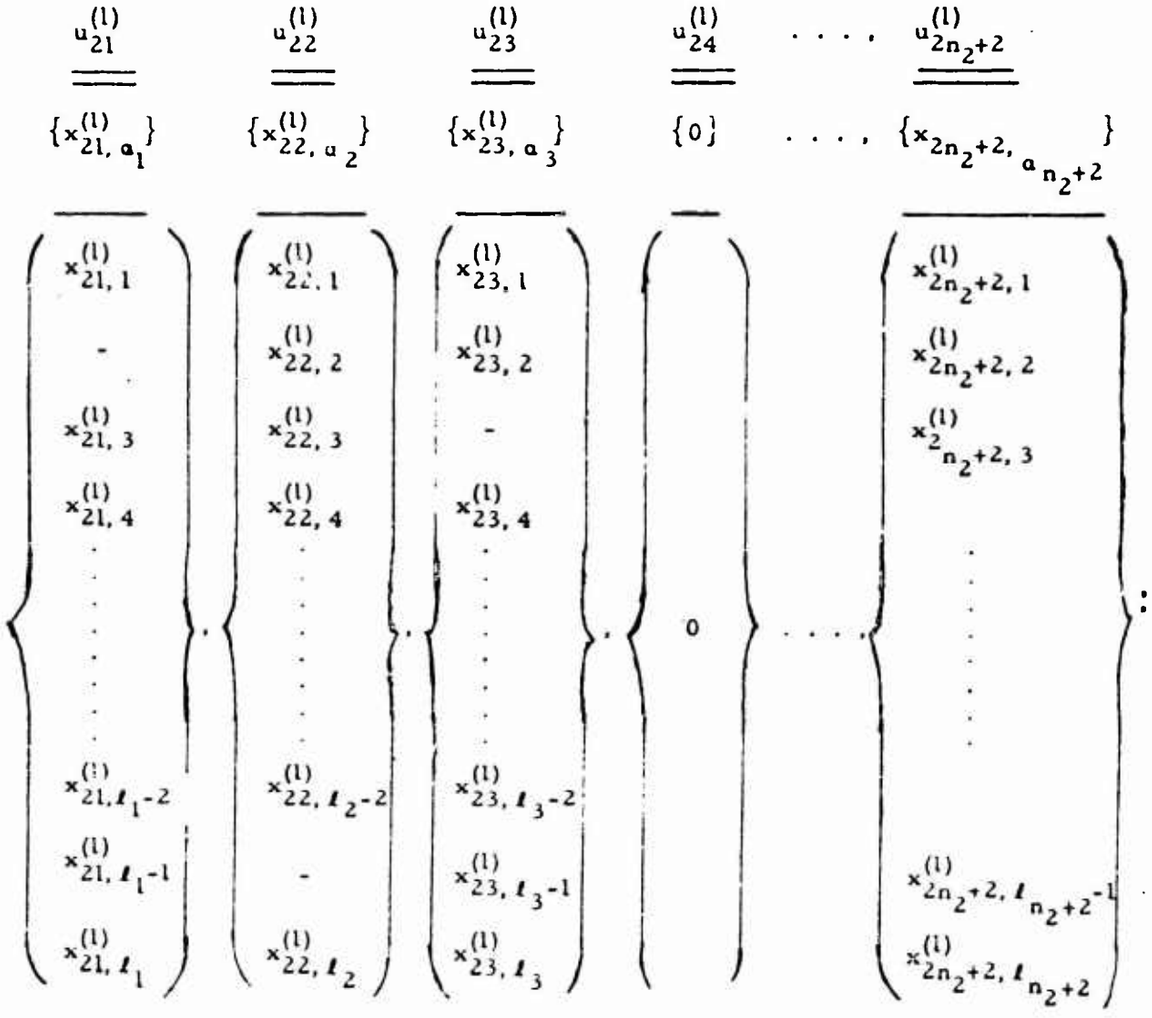
Subsystem $S^{(1)}_{1n_1+1}$:

$$\begin{array}{cccccc}
u^{(1)}_{11} & & u^{(1)}_{12} & & u^{(1)}_{13} & \cdots\cdots\cdots, & u^{(1)}_{1n_1+1} \\
\{x^{(1)}_{11,\,a_1}\} & & \{0\} & & \{x^{(1)}_{13,\,a_3}\} & \cdots\cdots, & \{x^{(1)}_{1n_1+1,\,a_{n_1+1}}\} \\
\left\{\begin{array}{l} x^{(1)}_{11,1} \\ x^{(1)}_{11,2} \\ x^{(1)}_{11,3} \\ \vdots \\ x^{(1)}_{11,\,m_1-2} \\ \cdots \\ x^{(1)}_{11,m_1} \end{array}\right\}, & & \left\{\begin{array}{l} \\ \\ \\ \\ 0 \\ \\ \\ \end{array}\right\}, & & \left\{\begin{array}{l} x^{(1)}_{13,1} \\ \cdots \\ x^{(1)}_{13,3} \\ \vdots \\ x^{(1)}_{13,\,m_3-2} \\ x^{(1)}_{13,\,m_3-1} \\ x^{(1)}_{13,m_3} \end{array}\right\}, \cdots, & \left\{\begin{array}{l} x^{(1)}_{1n_1+1,1} \\ x^{(1)}_{1n_1+1,2} \\ x^{(1)}_{1n_1+1,3} \\ \vdots \\ x^{(1)}_{1n_1+1,\,m_{n_1+1}-2} \\ \cdots \\ x^{(1)}_{1n_1+1,\,m_{n_1+1}} \end{array}\right\}; \\
\end{array}$$

Set of Values Assigned to Parameters in the Subsystem $S^{(1)}_{1\,n_1+1}$

FIGURE 9

Subsystem $S^{(1)}_{2n_2+2}$:



Set of Values Assigned to Parameters in the Subsystem $S^{(1)}_{2n_2+2}$

FIGURE 10

$$S^{(1)}_{1n_1+1} = \{u^{(1)}_{11},\ -,\ u^{(1)}_{13},\ u^{(1)}_{14},\ \ldots,\ u^{(1)}_{1n_1},\ u^{(1)}_{1n_1+1}\};$$

$$S^{(1)}_{2n_2+2} = \{u^{(1)}_{21},\ u^{(1)}_{22},\ u^{(1)}_{23},\ -,\ u^{(1)}_{25},\ \ldots,\ u^{(1)}_{2n_2},\ u^{(1)}_{2n_2+1},\ u^{(1)}_{2n_2+2}\};$$

$$S^{(1)}_{3n_3+1} = \{u^{(1)}_{31},\ -\ u^{(1)}_{33},\ -\ ,u^{(1)}_{35},\ldots,\ u^{(1)}_{3n_3},\ u^{(1)}_{3n_3+1}\};$$

$$S^{(1)}_{4n_4} = \{u^{(1)}_{41},\ -,\ -,\ u^{(1)}_{44},\ u^{(1)}_{45},\ \ldots\ldots,\ u^{(1)}_{4n_4}\}$$

Distinct Parameters of Subsystems $S^{(1)}_{in_i}$; i = 1 to 4

FIGURE 11

No.	$S^{(1)}_{1n_1+1}$	$S^{(1)}_{2n_2+2}$	$S^{(1)}_{3n_3+1}$	$S^{(1)}_{4n_4}$
1	-	-	-	-
2	$u^{(1)}_{12} \rightarrow u^{(1)}_{2n_2+1}$		$u^{(1)}_{32} \rightarrow u^{(2)}_{2n_2+1}$	$u^{(1)}_{42} \rightarrow u^{(1)}_{2n_2+2}$
3				$u^{(1)}_{43} \rightarrow u^{(1)}_{3n_3+1}$
4		$u^{(1)}_{24} \rightarrow u^{(1)}_{n_1+1}$	$u^{(1)}_{34} \rightarrow u^{(2)}_{3n_3+1}$	
5	-	-	-	-
.	.	.	.	.
.	.	.	.	.
.	.	.	.	.
.	.	.	.	.
.	.	.	.	.
.	.	.	.	.
.	.	.	.	.
n_i				
n_i+1	$u^{(1)}_{1n_1+1}$ from $u^{(1)}_{24}$	$u^{(1)}_{2n_2+1}$ from $u^{(1)}_{12}$	$u^{(1)}_{3n_3+1}$ from $u^{(1)}_{43}$	
n_i+2		$u^{(1)}_{2n_2+2}$ from $u^{(1)}_{42}$		

Input into the System $S^{(1)}$ and Output for the System $S^{(1)}$

FIGURE 12

parameters $u^{(l)}_{ln_l+l}$ in the subsystem $S^{(l)}_{ln_l+l}$:

$$\sum_{a_1=1}^{m_1} p_{a_1}\,(u^{(l)}_{ll} = x^{(l)}_{ll,\,a_1}) = 1; \qquad 0 \le p_{a_1} \le 1;$$

$$\sum_{a_3=1}^{m_3} p_{a_3}\,(u^{(l)}_{l3} = x^{(l)}_{l3,\,a_3}) = 1; \qquad 0 \le p_{a_3} \le 1;$$

$$\cdot \qquad \cdot \qquad \cdot \qquad \cdot \qquad \cdot \qquad \cdot$$

$$\sum_{a_{n_l+1}}^{m_{n+1}} p_{a_{n_l+1}}\,(u^{(l)}_{ln_l+l} = x^{(l)}_{ln_l+l,\,a_{n_l+1}}) = 1; \qquad 0 \le p_{a_{n_l+1}} \le 1;$$

parameters $u^{(l)}_{2n_2+2}$ in the subsystem $S^{(l)}_{2n_2+2}$:

$$\sum_{a_1=1}^{\ell_1} p_{a_1}\,(u^{(l)}_{21} = x^{(l)}_{21,\,a_1}) = 1; \qquad 0 \le p_{a_1} \le 1;$$

$$\sum_{a_2=1}^{\ell_2} p_{a_2}\,(u^{(l)}_{22} = x^{(l)}_{22,\,a_2}) = 1; \qquad 0 \le p_{a_2} 1;$$

$$\cdot \qquad \cdot \qquad \cdot \qquad \cdot \qquad \cdot \qquad \cdot$$

$$\sum_{a_{n_2+2}}^{\ell_{n_2+2}} p_{a_{n_2+2}}\,(u_{2n_2+2} = x_{2n_2+2,a_{n_2+2}}) = 1; \qquad 0 \le p_{a_{n_2+2}} \le 1;$$

parameters $u^{(l)}_{4n_4}$ in the subsystem $S^{(l)}_{4n_4}$:

The Probabilities Associated with Each Parameter Normalized to Unity

FIGURE 13

Parameter u_{11}: $u_{11}^{(0)} \longrightarrow u_{11}^{(1)}$ in the subsystems $S_{1n_1}^{(0)} \longrightarrow S_{1n_1+1}^{(1)}$:

$$se_{11}^{(0,1)} = \frac{\sum_{a_1=1}^{m_1} p_{a_1}(u_{11}^{(0)} = x_{11,a_1}^{(0)}) \log p_{a_1} - \sum_{a_1=1}^{m_1} p_{a_1}(u_{11}^{(1)} = x_{11,a_1}^{(1)}) \log p_{a_1}}{\sum_{a_1=1}^{m_1} p_{a_1}(u_{11}^{(0)} = x_{11,a_1}^{(0)}) \log p_{a_1}} \qquad (1.3.23)$$

where the superscript (0, 1) denotes that the parameter $u_{11}^{(0)}$ was subjected to the transformation from state 0 to state 1.

Parameter u_{1n_1}: $u_{1n_1}^{(0)} \longrightarrow u_{1n_1}^{(1)}$ in the subsystems $S_{1n_1}^{(0)} \longrightarrow S_{1n_1+1}^{(1)}$:

$$se_{1n_1}^{(0,1)} = \frac{\sum_{a_{n_1}=1}^{m_{n_1}} p_{a_{n_1}}(u_{1n_1}^{(0)} = x_{1n_1,a_{n_1}}^{(0)}) \log p_{a_{n_1}} - \sum_{a_{n_1}=1}^{m_{n_1}} p_{a_{n_1}}(u_{1n_1}^{(1)} = x_{1n_1,a_{n_1}}^{(1)}) \log p_{a_{n_1}}}{\sum_{a_{n_1}=1}^{m_{n_1}} p_{a_{n_1}}(u_{1n_1}^{(0)} = x_{1n,a_{n_1}}^{(0)}) \log p_{a_{n_1}}} \qquad (1.3.24)$$

Sensitivity Coefficients of Particular Parameters

FIGURE 14

$$S^{(0)}_{1n_1} \longrightarrow S^{(1)}_{1n_1+1} :$$

$$Se^{(0,1)}_{1n_1} = \frac{H(S^{(0)}_{1n_1}) - H(S^{(1)}_{1n_1+1})}{H(S^{(0)}_{1n_1})} ;$$

subsystem S_{2n_2} :

$$Se^{(0,1)}_{2n_2} = \frac{H(S^{(0)}_{2n_2}) - H(S^{(1)}_{2n_2+2})}{H(S^{(0)}_{2n_2})}$$

subsystem S_{4n_4} :

$$Se^{(0,1)}_{4n_4} = \frac{H(S^{(0)}_{4n_4}) - H(S^{(1)}_{4n_4})}{H(S^{(0)}_{4n_4})} \quad ; \text{ etc.}$$

Sensitivity Coefficients of Subsystems

FIGURE 15

Efficiency Coefficients of Subsystems(continued)

Subsystem $S^{(0)}_{3n_3} \longrightarrow S^{(1)}_{3n_3}$:

$$Se^{(0)}_{3n_3} = \frac{111.203 - 66.531}{111.203} = \frac{44.672}{111.203} = 0.401$$

Subsystem $S^{(0)}_{4n_4} \longrightarrow S^{(1)}_{4n_4}$:

$$Se^{(0)}_{4n_4} = \frac{85.850 - 52.255}{85.850} = \frac{33.595}{85.850} = 0.391$$

FIGURE 16

$$\sum_{a_1=1}^{m_1} p_{a_1} \left(u_{11}^{(2)} = x_{11,a_1}^{(2)}\right) = 1 ; \qquad 0 \leq p_{a_1} \leq 1 ;$$

. . . .
. . . .
. . . .

$$\sum_{a_3=1}^{m_3} p_{a_3} \left(u_{13}^{(2)} = x_{13,a_3}^{(2)}\right) = 1 ; \qquad 0 \leq p_{a_3} \leq 1 ;$$

. . . .
. . . .
. . . .

$$\sum_{a_{n_1}=1}^{m_{n_1}} p_{a_{n_1}} \left(u_{1n_1}^{(2)} = x_{1n_1}^{(2)}\right) = 1 ; \qquad 0 \leq p_{a_{n_1}} \leq 1 ;$$

parameters $u_{2n_2+1}^{(2)}$ in the subsystem $S_{2n_2+1}^{(2)}$:

$$\sum_{a_1=1}^{\ell_1} p_{a_1} \left(u_{21}^{(2)} = x_{21,a_1}^{(2)}\right) = 1; \qquad 0 \leq p_{a_1} \leq 1$$

$$\sum_{a_2=1}^{\ell_2} p_{a_2} \left(u_{22}^{(2)} = x_{22,a_2}^{(2)}\right) = 1 ; \qquad 0 \leq p_{a_2} \leq 1 ;$$

. . . .
. . . .
. . . .

Normalization of Probabilities for Parameters in Subsystems $S_{1n_1}^{(2)}$ and $S_{2n_2+1}^{(2)}$

FIGURE 17

$$\sum_{a_{n_2+1}=1}^{l_{n_2+1}} p_{a_{n_2+1}} (u^{(2)}_{2n_2+1} = x^{(2)}_{2n_2+1,\, a_{n_2+1}}) = 1 \; ; \; 0 \leq p_{a_{n_2+1}} \leq 1;$$

$(S^{(2)}_{2n_2+1})$

parameters $u^{(2)}_{4n_4}$ in the subsystem $S^{(2)}_{4n_4}$:

$$\sum_{a_1=1}^{s_1} p_{a_1} (u^{(2)}_{41} = x^{(2)}_{41,\, a_1}) = 1 \; ; \qquad 0 \leq p_{a_1} \leq 1 \; ;$$

$$\sum_{a_2=1}^{s_2} p_{a_2} (u^{(2)}_{42} = x^{(2)}_{42,\, a_2}) = 1; \qquad 0 \leq p_{a_2} \leq 1 \; ;$$

. . . .
. . . .
. . . .

. .
. .
. .

$$\sum_{a_{n_4}}^{s_{n_4}} p_{a_{n_4}} (u^{(2)}_{4n_4} = x^{(2)}_{4n_4,\, a_{n_4}}) = 1 \; ; \qquad 0 \leq p_{a_{n_4}} \leq 1.$$

Normalization of Probabilities for Parameter in Subsystem $S^{(2)}_{4n_4}$

FIGURE 18

The subsystem $S^{(1)}_{1n_1+1}$:

$$H(S^{(1)}_{1n_1+1}) = -\sum_{a_1=1,\ a_3=1,\ \ldots,\ a_{n_1+1}=1}^{m_1,\ m_3,\ \ldots,\ m_{n_1+1}} p_{a_j}\,(u^{(1)}_{1j} = x^{(1)}_{1j,\ a_j}) \cdot \log p_{a_j},$$

The subsystem $S^{(1)}_{2n_2+2}$:

$$H(S^{(1)}_{2n_2+2}) = -\sum_{a_1=1,\ a_2=1,\ \ldots,\ a_{n_2+2}=1}^{l_1,\ l_2,\ l_3,\ \ldots,\ l_{n_2+2}} p_{a_j}\,(u^{(1)}_{2j} = x^{(1)}_{2j,\ a_j}) \cdot \log p_{a_j},\quad j = 1,\ 2,\ 3,\ \ldots,\ n_2+2;$$

$$H(S^{(1)}_{4_{n_4}}) = -\sum_{a_1=1,\ a_2=1,\ \ldots,\ a_{n_4}=1}^{s_1,\ s_2,\ \ldots,\ s_{n_4}} \cdot p_{a_j}\,(u^{(1)}_{4j} = x^{(1)}_{4j,\ a_j}) \cdot \log p_{a_j},\quad j = 1,\ 2,\ 3,\ \ldots,\ n_4.$$

Entropies of Subsystems

FIGURE 19

As the next step we calculate some sensitivity coefficients. Subsystem S_{1n_1} when it is transformed from state 1 to state 2, i.e.,

$$S^{(1)}_{1n_1+1} \Longrightarrow S^{(2)}_{1n_1} :$$

$$Se^{(1,2)}_{1n_1+1} = \frac{H(S^{(1)}_{1n_1+1}) - H(S^{(2)}_{1n_1})}{H(S^{(1)}_{1n_1+1})} ;$$

Subsystem S_{2n_2+2} :

$$Se^{(1,2)}_{2n_2+2} = \frac{H(S^{(1)}_{2n_2+2}) - H(S^{(2)}_{2n_2+1})}{H(S^{(1)}_{2n_2+2})} ;$$

Subsystem S_{4n_4} :

$$Se^{(1,2)}_{4n_4} = \frac{H(S^{(1)}_{4n_4}) - H(S^{(2)}_{4n_4})}{H(S^{(1)}_{4n_4})} .$$

Sensitivity Coefficients of Transformation (1)—> (2)

FIGURE 20

The subsystems $S^{(2)}_{in_i}$ have the following structure:

$$S^{(2)}_{1n_1} = \{ u^{(2)}_{11}, u^{(2)}_{12}, \ldots\ldots, \ldots\ldots, u^{(2)}_{1n_1} \} ;$$

$$S^{(2)}_{2n_2+1} = \{u^{(2)}_{21}, u^{(2)}_{22}, \ldots., u^{(2)}_{2n_2}, u^{(2)}_{2n_2+1}\};$$

$$S^{(2)}_{3n_3+1} = \{u^{(2)}_{31}, u^{(2)}_{32}, - u^{(2)}_{34}, \ldots, u^{(2)}_{3n_3}, u^{(2)}_{3n_3+1}\};$$

$$S^{(2)}_{4n_4} = \{ u^{(2)}_{41}, u^{(2)}_{42}, \ldots\ldots\ldots, u^{(2)}_{4n_4} \}.$$

The Parameters of $S^{(2)}_{in_i}$

FIGURE 21

No.	$S^{(2)}_{1n_1}$	$S^{(2)}_{2n_2+1}$	$S^{(2)}_{3n_3+1}$	$S^{(2)}_{4n_4}$
1	$u^{(2)}_{11}$	$u^{(2)}_{21}$	$u^{(2)}_{31}$	$u^{(2)}_{41}$
2	$u^{(2)}_{12}$	$u^{(2)}_{22}$	$u^{(2)}_{32}$	$u^{(2)}_{42}$
3	$u^{(2)}_{13}$	$u^{(2)}_{23}$	--	$u^{(2)}_{43}$
	. . .	. . .	. . .	. . .
n_i	$u^{(2)}_{1n_1}$	$u^{(2)}_{2n_2}$	$u^{(2)}_{3n_3}$	$u^{(2)}_{4n_4}$
n_i+1		$u^{(2)}_{2n_2+1}$	$u^{(2)}_{3n_3+1}$	

System $S^{(2)}$ After the Transmission of Information is Fully Completed

FIGURE 22

	$S^{(2)}_{in_1}$	$S^{(2)}_{2n_2+1}$	$S^{(2)}_{3n_3+1}$	$S^{(2)}_{4n_4}$
1				
2			$u^{(2)}_{32} \rightarrow u^{(3)}_{43}$	
3				
4				
5				
n_i				
n_{i+1}		$u^{(2)}_{2n_2+1}$ from $u^{(1)}_{32}$	$u^{(2)}_{3n_3+1}$ from $u^{(1)}_{34}$	

Input into the System $S^{(2)}$ and Output from the System $S^{(2)}$

FIGURE 23

Efficiency Coefficients of Subsystems (numerical calculations)

	STATE $S^{(0)}$			STATE $S^{(1)}$
H FOR SUBSYSTEM	$S^{(0)}_{1n_1}$	6.160 bits	⟶	$S^{(1)}_{1n_1}$ 51.737 bits
	$S^{(0)}_{2n_2}$	39.553 bits	⟶	$S^{(1)}_{2n_2}$ 59.382 bits
	$S^{(0)}_{3n_3}$	111.203 bits	⟶	$S^{(1)}_{3n_3}$ 66.531 bits
	$S^{(0)}_{4n_4}$	85.850 bits	⟶	$S^{(1)}_{4n_4}$ 52.255 bits
H FOR THE SYSTEM		242.766 bits		229.905 bits

The efficiency coefficient of the entire system is:

$$Se^{(0,1)}(S) = \frac{242.766 - 229.905}{242.766} = \frac{12.861}{242.766} = 0.0528$$

During the transformation from the state $S^{(0)}$ to the state $S^{(1)}$ the efficiency coefficients of particular subsystems are:

Subsystem $S^{(0)}_{1n_1} \longrightarrow S^{(1)}_{1n_1}$:

$$Se^{(0)}_{1n_1} = \frac{6.160 - 51.737}{6.160} = -\frac{45.577}{6.160} = -7.4$$

Subsystem $S^{(0)}_{2n_2} \longrightarrow S^{(1)}_{2n_2}$:

$$Se^{(0)}_{2n_2} = \frac{39.553 - 59.382}{39.553} = -\frac{19.829}{39.553} = -0.502$$

FIGURE 24

Efficiency Coefficients after the Transformation from the State S(0) to the State S(1)

Subsystem or Total System	H = entropy in bits	Efficiency Coefficients of Subsystems and Total System	
		Symbol	Value
$S^{(0)}_{1n_1}$	48.074	$Se^{(0)}_{1n_1}$	-0.369
$S^{(1)}_{1n_1}$	65.797		
$S^{(0)}_{2n_2}$	81.837	$Se^{(0),(1)}_{2n_2}$	0.412
$S^{(1)}_{2n_2}$	48.062		
$S^{(0)}_{3n_3}$	30.510	$Se^{(0),(1)}_{3n_3}$	-0.815
$S^{(1)}_{3n_3}$	55.011		
$S^{(0)}_{4n_4}$	80.981	$Se^{(0),(1)}_{4n_4}$	0.3715
$S^{(1)}_{4n_4}$	59.573		
Total System $S^{(0)}$	241.402	$Se^{(0,1)}(S)$	0.0536
Total System $S^{(1)}$	228.443		

FIGURE 25

Efficiency Coefficients after the Transformation
from the State S(2) to the State S(3)

Subsystem or Total System	H = entropy in bits	Efficiency Coefficients of Subsystems and Total System	
		Symbol	Value
$S^{(2)}_{1n_1}$	68.056	$Se^{(2,3)}_{1n_1}$	-0.1626
$S^{(3)}_{1n_1}$	79.143		
$S^{(2)}_{2n_2}$	76.687	$Se^{(2,3)}_{2n_2}$	0.1045
$S^{(3)}_{2n_2}$	68.675		
$S^{(2)}_{3n_3}$	77.746	$Se^{(2,3)}_{3n_3}$	0.326
$S^{(3)}_{3n_3}$	52.395		
$S^{(2)}_{4n_4}$	79.413	$Se^{(2,3)}_{4n_4}$	0.1909
$S^{(3)}_{4n_4}$	64.279		
Total System $S^{(2)}$	301.902	$Se^{(2,3)}_{(S)}$	0.1240
Total System $S^{(3)}$	264.492		

FIGURE 26

(0, 1): From State 0 to State 1

$$S_e^{(0,1)}(S) = \frac{H(S^{(0)}) - H(S^{(1)})}{H(S^{(0)})}$$

(1, 2): From State 1 to State 2

$$S_e^{(1,2)}(S) = \frac{H(S^{(1)}) - H(S^{(2)})}{H(S^{(1)})}; \text{ etc.}$$

(i, p): From State i to State p
(i < p)

$$S_e^{(i,p)}(S) = \frac{H(S^{(i)}) - H(S^{(p)})}{H(S^{(i)})}$$

Sensitivity Coefficients of Entire System

FIGURE 27

The State 0 :

$$H(S^{(0)}) = H(S_{1n_1}^{(0)}) + H(S_{2n_2}^{(0)}) + H(S_{3n_3}^{(0)}) + H(S_{4n_4}^{(0)})$$

The State 1 :

$$H(S^{(1)}) = H(S_{1n_1}^{(1)}) + H(S_{2n_2}^{(1)} + 2) + \ldots + H(S_{4n_4}^{(1)})$$

The State 2 :

$$H(S^{(2)}) = H(S_{1n_1}^{(2)}) + \ldots + H(S_{4n_4}^{(2)}), \text{ etc.}$$

The Entropy of the Total System

TABLE OF STATES IN RADAR TARGET DETECTION

STATE		
	U(1)	TIME OF APPEARANCE NEAR TARGET
	U(2)	WEATHER
	U(3)	TIME OF DAY
	U(4)	DEFENSE
	U(5)	PILOT'S CONDITION
	U(6)	VISIBILITY
	U(7)	REFLECTION FROM TARGET
	U(8)	ELECTROMAGNETIC NOISE

FIGURE 2

CHANGES IN STATES IN RADAR TARGET DETECTION

CHANGED STATES FROM MISSION	MISSION NUMBER	TOTAL ENTROPY FOR THE MISSION
	1	7.092 bits
	2	7.240 bits
	3	7.202 bits
	4	6.854 bits
	5	7.177 bits
U(2) $\not\subset$ U(3)	6	7.521 bits
	7	7.162 bits
	8	7.162 bits
	9	7.200 bits
	10	6.756 bits
	11	6.856 bits
	12	7.232 bits
U(1) $\not\subset$ U(2)	13	7.690 bits
	14	7.091 bits
	15	6.930 bits
	16	7.907 bits
	17	8.082 bits
U(1) $\not\subset$ U(3)	18	8.316 bits
	19	8.237 bits
	20	7.083 bits
	21	6.935 bits

FIGURE 30

CHANGES IN STATES IN RADAR TARGET DETECTION

	22	7.092 bits
	23	7.208 bits
U(2) ⊄ U(6)	24	6.781 bits
	25	6.716 bits
	26	6.750 bits
	27	7.161 bits
U(2) ⊄ U(8)	28	7.104 bits
	29	7.052 bits
	30	6.878 bits
	31	7.299 bits
U(1) ⊄ U(4)	32	7.142 bits
	33	7.354 bits
	34	6.984 bits
	35	7.004 bits
U(4) ⊄ U(5)	36	7.230 bits
	37	7.746 bits
	38	7.895 bits
	39	7.674 bits

FIGURE 31

CHANGES IN STATES IN RADAR TARGET DETECTION (contd)

CHANGED STATES FROM MISSION	MISSION NUMBER	TOTAL ENTROPY FOR THE MISSION
	40	7.140 bits
	41	7.092 bits
U(4) ℰ U(6)	42	6.956 bits
	43	7.004 bits
	44	7.624 bits
	45	7.240 bits
U(3) ℰ U(8)	46	7.140 bits
	47	7.414 bits

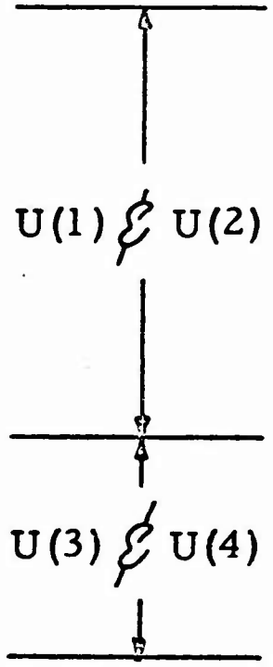
FIGURE 32

TABLE OF STATES IN INFRARED TARGET DETECTION

STATE		
	U(1)	CAMOUFLAGE
	U(2)	WEATHER
	U(3)	ALTITUDE
	U(4)	EMISSION AND REFLECTION FROM TARGET
	U(5)	TIME OF DAY
	U(6)	TIME OF APPEARANCE NEAR TARGET
	U(7)	CONDITION OF INFRARED DETECTOR
	U(8)	ELECTROMAGNETIC NOISE IN ATMOSPHERE

FIGURE 33

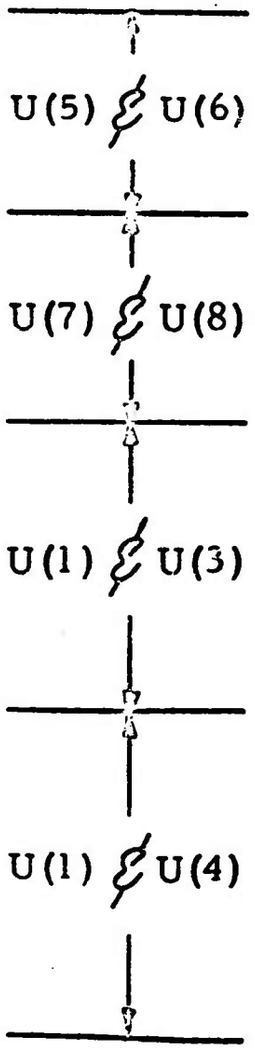
CHANGES IN STATES IN INFRARED TARGET DETECTION



MISSION NUMBER	TOTAL ENTROPY FOR THE MISSION
1	8.105 bits
2	9.325 bits
3	9.470 bits
4	9.482 bits
5	10.298 bits
6	9.637 bits
7	7.259 bits
8	7.689 bits
9	8.816 bits
10	7.586 bits
11	8.529 bits
12	9.401 bits
13	9.495 bits
14	9.557 bits
15	9.037 bits

FIGURE 34

CHANGES IN STATES IN INFRARED TARGET DETECTION



16	8.366 bits
17	8.145 bits
18	7.874 bits
19	7.977 bits
20	8.133 bits
21	8.962 bits
22	8.893 bits
23	9.934 bits
24	8.452 bits
25	9.996 bits
26	9.086 bits
27	8.465 bits
28	9.134 bits
29	9.193 bits
30	8.275 bits
31	8.253 bits
32	7.720 bits
33	9.325 bits
34	8.681 bits
35	8.979 bits
36	8.527 bits
37	9.446 bits
38	8.319 bits
39	8.319 bits
40	8.681 bits

FIGURE 35

CHANGES IN STATES IN INFRARED TARGET DETECTION (contd)

CHANGED STATES FROM MISSION	MISSION NUMBER	TOTAL ENTROPY FOR THE MISSION
	41	7.472 bits
	42	7.828 bits
	43	7.771 bits
U(1) ξ U(5)	44	7.455 bits
	45	7.357 bits
	46	7.625 bits
	47	7.175 bits
	48	6.952 bits
	49	8.964 bits
U(1) ξ U(6)	50	9.565 bits
	51	9.716 bits
	52	10.420 bits
	53	9.686 bits
	54	9.254 bits
U(4) ξ U(2)	55	8.270 bits
	56	8.725 bits
	57	9.283 bits
	58	8.805 bits
	59	8.276 bits
	60	9.475 bits
	61	8.584 bits
	62	8.656 bits

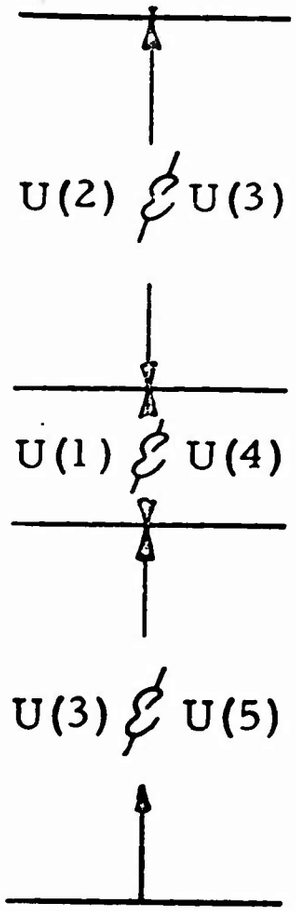
FIGURE 36

CHANGES IN STATES IN VISUAL TARGET DETECTION

CHANGED STATES FROM MISSION	MISSION NUMBER	TOTAL ENTROPY FOR THE MISSION
	1	5.279 bits
	2	5.320 bits
	3	5.347 bits
	4	5.364 bits
U(1) ≠ U(2)	5	5.452 bits
	6	5.676 bits
	7	5.656 bits
	8	5.860 bits
	9	5.255 bits
	10	5.142 bits
	11	6.002 bits
	12	6.232 bits
	13	5.323 bits
U(1) ≠ U(3)	14	5.027 bits
	15	5.100 bits
	16	4.732 bits
	17	5.006 bits
	18	4.880 bits
	19	5.543 bits
	20	5.922 bits

FIGURE 37

CHANGES IN STATES IN VISUAL TARGET DETECTION



21	4.706 bits
22	4.573 bits
23	4.445 bits
24	5.750 bits
25	6.089 bits
26	4.732 bits
27	5.438 bits
28	4.578 bits
29	5.840 bits
30	5.416 bits
31	5.076 bits
32	5.134 bits
33	4.835 bits
34	5.145 bits
35	5.664 bits
36	5.810 bits
37	5.404 bits
38	5.336 bits
39	5.875 bits

FIGURE 38

CHANGES IN STATES IN VISUAL TARGET DETECTION (contd)

CHANGED STATES FROM MISSION	MISSION NUMBER	TOTAL ENTROPY FOR THE MISSION
	40	5.936 bits
	41	6.378 bits
U(4) ⫰ U(6)	42	6.029 bits
	43	6.137 bits
	44	6.087 bits
	45	6.227 bits
	46	6.759 bits
U(5) ⫰ U(6)	47	7.096 bits
	48	6.041 bits
	49	5.798 bits
	50	6.379 bits
U(4) ⫰ U(6)	51	5.577 bits
	52	5.893 bits

FIGURE 39

REFERENCES

1. BISER, E.: Cybernetics and Statistical Concepts of Entropy and Correlation Relating to Systems Analysis and Synthesis (Partition of Discrete Information Spaces) ECOM Technical Report 2575, April 1965.

2. BISER, E.. Partitions of Discrete Information Spaces with Some Systems Applications, Transactions of the Tenth Conference of Army Mathematicians, ARO-D Number 65-2, June 1965.

3. BISER, E.: Cybernetic and Information Theoretic Concepts with Application to System Analysis Lecture Presented at MATHEMATICA, Princeton, NJ. Jan-May, 1968, Course: Modern Analytic Techniques for Decision-Making.

4. Effect of Subsystem Information Feedback on the Entropy of the Whole System. Parts I, II, III, IV Research & Development Technical Reports: ECOM 0586-1, 0586-2, 0586-3, 0586-4. Prepared by Division of Engineering Research, Michigan State University, East Lansing, Michigan, April 1968 under contract DAAB07-67-C-0586.

ACKNOWLEDGEMENTS

We are glad to express our indebtendess to Mr. Melvin M. Albee, Avionics Laboratory, for his aid and discussions on the relevance of these concepts to radar and infrared detection systems.

Our gratitude is cordially extended to Dr. Biser's former secretary, Mrs. Shirley Grissom for her aid and unstinted efforts in the preparation of this paper. We also wish to thank Miss Sue Diglio for coming to our aid in finishing this report.

TENSOR CONCEPTS APPLIED TO PROJECTIVE GEOMETRY

Shunsuke Takagi
U. S. Army Cold Regions Research and Engineering Laboratory
Hanover, New Hampshire

SUMMARY

A point, instead of a line segment, may be chosen as a vector in a Euclidean space, which, when the linear transformation of point vectors is introduced, becomes a projective space.

In addition to the usual operation of linear combination of vectors, a new product called a "tensor product" of vectors is introduced. The incidence product is then defined as a special tensor product expressing the incidence relationships among the geometric elements in the projective space.

1. Point as a vector

In the axiomatic theory of vector space (for example [1, 2]), a vector is an "undefined element". We may choose, therefore, a point, instead of a line segment, as a vector in a Euclidean space.

Let $\mathcal{X}$ be a point in an n-dimensional Euclidean space. Then we may write

$$\mathcal{X} = \sum_{i=1}^{n} \bar{x}^i \mathcal{A}_i + \mathcal{A}_{n+1}, \tag{1.1}$$

where $\mathcal{A}_{n+1}$ expresses the origin, $\mathcal{A}_1, \cdots, \mathcal{A}_n$ are the unit orthogonal vectors spanning the n-dimensional Euclidean space, and $\bar{x}^1, \cdots, \bar{x}^n$ are the coordinates of point $\mathcal{X}$ in the usual sense. To include points at infinity in our algebra, let

$$\bar{x}^1 : \cdots : \bar{x}^n : 1 = x^1 : \cdots : x^n : x^{n+1}. \tag{1.2}$$

This article has been reproduced photographically from the author's manuscript.

We then write (1.1) as

$$\mathcal{X} = x^i \mathcal{A}_i \quad , \tag{1.3}$$

where i is a summation index ranging over 1, ... , n+1. Only the ratio $x^1 : \cdots : x^{n+1}$ has a meaning in this notation, and the absolute magnitudes of $x^1 , \cdots , x^{n+1}$ are not important. Vector $\mathcal{A}_i$ (i=1, ... , n) may then be interpreted as the representation of a point at infinity with coordinates $\bar{x}^i = 1$ and $\bar{x}^j = 0$ for $j \neq i$.

When a ratio $x^1 : \cdots : x^{n+1}$ is given, a point $\mathcal{X}$ defined by (1.3) is unique. A sum of two given points, however, is not unique, because a set of coordinates may be multiplied by any number. The ambiguity can be removed by choosing another point called a unit point, as shown in the following. For simplicity, the procedure will first be shown in one dimension.

Theorem 1.1. Given three different points,

$$\mathcal{A} = a^1 \mathcal{A}_1 + a^2 \mathcal{A}_2 \quad , \tag{1.4}$$

$$\mathcal{B} = b^1 \mathcal{A}_1 + b^2 \mathcal{A}_2 \quad , \tag{1.5}$$

and

$$\mathcal{U} = u^1 \mathcal{A}_1 + u^2 \mathcal{A}_2 \quad , \tag{1.6}$$

in a one-dimensional Euclidean space, there exist vectors $\mathcal{P}_1$ and $\mathcal{P}_2$, such that $\mathcal{P}_1$ and $\mathcal{P}_2$ are scalar multiples of $\mathcal{A}$ and $\mathcal{B}$, respectively,

and their magnitudes are proportional only to the magnitude of u. They are expressed as

$$p_1 = \frac{\begin{vmatrix} u' & u^2 \\ \beta' & \beta^2 \end{vmatrix}}{\begin{vmatrix} a' & a^2 \\ \beta' & \beta^2 \end{vmatrix}} \alpha \tag{1.7}$$

and

$$p_2 = \frac{\begin{vmatrix} a' & a^2 \\ u' & u^2 \end{vmatrix}}{\begin{vmatrix} a' & a^2 \\ \beta' & \beta^2 \end{vmatrix}} \beta \, . \tag{1.8}$$

In terms of p_1 and p_2, u becomes

$$u = p_1 + p_2 \, . \tag{1.9}$$

Proof. Solving (1.4) and (1.5) for α_1 and α_2, we obtain

$$\alpha_1 = \frac{\begin{vmatrix} \alpha & a^2 \\ \beta & \beta^2 \end{vmatrix}}{\begin{vmatrix} a' & a^2 \\ \beta' & \beta^2 \end{vmatrix}} \tag{a}$$

and

$$\alpha_2 = \frac{\begin{vmatrix} a' & \alpha \\ \beta' & \beta \end{vmatrix}}{\begin{vmatrix} a' & a^2 \\ \beta' & \beta^2 \end{vmatrix}} \, . \tag{b}$$

The substitution of (a) and (b) into (1.6) transforms it to (1.9). The $\mathbb{P}_1$ and $\mathbb{P}_2$ thus obtained prove the theorem.

A set of <u>base points</u> on a one-dimensional Euclidean space is a set of points $\mathbb{P}_1$, $\mathbb{P}_2$ whose coefficients are in proportion to one and same number; i.e. the ratio of the components $p_1^1 : p_1^2 : p_2^1 : p_2^2$ of a set of vectors $\mathbb{P}_1$, $\mathbb{P}_2$, where $\mathbb{P}_1 = p_1^i \mathbb{e}_i$ and $\mathbb{P}_2 = p_2^i \mathbb{e}_i$, is constant. Point $\mathbb{U}$ is called a unit point.

The use of base points $\mathbb{P}_1$, $\mathbb{P}_2$ enables us to define y^1, y^2 in

$$\mathbb{x} = y^1 \mathbb{P}_1 + y^2 \mathbb{P}_2 \ . \tag{1.10}$$

The ratio $y^1 : y^2$ is called the <u>projective coordinates</u> of point $\mathbb{x}$ referred to $\mathbb{P}_1$, $\mathbb{P}_2$, $\mathbb{U}$, and denoted by

$$y^1 / y^2 = (\mathbb{x}, \mathbb{U}, \mathbb{P}_2 , \mathbb{P}_1) . \tag{1.11}$$

The ratio $y^1 : y^2$ is traditionally called the <u>cross ratio</u> or the <u>double ratio</u> of the four points $\mathbb{x}$, $\mathbb{U}$, $\mathbb{P}_2$, $\mathbb{P}_1$.

The one-dimensional theorem can readily be extended to n dimensions.

<u>Theorem 1.2.</u> Assume that n+2 points $\mathbb{a}_1 = a_1^i \mathbb{e}_i$, ... , $\mathbb{a}_{n+1} = a_{n+1}^i \mathbb{e}_i$, and $\mathbb{U} = u^i \mathbb{e}_i$ in an n-dimensional Euclidean space, where <u>i</u> is a summation index ranging over 1, ... , n+1, satisfy the condition that none of the determinants of the coefficients of an arbitrary set of n+1 points is zero. Then, there exist vectors $\mathbb{P}_1$, ... , $\mathbb{P}_{n+1}$ such that $\mathbb{P}_1$, ... , $\mathbb{P}_{n+1}$ are scalar multiples of $\mathbb{a}_1$, ... , $\mathbb{a}_{n+1}$, respectively, and the magnitudes of $\mathbb{P}_1$, ... , $\mathbb{P}_{n+1}$ are proportional only to the

magnitude of u. They are expressed as

$$\rho_1 = \frac{1}{\Delta} \begin{vmatrix} u' & \cdots & u^{n+1} \\ a_2' & \cdots & a_2^{n+1} \\ \cdots & & \cdots \\ a_{n+1}' & \cdots & a_{n+1}^{n+1} \end{vmatrix} a_1 , \tag{1.12}$$

$$\rho_{n+1} = \frac{1}{\Delta} \begin{vmatrix} a_1' & & a_1^{n+1} \\ \cdots & & \cdots \\ a_n' & \cdots & a_n^{n+1} \\ u' & \cdots & u^{n+1} \end{vmatrix} a_{n+1} , \tag{1.13}$$

where

$$\Delta = \begin{vmatrix} a_1' & \cdots & a_1^{n+1} \\ \cdots & & \cdots \\ a_{n+1}' & \cdots & a_{n+1}^{n+1} \end{vmatrix} . \tag{1.14}$$

In terms of $\rho_1, \ldots, \rho_{n+1}$,

$$u = \rho_1 + \cdots + \rho_{n+1} . \tag{1.15}$$

(End of Theorem 2)

A set of base points is a set of points $\rho_1, \ldots, \rho_{n+1}$ whose coordinates are in proportion to one and same number; i.e. the ratio of the

components $p_1' : \cdots : p_{n+1}^{n+1}$ of a set of vectors $\mathfrak{p}_1 , \cdots , \mathfrak{p}_{n+1}$, where $\mathfrak{p}_1 = p_1^i \mathfrak{a}_i , \cdots ,$ and $\mathfrak{p}_{n+1} = p_{n+1}^i \mathfrak{a}_i$, is constant. Point $\mathfrak{u}$ is called a unit point.

The use of base points $\mathfrak{p}_1 , \cdots , \mathfrak{p}_{n+1}$ enables us to define $y^1 , \cdots , y^{n+1}$ in

$$\mathfrak{x} = y^1 \mathfrak{p}_1 + \cdots + y^{n+1} \mathfrak{p}_{n+1} . \tag{1.16}$$

The ratio $y^1 : \cdots : y^{n+1}$ is called the projective coordinates of point $\mathfrak{x}$ referred to points $\mathfrak{p}_1 , \cdots , \mathfrak{p}_{n+1} , \mathfrak{u}$.

Thus a linear combination of a set of base points represents a definite point. Totality of the points that are linearly dependent on the base points form a projective space. A projective space is n dimensions, when the number of base points is n + 1. When a measure is given to a set of points in a projective space, its geometry becomes that of a Euclidean, or of a non-Euclidean, space.

The vectors $\mathfrak{a}_1 , \cdots , \mathfrak{a}_{n+1}$ are called projective Cartesian base vectors; and those components in which the last member x^{n+1} is reduced to 1 are called Euclidean components. The introduction of Euclidean components gives a Euclidean measure to the projective space.

2. Tensor Product

Juxtaposing vectors $\mathfrak{a}$ and $\mathfrak{B}$ in this order is to write $\mathfrak{a}$ and $\mathfrak{B}$ side by side forming $\mathfrak{a}\mathfrak{B}$, which was called a dyad by Gibbs and Wilson [3]. Note that dyads $\mathfrak{a}\mathfrak{B}$ and $\mathfrak{B}\mathfrak{a}$ are different, if $\mathfrak{a}$ and $\mathfrak{B}$ are different.

Juxtapositions of three, four, five, six, ... , r vectors are called

triads, tetrads, pentads, hexads, ... , r-ads, respectively. They are collectively called multiads [3].

Products defined by juxtaposition are called tensor products.

The axioms of tensor products are as follows:

In r-ad $a_1 \cdots a_r$, vectors a_1 , ... , a_r are called the first, ... , rth members, respectively.

Axiom 1. r-ad $a_1 \cdots a_r$ and s-ad $B_1 \cdots B_s$ are equal when, and only when, r=s and the first, second, ... , and rth members are equal.

Axiom 2. Tensor products are associative.

For example,

$$(A_r B_s) C_t = A_r (B_s C_t) ,$$

which, therefore, may be written $A_r B_s C_t$.

Axiom 3. Tensor products are distributive.

For example,

$$A_r (B_s + C_s) D_t = A_r B_s D_t + A_r C_s D_t .$$

Axiom 4. A multiple of one of the factors of a tensor product by a scalar is equal to the multiple of the tensor product by the scalar.

For example,

$$A_r \cdots (aB_s) \cdots C_t = a(A_r \cdots B_s \cdots D_t) ,$$

where a is a scalar.

Given n+1 independent vectors, the total number of independent r-ads is $(n+1)^r$. A linear combination of the r-ads is called an n-dimensional rth-order tensor. The totality of n-dimensional rth-order tensors forms a vector space of $(n+1)^r$ dimensions.

3. Wedge Product

The permutation symbol $\pi^{p_1 \cdots p_n}_{a_1 \cdots a_n}$ represents 1 , -1 , or 0 , when the permutation $p_1 \cdots p_n$ is an even permutation, an odd permutation, or not a permutation derived from $a_1 \cdots a_n$, respectively. When one of the permutations $a_1 \cdots a_n$ and $p_1 \cdots p_n$ in $\pi^{p_1 \cdots p_n}_{a_1 \cdots a_n}$ is 123 ... n, we usually omit it and simply write $\pi^{p_1 \cdots p_n}$ or $\pi_{a_1 \cdots a_n}$, respectively.

The following proposition, although not used explicity in this paper, is noted for the sake of potential usefulness.

Proposition 3.1

$$\pi^{j_1 \cdots j_n}_{i_1 \cdots i_n} = \begin{vmatrix} \delta_{i_1}^{j_1} & \delta_{i_1}^{j_2} & \cdots & \delta_{i_1}^{j_n} \\ \cdots & \cdots & \cdots & \cdots \\ \delta_{i_n}^{j_1} & \delta_{i_n}^{j_2} & \cdots & \delta_{i_n}^{j_n} \end{vmatrix} . \qquad (3.1)$$

Proof An exchange of indexes in one side of (3.1) causes the same sign change on the other side, hence proving the proposition.

The wedge product (sometimes called the Grassmann product or the exterior product) of vectors $\alpha_1 , \cdots , \alpha_n$, denoted by

$$\alpha_1 \wedge \cdots \wedge \alpha_n ,$$

is defined as a linear combination of the $n!$ tensor products using permutation symbols as the coefficients:

$$\alpha_1 \wedge \cdots \wedge \alpha_n = \pi^{p_1 \cdots p_n} \alpha_{p_1} \cdots \alpha_{p_n} , \qquad (3.2)$$

where $p_1, \ldots, p_n$ are summation indexes ranging over 1, ... , n. The order of vectors $\alpha_1, \ldots, \alpha_n$ in $\alpha_1 \wedge \cdots \wedge \alpha_n$ is said to define the orientation of $\alpha_1 \wedge \cdots \wedge \alpha_n$.

Wedge products of two, three, ... , and n vectors are called bivectors, trivectors, ... , and n-vectors, respectively. They are collectively called multivectors.

The right-hand side of (3.2) may be expressed as an array of n columns, called a column tensor determinant:

$$\alpha_1 \wedge \cdots \wedge \alpha_n = \begin{vmatrix} \alpha_1 & \vdots & \alpha_1 \\ \vdots & \vdots & \vdots \\ \alpha_n & \vdots & \alpha_n \end{vmatrix}, \tag{3.3}$$

or as an array of n rows, called a row tensor determinant:

$$\alpha_1 \wedge \cdots \wedge \alpha_n = \begin{vmatrix} \alpha_1 & \cdots & \alpha_n \\ \cdots & \cdots & \cdots \\ \alpha_1 & \cdots & \alpha_n \end{vmatrix}. \tag{3.4}$$

The tensor determinant (3.3), or (3.4), is reduced to (3.2) by applying the convention that the first, second, ... , nth number of the n-ads are taken from the first, second, ... , nth column, or row, respectively.

4. Geometric meaning of the wedge product

The linear space passing through points $\alpha_1, \ldots, \alpha_r$ is defined as a scalar multiple of $\alpha_1 \wedge \cdots \wedge \alpha_r$.

Theorem 4.1. A linear space passing through r points that are linearly dependent on points $\alpha_1, \ldots, \alpha_r$ is the linear space $\alpha_1 \wedge \cdots \wedge \alpha_r$.

Proof. Let

$$y_i = y_i^j \alpha_j .$$

Then

$$y_1 \wedge \cdots \wedge y_r = y_1^{j_1} \cdots y_r^{j_r} \alpha_{j_1} \wedge \cdots \wedge \alpha_{j_r}$$

$$= \pi_{j_1 \cdots j_r} y_1^{j_1} \cdots y_r^{j_r} \alpha_1 \wedge \cdots \wedge \alpha_r$$

$$= \begin{vmatrix} y_1^1 & \cdots & y_1^r \\ \cdots & \cdots & \cdots \\ y_r^1 & \cdots & y_r^r \end{vmatrix} \alpha_1 \wedge \cdots \wedge \alpha_r .$$

The theorem is thus proved.

Let us assume that a set of projective Cartesian base vectors can be found in the projective space spanned by points $\alpha_1, \ldots, \alpha_r$; then we can have the Euclidean interpretation of multivector $\alpha_1 \wedge \cdots \wedge \alpha_r$.

Corollary 4.1. Given the Euclidean measure, the multivector $\alpha_1 \wedge \cdots \wedge \alpha_{r+1}$ is an r-dimensional oriented volume of the r-dimensional parallelepiped spanned by the ordered point set $\alpha_1, \ldots, \alpha_{r+1}$.

Proof. Express $\alpha_1, \ldots, \alpha_{r+1}$ with their Euclidean components as

$$\alpha_i = \sum_{p=1}^{r} x_i^p \mathscr{A}_p + \mathscr{A}_{r+1} .$$

Then

$$\alpha_1 \wedge \cdots \wedge \alpha_{r+1} = \begin{vmatrix} x_1^1 & \cdots & x_1^r & 1 \\ \cdots & \cdots & \cdots & \cdots \\ x_{r+1}^1 & \cdots & x_{r+1}^r & 1 \end{vmatrix} \mathscr{A}_1 \wedge \cdots \wedge \mathscr{A}_{r+1} . \qquad (a)$$

The determinant on the right-hand side of (a) means the r-dimensional oriented volume of the r-dimensional paralleleped spanned by the ordered point set $\alpha_1, \ldots, \alpha_{r+1}$. The interpretation stated in the corollary therefore may be applied to the multivectors. The corollary is thus proved.

The bivector $\alpha \wedge y$ in a Euclidean space is a "free vector" that can move freely on the line spanned by points α and y. Similarly a multivector in a Euclidean space can move freely in the space in which the multivector is defined.

5. Incidence product

The wedge product will be re-defined so that it can represent the incidence relationships.

If all the geometric elements of interest are contained in the space $\mathscr{E}$, and if a space that embeds $\mathscr{E}$ need not be considered, then

it is called the universe.

Let the universe be n dimensions. Wedge product of an r-ad,

$$\mathbb{R} = \alpha_1 \wedge \cdots\cdots \wedge \alpha_r , \tag{5.1}$$

and an s-ad,

$$\mathbb{S} = \alpha_{r+1} \wedge \cdots\cdots \wedge \alpha_{r+s} , \tag{5.2}$$

is defined as

$$\mathbb{R} \wedge \mathbb{S} = \alpha_1 \wedge \cdots \wedge \alpha_r \wedge \alpha_{r+1} \wedge \cdots \wedge \alpha_{r+s} . \tag{5.3}$$

Eq. (5.3) may be written as

$$\begin{aligned} &\pi^{i_1 \cdots i_r}_{1 \cdots r} \alpha_{i_1} \cdots \alpha_{i_r} \wedge \pi^{i_{r+1} \cdots i_{r+s}}_{(r+1) \cdots (r+s)} \alpha_{i_{r+1}} \cdots \alpha_{i_{r+s}} \\ &= \pi^{i_1 \cdots i_r i_{r+1} \cdots i_{r+s}} \alpha_{i_1} \cdots \alpha_{i_{r+s}} . \end{aligned} \tag{5.4}$$

A wedge product is said to be saturated, if it is comprised of more than n+1 n-dimensional vectors including n+1 linearly independent vectors.

Rule (1) of saturation. One cannot interchange the position of the same vector appearing more than once in a saturated multivector. One can interchange vectors, whether the same or different, in an unsaturated multivector, and different vectors in a saturated multivector, changing the sign of the multivector at each such interchange.

Rule (2) of saturation. A multivector $\mathcal{R}$ with $\mathcal{E}$ wedged from the right is equal to $\mathcal{R}$; i.e.

$$\mathcal{R} \wedge \mathcal{E} = \mathcal{R}. \tag{5.5}$$

The re-defined wedge product is called the incidence product.

Example 1. The intersection $\mathcal{Z}$ of coplanar lines ξ and η is given as

$$\mathcal{Z} = \xi \wedge \eta ,$$

when the plane is in the universe.

Proof. Let

$$\xi = y \wedge z \tag{a}$$

and

$$\eta = z \wedge x . \tag{b}$$

Then

$$\xi \wedge \eta = - z \wedge (y \wedge z \wedge x). \tag{c}$$

Because $y \wedge z \wedge x$ represents the universe, (c) proves the example.

The example can readily be extended to intersections in a space of higher dimensions.

6. Dual Base Vectors

For simplicity, the universe in this section is three-dimensional.

The base points $\mathbb{P}_1$, $\mathbb{P}_2$, $\mathbb{P}_3$, $\mathbb{P}_4$ span the universe:

$$\mathbb{P}_1 \wedge \mathbb{P}_2 \wedge \mathbb{P}_3 \wedge \mathbb{P}_4 = \mathbb{E} . \tag{6.1}$$

Superindexed vectors will represent planes, while subindexed vectors will continue to describe points.

Base planes $\mathbb{P}^i$ (i=1, 2, 3, 4) are defined as

$$\mathbb{P}^i = \pi^{ijkh} \mathbb{P}_j \mathbb{P}_k \mathbb{P}_h \tag{6.2}$$

$$= \frac{1}{3!} \pi^{ijkh} \mathbb{P}_j \wedge \mathbb{P}_k \wedge \mathbb{P}_h . \tag{6.3}$$

Vectors $\mathbb{P}_i$ and $\mathbb{P}^i$ will be called subindexed and superindexed base vectors, respectively.

Proposition 6.1.

$$\mathbb{P}_i \wedge \mathbb{P}^j = \delta_i^j \mathbb{E} \tag{6.4}$$

$$\mathbb{P}^j \wedge \mathbb{P}_i = \delta_i^j \mathbb{E} \tag{6.5}$$

Proof. The substitution of (6.3) into $\mathbb{P}_i \wedge \mathbb{P}^j$ yields

$$\mathbb{P}_i \wedge \mathbb{P}^j = \mathbb{P}_i \wedge \frac{1}{3!} \pi^{jabc} \mathbb{P}_a \wedge \mathbb{P}_b \wedge \mathbb{P}_c ,$$

which becomes

$$\mathbb{P}_i \wedge \mathbb{P}^j = \frac{1}{3!}\pi^{jabc}\pi_{iabc}\mathbb{E}\,, \qquad \text{(a)}$$

where (6.1) is used. Eq. (a) reduces to (6.1) by use of the formula

$$\pi^{jabc}\pi_{iabc} = 3!\,\delta_i{}^j. \qquad (6.6)$$

Eq. (6.5) can be found similarly. The proposition is thus proved.

Bivectors $\mathbb{P}_i \wedge \mathbb{P}_j$, $\mathbb{P}^i \wedge \mathbb{P}^j$ are bases of straight lines. They are related as follows:

Proposition 6.2.

$$\mathbb{P}^i \wedge \mathbb{P}^j = \pi^{ijab}\mathbb{P}_a \wedge \mathbb{P}_b \qquad (6.7)$$

$$\mathbb{P}_i \wedge \mathbb{P}_j = \pi_{ijab}\mathbb{P}^a \wedge \mathbb{P}^b \qquad (6.8)$$

Proof. The use of (6.3) yields

$$\mathbb{P}^i \wedge \mathbb{P}^j = \frac{1}{3!}\pi^{iabc}\mathbb{P}_a \wedge \mathbb{P}_b \wedge \mathbb{P}_c \wedge \mathbb{P}^j. \qquad \text{(a)}$$

By (6.4), $\mathbb{p}_c \wedge \mathbb{p}^j$ in the right-hand side is equal to $\delta_c^j \mathbb{E}$. Applying the rule of saturation, (a) becomes (6.6). Eq. (6.7) can be proved similarly.

Proposition 6.3.

$$\mathbb{p}_i = \pi_{ijkh} \mathbb{p}^j \mathbb{p}^k \mathbb{p}^h \tag{6.9}$$

$$= \frac{1}{3!} \pi_{ijkh} \mathbb{p}^j \wedge \mathbb{p}^k \wedge \mathbb{p}^h \tag{6.10}$$

Proof. The use of (6.6) yields

$$\mathbb{p}^j \wedge \mathbb{p}^k \wedge \mathbb{p}^h = \pi^{jkab} \mathbb{p}_a \wedge \mathbb{p}_b \wedge \mathbb{p}^h \tag{a}$$

The use of (6.4) and the rule of saturation changes (a) to

$$\mathbb{p}^j \wedge \mathbb{p}^k \wedge \mathbb{p}^h = \pi^{jkah} \mathbb{p}_a . \tag{b}$$

By multiplying (b) by π_{ijkh} (j, k, and h are summation indexes) and using the formula (6.6) one obtains (6.9). The proposition is thus proved.

Proposition 6.4.

$$\mathbb{p}^1 \wedge \mathbb{p}^2 \wedge \mathbb{p}^3 \wedge \mathbb{p}^4 = \mathbb{E} \tag{6.11}$$

Proof. The substitution of (6.10) into $\mathbb{p}_i \wedge \mathbb{p}^j$ yields

$$\mathbb{p}_i \wedge \mathbb{p}^j = \frac{1}{3!} \pi_{iabc} \mathbb{p}^a \wedge \mathbb{p}^b \wedge \mathbb{p}^c \wedge \mathbb{p}^j$$

which becomes

$$\mathbb{P}_i \wedge \mathbb{P}^j = -\delta_i^j \mathbb{P}^1 \wedge \mathbb{P}^2 \wedge \mathbb{P}^3 \wedge \mathbb{P}^4, \qquad \text{(a)}$$

where the formula (6.6) is used. Comparing (a) with (6.4) proves the proposition. Comparison of (a) with (6.4) yields (6.10). The proposition is thus proved.

Proposition 6.5.

$$\mathbb{E} = \mathbb{P}_i \mathbb{P}^i = \mathbb{P}^i \mathbb{P}_i \qquad (6.12)$$

Proof. The use of (6.2) yields

$$\mathbb{P}_i \mathbb{P}^i = \pi^{ijkh} \mathbb{P}_i \mathbb{P}_j \mathbb{P}_k \mathbb{P}_h,$$

which becomes

$$\mathbb{P}_i \mathbb{P}^i = \mathbb{E}$$

by use of (6.1). The relation

$$\mathbb{P}^i \mathbb{P}_i = \mathbb{E}$$

can be proved similarly. The proposition is thus proved.

Proposition 6.5 shows that the unit tensor $\mathbb{I}$, used in the Euclidean tensor analysis as the unit for scalar products [6,7], is equal to $\mathbb{E}$ in the projective tensor analysis.

It is now seen that the tensor analysis developed by Takagi [4,5,6,7] following the treatment of Gibbs and Wilson [3] can be extended to projective geometry.

REFERENCES

[1] Halmos, P. R. Finite-Dimensional Vector Analysis. D. Van Nostrand Company, Inc., 1958.

[2] Nickerson, H. K., Spencer, D. C., Steenrod, N. E. Advanced Calculus, D. Van Nostrand Company, Inc., 1959.

[3] Gibbs, J. W. and Wilson E. S. Vector Analysis, 1901; Dover Publications (republication, 1960).

[4] Takagi, S. Tensor Analysis with Tensor Bases. Transactions of the Eleventh Conference of Army Mathematicians, (1965), 131-168.

[5] Takagi, S. Canonical forms of general second-order tensors. Transactions of the Twelfth Conference of Army Mathematicians, (1966) 349-378.

[6] Takagi, S. Unified treatment of vectors and tensors in n-dimensional Euclidean space. Research Report 207, Cold Regions Research & Engineering Laboratory, Hanover, N. H., (1968)

[7] Takagi, S. The Gibbs-Einstein tensor analysis with application to continuum mechanics and canonical forms of general second-order tensors. Recent Advances in Engineering Science (1968) 225-284. Gordon and Breach Science Publishers Ltd., London; Research Report 221, Cold Regions Research & Engineering Laboratory, Hanover, N. H., (1968)

A GENERAL THEORY OF STRESSES AND DISPLACEMENTS IN ELASTIC AND VISCOELASTIC LAYERED SYSTEMS

Y. T. Chou
U. S. Army Engineer Waterways Experiment Station
Vicksburg, Mississippi

ABSTRACT. A multilayered, linear, elastic, and viscoelastic half space under stationary and moving axisymmetric loads is analyzed. Solutions are presented for normal stress, radial stress, tangential stress, shear stress, vertical deflection, and radial displacement at any point within the half space. The elastic solutions are obtained by Love's stress function and the Fourier-Hankel transform; the viscoelastic solutions, based on the elastic-viscoelastic correspondence principle, are obtained by applying the Laplace transformation to replace the time variable with a transformed variable. The time-dependent problem is then changed to an associated elastic problem. Inversion of the solution of the associated elastic problem into the real time variable solves the viscoelastic problem. By neglecting the inertia effect, the static viscoelastic solution has been extended to the moving load case.

Numerical examples are given to illustrate the response of the materials to a normal point load. Such an analysis is believed to be an essential step in the development of a rational method for designing airport and highway flexible pavements.

INTRODUCTION. A rational design method for airport and highway flexible pavements requires knowledge of the stresses and displacements within the layered systems. Once these quantities are numerically determined, other design criteria, such as fatigue and failure considerations, can then be taken into account.

This paper presents an analysis of linear, elastic and viscoelastic, multilayered systems under both stationary and moving axisymmetric loads. These loads were comprised of normal point load, uniform and parabolic normal loads, and tangential load, which are commonly found on pavements. Expressions for stresses and displacements under stationary loads at points within the systems were developed by Love's stress function[1] and the Fourier-Hankel transform. Expressions were developed for viscoelastic cases under stationary and moving loads, based on the elastic-viscoelastic correspondence principle.[2] This was accomplished by applying the Laplace transform to replace the time variable with a transformed variable p. The time-dependent problem was thus changed to an associated elastic problem. Inversion of the solution for the associated elastic problem into the real time variable solved the viscoelastic problem. Inertial effects were not considered in the derivation of equations for moving loads.

In deriving equations, a "rough" interface was assumed; i.e., the displacement in the horizontal direction and the shearing stress were continuous across the interface. These conditions were felt to be better descriptions of the actual conditions of flexible pavement structures.

STATIC ELASTIC SOLUTION. The elastic solution for two-and three-layered systems was developed by Burmister[3] and later extended to multilayer systems by Mehta and Veletsos.[4] An n-layer elastic system, subjected to an axisymmetrically distributed load, is shown in Figure 1. Cylindrical coordinates are used to facilitate the solution of the problem, since axial symmetry exists. The general method of analysis involves the determination of a stress function that satisfied the governing differential equation

$$\nabla^4 \phi = 0 \tag{1}$$

in which

$$\nabla^2 = \frac{\partial^2}{\partial r^2} + \frac{1}{r}\,\frac{\partial}{\partial r} + \frac{\partial^2}{\partial z^2}$$

for each of the layers. The stresses and displacements for the various layers are expressed in terms of the stress function ϕ.[1]

Consider a stress function of the form:

$$\phi_j = G_j(z)\, J_o(mr)$$

where

$G_j(z)$ = a function of depth z only,

$J_o(mr)$ = the Bessel function of the first kind and order of 0

m = a parameter

Subscript j = the quantities corresponding to the j^{th} layer

Substitutions can easily verify that

$$\phi_j = \frac{H^3 J_o(m\rho)}{m^2} \left\{ A_j \exp[-m(\lambda_j - \lambda)] - B_j \exp[-m(\lambda - \lambda_{j-1})] \right. \tag{2}$$
$$\left. + C_j m\lambda \exp[-m(\lambda_j - \lambda)] - D_j m\lambda \exp[-m(\lambda - \lambda_{j-1})] \right\}$$

is a stress function for the j^{th} layer that satisfies equation 1, where

A, B, C, D = integration constants

ρ = r/H

λ = z/H

H = the distance from the surface to the upper boundary of the lowest layer

The stresses and displacements determined from the stress functions are:

$$(\sigma_z^{**})_j = -m\, J_o(m\rho)\, \{[A_j - C_j(1-2\nu_j - m\lambda)]\, \exp[-m(\lambda_j - \lambda)] + [B_j + D_j(1-2\nu_j + m\lambda)]\, \exp[-m(\lambda - \lambda_{j-1})]\} \quad (3a)$$

$$(\sigma_r^{**})_j = \left[mJ_o(m\rho) - \frac{J_1(m\rho)}{\rho}\right] \{[A_j + C_j(1+m\lambda)]\, \exp[-m(\lambda_j - \lambda)] + [B_j - D_j(1-m\lambda)]\, \exp[-m(\lambda - \lambda_{j-1})\} + 2\nu_j m J_o(m\rho) \{C_j \exp[-m(\lambda_j - \lambda)] - D_j \exp[-m(\lambda - \lambda_{j-1})\} \quad (3b)$$

$$(\sigma_\theta^{**})_j = \frac{J_1(m\rho)}{\rho} \{[A_j + C_j(1+m\lambda)]\, \exp[-m\lambda_j - \lambda)] + [B_j - D_j(1-m\lambda)]\, \exp[-m(\lambda - \lambda_{j-1})]\} + 2\nu_j m J_o(m\rho) \{C_j \exp[-m(\lambda_j - \lambda)] - D_j \exp[-m(\lambda - \lambda_{j-1})]\} \quad (3c)$$

$$(\tau_{rz}^{**})_j = mJ_1(m\rho) \cdot \{[A_j + C_j(2\nu_j + m\lambda)]\, \exp[-m(\lambda_j - \lambda)] - [B_j - D_j(2\nu_j - m\lambda)]\, \exp[-m(\lambda - \lambda_{j-1})]\} \quad (3d)$$

$$(w^{**})_j = \frac{1+\nu_j}{E_j} J_o(m\rho) \cdot \{[A_j - C_j(2-4\nu_j-m\lambda)] \exp[-m(\lambda_j-\lambda)] - [B_j + D_j(2-4\nu_j+m\lambda)] \exp[-m(\lambda-\lambda_{j-1})]\} \quad (3e)$$

$$(u^{**})_j = \frac{1+\nu_j}{E_j} J_1(m\rho) \{[A_j + C_j(1+m\lambda)] \exp[-m(\lambda_j-\lambda)] + [B_j - D_j(1-m\lambda)] \exp[-m(\lambda-\lambda_{j-1})]\} \quad (3f)$$

where

σ_z, σ_r, and σ_θ = stresses in z, r, and θ directions, respectively.

w and u = vertical and horizontal displacements, respectively.

J_1 = Bessel function of the first kind and order of 1.

The double asterisks indicate that these quantities are not the actual stresses and displacements due to the actual load, but are those due to a vertical load, $-mJ_o(m\rho)$, and a horizontal shearing force, $mJ_1(m\rho)$. From equations 3a and 3d, at the upper surface ($j = 1$, $\lambda = 0$), $\sigma_z = -mJ_o(m\rho)$ and $\tau_{rz} = mJ_1(m\rho)$, when the respective expression in the brackets is taken as unity.

The boundary and interface conditions are:

a. <u>At the upper surface</u>, $j = 1$ and $\lambda = 0$

$$(\sigma_z^{**})_1 = -mJ_o(m\rho) \quad (4a)$$

$$(\tau_{rz}^{**})_1 = mJ_1(m\rho) \quad (4b)$$

If the influence of normal loads is considered alone, then $(\tau_{rz}^{**})_1 = 0$ in equation 4b; if only the horizontal force exists, then $(\sigma_z^{**})_1 = 0$ in equation 4a. In the following discussion, the effects of normal and horizontal loads are considered separately.

b. <u>At the interface</u>,

$$(\sigma_z^{**})_j = (\sigma_z^{**})_{j+1} \quad (5a)$$

$$(\tau_{rz}^{**})_j = (\tau_{rz}^{**})_{j+1} \quad (5b)$$

$$(w^{**})_j = (w^{**})_{j+1} \tag{5c}$$

$$(u^{**})_j = (u^{**})_{j+1} \tag{5d}$$

Since the stresses and displacements must vanish as λ approaches infinity, it can be concluded from equation 2 that for the lowermost layer ($i = n$), $A_n = C_n = 0$.

The remaining 4n-2 integration constants can be evaluated from the 4n-2 simultaneous equations obtained by satisfying equations 4 and 5 for each of the n-1 interfaces. After the integration constants are determined, they can be substituted into equation 3 to get the stresses and displacements due to loadings $-mJ_o(m\rho)$ or $mJ_1(m\rho)$.

To find the stresses and displacements due to various types of surface loading, the Hankel transform is used. For a normal load of constant intensity q distributed over a circular area of radius a:

$$\bar{f}(m) = \int_0^{\alpha} q\rho \; J_o(m\rho)d\rho = \frac{q\alpha}{m} \; J_1(m\alpha)$$

where

$$\alpha = \frac{a}{H}$$

The Hankel inversion of $\bar{f}(m)$ is

$$q(\rho) = \int_0^{\infty} \bar{f}(m) \; mJ_o(m\rho)dm = q\alpha \int_0^{\infty} J_o(m\rho) \; J_1(m\alpha)dm$$

If Y* is the stress or displacement in equation 3 due to the vertical loading $-mJ_o(m\rho)$ and Y is that due to the load -q, then:

$$Y = q\alpha \int_0^{\infty} \frac{Y^*}{m} \; J_1(m\alpha)dm \tag{6}$$

For a concentrated normal load $-q_o$:

$$\bar{f}(m) = \lim_{\alpha \to 0} \left[\frac{-q\alpha}{m} J_1(m\alpha) \right] = \frac{-q_o}{2\pi H^2}$$

$$q_o(\rho) = \frac{-q_o}{2\pi H^2} \int_0^\infty m J_o(m\rho)\, dm$$

$$Y = \frac{q_o}{2\pi H^2} \int_0^\infty Y^*\, dm \qquad (7)$$

For a parabolically distributed normal load over a circular area of radius a with $q(r) = -q\left(1 - \frac{r^2}{a^2}\right)$:

$$\bar{f}(m) = \int_0^\alpha -\frac{q}{a^2} (a^2 - r^2)\rho \; J_o(m\rho)\, d\rho$$

$$= \frac{-2q}{m^2} \left[\frac{2}{\alpha m} J_1(m\alpha) - J_o(m\alpha) \right]$$

$$q(\rho) = \int_0^\infty \bar{f}(m) m J_o(m\rho)\, dm$$

$$= -2q \int_0^\infty \frac{1}{m} \left[\frac{2}{\alpha m} J_1(m\alpha) - J_o(m\alpha) \right] J_o(m\rho)\, dm$$

$$Y = 2q \int_0^\infty \frac{1}{m^2} \left[\frac{2}{\alpha m} J_1(m\alpha) - J_o(m\alpha) \right] Y^*\, dm \qquad (8)$$

For a horizontal shear force of constant intensity T distributed over a circular area of radius a:

$$\bar{f}(m) = \int_0^\alpha T \rho \, J_1'(m\rho)\, d\rho$$

For a given value of m, $\bar{f}(m)$ can be found by numerical integration.

$$T(\rho) = \int_0^\infty \bar{f}(m)\ mJ_1(m\rho)dm$$

$$Y = \int_0^\infty \bar{f}(m)\ Y^*\ dm \qquad (9)$$

Similarly, the same procedure may be employed for other types of axisymmetric loads.

The analysis of elastic layered systems can, therefore, be summarized in the following steps: (a) assign successifve values of m to any one of equations 6 to 9, depending upon the surface loading conditions, starting from zero to a rather large positive number until Y converges; (b) for each value of m, establish the simultaneious equations from equations 3, 4, and 5, and solve for the constants of integration; and, (c) substitute the constants into equation 3 to obtain Y* and determine Y from one of equations 6 to 9 by numerical integration.

To illustrate - the vertical displacement w_o at the surface, the vertical displacement w_B, and the vertical stress σ_B at a point $2h_1$ below the surface for an incompressible, two-layer elastic system due to a vertical load $-mJ_o(m\rho)$ are

$$W_o^{**} = \frac{1}{2G_1}\ J_o(m\rho)\ V_o \qquad (10a)$$

$$W_B^{**} = \frac{1}{2G_2}\ J_o(m\rho)\ V_B \qquad (10b)$$

$$\sigma_B^{**} = -J_o(m\rho)\ V_\sigma \qquad (10c)$$

where

$$V_o = \frac{1+4Nm\ \exp(-2m) - N^2\ \exp(-4m)}{1-2N(1+2m^2)\ \exp(-2m) + N^2\ \exp(-4m)}$$

$$V_B = (1-N)\frac{(1+2m)\exp(-2m) - N(1-2m^2)\exp(-4m)}{1-2N(1+2m^2)\exp(-2m) + N^2\exp(-4m)}$$

$$V_\sigma = mV_B$$

$$N = \frac{G_1 - G_2}{G_1 + G_2}$$

The corresponding expressions w_o, w_B, and σ_B due to a normal point load $-q_o$ can be obtained from equation 7:

$$w_o = \frac{q_o}{4\pi h_1^2 G_1}\int_0^\infty J_o(m\rho)\, V_o\, dm \qquad (11a)$$

$$w_B = \frac{q_o}{4\pi h_1^2 G_2}\int_0^\infty J_o(m\rho)\, V_B\, dm \qquad (11b)$$

$$\sigma_B = -\frac{q_o}{2\pi h_1^2}\int_0^\infty J_o(m\rho)\, V\, dm \qquad (11c)$$

where V_o, V_B, and V_σ are the same as in equation 10.

The expressions for stresses and displacements at any point in the layered system induced by other axisymmetric normal loads have the same form as shown in equation 11. For example, equation 11 for a uniform circular load $-q$ can be written:

$$w_o = \frac{q\alpha}{2G_1}\int_0^\infty \frac{J_o(m\rho)}{m} J_1(m\alpha)\, V_o\, dm \qquad (12a)$$

$$w_B = \frac{q\alpha}{2G_2}\int_0^\infty \frac{J_o(m\rho)}{m} J_1(m\alpha)\, V_B\, dm \qquad (12b)$$

$$\sigma_B = -q\alpha\int_0^\infty \frac{J_o(m\rho)}{m} J_1(m\alpha)\, V_\sigma dm \qquad (12c)$$

where V_o, V_B, and V_σ are the same as in equation 10.

Note that singularity exists in surface displacement w_o under a normal point load, as shown in equation 11a. The value of the Bessel function becomes 1 when the value of ρ is zero, and the value of V_o converges to 1 when m becomes larger than 10.

When the number of layers is increased, the equations for stresses and displacements have the same form as equation 11; but the terms V_o, V_B, V_σ, which contain expressions for material properties of the components of each layer, become more complicated.

STATIC VISCOELASTIC SOLUTIONS. The viscoelastic stress-strain relations used throughout this paper are based on the principle of elastic-viscoelastic correspondence developed by Lee[2] and are defined by linear differential operators with respect to time. For a linear, homogeneous, and isotropic material, the stress-strain relation can be represented by two pairs of operators, one of which relates the deviatoric stress to the deviatoric strain, the other the mean normal dilatational stress to the mean normal strain. Thus:

$$P'S_{ij} = 2Q'e_{ij} \tag{13a}$$

$$P''\sigma_{ii} = 3Q''\epsilon_{ii} \tag{13b}$$

where

S_{ij} = deviatoric stress = $\sigma_{ij} - \frac{1}{3}\sigma_{KK}\delta_{ij}$

e_{ij} = deviatoric stress = $\epsilon_{ij} - \frac{1}{3}\epsilon_{KK}\delta_{ij}$

σ_{ij} = stress tensors

ϵ_{ij} = strain tensors

δ_{ij} = Kronecker delta; i.e., $\delta_{ij} = 1$, $i = j$, $\delta_{ij} = 0$, $i \neq j$

The analogous equations for the elastic solid are:

$$S_{ij} = 2Ge_{ij} \tag{14a}$$

$$\sigma_{ii} = 3K\epsilon_{ii} \tag{14b}$$

where G is the shear modulus and K the bulk modulus.

Compare equations 13 and 14

$$G = \frac{Q'}{P'} \tag{15a}$$

$$K = \frac{Q''}{P''} \tag{15b}$$

where Q', P', Q", and P" are linear operators of the form $\sum_{r=0}^{n} a_r \frac{\partial^r}{\partial t^r}$. The coefficients a_r and the integer n are, in general, different for each operator. Linearity requires that a_r be independent of stress and strain, and the assumption of homogenity and isotropy eliminates the dependence of a_r on location and orientation of stress within the system. The Young's modulus E and the Poisson's ratio ν are related to G and K by the formulas

$$E = \frac{9KG}{3K + G} \tag{16a}$$

$$\nu = \frac{3K - 2G}{6K + 2G} \tag{16b}$$

In elastic problems, K, G, E, and ν are time-independent constants; but in viscoelastic problems, they are not constants, but are linear differential operators, as shown in equation 15.

To eliminate the time variable t, the Laplace transform with respect to t can be applied to equation 13. The transforms of stresses and strains are denoted by an asterisk on the corresponding function. If the system is initially undisturbed; i.e., with initial stress and strain conditions equal to zero, and the operator in $\partial/\partial t$ merely becomes the same function of the transformed variable p,[2] equation 13 becomes:

$$P'(p)S_{ij}^{*} = 2Q'(p)\, e_{ij}^{*} \tag{17a}$$

$$P''(p)\sigma_{ii}^{*} = 3Q''(p)\epsilon_{ii}^{*} \tag{17b}$$

where P'(p), Q'(p), P"(p), and Q"(p) are polynomials of the form $\sum_{r=0}^{n} a_r p^r$.

If the Laplace transforms of the stresses and strains are considered, and if G* and K* are defined as follows:

$$G^* = \frac{S_{ij}^*}{2e_{ij}^*} = \frac{Q'(p)}{P'(p)} \tag{18a}$$

$$K^* = \frac{\sigma_{ii}^*}{3\epsilon_{ii}^*} = \frac{Q''(p)}{P''(p)} \tag{18b}$$

then by replacing G, K, and load q_o (or q, T) in the elastic equations for stresses and displacements with G*, K*, and q_o^*, respectively, the equations for the Laplace transforms of stresses and displacements are obtained. These equations are functions of the transformed variable, p, and their inversions give the stresses and displacements in terms of the time variable, t.

The corresponding equations in the transformed domain for equation 11 are:

$$w_o^* = \frac{1}{4\pi h_1^2} \int_0^\infty J_o(m\rho)\, V_o^*\, dm \tag{19a}$$

$$w_B^* = \frac{1}{4\pi h_1^2} \int_0^\infty J_o(m\rho)\, V_B^*\, dm \tag{19b}$$

$$\sigma_B = -\frac{1}{2\pi h_1^2} \int_0^\infty J_o(m\rho)\, V_\sigma^*\, dm \tag{19c}$$

where

$$V_o^* = \frac{q_o^*}{G_1^*} \; \frac{1+4N^*m\exp(-2m) - (N^*)^2\exp(-4m)}{1-2N^*(1+2m^2)\exp(-2m) + (N^*)^2\exp(-4m)} \tag{20a}$$

$$V_B^* = \frac{q_o^*(1-N^*)}{G_2^*} \; \frac{(1+2m)\exp(-2m) - N^*(1-2m^2)\exp(-4m)}{1-2N^*(1+2m^2)\exp(-2m) + (N^*)^2\exp(-4m)} \tag{20b}$$

$$V_\sigma^* = q_o^* \, m(1-N^*) \frac{(1+2m)\exp(-2m) - N^*(1-2m^2)\exp(-4m)}{1-2N^*(1+2m^2)\exp(-2m) + (N^*)^2\exp(-4m)} \tag{20c}$$

$$N^* = \frac{G_1^* - G_2^*}{G_1^* + G_2^*} \tag{20d}$$

$$q_o^* = \frac{q_o}{p} \tag{20e}$$

G_1^* and G_2^*, which characterize the material properties, can be obtained from the linear differential operators as shown in equation 18a. For a given mechanical model that properly characterizes the shear behavior of the material, the transformed shear modulus G* can be substituted into equation 20. V_o^*, V_B^*, and V_σ^* will be found to be the ratios of two polynomials, the polynomial in the denominator having degrees higher than that in the numerator. Consequently, V_o^*, V_B^*, and V_σ^* can be partial-fractioned, and the direct Laplace inversion can be applied. By substituting V_o, V_B, and V_σ into equation 11, the viscoelastic solution can be obtained. The resulting integrals can be evaluated numerically by the Gaussian quadrature formula.[5] However, when the polynomial is of such a high degree that finding its roots becomes very tedious, the collocation method is suggested, which will be explained later. For other types of surface loads, similar procedures can be used to obtain solutions.

MOVING LOADS. Since the speeds of the loads of vehicles traveling on pavements are much less than the speeds of the shear and compression waves propagated in the pavement structures, inertial effects can be assumed negligible. The system is assumed to be at rest initially. For time greater than zero, the surface of the system is subject to an axisymmetrical loading moving along the x-axis with constant velocity v. A point load $-q_o(t)$ is shown in Figure 2. At any instant the stresses and displacement at the point (x, 0, z) directly under the path of the load in the elastic problem with this point load are given in equation 11 with r replaced by $(x-\alpha t)$, since the directions of x and r are the same at the point in question, and the radians of the point (x, 0, z) relative to cylindrical coordinates based on the load axis is $(x-vt)$. Equation 19 for the case of a moving load can be written:

$$w_o^* = \frac{1}{4\pi l_1^2} \int_0^\infty \{q_o J_o [m(X-V\tau')]\}^* V_o^* \, dm \tag{21a}$$

$$w_B^* = \frac{1}{4\pi h_1^2} \int_0^\infty \{q_o J_o[m(X-V\tau')]\}^* V_B^* \, dm \qquad (21b)$$

$$\sigma_B^* = \frac{-1}{2\pi h_1^2} \int_0^\infty \{\alpha q_o J_o[m(X-V\tau')]\}^* V_\sigma^* \, dm \qquad (21c)$$

where $X = \frac{x}{H}$, V_o^*, V_B^*, and V_σ^* are the same as shown in equation 20, except that q_o^* does not appear in the expression.

Moreover, the viscoelastic solution can be obtained by using the convolution integral. After the exchange of integrals we have:

$$w_o = \frac{4\pi}{q_o} w_o(t) = \frac{1}{h_1^2} \int_0^t \int_0^\infty J_o[m(X-V\tau')] \, V_o(t-\tau')dmd\tau' \qquad (22a)$$

$$w_B = \frac{4\pi}{q_o} w_B(t) = \frac{1}{h_1^2} \int_0^t \int_0^\infty J_o[m(X-V\tau')] \, V_B(t-\tau')dmd\tau' \qquad (22b)$$

$$\sigma_B = -\frac{2\pi}{q_o} \sigma_B(t) = \frac{1}{h_1^2} \int_0^t \int_0^\infty \alpha J_o[m(X-V\tau')] V_\sigma(t-\tau')dmd\tau' \qquad (22c)$$

where τ' is time varying from zero to t, and the expression $(t - \tau')$ means that V_o, V_B, and V_σ are functions of $(t - \tau')$.

Mathematically, the exchange of integrals is possible because the inner integrals of equation 22 are uniformly convergent in the range $0 \leq \tau' \leq t$.[6] This exchange is desirable, since it greatly reduces the computation time.

The value of V_o, V_B, and V_σ in equation 22 can be obtained by inverting V_o^*, V_B^*, and V_σ^*, as in the case of a stationary load. For cases of incompressible two-layer systems, where the material in each layer is characterized by simple models, the direct inversion method may also be used. To solve the double integral shown in equation 22, the inner integral can be evaluated by the Gaussian quadrature formula, and the outer integral by Simpson's rule. In equation 22, the dimensionless factor X(=x/H) cannot be factored out of the Bessel function $J_o[m(X-V_\tau')]$, as in the case of the load q_o; therefore, a value should be assigned to X in numerical computations.

The singularity that exists in equation 22a can be treated by separate consideration of the conditions where the load approaches the point and those where it moves away from the point. Equation 22a can be written:

$$w_o = \int_0^{\frac{x}{v}(1-\epsilon)} \int_0^{\infty} J_o[m(X-V\tau')]\, V_o(t-\tau')\,dm\,d\tau + \int_{\frac{x}{v}(1+\epsilon)}^{t} \int_0^{\infty} J_o[m(X-V\tau')]\, V_o(t-\tau')\,dm\,d\tau' \tag{23}$$

where ϵ is any positive number less than unity.

Equation 22 is for two-layer systems under point load; the same procedure can be applied to obtain stresses and displacements for other types of surface loads.

COLLOCATION METHOD. For multilayer systems or compressible material, the mathematical work required for the direct inversion method becomes very tedious, and the polynomial that results is of such a high degree that its roots are almost impossible to find. Therefore, the direct inversion method is used mainly when equations can be reduced to a sum of simple partial fractions. For multilayer or compressible material, an approximate method is developed. This method was originally proposed by Schapery,[7,8] based on results obtained from irreversible thermodynamics and variational principles. Schapery concluded that the class of problems to which the elastic-viscoelastic analogy may be applied has time-dependent solutions of the form:

$$\psi(t) = \psi' + \psi''t + \Delta\psi(t) \tag{24}$$

where ψ' and ψ'' are constants with respect to time, and $\Delta\psi(t)$ is the transient component of the solution defined as

$$\Delta\psi(t) = \int_0^{\infty} \phi(\tau')\, \exp(-\tfrac{t}{\tau'})\, d\tau' \tag{25}$$

The function $\phi(\tau')$, referred to as a spectral function of the variable τ', may consist either entirely or partly of Dirac delta functions. If $\Delta\psi(t)$

is expressed approximately by a Dirichlet series of decaying exponentials,

$$\Delta\psi(t) \simeq \Delta\psi_o = \sum_{i=1}^{n} S_i \exp\left(-\frac{t}{\gamma_i}\right) \tag{26}$$

Since viscoelastic materials have exponential stress-relaxation characteristics, equation 26 allows a wide spectrum of relaxation times; e.g., a reasonably large number of springs and dashpots may be incorporated in the material representation. Values of γ_i are positive constants prescribed in such a way as to provide adequate coverage of the time spectrum, and the S_i are unspecified coefficients to be evaluated by minimizing the total square error between the actual $\Delta\psi(t)$ and $\Delta\psi_D$, as given by the series. The minimization process will result in the expression:

$$\int_0^\infty \Delta\psi \exp\left(-\frac{t}{\gamma_i}\right) dt = \int_0^\infty \Delta\psi_D \exp\left(-\frac{t}{\gamma_i}\right) dt \quad i=1,2,\ldots n \tag{27}$$

Equation 27 essentially means that, for the mean square error of the approximation to be a minimum, the Laplace transform of the approximation must equal the Laplace transform of the exact function, at least at the n points $p = 1/\gamma_i$, $i=1,2,\ldots n$. Therefore, n relations are available for the Laplace transforms of $\Delta\psi(t)$ and evaluated at $p = 1/\gamma_i$; i.e.,

$$\Delta\psi^*_{(1/\gamma_i)} = \Delta\psi^*_{D(1/\gamma_i)} \qquad i=1,2,\ldots n \tag{28}$$

A more convenient form is obtained by multiplying these by $1/\gamma_i$ which yields:

$$(p\Delta\psi^*(p))_{p=1/\gamma_i} = (p\Delta\psi_D{}^*(p))_{p=1/\gamma_i} \qquad i=1,2,\ldots n \tag{29}$$

Since $\Delta\psi(t)$ was assumed to be of the form indicated by equation 26, equation 29 reduces to the series of equations:

$$(p\Delta\psi^*(p))_{p=1/\gamma_i} = \sum_{j=1}^{n} \frac{S_i}{1 + \frac{\gamma_i}{\gamma_j}} \qquad i=1,2,\ldots n \tag{30}$$

which constitutes a set of simultaneous equations for different values of p, which are solved for S_i. Thus, the collocation consists of matching the summation on the left-hand side of equation 30 with the calculated values of $p\Delta\psi^*(\rho)$ for various values of real, positive p. Hence, the inversion procedure consists essentially in being able to determine the values of the transform all along the positive real p-axis.

The constants ψ' and ψ'' in equation 24 are determined from given initial and boundary conditions. For the special case of a moving load, the viscoelastic pavement system is assumed to be initially undistrubed, and at infinite time; i.e., the load has passed over the station for a very long time, the stresses and displacements induced by the moving load approach zero. Therefore, the constants ψ' and ψ'' are equal to zero.

If we are interested in the time interval between zero to 1000 seconds for the moving point load case, 10 values of p, i.e., 100, 0.1, 0.055, 0.031, 0.018, 0.01, 0.0055, 0.0031, 0.0018, and 0.001, may be used; so equation 11 with ρ replaced by (X-Vt) becomes

$$\psi(t) = S_1 \exp(-100t) + S_2 \exp(-0.1t) + S_3 \exp(-0.055t) + \ldots\ldots + S_{10} \exp(-0.001t) \tag{31}$$

Take the Laplace transform of equation 31 and then multiply by p:

$$p\psi(p)^* = \frac{S_1}{1 + \frac{100}{p}} + \frac{S_2}{1 + \frac{0.1}{p}} + \frac{S_3}{1 + \frac{0.055}{p}} + \ldots\ldots + \frac{S_{10}}{1 + \frac{0.001}{p}} \tag{32}$$

By assigning successively p = 100, 0.1, 0.055, 0.031, 0.018, 0.01, 0.0055, 0.0031, 0.0018, and 0.001 in equation 32, 10 equations are obtained, which will give a solution to the 10 unknowns, S_1 through S_{10}.

$$
\begin{bmatrix}
\frac{1}{1+\frac{100}{100}} & \frac{1}{1+\frac{0.1}{100}} & \frac{1}{1+\frac{0.055}{100}} & \cdots & \frac{1}{1+\frac{0.001}{100}} \\
\frac{1}{1+\frac{100}{0.1}} & \frac{1}{1+\frac{0.1}{0.1}} & \frac{1}{1+\frac{0.055}{0.1}} & \cdots & \frac{1}{1+\frac{0.001}{0.1}} \\
\frac{1}{1+\frac{100}{0.055}} & \frac{1}{1+\frac{0.1}{0.055}} & & & \\
\vdots & & & & \\
\frac{1}{1+\frac{100}{0.001}} & \cdots & & & \frac{1}{1+\frac{0.001}{0.001}}
\end{bmatrix}
\begin{Bmatrix} S_1 \\ S_2 \\ S_3 \\ \vdots \\ S_{10} \end{Bmatrix}
=
\begin{Bmatrix} p\psi(p)^*_{p=100} \\ p\psi(p)^*_{p=0.1} \\ \vdots \\ p\psi(p)^*_{p=0.001} \end{Bmatrix}
\tag{33}
$$

The values of p used in the example are quarter decades, spaced in the time interval between 10 and 1000 seconds. Basically, the accuracy of the inversion can be improved by adding more terms to the series in equation 26, but "ill condition" may be encountered in solving the simultaneous equations if the p values selected are too close to each other.

The most basic aspect of viscoelastic response is that the complete time history of the event must be taken into consideration to determine the present state of the material. Therefore, the criterion for the selection of an effective solution range is that the p-multiplied transform, i.e. $p\Delta\psi^*(p)$, should go from a constant value (before any actual response takes place), through its "transition" range, to a final (long-time) constant value. Since the solution at any given time is basically a function of the value of the Laplace transform throughout its entire range, the time span of the solution should be as wide as possible.

NUMERICAL EXAMPLES AND DISCUSSIONS. The effect of E_1/E_2 on vertical stress and vertical displacement for a two-layer incompressible elastic system under a stationary normal point load is shown in Figure 3; E_1 and E_2

are the Young's moduli of layers 1 and 2, respectively. When E_1/E_2 is less than unity, the stress and displacement decreases slowly with increasing values of E_1/E_2; but when E_1/E_2 is greater than unity, the stress and displacement decrease rapidly, and the stress decreases faster than the displacement.

The stress factors in the same elastic system are listed in Table 1. The stress factors, S_B, are compressive when the distance, R, is less than 7.5, and oscillate between compression and tension when the values of R are greater than 7.5.

The stress and displacement in a viscoelastic two-layer incompressible system are shown in Figure 4. The response of the material in each layer to deviatoric stress is characterized by a simple Kelvin model. The displacement has a very small value initially, but the value increases slowly with time. The stress, on the other hand, has a value about one-third its maximum at 0.1 second; the value then increases slowly with time. At longer times, the stress and displacement factors reach the elastic solutions having the ratio $G_1/G_2 = 10$.

The values of the stress factor, S_B, in an incompressible viscoelastic two-layer system at a point 2 ft. below the surface are shown in Table 2. T, a dimensionless time factor, is the ratio of the real time, t, to the retardation time, τ_2, of the bottom layer. For longer periods of time, i.e., T = 100, values of the stress factor, S_B, for a viscoelastic case approach the elastic case values. Also, interesting is the fact that the stress factor, S_B, for a given value of R may either oscillate in sign between compression and tension, or decrease in value when the time factor, T, increases from 0 to 100.

The effect of the speed of a moving point load on the displacement at a point 2 ft. below the surface of a viscoelastic half space is shown in Figure 5. The displacement decreases as the speed of the load increases. At low speed of the load, the displacement curves rebound as soon as the load moves away from the station; as the speed of the load increases, the displacement subsequently increases as the load moves away from the station.

The surface displacement for an incompressible two-layer viscoelastic system under a moving point load is shown in Figure 6. The discontinuities shown in the figure are caused by the singularity that exists when the load is acting directly over the point under consideration. The shapes of the curves are similar to those in Figure 5.

In multilayer systems, the collocation method replaces the direct inversion method. The former method requires long computer time to

evaluate the stresses or displacements in their transformed domain. The collocation method was used to obtain the displacement at the second interface in a viscoelastic incompressible three-layer system under a moving point load, with each layer having the same material properties. The solutions obtained were then compared with those for a viscoelastic semi-infinite solid. The computed results, with five collocated points, are shown in Figure 7. The collocation method is applicable to moving loads on multilayer systems.

SUMMARY. An analysis of a multilayered, linear, elastic, and viscoelastic half space under stationary and moving axisymmetric loads has been made. Solutions have been presented for the normal stress, σ_z, radial stress σ_r, tangential stress, σ_θ, shear stress, τ_{rz}, vertical deflection, w, and radial displacement u, at any point within the half space, in terms of integral equations. Numerical examples have been given for illustration.

REFERENCES

1. Love, A. E. H., "A Treatise on the Mathematical Theory of Elasticity," 4th ed, Dover Publications, New York, 1944.

2. Lee, E. H., "Stress Analysis in Viscoelastic Bodies," Quarterly of Applied Mathematics, Vol. 13, 1955, pp. 183-190.

3. Burmister, D. M., "The General Theory of Stresses and Displacements in Layered Soil Systems," Journal of Applied Physics, Vol. 16, 1945, pp. 89-94, 126-127, 296-302.

4. Mehta, M. R., and Veletsos, A. S., "Stresses and Displacements in Layered Systems," Structural Research Series No. 178, 1959, University of Illinois, Champaign, Ill.

5. Hilderbrand, F. P., Introduction to Numerical Analysis, 1956, McGraw-Hill, New York, pp. 323-325.

6. Titchmarsh, E. C., The Theory of Functions, 1939, Oxford University Press, England, pp. 53.

7. Schapery, R. A., "Approximate Methods of Transform Inversion for Visco-Elastic Stress Analysis," Proceedings of the Fourth U. S. National Congress of Applied Mechanics, 1962, pp. 1075-1085.

8. Schapery, R. A., "Application of Thermodynamics to Thermomechanical, Fracture, and Birefringement Phenomena in Viscoelastic Media," Journal of Applied Physics, Vol. 35, 1964.

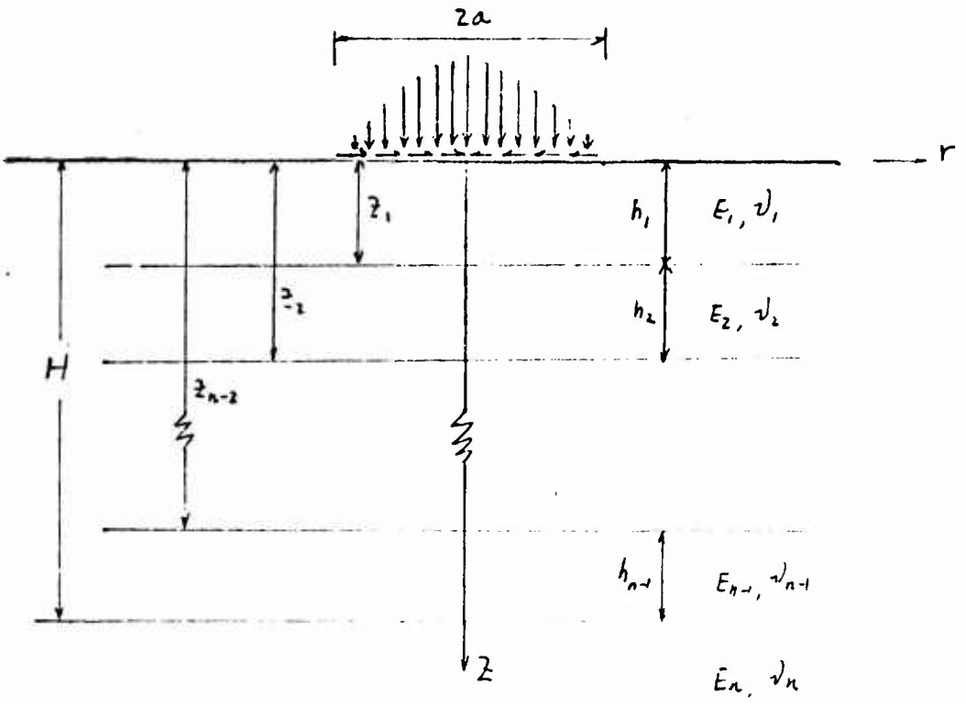


Fig. 1. An n-layer elastic system.

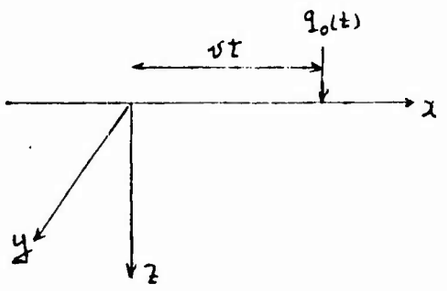


Fig. 2

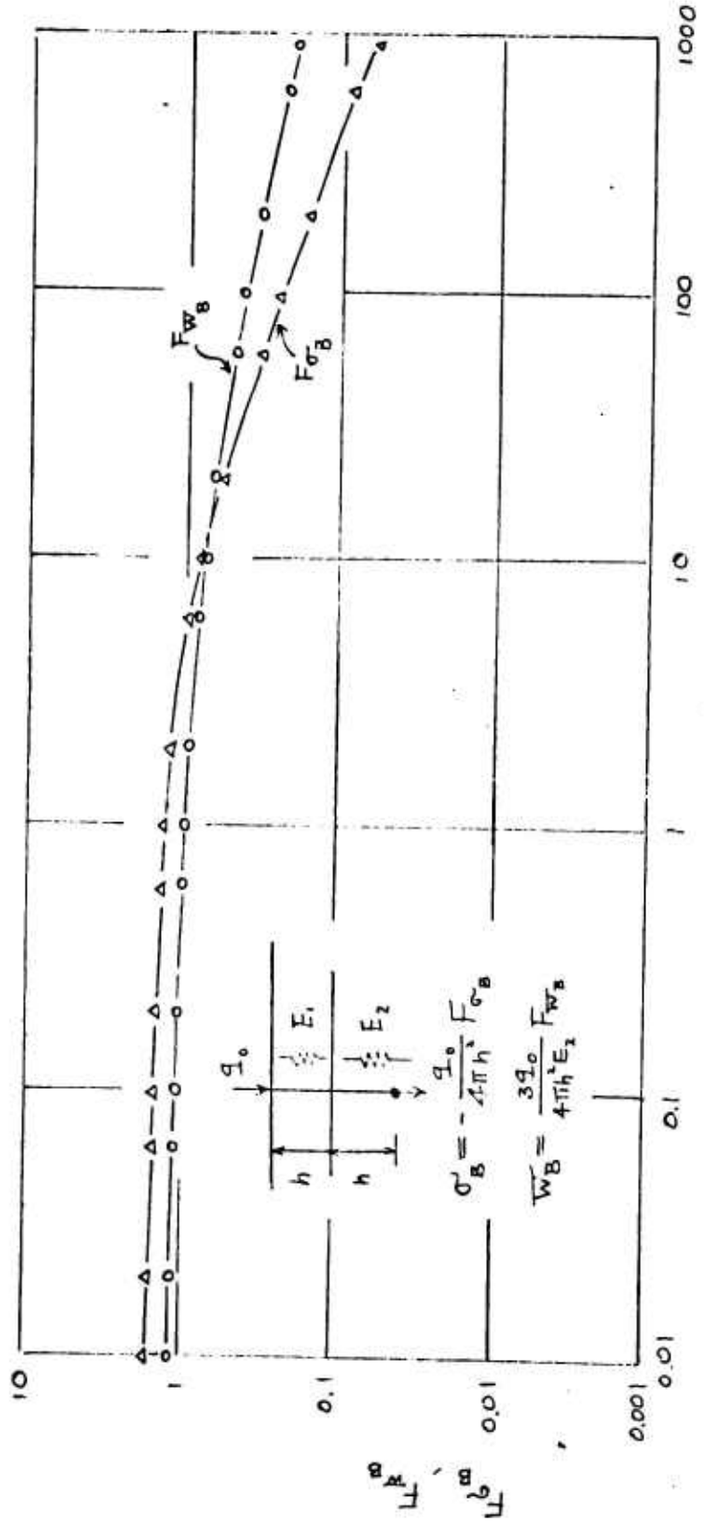


Fig. 3. Effect of E_1/E_2 on stress and displacement factors.

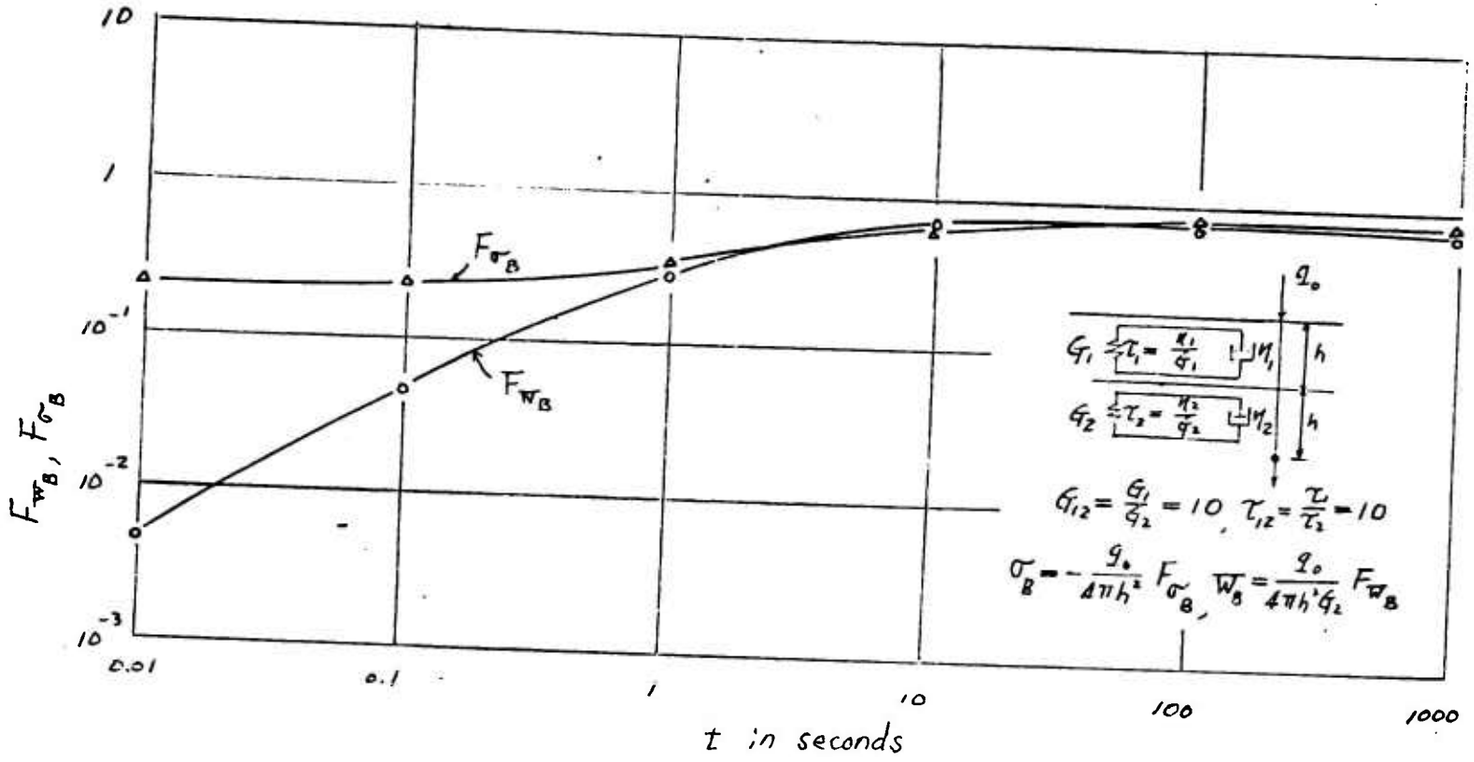


Fig. 4. Stress and displacement factors under a stationary point load.

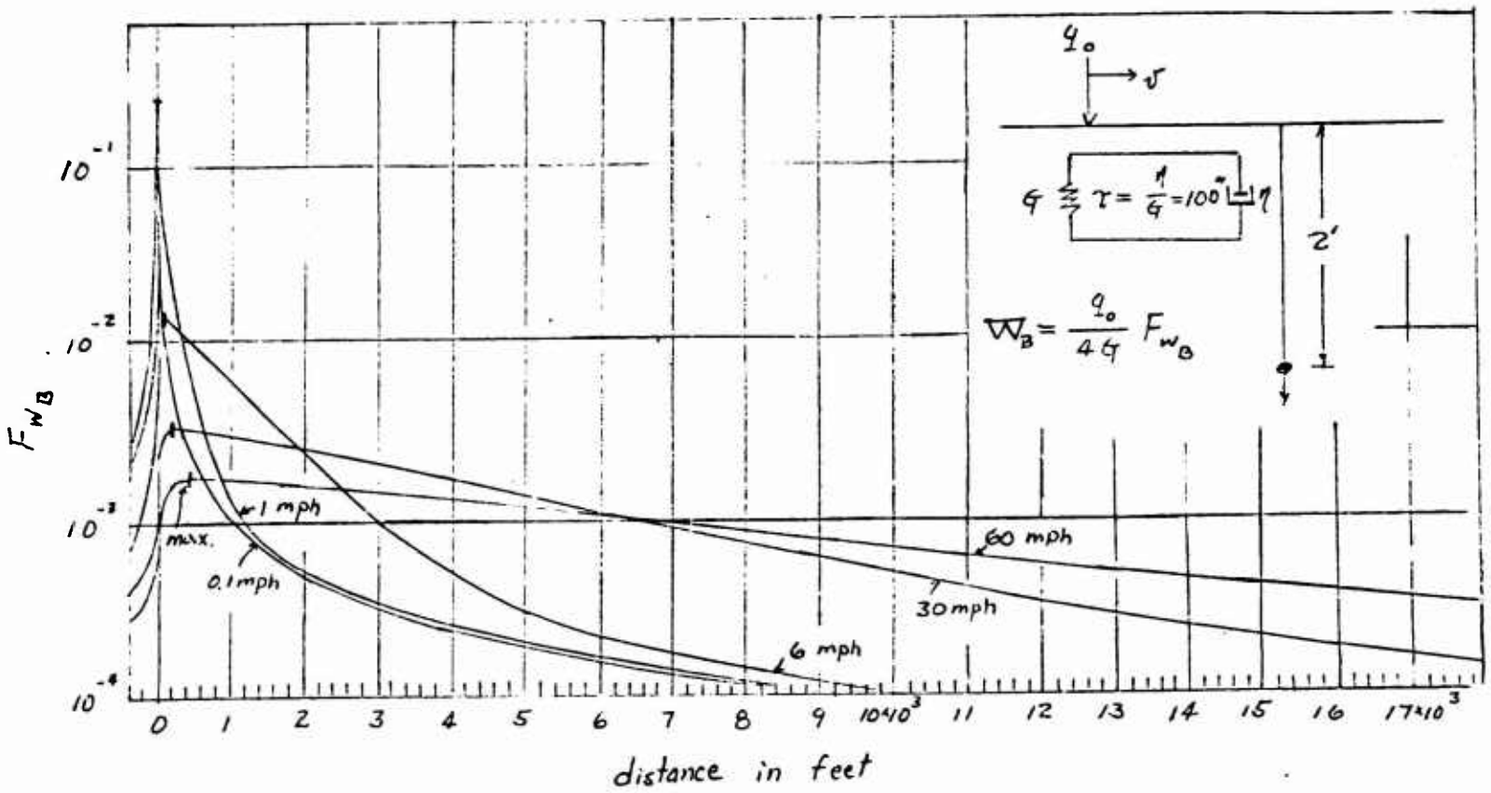


Fig. 5. Effects of speed on the displacement factor F_{W_B}

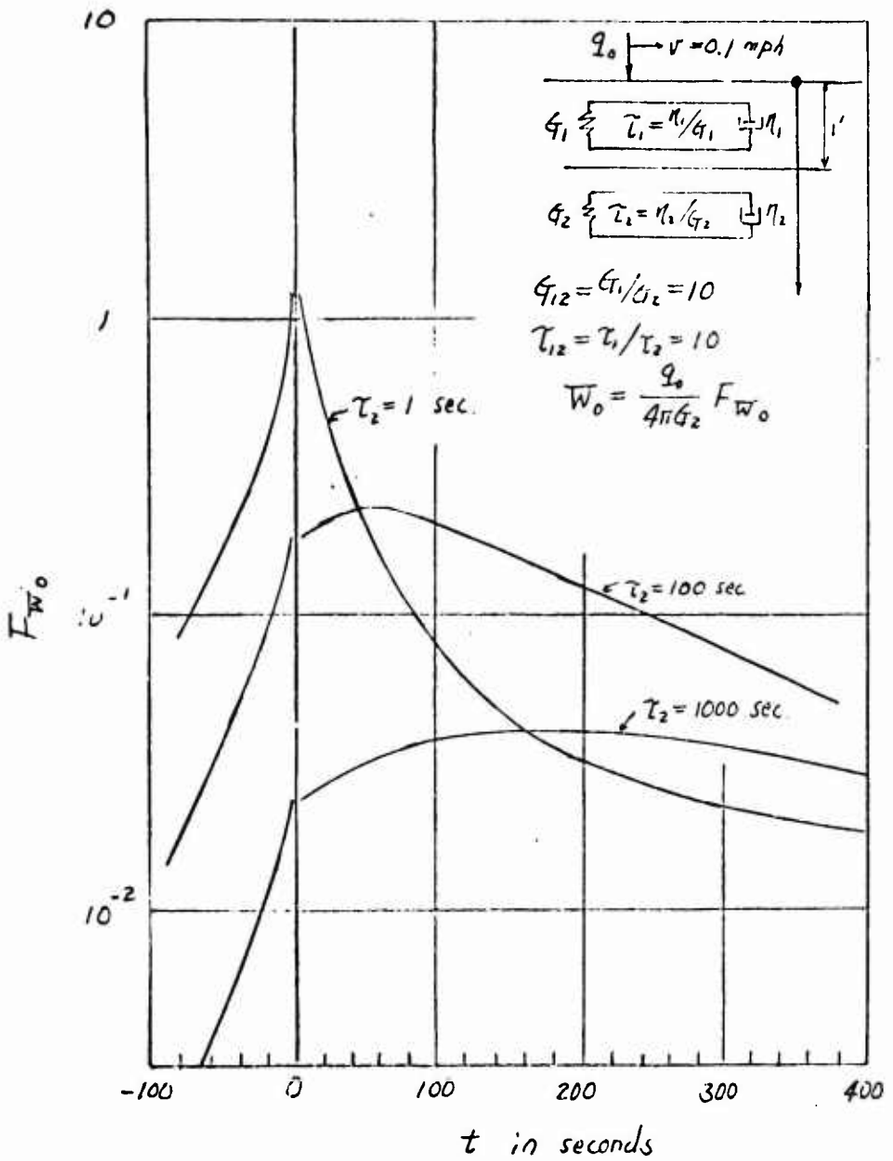


Fig. 6. Effect of τ_2 on surface displacement factor F_{w_0}

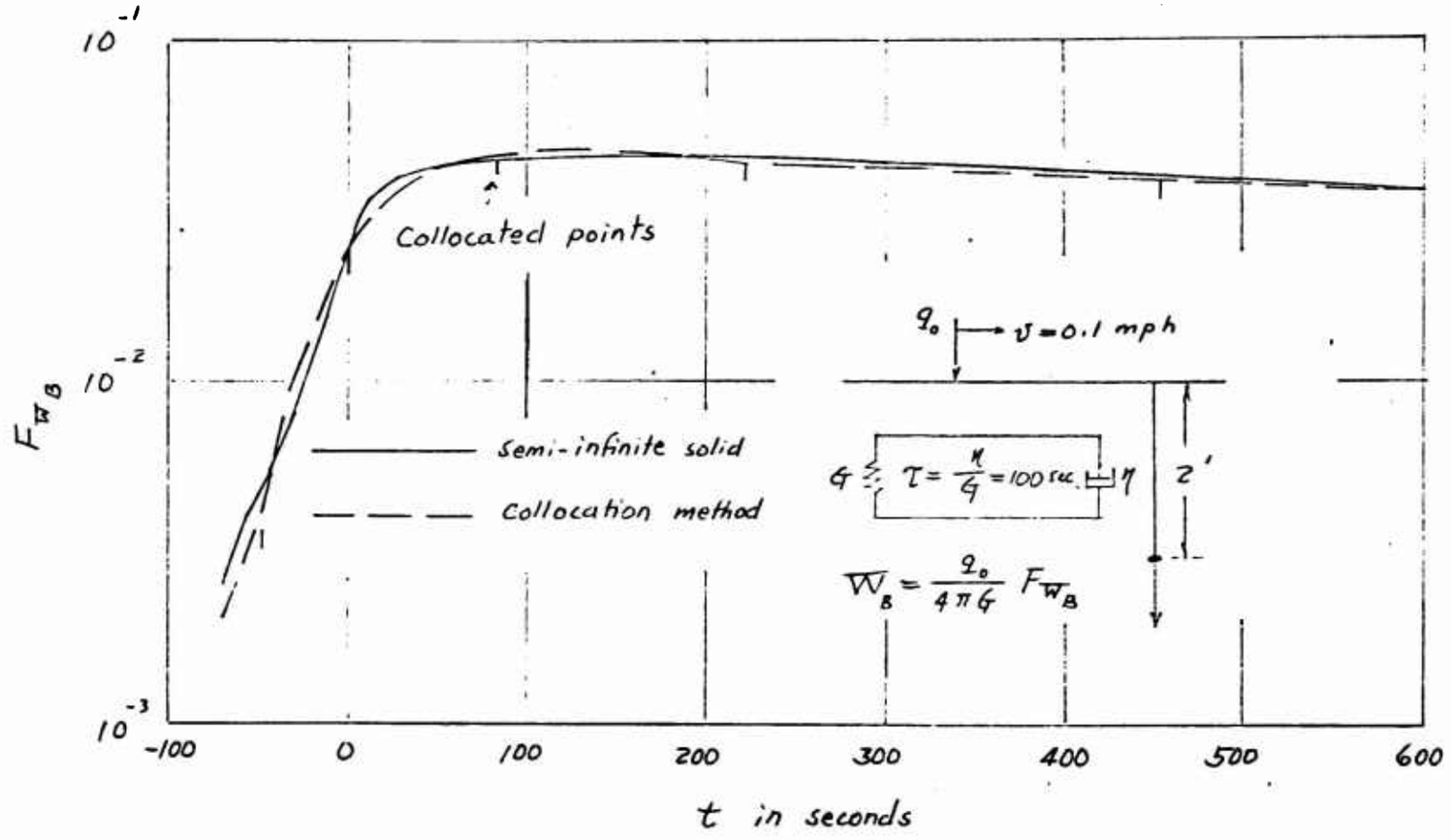


Fig. 7. Collocation Method - Comparison of results
(displacement factor 2 ft below the surface)

Table 1

Stress Factors in a Two-Layer Incompressible Elastic System

Under a Stationary Point Load, $\sigma_B = \frac{-q_o}{2\pi} S_B$

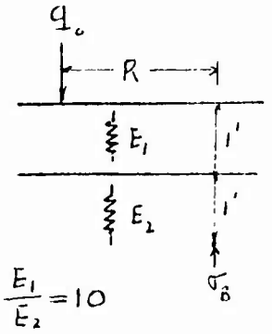
R	S_B	R	S_B	R	S_B	R	S_B	Sketch
0.0	3.91 @ -1	0.4	3.71 @ -1	1.0	2.88 @ -1	1.6	1.99 @ -1	
2.4	1.11 @ -1	3.2	0.57 @ -1	4.0	2.81 @ -2	5.0	1.01 @ -2	
6.0	2.89 @ -3	7.5	-0.95 @ -4	9.0	-3.33 @ -4	13.5	-2.72 @ -5	
15.0	-3.02 @ -5	18.0	-2.00 @ -5	22.0	2.07 @ -6	30.0	1.71 @ -5	

Table 2

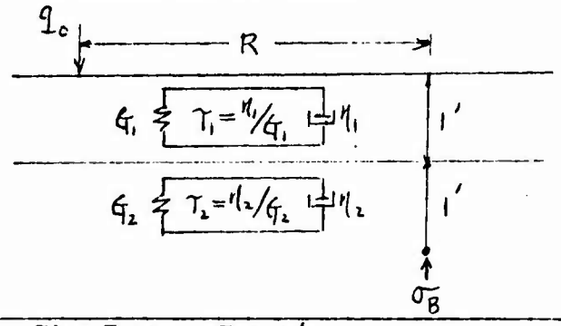
Stress Factors S_B in a Two-Layer Incompressible Viscoelastic System Under a Stationary Point Load

$G_{12} = G_1/G_2 = 10$

$\tau_{12} = \tau_1/\tau_2 = 10$

$T = t/\tau_2$

$\sigma_B = -\frac{q_o}{2\pi} S_B$



R	Time Factor $T = t/\tau_2$				
	0.01	0.1	1	10	100
0.0	1.29 @ -1	1.35 @ -1	1.82 @ -1	3.49 @ -1	3.91 @ -1
1.0	1.12 @ -1	1.17 @ -1	1.54 @ -1	2.68 @ -1	2.88 @ -1
2.0	0.84 @ -1	0.87 @ -1	1.07 @ -1	1.51 @ -1	1.50 @ -1
5.0	2.68 @ -2	2.67 @ -2	2.49 @ -2	1.13 @ -2	1.01 @ -2
7.5	0.81 @ -2	0.77 @ -2	4.50 @ -3	-0.84 @ -3	-0.95 @ -4
13.5	-3.24 @ -4	-3.66 @ -4	-0.52 @ -3	3.89 @ -5	-2.72 @ -5
22.0	-0.76 @ -4	-0.66 @ -4	-0.51 @ -5	-1.00 @ -6	2.07 @ -6
30.0	-3.89 @ -6	-2.96 @ -6	1.61 @ -6	1.21 @ -5	1.71 @ -5

ADAPTATION OF VALANIS' METHOD TO THE KINETICS OF VISCOELASTIC PLATES

Struan R. Robertson
Maggs Research Center
Watervliet, New York

ABSTRACT. Valanis' method for solution to dynamic problems of viscoelastic media having a constant Poisson's ratio, is adapted to the analysis of viscoelastic plates. Three cases are treated: first, the dynamic load; second, the dynamic moment on the boundary; and, third, a dynamic displacement on the boundary.

INTRODUCTION. A method developed by Valanis[1*] for a general linear viscoelastic kinetic problem is adapted to the classical theory of plates. Two assumptions are made by Valanis in his method; firstly, and most important, is the assumption of constant Poisson's ratio and secondly is that the forcing function is separable in time and space. These assumptions lead to reducing the viscoelastic problem to the superposition of a static problem and an eigenvalue problem in elasticity and the solution of a Volterra integrodifferential equation. Correspondingly, in the present paper the problem of the linear viscoelastic plate is reduced to a static problem and an eigenvalue problem in elastic plates and the solution of an integrodifferential equation.

Three cases are treated for the plate which give different results. They are: the forced motion with homogeneous boundary conditions; specified moment on part of the boundary; and, a specified displacement on part of the boundary.

GOVERNING EQUATIONS. In the following cartesian coordinates, x_i, are used. The usual index notation is followed with repeated indices denoting summation over the range of the indices and a comma preceding an index denotes partial differentiation with respect to the corresponding coordinate direction. Thus, Hooke's law for a linear viscoelastic medium can be written

$$\sigma_{ij} = \delta_{ij} \cdot \lambda^* \epsilon_{kk} + 2\mu^* \epsilon_{ij} \qquad i = 1,2,3 \qquad (1)$$

where * indicates the convolution integral

$$f^*g = \int_0^t [f(t-\tau)\ \partial g(\tau)/\partial\tau]d\tau. \qquad (2)$$

*Subscript after a name refers to references at the end of the paper.

PRECEDING PAGE BLANK

Taking the Laplace transform of (1) gives

$$\bar{\sigma}_{ij} = \delta_{ij}\, s\bar{\lambda}\bar{\epsilon}_{kk} + 2\bar{\mu}s\bar{\epsilon}_{ij} \tag{3}$$

or

$$\bar{\epsilon}_{ij} = [\,\bar{\sigma}_{ij} - \delta_{ij}\,\bar{\lambda}\bar{\sigma}_{kk}/(3\bar{\lambda} + 2\bar{\mu})\,]/2s\bar{\mu} \tag{4}$$

where s is the Laplace transform variable and the superbar indicates the Laplace transform.

The assumption of a constant Poisson's ratio is now employed. This assumption gives the following simplification

$$\mu = \mu_o G, \qquad \lambda = \lambda_o G \tag{5}$$

with μ_o and λ_o being constants and G is essentially the relaxation modulus in shear. If J is essentially the creep function in shear then

$$s\bar{G} = 1/s\bar{J}\ . \tag{6}$$

Employing (5) in (4) gives

$$\bar{\epsilon}_{ij} = [\bar{\sigma}_{ij} - \delta_{ij}\lambda_o\bar{\sigma}_{kk}/(3\lambda_o + 2\mu_o)]/2\mu_o s\bar{G} \tag{7}$$

with

$$\nu_o = \lambda_o/2(\lambda_o + \mu_o), \qquad E_o = \mu_o(3\lambda_o + 2\mu_o)/(\lambda_o + \mu_o) \tag{8}$$

the constitutive relations for viscoelastic plates becomes

$$\bar{\epsilon}_{\alpha\beta} = [(1 + \nu_o)\bar{\sigma}_{\alpha\beta} - \delta_{\alpha\beta}\,\nu_o\,\bar{\sigma}_{\gamma\gamma}]/E_o s\bar{G} \qquad \alpha = 1,2 \tag{9}$$

The strain displacement relations are

$$\epsilon_{\alpha\beta} = \frac{1}{2}\,(u_{\alpha,\beta} + u_{\beta,\alpha}) \tag{10}$$

Using the usual plate assumptions

$$u = -z\,\partial w/\partial x, \qquad v = -z\partial w/\partial y \tag{11}$$

$$w = w(x,y,t)$$

the stress-displacement relations become

$$\begin{aligned}
\bar{\sigma}_{xx} &= -[\bar{w}_{xx} + \nu_o\,\bar{w}_{yy}]\; z\,E_o s\bar{G}/(1-\nu_o^2) \\
\bar{\sigma}_{yy} &= -[\bar{w}_{yy} + \nu_o\,\bar{w}_{xx}]\; z\,E_o s\bar{G}/(1-\nu_o^2) \\
\bar{\sigma}_{xy} &= -\,\bar{w}_{xy}\; z\,E_o s\bar{G}/(1-\nu_o)
\end{aligned} \tag{12}$$

As usual in the derivation of the classical plate equations, see Filonenko-Borodich's book,[2] the equations of motion are taken as

$$\sigma_{ij,j} = \rho\ddot{u}_i \qquad i = 1,2,3 \tag{13}$$

with

$$\ddot{u}_1 = \ddot{u}_2 = 0$$

and the boundary conditions

$$\begin{aligned}
\sigma_{xz} &= \sigma_{yz} = 0 && z = \pm\, h/2 \\
\sigma_{zz} &= \begin{cases} 0 \\ q(x,y,t) \end{cases} && z = h/2 \\
& && z = -h/2
\end{aligned} \tag{14}$$

Figure 1 serves to illustrate the geometry. Using (12) integrate the first two equations through the plate thickness to get

$$\sigma_{\alpha z} = \frac{E_o(z^2 - h^2/4)}{2(1 - \nu_o^2)} \frac{\partial \nabla^2}{\partial \alpha} \bar{w}\, s\bar{G} \qquad \alpha = x,y \tag{15}$$

Then, using (15) and (12) in the remaining equation of motion integrate through the plate thickness to obtain

$$\frac{E_o h^3}{12(1 - \nu_o^2)} s\bar{G}\, \nabla^4 \bar{w} + \rho h(s^2 \bar{w} - sw(0) - \dot{w}(0)) = \bar{q} \tag{16}$$

Letting

$$D_o = E_o h^3/12(1-\nu_o^2) \tag{17}$$

the equation of motion for the viscoelastic plate becomes

$$D_o G^* \nabla^4 w + \rho h \ddot{w} = q \tag{18}$$

The moments and shearing forces are direct analogs to those of classical plate theory and are found to be:

the moment about the x-axis

$$\bar{M}_x = D_o s\bar{G}[\bar{w}_{yy} + \nu_o \bar{w}_{xx}]$$

the moment about the y-axis

$$\bar{M}_y = D_o s\bar{G}\,[\bar{w}_{xx} + \nu_o \bar{w}_{yy}]$$

the twisting moment (19)

$$\bar{H} = -D_o\,(1-\nu_o)\, s\bar{G}\, \bar{w}_{xy}$$

and the shearing forces

$$\bar{N}_x = -D_o s\bar{G}\partial\nabla^2 \bar{w}/\partial x$$

$$\bar{N}_y = -D_o s\bar{G}\partial\nabla^2 \bar{w}/\partial y$$

where the super-bar denotes the Laplace transform. The similarity between equations (16) and (19) and those of elastic plates was to be expected. The equations (16) and (19) may be simply arrived at by taking the equations for elastic plates, taking their Laplace transform and replacing the flexural rigidity D by $D_o s\bar{G}$. This is just the usual correspondence principle as given in Bland's book,[3] for example.

The boundary condition will be, of course, the same as elastic plates. Thus, with the aid of figure 2, at the clamped edge

$$w = 0, \qquad \partial w/\partial x = 0 \qquad (x = 0) \qquad (20)$$

at the simply supported edge

$$w = 0, \qquad M_x = 0 \qquad (y = b) \qquad (21)$$

$M_x = 0$ implies that

$$D_o s\bar{G} \left[\partial^2 \bar{w}/\partial y^2 + \nu_o \partial^2 \bar{w}/\partial x^2\right] = 0$$

and since $D_o s\bar{G} \neq 0$

$$\partial^2 w/\partial y^2 + \nu_o \partial^2 w/\partial x^2 = 0 \qquad (21a)$$

and at the free edge

$$M_y = 0, \qquad N_x + \partial H/\partial y = 0 \qquad (x = a) \qquad (22)$$

which leads to

$$\partial^2 w/\partial x^2 + \nu_o \partial^2 w/\partial y^2 = 0 \qquad (22a)$$

$$\partial^3 w/\partial y^3 + (2-\nu_o)\partial^3 w/\partial x \partial y^2 = 0 \ .$$

FORCED MOTION.

Case I. Solution of the Inhomogeneous Equation of Motion with Homogeneous Boundary Conditions

In this case there will be no need to seek a solution to the static problem. This is due to the fact that the boundary conditions

are homogeneous and that the static equation is also homogeneous; thus, leading to a trivial solution. The problem is solved by employing Valanis' approach, which will reduce it to an eigenvalue problem in elastic plates plus an integrodifferential equation.

The equation of motion is

$$D_o G^* \nabla^4 w + \rho h \ddot{w} = q(x,y,t) \tag{23}$$

together with the initial conditions

$$w = p_1(x,y), \qquad \dot{w} = p_2(x,y) \qquad (t = 0) \tag{24}$$

and homogeneous boundary conditions appropriate to whatever plate is being considered. For example, if the plate is simply supported at $x = 0, a$ and clampled at $y = 0,b$ then

$$w(0,y) = M_y(0,y) = w(a,y) = M_y(a,y) = w(x,0) =$$

$$\partial w(x,0)/\partial x = w(x,b) \qquad \partial w(x,b)/\partial y = 0.$$

In order to reduce the problem to an eigenvalue problem it is necessary to seek solutions to the homogeneous equation

$$D_o G^* \nabla^4 V + \rho h \ddot{V} = 0 \tag{25}$$

Expand V in the series

$$V = \sum_n A_n u^{(n)}(x,y)\, f_n(t) \tag{26}$$

then

$$D_o G^* f_n \nabla^4 u^{(n)} + \rho h u^{(n)} \ddot{f}_n = 0 \tag{27}$$

Require that f_n satisfy

$$\ddot{f}_n / G^* f_n = -k_n^2 \tag{28}$$

then $u^{(n)}$ satisfies

$$D_o \nabla^4 u^{(n)} - k_n^2 \rho h u^{(n)} = 0 \tag{29}$$

together with the appropriate boundary conditions. Thus, the eigenfunctions for the elastic plate are sought. Note that no initial conditions were specified for V so that the initial conditions associated with (28) are arbitrary. However, $f_n(t)$ is not, as will become apparent, needed.

Expand the desired solution w in terms of the eigenfunctions as follows

$$w = \sum_n B_n u^{(n)} g_n(t) \tag{30}$$

and assume that

$$q(x,y,t) = Q(x,y)F(t) \tag{31}$$

Thus the equation of motion (25) becomes

$$\sum_n [D_o(G*g_n) B_n \nabla^4 u^{(n)} + \rho h \ddot{g}_n B_n u^{(n)}] = Q(x,y)F(t) \tag{32}$$

Employing (29) in (32) gives

$$\sum_n [G*g_n B_n \rho h k_n^2 u^{(n)} + \rho h g_n B_n u^{(n)}] = QF \tag{33}$$

For the usual homogeneous boundary conditions the eigenfunctions are orthogonal thus, multiplying (33) by $u^{(m)}$ and integrating over the plate gives

$$G*g_n B_n \rho h k_n^2 + \rho h \ddot{g} B_n = \frac{F \iint Q u^{(n)} dxdy}{\iint u^{(n)} u^{(n)} dxdy} \tag{34}$$

or

$$G^* g_n k_n^2 + \ddot{g}_n = \frac{C_n}{\rho h B_n} F \tag{35}$$

The k_n are the eigenvalues of (29) so in order to complete the solution the B_n must be determined along with initial conditions for (35). This is accomplished by considering the initial conditions for w.

If $p_1 \neq 0$ and $p_2 = 0$ then

$$\begin{aligned} \sum_n B_n \, g(0) u^{(n)} &= p_1 \\ \sum_n B_n \, \dot{g}(0) u^{(n)} &= 0 \end{aligned} \tag{36}$$

Taking

$$g(0) = 1, \qquad \dot{g}(0) = 0 \tag{37}$$

gives

$$B_n = \frac{\iint p_1 u^{(n)} \, dxdy}{\iint u^{(n)} u^{(n)} dxdy} \tag{38}$$

If $p_1 = 0$ and $p_2 \neq 0$ then

$$\begin{aligned} \sum_n B_n g(0) \, u^{(n)} &= 0 \\ \sum_n B_n \dot{g}(0) \, u^{(n)} &= p_2. \end{aligned} \tag{39}$$

Taking

$$g(0) = 0, \qquad \dot{g}(0) = 1 \tag{40}$$

gives

$$B_n = \frac{\iint P_2 u^{(n)}\, dxdy}{\iint u^{(n)} u^{(n)} dxdy} \quad . \tag{41}$$

If $p_1 \neq 0$ and $p_2 \neq 0$ superimpose the solutions resulting from the two above cases.

If $p_1 = 0$ and $p_2 = 0$ take

$$B_n = 1 \tag{42}$$

then

$$g_n(0) = \dot{g}_n(0) = 0 \quad . \tag{43}$$

Now the B_n are determined and the appropriate initial conditions for g_n found the solution to (35) can be found. One method is to employ the Laplace transform. Considering, for example, the case when $p_1 \neq 0$ and $p_2 = 0$ this gives for (35)

$$s\bar{G}\,\bar{g}_n k_n^2 + s^2\bar{g}_n - s = C_n\bar{F}/\rho h B_n \tag{44}$$

or

$$\bar{g}_n = (s + C_n\bar{F}/\rho h B_n)/(s\bar{G}k_n^2 + s^2) \tag{45}$$

If a system of springs and dashpots is used to represent the relaxation function G then $\bar{G}$ is the ratio of polynomials in s and if F is of the form such that $\bar{F}$ is also a ratio of polynomials in s then, of course, $\bar{g}_n$ is the ratio of polynomials in s which can be easily inverted by finding the roots of the denominator on a computer. Note that there will be a $g_n(t)$ corresponding to each eigenvalue k_n.

Case II. Specified Moment of Kirchoff Boundary Condition as a Function of Time

In this case it will be necessary to seek the solution to a static problem in elastic plates as well as that of the eigenvalue problem.

The moment on the boundary takes the form

$$M_\alpha = -D_o G^*[\partial^2 w/\partial\beta^2 + \nu_o \partial^2 w/\partial\alpha^2]$$

$$= g_1(x,y,t) \qquad \alpha = x,y \tag{46}$$

and the Kirchoff condition is

$$N_\alpha + \partial H/\partial\beta = -D_o G^*[\partial^3 w/\partial\alpha^3 + (2-\nu_o)\partial^3 w/\partial\alpha\partial\beta^2]$$

$$= g_2(x,y,t) \qquad \alpha = x,y \tag{47}$$

Assume that

$$g_{1,2} = g(x,y)E(t). \tag{48}$$

Equations (46) and (47) are of the form

$$-D_o G^* L\{w\} = g(x,y)E(t) \tag{49}$$

where L is a linear differential operator.

The equation of motion is

$$D_o G^* \nabla^4 w + \rho h \ddot{w} = 0 \tag{50}$$

with the initial conditions

$$w = \dot{w} = 0 \qquad (t = 0) \tag{51}$$

and the boundary condition

$$-D_o G^* L\{w\} = g(x,y)E(t) \tag{52}$$

plus other homogeneous boundary conditions appropriate to the particular problem being considered.

Look for an auxiliary solution defined by

$$\bar{w} = \frac{\bar{E}}{\bar{G}} \bar{w}_{Aux} \tag{53}$$

Now define the auxiliary problem as

$$D_o G^* \nabla^4 w_{Aux} + \rho h \ddot{w}_{Aux} = 0 \tag{54}$$

with

$$w_{Aux} = \dot{w}_{Aux} = 0 \tag{55}$$

and (52) becomes

$$-D_o L\{ \bar{w}_{Aux} \} = g/s \tag{56}$$

or

$$D_o L \{w_{Aux}\} = g\, H(t) \tag{57}$$

plus other homogeneous boundary conditions on w. Note that by using (53) the convolution was removed from (52).

Define a static problem by*

$$\nabla^4 U = 0 \tag{58}$$

with the boundary condition

$$-D_o L \{U\} = g(x,y) \tag{59}$$

plus other homogeneous boundary terms for w. The initial conditions are identically satisfied.

Now define a dynamic problem with homogeneous boundary conditions by

$$D_o G^* \nabla^4 V + \rho \ddot{V} h = 0 \tag{60}$$

with

$$V = U, \qquad \dot{V} = 0 \qquad (t = 0) \tag{61}$$

*To clarify where (58) comes from consider $G^* \nabla^4 U = 0$. The convolution states that either $G = 0$ or $\nabla^4 U = 0$ or they both equal zero and $G \neq 0$ so $\nabla^4 U = 0$.

and the boundary term

$$L\{V\} = 0 \tag{62}$$

plus other homogeneous boundary terms on w. Following the procedure used in treating (26) expand V in the series

$$V = \sum_n A_n v^{(n)} f_n(t) \tag{63}$$

and take

$$\ddot{f}_n / G^* f_n = -k_n^2 \tag{64}$$

then $v^{(n)}$ satisfies

$$\nabla^4 v^{(n)} = k_n^2 \rho h v^{(n)} / D_o \tag{65}$$

with

$$L\{v^{(n)}\} = 0 \tag{66}$$

plus other appropriate, homogeneous boundary terms. Thus $v^{(n)}$ is an eigenfunction of the elastic plate problem.

The initial conditions require that

$$\begin{aligned} \sum A_n v^{(n)} f_n(0) &= U \\ \sum A_n v^{(n)} \dot{f}_n(0) &= 0 \end{aligned} \tag{67}$$

so that taking

$$\begin{aligned} f_n(0) &= 1 \\ \dot{f}_n(0) &= 0 \end{aligned} \tag{68}$$

gives

$$A_n = \frac{\iint U\, v^{(n)}\, dxdy}{\iint v^{(n)} v^{(n)}\, dxdy} \tag{69}$$

The solution to the auxiliary problem is found by the superposition

$$w_{Aux} = U - V \tag{70}$$

Equation (64) with (68) can be used to determine f_n as follows

$$s^2 \bar{f}_n - s + k_n^2\, s\bar{G}\, \bar{f}_n = 0$$

$$\bar{f}_n = s/(s\bar{G}\, k_n^2 + s^2)$$

which is the ratio of two polynomials in s when G is represented by a system of springs and dashpots and can be easily inverted as mentioned earlier.

As an example consider figure 2 with a forced moment at x = a. Then for the static problem the boundary conditions are

$$\left.\begin{aligned} -D_o\left(\frac{\partial^2 U}{\partial x^2} + \nu_o \frac{\partial^2 U}{\partial y^2}\right) &= g(a,y) \\ \frac{\partial^3 U}{\partial x^3} + (2-\nu_o)\frac{\partial^3 U}{\partial x \partial y^2} &= 0 \end{aligned}\right\} \quad (x = a)$$

$$\left.\begin{aligned} U &= 0 \\ \frac{\partial U}{\partial y} &= 0 \end{aligned}\right\} \quad (y = 0,b)$$

$$\left.\begin{aligned} U &= 0 \\ \frac{\partial^2 U}{\partial x^2} + \nu_o \frac{\partial^2 U}{\partial y^2} &= 0 \end{aligned}\right\} \quad (x = 0)$$

and for the eigenvalue problem they are

$$\left.\begin{aligned} &\frac{\partial^2 U}{\partial x^2} + \nu_o \frac{\partial^2 U}{\partial y^2} = 0 \\ &\frac{\partial^3 U}{\partial x^3} + (2-\nu_o) \frac{\partial^3 U}{\partial x \partial y^2} = 0 \end{aligned}\right\} \quad (x = a)$$

$$\left.\begin{aligned} &U = 0 \\ &\frac{\partial U}{\partial y} = 0 \end{aligned}\right\} \quad (y = 0,b)$$

$$\left.\begin{aligned} &U = 0 \\ &\frac{\partial^2 U}{\partial x^2} + \nu_o \frac{\partial^2 U}{\partial y^2} = 0 \end{aligned}\right\} \quad (x = 0)$$

Case III. Specified Displacement

The procedure is similar to Case II, the only difference being the definition of the auxiliary solution. If the displacement is specified on part of the boundary as

$$w = \phi(x,y)E(t) \tag{71}$$

then

$$\overline{w} = \phi\overline{E}$$

so the auxiliary solution is given by

$$\overline{w} = \overline{E}\overline{s}\overline{w}_{Aux} \tag{72}$$

and the boundary condition (71) becomes for the auxiliary problem

$$w_{Aux} = \phi E(t) \tag{73}$$

Thus the static problem is

$$\nabla^4 U = 0 \tag{74}$$

with the boundary condition

$$U = \phi \tag{75}$$

plus additional homogeneous boundary conditions.

The dynamic problem is

$$D_o G^* \nabla^4 V = - \rho h V \tag{76}$$

with the boundary condition

$$V = 0 \tag{77}$$

on part of the boundary plus the other appropriate homogeneous boundary conditions. The remainder of the procedure is the same as in (63) to (69) in Case II. The auxiliary solution is thus

$$w_{Aux} = U - V \tag{78}$$

As an example, consider figure 2 with a forced displacement at $x = 0$. Then for the static problem

$$\left.\begin{aligned} U &= \phi(0,y) \\ \frac{\partial^2 U}{\partial x^2} &+ \nu_o \frac{\partial^2 U}{\partial y^2} = 0 \end{aligned}\right\} \quad (x = 0)$$

$$\left.\begin{aligned} U &= 0 \\ \frac{\partial U}{\partial y} &= 0 \end{aligned}\right\} \quad (y = 0, b)$$

$$\left.\begin{aligned} &\frac{\partial^2 U}{\partial x^2} + \nu_o \frac{\partial^2 U}{\partial y^2} = 0 \\ &\frac{\partial^3 U}{\partial x^3} + (2-\nu_o) \frac{\partial^3 U}{\partial x \partial y^2} = 0 \end{aligned}\right\} \quad (x = a)$$

and for the dynamic problem

$$\left.\begin{aligned} &V = 0 \\ &\frac{\partial^2 V}{\partial x^2} + \nu_o \frac{\partial^2 V}{\partial y^2} = 0 \end{aligned}\right\} \quad (x = 0)$$

$$\left.\begin{aligned} &V = 0 \\ &\frac{\partial V}{\partial y} = 0 \end{aligned}\right\} \quad (y = 0, b)$$

$$\left.\begin{aligned} &\frac{\partial^2 V}{\partial x^2} + \nu_o \frac{\partial^2 V}{\partial y^2} = 0 \\ &\frac{\partial^3 V}{\partial x^3} + (2-\nu_o) \frac{\partial^3 V}{\partial x \partial y^2} = 0 \end{aligned}\right\} \quad (x = a)$$

CONCLUSION. Other cases than the three treated here are certainly possible and the methods used to threat these cases should be easily adapted to ones such as forced motion of a plate with an elastic support on part of the boundary. However, it was the intent here to give an outline that illustrated the pertinent features of the method and which could be modified to suit the needs of particular cases and not to treat a wide variety of them.

REFERENCES

1. Valanis, K. C., "Exact and Variational Solutions to a General Viscoelasto-Kinetic Problem," Trans. ASME, Journal of Applied Mechanics, Vol. 33 Series E No. 4, Dec. 1966, pp. 868-892.

2. Filonenko-Borodich, M., "Theory of Elasticity," Dover Publications, Inc., New York, 1965, pp. 303-317.

3. Bland, D. R., "The Theory of Linear Viscoelasticity," Pergamon Press, New York, 1960.

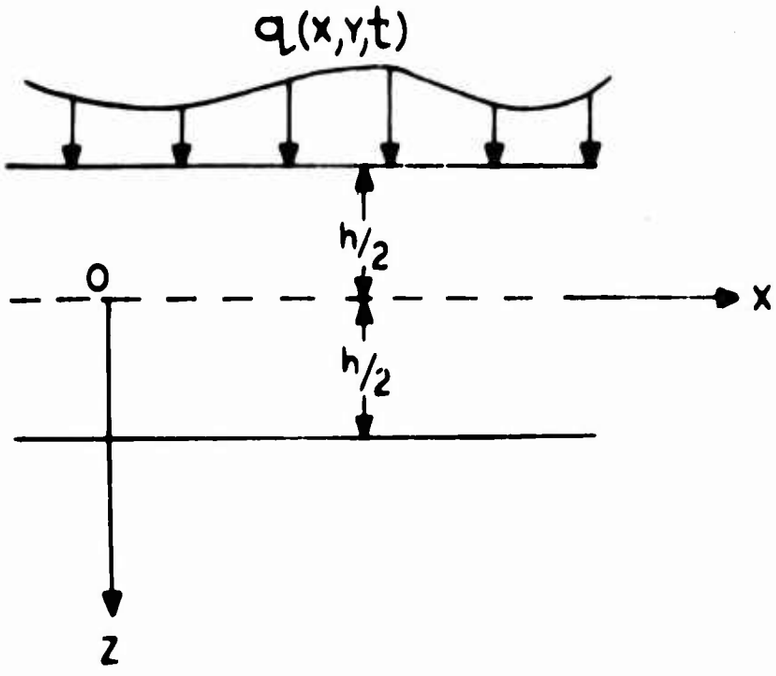


FIG. 1

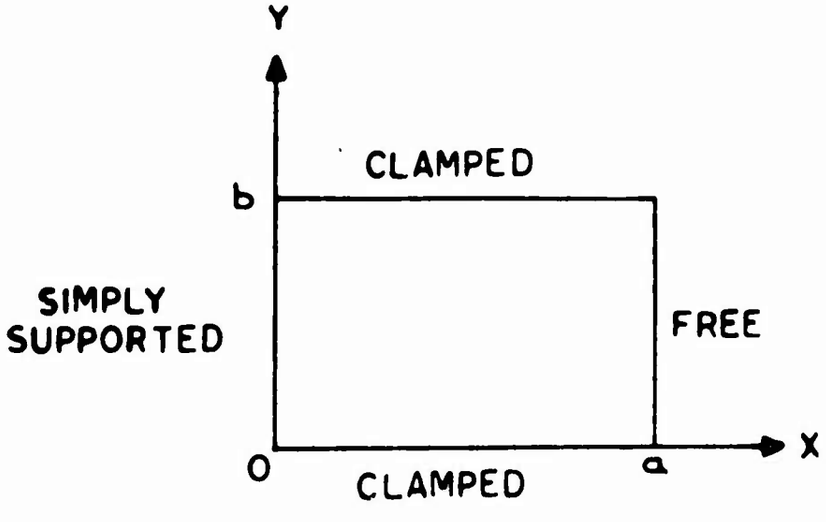


FIG. 2

Third Order Positive Cyclic Systems of Linear Differential Equations* **

GARRETT BIRKHOFF

Harvard University, Cambridge, Massachusetts 02138

AND

LEON KOTIN

Institute for Exploratory Research,
U. S. Army Electronics Command, Fort Monmouth, New Jersey 07703

Received October 23, 1967

1. INTRODUCTION. Our original aim was to find analogs of Sturm's theorems for linear, homogenous third-order differential equations of the special form $x'''(t) = p(t)\,x$. Negative results concerning such analogs for the general third order linear homogeneous differential equation were established in 1911 by G. D. Birkhoff [1]. He proved that an integral curve (i.e., one whose components are three linearly independent solutions) in the projective plane can have no point of inflection, but that any smooth curve without points of inflection can be an integral curve of a third-order equation. From this, he showed that there exist third-order differential equations with three solutions whose zeros occur in any arbitrarily prescribed order. This destroyed any hope that there might be a simple analog of Sturm's classical separation theorem to general third-order differential equations.

However, as we shall see below, much can be proved in the special case of $x'''(t) = p(t)\,x$, with $p(t) \neq 0$. More generally, much can be proved for any piecewise continuous (n-th order) *positive cyclic system* of the form

$$x_i'(t) = p_i(t)\,x_{i+1}, \qquad p_i(t) > 0, \qquad i = 1, 2, \ldots, n. \tag{1}$$

Remark. The condition that all $p_i > 0$ in (1) can be weakened to the conditions that each $p_i(t)$ has constant sign and that $\prod_{j=1}^{n} p_j(t) > 0$. For, upon replacing x_i for $i = 2, \ldots, n$ by $[\prod_{j=1}^{i-1} \operatorname{sgn} p_j(t)]\,x_i = y_i$, we get a positive cyclic system. When n is odd, it suffices to assume that each $p_i(t)$ has constant sign, since the substitution $t \to -t$ reverses the sign of $\prod_{j}^{n} p_j(t)$.

Stronger results can be obtained if one assumes that, for suitable positive constants m and M,

$$m < p_i(t) < M, \qquad 0 < m < M < \infty. \tag{1'}$$

---

*This paper has been published in the Journal of Differential Equations, Vol. 5, No. 1, January, 1969, pp. 182-196. We appreciate the fact that the Editor of this Journal, which is copyrighted by Academic Press, gave his permission to republish this article in these Transactions.

**This article has been reproduced photographically.

Namely, using the theory of positive linear operators [2], one can prove the existence and *projective uniqueness* (i.e., to within a constant scalar factor) of a solution $\mathbf{f}$ whose n components are positive for all t. This positive solution grows exponentially as $t \to +\infty$. Indeed, if a solution $\mathbf{x}(t)$ of (1)-(1′) ever becomes positive, then for all sufficiently large t

$$ce^{mt} \leqslant x_i(t) \leqslant Ce^{Mt}$$

where c and C are suitable positive constants.

The adjoint equation $d\mathbf{x}/dt = -P^T(t)\,\mathbf{x}$ also has a projectively unique positive solution $\mathbf{g}(t)$. Both $\mathbf{g}$ and $\mathbf{f}$ remain for all t in a positive cone in the interior of the positive orthant. Letting $\mathbf{g}^\perp(t)$ denote the $(n-1)$-space orthogonal to $\mathbf{g}(t)$, any solution $\mathbf{x}(t)$ of (1) either lies in $\mathbf{g}^\perp(t)$ for all t or never intersects it at all. If $\mathbf{x} \in \mathbf{g}^\perp$ then $\mathbf{x} = o(\mathbf{f})$ as $t \to +\infty$, and conversely. This is equivalent to the condition that $\mathbf{x}$ is never positive or negative. On the other hand, if $\mathbf{x}$ is ever positive, then $\mathbf{x} \sim k\mathbf{f}$ for some suitable constant k as $t \to +\infty$.

When $n = 3$, stronger results can be obtained (see Part II). $\mathbf{g}^\perp(t)$ is then the 2-space composed of all oscillatory solutions at time t, an oscillatory solution being one whose components all have an infinite number of zeros going to $+\infty$ with t. From the general case then, $\mathbf{x}$ is an oscillatory solution if and only if $\mathbf{x} = o(\mathbf{f})$ as $t \to +\infty$, where $\mathbf{f}$ is a positive solution of (1)-(1′) (with $n = 3$). Likewise, if $\mathbf{x}$ is nonoscillatory then $\mathbf{x} \sim k\mathbf{f}$ as $t \to +\infty$.

These results have their duals as $t \to -\infty$; e.g., if $\mathbf{u}$ and $\mathbf{v}$ are any linearly independent oscillatory solutions, then $\mathbf{f} = o(\mathbf{u})$ as $t \to -\infty$; and if $\pm\,\mathbf{x}$ is not positive, then $\mathbf{x} \sim a\mathbf{u} + b\mathbf{v}$ as $t \to -\infty$.

Because of the negative character of the adjoint equation, its solutions behave, as $t \to +\infty$, like those of (1)-(1′) as $t \to -\infty$. Thus any positive solution $\mathbf{g}(t)$ of the adjoint system approaches zero exponentially as $t \to +\infty$. Similarly, if $\mathbf{u}$ and $\mathbf{v}$ are any linearly independent oscillatory solutions, then $\mathbf{g} = o(\mathbf{u})$; and if $\mathbf{y}$ is a nonpositive and nonnegative solution, then $\mathbf{y} \sim a\mathbf{u} + b\mathbf{v}$ as $t \to +\infty$.

I. The nth Order Case

2. Positive Cyclic Systems. Sharpening the results of [3] and [4], we first prove the existence and uniqueness of positive solutions of the nth order piecewise continuous positive cyclic system

$$x_i'(t) = p_i(t)\,x_{i+1}, \qquad i = 1, 2, \ldots, n, \tag{2}$$

with the uniform bounds

$$0 < m \leq p_i(t) \leq M \leq Nm, \qquad i = 1, 2, \ldots, n, \tag{2'}$$

all subscripts taken modulo n here, as throughout the paper.

We shall normalize (2)-(2') by substituting for t a new variable τ, defined by

$$\tau = \int_0^t \lambda(s)\, ds, \qquad \lambda(t) = \left[\prod_{i=1}^{n} p_i(t)\right]^{1/n}. \tag{3}$$

This substitution yields from (2) another nth order cyclic system

$$dx_i/d\tau = q_i(\tau)\, x_{i+1}, \qquad i = 1, 2, \ldots, n, \tag{4}$$

where $q_i(\tau) = p_i(t)/\lambda(t)$, thereby reducing (2) to a system of the same form, with $\prod_{i=1}^{n} q_i(\tau) = 1$. Indeed,

$$1/N \leq q_i(\tau) \leq N \qquad \text{and} \qquad \prod_{i=1}^{n} q_i(\tau) = 1. \tag{5}$$

Moreover, trivially for t and τ as in (3),

$$\sup_{t,i,j}[q_i(\tau)/q_j(\tau)] = \sup_{t,i,j}[p_i(t)/p_j(t)] \leq N.$$

Finally, (2') implies that $m \leq \lambda(t) \leq M$, so that τ ranges over $(-\infty, +\infty)$ with t.

Example 1. In the constant coefficient case $N = 1$, $p_i(t) = p_i = \text{const.}$ in (2), the preceding normalization gives $q_i(\tau) \equiv q_i = \text{const.}$ with $\Pi q_i = 1$. The characteristic equation of the coefficient matrix Q of the associated (constant-coefficient) vector system

$$\mathbf{x}'(\tau) = Q\mathbf{x}, \qquad Q = \begin{pmatrix} 0 & q_1 & 0 \cdots 0 \\ 0 & 0 & q_2 \cdots 0 \\ \cdots & \cdots & \cdots \\ 0 & 0 & 0 \cdots q_{n-1} \\ q_n & 0 & 0 \cdots 0 \end{pmatrix}, \tag{6}$$

is then $\lambda^n = 1$. Hence (6) has a positive solution

$$\mathbf{x}_0(\tau) = e^{\tau}\mathbf{g}_0. \tag{7}$$

Moreover, writing $\alpha = 2\pi/n$, the other solutions of the characteristic basis[1] have the *oscillatory* form

$$\begin{Bmatrix} \mathbf{x}_k(\tau) \\ \mathbf{y}_k(\tau) \end{Bmatrix} = e^{(\cos k\alpha)\tau} \begin{pmatrix} |g_{1k}| \begin{Bmatrix} \cos \\ \sin \end{Bmatrix} [(\sin k\alpha)\tau + \arg g_{1k}] \\ \cdots\cdots\cdots\cdots\cdots\cdots \\ |g_{nk}| \begin{Bmatrix} \cos \\ \sin \end{Bmatrix} [(\sin k\alpha)\tau + \arg g_{nk}] \end{pmatrix}$$

where $k = 1, 2, \ldots, [(n-1)/2]$, and $\mathbf{g}_k = (g_{1k}, \ldots, g_{nk})^T$ is the kth eigenvector of Q, with eigenvalue $\lambda^k = e^{k\alpha i}$. If n is even, we have also a decreasing solution $\mathbf{x}_{n/2}(\tau) = e^{-\tau}\mathbf{g}_{n/2}$.

In particular, if $n = 3$, (6) has a subspace of decaying oscillatory solutions, whose components have interlacing zeros, of the form

$$e^{-\tau/2} \begin{pmatrix} q_1 q_2 q_3 \begin{Bmatrix} \cos \\ \sin \end{Bmatrix} \sqrt{3}\tau/2 \\ q_2 q_3 \begin{Bmatrix} \cos \\ \sin \end{Bmatrix} (\sqrt{3}\tau/2 + 2\pi/3) \\ q_3 \begin{Bmatrix} \cos \\ \sin \end{Bmatrix} (\sqrt{3}\tau/2 - 2\pi/3) \end{pmatrix}. \tag{8}$$

Now we shall prove that there exists a unique positive solution of the system (2)-(2′). We introduce as in [3] the two-parameter family of nonnegative linear operators

$$P(s, t) = \overset{\frown}{\int_s^t} P(u)\, du, \tag{9}$$

the product integral or matrizant of the system (2)-(2′), whence

$$P(s, t)\, \mathbf{x}(s) = \mathbf{x}(t).$$

This product integral is a positive matrix ([2], p. 387, Example 4), whose entries $p_{i,j}$ are easily expressed as sums of multiple integrals by expanding the product integral in a Peano series. Thus, for small h we have cyclically, generalizing ([3], (3)):

$$\begin{aligned} p_{i,i}(s, s+h) &= 1 + O(h^n) \\ p_{i,i+1}(s, s+h) &= p_i(s)\, h + O(h^2) \\ p_{i,i+2}(s, s+h) &= p_i(s)\, p_{i+1}(s)\, h^2/2! + O(h^3) \\ &\cdots\cdots\cdots\cdots \\ p_{i,i-1}(s, s+h) &= \Big(\prod_{j \neq i-1} p_j(s)\Big) h^{n-1}/(n-1)! + O(h^n). \end{aligned}$$

[1] By a *characteristic basis* of a real linear system with constant coefficients, we mean a basis of solutions of the form $ce^{\lambda t}$ (λ real), or Re $[ce^{\lambda t}]$ and Im $[ce^{\lambda t}]$ (λ complex).

In view of the uniform inequality $m < p_i(s) < M$, it follows that (for sufficiently small h) we can write

$$p_{i,i+k}(s, s+h) = Rh^k, \qquad k = 0, 1, \ldots, n-1, \tag{10}$$

where the $R = R(i, k, s, h) > 0$ are uniformly bounded away from 0 and ∞: e.g., when $m < 1 < M$,

$$m^{n-1}/(n-1)! - O(h) < R < M^{n-1}/(n-1)! + O(h).$$

Consequently, the projective diameter $\Delta(s, s+h)$ of the transform of the positive orthant under the action of $P(s, s+h)$ satisfies (for small h)

$$\begin{aligned} \Delta(s, s+h) &= \sup_{i,j} \ln[p_{i,i}p_{j,j}/p_{i,j}p_{j,i}] \\ &= \ln(h^{-n}/R^2) \end{aligned} \tag{11}$$

where R^2 represents the product of two suitable R's. This projective diameter is bounded uniformly in s. It follows that the family $\{P(s, t)\}$ of positive linear operators is uniformly semi-primitive [2] for increasing and decreasing time. We thus obtain the following result as a corollary of ([2], p. 389, Theorem 9).

THEOREM 1. *The system* (2)-(2′) *has a projectively unique positive solution, i.e., with all components positive everywhere in* $(-\infty, +\infty)$.

3. POSITIVE SOLUTIONS. It is easy to derive bounds on the rate of growth of positive solutions of any positive cyclic system (2) satisfying the uniform inequalities (2′). This is because positive solutions are *isotone* both in their initial values $x_i(0)$ and in the $p_i(t)$. As a result, from a simple comparison with the solution of the systems $x_i'(t) = mx_{i+1}$, $x_i'(t) = Mx_{i+1}$ for the initial condition $x_i(0) = 1$, we infer

THEOREM 2. *If* $\mathbf{x}(t)$ *is any solution of a uniformly positive cyclic system* (2)-(2′) *with* $\mathbf{x}(a) > 0$ *for some real* a, *then for some* c, $C > 0$ *we have*:

$$ce^{mt} \leqslant x_i(t) \leqslant Ce^{Mt} \qquad \text{for all} \quad t \geqslant a. \tag{12}$$

Proof. By hypothesis, all $x_i(a) > 0$; let

$$c = e^{-ma} \operatorname{Min}_i x_i(a), \qquad C = e^{-Ma} \operatorname{Max}_i x_i(a).$$

The inequality now follows by comparison with the systems $x_i'(t) = mx_{i+1}$ and $x_i'(t) = Mx_{i+1}$, for the initial conditions $x_i(a) = ce^{ma}$ and Ce^{Ma} respectively. This is because the hypotheses $p_i(t) \geqslant q_i(t) \geqslant 0$ and

$x_i(a) \geq y_i(a) \geq 0$ imply $x_i(t) \geq y_i(t) \geq 0$ for any solutions of (1) and the analogous positive cyclic system $y_i'(t) = q_i(t)\, y_{i+1}$.

Likewise, we can prove that any nonpositive and nonnegative solution of a uniformly positive cyclic system (2)-(2′) is dominated by any ultimately positive solution. This is an immediate corollary of the following general theorem, which seems to be new.

THEOREM 3. *Let* $\mathbf{f}(t)$ *be any somewhere positive function consistent with a uniformly semi-primitive multiplicative process, and let* $\mathbf{x}(t)$ *be any other consistent function which is nowhere positive or negative. Then* $\mathbf{x}(t) = o(\mathbf{f}(t))$ *in the sense that, for any* $\epsilon > 0$, $-2\epsilon\mathbf{f}(t) \leq \mathbf{x}(t) \leq 2\epsilon\mathbf{f}(t)$ *for all sufficiently large* t.

Proof. Let $\mathbf{x}(0) = \mathbf{c}$ be decomposed into its positive and negative parts $\mathbf{c}^+$, $\mathbf{c}^-$, and let $\mathbf{x}_1(t)$, $\mathbf{x}_2(t)$ be the (ultimately positive) solutions which satisfy the initial conditions $\mathbf{x}_1(0) = \mathbf{c}^+$, $\mathbf{x}_2(0) = -\mathbf{c}^-$. Then, by uniform semi-primitivity[2], there exist constants $M_i (i = 1, 2)$ such that $\mathbf{x}_i(t) \sim M_i\mathbf{f}(t)$ in the sense that, for any $\epsilon > 0$ and all large enough t,

$$(M_i - \epsilon)\,\mathbf{f}(t) \leq \mathbf{x}_i(t) \leq (M_i + \epsilon)\,\mathbf{f}(t). \tag{13}$$

Unless $M_1 = M_2$, clearly $\mathbf{x}(t) = \mathbf{x}_1(t) - \mathbf{x}_2(t)$ will ultimately become positive or negative, contrary to hypothesis. Hence $M_1 = M_2$ and so, subtracting the two inequalities of (13),

$$-2\epsilon\mathbf{f}(t) \leq \mathbf{x}(t) = \mathbf{x}_1(t) - \mathbf{x}_2(t) \leq (M_1 + \epsilon)\,\mathbf{f}(t) - (M_1 - \epsilon)\,\mathbf{f}(t) = 2\epsilon\mathbf{f}(t),$$

as claimed.

Now recall that the family $\{P(s, t)\}$ of product integrals defined in (9) is uniformly semi-primitive, and that a function $\mathbf{f}(t)$ is consistent with this process if and only if it is a solution of the positive cyclic system (2)-(2′). Because of this, Theorem 3 has the following corollary.

COROLLARY. *Let* $\mathbf{x}(t)$ *be any nowhere positive or negative solution, and let* $\mathbf{f}(t)$ *be any ultimately positive solution of* (2)-(2′). *Then* $\mathbf{x}(t) = o(\mathbf{f}(t))$ *as* $t \to +\infty$.

4. THE ADJOINT SYSTEM. Since the adjoint of any linear system $\mathbf{x}'(t) = A\mathbf{x}$ is $\mathbf{y}'(t) = -A^T\mathbf{y}$, the adjoint of any positive cyclic system (2) is the system

$$g_i'(t) = -p_{i-1}(t)\, g_{i-1}, \tag{14}$$

[2] The details of the argument resemble those of the proof of Theorem 4 in G. Birkhoff, Trans. Am. Math. Soc. 85 (1957), 219–227; see also J. Math. Mech. 3 (1965), 507–512.

which is *cyclic* for the reverse ordering p_n , p_{n-1} ,..., p_1 . If (2) is normalized, then so is (14). Moreover the adjoint system (14) is *positive* for the independent variable $-t$, assuming

$$0 < m \leqslant p_i(t) \leqslant M. \tag{14'}$$

If we apply the same considerations to the adjoint (14)-(14') as to (2)-(2'), obtaining a two-parameter family of positive operators for increasing $-t$ (i.e., decreasing t), we arrive at the following dual of Theorem 1.

THEOREM 1'. *The system* (14)-(14') *has a projectively unique* (*strictly*) *positive solution.*

Actually, no two linearly independent solutions can be strictly positive even on (a, ∞), i.e., even for all sufficiently large t.

If we permute the $x_i's$ and replace t by $-t$, the adjoint system (14) can be made positive cyclic. Therefore (14) behaves for positive t like (3) does for negative t; e.g., any ultimately positive solution $\mathbf{x}$ of (14) satisfies

$$ce^{-Mt} \leqslant x_i \leqslant Ce^{-mt}$$

for t sufficiently large, whence positive solutions approach zero exponentially.

We now appeal to the following easily proved result [5, p. 71].

LEMMA 1. *The inner product*

$$(\mathbf{g}(t), \mathbf{x}(t)) \equiv \sum g_k(t)\, x_k(t) = \text{const.}$$

for every solution $\mathbf{x}(t)$ *of* (2) *if and only if* $\mathbf{g}(t)$ *satisfies* (14).

Thus any solution $\mathbf{x}(t)$ of (2)-(2') which is orthogonal at t_0 to a positive solution $\mathbf{g}(t)$ of its adjoint (14) is identically orthogonal to it; i.e., if $\mathbf{x}(t_0) \in \mathbf{g}^{\perp}(t_0)$, then $\mathbf{x}(t) \in \mathbf{g}^{\perp}(t)$ for all t. Here $\mathbf{g}^{\perp}(t)$ denotes the space of all solutions $\mathbf{x}(t)$ which satisfy $(\mathbf{g}(t), \mathbf{x}(t)) \equiv 0$.

THEOREM 4. *Let* $\mathbf{x}(t)$ *be a solution of* (2)-(2') *and let* $\mathbf{f}(t)$ *be a positive solution. Then the following conditions are equivalent*: (i) $\mathbf{x}(t) = o(\mathbf{f}(t))$ *as* $t \to +\infty$; (ii) $\mathbf{x}(t) \in \mathbf{g}^{\perp}(t)$; (iii) $\mathbf{x}(t)$ *is nowhere positive or negative*; (iv) $\mathbf{x}(t)$ *is not ultimately positive or negative.*

Proof. To prove the equivalence of the first two conditions, consider the set of all solutions $\mathbf{x}$ with the property that $\mathbf{x} = o(\mathbf{f})$, which is trivially a subspace of the n-dimensional vector space of all solutions. This set is proper since it fails to contain $\mathbf{f}(t)$. From the Corollary of Theorem 3, it contains $\mathbf{g}^{\perp}(t)$; for, any solution in $\mathbf{g}^{\perp}$ cannot be positive or negative since no two

positive solutions can be orthogonal. Finally, since $\mathbf{g}^+(t)$ is $(n-1)$-dimensional, the subspace is $\mathbf{g}^+(t)$.

To prove the equivalence of conditions (ii) and (iii), suppose $\mathbf{x}(a)$ is positive or negative. Then clearly $\mathbf{x} \notin \mathbf{g}^+$. Conversely, if $\mathbf{x}$ is nowhere positive or negative, then $\mathbf{x} = o(\mathbf{f})$ from the Corollary of Theorem 3. But this condition is equivalent to $\mathbf{x} \in \mathbf{g}^+$. Finally, (iv) is immediate from (iii); conversely, if $\mathbf{x}(a)$ is positive or negative, then it remains so for $t > a$. This completes the proof.

COROLLARY. *If $\mathbf{x}(t)$ is an ultimately positive or negative solution of (2)-(2'), then $\mathbf{x}(t) \sim c\mathbf{f}(t)$ as $t \to +\infty$ for some constant c.*

Proof. Let $\mathbf{u}^1, \mathbf{u}^2, \ldots, \mathbf{u}^{n-1}$ be a set of linearly independent solutions in $\mathbf{g}^+$. These, together with $\mathbf{f}$, form a basis of solutions of (2)-(2'). Then $\mathbf{x} = c_1\mathbf{u}^1 + c_2\mathbf{u}^2 + \cdots + c_{n-1}\mathbf{u}^{n-1} + c_n\mathbf{f}$ for suitable constants $c_1, \ldots, c_n$. From Theorem 4, each $\mathbf{u}^i = o(\mathbf{f})$. Since $\pm\mathbf{x}$ is ultimately positive, $c_n \neq 0$.

II. The Third-Order Case

5. General Results. We now restrict our attention to the third-order case of (2)-(2'):

$$dx_i/dt = p_i(t)\, x_{i+1}, \qquad i = 1, 2, 3, \tag{15}$$

$$0 < m \leqslant p_i \leqslant M. \tag{15'}$$

Letting $\mathbf{g}(t) = (g_1, g_2, g_3)^T$ denote a positive solution of the adjoint (14) with $n = 3$ now, we consider the subspace $\mathbf{g}^+(t)$ of all solutions $\mathbf{x}(t)$ of (15)-(15') which satisfy

$$g_1(t)\, x_1(t) + g_2(t)\, x_2(t) + g_3(t)\, x_3(t) = 0. \tag{16}$$

This condition characterizes the oscillatory solutions, i.e., the solutions whose components each have arbitrarily large positive zeros.

THEOREM 5. *A solution of (15)-(15') is oscillatory if and only if it satisfies (16), where $\mathbf{g}(t)$ is a positive solution of (14).*

Proof. It is immediate from Theorem 4 that any oscillatory solution of (15)-(15') satisfies (16). To prove the converse, suppose there were a solution $\mathbf{x}(t)$ which satisfied (16) and did not oscillate. With no loss in generality, we may then assume that for some suitable t_0, $x_1(t) > 0$, $x_2(t) \geqslant 0$, and $x_3(t) \leqslant 0$ for all $t \geqslant t_0$. Then, from (15)-(15'), $0 < x_1 \uparrow$, and $x_3 \uparrow \text{const.} \leqslant 0$,

Thus $\liminf_{t\to\infty} x_3' = 0$. Since $x_3' = p_3 x_1$ and $p_3 \geqslant m > 0$, we arrive at the contradiction that $\liminf_{t\to\infty} x_1 = 0$. (Similarly, (16) implies that each $x_i(t)$ vanishes infinitely often as t *decreases*). This completes the proof.

Thus the oscillatory solutions of (15)-(15′) *comprise* the plane $\mathbf{g}^{\perp}(t)$ orthogonal to $\mathbf{g}(t)$. This is noteworthy in that the oscillatory solutions do *not* generally form a subspace. More typical in this respect is the system

$$d\mathbf{x}/dt = \begin{pmatrix} 0 & 1 & 0 \\ 0 & 0 & 1 \\ -1 & -1 & -1 \end{pmatrix} \mathbf{x}$$

which has a basis of solutions

$$\mathbf{x}^1 = e^{-t}\begin{pmatrix} 1 \\ -1 \\ 1 \end{pmatrix}, \qquad \mathbf{x}^2 = \begin{pmatrix} \cos t \\ -\sin t \\ -\cos t \end{pmatrix}, \qquad \mathbf{x}^3 = \begin{pmatrix} \sin t \\ \cos t \\ -\sin t \end{pmatrix}.$$

Thus the solutions $\mathbf{x}^1 + \mathbf{x}^2$ and $\mathbf{x}^2$ are oscillatory, but their difference is not. This example is also typical in that the components of oscillatory solutions (as $t \to +\infty$) do not generally vanish infinitely often as $t \to -\infty$, in contrast to the behavior of the oscillatory solutions of (15)-(15′).

Since the oscillatory solutions of (15)-(15′) lie in the plane $\mathbf{g}^{\perp}(t)$, which makes them linearly independent of $\mathbf{f}$, we obtain a natural basis of solutions.

THEOREM 6. *Any two linearly independent oscillatory solutions of the third-order positive cyclic system* (15)-(15′) *constitute, together with any positive solution, a basis of solutions.*

The equivalence of the space of oscillatory solutions and the plane $\mathbf{g}^{\perp}$ has other consequences. Following are two which are immediate from Theorem 4.

COROLLARY 1. *If* $\mathbf{x}(t)$ *is a nonoscillatory solution of* (15)-(15′), *then* $\mathbf{x}(t) \sim c\mathbf{f}(t)$ *as* $t \to +\infty$, *where* $\mathbf{f}$ *is any positive solution and* c *is a suitable constant.*

COROLLARY 2. *A solution* $\mathbf{u}(t)$ *of* (15)-(15′) *is oscillatory if and only if* $\mathbf{u} = o(\mathbf{f})$ *as* $t \to +\infty$.

6. DECREASING t. As $t \to -\infty$, on the other hand, it is the oscillatory solutions which are dominant. The following results are the duals, as $t \to -\infty$, of some results stated above. Some of them are related to results of Lazer [6]; note that his x plays the role of our $-t$. See especially his Theorems 1.4, 1.5, and 2.3.

LEMMA 2. *Let* $\mathbf{u}(t)$ *be any oscillatory solution and let* $\mathbf{f}(t)$ *be any positive solution of* (15)-(15′). *Then* $\mathbf{f}(t) = o(\mathbf{u}(t))$ *as* $t \to -\infty$.

Proof. Let $\mathbf{v}$ be an oscillatory (for negative t) and $\mathbf{g}$ a positive solution of the adjoint (14); select $\mathbf{v}$ so that the inner product $(\mathbf{u}(0), \mathbf{v}(0)) \neq 0$. By the dual of Corollary 2 above, $\mathbf{v} = o(\mathbf{g})$ as $t \to -\infty$. From Lemma 1,

$$(\mathbf{f}, \mathbf{g}) = |\mathbf{f}|\,|\mathbf{g}| \cos \alpha(t) \equiv \text{const.}$$

$$(\mathbf{u}, \mathbf{v}) = |\mathbf{u}|\,|\mathbf{v}| \cos \beta(t) \equiv \text{const.},$$

whence

$$|\mathbf{f}|/|\mathbf{u}| = \text{const.}\,|\mathbf{v}| \cos \beta/|\mathbf{g}| \cos \alpha. \tag{17}$$

Since $\mathbf{v} = o(\mathbf{g})$ as $t \to -\infty$, and since $\mathbf{f}$ and $\mathbf{g}$ can be shown to be bounded away from the coordinate planes (cf. Section 8), $\cos \alpha \geqslant \epsilon > 0$. Hence the right side of (17) tends to 0; i.e., $\mathbf{f} = o(\mathbf{u})$ as $t \to -\infty$.

COROLLARY 1. *Let* $\mathbf{x}(t)$ *be any solution, and let* $\mathbf{u}(t)$ *and* $\mathbf{v}(t)$ *be linearly independent oscillatory solutions of* (15)-(15′). *Then either*: (i) $\mathbf{x}(t) \sim a\mathbf{u}(t) + b\mathbf{v}(t)$ *as* $t \to -\infty$ *for suitable constants* a *and* b, *or* (ii) $\mathbf{x}(t)$ *is either positive or negative.*

Proof. Since $\mathbf{f}$, $\mathbf{u}$, and $\mathbf{v}$ form a basis from Theorem 6, $\mathbf{x} = a\mathbf{u} + b\mathbf{v} + c\mathbf{f}$ for suitable constants a, b, c. Then

$$\frac{|\mathbf{x} - (a\mathbf{u} + b\mathbf{v})|}{|a\mathbf{u} + b\mathbf{v}|} = \frac{|c\mathbf{f}|}{|a\mathbf{u} + b\mathbf{v}|} \to 0$$

as $t \to -\infty$, from Lemma 2.

This, together with the parenthetical remark in the proof of Theorem 5, immediately yields

COROLLARY 2. *Any solution of* (15)-(15′) *which is neither positive nor negative is oscillatory as* $t \to -\infty$.

Corollary 2 of Theorem 6 and Corollary 1 above have the following duals.

COROLLARY 3. *Let* $\mathbf{v}(t)$ *be any oscillatory solution of* (14)-(14′) *with* $n = 3$, *and let* $\mathbf{g}(t)$ *be a positive solution. Then* $\mathbf{g}(t) = o(\mathbf{v}(t))$ *as* $t \to +\infty$.

COROLLARY 4. *Let* $\mathbf{y}(t)$ *be any solution of* (14)-(14′) *with* $n = 3$, *and let* $\mathbf{u}(t)$ *and* $\mathbf{v}(t)$ *be any two linearly independent oscillatory solutions. Then either*: (i) $\mathbf{y} \sim a\mathbf{u} + b\mathbf{v}$ *as* $t \to +\infty$ *for appropriate constants* a *and* b, *or* (ii) $\mathbf{y}(t)$ *is positive or negative* (*for all* t).

7. Oscillatory Solutions. Any oscillatory solution of (15) satisfies (16) and, if nontrivial, must therefore have components of both signs. Since $-\mathbf{x}(t)$ also satisfies (16), we can assume two positive components and one negative component for an arbitrary $t = t_0$ where all $x_i(t_0) \neq 0$. By cyclic symmetry, we can assume $x_1(t_0) > 0$, $x_2(t_0) > 0$, and $x_3(t_0) < 0$. By positivity, this implies $dx_1/dt > 0$, $dx_2/dt < 0$ and $dx_3/dt > 0$ at t_0 ; hence x_1 cannot change sign until x_2 does. By (16), however, x_3 cannot become positive until x_1 or x_2 becomes negative. Hence x_2 must change sign first. Generalizing by cyclic symmetry and replacement of $\mathbf{x}(t)$ by $-\mathbf{x}(t)$, we find that as t increases, each sign change must affect the second of the two components having like sign. This yields the following result.

Theorem 7. *If $\mathbf{x}(t)$ is any nontrivial oscillatory solution of* (15), *then the signs of its components permute cyclically*:
$(+, +, -)$, $(+, -, -)$, $(+, -, +)$, $(-, -, +)$, $(-, +, +)$, $(-, +, -)$, *etc. Hence the x_i's vanish cyclically, in increasing order mod* 3 *and, as t increases, $\mathbf{x}(t)$ rotates clockwise as viewed from the positive octant.*

Figure 1 shows a typical solution $\mathbf{x}(t)$ of (15) with positive component $\mathbf{f}(t)$ and oscillatory component $\mathbf{u}(t)$ lying in $\mathbf{g}^{\perp}(t)$.

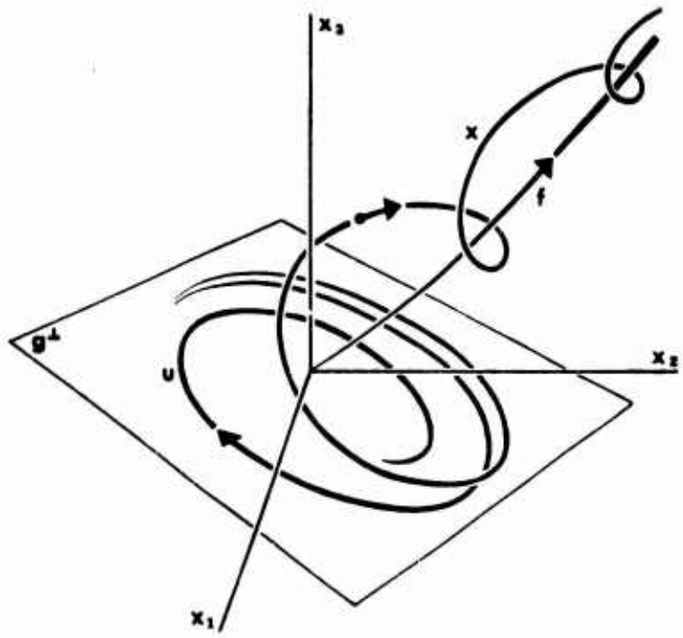


Fig. 1

The following observation is of help in the qualitative study of the order of magnitude of oscillatory solutions of (15). Let $X(t)$ be any matrix solution of (15). Since

$$\det X(t) = \det X(0) \exp\left(\int_0^t \operatorname{Tr} P(s)\, ds\right)$$

and $\operatorname{Tr} P(s) \equiv 0$, the mapping which takes $X(0)$ into $X(t)$ is volume preserving.

In particular, if (15′) holds and the columns of the matrix

$$X = \begin{pmatrix} f_1 & u_1 & v_1 \\ f_2 & u_2 & v_2 \\ f_3 & u_3 & v_3 \end{pmatrix}$$

are the positive solution $\mathbf{f}$ of (15) and two oscillatory solutions $\mathbf{u}$ and $\mathbf{v}$, then the parallelepiped spanned by $\mathbf{f}$, $\mathbf{u}$, $\mathbf{v}$ has constant volume for all t. Since $\mathbf{f}(t)$ grows exponentially and is bounded away from $\mathbf{g}^{\perp}$ (see Section 8), the area of the parallelogram determined by the two oscillatory solutions approaches zero exponentially. It does not follow, however, that every oscillatory solution tends to zero, as the following example shows.

Example 2. In the interval $0 < t < t_0 = \pi/\sqrt{3}$, consider the system

$$\mathbf{x}'(t) = C\mathbf{x}, \qquad C = \begin{pmatrix} 0 & c_1 & 0 \\ 0 & 0 & c_2 \\ c_3 & 0 & 0 \end{pmatrix}$$

where, in terms of the arbitrary constant $k > 1$,

$$c_1 = \frac{1}{k(e^{2t_0} + \sqrt{3}e^{t_0/2})}, \qquad c_2 = \frac{1}{k}(e^{-2t_0} + \sqrt{3}e^{-t_0/2}),$$

$$c_3 = k^2 \frac{e^{2t_0} + \sqrt{3}e^{t_0/2}}{e^{-2t_0} + \sqrt{3}e^{-t_0/2}}.$$

The coefficient matrix C is then permuted cyclically in $(t_0, 2t_0)$, etc. It is easily confirmed that the solution initially at $(1, -ke^{2t_0}, 0)^T$ goes into $k(0, -1, ke^{2t_0})^T$ at time t_0 ; i.e.,

$$e^{Ct_0}\begin{pmatrix} 1 \\ -ke^{2t_0} \\ 0 \end{pmatrix} = k\begin{pmatrix} 0 \\ -1 \\ ke^{2t_0} \end{pmatrix}.$$

Now if we permute c_1 , c_2 , c_3 and x_1 , x_2 , x_3 cyclically, we obtain a piecewise

continuous differential system and an oscillatory solution whose magnitude at nt_0 increases exponentially; i.e., $|\mathbf{x}(n\pi/\sqrt{3})| = k^n |\mathbf{x}(0)|$.

Although an oscillatory solution may grow like k^n for any $k > 0$, it must still be of smaller order than the positive solution, as the Corollary of Theorem 3 shows.

The bounds on the periods, in contrast to the magnitude, of an oscillatory solution permit a more quantitative analysis. We first introduce the following definitions. The triplet of signs $\mathbf{s}(t) \equiv (\operatorname{sgn} x_1, \operatorname{sgn} x_2, \operatorname{sgn} x_3)$ of the components of a solution $\mathbf{x}(t)$ will be called the *signature* of x. If $\mathbf{s}(t_1) = \mathbf{s}(t_2)$ for $t_2 > t_1$ and a component of $\mathbf{s}(t_i)$ is zero, then $t_2 - t_1$ will be called a *signature cycle* of $\mathbf{x}$. A *phase* is a maximum t-interval of constant signature. By Theorem 7, the signature of a solution changes cyclically in six phases.

THEOREM 8. *Let* $\mathbf{g}(t)$ *be a positive solution of* (14) *and* $\mathbf{u}(t)$ *an oscillatory solution of* (15)-(15′). *Then the duration of any phase of* $\mathbf{u}$ *is at least* $\inf_{i,j,t}(g_i/Mg_j)$.

Proof. We shall determine the interval between a zero of u_i and the next zero of u_{i+1}. Without loss in generality, suppose $\mathbf{u}(t_1) = (0, 1, -k)^T$ and $\mathbf{u}(t_2) = (a, 0, -b)^T$ for suitable positive a, b, k. Then from (15)-(15′),

$$0 = u_2(t_2) = 1 + \int_{t_1}^{t_2} p_2(s)\, u_3(s)\, ds$$

$$\geqslant 1 - Mk(t_2 - t_1)$$

whence $t_2 - t_1 \geqslant 1/Mk$. But $u_1g_1 + u_2g_2 + u_3g_3 \equiv 0$. Thus $k = g_2(t_1)/g_3(t_1)$, and $t_2 - t_1 \geqslant \inf(g_i/Mg_j)$.

8. *N*-STABLE POSITIVE CONES. To prove the positivity of $\inf(f_i/f_j)$ and $\inf(g_i/g_j)$ for $i, j = 1, 2, 3$ and $-\infty < t < +\infty$, we shall introduce another concept, expressed in terms of the $N = M/m$ of (2′).

DEFINITION. *An N-stable positive cone* is a closed cone C in the positive octant with the following *stability* property: if $\mathbf{x}(t)$ is a solution of (15)-(15′) with $M = Nm$, and $\mathbf{x}(a) \in C$, then $\mathbf{x}(t) \in C$ for all $t \geqslant a$.

LEMMA 3. *If* C *is any N-stable positive cone, then* $\mathbf{f}(t) \in C$ *and* $\mathbf{g}(t) \in C$, *where* $\mathbf{f}$ *and* $\mathbf{g}$ *are positive solutions of* (2) *and* (14) *respectively.*

Proof. For any $T > 0$ and t_0, and any solution $\mathbf{x}(t)$ of (2) with $\mathbf{x}(t_0 - T) \in C$, we may consider $\Theta(t) = \Theta(\mathbf{x}(t), \mathbf{f}(t))$, Hilbert's projective quasi-metric ([2], p. 381). By uniform semiprimitivity, $\Theta(t_0) < \epsilon$ for sufficiently large $T = T(\epsilon)$, yet $\mathbf{x}(t_0) \in C$. Since C is closed (in the projective

quasi-metric), this implies $\mathbf{f}(t_0) \in C$. But t_0 was arbitrary; hence $\mathbf{f}(t) \in C$. From the dual behavior of the adjoint, the same is true of $\mathbf{g}(t)$.

Clearly, the (closed) positive octant Δ is N-stable. To construct an N-stable positive cone in the *interior* of Δ, we now define the pseudo-Liapounov function

$$U = x_1/x_2 + x_2/x_3 + x_3/x_1 \tag{18}$$

in Int Δ. This function has the property that $U = 3$ when $x_1 = x_2 = x_3$ and $U > 3$ elsewhere. Differentiating both sides of (18), we compute

$$dU/dt = \sum p_i(t)[1 - x_{i+1}x_{i+2}/x_i^2]. \tag{19}$$

If $x_i^2 \leqslant x_{i+1}x_{i+2}/3N$ for even one i, then $dU/dt \leqslant 0$ at $\mathbf{x}$, since in that event the corresponding negative term dominates the sum of all three terms. We therefore define the domain $E \subset \Delta$ by

$$E = \{\mathbf{x} \mid \mathbf{x} > \mathbf{0} \text{ and } x_i^2 \leqslant x_{i+1}x_{i+2}/3N \text{ for some } i = 1, 2, 3\}, \tag{20}$$

with the assurance that

$$dU/dt \leqslant 0 \qquad \text{in} \quad E.$$

Now consider the closure $\overline{\Delta - E}$ of the set-theoretic complement of E:

$$\Delta - E = \{\mathbf{x} \mid \mathbf{x} > \mathbf{0} \text{ and } x_i^2 > x_{i+1}x_{i+2}/3N \text{ for all } i = 1, 2, 3\}. \tag{21}$$

This is a curvilinear triangular cone strictly *interior* to Δ; hence

$$\operatorname{Max}_{\mathbf{x} \in \overline{\Delta - E}} U(\mathbf{x}) \equiv A < +\infty. \tag{22}$$

Finally, we define the cone $C \supset \overline{\Delta - E}$ as the domain

$$C = \{\mathbf{x} \mid \mathbf{x} \geqslant \mathbf{0} \text{ and } U(\mathbf{x}) \leqslant A\}. \tag{23}$$

Clearly C is closed and lies in the interior of the positive octant. Moreover, this domain is N-stable because its boundary lies in E, whence $dU/dt \leqslant 0$ on it. This proves the following result.

THEOREM 9. *If A is defined by* (21)-(22), *then the interior cone* $C = \{\mathbf{x} \mid \mathbf{x} \geqslant \mathbf{0}$ and $U(\mathbf{x}) < A\}$ *is N-stable.*

This, together with Lemma 3, gives us the

COROLLARY. *The components of the positive solutions* $\mathbf{f}$ *and* $\mathbf{g}$ *of* (15)-(15′) *and its adjoint satisfy* $1/A^2 < x_i/x_j < A^2$, $A = 3N + 1 + 1/3N$.

Proof. Let $\mathbf{x}$ be any solution of (15)–(15′) lying in C. It can be shown that in $\overline{\Delta - E}$, $U(\mathbf{x})$ attains its maximum value A at any vertex of $\overline{\Delta - E}$, whence

$$A = U(3N, 1, 1) = 3N + 1 + 1/3N.$$

But $x_i/x_{i+1} < U \leqslant A$, so $x_{i+1}/x_i > 1/A$ for each i. Furthermore,

$$x_i/x_{i+1} = 1/(x_{i+1}/x_{i+2})(x_{i+2}/x_i) > 1/A^2.$$

Consequently, $x_i/x_j > 1/A^2$ for each i, j. Clearly then $x_i/x_j < A^2$ for all i, j. An application of Lemma 3 completes the proof for $\mathbf{f}$. The same inequalities for $\mathbf{g}$ follow from the dual behavior of the adjoint.

Actually, we have computed the *minimal* stable cone by other methods for the family of positive cyclic systems (15)-(15′). These methods will be described in another paper.

References

1. Birkhoff, G. D., On solutions of ordinary linear homogeneous differential equations of the third order. *Ann. Math.* **12** (1911), 103–127.
2. Birkhoff, G., "Lattice Theory", 3rd ed., *Am. Math. Soc.*, 1967.
3. Birkhoff, G. and Kotin, L., Essentially positive systems of linear differential equations. *Bull. Amer. Math. Soc.* **71** (1965), 771–772.
4. Birkhoff, G. and Kotin, L., Linear second order differential equations of positive type. *J. d'Analyse Math.* **18** (1967), 43–52.
5. Coddington, E. A. and Levinson, N., "Theory of Ordinary Differential Equations." McGraw-Hill, New York, 1955.
6. Lazer, A. C., The behavior of solutions of $y''' + p(x)y' + q(x)y = 0$. *Pacific J. Math.* **17** (1966), 435–66.
7. Sansone, G., Studi sulle equazioni differenziali lineari omogenee di terzo ordine nel campo reale. *Univ. Nac. Tacumán. Revista A.* **6** (1948), 195–253.

PERTURBATIONS OF FUNCTIONAL DIFFERENTIAL SYSTEMS

G. A. Shanholt*
U. S. Army Engineer Topographic Laboratories
Fort Belvoir, Virginia

1. INTRODUCTION. In a recent series of papers [1-4], A. Strauss and J. A. Yorke have investigated "eventual" stability properties for systems of ordinary differential equations. In this paper, we extend two of their results to functional differential systems.

The following notation will be used in this paper: E^n is the space of n-vectors, and for x in E^n, $|x|$ denotes any vector norm. For a given number $\tau > 0$, C denotes the linear space of continuous functions mapping the interval $[-\tau, 0]$ into E^n, and for ϕ in C, $||\phi|| = \sup |\phi(\theta)|$, $-\tau \leq \theta \leq 0$. For $H > 0$, C_H denotes the set of ϕ in C for which $||\phi|| < H$. For any continuous function $x(u)$ whose domain is $-\tau \leq u \leq a$, $a \geq 0$, and whose range is in E^n, and any fixed t, $0 \leq t \leq a$, the symbol x_t will denote the function $x_t(\theta) = x(t + \theta)$, $-\tau \leq \theta \leq 0$; that is, x_t is in C, and is that segment of the function $x(u)$ defined by letting u range in the interval $t - \tau \leq u \leq t$.

Let $F(t, \phi)$ be a function defined on $D_H = [0, \infty) \times C_H$ into E^n, and let $\dot{x}(t)$ denote the right hand derivative of $x(u)$ at $u = t$. Consider the functional differential system

$$\dot{x}(t) = F(t, x_t). \tag{1.1}$$

Let (s, ϕ) be in D_H. A function $x(s, \phi)(t)$ is said to be a solution of (1.1) with initial function ϕ at $t = s$ if there exists a number $b > 0$ such that

i) for each t, $s \leq t < s + b$, $x_t(s, \phi)$ is defined and in C_H;

ii) $x_s(s, \phi) = \phi$;

iii) $x(s, \phi)(t)$ satisfies (1.1) for $s \leq t < s + b$.

---

*Dr. G. A. Shanholt is now at the Radar Research Department, Bell Telephone Laboratories, Whippany, New Jersey 07981.

PRECEDING PAGE BLANK

$x(s, \phi)(t)$ is unique if every other solution with the same initial function ϕ at $t = s$ agrees with $x(s, \phi)(t)$ in their common domain of definition.

If F is continuous on D_H, then for every (s, ϕ) in D_H there is at least one solution of (1.1) with initial function ϕ at $t = s$ [7]. If, moreover, F is Lipschitzian in ϕ, i.e., there is a constant L such that for every ϕ_1, ϕ_2 in C_H

$$| F(t, \phi_1) - F(t, \phi_2)| \leq L || \phi_1 - \phi_2|| \tag{1.2}$$

for $t \geq 0$, then there is only one such solution. Generally, under such assumptions, one can only expect a solution to exist over a finite interval.

2. PRELIMINARIES. We now define the stability concepts to be used herein. These definitions are stated for equation (1.1) in which it is assumed that for some H, $0 < H \leq \infty$, F is continuous and Lipschitzian on D_H.

Definition 2.1. The origin is eventually uniformly stable (EvUS) if for every $\varepsilon > 0$, there exists $\delta = \delta(\varepsilon) > 0$ and $\alpha = \alpha(\varepsilon) \geq 0$ such that $||x_t(s, \phi)|| < \varepsilon$ for all $||\phi|| < \delta$ and $t \geq s \geq \alpha$. It is uniformly stable (US) if one can choose $\alpha(\varepsilon) = 0$.

Definition 2.2. The origin is eventually uniformly attracting (EvUA) if there exists constants $\eta > 0$ and $\beta \geq 0$, and if for every $\varepsilon > 0$ there exists a $T = T(\varepsilon) > 0$ such that $||x_t(s, \phi)|| < \varepsilon$ for $||\phi|| < \eta$, $s \geq \beta$, and $t \geq s + T$. It is uniformly attracting (UA) if one can choose $\beta = 0$.

Definition 2.3. The origin is eventually uniform-asymptotically stable (EvUAS) if it is both EvUS and EvUA. It is uniform-asymptotically stable (UAS) if it is both US and UA.

It should be noted that in the above definitions we do not assume that the zero function is a solution of (1.1). When the origin is US, this implies that the zero function is a unique solution of (1.1) for any $s \geq 0$. Thus, we see that EvUS (EvUAS) is a natural generalization of US (UAS) in which it is not assumed that the zero function is a solution. Finally, it is important to note that UA does not imply that the zero function is a solution [2, example 2.9].

Definition 2.4. Let $V(t, \phi)$ be a functional defined for (t, ϕ) in D_H. The derivative of V along solutions of (1.1) will be denoted by

$\dot{V}$ (1.1) $(t, x_t (s, \phi))$ and is defined to be

$$\dot{V} \text{ (1.1) } (t, s_t (s, \phi)) = \limsup_{h \to 0+} \frac{1}{h} \left[V(t+h, x_{t+h}(s, \phi)) - V (t, x_t(s, \phi)) \right] .$$

If F is continuous and Lipschitzian, and if the origin is either EvUS or EvUAS, then the existence of a Lyapunov type functional can be established. By following D. Wexler [5] and A. Halanay [6], one easily proves the following two theorems.

Theorem 2.1. Let F be continuous and Lipschitzian on D_H, and let the origin be EvUS. Then there exists a number K, $0 < K < H$, and a functional $V (t, \phi)$ with the following properties:

1. There exists functions a(r), b(r) continuous, positive, and monotone increasing for $r > 0$, with $a(0) = b(0) = 0$, such that for m in (0, K],

$$a (||\phi||) \leq V(t, \phi) \leq b (||\phi||)$$

for $m \leq ||\phi|| \leq K$, $t \geq d (m)$, where d(r) is a continuous, nonnegative, and nonincreasing function for $r > 0$.

2. $V (t, x_t (s, \phi))$ is a monotone-decreasing function of t for $||\phi|| \leq K$, $t \geq s \geq d (k)$.

Theorem 2.2. Let F be continuous and Lipschitzian on D_H, and let the origin be EvUAS. Then there exists a number K, $0 < K < H$, and a functional $V(t, \phi)$ satisfying the conclusions of the above theorem, with the additional properties.

1. There exists a function c(r) continuous, positive, and monotone-increasing for $r > 0$, with $c(0) = 0$, such that

$$\dot{V} (1.1)(t, x_t (s, \phi)) \leq - c (||x_t (s, \phi)||)$$

for $||\phi|| \leq K$, $t \geq s \geq d (k)$.

2. $| V (t, \phi_1) - V (t, \phi_2) | \leq M(r) || \phi_1 - \phi_2 ||$

for $0 < r \leq || \phi_i || \leq K$, $t \geq d(k)$, where M(r) is continuous and monotone-decreasing on (0,K].

3. PERTURBED EQUATIONS. We now prove two theorems which show that the eventual stability behavior of the origin of the nominal equation

$$\text{(N)} \qquad \dot{y}(t) = F(t, y_t)$$

is preserved for the perturbed equation

$$\text{(P)} \qquad \dot{x}(t) = F(t, x_t) + G(t, x_t)$$

when F and G satisfy certain conditions.

Consider the conditions

(A): For every m, $0 < m < H$, there exists $\gamma_m \geq 0$ and a function $g_m(t)$ continuous on $[\gamma_m, \infty)$ such that for $m \leq ||\phi|| < H$, $t \geq \gamma_m$

$$| G(t, \phi) | \leq g_m(t) \text{ and } \int_{\gamma_m}^{\infty} g_m(t)\, dt < \infty.$$

(B): For every m, $0 < m < H$, there exists $\gamma_m \geq 0$ and a function $g_m(t)$ continuous on $[\gamma_m, \infty)$ such that for $m \leq ||\phi|| < H$, $t \geq \gamma_m$

$$| G(t, \phi) | \leq g_m(t) \text{ and}$$

$$I_m(t) = \int_t^{t+1} g_m(s)\, ds \to 0 \text{ as } t \to \infty.$$

REMARKS. If condition (A) is satisfied, then so is condition (B). Moreover, if $g_m(t) \to 0$ as $t \to \infty$, then also condition (B) is satisfied. Condition (B), however, does not imply (A) [1, example 3.3].

In [3], Strauss and Yorke proved:

Theorem 3.1. If the origin is US for the continuous linear system

$$\dot{x}(t) = A(t)\, x(t)$$

and if G (t, x), which is continuous on [0, ∞) x E^n, satisfies the condition that for some r > 0 and every m satisfying 0 < m < r there exists a function g_m (t) continuous for t ≥ 0 such that for m ≤ |x| ≤ r, t ≥ 0

$$| G (t, x) | \leq g_m (t) \text{ and } \int_0^\infty g_m (t)\, dt < \infty,$$

then the origin is EvUS for

$$\dot{x} (t) = A (t) x (t) + G (t, x (t)).$$

We now extend theorem 3.1 to functional differential equations.

Theorem 3.2. Suppose that F and G are continuous and Lipschitzian on D_H, that G satisfies condition (A), that the origin is EvUS for (N), and that a functional V(t, φ) whose existence is guaranteed by theorem 2.1 satisfies condition 2 of theorem 2.2. Then the origin is EvUS for (P).

PROOF. Let 0 < ε ≤ K, and choose $||\phi|| < \delta (\varepsilon) = b^{-1} (a (\varepsilon) /2)$, α (ε) = max (d (δ), θ (ε)), where θ (ε) ≥ γ_δ and is such that

$$\int_\theta^\infty g_\delta (t)\, dt < \frac{a (\varepsilon)}{2LM (\delta)} .$$

Then for t ≥ s ≥ α(ε), $|| x_t (s, \phi) || < \varepsilon$. Suppose chis is not the case, i.e., for some t ≥ s $|| x_t (s, \phi) || = \varepsilon$. Let q be the first t-value greater than s for which $|| x_q (s, \phi) || = \varepsilon$, and let p be the last t-value less than q for which $|| x_p (s, \phi) || = \delta$. Then

$$\delta \leq || x_t (s, \phi) || \leq \varepsilon, \; p \leq t \leq q. \tag{3.1}$$

For t in an interval on which x (s, φ) (t) exists, we evaluate

$$\dot{V}_{(P)} (t, x_t (s, \phi))$$

$$\leq \dot{V}_{(N)} (t, y_t (t, x_t (s, \phi))) +$$

$$+ \limsup_{h \to 0^+} \frac{1}{h} \Big| V(t+h,\ x_{t+h}(t, x_t(s, \phi))) - V(t+h,\ y_{t+h}(t, x_t(s, \phi))) \Big|$$

$$- \limsup_{h \to 0^+} \frac{M}{h} \Big| \| x_{t+h}(t, x_t(s, \phi)) - y_{t+h}(t, x_t(s, \phi)) \| \Big|$$

since V is Lipschitzian and decreasing along solutions of equation (N). By assuming - with no loss of generality - that the Lipschitz constant L is greater than one, the result on pages 340-1 of Halanay's book [6] when used in the above inequality yields

$$\dot{V}_{(P)}(t, x_t(s, \phi)) \leq L M \, | G(t, x_t(s, \phi)) | .$$

By integrating both sides of the above inequality from p to q, and by using condition (A) and equation (3.1), we obtain

$$V(q, x_q(s, \phi)) \leq V(p, x_p(s, \phi)) + L M \int_q^p g_\delta(t)\, dt$$

$$a(\varepsilon) \leq b(\delta) + L M \int_\theta^\infty g_\delta(t)\, dt$$

$$a(\varepsilon) < \frac{a(\varepsilon)}{2} + \frac{a(\varepsilon)}{2} = a(\varepsilon).$$

Thus, we arrive at a contradiction, and this proves the theorem.

The second result of Strauss and Yorke [2] which we shall extend is

Theorem 3.3. If F (t, x) and G (t, x) are continuous in the cylinder $(0, \infty) \times \{x : |x| < H\}$, if F is Lipschitzian, and if G satisfies the condition that for some $r > 0$ and every m satisfying $0 < m < r$, there exists a function $g_m(t)$ continuous on $(0, \infty)$ such that for $t \geq 0$,

$m \leq |x| \leq r$

$$| G (t, x) | \leq g_m (t), \int_t^{t+1} g_m (s)\, ds \to 0 \text{ as } t \to \infty,$$

then the EvUAS of the origin of

$$\dot{x} (t) = F (t, x (t))$$

implies the same stability property for

$$\dot{x} (t) = F (t, x (t)) + G (t, x (t)).$$

We now state and prove our extension.

Theorem 3.4. Suppose that F and G are continuous and Lipschitzian on D_H, that G satisfies condition (B), and that the origin is EvUAS for (N). Then the origin is EvUAS for (P).

PROOF. Define $J_m (t) = \sup (I_m (s) : t-1 \leq s < \infty)$ for $t \geq 1$. Condition (B) implies that $J_m (t) \to 0$ monotonically as $t \to \infty$.

Let $0 < \varepsilon \leq K$, and choose $||\phi|| < \delta (\varepsilon) = b^{-1} (a (\varepsilon) /2)$, $\theta = \theta (\varepsilon) \geq 0$ and such that

$$2 L M (\delta) J_\delta(t) < \min (a (\varepsilon), c (\delta)) \tag{3.2}$$

for $t \geq \theta$. Then for $t \geq s \geq \alpha (\varepsilon) = \max (1, \theta (\varepsilon), d (\delta))$, $|| x_t (s, \phi) || < \varepsilon$. Suppose not, i.e., there exists t-values p and q, as defined in the proof of theorem 3.2, which satisfy inequality (3.1). Proceeding as before, we find that

$$\dot{V}_{(P)} (t, x_t (s, \phi)) \leq \dot{V}_{(N)} (t, y_t (t, x_t (s, \phi))) + L M | G (t, x_t(s, \phi)) |$$

$$\leq -c (|| x_t (s, \phi) ||) + L M | G (t, x_t (s, \phi)) |.$$

Using equation (3.1) and condition (B), we have upon integrating the above from p to q

$$a (\varepsilon) \leq b (\delta) - (q-p)\, c (\delta) + L M \int_p^q g_\delta (t)\, dt. \tag{3.3}$$

Using the easily shown fact that

$$\int_u^t g_m(s)\,ds \leq \int_{u-1}^t I_m(s)\,ds,\quad t \geq u \geq 1,$$

and equations (3.2) and (3.3), we see that

$$a(\varepsilon) \leq b(\delta) - (q-p)\,c(\delta) + L\,M\,(q-p+1)\,J_\delta(p)$$

$$a(\varepsilon) < b(\delta) + a(\varepsilon)/2 = a(\varepsilon).$$

Hence, we arrive at a contradiction which shows that the origin is EvUS.

Let $\eta = \delta(K)$, $\beta = \alpha(K)$, and

$$T(\varepsilon) = \alpha(\varepsilon) + 2\,(L\,M\,J_\delta(1) + b(K))/c(\delta). \tag{3.4}$$

Consider $s \geq \beta$ and $||\phi|| < \eta$. Thus, the solution $x(s, \phi)(t)$ exists for all $t \geq s$. Moreover, since the origin is EvUS, to prove EvUA it is sufficient to show the existence of a u, $s + \alpha \leq u \leq s + T$, such that $||x_u(s, \phi)|| < \delta(\varepsilon)$. Assume the contrary, i.e.,

$$\delta \leq ||x_t(s, \phi)|| \leq K,\quad s + \alpha \leq t \leq s + T.$$

Employing the same procedure as above, we arrive at the estimate

$$a(\delta) < b(K) - (T-\alpha)\,c(\delta) + M\,L\,(T-\alpha+1)\,J_\delta(s+\alpha).$$

Using the monotonicity of J_δ and equations (3.2) and (3.4) we compute

$$a(\delta) < b(K) - \frac{c(\delta)}{2}(T-\alpha) + M\,L\,J_\delta(1) = 0.$$

This contradiction then completes the proof of this theorem.

REMARK. The author wishes to acknowledge that the proofs given herein were modeled on those of A. Strauss and J. A. Yorke.

REFERENCES

1. Strauss, A. and Yorke, J. A., Perturbation Theorems for Ordinary Differential Equations, J. Differential Equations 3 (1967), 15-30.

2. Strauss, A. and Yorke, J. A., Perturbing Uniform Asymptotically Stable Nonlinear Systems, U. Maryland Tech. Note BN-539, 1968.

3. Strauss, A. Yorke, J. A., Perturbing Uniformly Stable Linear Systems with and Without Attraction, U. Maryland Tech. Note BN-540, 1968.

4. Strauss, A. and Yorke, J. A., Perturbing Asymptotically Stable Differential Equations, Bull. Amer. Math. Soc. 74 (1968), 992-996.

5. Wexler, D., Note on the Eventual Stability, Rev. Roum. Math. Pures et Appl. 11 (1966), 819-824.

6. Halanay, A., Differential Equations, Academic Press, New York, 1966.

7. Oguztoreli, N. N., Time-Lag Control Systems, Academic Press, New York, 1966.

STRESS WAVE PROPAGATION IN A CLASS OF NONHOMOGENEOUS ELASTIC MEDIA*

Shun-Chin Chou
Army Materials and Mechanics Research Center
Watertown, Massachusetts

R. Greif
Tufts University, Medford, Massachusetts

D. E. Johnson
Avco Corporation, Wilmington, Massachusetts

ABSTRACT. A scheme for changing one of the independent variables is used to transform the curvilinear characteristics associated with continuously nonhomogeneous material properties into straight lines of equal slope. By using this scheme some of the practical difficulties caused by curvilinear characteristics are alleviated. The characteristic relations and appropriate jump conditions in the transformed space-time plane are derived for a hyperbolic system of quasi-linear partial differential equations of first order for two functions of two independent variables. The resulting equations are solved numerically. Accurate results are obtained for several cases in which previous investigators had encountered difficulties. In addition to checking against existing solutions, the method is also applied to problems for which solutions had not previously been obtained.

INTRODUCTION. Recently, there has been a great deal of research done on stress wave propagation in various types of elastic media. Analytical techniques usually incorporating transform methods have been successful on several problems[1], however, direct numerical analysis on the governing equations appears to be amenable to a wider class of problems. Examples of this latter procedure has been the work of P. C. Chou and Loenig[2] using the characteristic method, and S. C. Chou and Greif[3] using a technique which combines features of both the finite difference and characteristic methods. In these methods, the characteristic lines along which the stresses and velocities are related by total derivatives are straight lines of constant slope because of the homogeneity of the material. This property of straight line characteristics is a great simplification in the resulting numerical analysis since a constant time and space increment may be used throughout the entire region of interest. Consequently, even the nonhomogeneous multilayer stress wave problem can be done in a relatively straightforward manner as long as the properties remain constant within each layer.[3]

*This paper has been accepted by AIAA for publication.

PRECEDING PAGE BLANK

However, in recent aerospace applications a need has arisen for the analysis of stress wave propagation in bodies in which the material properties continuously vary with position. Accordingly, a certain class of bars in which the elastic modulus varies as a power of the spatial coordinate has been analyzed theoretically by Payton[4] and by Lindholm and Doshi[5]. In addition, the plane stress problem in polar coordinates in which rotary motion is caused by an axially symmetric shear loading applied at the inner circular hole of an elastic medium has been investigated. This cylindrical shear wave problem, in which the shear modulus varies as an arbitrary power of the radial coordinate, has been studied by Sternberg and Chakravorty[6] using a Laplace transform technique and by Chou and Schaller[7] using numerical integration of the characteristic equations.

All the foregoing nonhomogeneous problems have governing equations of hyperbolic type which may be solved by numerical integration of the characteristic equations along the characteristic lines. However, for these cases, the characteristics are curved lines in the space-time regime. Consequently, the grid size will vary as the numerical procedure continues and, indeed, if the curvature involved is too great, inaccurate results may be obtained as has been noted in Ref. 7. In the present paper, a method in a general form is introduced that will alleviate the difficulties caused by curvilinear characteristics. The essence of the method is to introduce a new independent variable to replace the space variable so that the characteristic lines in the new space-time regime are straight lines. The grid sizes now involved will be uniform, and accurate integration of the new characteristic equations along these characteristic lines may be easily accomplished.

To cover the widest class of problems, this method is introduced for a hyperbolic system of quasi-linear[8] partial differential equations of the first order for two functions of two independent variables. For this general system, characteristic relations are derived as well as the appropriate jump conditions across the characteristics. These latter conditions are necessary when the elastic media under study is subjected to an instantaneous disturbance in time. The numerical method of solution for this system is explained in detail so that specialized problems may be done in a uniform manner. Among the specialized cases for which numerical results are found are the previously mentioned cylindrical shear wave and plane wave problems, respectively. Results are checked against existing solutions with several discrepancies being explained. The method is then extended to problems involving geometries for which solutions have not been previously solved. For example, the important case of cylindrical shear waves in a structure with a finite outer boundary is solved for various types of nonhomogeneity and boundary conditions. In addition, several finite bar solutions are found for cases not previously done.

THEORETICAL ANALYSIS.

Characteristic Relations

For a wide class of stress wave problems the governing equations may be represented by the following system of quasi-linear partial differential equations of the first order for two functions of two independent variables

$$L_1 = A_1 s_r + B_1 s_t + C_1 v_r + D_1 v_t + E_1 = 0 \qquad (1)$$

$$L_2 = A_2 s_r + B_2 s_t + C_2 v_r + D_2 v_t + E_2 = 0 \qquad (2)$$

In these equations s and v represent stress and velocity, respectively, and the subscripts indicate differentiation with respect to either the space variable r or the time variable t. The coefficients A_1, A_2,... ...D_1, D_2 are assumed to be known functions of r, t while E_1 and E_2 are known functions of r, t and also possibly nonlinear functions of s and v. According to Courant and Hilbert[8] this particular type of quasi-linear system is called semi-linear. Of course, if E_1 and E_2 were linear functions of s and v the system would be linear. In equations (1) and (2) all functions are assumed to be continuous and to have as many continuous derivatives as required. It is further assumed that nowhere does $A_1/A_2 = B_1/B_2 = C_1/C_2 = D_1/D_2$. Following the work of Ref. (8), (9), and (10), the characteristic lines and characteristic forms of equations (1) and (2) will be found. Then the associated problem of propagation of discontinuities will be investigated.

In (1) and (2) s and v are differentiated with respect to both space and time and it would be advantageous to derive new equations each involving only total derivatives in a particular direction in the r, t plane. These lines are called the characteristic lines or "characteristics" and the equivalent equations written in these directions are called characteristic equations. A linear combination of L_1 and L_2 is formed as follows:

$$\begin{aligned} L &= \lambda L_1 + L_2 \\ &= (\lambda A_1 + A_2)\, s_r + (\lambda B_1 + B_2)\, s_t \\ &\quad + (\lambda C_1 + C_2)\, v_r + (\lambda D_1 + D_2)\, v_t + (\lambda E_1 + E_2) \end{aligned} \qquad (3)$$

where λ is to be found so that the partial derivatives in (3) combine to form total derivatives of s and v in the same direction as the characteristic line $r(\gamma)$, $t(\gamma)$ where γ is an arbitrary parameter. For these terms involving s and v to combine in the form

$$s_r r_\gamma + s_t t_\gamma = ds/d\gamma$$
$$v_r r_\gamma + v_t t_\gamma = dvd\gamma \tag{4}$$

it follows from (3) that

$$\frac{\lambda B_1 + B_2}{\lambda A_1 + A_2} = \frac{dt/d\gamma}{dr/d\gamma} \tag{5a}$$

$$\frac{\lambda D_1 + D_2}{\lambda C_1 + C_2} = \frac{dt/d\gamma}{dr/d\gamma} \tag{5b}$$

where dt/dr is the required slope of the characteristic line. Equating (5a) and (5b) forms a quadratic in λ which yields

$$\lambda_{\pm} = \frac{b \pm \sqrt{b^2 - 4ac}}{2a} \tag{6}$$

where

$$b = D_1 A_2 + D_2 A_1 - B_1 C_2 - B_2 C_1$$
$$a = B_1 C_1 - D_1 A_1 \tag{7}$$
$$c = B_2 C_2 - D_2 A_2$$

The characteristic slope may now be written from (5a) and (5b) in either one of the two following forms

$$\frac{dt}{dr} = \frac{B_1 \cdot \lambda_{\pm} + B_2}{A_1 \cdot \lambda_{\pm} + A_2} = \zeta_{\pm} \tag{8a}$$

$$\frac{dt}{dr} = \frac{D_1 \cdot \lambda_{\pm} + D_2}{C_1 \cdot \lambda_{\pm} + C_2} = \zeta_{\pm} \tag{8b}$$

For the hyperbolic case $b^2 - 4ac > 0$. Since the coefficients $A_1, A_2, \ldots, D_1, D_2$ involved in (7) are all known functions of r and t the equations $dt/dr = \zeta_{\pm}$ are two separate ordinary differential equations of the first order which define the two real families of characteristics I^+ and I^- (Fig. 1).

Conceptually, the solution of (1) and (2) may now be established by integrating the appropriate characteristic equations along the characteristics defined in (8a) and (8b). Since in general the characteristics are curved lines, the resulting variation of grid size along these lines may become quite large and lead to inaccuracies[7]. Consequently, it is desirable at this point to introduce new variables so that the characteristics in a new space-time plane are straight lines of equal slope. The constant grid size now involved tends to make the resulting integration simpler and more accurate than previously. From Figure 1 seeking ξ such that

$$I^+ : dt/d\xi = +K \tag{9a}$$

$$I^- : dt/d\xi = -K \tag{9b}$$

where K is an arbitrary constant, and comparing these relations to (8a) and (8b) yields

$$I^+ : Kd\xi = \zeta_+ dr \tag{10a}$$

$$I^- : Kd\xi = -\zeta_- dr \tag{10b}$$

as the required equations linking ξ to r on the two families of

characteristics. The success of solving problems in (t, ξ) depends to a great extent on being able to integrate (10) in closed form. Once this is done, the equations valid along the characteristics in (t, ξ) can be obtained by multiplying (3) by dt and employing (8) - (10) to give

$$I^+: (\lambda_+ B_1 + B_2)ds + (\lambda_+ D_1 + D_2)dv + (\lambda_+ E_1 + E_2)dt = 0, (dt = K d\xi) \tag{11a}$$

$$I^-: (\lambda_- B_1 + B_2)ds + (\lambda_- D_1 + D_2)dv + (\lambda_- E_1 + E_2)dt = 0, (dt = -K d\xi) \tag{11b}$$

where $\lambda_{\pm}$ can be calculated from (6).

If the elastic media under study is subjected to an instantaneous disturbance, jumps in s and v will occur across I^+ and I^- as the wave front propagates. In order to solve a problem of this type completely it is necessary to determine both the relationship between the jumps and the variation of the magnitude of these jumps as they propagate through the nonhomogeneous media. Consider the points m and n on either side of an I^+ characteristic as shown in Figure 1. If s is discontinuous across I^+ then $s_m - s_n$ has a finite value δs as m and n approach I^+ from either side. Using the characteristic equation along I^- from (11b) it follows that in this limit as dt approaches zero

$$(\lambda_- B_1 + B_2) \cdot \delta s + (\lambda_- D_1 + D_2) \cdot \delta v = 0 \tag{12}$$

At all points along I^+, the jumps δs and δv across this characteristic are related by (12).

The variation in magnitude of δs and δv as they propagate along I^+ is obtained by writing (11a) along I_1^+ and I_2^+ (Figure 1) and subtracting the two equations. As m and n approach I^+ from either side, it is found that

$$(\lambda_+ B_1 + B_2)d(\delta s) + (\lambda_+ D_1 + D_2)d(\delta v) + F(\lambda_+, r, t, s, v, \delta s, \delta v)dt = 0 \tag{13}$$

where

$$F = \lim_{\substack{I_1^+ \to I^+ \\ I_2^+ \to I^+}} \left[(\lambda_+ E_1 + E_2)_m - (\lambda_+ E_1 + E_2)_n\right] \tag{14}$$

In general, F will be a nonlinear function. Integration of (13) after eliminating δv by use of (12) and after substituting the functional form of the coefficients B_1, B_2, D_1, D_2 will give the variation of the jump δs along the I^+ characteristic. The corresponding variation of δv follows immediately from (12).

In a similar manner it is easy to show that jumps across I^- are related by

$$(\lambda_+ B_1 + B_2) \cdot \delta s + (\lambda_+ D_1 + D_2) \cdot \delta v = 0 \tag{15}$$

while the variation in magnitude of these jumps along I^- are dependent upon integration of the following equation

$$(\lambda_- B_1 + B_2)\,d(\delta s) + (\lambda_- D_1 + D_2)\,d(\delta v) + G(\lambda_-, r, t, s, v, \delta s, \delta v)\,dt = 0 \tag{16}$$

In (16) the function G represents the limit of the difference of $(\lambda_- E_1 + E_2)$ on either side of I^- in a manner similar to (14).

Special Cases

In the following two sections the foregoing characteristic relations will be specialized to certain problems involving cylindrical shear waves and plane waves, respectively, in nonhomogeneous elastic media.

Cylindrical Shear Waves

Consider the plane stress problem in polar coordinates in which rotary motion is caused by a shear loading or tangential velocity applied uniformly around an innter circular hole of radius r_o. The equations governing this motion are

$$\frac{\partial \bar{\tau}}{\partial \bar{r}} + \frac{2\bar{\tau}}{\bar{r}} = \bar{\rho}\,\frac{\partial^2 \bar{u}}{\partial \bar{t}^2} \tag{17}$$

$$\bar{\tau} = \bar{G}\left(\frac{\partial \bar{u}}{\partial \bar{r}} - \frac{\bar{u}}{\bar{r}}\right) \tag{18}$$

where $\bar{\tau}$ is the shear stress, $\bar{r}$ radius, and $\bar{u}$ tangential displacement. The density $\bar{\rho}$ and the shear modulus $\bar{G}$ may be assumed to be (different) functions of radius. For the present analysis the most convenient form of the equations is two equations with shear stress $\bar{\tau}$ and velocity $\bar{v}$

as the dependent variables. This is obtained by differentiating (18) with respect to time and letting $\bar{v} = \partial\bar{u}/\partial\bar{t}$. Dimensionless variables are now introduced as follows:

$$\tau = \frac{\bar{\tau}}{\tau_o}, \quad r = \frac{\bar{r}}{r_o}, \quad t = \frac{\bar{t}c_o}{r_o}, \quad G = \frac{\bar{G}}{G_o}, \quad v = \frac{G_o}{\tau_o c_o}\bar{v}, \quad \rho = \frac{\bar{\rho}}{\rho_o}, \quad c = \frac{\bar{c}}{c_o} \tag{19}$$

where the quantities with the zero subscripts are reference values. The quantity c_o represents the velocity of shear waves in a <u>homogeneous</u> plate in plane stress with shear modulus G_o and density ρ_o; i.e., $c_o^2 = G_o/\rho_o$. Employing these relations, (17) and (18) become

$$\frac{\partial\tau}{\partial r} - \rho(r)\cdot\frac{\partial v}{\partial t} + \frac{2\tau}{r} = 0 \tag{20}$$

$$\frac{\partial\tau}{\partial t} - G(r)\cdot\frac{\partial v}{\partial r} + \frac{G(r)v}{r} = 0 \tag{21}$$

Comparison of (20) and (21) with (1) and (2) leads to $s = \tau$, $A_1 = 1$, $D_1 = -\rho$, $E_1 = 2\tau/r$, $B_1 = C_1 = 0$ and $B_2 = 1$, $C_2 = -G$, $E_2 = Gv/r$, $A_2 = D_2 = 0$. From (6), (7), and (8), it follows that $\lambda_{\pm} = \pm\ G/\rho$ and $\zeta_{\pm} = \pm\ \sqrt{\rho/G}$. Substitution into (11a) and (11b) gives the appropriate characteristic relations

$$I^{+}: \ d\tau - \sqrt{\rho G}\ dv + 2\sqrt{\frac{G}{\rho}}\frac{\tau}{r(\xi)}\,dt + \frac{Gv}{r(\xi)}\,dt = 0, \quad (dt = Kd\xi) \tag{22a}$$

$$I^{-}: \ d\tau + \sqrt{\rho G}\ dv - 2\sqrt{\frac{G}{\rho}}\frac{\tau}{r(\xi)}\,dt + \frac{Gv}{r(\xi)}\,dt = 0, \quad (dt = -Kd\zeta) \tag{22b}$$

where G and ρ are arbitrary functions of radius r that are related to ξ by equation (10), namely

$$Kd\xi = \sqrt{\frac{\rho}{G}}\ dr \tag{23}$$

From (12) and (15) it follows that the jumps across the characteristics are related by

$$I^{+} : \delta\tau + (\rho G)^{\frac{1}{2}}\, \delta v = 0 \tag{24a}$$

$$I^{-} : \delta\tau - (\rho G)^{\frac{1}{2}}\, \delta v = 0 \tag{24b}$$

The differential equation governing the change in $\delta\tau$ as one proceeds along I^{+} follows from (13), (14) and (24a)

$$\frac{d(\delta\tau)}{\delta\tau} = \frac{d(\sqrt{\rho\, G})}{2\sqrt{G}} - \frac{K}{2}\sqrt{\frac{G}{\rho}}\,\frac{d\xi}{r(\xi)} \tag{25}$$

Solution of this differential equation may be obtained by integrating between two points on I^{+} in (t, ξ). However, because of difficulties with the term containing $d\xi$ it is best to integrate between the corresponding two points in (t, r) making use of the relation (23). The resulting solution is

$$(\delta\tau)_2 = (\delta\tau)_1 \cdot \left[\left(\frac{G_2\ \rho_2}{G_1\ \rho_1}\right)^{\frac{1}{2}} \frac{r_1}{r_2}\right]^{\frac{1}{2}} \tag{26}$$

It then follows from (24) that the jumps in velocity obey the equation

$$(\delta v)_2 = (\delta v)_1 \cdot \left[\left(\frac{G_1\ \rho_1}{G_2\ \rho_2}\right)^{\frac{1}{2}} \frac{r_1}{r_2}\right]^{\frac{1}{2}} \tag{27}$$

Equations (26) and (27) show how the jumps across I^{+} vary in magnitude at two points 1 and 2 on I^{+}. It can be shown by a similar calculation that jumps across I^{-} obey identical relations as they propagate along I^{-}.

Plane Waves

Consider a bar undergoing axial motion due to a loading or velocity applied at one end. Denoting the axial coordinate by $\bar{x}$, the governing equations are

$$\frac{\partial \bar{\sigma}}{\partial \bar{x}} = \bar{\rho}\,(\bar{x})\,\frac{\partial \bar{v}}{\partial \bar{t}} \tag{28}$$

$$\frac{\partial \bar{\sigma}}{\partial \bar{t}} = \bar{E}(\bar{x})\,\frac{\partial \bar{v}}{\partial \bar{x}} \tag{29}$$

where $\bar{\sigma}$ is the direct stress, $\bar{E}$ is Young's modulus, and $\bar{v}$ now is interpreted as the axial velocity of the bar. Introducing the dimensionless variables

$$\sigma = \frac{\sigma}{\sigma_o},\ x = \frac{\bar{x}}{x_o},\ E = \frac{\bar{E}}{E_o},\ v = \frac{E_o \bar{v}}{\sigma_o c_o},\ t = \frac{\bar{t}\, c_o}{x_o},\ \rho = \frac{\bar{\rho}}{\rho_o},\ c = \frac{\bar{c}}{c_o} \tag{30}$$

where the subscripted quantities are reference values and the quantity c_o now represents the velocity of axial waves in a <u>homogeneous</u> bar with elastic modulus E_o and density ρ_o, i.e., $c_o^2 = E_o/\rho_o$. Employing these relations (28) and (29) become

$$\frac{\partial \sigma}{\partial x} - \rho(x)\,\frac{\partial v}{\partial t} = 0 \tag{31}$$

$$\frac{\partial \sigma}{\partial t} - E(x)\,\frac{\partial v}{\partial x} = 0 \tag{32}$$

Comparing these relations to (1) and (2) leads to $s = \sigma$, $r = x$, and $A_1 = 1$, $D_1 = -\rho$, $B_2 = 1$, $C_2 = -E$ with the rest of the coefficients being zero. It then follows that $\lambda_{\pm} = \pm\sqrt{E/\rho}$ and $\zeta_{\pm} = \pm\sqrt{\rho/E}$. The equations valid along the characteristics are

$$I^+ : d\sigma - \sqrt{E\rho}\ dv = 0 \tag{33a}$$

$$I^- : d\sigma + \sqrt{E\rho}\ dv = 0 \tag{33b}$$

where E and ρ are arbitrary functions of x that are related to ξ by equation (10), namely,

$$K d\xi = (\rho/E)^{\frac{1}{2}}\ dx \tag{34}$$

From (12) and (15) it follows that the jumps across the characteristics are related by

$$I^+ : \delta\sigma + (E\rho)^{\frac{1}{2}}\ \delta v = 0 \tag{35a}$$

$$I^- : \delta\sigma - (E\rho)^{\frac{1}{2}}\ \delta v = 0 \tag{35b}$$

Following the same procedure as for the cylindrical shear wave problem, the variation of the jumps along both the I^+ and I^- characteristics satisfy

$$(\delta\sigma)_2 = (\delta\sigma)_1\ (E_2\ \rho_2/E_1\ \rho_1)^{\frac{1}{4}} \tag{36a}$$

$$(\delta v)_2 = (\delta v)_1\ (E_1\ \rho_1/E_2\ \rho_2)^{\frac{1}{4}} \tag{36b}$$

NUMERICAL ANALYSIS. The foregoing equations can now be solved numerically. The (t, ξ) space, as shown in Figure 1, is divided into a mesh formed by the intersecting families of I^+ and I^- characteristic lines. Assuming that the stress and velocity functions vary linearly in the small intervals between the grid points in (t, ξ), the appropriate characteristic equations (22) or (33) may be integrated to yield their finite difference equivalent. (It should be noted that the assumed linear variation in stress or velocity between grid points in (t, ξ) will, in general, lead to a nonlinear variation between grid points in (t,r)). Studying the typical points A, D, C, E in Figure 1, this integration along I^+ produces an equation containing quantities at A and D while integration along I^- leads to quantities evaluated at C and D. Assuming that all the unknowns in the problem have been determined up to the time represented by the points A and C, then the results obtained may be considered as two equations in two unknowns; namely, the unknown stress and velocity at point D. These equations are solved simultaneously for the quantities at the point D and then programmed for the computer.

For discontinuities in stress and velocity due to the propagation of abrupt wave fronts the above procedure is modified by using the exact value of the jump at points in (t, ξ) where the wave front is currently located.

The boundary points are treated in a similar manner to that of the interior points. However, now integration is needed only along one characteristic line since the extra condition supplied by the boundary data is sufficient to determine the unknown quantity at the boundary.

Specific Examples

In the following work, results will be found for several problems involving shear waves and plane waves, respectively. For all of these problems it is assumed that the density ρ is a constant while the elastic modulus varies with distance. It should be noted that a study of the relevant equations involved shows that variable ρ may be retained without difficulty; indeed the characteristic equations (22) and (33) are derived for variable ρ as well as variable E. However, for many problems, particularly those for which the inhomogeneity is due to a temperature gradient, the density changes are rather small, while the elastic modulus is often highly temperature dependent and, consequently, the foregoing assumption is justified. Structures with infinite outer boundaries are studied and results are compared with those of other authors with several discrepancies being explained. The finite problem is then run with different boundary conditions and design considerations are studied. For maximum convenience, all the computer runs were made for the characteristic lines in (t, ξ) being an orthogonal network with $K = 1$ (Figure 1).

Cylindrical Shear Waves

Consider a plate with inner radius of $r_o = 1$ (Figure 2) for which the shear modulus varies as a power of the radial coordinate

$$G = r^{\alpha} \tag{37}$$

where α is a real number not restricted to being an integer. The density is assumed to be a constant so that $\rho = 1$. For this problem, ξ may be found as a function of r by integration of (23)

$$\xi = 1 + \frac{1}{1 - \frac{\alpha}{2}} \left(r^{1 - \frac{\alpha}{2}} - 1 \right) \qquad \alpha \neq 2 \tag{38a}$$

$$\xi = 1 + \ell n\, r \qquad \alpha = 2 \tag{38b}$$

where ξ is arbitrarily fixed to be $\xi = 1$ when $r = 1$. The relationships of (38) are plotted in Figure 2. The particular I^+ equations for this shear case in (t, ξ) for $\alpha \neq 2$ follow from (22), (24), (26), (27), and (38a),

$$d\tau - \left[\xi - \frac{\alpha}{2}(\xi - 1)\right]^{\frac{\alpha}{2-\alpha}} dv + \frac{2\tau dt}{\left[\xi - \frac{\alpha}{2}(\xi - 1)\right]} + \frac{v\, dt}{\left[\xi - \frac{\alpha}{2}(\xi - 1)\right]^{2(1-\alpha)/(2-\alpha)}} = 0,$$

$$\delta\tau + \left[\xi - \frac{\alpha}{2}(\xi - 1)\right]^{\frac{\alpha}{2-\alpha}} \delta v = 0 \quad , \tag{39}$$

$$(\delta\tau)_2 = (\delta\tau)_1 \left\{\left[\xi_1 - \frac{\alpha}{2}(\xi_1 - 1)\right] \Big/ \left[\xi_2 - \frac{\alpha}{2}(\xi_2 - 1)\right]\right\}^{\frac{1}{2}} ,$$

$$(\delta v)_2 = (\delta v)_1 \left\{\left[\xi_1 - \frac{\alpha}{2}(\xi_1 - 1)\right] \Big/ \left[\xi_2 - \frac{\alpha}{2}(\xi_2 - 1)\right]\right\}^{\frac{1}{2}\left(\frac{2+\alpha}{2-\alpha}\right)}$$

The I^- equations may be derived in a similar manner. Equations (39) are actually used in the computer program to obtain numerical results.

As a check on the accuracy of the present method a comparison was made with previous results[7] for the case with $\alpha = 1$ and an infinite outer boundary. The shear stress at the inner boundary is taken as a step function in time. As may be seen from Figure 3, the comparison is excellent. The shear stress is zero at (dimensionless) radius $r = 4$ until the discontinuous wave front arrives at (dimensionless) time $t = 2$. Then, there is an instantaneous jump followed by oscillations and finally the shear stress asymptotically approaches its static value. Actually, the case with $\alpha = 1$ does not bring out the practical advantages of the transformation from (t, r) to (t, ξ) since the degree of inhomogeneity involved is "relatively mild" and the resulting relationship between r and ξ in Figure 2 is "relatively smooth." On the other

hand, the case with $\alpha = 10$ represents a highly inhomogeneous material with the resulting large radial variation in Figure 2 corresponding to a small variation in ξ. It is now quite advantageous to transform to (t, ξ) and integrate the characteristic equations after assuming that the shear stress and velocity vary linearly between the closely spaced grid points. The stress-time history at two different radii is shown in Figure 4 for this case of $\alpha = 10$. The stress is zero until the wave front arrives, at which time the shear stress jumps to a value which it maintains essentially as a constant until affected by the stress wave reflected from the outer boundary $r = 2.66$. This same problem was done by Chou and Schaller[7] for an infinite outer boundary by numerical integration of the characteristic relations along the characteristics in (t, r). Their numerical results showed that the shear stress erroneously increased for $t > .25$, but they correctly diagnosed the trouble as due to inaccuracies associated with large distorted grids in (t, r). The present technique eliminates this trouble giving the correct stresses which remain essentially constant in time.[6] On this diagram, the effect of the stress free outer boundary is clearly shown. At any radius, the stress abruptly drops approximately to zero and stays at this value until the stress wave reflects off the inner boundary and reaches this same radius again; then, the cycle starts anew. These results were obtained for a mesh size $\Delta\xi = \Delta t = .005$ and checked for accuracy with a mesh size $\Delta\xi = \Delta t = .001$.

The effect of variation of the degree of nonhomogeneity is shown on Figure 5 for two cases of $\alpha = 4$ and 6. Both runs are made for a body which is stress free at its outer boundary $r = 2$ and subjected to a step loading in time at its inner boundary. The shear stress is plotted against radius for the fixed time of $t = .475$. The wave front for the stiffer structure, $\alpha = 6$, at this time has already reflected off the stress free outer surface and is now located at $r = 1.4907$. The wave front for the softer structure, $\alpha = 4$, has a slower wave speed associated with its wave front and consequently at this time the front has not yet reached the outer boundary.

In Figure 6, for the same conditions as in Figure 5 for $\alpha = 6$, the shear stress is plotted against time for a fixed radius of $r = 1.35$. The sudden boosts in the stress due to the incoming and outgoing wave fronts are clearly shown in the figure. It is interesting to compare qualitatively the $\alpha = 10$ results of Figure 4 with the $\alpha = 6$ results of Figure 6. For example, it is of interest to know from the design viewpoint whether the shear stress at any point of the finite inhomogeneous structure may be determined from the corresponding quantity of the infinite inhomogeneous structure. From the figures it may be seen that for $G \propto r^{10}$ the vibratory effects are negligible and consequently the infinite domain results are also applicable to the finite domain. However, when $G \propto r^6$ (which is still relatively stiff) the vibratory effects for the finite problem are important, causing a 90% increase in shear stress (at the radius $r = 1.35$) over that which would occur for the infinite domain.

The response of a body with $\alpha = 6$ which is fixed (zero velocity condition) at its outer boundary $r = 2$ and subjected to a step loading in time at its innter boundary is plotted in Figure 7 for the fixed time of $t = .475$. For comparison purposes the response curve of Figure 5 for the same body, but with a stress free outer boundary, is also shown in Figure 7. Since the wave speeds in both cases are identical, both curves show the wave front at $r = 1.4907$ for this time. For the case with the fixed outer boundary, the discontinuous wave front pushes the shear stress abruptly higher while for the free end case the front acts as a relieving wave by suddenly decreasing the shear stress.

Plane Waves

Consider a bar of length L for which the wave speed varies as a quadratic in $\bar{x}$ for $0 < \bar{x} < \ell$ and is a constant c_o for $\ell \leq \bar{x} < L$, according to the following dimensionless relations

$$\begin{aligned} c(x) &= ax^2 + mx + b \qquad && 0 < x < 1 \\ c(x) &= 1 \qquad && 1 \leq x < (L/\ell) \end{aligned} \tag{40}$$

where the reference value x_o is taken to be the length of the non-homogeneous portion of the bar; namely, $x_o = \ell$. The constant coefficients a and m may be determined from the condition that both c(x) and dc/dx are continuous at x = 1 while b, the wave speed at x = 0, is taken as an arbitrarily predetermined constant. There is a discontinuity in the second derivative d^2c/dx^2 at x = 1 which apparently leads to a wave reflection from x = 1; however, the magnitude of this reflected wave for the cases examined turns out to be too small to be seen in the graphical results.

For this problem the relationship between ξ and x may be found from integration of (34),

$$\xi = \frac{1}{Q}\left[\ell n \left(\frac{Q - m - 2ax}{Q + m + 2ax}\right) - \ell n \left(\frac{Q - m}{Q + m}\right)\right], \quad 0 < x < 1$$

$$Q = \sqrt{m^2 - 4\,ab}\,, \qquad Q^2 > m^2 > 0 \tag{41}$$

$$\xi = x\,, \qquad 1 \leq x < L/\ell$$

The equations to be used in this problem then follow from (33) - (36). Integration of the characteristic equations then yields the appropriate finite difference relations. Quantities at the intersection x = 1 are handled by simultaneous solution of the equations obtained by integrating the I^+ relations with the nonhomogeneous properties and the I^- relations with the homogeneous properties.

Payton[4] investigated the semi-infinite equivalent of this bar problem ($L \to \infty$) using a Laplace transform method and asymptotic techniques for the inversion. He used b = 1/1.21 so that the wave speed quadratically increases as the intersection x = 1 is approached from the loaded end x = 0. The loading condition at this end is a pressure step in time, $\sigma(x = 0) = -P_o H(t)$.

In Figures 8 and 9, results are shown at $\bar{x} = 2\ell$ for these conditions for a finite bar with $\ell = 0.3L$. These results should check with those of Reference 4 up until the time that the point $\bar{x} = 2\ell$ is affected by wave reflection from the finite end $\bar{x} = L$. The results do compare very well for arrival time and for the jump value at $\bar{x} = 2\ell$. However, there is a discrepancy in that the present results imply an asymptotic value $\sigma/P_o \to -1$ for the semi-infinite bar while those of Reference 4 seem to imply a slightly larger asymptotic value. In Figure 8, for the finite bar with the free end, the familiar patterns of stress wave relief due to reflections from the free end are shown clearly. It also follows from this figure that the stress reflections and vibratory effects make it necessary to consider the finite bar for design purposes rather than the results of the (mathematically simpler) semi-infinite bar. In Figure 9, a plot is shown for the response at $\bar{x} = 2\ell$ for a finite bar with a fixed end.

Another inhomogeneous bar problem has been analyzed by Lindholm and Doshi[5] for the case where the elastic modulus varies with the distance $\bar{x}$ from the loaded end

$$\bar{E} = \bar{E}_o \left(\frac{\bar{x} + k\ell}{k\ell} \right)^n \qquad 0 \leq \bar{x} \leq \ell \qquad (42)$$

where k is an arbitrary prescribed constant, $\bar{E}_o$ is the modulus at $\bar{x} = 0$, the exponent n is any real number, and ℓ is the length of the bar. The relation of (42) is equivalent to specifying the wave speed since the density is assumed to be constant. Taking the reference length x_o to be equal to $k\ell$, equation (42) may be written in the following dimensionless form

$$E = (x + 1)^n \qquad 0 \leq x \leq 1/k \qquad (43)$$

For this problem integration of (34) yields

$$\xi = \left[(x+1)^{1-\frac{n}{2}} - 1\right] \Big/ \left(1 - \frac{n}{2}\right) \qquad n \neq 2$$

$$\xi = \ln (x+1) \qquad n = 2 \tag{44}$$

The equations to be used in this problem then follow from (33) - (36).

Lindholm and Doshi investigated several bars through use of an eigenfunction expansion in conjunction with the principle of virtual work. The loading condition is a half sine wave at the x = 0 end of a free-free bar. These results compare very well with the results based on the numerical method for a free-free bar, with a linearly varying modulus, subjected to a pressure step in time at the x = 0 end. The stress is plotted in Figure 10 at a fixed station x = .2 and the discontinuities due to the reflecting wave fronts are easily distinguished.

CONCLUDING REMARKS. It has been demonstrated that for certain types of continuously nonhomogeneous media, it is beneficial to transform the resulting characteristic problem to a new space-time regime in which the characteristics are straight lines of equal slope that form a closely spaced uniform grid. Although results were shown only for step pressure loadings of nonhomogeneous elastic media with variable elastic modulus but constant density it should be noted that these assumptions are not necessarily restrictive. Boundary conditions on velocity are as easy to handle as boundary conditions on stress. Loadings of a continuous nature are easily handled since there is no need to invoke the jump conditions. Finally, variable density may be included in the analysis with only minor modifications for many problems.

REFERENCES

1. Goodier, J. N. and Jahsman, W. E., "Propagation of a Sudden Rotary Disturbance in an Elastic Plate in Plane Stress," Journal of Applied Mechanics, Vol. 23, Trans ASME, Vol. 78, 1956, pp. 284-286.

2. Chou, P. C. and Koenig, H. A., "A Unified Approach to Cylindrical and Spherical Elastic Waves by Method of Characteristics," Journal of Applied Mechanics, Vol. 33, March 1966, pp. 195-167.

3. Chou, S. C. and Greif, R., "Numerical Solution of Stress Waves in Layered Media," AIAA Journal, Vol. 6, No. 6, June 1968, pp. 1067-1074.

4. Payton, R. G., "Elastic Wave Propagation in a Nonhomogeneous Rod," Quart. Journ. Mech. and Applied Math, Vol. XIX, Pt. 1, 1966, pp. 83-91.

5. Lindholm, U. S. and Doshi, K. D., "Wave Propagation in an Elastic Nonhomogeneous Bar of Finite Length," Journal of Applied Mechanics, Vol. 32, 1965, pp. 135-142.

6. Sternberg, E. and Chakravorty, J. G., "On the Propagation of Shock Waves in a Nonhomogeneous Elastic Medium," Journal of Applied Mechanics, Vol. 26, December 1959, pp. 528-536.

7. Chou, P. C. and Schaller, R. J., "Propagation of Cylindrical Shear Waves in Nonhomogeneous Elastic Media," AIAA Paper No. 66-444, presented at AIAA 4th Aerospace Sciences Meeting, Los Angeles, California, June 27-29, 1966.

8. Courant, R. and Hilbert, D., Methods of Mathematical Physics, Vol. II, Interscience Publishers, July 1966, Chapter V.

9. Courant, R. and Friederichs, K. O., Supersonic Flow and Shock Waves, Interscience Publishers, 1956, Chapters II-III.

10. Leonard, R. W. and Budiansky, B., "On Traveling Waves in Beams," NACA Report 1173, 1954.

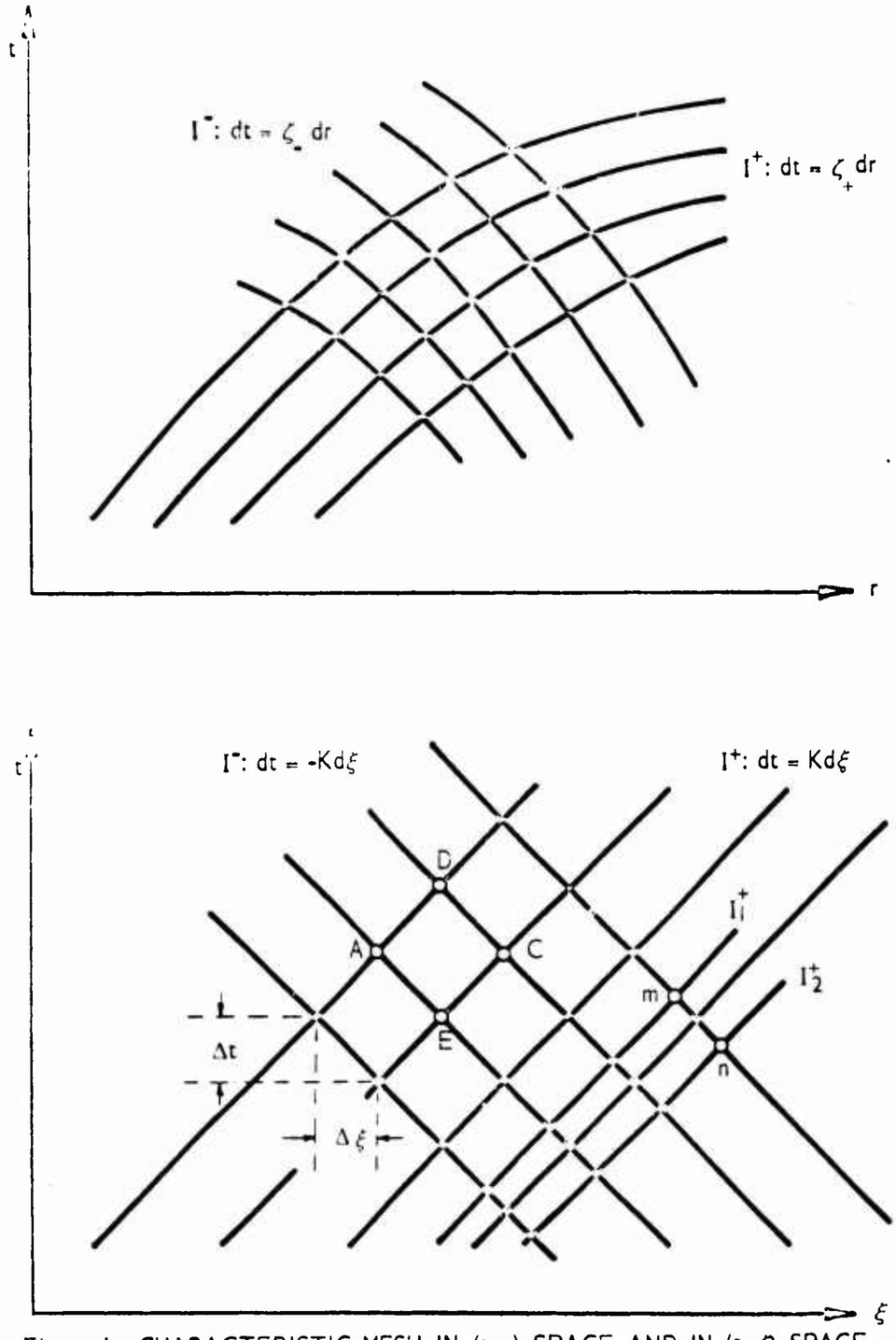


Figure 1. CHARACTERISTIC MESH IN (t, r) SPACE AND IN (t, ξ) SPACE

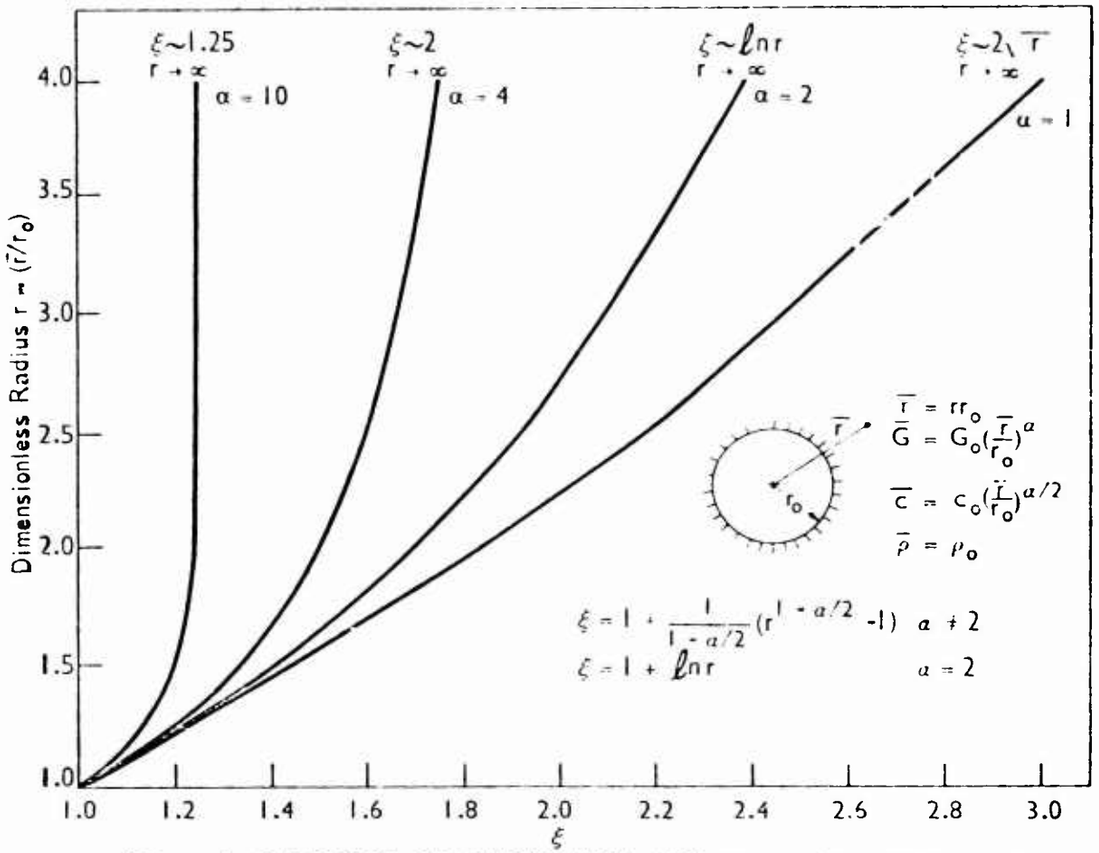


Figure 2. VARIATION OF RADIUS WITH NEW VARIABLE ξ FOR $G = r^{\alpha}$

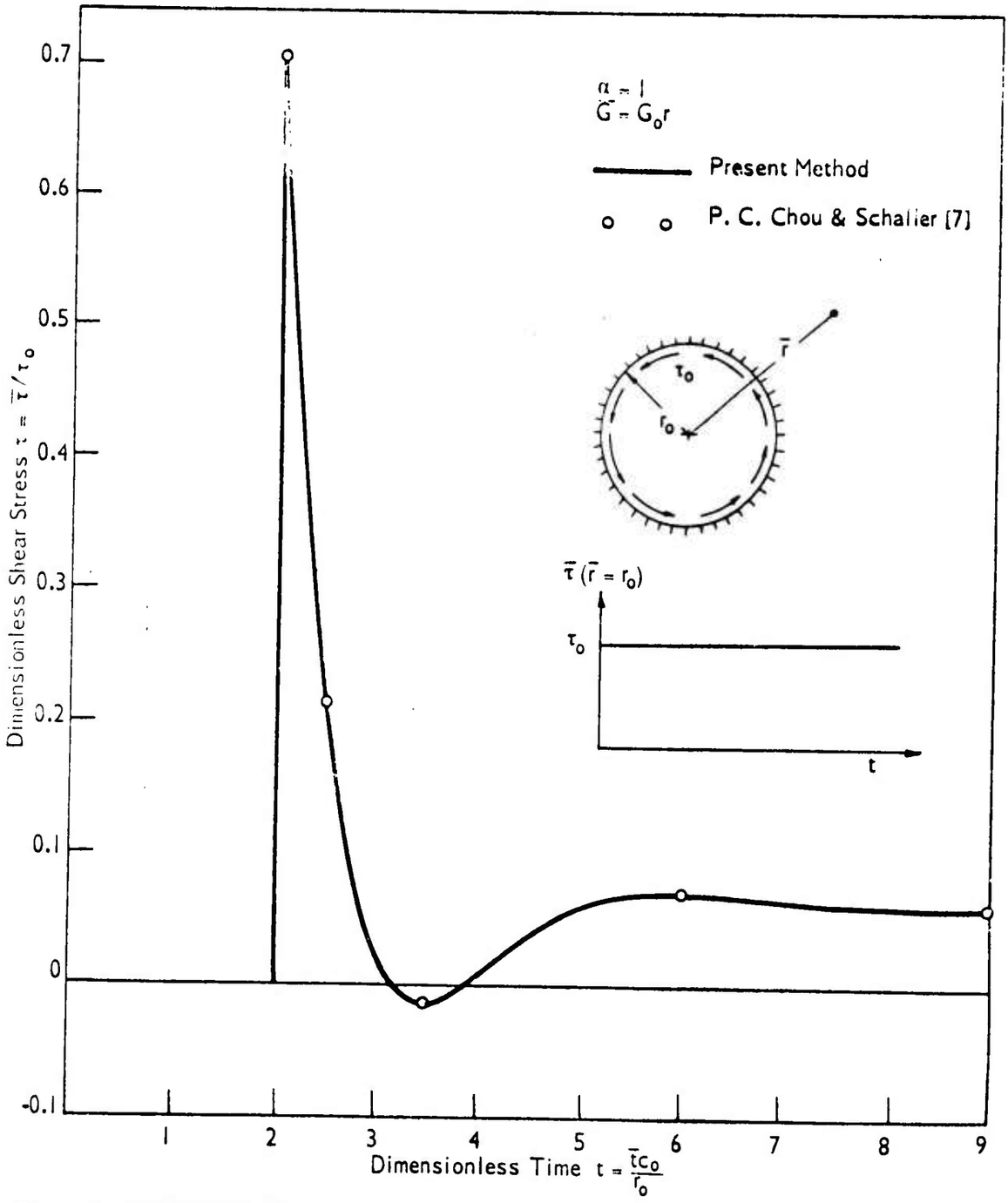


Figure 3. RESPONSE AT $\bar{r} = 4r_0$ DUE TO STEP LOADING AT INNER RADIUS FOR $\alpha = 1$

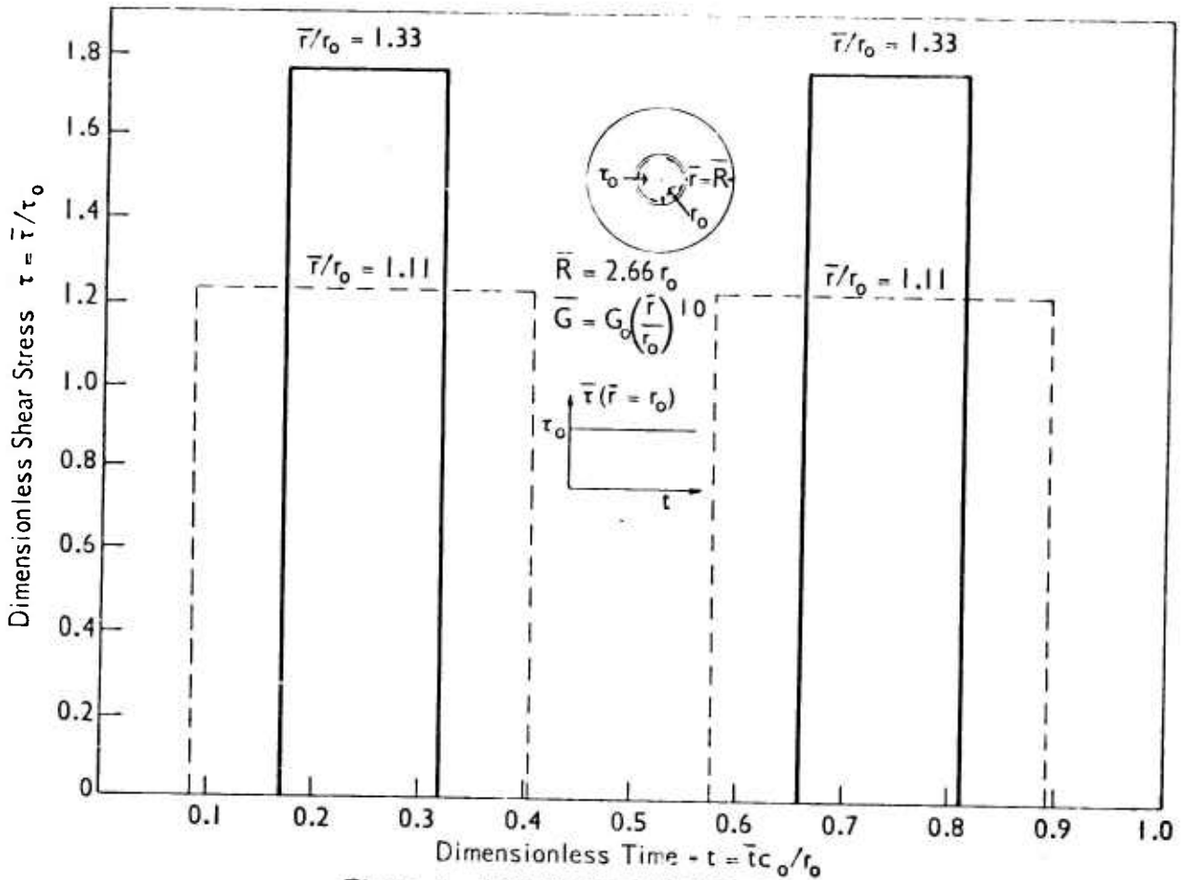


Figure 4. RESPONSE CURVES FOR $\alpha = 10$

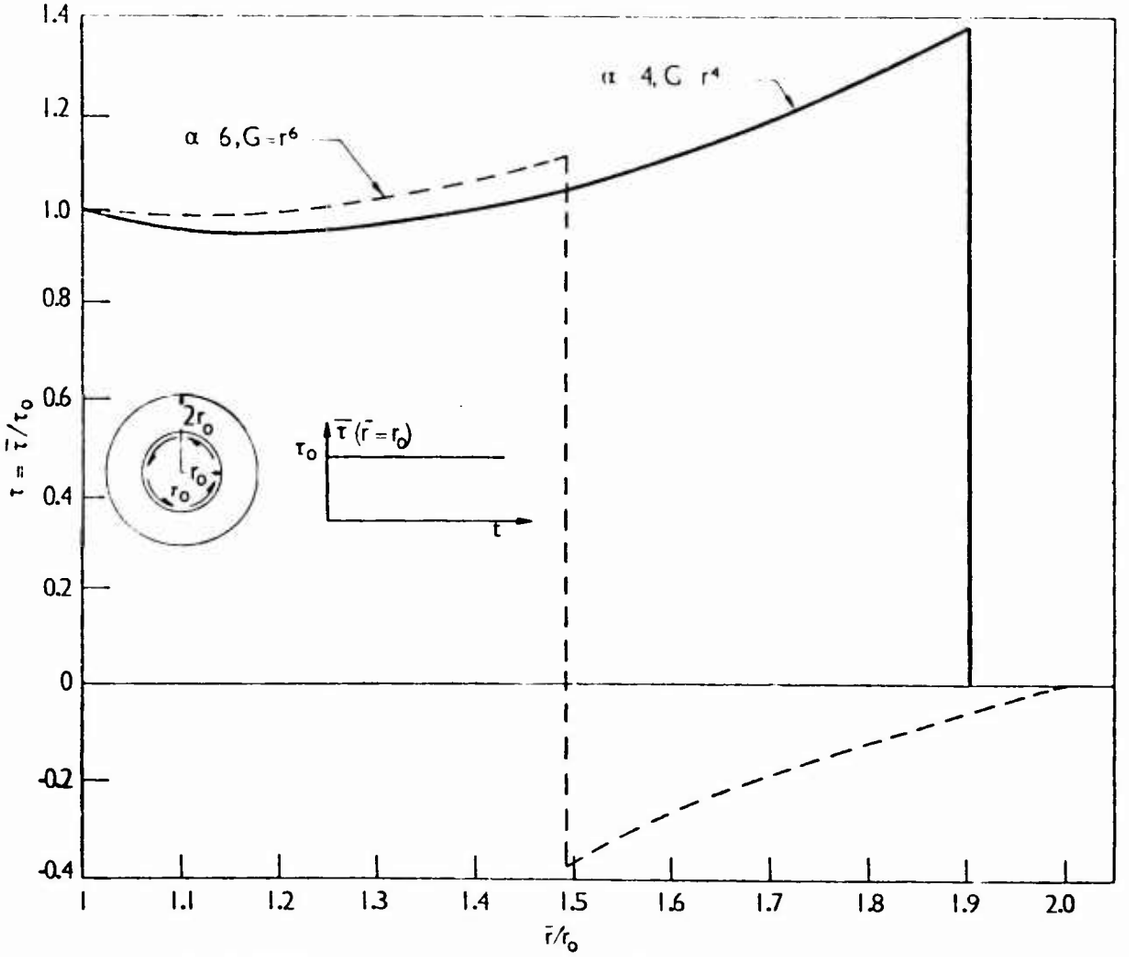


Figure 5. RESPONSE FOR $\alpha = 4$ AND $\alpha = 6$ FOR DIMENSIONLESS TIME $t = 0.475$

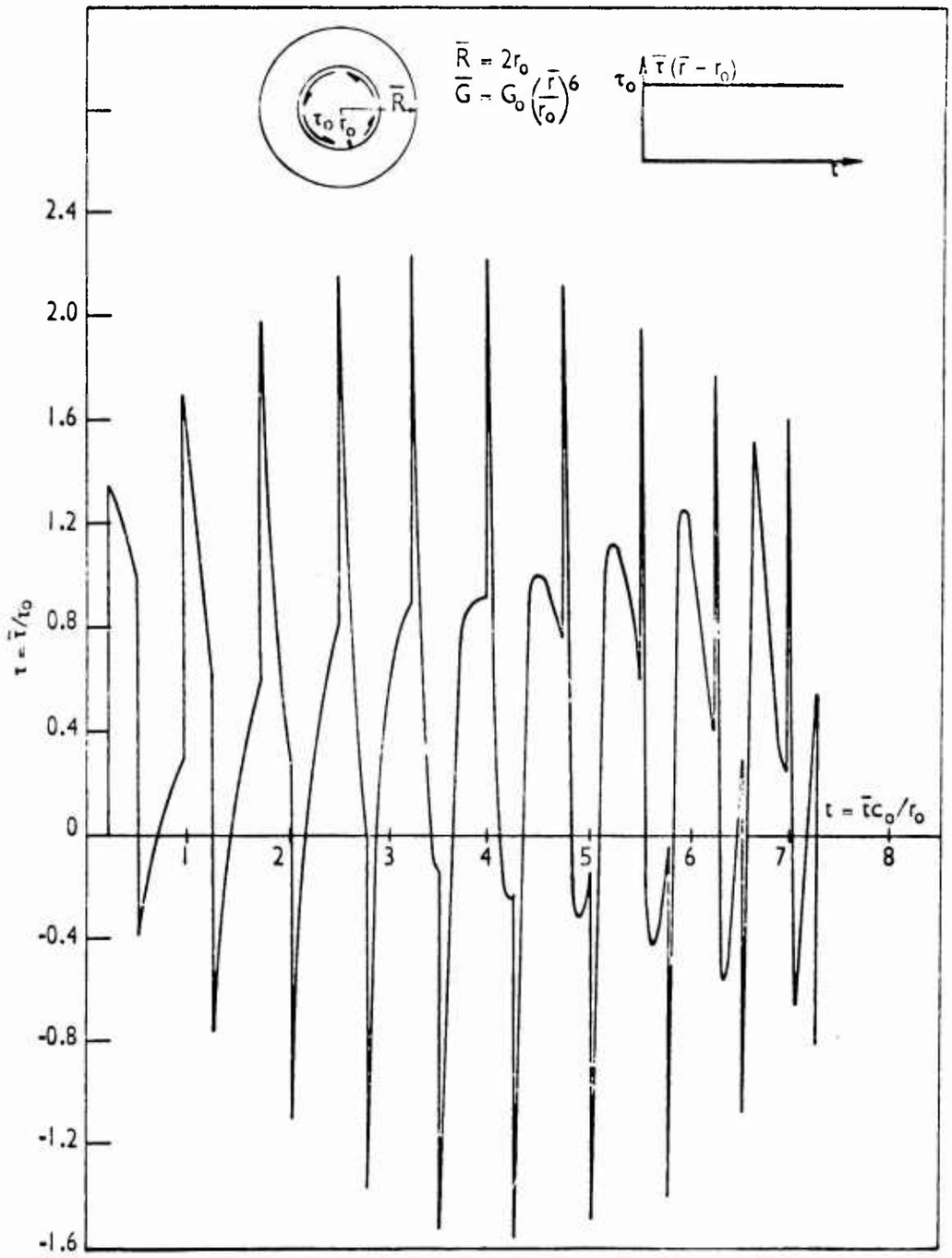


Figure 6. STRESS TIME HISTORY AT $\bar{r} = 1.35r_o$ FOR $\alpha = 6$

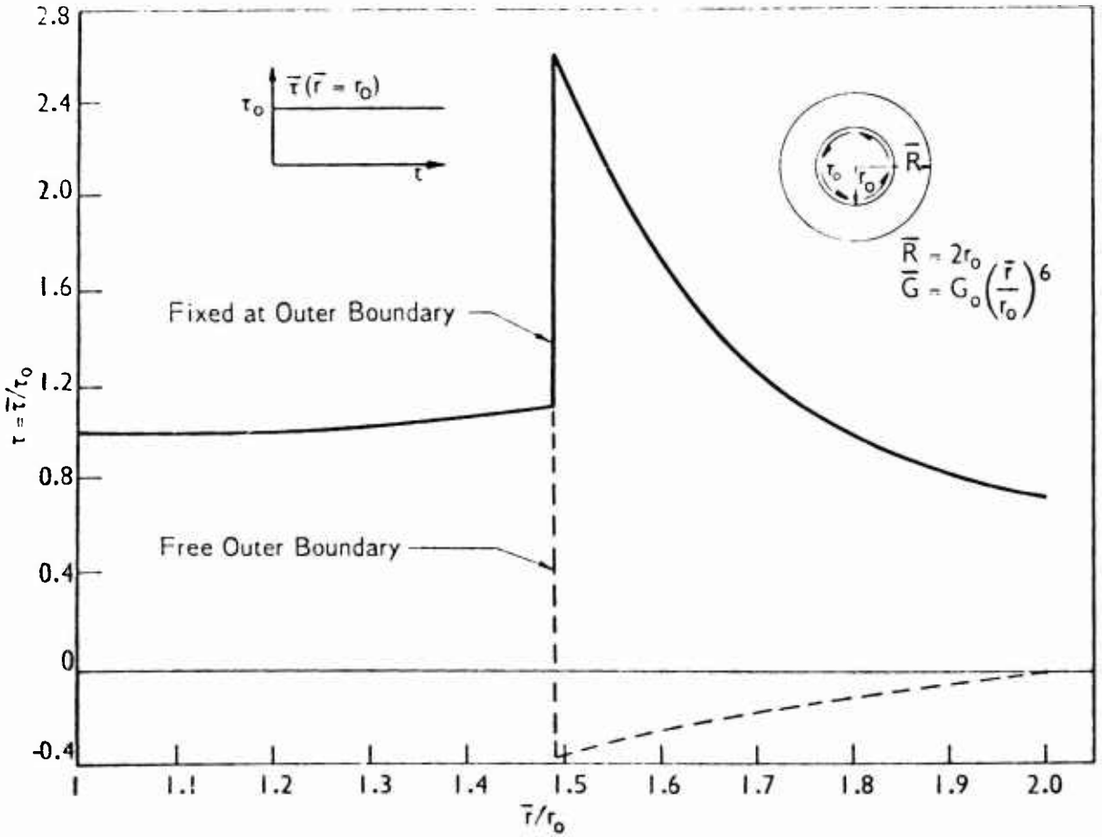


Figure 7. COMPARISON OF RESPONSE FOR STRUCTURE WITH **FIXED** OUTER BOUNDARY AND **FREE** OUTER BOUNDARY FOR $\alpha = 6$ AND $t = 0.475$

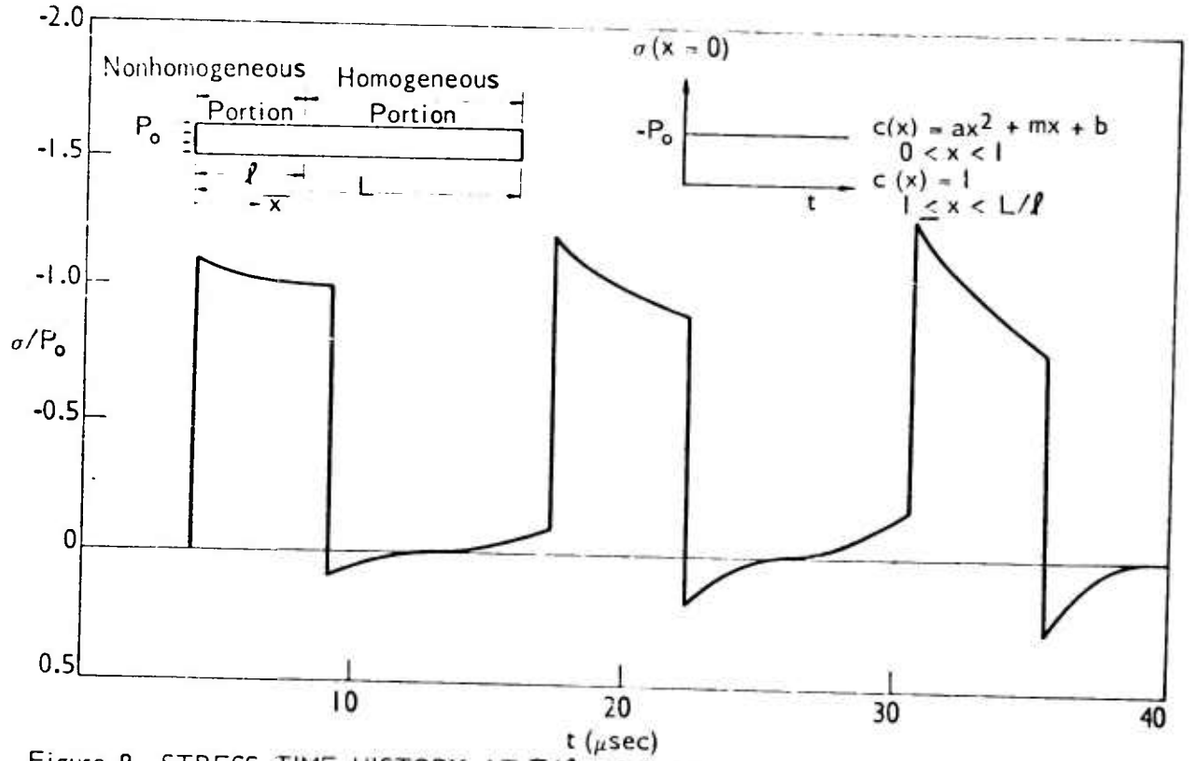


Figure 8. STRESS TIME HISTORY AT $\bar{x}/\ell = 2.0$ OF A FREE END BAR WITH $\ell = 0.3L$

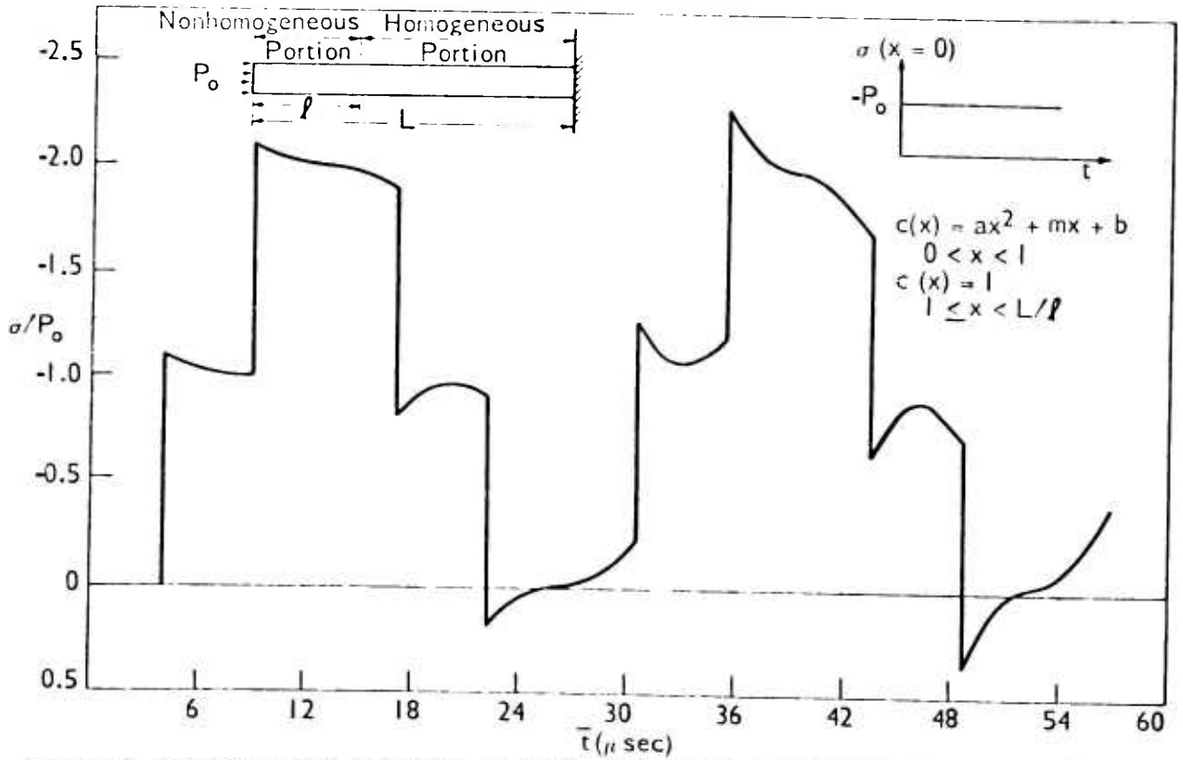


Figure 9. STRESS TIME HISTORY AT $\bar{x}/\ell = 2.0$ OF A **FIXED** END BAR WITH $\ell = 0.3L$

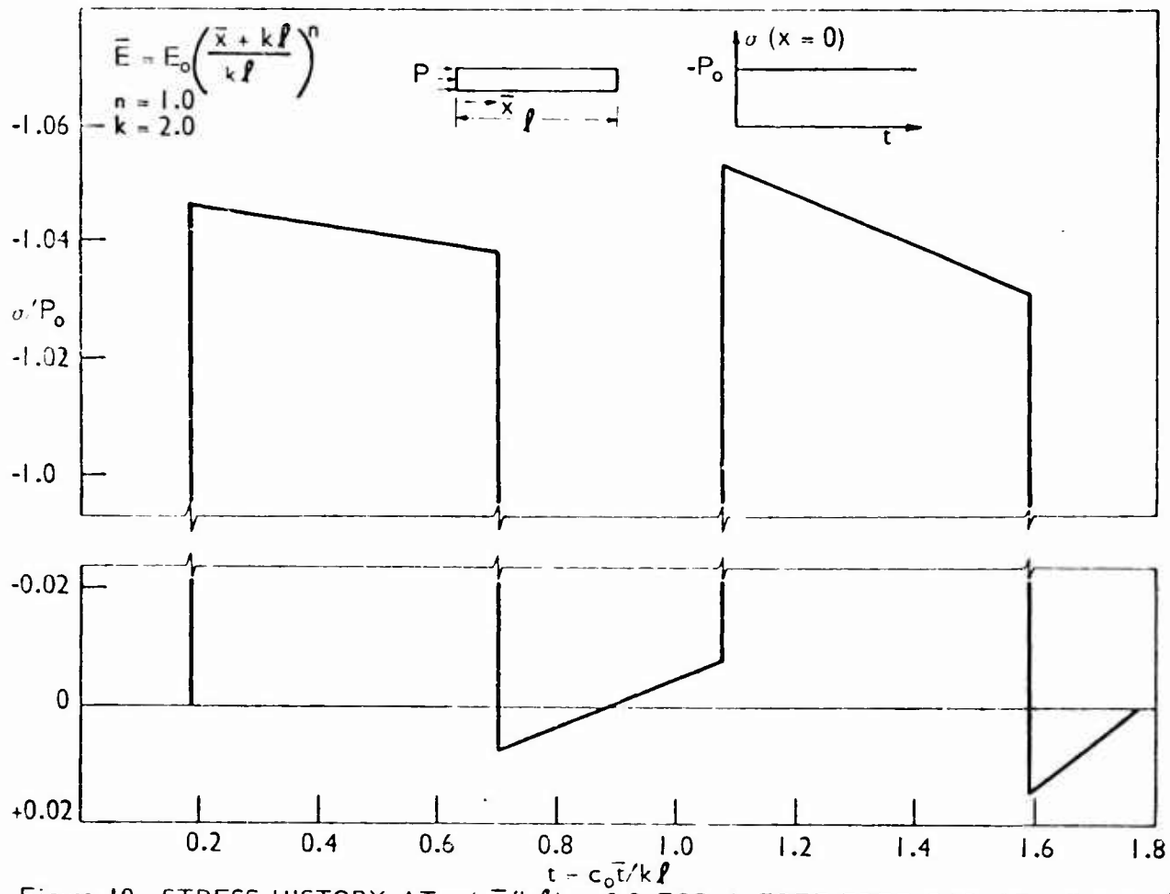


Figure 10. STRESS HISTORY AT $x(=\bar{x}/k\ell) = 0.2$ FOR A FREE-FREE BAR OF LENGTH ℓ

FREE EXTENSIONAL VIBRATIONS IN PLATE STRIPS

Gary L. Anderson
Maggs Research Center, Watervliet Arsenal
Watervliet, New York

ABSTRACT. The Kane-Mindlin equations for the extensional motion of an isotropic elastic plate are solved and the frequency spectrum of an infinite plate strip is investigated for three types of boundary conditions: (i) both edges of the strip are free of traction; (ii) both edges are clamped; and, (iii) one edge is free and the other is clamped. The resulting transcendental frequency equations corresponding to these boundary conditions must be solved numerically with a digital computer. The frequency spectra obtained from the Kane-Mindlin theory are compared with the corresponding curves as derived from the theory of generalized plane stress. The orthogonality condition which the plate-displacements, subject to the above mentioned three sets of boundary conditions, satisfy is also derived.

1. INTRODUCTION. It is well known that straight-crested waves traveling in an infinite plate with traction-free surfaces are dispersed and consist of two uncoupled modes - one symmetric and one antisymmetric with respect to the middle plane of the plate. The character of the dispersion relations in this problem as determined from the equations of elasticity was first discussed by Rayleigh [1] and by Lamb [2]. In particular, it has been pointed out by Lamb that in the limit of very long waves relative to the thickness of the plate the phase speed of the lowest symmetric mode tends to a value independent of wave-length. This is in exact agreement with the phase speed of straight-crested waves in an infinite plate as computed from the theory of generalized plane stress which is formulated on the basis that the transverse component of the plate's displacement is negligible in comparison with the longitudinal displacements in the middle plane of the plate. In other words, the theory of generalized plane stress attempts to approximate the extensional motion of a plate.

It is generally true that the theory of generalized plane stress will provide accurate values of the extensional frequencies of vibration of finite plates only in the low frequency range and these values are usually reliable only in the first few modes. Two exceptions to this will be discussed in Section 3. The reason for the poor agreement at higher frequencies is due to the fact that the transverse displacement of the plate, and hence the coupling with the lowest thickness-stretch mode, is ignored in the theory of generalized plane stress.

Kane and Mindlin [3] have developed a set of differential equations and boundary conditions which describe the extensional motion of a plate much more accurately in the high frequency range than does the classical theory of generalized plane stress. This has been accomplished by taking into account the coupling between the extensional motions and the first mode of thickness vibration by retaining the transverse displacement u_z and the "pinching" stress σ_{zz}. When Poisson's ratio, ν, is greater than 1/3, the frequency of the lowest thickness-stretch mode in an infinite plate is higher than the frequency, independent of ν, of the lowest symmetric thickness-shear mode in an infinite plate. In the range of Poisson's ratio commonly encountered, both thickness modes can couple with face modes and with each other. This circumstance has a marked influence on phase and group velocities of waves and on the frequencies and shapes of high-frequency vibrational modes. Moreover, for $\nu \geq 1/3$, the Kane-Mindlin theory does not yield accurate values of the natural frequencies of vibration of plates. For these reasons, Medick and Mindlin [4] have derived a system of approximate, two-dimensional equations of extensional motion of isotropic, elastic plates which take into account the coupling between extensional, symmetric thickness-stretch and symmetric thickness-shear modes and which also includes the two face-shear modes.

The propagation of variable crested waves in an infinite plate strip, sometimes called edge waves because they are analogous to Rayleigh surface waves which propagate near the surface of a semi-infinite medium, has been studied by Kumar [5] who investigated the problem using the equations of motion from the theory of generalized plane stress. Gazis and Mindlin [6], using the equations of the Kane-Mindlin theory, have investigated the influence of width on phase velocities of waves in plate strips in the transition region between the states of generalized plane stress and plane strain.

This paper is concerned with a special limiting case of the problems discussed in References [5] and [6] in that the frequency spectrum of standing waves is determined for an infinite plate strip, the edges of which are subject to three types of boundary conditions: (i) both edges of the strip are free of traction; (ii) both edges are clamped; and, (iii) one edge is free and the other is clamped. We shall obtain the frequency equations within the framework of the Kane-Mindlin theory; however, these equations cannot be solved analytically, so we must obtain numerical solutions with the aid of an electronic computer. The corresponding problems formulated in terms of the theory of generalized plane stress are also solved, and the results are presented in the Appendix.

2. THE EQUATIONS OF MOTION. The Kane-Mindlin equations [3] of motion for the free extensional vibrations of a plate of thickness h are

$$h\mu\nabla^2\underset{\sim}{v} + h(\lambda+\mu)\ \nabla\ (\nabla\cdot\underset{\sim}{v}) + 2\lambda\kappa\nabla\ v_z = \rho h\ddot{\underset{\sim}{v}}, \tag{1}$$

$$\frac{1}{6}\ \mu h^2\nabla^2 v_z - 2\kappa^2(\lambda+2\mu)\ v_z - \lambda h\kappa\nabla\cdot\underset{\sim}{v} = \frac{1}{6}\ \rho h^2\ddot{v}_z, \tag{2}$$

where μ and λ are the Lamé constants, κ is a correction factor with the value $\kappa^2 = \pi^2/12$, ρ is the density of the material, $\underset{\sim}{v} = v_x(x,y,t)\underset{\sim}{i} + v_y(x,y,t)\underset{\sim}{j}$, $v_z = v_z(x,y,t)$ and ∇ and ∇^2 are the usual two-dimensional Laplacian operators

$$\nabla = \underset{\sim}{i}\ \frac{\partial}{\partial x} + \underset{\sim}{j}\ \frac{\partial}{\partial y}, \qquad \nabla^2 = \frac{\partial^2}{\partial x^2} + \frac{\partial^2}{\partial y^2}.$$

The plate-strain-displacement relations are

$$\left.\begin{aligned} e_{xx} &= -\frac{\partial v_x}{\partial x}, \quad e_{yy} = \frac{\partial v_y}{\partial y}, \quad e_{xy} = \frac{1}{2}\left(\frac{\partial v_x}{\partial y} + \frac{\partial v_y}{\partial x}\right), \\ e_{xz} &= \frac{1}{h}\ \frac{\partial v_z}{\partial x}, \quad e_{yz} = \frac{1}{h}\ \frac{\partial v_z}{\partial y}, \quad e_{zz} = \frac{2}{h}\ v_z, \end{aligned}\right\} \tag{3}$$

and the plate-stress resultants are

$$\left.\begin{aligned} N_{xx} &= 2\mu h e_{xx} + h\ \lambda(e_{xx} + e_{yy} + \kappa e_{zz}), \\ N_{yy} &= 2\mu h e_{yy} + h\lambda(e_{xx} + e_{yy} + \kappa e_{zz}), \\ N_{xy} &= 2\mu h e_{xy}, \quad R_x = 2\mu I_z e_{xz}, \quad R_y = 2\mu I_z e_{yz}, \\ N_{zz} &= 2\mu h\kappa^2 e_{zz} + \lambda h\kappa(e_{xx} + e_{yy} + \kappa e_{zz}), \end{aligned}\right\} \tag{4}$$

where $I_z = h^3/12$. The boundary conditions on the edge of the plate consist of one condition from each of the following three sets:

$$\left.\begin{aligned} &\text{(a) either } N_{nn} = 0 \text{ or } v_n = 0, \\ &\text{(b) either } N_{ns} = 0 \text{ or } v_s = 0, \\ &\text{(c) either } R_n = 0 \text{ or } v_z = 0, \end{aligned}\right\} \tag{5}$$

where the subscripts n and s refer to the normal and tangential directions to the boundary curve of the plate, respectively.

We shall consider an infinite strip of an isotropic elastic material of thickness h and width a, with the coordinate directions as shown in Figure 1. We shall confine our attention to a motion in which the plate-displacements are of the form

$$v_x = 0, \quad v_y = v_y(y,t), \quad v_z = v_z(y,t). \tag{6}$$

Under this assumption (1) and (2) reduce to

$$\left.\begin{aligned} &h(\lambda+2\mu)\ \frac{\partial^2 v_y}{\partial y^2} + 2\lambda\kappa\ \frac{\partial v_z}{\partial y} = \rho h\ \frac{\partial^2 v_y}{\partial t^2}, \\ &\mu h^2\ \frac{\partial^2 v_z}{\partial y^2} - 12\kappa^2(\lambda+2\mu)v_z - 6\lambda h\kappa\ \frac{\partial v_y}{\partial y} = \rho h^2\ \frac{\partial^2 v_z}{\partial t^2}. \end{aligned}\right\} \tag{7}$$

Following Kane and Mindlin [3], we reduce the system (7) to a pair of ordinary differnetial equations by assuming harmonic vibrations and setting

$$v_y(y,t) = \psi'(y) \cos\ \omega t, \quad v_z(y,t) = u(y) \cos\ \omega t, \tag{8}$$

where ω denotes the natural circular frequency of vibration of the strip and the prime denotes differentiation with respect to y. Substitution of (8) into (7) leads to

$$\left.\begin{aligned} &\rho h c_1^2 \psi'' + 2\lambda\kappa u + \rho h\omega^2 \psi = 0, \\ &\rho c_2^2\, u'' - \pi^2 \rho\ c_1^2 u - 6\lambda h\kappa\ \psi'' + \rho h\omega^2 u = 0, \end{aligned}\right\} \tag{9}$$

where $c_1^2 = (\lambda+2\mu)/\rho$ and $c_2^2 = \mu/\rho$, and elimination of u between the equations in (9) yields

$$\psi^{IV}(y) + p[(\alpha+\beta)\Omega^2 - 1]\ \psi''(y) - p^2\alpha\beta\Omega^2(1-\Omega^2)\psi(y) = 0, \tag{10}$$

where

$$p = \frac{\pi^2}{\beta h^2}, \quad \alpha = \frac{c_1^2}{c_3^2}, \quad \beta = \frac{c_2^2}{c_3^2}, \quad c_3^2 = \frac{4\mu(\lambda+\mu)}{\rho(\lambda+2\mu)}, \quad \Omega = \frac{\omega}{\bar{\omega}}, \quad \bar{\omega} = \frac{\pi c_1}{h},$$

with $\bar{\omega}$ denoting the lowest circular frequency of symmetric thickness-stretch vibration of an infinite plate of thickness h. Since all the coefficients in (10) are constants, it is convenient to rewrite it as

$$(D^2 + \delta_1^2)\ (D^2 + \delta_2^2)\ \psi = 0, \quad D = d/dy, \tag{11}$$

where

$$\delta_1^2 = \frac{1}{2}\, p[(\alpha+\beta)\Omega^2 - 1 + \gamma], \quad \delta_2^2 = \frac{1}{2}\, p[(\alpha+\beta)\Omega^2 - 1 - \gamma], \tag{12}$$

$$\gamma^2 = [(\alpha+\beta)\Omega^2 - 1]^2 + 4\alpha\beta\Omega^2(1-\Omega^2).$$

Therefore, in view of the form of (11), we may solve two second order ordinary differential equations

$$(D^2 + \delta_j^2)\,\psi_j = 0, \quad j = 1,2, \tag{13}$$

such that ψ is obtained by superposition:

$$\psi = \psi_1 + \psi_2. \tag{14}$$

It is not difficult to show that $\delta_1^2 > 0$ for all real values of Ω and that $\delta_2^2 < 0$ if $\Omega < 1$, $\delta_2^2 = 0$ if $\Omega = 1$, and $\delta_2^2 > 0$ if $\Omega > 1$. Hence, the form of the solution of $(D^2 + \delta_2^2)\,\psi_2 = 0$ will depend upon the frequency range.

A convenient expression for u(y) can be obtained from the first equation in (9), in conjunction with (13) and (14):

$$2\alpha u(y) = ph(c_1^2\delta_1^2 - \omega^2)\psi_1(y) + ph(c_1^2\delta_2^2 - \omega^2)\psi_2(y). \tag{15}$$

It is our objective to determine the natural circular frequencies of vibration of an infinite plate strip subject to the following sets of boundary conditions on the edges $y = \pm a/2$ (see Eq. 5):

(i) Free Edges, $N_{yy} = 0$, $R_y = 0$, or, equivalently,

$$h(\lambda+2\mu)\frac{\partial v_y}{\partial y} + 2\lambda\kappa v_z = 0, \quad \frac{\partial v_z}{\partial y} = 0, \text{ on } y = \pm a/2 \qquad (16)$$

However, in view of (8) and (15), the conditions (16) become

$$\psi_1 + \psi_2 = 0, \ (c_1^2\delta_1^2-\omega^2)\psi_1' + (c_1^2\delta_2^2-\omega^2)\psi_2' = 0, \text{ on } y = \pm a/2; \qquad (17)$$

(ii) Clamped Edges, $v_y = v_z = 0$, i.e.,

$$\psi_1' + \psi_2' = 0, \ (c_1^2\delta_1^2-\omega^2)\psi_1 + (c_1^2\delta_2^2-\omega^2)\psi_2 = 0, \text{ on } y = \pm a/2; \qquad (18)$$

(iii) Mixed Edge Conditions, $y = a/2$ is a clamped edge and $y = -a/2$ is a free edge:

$$\psi_1' + \psi_2' = 0, \ (c_1^2\delta_1^2-\omega^2)\psi_1 + (c_1^2\delta_2^2-\omega^2)\psi_2 = 0, \text{ on } y = a/2, \qquad (19)$$

$$\psi_1 + \psi_2 = 0, \ (c_1^2\delta_1^2-\omega^2)\psi_1' + (c_1^2\delta_2^2-\omega^2)\psi_2' = 0, \text{ on } y = -a/2. \qquad (20)$$

3. SOLUTIONS OF EQUATIONS OF MOTION.

3a. Case (i). Free Edges.

If $\Omega > 1$, then $\delta_2^2 > 0$ and the solutions of (13) are

$$\psi_1 = A\cos(\delta_1 y) + B\sin(\delta_1 y), \quad \psi_2 = C\cos(\delta_2 y) + E\sin(\delta_2 y), \qquad (21)$$

where A, B, C, and E are constants. Substitution of (21) into the boundary conditions (17) yields, after some rearrangement, two uncoupled systems of homogeneous algebraic equations in A, B, C, and E:

$$A \cos (\delta_1 a/2) + C \cos (\delta_2 a/2) = 0,$$

$$\delta_1(c_1^2\delta_1^2-\omega^2)A \sin (\delta_1 a/2) + \delta_2(c_1^2\delta_2^2-\omega^2)\, C \sin (\delta_2 a/2) = 0 \tag{22}$$

and

$$B \sin (\delta_1 a/2) + E \sin (\delta_2 a/2) = 0,$$

$$\delta_1(c_1^2\delta_1^2-\omega^2)\, B \cos (\delta_1 a/2) + \delta_2(c_1^2\delta_2^2-\omega^2)\, E \cos (\delta_2 a/2) = 0. \tag{23}$$

From the first equation in (24) it follows that

$$C = -A \cos (\delta_1 a/2) \,/\, \cos (\delta_2 a/2),$$

and hence, by virtue of (14),

$$\psi(y) = A \sec (\delta_2 a/2)\, [\cos (\delta_2 a/2) \cos \delta_1 y - \cos (\delta_1 a/2) \cos \delta_2 y], \tag{24}$$

which, henceforth, we shall call the <u>symmetric mode</u> of vibration. Similarly, starting with the first of (23), we obtain the <u>antisymmetric mode</u>

$$\psi(y) = B \csc (\delta_2 a/2)\, [\sin (\delta_2 a/2) \sin \delta_1 y - \sin (\delta_1 a/2) \sin \delta_2 y]. \tag{25}$$

In order that the systems of equations (22) and (23) have nontrivial solutions, we must require that the determinants of their coefficient matrices vanish. For the <u>symmetric mode</u>, we obtain

$$\frac{\tan \xi\gamma}{\tan \gamma} = \frac{1 - \eta}{\xi(\xi^2 - \eta)}, \quad (\Omega > 1), \tag{26}$$

where $\gamma = \delta_1 a/2$,

$$\xi^2 = \frac{\delta_2^2}{\delta_1^2} = \frac{(\alpha+\beta)\Omega^2-1-\sigma}{(\alpha+\beta)\Omega^2-1+\sigma}, \quad \eta = \left(\frac{\omega}{c_1\delta_1}\right)^2 = (1-\nu)\Omega^2[(\alpha+\beta)\Omega^2-1+\sigma]^{-1}. \tag{27}$$

For the <u>antisymmetric mode</u> the corresponding result is

$$\frac{\tan \xi\gamma}{\tan \gamma} = \frac{\xi(\xi^2 - \eta)}{1 - \eta}, \quad (\Omega < 1). \tag{28}$$

Because of the complexity of the transcendental equations (26) and (28), it is necessary to solve them numerically with an electronic computer. In order to display the variation of the frequency ratio Ω versus the width-to-thickness ratio a/h of the strip for a given value of Poisson's ratio ν, we select values of $\Omega > 1$ and solve (26) and (28) for γ since ξ and η are known from (27) once Ω and ν are specified. Then a/h can be computed from

$$\frac{a}{h} = \frac{2\gamma}{\pi\Omega}\sqrt{1 - \eta}. \tag{29}$$

The discussion of the numerical results associated with (26) and (28) will be postponed until the cases $\Omega < 1$ and $\Omega = 1$ have been examined.

Next, if $\Omega < 1$, then set $\delta_3^2 = -\delta_2^2 > 0$, so that the equation for ψ_2 in (13) becomes $\psi_2''(y) - \delta_3^2 \psi_2(y) = 0$, which has the solution

$$\psi_2(y) = C \cosh \delta_3 y + E \sinh \delta_3 y. \tag{30}$$

Proceeding as before, we can show that

$$\psi(y) = A \operatorname{sech} (\delta_3 a/2) [\cosh (\delta_3 a/2) \cos \delta_1 y - \cos (\delta_1 a/2) \cosh \delta_3 y], \tag{31}$$

and

$$\frac{\tanh \tilde{\xi}\gamma}{\tan \gamma} = \frac{1 - \eta}{\tilde{\xi}(\tilde{\xi}^2 + \eta)}, \quad (\tilde{\xi} < 1), \tag{32}$$

where $\tilde{\xi} = \delta_3/\delta_1$, for the <u>symmetric mode</u>, whereas

$$\psi(y) = B \operatorname{csch} (\delta_3 a/2) [\sinh (\delta_3 a/2) \sin \delta_1 y - \sin (\delta_1 a/2) \sinh \delta_3 y], \tag{33}$$

and

$$\frac{\tanh \tilde{\xi}\gamma}{\tan \gamma} = \frac{-\tilde{\xi}(\tilde{\xi}^2 + \eta)}{1 - \eta}, \quad (\tilde{\xi} < 1), \tag{34}$$

for the <u>antisymmetric mode</u>.

Finally, we turn our attention to the case in which $\Omega = 1$, i.e., the natural circular frequency of the strip is equal to the lowest circular frequency of symmetric thickness-stretch vibrations of an infinite plate. It follows from (12) that

$$\delta_1^2 = p(\alpha + \beta - 1), \qquad \delta_2^2 = 0, \tag{35}$$

when $\Omega = 1$ since $\sigma = \alpha + \beta - 1$. With $\delta_2 = 0$, the differential equation for ψ_2 in (13) becomes $\psi_2'' = 0$, whence

$$\psi_2(y) = C + Ey. \tag{36}$$

Substituting the first of (21) and (36) into the boundary conditions (17), we obtain for the symmetric mode

$$A \cos(\delta_1 a/2) + C = 0, \quad \delta_1(c_1^2\delta_1^2 - \bar{\omega}^2) A \sin(\delta_1 a/2) = 0, \tag{37}$$

and for the antisymmetric mode

$$B \sin(\delta_1 a/2) + a E/2 = 0, \quad \delta_1(c_1^2\delta_1^2 - \bar{\omega}^2) B \cos(\delta_1 a/2) - \bar{\omega}^2 E = 0. \tag{38}$$

Since it can be shown that $\delta_1 \neq 0$ and $c_1^2\delta_1^2 - \bar{\omega}^2 \neq 0$, it follows from (37) that $\sin(\delta_1 a/2) = 0$. Hence

$$\delta_1 = 2n\pi/a, \quad n = 1,2,3,\ldots, \tag{39}$$

and from (35) and (39), we obtain

$$\frac{a}{h} = 2n\beta^{\frac{1}{2}}(\alpha + \beta - 1)^{-\frac{1}{2}} = 2n\left[\frac{(1-\nu)(1-2\nu)}{1-3\nu+4\nu^2}\right]^{\frac{1}{2}}, \quad n=1,2,3,\ldots, \tag{40}$$

which holds for $\Omega = 1$ in the symmetric mode. For the antisymmetric mode, it follows from (38) that γ is to be determined from

$$\tan\gamma = (\eta - 1)/\gamma\eta, \tag{41}$$

where in this case

$$\eta = \beta(\alpha + \beta - 1)^{-1} \quad \text{and} \quad a/h = 2\gamma\eta^{\frac{1}{2}}/\pi.$$

Let us now investigate some limiting cases of the equations (26), (28), (32), (34), and (41).

Low Frequencies, Wide Plates. For $\Omega \ll 1$ and $a/h \gg 1$, we can show that

$$\tilde{\xi}^2 \simeq 1/(\alpha\beta\Omega^2) \qquad \text{and} \qquad \eta \simeq 1/\alpha \tag{42}$$

From (42) and (29), it follows that

$$\Omega = \frac{2\gamma}{\pi\alpha^{\frac{1}{2}}} \cdot \frac{h}{a} \qquad \text{or} \qquad \omega = 2\gamma c_3/a, \tag{43}$$

where γ must be determined from (32) and (34) for the symmetric and antisymmetric modes, respectively. But, in view of (42) and (43), we know that

$$\tilde{\xi}\gamma = \frac{\pi}{\alpha\beta^{\frac{1}{2}}} \cdot \frac{a}{h}$$

i.e., $\tilde{\xi}\gamma \gg 1$ since $a/h \gg 1$. Thus, we are justified in making the approximation $\tanh \tilde{\xi}\gamma \simeq 1$, so that (32) and (34) are reduced to $\cos\gamma = 0$ and $\sin\gamma = 0$, for the symmetric and antisymmetric modes, respectively. Consequently,

$$\gamma = (2n+1)\pi/2, \quad n = 0,1,2,\ldots \qquad \text{and} \qquad \gamma = n\pi, \quad n = 1,2,3\ldots,$$

so that in the present approximation of low frequencies in wide plates we find from (43)

$$\omega_n = (2n+1)\pi c_3/a \qquad \text{and} \qquad \omega_n = 2n\pi c_3/a$$

for the symmetric and antisymmetric modes, respectively. These frequencies are identical to those obtained from the theory of generalized plane stress in (A.15) and (A.13) of the Appendix.

High Frequencies, Narrow Plates. For $\Omega \gg 1$ and $a/h \ll 1$, we can show that

$$\xi_1^2 \simeq \pi^2 \omega^2/\beta h^2, \quad \xi_2^2 = \pi^2 \omega^2/h^2, \quad \xi^2 = \pi^2/\alpha,$$

$$\frac{a}{h} = \frac{2\gamma}{\pi} \eta^{\frac{1}{2}} \simeq 2\xi_1/\pi\alpha, \tag{44}$$

where γ is the solution of (26) and (28) for the symmetric and antisymmetric modes, respectively. However, in view of the fact that $\xi^2 - \eta \doteq 0$, (26) and (28) reduce to $\cos\xi\gamma = 0$ and $\sin\xi\gamma = 0$, respectively. Hence

$$\xi\gamma = (2n+1)\pi/2, \quad n = 0,1,2\ldots, \qquad \text{and} \quad \xi\gamma = n\pi, \quad n = 1,2,3,\ldots,$$

so that (44) leads to

$$\omega_n = (2n+1)\pi c_1/a \qquad \text{and} \qquad \omega_n = 2n\pi c_1/a \tag{45}$$

for the symmetric and antisymmetric modes, respectively. The frequencies given in (45) are identical to the natural circular frequencies of symmetric and antisymmetric thickness-stretch vibrations of an infinite plate of thickness a.

Intermediate Frequency, $\Omega = 1$. In (40) we gave the value of the width-to-thickness ratio for the special case of symmetric vibrations with frequency ratio $\Omega = 1$. The antisymmetric mode is not quite so simple, but a convenient approximate expression can be derived from (41). Since in this case

$$\eta = \beta/(\alpha + \beta - 1) \qquad \text{and} \qquad a/h = 2\gamma\eta^{\frac{1}{2}}/\pi, \tag{46}$$

it follows that

$$(\eta - 1)/\eta = -s,$$

where s is a function of Poisson's ratio given by

$$s = 2\nu^2/(1 - \nu)(1 - 2\nu).$$

Therefore, (41) may be written as

$$\tan\gamma = -s\gamma. \tag{47}$$

Now the larger roots of (47) are near $(2n+1)\pi/2$, n being a positive integer, and the larger value of n the better the approximation. To obtain an improved approximation, we put $\gamma = (2n+1)\pi/2 + \varepsilon$, where it is understood that $|\varepsilon| << \pi/2$. We can easily show that to a first approximation ε has the value

$$\varepsilon \doteq 2/s(2n+1)\pi$$

so that

$$\nu \simeq \frac{(2n+1)\pi}{2}\left[1 + \frac{2(1-\nu)(1-2\nu)}{(\pi\nu)^2\,(2n+1)^2}\right], \tag{48}$$

and consequently, inserting (48) into (46), we obtain

$$\frac{a}{h} \simeq (2n+1)\left[\frac{(1-\nu)(1-2\nu)}{1-3\nu+4\nu^2}\right]^{\frac{1}{2}}\left[1 + \frac{2(1-\nu)(1-2\nu)}{(\pi\nu)^2\,(2n+1)^2}\right],$$

for the antisymmetric mode in the special case that $\Omega = 1$.

The variation of the frequency ratio Ω with the width-to-thickness ratio a/h for the first three symmetric and antisymmetric modes for $\nu = 0.3$ is shown in Figures 2 and 3, respectively. For the sake of comparison, the generalized plane stress and the Kane-Mindlin results are plotted on the same set of axes. Clearly, the frequencies as computed from these theories are in agreement only in the low frequency range (i.e., very wide strips relative to the thickness), and the range of agreement decreases as the mode number n increases. While the theory of generalized plane stress predicts that the frequency of the lowest mode becomes unbounded as the width-to-thickness ratio tends to zero, the Kane-Mindlin theory indicates that Ω approaches a finite value less than unity as a/h tends to zero.

3b. Case (ii). Clamped Edges.

For a plate strip with clamped edges, the boundary conditions are now (18). Repeating the procedures outlined in Section 3a above, we can show that the secular equations become

$$\left.\begin{aligned} \frac{\tanh \tilde{\xi}\gamma}{\tan \gamma} &= \frac{\tilde{\zeta}^2 + \eta}{\tilde{\xi}(1-\eta)}, \quad (\Omega < 1), \quad \sin \gamma = 0, \ (\Omega = 1), \\ \frac{\tan \xi\gamma}{\tan \gamma} &= \frac{\zeta^2 - \eta}{\xi(1-\eta)}, \quad (1 < \Omega), \end{aligned}\right\} \tag{49}$$

for the symmetric mode, and

$$\frac{\tanh \tilde{\xi}\gamma}{\tan \gamma} = \frac{\tilde{\xi}(\eta - 1)}{\tilde{\xi}^2 + \eta}, \quad (\Omega < 1), \qquad \tan \gamma = \frac{\eta\gamma}{\eta - 1}, \quad (\Omega = 1),$$

$$\frac{\tan \xi\gamma}{\tan \gamma} = \frac{\xi(1 - \eta)}{\xi^2 - \eta}, \quad (1 < \Omega), \tag{50}$$

for the antisymmetric mode. As in the case of the strip with free edges, once the transcendental equations (49) and (50) are solved for γ, the width-to-thickness ratio may be computed from (29). We turn our attention next to some limiting forms of the secular equations given above.

Low Frequencies, Wide Plates. Assuming that $\Omega << 1$ and $a/h >> 1$, we again adopt the approximate expressions (42). Since $\tilde{\xi} >> 1$, it follows that $\tanh \tilde{\xi}\gamma \simeq 1$, so the first equations in (49) and (50) can be approximated by

$$\tan \gamma \simeq \Omega \cdot (\beta/\alpha)^{\frac{1}{2}} \qquad \text{and} \qquad \cot \gamma \simeq \Omega \cdot (\beta/\alpha)^{\frac{1}{2}}$$

respectively. Since we are concerned with very low frequencies, we replace these last expressions by $\sin \gamma = 0$, which implies that $\gamma = n\pi$, $n = 1,2,3,\ldots$, for the symmetric mode and $\cos \gamma = 0$, whence $\gamma = (2n+1)\pi/2$, $n = 0,1,2,\ldots$ for the antisymmetric mode. Hence, by (29) we have $\Omega \simeq 2n\alpha^{\frac{1}{2}}h/a$ for the symmetric mode and $\Omega \simeq (2n + 1)\alpha^{\frac{1}{2}}(h/a)$ for the antisymmetric mode, which are identical to the corresponding results computed within the framework of generalized plane stress, which are given in (A.17) and (A.16), respectively, of the Appendix.

High Frequencies, Narrow Plates. Here we assume that $\Omega >> 1$ and $a/h << 1$. As discussed above, $\xi^2 - \eta \simeq 0$ in the high frequency range, so the third equations in (49) and (50) reduce to $\tan \xi\gamma = 0$ which leads to $\xi\gamma = n\pi$, $n = 1,2,3\ldots$, for the symmetric mode, and $\tan \xi\gamma = \infty$, i.e., $\xi\gamma = (2n+1)\pi/2$, $n = 0,1,2,\ldots$, for the antisymmetric mode. Because $a/h \simeq 2\xi\gamma/\pi\Omega$ in the high frequency range, it follows that $\Omega = 2nh/a$ for the symmetric mode and $\Omega = (2n+1)h/a$ for the antisymmetric mode. These frequency ratios are identical to those which can be computed from the exact theory of elasticity for the thickness-stretch type of vibration of an infinite plate of thickness a which has its faces rigidly clamped.

Intermediate Frequency, $\Omega = 1$. We have already observed that in the symmetric mode γ is to be computed from $\sin \gamma = 0$ when $\Omega = 1$, which implies that $\gamma = n\pi$, with $n = 1,2,3,\ldots$. In this situation (29) yields

$$\frac{a}{h} = n\eta^{\frac{1}{2}} = 2n\left[\frac{(1-\nu)(1-2\nu)}{1-3\nu+4\nu^2}\right]^{\frac{1}{2}}.$$

For the antisymmetric mode, γ is to be found from

$$s \tan \gamma = -\gamma , \tag{51}$$

where $s = 2\nu^2/(1-\nu)\cdot(1-2\nu)$. It is a straightforward matter to show that the larger roots of (51) may be approximated by

$$\gamma \simeq \frac{(2n+1)\pi}{2}\left[1 + \frac{4s}{(2n+1)^2\pi^2}\right],$$

and hence an approximate expression for the width-to-thickness ratio is

$$\frac{a}{h} \simeq (2n+1)\left[\frac{(1-\nu)(1-2\nu)}{1-3\nu+4\nu^2}\right]^{\frac{1}{2}}\left[1 + \frac{8\nu^2}{(2n+1)^2\pi^2\,(1-\nu)(1-2\nu)}\right].$$

In Figures 4 and 5, graphs of Ω versus a/h have been plotted for $\nu = 0.3$ for the symmetric and antisymmetric modes in an infinite plate strip with clamped edges. We note that the Kane-Mindlin and generalized plane stress theories are in agreement only for plates very wide relative to the thickness in the symmetric mode in Figure 4. However, in Figure 5 the frequency spectrum for the lowest antisymmetric mode in an infinite plate strip with clamped edges as computed from the Kane-Mindlin theory coincides almost exactly with that computed according to the theory of generalized plane stress over the entire transition from very narrow plate strips to very wide strips. As before, though, the higher modes agree only in the low frequency range.

We can show that the displacement potential $\psi(y) = \psi_1(y) + \psi_2(y)$ is given by

$$\psi(y) = \begin{cases} A\tilde{\xi}^{-1}\operatorname{csch}\tilde{\xi}\gamma[\sinh\tilde{\xi}\gamma\cos\delta_1 y - \sin\gamma\cosh\delta_3 y], & \Omega<1, \\ A\eta^{-1}[\eta\cos\delta_1 y + (1-\eta)\cos\gamma], & \Omega = 1, \\ A\xi^{-1}\csc\xi\gamma\,[\xi\sin\xi\gamma\cdot\cos\delta_1 y - \sin\gamma\cdot\cos\delta_2 y], & \Omega>1, \end{cases} \tag{52}$$

and with (15) it follows that

$$2\lambda Ku(y) = \begin{cases} AQ\tilde{\xi}^{-1}\,\mathrm{csch}\tilde{\xi}\gamma[(1-\eta)\tilde{\xi}\sinh\tilde{\xi}\gamma\,\cos\delta_1 y + (\tilde{\xi}^2+\eta)\,\sin\gamma\cosh\,\delta_3 y], & \Omega<1, \\ AQ(1-\eta)\,(\cos\delta_1 y - \cos\gamma), & \Omega = 1 \\ AQ\xi^{-1}\,\mathrm{csc}\xi\gamma[\xi(1-\eta)\sin\xi\gamma\cos\delta_1 y-(\xi^2-\eta)\sin\gamma\cos\delta_2 y], & \Omega>1, \end{cases} \tag{53}$$

for the symmetric mode, and

$$\psi(y) = \begin{cases} B\tilde{\xi}^{-1}\,\mathrm{sech}\tilde{\xi}\gamma[\tilde{\xi}\cosh\tilde{\xi}\gamma\sin\delta_1 y - \cos\gamma\sinh\delta_3 y], & \Omega<1, \\ B(\sin\delta_1 y-\delta_1 y\,\cos\,\gamma), & \Omega = 1, \\ B\xi^{-1}\,\mathrm{sec}\xi\gamma[\xi\cos\xi\gamma\sin\delta_1 y - \cos\gamma\,\sin\delta_2 y], & \Omega>1, \end{cases} \tag{54}$$

and

$$2\lambda Ku(y) = \begin{cases} BQ\tilde{\xi}^{-1}\mathrm{sech}\tilde{\xi}\gamma[\tilde{\xi}(1-\eta)\cosh\tilde{\xi}\gamma\sin\delta_1 y+(\tilde{\xi}^2+\eta)\cos\gamma\,\sinh\delta_3 y], & \Omega<1, \\ BQ[(1-\eta)\sin\delta_1 y + \delta_1\eta y], & \Omega = 1, \\ BQ\xi^{-1}\mathrm{sec}\xi\gamma[\xi(1-\eta)\cos\xi\gamma\sin\delta_1 y - (\xi^2-\eta)\,\cos\gamma\,\sin\delta_2 y], & \Omega>1, \end{cases} \tag{55}$$

for the antisymmetric mode, where $Q = \rho h(c_1\delta_1)^2$.

3c. Case (iii). Mixed Edge Conditions

Finally, we wish to solve the pair of differential equations in (13) subject to the boundary conditions (19) and (20). Upon repetition of the steps outlined in Section 3a, we can show that in the case of mixed edge conditions the symmetric and antisymmetric modes do not uncouple. In the usual fashion we find the secular equation to be

$$\xi[(\xi^2-\eta)^2 + (1-\eta)^2]\,\cos\,2\gamma\,\cos\,2\xi\gamma - 2\xi(1-\eta)(\xi^2-\eta) + \\ + (1-\eta)(\xi^2-\eta)(1+\xi^2)\,\sin\,\,2\gamma\,\sin 2\xi\gamma = 0, \tag{56}$$

for $\Omega>1$,

$$\gamma\tan\,2\gamma - \sec\,2\gamma\, = (1-2\eta\, + 2\eta^2)/2\eta(1-\eta), \tag{57}$$

for $\Omega = 1$, and

$$\tilde{\xi}[(\tilde{\xi}^2+\eta)^2 + (1-\eta)^2] \cos 2\gamma \cosh 2\tilde{\xi}\gamma + 2\tilde{\xi}(1-\eta)(\tilde{\xi}^2+\eta)$$

$$= (1-\eta)(\tilde{\xi}^2-\eta)(1-\tilde{\xi}^2) \sin 2\gamma \sinh 2\tilde{\xi}\gamma . \tag{58}$$

The variation of Ω with a/h, as determined from (56), (57), (58), and (29), for plate strips with mixed edge conditions is shown in Figure 6 for $\nu = 0.3$. As in the case of the antisymmetric mode of vibration of a plate strip with clamped edges (see Figure 5), it is evident that the theory of generalized plane stress predicts rather accurately the variation of Ω with a/h for the lowest mode for all values of a/h. Clearly, the higher modes are in agreement only when the width of the strip is very large relative to its thickness.

4. ORTHOGONALITY RELATION. In terms of the plate-stress resultants, the Kane-Mindlin [3] equations of extensional motions of plates are of the form

$$N_{\alpha\beta,\beta} = \rho h \ddot{v}_\alpha, \qquad R_{\alpha,\alpha} - N_{zz} = 2\rho(I_z/h)\ddot{v}_z$$

for free vibrations, where the comma denotes differentiation with respect to x_α, with $x_1 = x$ and $x_2 = y$ and the subscripts $\alpha,\beta = 1,2$. By virtue of (4) and (6), these reduce to

$$N_{yy,y} = \rho h \ddot{v}_y, \quad R_{y,y} - N_{zz} = 2\rho(I_z/h)\ddot{v}_z, \tag{59}$$

where

$$N_{yy} = h(\lambda+2\mu)v_{y,y} + 2\lambda\kappa v_z, \quad R_y = 2\mu(I_z/h)v_{z,y},$$

$$N_{zz} = 2(2\mu+\lambda)\kappa^2 v_z + \lambda k h v_{y,y}. \tag{60}$$

Denoting the natural circular frequencies of vibration of the strip by ω_n (n=1,2,3...) for any of the sets of boundary conditions discussed in Section 3, let

$$v_y(y,t) = w_n(y) \cos \omega_n t, \qquad v_z(y,t) = u_n(y) \cos \omega_n t,$$

$$N_{yy}(y,t) = N_n(y) \cos \omega_n t, \qquad R_y(y,t) = R_n(y) \cos \omega_n t,$$

$$N_{zz}(y,t) = M_n(y) \cos \omega_n t,$$

and substitute these into (59) and (60):

$$N_n' = -\rho h \omega_n^2 w_n, \qquad R_n' = -2\rho (I_z/h) \omega_n^2 u_n, \tag{61}$$

$$\left.\begin{aligned} N_n &= h(\lambda+2\mu) w_n' + 2\lambda\kappa u_n, \quad R_n = 2\mu (I_z/h) u_n', \\ M_n &= 2(2\mu+\lambda)\kappa^2 u_n + \lambda h \kappa w_n' . \end{aligned}\right\} \tag{62}$$

Multiply the first equation in (61) by w_k and integrate the result over the interval $-a/2 \leq y \leq a/2$:

$$\int_{-a/2}^{a/2} w_k' N_n \, dy = \rho h \omega_n^2 \int_{-a/2}^{a/2} w_k w_n \, dy, \tag{63}$$

where we have integrated by parts, using the fact that $w_k N_n = 0$ on $y = \pm a/2$ for any of the sets of boundary conditions considered in Section 3. Upon interchanging k and n in (63), we obtain

$$\int_{-a/2}^{a/2} w_n' N_k \, dy = \rho h \omega_k^2 \int_{-a/2}^{a/2} w_k w_n \, dy. \tag{64}$$

We now form the difference of (63) and (64):

$$\rho h (\omega_n^2 - \omega_k^2) \int_{-a/2}^{a/2} w_n w_k \, dy = \int_{-a/2}^{a/2} (w_k' N_n - w_n' N_k) \, dy. \tag{65}$$

Next, multiply the second equation in (61) by u_k and repeat essentially the same steps which were outlined in the previous paragraph. In this way, it can be shown that

$$\int_{-a/2}^{a/2} u_k' R_n \, dy + \int_{-a/2}^{a/2} u_k M_n \, dy = 2\rho (I_z/h) \omega_n^2 \int_{-a/2}^{a/2} u_k u_n \, dy,$$

where we have used the fact that $u_k R_n = 0$ on $y = \pm a/2$ by virtue of the boundary conditions considered in Section 3. As before, we find

$$2\rho(I_z/h)(\omega_n^2 - \omega_k^2) \int_{-a/2}^{a/2} u_k\, u_n\, dy = \int_{-a/2}^{a/2} (u_k' R_n + \\ + u_k M_n - u_n' R_k - u_n M_k)\, dy. \tag{66}$$

Finally, multiply (66) by 2/h and add the result to (65):

$$\frac{1}{3}\rho h(\omega_n^2 - \omega_k^2) \int_{-a/2}^{a/2} (3w_n w_k + u_n u_k)\, dy = \int_{-a/2}^{a/2} (F_{nk} - G_{kn})\, dy, \tag{67}$$

where

$$F_{nk} = w_k' N_n + \frac{2}{h} u_k' R_n + \frac{2}{h} u_k M_n, \quad G_{kn} = w_n' N_k + \frac{2}{h} u_n' R_k + \frac{2}{h} u_n M_k \tag{68}$$

But, substituting (62) into (68), we can show that $F_{nk} = G_{kn}$, and hence (67) reduces to

$$\int_{-a/2}^{a/2} (3\, w_n w_k + u_n u_k)\, dy = 0, \quad n \neq k$$

which is the orthogonality condition which the plate-displacements for the plate-strip problem must satisfy.

REFERENCES

1. Lord Rayleigh 1889 Proc. London Math. Soc. 29, 225. On the free vibrations of an infinite plate of homogeneous elastic matter.

2. H. Lamb 1917 Proc. Royal Soc. London, Series A 93, 114. On waves in an elastic plate.

3. T. R. Kane and R. D. Mindlin 1956 J. Appl. Mech. 23, 277. High frequency extensional vibrations of plates.

4. R. D. Mindlin and M. A. Medick 1959 J. Appl. Mech. 26, 561. Extensional vibrations of elastic plates.

5. S. Kumar 1960 International Symposium on Stress Wave Propagation in Macerials (Norman Davids, Editor) 119. Edge waves in plates. New York: Interscience Publishers.

6. D. C. Gazis and R. D. Mindlin 1957 J. Appl. Mech. 24, 541. Influence of width on velocities of long waves in plates.

7. I. S. Sokolnikoff 1960 Mathematical Theory of Elasticity. New York: McGraw-Hill.

8. R. D. Mindlin 1955 An Introduction to the Mathematical Theory of Vibrations of Elastic Plates. Fort Monmouth, New Jersey: Signal Corps Engineering Laboratories.

APPENDIX

GENERALIZED PLANE STRESS FORMULATION. Neglecting body forces, the differential equation of motion of an isotropic elastic solid within the framework of the theory of generalized plane stress is

$$\mu\nabla^2\underset{\sim}{v} + \mu\left(\frac{3\lambda + 2\mu}{\lambda + 2\mu}\right)\nabla(\nabla\cdot\underset{\sim}{v}) = \rho\ddot{\underset{\sim}{v}} \tag{A.1}$$

where $\underset{\sim}{v} = v_x\underset{\sim}{i} + v_y\underset{\sim}{j}$, μ and λ are Lame's elastic constants, ρ is the density of the material, and $\nabla^2 = \partial^2/\partial x^2 + \partial^2/\partial y^2$. According to Sokolnikoff [7], the stress-displacement equations are

$$\left.\begin{aligned}
\sigma_{xx} &= \frac{2\mu}{\lambda + 2\mu}\left[2(\lambda+\mu)v_{x,x} + \lambda v_{y,y}\right], \\
\sigma_{yy} &= \frac{2\mu}{\lambda + 2\mu}\left[\lambda v_{x,x} + 2(\lambda+\mu)v_{y,y}\right], \\
\sigma_{xy} &= \mu(v_{x,y} + v_{y,x}).
\end{aligned}\right\} \tag{A.2}$$

Let us assume that $v_x = 0$ and $v_y = v_y(y,t)$, so that (A.1) reduces to

$$c_3^2\, v_{y,yy} = \ddot{v}_y, \quad c_3^2 = \frac{4\mu(\lambda+\mu)}{\rho(\lambda + 2\mu)} = \frac{E}{\rho(1-\nu^2)}, \tag{A.3}$$

where E is Young's modulus and ν is Poisson's ratio. With reference to Figure 1, we shall consider the following three sets of boundary conditions:

(i) free edges: $\sigma_{yy} = 0$ on $y = \pm a/2$, or

$$v_{y,y}(\pm a/2, t) = 0; \tag{A.4}$$

(ii) clamped edges

$$v_y(\pm a/2, t) = 0; \tag{A.5}$$

(iii) mixed edge conditions: the edge $y = a/2$ is clamped and the edge $y = -a/2$ is free

$$v_y(a/2,t) = 0, \qquad v_{y,y}(-a/2,t) = 0. \tag{A.6}$$

In all three cases we shall seek a solution of (A.3) of the form

$$v_y(y,t) = w(y)\cos\omega t, \tag{A.7}$$

so that (A.3) is reduced to the ordinary differential equation

$$w''(v) + b^2 w(y) = 0, \tag{A.8}$$

where $b = \omega/c_3$, subject to the following boundary conditions, obtained from (A.4) to (A.6):

(i) free edges, $w'(\pm a/2) = 0$, (A.9)

(ii) clamped edges, $w(\pm a/2) = 0$, (A.10)

(iii) mixed edge conditions, $w(a/2) = w'(-a/2) = 0$. (A.11)

The solution of (A.8) is

$$w(y) = A\cos by + B\sin by, \tag{A.12}$$

where the boundary conditions (A.9) to (A.11) serve to determine the eigenvalue and the ratio A/B.

Case (i). Free Edges. Substituting (A.12) into (A.9), we obtain two uncoupled systems of equations, which lead to

$$\omega_n = 2n\pi c_3/a, \tag{A.13}$$

or in terms of the dimensionless frequency ratio Ω_n, (A.13) becomes

$$\Omega_n = \omega_n/\omega = 2n\alpha^{-\frac{1}{2}}(h/a), \tag{A.14}$$

for the antisymmetric mode, where $\alpha = c_1^2/c_3^2$ and $\bar{\omega} = \pi c_1/h$, with $c_1^2 = (\lambda + 2\mu)/\rho$, which is the lowest natural circular frequency of symmetric thickness-stretch vibrations of an infinite plate of thickness h (see Mindlin [8]). For the symmetric mode we find

$$\omega_n = (2n + 1)\pi c_3/a \qquad \text{or} \qquad \Omega_n = (2n + 1)\alpha^{-\frac{1}{2}}\,(h/a), \qquad (A.15)$$

with $n = 0,1,2,\ldots$.

Case (ii). Clamped Edges. We record only the results here since the details are essentially the same as in Case (i). For the anti-symmetric mode the frequency ratio is

$$\Omega_n = (2n + 1)\alpha^{-\frac{1}{2}}\,(h/a), \quad n = 0,1,2,\ldots, \qquad (A.16)$$

and for the symmetric mode the corresponding result is

$$\Omega_n = 2n\alpha^{-\frac{1}{2}}\,(h/a), \quad n = 1,2,3,\ldots. \qquad (A.17)$$

Case (iii). Mixed Edge Conditions. Inserting (A.12) into (A.11), we obtain the system of equations

$$A\cos(ba/2) + B\sin(ba/2) = 0$$
$$A\sin(ba/2) + B\cos(ba/2) = 0.$$

This homogeneous system of algebraic equations will have a solution other than the trivial one if the determinant of the coefficient matrix vanishes. After some manipulation, we can show that this is equivalent to $\cos(ba) = 0$, which possesses the solutions $b_n = (2n + 1)\,\pi/2a$, $n = 0,1,2,\ldots$, which leads us to

$$\Omega_n = \frac{1}{2}(2n + 1)\alpha^{-\frac{1}{2}}\,(h/a). \qquad (A.18)$$

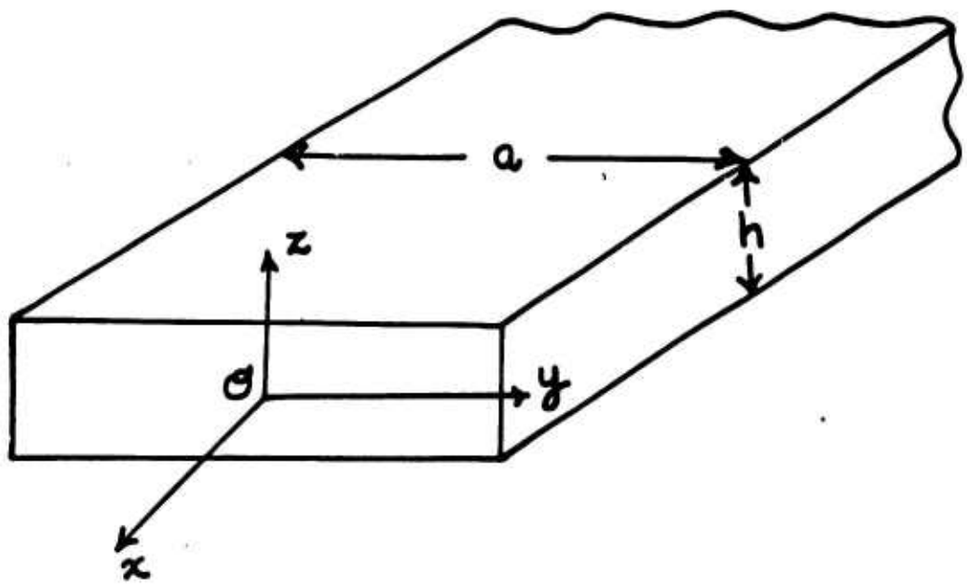
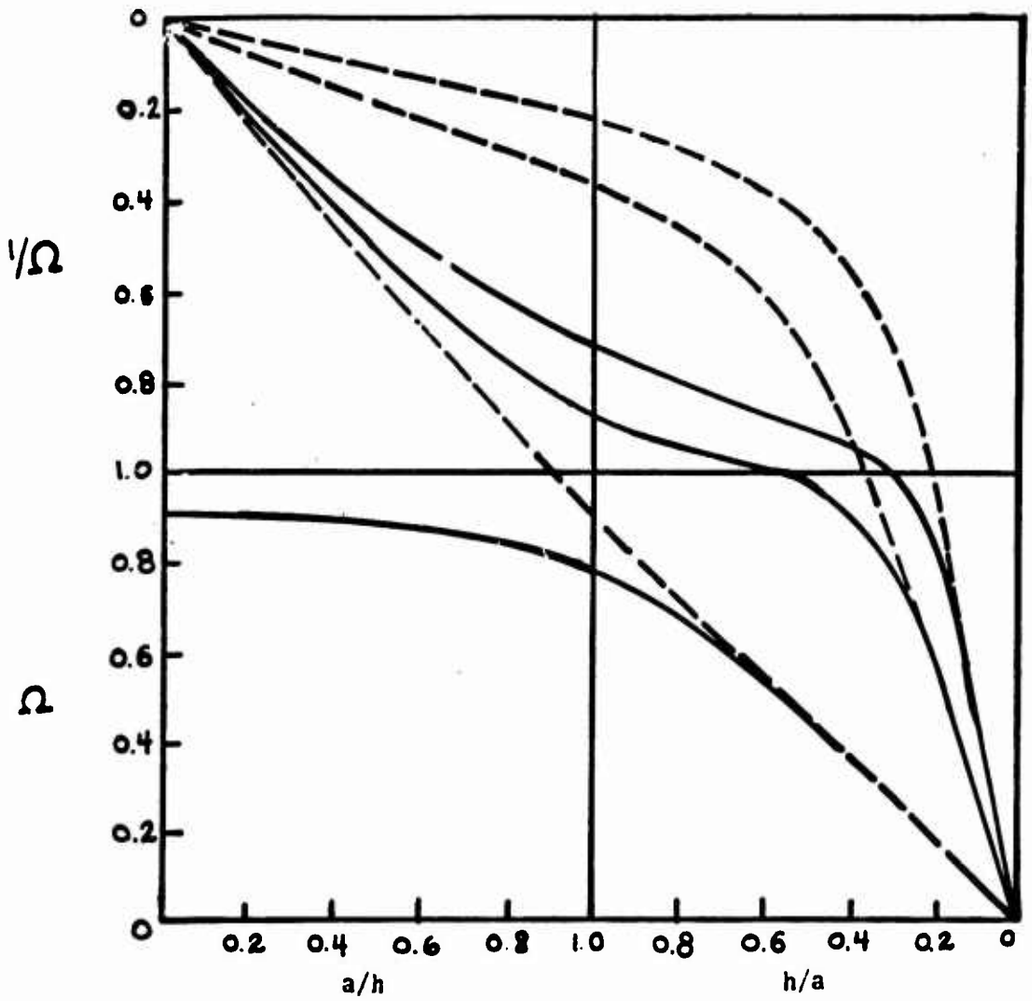


Figure 1. Reference coordinates and dimensions.



Dashed curves: theory of generalized plane stress

Solid curves: Kane-Mindlin theory

Figure 2. Free edge conditions, symmetric mode. Variation of frequency ratio Ω with width to thickness ratio a/h ($\nu = 0.3$).

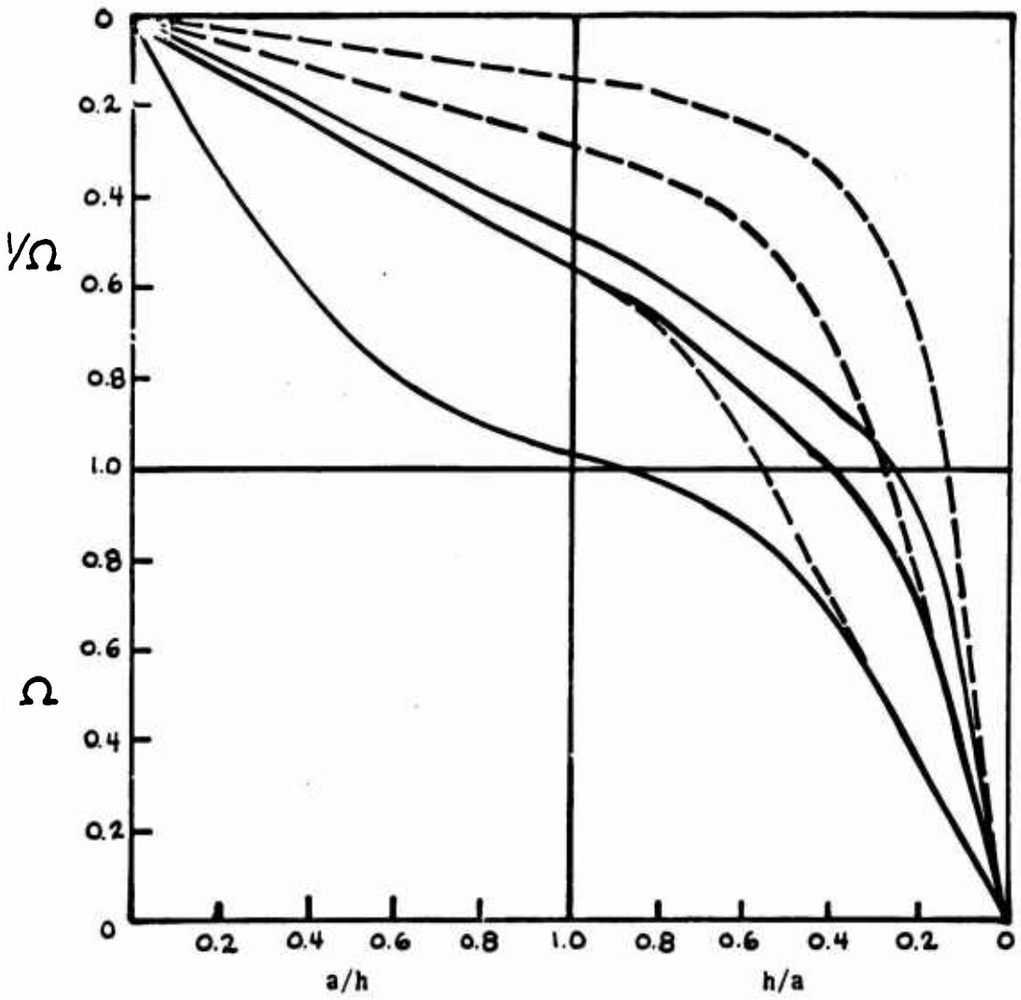


Figure 3. Free edge conditions, antisymmetric mode. Variation of frequency ratio Ω with width to thickness ratio a/h (ν = 0.3).

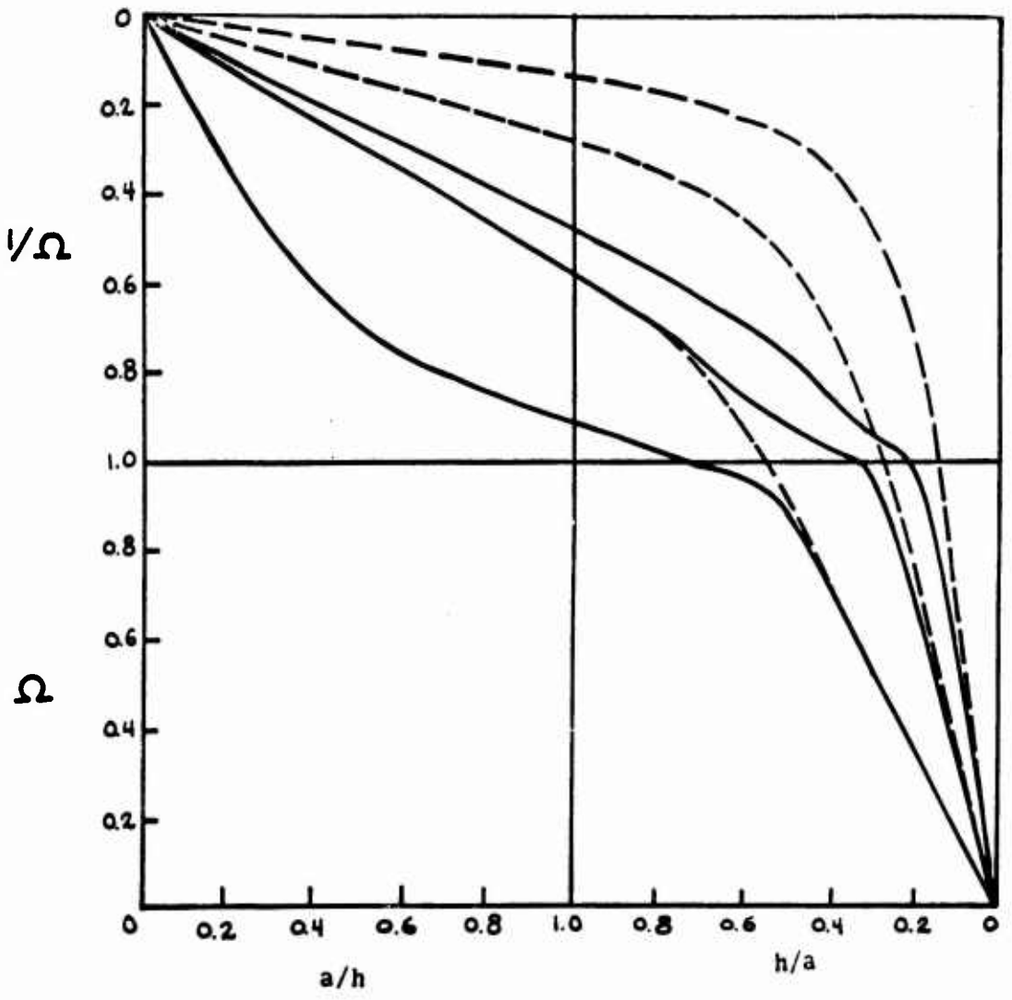


Figure 4. Clamped edge conditions, symmetric mode. Variation of frequency ratio Ω with width to thickness ratio a/h (ν = 0.3).

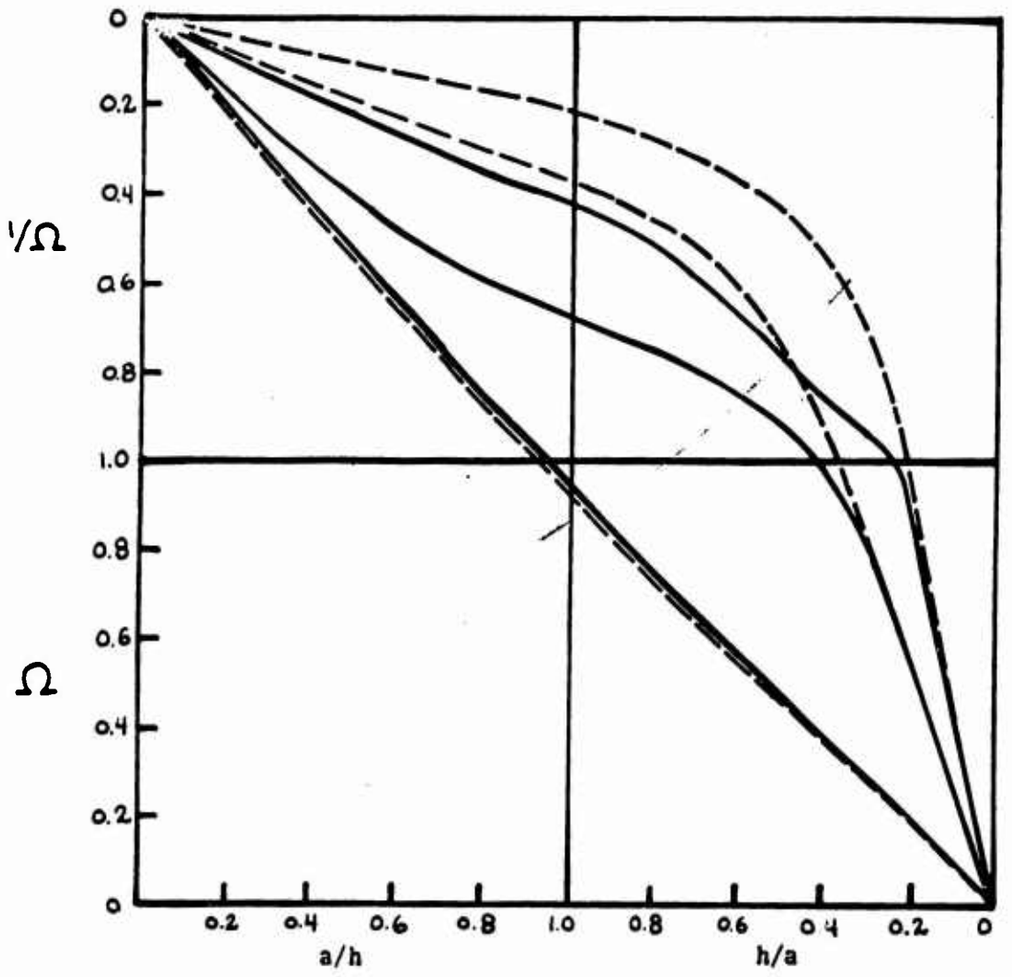


Figure 5. Clamped edge conditions, antisymmetric mode. Variation of frequency ratio Ω with width to thickness ratio a/h (ν = 0.3).

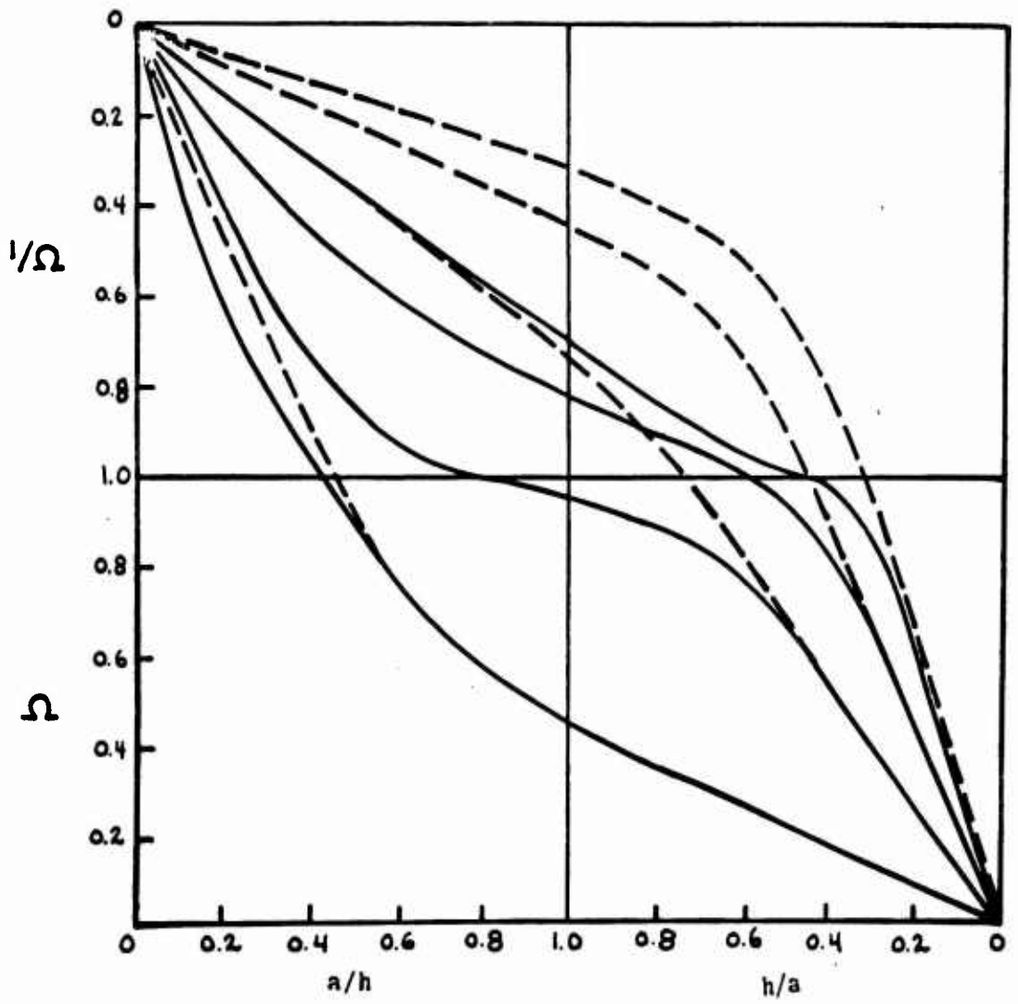


Figure 6. Mixed edge conditions. Variation of frequency ratio Ω with width to thickness ratio a/h (ν = 0.3).

FORCED OSCILLATION OF A MASS WITH A BILINEAR SPRING

Royce Beckett and K. C. Pan
Systems Analysis Directorate, Army Weapons Command
Rock Island, Illinois

ABSTRACT. The response of a mechanical assembly in a vibration environment is strongly dependent upon the tolerance between parts. An increase in the looseness in an assembly may increase the amplitude of the response which can cause premature damage or failure. Of particular concern is the packaging of electronic components and fatigue failure of mechanical parts. This paper gives a numerical solution for the motion of a mass that is forced to vibrate between two springs which allow some free travel at the center. Coulomb or viscous dissipation is admitted. Results are presented in the form of amplification curves which are plotted against a dimensionless excitation frequency.

INTRODUCTION. Acceptance tests for assemblies and subassemblies of complex systems often require forced vibration at some level over a wide spectrum of frequencies. In the design of these assemblies, it is helpful to predict the response so that harmful effects can be minimized. In many instances tolerances may occur between mating parts and this complicates the analysis by causing the response to be non-linear.

It is also known that the service life of an assembly that is subject to a dynamic environment is adversely effected by tolerance buildup between parts [1]. Tests have shown that failures of assemblies are almost always preceded by an increase in the looseness between parts of the assembly.

This paper investigates the effect of looseness (tolerance) on the response of a simple spring mass system that is subjected to a vibration environment. Also included is an evaluation of the effect on the behavior of viscous damping which is sometimes present in a loose assembly - particularly those where some isolation from the environment may be sought..

Results of the study are presented in graphical form where the amplification factor is plotted against a dimensionless excitation frequency.

EQUATIONS OF BEHAVIOR. Figure 1 shows the problem that is considered. The mass m oscillates between the two springs with spring constant k. The tolerance in the system is represented by the two gaps of length a. The support is subjected to an excitation represented by x and the mass motion is defined by u. A representative spring force is graphed against the relative displacement z(z = u-x) in the Figure. Viscous and Coulomb damping may be included. The equation of motion for the mass is written

$$m\ddot{u} = -f-F \qquad (1)$$

where f is the spring force and F is the dissipation force.

$$f = 0 \qquad |u-x| \leq a \tag{2}$$

and it will depend upon the characteristics and deformation of the spring when $|u-x| > a$. The force F may represent any kind of dissipation force. Some computations have been carried out when F is a constant friction force that acts when the springs are in contact with the mass but the more interesting results are obtained when F is made to approximate the damping behavior of a visco-elastic spring. Then, it is assumed that the viscous drag will occur while the spring is being compressed, but will be zero when the spring is lengthened. The rationale for this assumption is that the spring is not attached to the mass.

SOLUTION OF EQUATIONS. The behavior is evaluated by two different methods. The first method requires that the springs be linear and equal, no damping, the excitation be harmonic and the response of the mass is suitably represented by a sine function. In the second method used, the equations of behavior are solved numerically and the springs may be unequal and non-linear, damping may exist and there is no requirement on the form of the response. The second method will, of course, handle many more cases; but, the former will give very good estimations of the response even for systems with substantial non-linearity provided the conditions cited above hold. Computation time for the first method is considerably less although this was not an important consideration when the work was done on a high speed third generation computer system.

If F is assumed to be zero, and if the springs are linear and symmetrical, then equation (1) can be written

$$m\ddot{u} = -f(u-x) \tag{3}$$

where

$$\begin{aligned} f &= 0 && |u-x| \leq a \\ f &= k(u-x-a) && u-x > a \\ f &= k(u-x+a) && u-x < a \end{aligned} \tag{4}$$

Equation (3) can be solved explicitly for the period T when x is harmonic and the response u is assumed to be harmonic [2].

$$\frac{T}{4} = \int_0^{\frac{T}{4}} dt = \int_0^{u_0} \frac{du}{\sqrt{\frac{2}{m}\int_{u_0}^{u} -f(u-x)\,du}} \tag{5}$$

where u_0 is the amplitude of motion of the mass. The integration in equation (5) is carried out for f as defined in equation (4) and for

$$x = \pm \frac{x_0}{u_0} u \tag{6}$$

The plus and minus signs give, respectively, the in-phase and out-of-phase response of the system. For the former:

$$\frac{T}{4} = \sqrt{\frac{m}{k}} \frac{1}{\sqrt{1 - \frac{x_0}{u_0}}} \left[\frac{a}{u_0 - x_0 - a} + \frac{\pi}{2} \right] \tag{7}$$

For the latter

$$\frac{T}{4} = \sqrt{\frac{m}{k}} \frac{1}{\sqrt{1 + \frac{x_0}{u_0}}} \left[\frac{a}{u_0 + x_0 - a} + \frac{\pi}{2} \right] \tag{8}$$

If T is replaced by its equivalent in terms of frequency, then equation (7) (or equation 8) is a relationship between frequency, level of input represented by x_0 and the amplitude of the output u_0.

The second method of solution used for equation (1) is based on numerically integrating the equation. The general objective in the numerical integration will be to generate a periodic solution under given conditions of excitation. This will be the steady state response to the excitation. In order to numerically integrate equation (1), two starting conditions on u must be known. If these starting conditions are correct, then a complete cycle of motion is generated in one period. In general, the two starting conditions are not known because the amplitude of the response is unknown and there is an unknown phase lag between the excitation and the response. The correct solution is generated by an iteration scheme that successively improves the starting values for the trial solution.

Figure 2 shows a trace of the excitation x and the response u versus time. The starting point is chosen where x = 0. The starting values for

u, i.e., u_0 and $\dot{u}_0$ will depend upon the amplification factor and the phase lag. When values are assigned to u_0 and $\dot{u}_0$, then the integration can proceed to time T. At time T the values for u and $\dot{u}$ should be the same as the starting values. In general, they will not be the same so that new starting values must be chosen. A Newton Raphson scheme is used to improve u_0 and $\dot{u}_0$ in the iteration.

In equation (1) let z = u-x, then

$$\ddot{z} = -\frac{1}{m} f - \frac{1}{m} F - \ddot{x} \tag{9}$$

The conditions assumed on f and F in the numerical solutions are as follows:

$$\begin{aligned} f &= 0 && |z| \leq a \\ &= k(z-a) && z > a \\ &= k(z+a) && z < a \end{aligned} \tag{10}$$

$$F(z) = 0 \qquad |z| \leq a$$

For z > a

$$\begin{aligned} F(z) &= c\dot{z} && \dot{z} > 0 \\ &= 0 && \dot{z} < 0 \end{aligned} \tag{11}$$

For z < a

$$\begin{aligned} F(z) &= c\dot{z} && \dot{z} < 0 \\ &= 0 && \dot{z} > 0 \end{aligned}$$

Rewriting equation (9) as two first order equations and using equations (10) and (11) gives

$$\begin{aligned} \dot{u} &= \text{constant} && |z| < a \\ \dot{z} &= y && |z| \leq a \\ \dot{y} &= -\frac{1}{m} f - \frac{1}{m} F - \ddot{x} \end{aligned} \tag{12}$$

Since x is known, starting values for u_0 and $\dot{u}_0$ give directly starting values for z and y.

Equation (12) is solved by a Runge-Kutta method. It is required that

$$u(T) = u_0$$
$$\dot{u}(T) = \dot{u}_0 \tag{13}$$

In general, equation (13) will not be satisfied by the first choice for u_0 and $\dot{u}_0$. Corrections are made to these starting values in the following way.

It is assumed that u(T) and $\dot{u}(T)$, denoted u_T and $\dot{u}_T$, have appropriate continuity with respect to u_0 and $\dot{u}_0$ so that the Taylor expansions in equations (14) and (15) will hold.

$$u_T(u_0+\Delta u_0, \dot{u}_0+\Delta\dot{u}_0) = u_T(u_0,\dot{u}_0) + \left.\frac{\partial u_T}{\partial u}\right|_0 \Delta u_0 + \left.\frac{\partial u_T}{\partial \dot{u}}\right|_0 \Delta\dot{u}_0 + \ldots \tag{14}$$

$$\dot{u}_T(u_0+\Delta u_0, \dot{u}_0+\Delta\dot{u}_0) = \dot{u}_T(u_0,\dot{u}_0) + \left.\frac{\partial \dot{u}_T}{\partial u}\right|_0 \Delta u_0 + \left.\frac{\partial \dot{u}_T}{\partial \dot{u}}\right|_0 \Delta\dot{u}_0 + \ldots \tag{15}$$

where the subscripts on the derivative terms indicate that the derivative is to be evaluated at $(u_0,\dot{u}_0)$.

From equations (14) and (15) values for $\dot{u}$ and $\dot{u}_0$ are sought that will make u_T and $\dot{u}_T$ equal to the starting values.

$$u_T(u_0+\Delta u_0, \dot{u}_0+\Delta\dot{u}_0) - (u_0+\Delta u_0) = 0 \tag{16}$$

$$\dot{u}_T(u_0+\Delta u_0, \dot{u}_0+\Delta\dot{u}_0) - (\dot{u}_0+\Delta\dot{u}_0) = 0 \tag{17}$$

Substituting for u_T and $\dot{u}_T$ gives two simultaneous equations in the correction terms Δu_0 and $\Delta\dot{u}_0$.

$$\left(1 - \left.\frac{\partial u_T}{\partial u}\right|_0\right)\Delta u_0 - \left.\frac{\partial u_T}{\partial \dot{u}}\right|_0 \Delta\dot{u}_0 = u_T(u_0,\dot{u}_0) - u_0 \tag{18}$$

$$-\left.\frac{\partial \dot{u}_T}{\partial u}\right|_0 \Delta u_0 + \left(1 - \left.\frac{\partial \dot{u}_T}{\partial \dot{u}}\right|_0\right)\Delta\dot{u}_0 = \dot{u}_T(u_0,\dot{u}_0) - \dot{u}_0 \tag{19}$$

The right hand side of equations (18) and (19) is the difference between u(or $\dot{u}$) at time T as found from the solution of equations (12) and the starting values. The derivative terms in the coefficients are evaluated numerically by making individual variations in u_0 and $\dot{u}_0$. Thus,

$$\left.\frac{\partial u_T}{\partial u}\right|_0 \doteq \frac{u_T(u_o+\delta u_0,\dot{u}_0) - u_T(u_0,\dot{u}_0)}{\delta u_0} \tag{20}$$

$u_T(u_0+\delta u_0,\dot{u}_0)$ is found by making a small change in u_0, i.e., δu_0, and then computing u_T from equation (12), etc.

RESULTS. Results of computer studies are presented in graphical form. Figure 3 shows a plot of the magnification curves for the system in Figure 1 when the dissipation is zero and the springs are equal and linear. Figure 4 shows the response with damping for the case of a small gap (non-linearity) and these do not differ significantly from the linear response. In Figure 5, the response curves are given for the same cases except that the tolerance gap has been increased. Points on the unstable portions of the curves in Figure 5 could not be obtained because the iteration would not converge to an unstable point. Figure 6 gives a plot of the phase angle for two values of the looseness. Here again the curve for a = 0.10 is not extended much beyond 90°, since the system is unstable in this region. The curves in Figure 6 and the curves for the magnification factor can be used for the evaluation of the forces acting in the system.

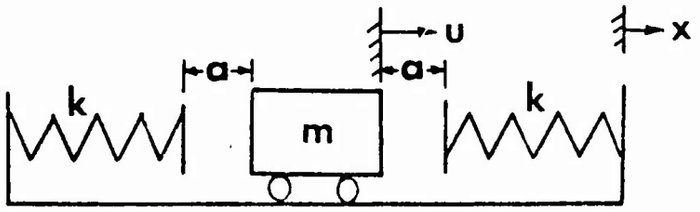
The results show that forced oscillation of a loose system gives higher amplitude response for in-phase motion, but that the out-of-phase response is almost non-existent (Figures 3 and 4). Very large increases in amplitude will occur when the looseness increases. For example, Figure 3 shows that for a "frequency ratio" of 0.6 that the magnification factor is increased by a factor of 2 when the looseness increases from zero to a value of 0.10 inches. Figure 4 shows that even for substantial damping there is a high magnification factor. This means that wear which increases the looseness of an assembly will have the effect of increasing the amplitude of the response to excitation and this will give a corresponding increase in the dynamic forces. Such a response confirms experiments reported in Ref. 1 on the effects of looseness on the life of mechanical assemblies.

It is also known that looseness is an important consideration in the packaging of all kinds of delicate equipment; particularly, in assemblies where a high reliability of performance is required. On the basis of the results presented here, it would appear that the control of looseness may be more effective than the introduction of damping in limiting the response in a vibration environment.

REFERENCES

1. Rim, K., and Louis, C., "Investigation of the Effect of Looseness of Imperfect Points on Structural Integrity," Fall Meeting of SESA, October, 1969.

2. Den Hartog, J. P., Mechanical Vibration, McGraw-Hill, 1956.



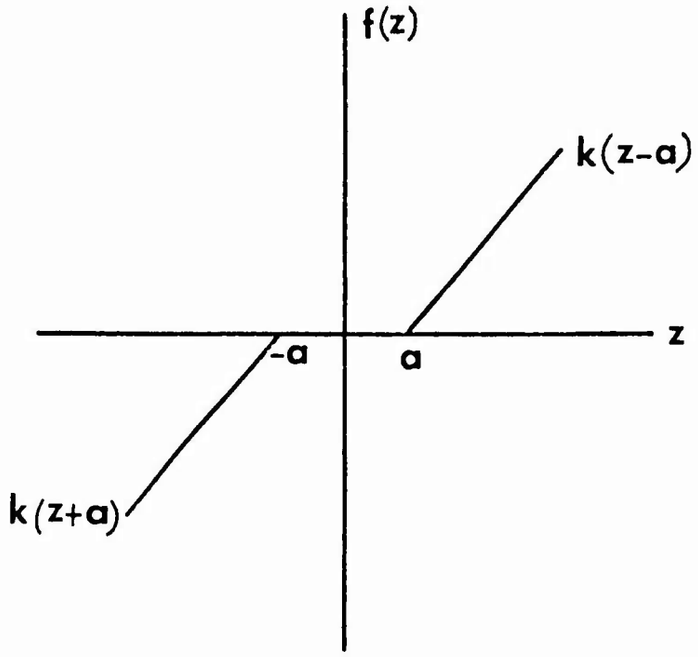


FIG. 1 SPRING MASS SYSTEM

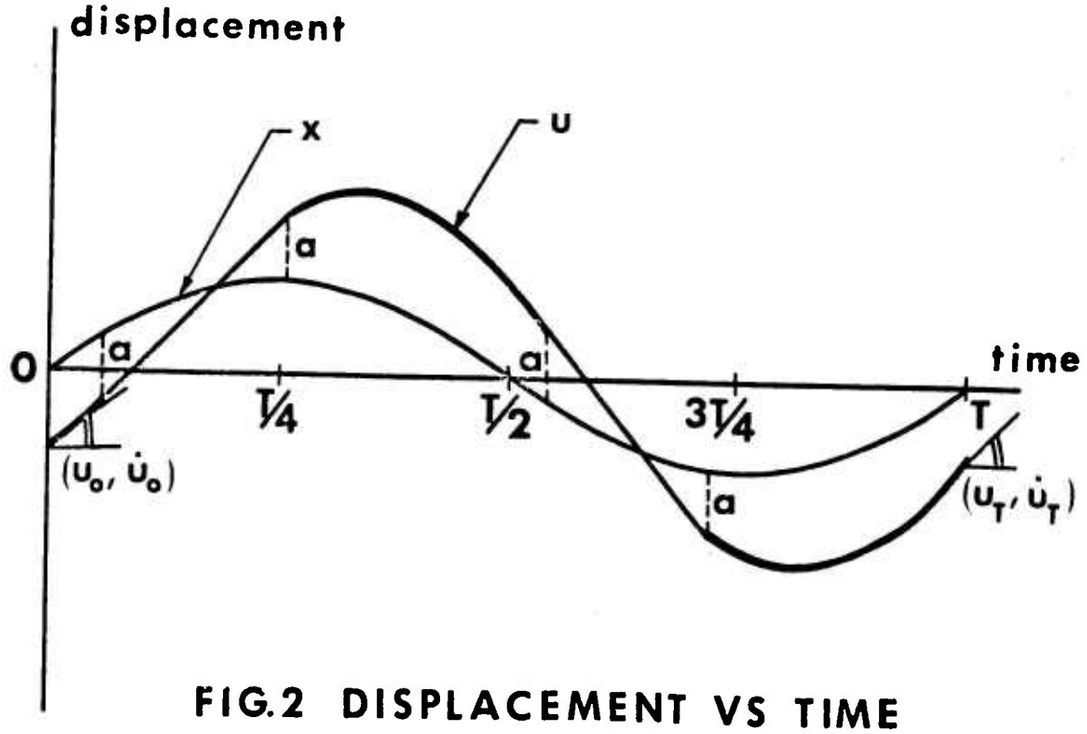


FIG.2 DISPLACEMENT VS TIME FOR DAMPED SYSTEM

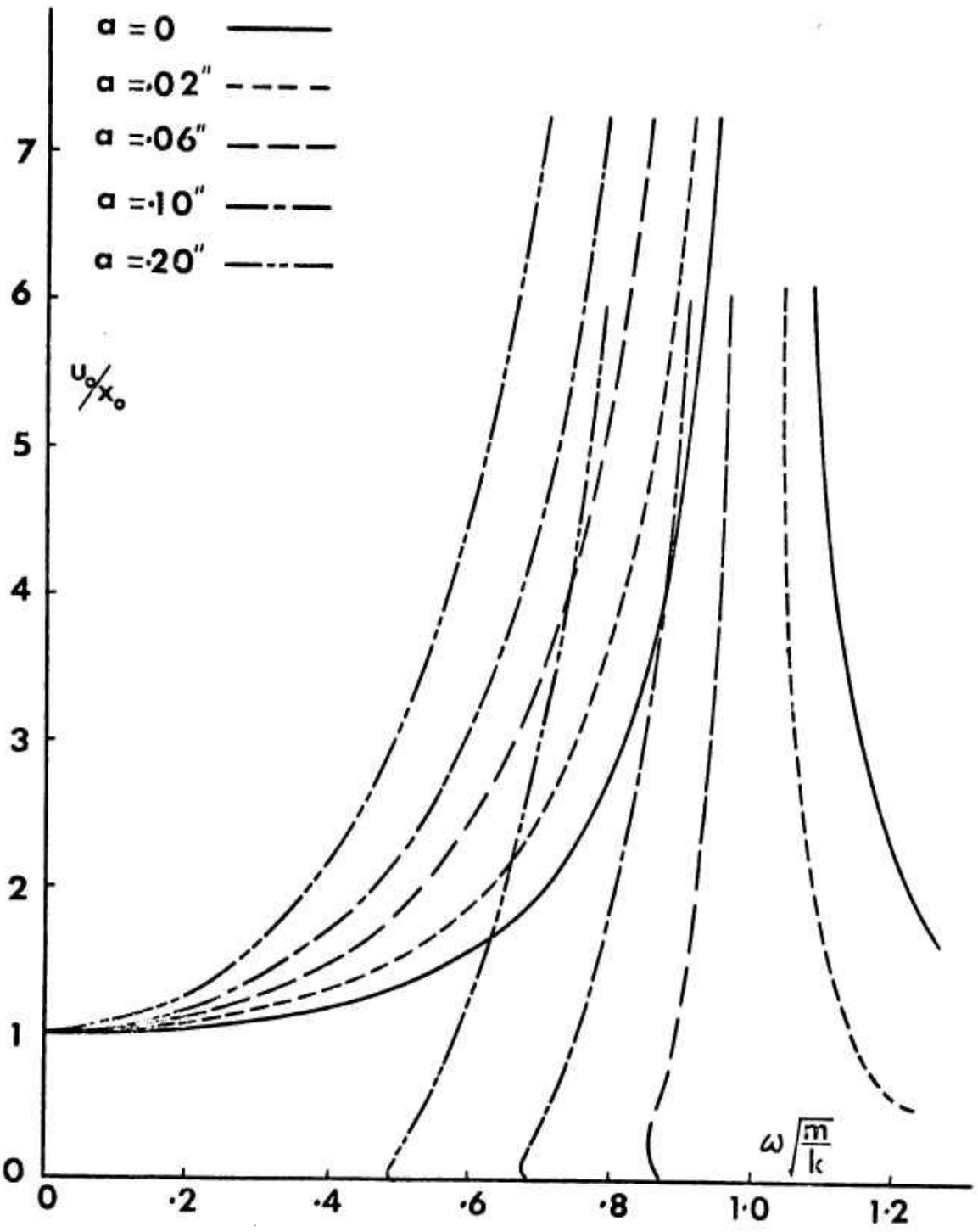


FIG. 3 MAGNIFICATION FACTOR VS FREQUENCY RATIO

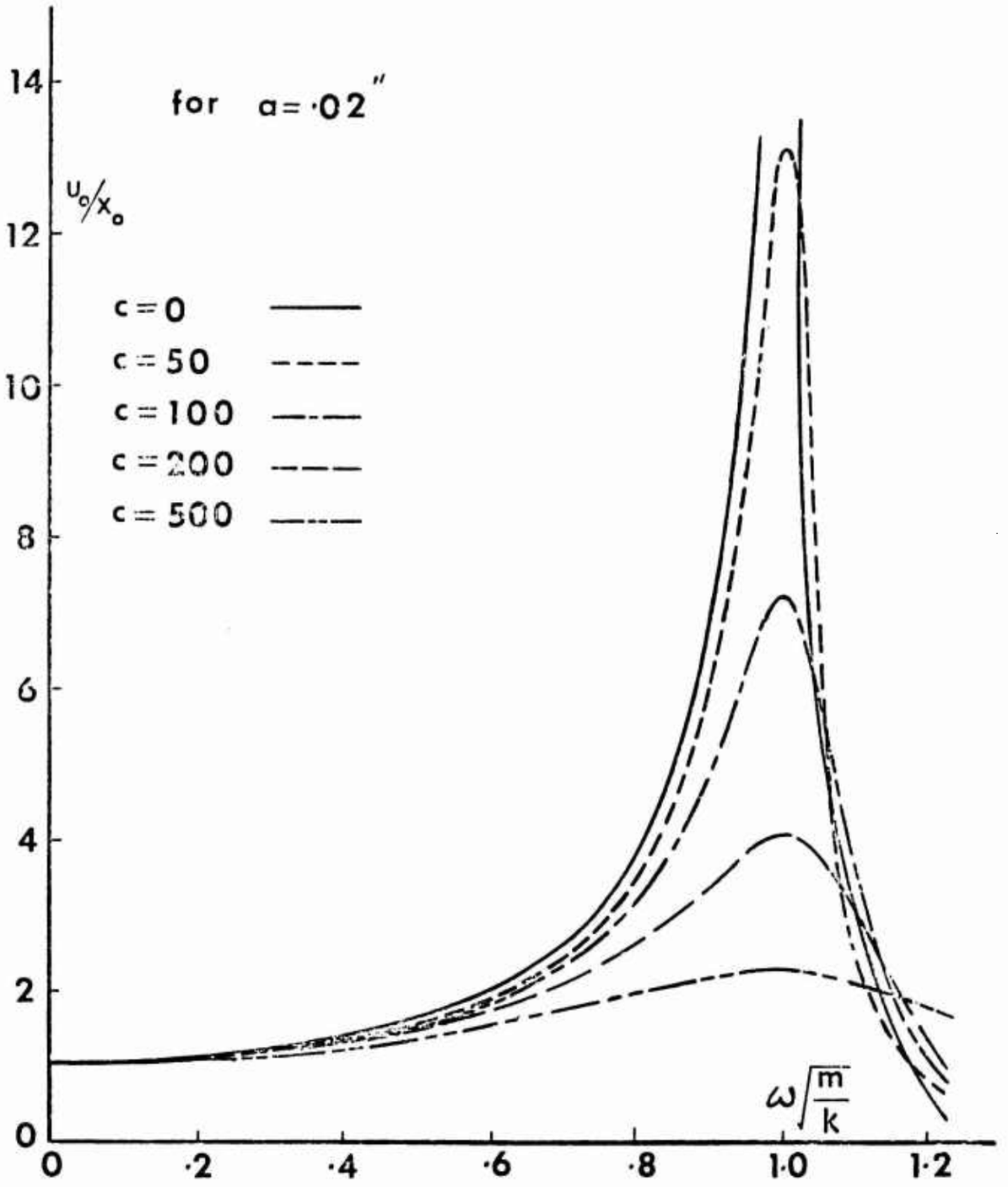


FIG.4 EFFECT OF DAMPING

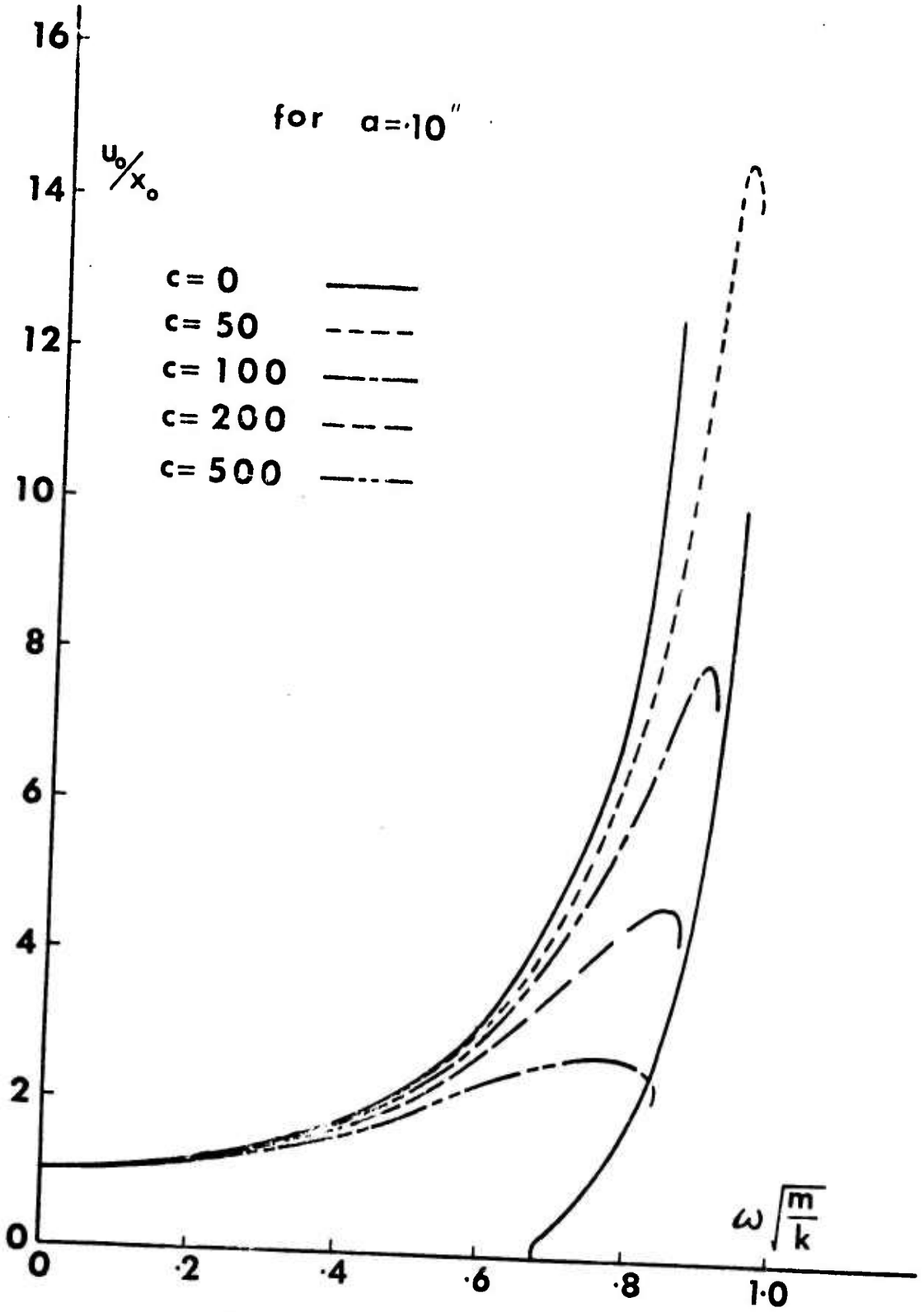


FIG. 5 EFFECT OF DAMPING

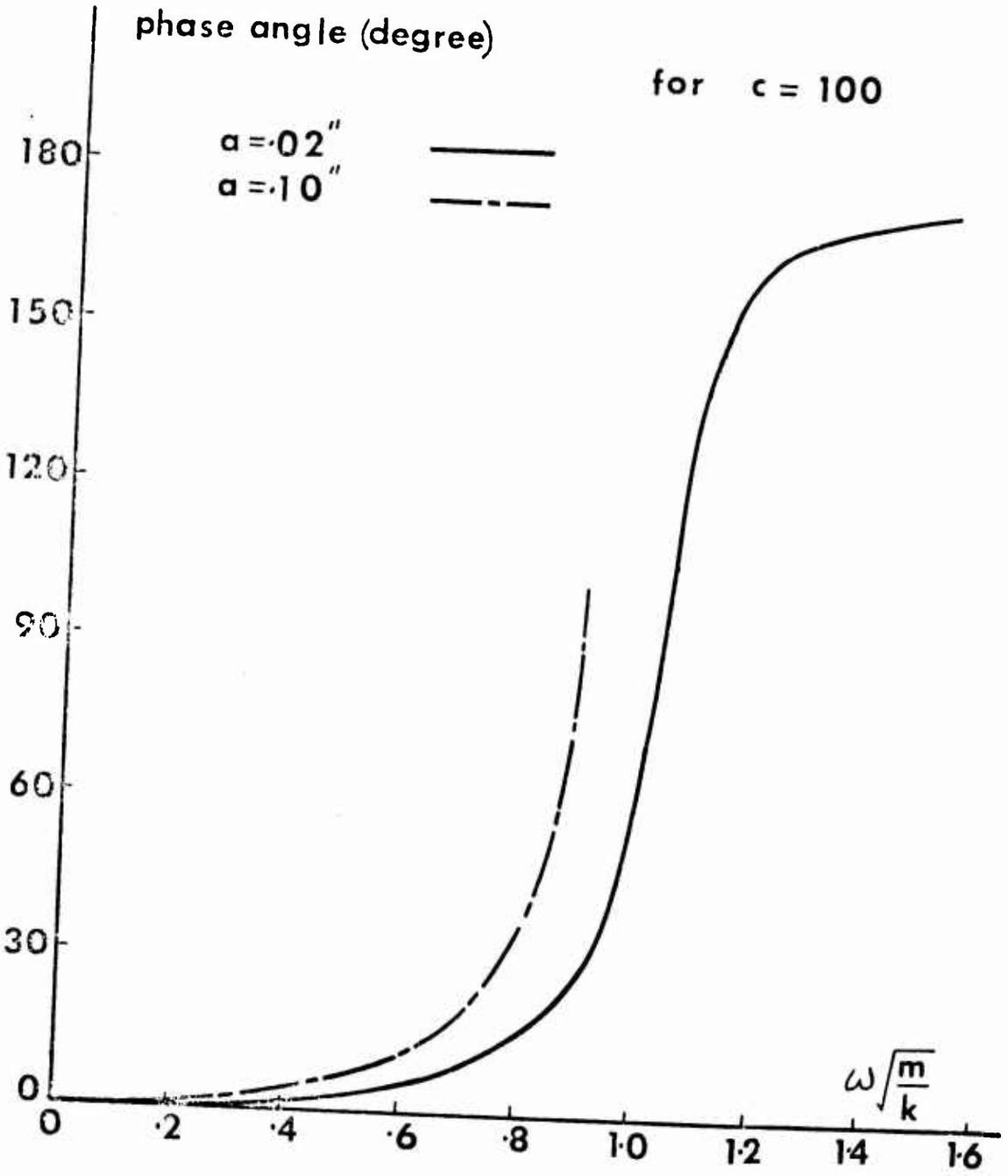


FIG.6 PHASE ANGLE VS FREQUENCY RATIO

ON EIGENVALUES AND STRUCTURE OF THE HURWITZ MATRIX

Siegfried H. Lehnigk
U. S. Army Missile Command
Redstone Arsenal, Alabama

SUMMARY. The set of special matrices investigated in the literature contains the Hurwitz matrix of a given polynomial. This matrix is of particular interest in the theory of stability of linear motions. In the special case that the given polynomial is real and Hurwitzian, its Hurwitz matrix has only positive eigenvalues and either these eigenvalues have all multiplicity one or there is one of multiplicity two. If, for a given real Hurwitzian polynomial, the Hurwitz matrix has an eigenvalue of multiplicity two, then it is nonderogatory, its set of eigenvectors is not complete; i.e., its Jordan normal form is not diagonal. The Hurwitz operator associated with the Hurwitz matrix has fixed points which are discussed briefly.

1. INTRODUCTION. In the theory of matrices with elements in the field $\tilde{C}$ of the complex numbers it is customary to investigate the eigenvalues (their reality or complexity, their location in the complex plane, their multiplicities) and the structure (number of linearly independent eigenvectors, canonical forms) of special matrices. As examples, we mention Hermitian and skew-Hermitian matrices, unitary matrices, (totally) nonnegative and oscillatory matrices.

This article deals with the eigenvalues and the structure of the Hurwitz matrix of a given polynomial with coefficients in $\tilde{C}$. The Hurwitz matrix is a fundamental tool in the theory of stability of linear motions [1; Chap. 4].

As it turns out, it seems to be rather hopeless to obtain usable results in the general case. Therefore, severe restrictions on the given polynomial will be introduced.

2. THE HURWITZ MATRIX. Let

$$f(z) = \sum_{\nu=0}^{n} a_\nu z^{n-\nu} \quad (a_o = 1) \qquad (1)$$

be a polynomial of degree $n \geq 1$ with $a_\nu \in \tilde{C}$ ($\nu = 0, 1, \ldots, n$). The $n \times n$ matrix $H = (H_{\mu\nu})$ with elements

$$H_{\mu\nu} = a_{2\nu-\mu} \quad (\mu,\nu = 1,\ldots,n;\ a_\alpha = 0 \text{ if } \alpha < 0 \text{ or } \alpha > n)$$

PRECEDING PAGE BLANK

ON EIGENVALUES AND STRUCTURE OF THE HURWITZ MATRIX

Siegfried H. Lehnigk
U. S. Army Missile Command
Redstone Arsenal, Alabama

SUMMARY. The set of special matrices investigated in the literature contains the Hurwitz matrix of a given polynomial. This matrix is of particular interest in the theory of stability of linear motions. In the special case that the given polynomial is real and Hurwitzian, its Hurwitz matrix has only positive eigenvalues and either these eigenvalues have all multiplicity one or there is one of multiplicity two. If, for a given real Hurwitzian polynomial, the Hurwitz matrix has an eigenvalue of multiplicity two, then it is nonderogatory, its set of eigenvectors is not complete; i.e., its Jordan normal form is not diagonal. The Hurwitz operator associated with the Hurwitz matrix has fixed points which are discussed briefly.

1. INTRODUCTION. In the theory of matrices with elements in the field $\tilde{C}$ of the complex numbers it is customary to investigate the eigenvalues (their reality or complexity, their location in the complex plane, their multiplicities) and the structure (number of linearly independent eigenvectors, canonical forms) of special matrices. As examples, we mention Hermitian and skew-Hermitian matrices, unitary matrices, (totally) nonnegative and oscillatory matrices.

This article deals with the eigenvalues and the structure of the Hurwitz matrix of a given polynomial with coefficients in $\tilde{C}$. The Hurwitz matrix is a fundamental tool in the theory of stability of linear motions [1; Chap. 4].

As it turns out, it seems to be rather hopeless to obtain usable results in the general case. Therefore, severe restrictions on the given polynomial will be introduced.

2. THE HURWITZ MATRIX. Let

$$f(z) = \sum_{\nu=0}^{n} a_\nu z^{n-\nu} \qquad (a_o = 1) \qquad (1)$$

be a polynomial of degree $n \geq 1$ with $a_\nu \in \tilde{C}$ ($\nu = 0, 1, \ldots, n$). The $n \times n$ matrix $H = (H_{\mu\nu})$ with elements

$$H_{\mu\nu} = a_{2\nu-\mu} \qquad (\mu,\nu = 1,\ldots,n;\ a_\alpha = 0 \text{ if } \alpha < 0 \text{ or } \alpha > n)$$

PRECEDING PAGE BLANK

is called the Hurwitz matrix of f. The odd-numbered rows and the even-numbered rows of H are cyclic; H is doubly cyclic. If the coefficients a_ν of f are real (in R) for $\nu = 0,1,\ldots,n$, the main principal minors $H_\rho = \det(H_{\mu\nu})_{\mu,\nu=1}^{\rho}$ $(\rho=1,\ldots,n)$ of H, the so-called Hurwitz determinants of H, can be used to determine the number of zeros of f with positive, negative, and vanishing real part [1;Th. 4.1, p. 101; Th.6.3, p. 118; Th.6.9, p. 150]. Other determinant criteria can be used for the same purpose (Hermite and Bilharz theorems [1; Th.2.1, p. 80; Th.6.2, p. 118; Th.6.8, p. 147; Th.3.2, p. 89]).

3. A FIRST LOOK AT THE EIGENVALUE PROBLEM OF THE HURWITZ MATRIX. To realize the complexity of the problem of the location of the eigenvalues of the Hurwitz matrix H of a given polynomial f, let us consider first two examples under the assumption that f is Hurwitzian; i.e., has only zeros with negative real part.

(i) $f(z) = z^3 + 8z^2 + 2z + 7$ (Hurwitzian); $h(z) = \det(zI - H) = (z - 7)(z - 1)(z - 9)$ has only zeros with positive real parts. (Throughout this article, I denotes the identity (unit) matrix of appropriate dimension.)

(ii) $f(z) = z^3 + (1 + 7i)z^2 + (1 + 4i)z + (10 + 30i)$ (Hurwitzian); $h(z) = \det(zI - H) = (z - (10 + 30i))(z^2 - (2 + 11i)z - (37 + 19i))$ has two zeros with positive real part and one with negative real part.

Next, let us look at the polynomial $f(z) = z^3 + (2 + 2i)z^2 + (2 - 2i)z + 5$; it is nonreal and non-Hurwitzian. The polynomial $h(z) = \det(zI - H) = (z - 1)(z - 3)(z - 5)$ is real and has only zeros with positive real part.

At present, it does not seem possible to establish relations between the zeros of f and those of $h = \det(zI - H)$ without imposition of restrictions on f. To determine the number of zeros with positive, negative and vanishing real part of the characteristic polynomial $h = \det(zI - H)$ of the Hurwitz matrix H of f we have to use any of the theorems mentioned in Sec. 2.

The particular form of the matrix H implies that

$$h(z) = \det(zI - H) = (z - a_n)\det(zI - R) \qquad (2)$$

where R is the $(n - 1) \times (n - 1)$ matrix obtained from H by omitting the last row and the last column. Therefore, only the eigenvalues of the matrix R; i.e., the zeros of the polynomial $h_R(z) = \det(zI - R)$ of degree $n - 1$, have to be investigated. The matrix R shall be

called the reduced Hurwitz matrix of f(z). For the coefficients of the polynomial

$$h_R(z) = \sum_{\nu=0}^{n-1} c_\nu z^{n-1-\nu}$$

we have the expressions $c_0 = 1$ and

$$c_\nu = (-1)^\nu \times (\text{sum of the principal minors of dimension } \nu \text{ of } R) \quad (\nu = 1, \ldots, n-1) \tag{3}$$

This is clear for n = 2 and easily established by induction for n > 2.

4. THE EIGENVALUES OF THE HURWITZ MATRIX OF A REAL HURWITZIAN POLYNOMIAL. Although the general problem we are interested in seems to be hopelessly complicated, one interesting and important solution of the special case in which the given polynomial f(z) has real coefficients and is Hurwitzian has been obtained recently [2]. It has been shown that, if f is real and Hurwitzian, the Hurwitz matrix H of f is totally nonnegative; i.e., all minors of H are nonnegative. Of course, the reduced Hurwitz matrix R of f is then also nonnegative. It has also been shown in [2] that there exists a positive integer q such that all minors of R^q are positive; i.e., R^q is totally positive. The matrix R is, therefore, oscillatory if f is real and Hurwitzian which implies that all eigenvalues of R are positive and distinct (of multiplicity one) [3; Vol.2, p. 105].

From the characteristic polynomial (2) of H we see now that, if f is real and Hurwitzian, all eigenvalues of H are positive and that either all eigenvalues of H are distinct or that a_n is an eigenvalue of H of multiplicity 2.

The following examples show that for n = 3 all possible locations of the eigenvalue a_3 relative to the other two can happen.

(i) $f(z) = z^3 + 8z^2 + 8z + 4$ (Hurwitzian); $h(z) = (z-4)(z-6)(z-10)$,

(ii) $f(z) = z^3 + 4z^2 + 4z + 4$ (Hurwitzian); $h(z) = (z-2)(z-4)(z-6)$,

(iii) $f(z) = z^3 + 4z^2 + 8z + 12$ (Hurwitzian); $h(z) = (z-2)(z-10)(z-12)$,

(iv) $f(z) = z^3 + 2z^2 + 2z + 1$ (Hurwitzian); $h(z) = (z-1)^2(z-3)$,

(v) $f(z) = z^3 + 4z^2 + 6z + 8$ (Hurwitzian); $h(z) = (z-2)(z-8)^2$.

5. THE STRUCTURE OF THE HURWITZ MATRIX OF A REAL HURWITZIAN POLYNOMIAL.

THEOREM. THE HURWITZ MATRIX OF A GIVEN REAL AND HURWITZIAN POLYNOMIAL IS NONDEROGATORY.

A matrix is called nonderogatory if its characteristic polynomial and its minimal polynomial are identical. In this case, to each of the distinct eigenvalues there corresponds only one linearly independent eigenvector.

If all eigenvalues of H are simple, the statement of our theorem is trivial. In this case, H is similar to a diagonal matrix; its Jordan normal form is diagonal.

If a_n is an eigenvalue of multiplicity 2, then H is not diagonal similar, its Jordan normal form is not diagonal.

To prove our theorem for the nontrivial case, we show that the matrix $H - a_n I$ has rank $n - 1$. This is clear if $n = 2$. To see this for $n \geq 3$, we show that the $(n - 1) \times (n - 1)$ submatrix A of $H - a_n I$ obtained by omitting the first row and the last column is nonsingular.

The particular form of H shows us that $\det A = \det B$ where B is the $(n-2) \times (n-2)$ matrix obtained from $H - a_n I$ by omitting the first two rows and the first and the last columns.

Let $C = (H_{\mu\nu})_{\mu,\nu=1}^{n-2}$ be that $(n-2) \times (n-2)$ matrix obtained from H by omitting the last two rows and the last two columns ($\det C = H_{n-2}$). Then, inspecting the particular form of B, we see that

$$B = C - a_r D \tag{4}$$

where D is the $(n-2) \times (n-2)$ matrix with the rows

$$\left.\begin{array}{ll} \text{(i) for } \mu=1,\ldots,n-3 : & (\underbrace{0,\ldots,0}_{\mu},1,\underbrace{0,\ldots,0}_{n-\mu-3}) \\ \text{(ii) for } \mu = n-2 : & (0,\ldots,0) \end{array}\right\} \tag{5}$$

i.e., D has n-3 non-zero columns. Thus, $\det B$ may be expressed as a sum of 2^{n-3} determinants. One of these determinants is the Hurwitz determinant $\det C = H_{n-2}$. Let us look at the remaining $2^{n-3} - 1$

determinants. Each one of them can be expressed as a product of an integral power of a_n and a minor of H. Under the assumption that f is Hurwitzian, all minors of H are nonnegative as we mentioned earlier. As (4) shows, a_n in connection with D appears with the negative sign. Furthermore, as (5) shows, in each of these $2^{n-3} - 1$ determinants, $-a_n$ stands at a place such that its cofactor has the sign factor -1. Consequently, det B = H_{n-2} + ($2^{n-3} - 1$) nonnegative terms. Since H_{n-2} is positive if f is Hurwitzian, it follows that det A = det B is positive.

6. FIXED POINTS OF THE HURWITZ OPERATOR. It is interesting to consider the transition from a given polynomial f(z) with coefficients in $\underset{\sim}{C}$ to the polynomial h(z) = det (zI - H), with H being the Hurwitz matrix of f, as being carried out by an operator. If f(z) is the polynomial given by (1) and if

$$h(z) = \sum_{\nu=0}^{n} b_\nu z^{n-\nu}$$

with $b_o = 1$, we may consider the operator $\underset{\sim}{H}_n$ from the complex vector space $\underset{\sim}{C}^n$ into itself defined by

$$b = \underset{\sim}{H}_n a$$

where $a = (a_1,\ldots,a_n)^T$ and $b = (b_1,\ldots,b_n)^T$ (T = transpose). We may then ask for fixed points of $\underset{\sim}{H}_n$, i.e., for points $a \in \underset{\sim}{C}^n$ for which $\underset{\sim}{H}_n a = a$. Since $h(z) = (z - a_n)h_R(z)$ with

$$h_R(z) = \sum_{\nu=0}^{n-1} c_\nu z^{n-1-\nu}$$

and $c_o = 1$ and $c_\nu (\nu = 1,\ldots, n-1)$ given by (3), we see that the coefficients $b_1,\ldots, b_n$ of h(z) are given by

$$b_\nu = (-1)^\nu \times \text{(sum of the principal minors of dimension } \nu \text{ of H)} \quad (\nu = 1,\ldots,n) \tag{6}$$

Thus, in checking for fixed points of $\underset{\sim}{H}_n$, we have to study the equations

$$a_\nu = b_\nu \ (\nu = 1,\ldots,n) \text{ with } b_\nu \text{ as function of } a_1,\ldots,a_n \text{ given by (6)} \tag{7}$$

For n = 3, e.g., these equations are

$$\left.\begin{aligned} a_1 &= -(a_1 + a_2 + a_3) \\ a_2 &= a_1a_2 - a_3 + a_1a_3 + a_2a_3 \\ a_3 &= -a_3\,(a_1a_2 - a_3) \end{aligned}\right\} \tag{8}$$

If we assume here $a_3 \neq 0$, the first and the last of these equations give us upon eliminating a_3

$$a_1a_2 + 2a_1 + a_2 + 1 = 0 \quad \text{(hyperbola)} \tag{9}$$

and, eliminating a_3 from the first and the second equation, we obtain

$$2a_1^2 + 2a_1a_2 + a_2^2 - 2a_1 = 0 \quad \text{(ellipse)} \tag{10}$$

From (9) and (10) we obtain the equation

$$2a_1^4 - 2a_1^3 - 4a_1^2 + 1 = 0$$

which has two real positive and two nonreal roots. Consequently, under the assumption that $a_3 \neq 0$, we obtain four fixed points of $\underset{\sim}{H}_3$, $a^{(1)}$, $a^{(2)}$, $a^{(3)}$, and $a^{(4)}$, two of which are in $\underset{\sim}{R}^3$ the other two being in $\underset{\sim}{C}^3$. It is also clear that (8) has the trivial solution $a^{(5)} = (0,0,0)^T$ and that $a^{(6)} = (1, -2, 0)^T$ is a solution of (8). Hence, the operator $\underset{\sim}{H}_3$ has four real and two nonreal fixed points. The operator $\underset{\sim}{H}_2$ has only two fixed points; namely, $a^{(1)} = (0,0)^T$ and $a^{(2)} = (1, -2)^T$.

In the general case of arbitrary n not much can be said. We observe, however, that, if a is a fixed point of the operator H_p, then the augmented vector $(a^T, \underbrace{0,\ldots,0}_{q})^T$ is a fixed point of the

of the operator H_{p+q}.

REFERENCES

1. S. H. Lehnigk, Stability Theorems for Linear Motions with an Introduction to Liapunov's Direct Method, Prentice-Hall, Englewood Cliffs, New Jersey, 1966.

2. B. A. Asner, On the Total Nonnegativity of the Hurwitz Matrix, Internal (unpublished) Report, Dep. of Eng. Sciences, Northwestern University, Evanston, Illinois.

3. F. R. Gantmacher, The Theory of Matrices, Chelsea, New York, N. W., 1959.

MATRIX SQUARE ROOT FORMULATION OF THE KALMAN FILTER COVARIANCE EQUATIONS

William S. Agee
Special Projects Branch
White Sands Missile Range, New Mexico

1. INTRODUCTION. In an effort to improve the quality of the reduction of flight test data at White Sands Missile Range, the Analysis and Computation Directorate has done a great deal of developmental work in the application of optimal, recursive smoothing and filtering theory. Many of the problems encountered in our applications of optimal estimation theory have been of the numerical type. It is one of these numerical problems and its solution which is presented here.

The set of equations displayed below define the application of the optimal linear filter, most often called the Kalman filter, to the sequential estimation of the state of a linear dynamic system for which we have observations taken at discrete instants of time.

Dynamic State Equation

The model of the process which we are observing is represented by the vector differential equation,

$$\underset{(nxl)}{\dot{x}} = \underset{(nxn)(nxl)}{A(t)x(t)} + \underset{(nxl)}{w(t)} \qquad (1)$$

where $x(t)$ is the state vector of the process and $w(t)$ is a random vector representing our uncertainties in how well the model defined by the homogeneous portion of the differential equation actually represents the system. We assume that $E[w(t)] = 0$ and $E[w(t)w^T(s)] = Q(t) \cdot \delta(t-s)$; i.e., mean zero and covariance matrix $Q(t)$.

Observation Equation

At discrete instants of time t_i, we have vector valued observations Z_i available. The Z_i are related to the state of the dynamic system by

$$\underset{(mxl)}{Z_i} = \underset{(mxn)(nxl)}{H_i\, x\,(t_i)} + \underset{(mxl)}{V_i} \qquad (2)$$

PRECEDING PAGE BLANK

where V_i is a random vector of measurement errors. We assume the V_i are mean zero and have covariance R_i, i.e., $E[V_i]=0$, $E[V_i V_j^T]=R_i\ \delta_{ij}$.

Predicted State Estimate

We denote by $\hat{x}_i$ the optimal estimate of $x(t_i)$ based on the set observations $Z_1, Z_2, \ldots, Z_i$, and by $\hat{x}_{i/i-1}$ the optimal estimate of x_i based on the set of observations $Z_1, Z_2, \ldots, Z_{i-1}$. We call $\hat{x}_{i/i-1}$ the predicted state estimate. It is defined by

$$\hat{x}_{k/k-1} = \Phi(t_k, t_{k-1})\ \hat{x}_{k-1} \tag{3}$$

where Φ satisfies

$$\dot{\Phi}(t, t_o) = A(t)\ \Phi(t, t_o),\quad \Phi(t_o, t_o) = I$$

Corrected State Estimate

The optimal estimate $\hat{x}_k$ is defined recursively by

$$\hat{x}_k = \hat{x}_{k/k-1} + P_k H_k^T R_k^{-1}\ (Z_k - H_k \hat{x}_{k/k-1}) \tag{4}$$

The (nxn) matrix P_k is the covariance of $\hat{x}_k$.

Posterior Covariance Matrix

$$P_k = E[x_k - \hat{x}_k)\ (x_k - \hat{x}_k)^T] \tag{5}$$

$$P_k = P_{k/k-1} - P_{k/k-1} H_k^T (R_k + H_k P_{k/k-1} H_k^T)^{-1} H_k P_{k/k-1}$$

or equivalently,

$$P_k = (P_{k/k-1}^{-1} + H_k^T R_k^{-1} H_k)^{-1} \tag{6}$$

Prior Covariance Matrix

The matrix $P_{k/k-1}$ appearing in equations (5) and (6) is the covariance of the predicted state estimate, $x_{k/k-1}$

$$P_{k/k-1} = E[(x_k - x_{k/k-1})\ (x_k - x_{k/k-1})^T]$$

$$P_{k/k-1} = P(t_k) \qquad \text{where}$$

$$\dot{P} = A(t)P + PA^T(t) + Q(t),\ P(t_{k-1}) = P_{k-1} \tag{7}$$

Equation (7) is a form of the matrix Ricatti equation.

2. THE PROBLEM. The difficulty in using the equations defined above for sequential computation of the optimal estimate lies in the calculation of the covariance matrices P_k and $P_{k/k-1}$. Due to loss in accuracy in the numerical computations accompanied many times by a nearly singular covariance matrix P_k, the computed matrices P_k and $P_{k/k-1}$ will often lose their required positive definite property during the course of the sequential estimation process, and the estimation process may eventually diverge. The situation sometimes becomes so bad that the diagonal elements of P_k which are the variances of the components of $\hat{x}_k$ become negative. This has happened often in the author's experience with filtering radar data from a re-entry vehicle.

Thus, the problem is to reformulate the equations for the predicted and posterior covariance matrices such that these matrices will retain their positive definite character during sequential computation. The method presented below for combating the numerical problem just described has been 100% successful. Since the incorporation of this technique into Kalman filtering programs at WSMR, we have been entirely free of computational instability arising from the covariance matrices not being positive definite. The basis for our solution to this problem is the following well known theorem on positive definite matrices.

Theorem: A square matrix M is positive definite if and only if, there exists a nonsingular matrix L such that $M = LL^T$. Using this theorem, we can restate the problem in two parts as follows:

1. Determine a nonsingular L_K such that $P_K = L_K L_K^T$.

2. Determine a nonsingular $L_{K/K-1}$ such that $P_{K/K-1} = L_{K/K-1} L_{K/K-1}^T$. Thus, L_K and $L_{K/K-1}$ are the matrix square roots of P_K and $P_{K/K-1}$, respectively.

3. FACTORIZATION OF P_K. The method proposed here for computing L_K such that $P_K = L_K L_K^T$ is an extension of the method proposed by Sorenson in Reference 1. Sorenson's development is restricted to the case where the components of the measurement error V_K are uncorrelated; i.e., R_K is diagonal, and there are no uncertainties in the process dynamics; i.e., $Q(t) = 0$. These restrictions are removed in the development that follows.

Recall the second definition of P_K given in equation (6),

$$P_K^{-1} = P_{K/K-1}^{-1} + H_K^T R_K^{-1} H_K.$$

In order to accomplish our purposes, we will first decompose the term $H_K^T R_K^{-1} H_K$ into a sum of symmetric dyads. Since R_K is positive definite, we can express R_K^{-1} as

$$R_K^{-1} = S_K S_K^T \tag{8}$$

The square root matrix is most easily determined numerically by the Choleski decomposition (see Reference 2). Then, we can write

$$H_K^T R_K^{-1} H_K = (H_K^T S_K)\ (H_K^T S_K)^T \tag{9}$$

If we partition $H_K^T S_K$ into its columns,

$$H_K^T S_K = [u_1, u_2, \ldots, u_m] \tag{10}$$

then

$$H_K^T R_K^{-1} H_K = \sum_{i=1}^{m} u_i u_i^T \tag{11}$$

Thus, we have a sum of symmetric dyads as desired. There are other ways of decomposing $H_K^T R_K^{-1} H_K$ into a sum of symmetric dyads which do not

resort to numerical techniques such as the Choleski decomposition. However, one must be careful in using any decomposition for which the coefficients of the dyads are not all positive.

Now, we can write the defining equation for P_K as

$$P_K^{-1} = P_{K/K-1}^{-1} + \sum_{i=1}^{m} u_i u_i^T \tag{12}$$

Define the finite sequence

$$P^{-1(i)} = P_K^{-1(i-1)} + u_i u_i^T \qquad i = 1,2,\ldots,m \tag{13}$$

Obviously, $P_K^{-1(m)} = P_K^{-1}$ and $P_K^{-1(o)} = P_{K/K-1}^{-1}$.

A very convenient method exists for inverting each term in the sequence given by Equation (13). This is the method which Householder (Ref. 3) calls the method of modification. This method gives $P_K^{(i)}$ as

$$P_K^{(i)} = P_K^{(i-1)} - \frac{P_K^{(i-1)} u_i u_i^T P_K^{(i-1)}}{1 + u_i^T P_K^{(i-1)} u_i} \tag{14}$$

Suppose $P_K^{(i-1)}$ is positive definite, then it is easily shown that $P_K^{(i)}$ is positive definite. Thus, we can write

$$P_K^{(i)} = L_K^{(i)} L_K^{(i)T} \text{ and } P_K^{(i-1)} = L_K^{(i-1)} L_K^{(i-1)T}$$

Using these relations in (14), we have

$$L_K^{(i)} L_K^{(i)T} = L_K^{(i-1)} \left(I - \frac{L_K^{(i-1)T} u_i u_i^T L_K^{(i-1)}}{\lambda_i} \right) L_K^{(i-1)T} \tag{15}$$

where $\lambda_i = 1 + u_i^T P_K^{(i-1)} u_i$.

If we can factor the term $(I - L_K^{(i-1)T} u_i u_i^T L_K^{(i-1)}/\lambda_i)$ as AA^T, we will immediately have a square root for $P_K^{(i)}$, $L_K^{(i)} = L_K^{(i-1)} A$. The reproducing property of dyads allows us to easily obtain the required square root matrix in the following way. Write

$$\left(I - \frac{L_K^{(i-1)T} u_i u_i^T L_K^{i-1}}{\lambda_i} \right) = \left(I - \theta_i L_K^{(i-1)T} u_i u_i^T L_K^{(i-1)} \right) \left(I - \theta_i L_K^{(i-1)T} u_i u_i^T L_K^{(i-1)} \right) \quad (16)$$

where θ_i is a scalar to be determined. A little manipulation of equation (16) shows that θ_i must satisfy a quadratic equation. The solution is given by

$$\theta_i = [\ 1 \pm 1/\lambda_i^{\frac{1}{2}}\ ] \ / \ (\lambda_i - 1) \quad (17)$$

It is permissible to use either sign in equation (17). Thus, we have obtained the matrix square root of each $P_K^{(i)}$ as

$$L_K^{(i)} = L_K^{(i-1)} (I - \theta_i L_K^{(i-1)T} u_i u_i^T L_K^{(i-1)}), \ i = 1,2,\ldots,m \quad (18)$$

This completes the solution of part 1 of the problem as stated previously. However, note that the sequence of matrices given in equation (18) requires a matrix $L_K^{(o)}$ as a starting point. Since $P_K^{(o)} = P_{K/K-1}$, $L_K^{(o)} = L_{K/K-1}$ so that we must solve part 2 of our problem as a starting point for part 1. Several alternatives for computing $L_{K/K-1}$ are available.

4. FACTORIZATION OF $P_{K/K-1}$. Recall that the prior covariance matrix $P_{K/K-1}$ was the terminal solution to the matrix Ricatti equation given in equation (7).

$$\dot{P} = A(t)P + PA^T(t) + Q(t) \quad , \quad P(t_{K-1}) = P_{K-1}$$

$$P_{K/K-1} = P(t_K) \tag{7}$$

METHOD I

Let $P(t) = C(t)\, C^T(t)$. A differential equation for $C(t)$ can be obtained by assuming the form $\dot{C} = A(t)C + M(t)$ and substituting this form and $P = CC^T$ into equation (7). The resulting differential equation for C is

$$\dot{C} = A(t)C + Q(t)C^{-T}/2, \; C(t_{K-1}) = L_{K-1} \tag{19}$$

Then $P_{K/K-1} = C(t_K)C^T(t_K)$.

The numerical solution of this equation for C is quite time consuming because of the matrix inverse term on the right hand side. The results from solving equation (18) numerically have otherwise been satisfactory.

METHOD II

This method is similar to Method I except that we factor the matrix Ricatti equation defining P^{-1}. It is easily verified that P^{-1} satisfies the following matrix Ricatti equation.

$$\dot{P}^{-1} = -P^{-1}\, A(t) - A^T(t)P^{-1} - P^{-1}Q(t)P^{-1} \tag{20}$$

Let $P^{-1} = S^T(t)S(t)$ and assume the form $\dot{S} = -SA + M(t)$. If these relations are substituted into equation (20), the resulting differential equation for S is

$$\dot{S} = -SA(t) - SQ(t)S^TS/2 \tag{21}$$

Then $P_{K/K-1} = S^{-1}(t_K)S^{-T}(t_K)$, $L_K^{(o)} = S^{-1}(t_K)$, $S(t_{K-1}) = L_{K-1}^{-1}$

This method requires two matrix inversions, while Method I may require more inversions depending on the numerical procedure used to integrate the differential equation.

METHOD III

The solution to the matrix Ricatti equation, equation (7) can be written as

$$P(t_K) = P_{K/K-1}=\Phi(t_K,t_{K-1})P_{K-1}\Phi^T(t_K,t_{K-1})+\int_{t_{K-1}}^{t_K}\Phi(t_K,\tau)Q(\tau)\Phi^T(t_K,\tau)d\tau \quad (22)$$

The following steps can be used to factor $P_{K/K-1}$ as $P_{K/K-1} = L_{K/K-1}L^T_{K/K-1}$:

1. Using some numerical technique, approximate the integral on the right side of equation (22). For example, applying the trapezoidal rule to the integral in equation (22), we can use the following computing formula for equation (22):

$$P_{K/K-1}=\Phi(t_K,t_{K-1})[P_{K-1}+.5(t_K-t_{K-1})Q(t_{K-1})]\Phi^T(t_K,t_{K-1})+.5(t_K-t_{K-1})Q(t_K) \quad (23)$$

2. After computing $P_{K/K-1}$; e.g., by equation (23), apply a Choleski decomposition to compute $L_{K/K-1}$, $P_{K/K-1} = L_{K/K-1}L^T_{K/K-1}$. The numerical results using Method III have been at least as good as those using Method I. Method III was also less time consuming than Method I.

REFERENCES

1. H. W. Sorenson, "Kalman Filtering Techniques," "Advances in Control Systems," Vol. 3, Academic Press, 1966.

2. R. S. Martinez, G. Peters, and J. H. Wilkinson, "Symmetric Decomposition of a Positive Definite Matrix," Numerische Mathematik, Band 7, P. 362-383, (1965).

3. A. S. Householder, "The Theory of Matrices in Numerical Analysis," Blaisdell Publishing Company, 1964.

SOLUTION OF THE FOURIER EQUATION AND ASSOCIATED BOUNDARY EQUATIONS USING ANALOG AND DIGITAL ALGORITHMS

Darrel M. Thomsen
Research and Engineering Directorate
U. S. Army Weapons Command
Rock Island, Illinois

ABSTRACT. The Fourier equation in cylindrical coordinates and the boundary equations utilized in gun tube transient heat-transfer analysis are discussed. Specifically, the problem involving thermal contact resistance between the interfaces of multilayer gun tubes is presented. Heat input is described as a function of time for both the analog and the digital calculation techniques. And, integration of the Fourier equation utilizing a finite-difference approximation on the digital computer, as well as a similar approximation on the analog computer, is given.

Results from both the analog and the digital solutions for the case involving thermal contact resistance are given. Accuracy of these two methods of calculation, along with stability criteria for the digital solution, is discussed. Finally, results of radial barrel temperatures, after 100 rounds fired, and transient barrel temperatures are presented.

INTRODUCTION. Firepower for current and past automatic weapons has been curtailed by excessive barrel temperatures. Therefore, in recent years, much effort has been directed toward gun barrel heat-transfer analysis. Gun barrel heat-transfer analysis is described in this paper in which the phenomenon of thermal contact resistance between multilayer gun barrels is considered.

An example of this application is that of a two-layer gun barrel with a bore liner and an outside sleeve, and variable thermal contact resistance between these layers. It follows that the greater the thermal contact resistance, the greater the temperature drop for a given heat dissipation. Hence, the contact resistance can be adjusted to maintain the outer sleeve at a significantly lower temperature than that of the bore liner. In fact, an optimum contact resistance can be obtained so that the outer sleeve is maintained at a sufficiently low temperature to guarantee that the allowable stress limits of the sleeve material will not be exceeded during sustained burst-firing. It follows that the bore liner will be fabricated of an exotic material with good high-temperature erosion and corrosion properties.

This analysis involves calculation of optimum contact resistances for various gun barrel configurations and firing schedules. Required input data are limited to heat-in, desired barrel configuration, and surrounding ambient conditions.

HEAT-TRANSFER ANALYSIS. Equations that govern the over-all heat-transfer process (only the radial direction is considered) are shown in Figure 1. Nomenclature utilized in this paper is presented in Figure 2. Heat convected into the bore is q_{in}, while q_{out} is the heat dissipated by the surrounding environment by free convection and radiation. The temperature distribution within the barrel is prescribed by the Fourier equation and by the thermal contact resistance equation. Thermal contact resistance is analogous to electrical contact resistance. The higher the thermal contact resistance, the greater the temperature drop for a given heat flow; whereas the greater the electrical resistance, the higher the voltage drop for a given current flow.

The general differential equations are given in Figure 3 in which subscripts pertain to radial locations and superscripts pertain to time. Semantically, these equations can be described as follows:

1. Heat convection into the bore equals that which is stored in the first radial increment plus that which is conducted from the first increment to the second increment.

2. Temperature distribution within the barrel wall is given by the Fourier equations.

3. Heat transferred through the thermal contact resistance section is given as the difference between the heat transferred into the leading increment and the heat stored in that increment.

4. Likewise, heat-out of the thermal contact resistance section is given as the sum of the heat leaving the increment outside the contact resistance and heat stored in this increment.

5. Heat dissipated by free convection and radiation equals that conducted into the outer wall increment minus heat stored in that increment.

These equations written in the form of a digital finite-difference approximation are given in Figure 4. Also in this figure is an example of the stability criteria used in the solution of these equations. For the Fourier equations, it can be seen that a negative coefficient for $T_i^{\theta-1}$, the temperature of increment i at time $\theta-1$, is prohibited. To have a negative coefficient for $T_i^{\theta-1}$, a high temperature for $T_i^{\theta-1}$ would result in a lower temperature for T_i^{θ} in violation of the first law of thermodynamics. This implies that $\Delta\theta$ and Δr must be adjusted to give a stable solution; however, it must be kept in mind that the smaller $\Delta\theta$, the longer the digital computer run-time. Hence, the positive coefficient criterion is given for solution convergence.

For both, the analog and the digital solutions, experimentally measured gas temperatures and bore convection coefficients are input as a function of time. For the digital solution, diffusivity and heat dissipated to the surrounding environment are calculated as a function of barrel temperature; whereas, for the analog solution, diffusivity and the exterior heat-transfer coefficients are input as constant values and corrected by use of an iterative technique. Therefore, it can be seen that this procedure would introduce a slight error in the analog solution. Also, a larger number of radial increments can be introduced in the digital solution without exceeding the capability of the facility by multiple circuitry requirements that would be inherent for the analog solution.

The same differential equations written in analog form are shown in Figure 5. From these equations, it can be seen that $\dot{T}$ (i.e. $dT/d\theta$), the differential of the temperature with respect to time, is continuously integrated to give temperature as a function of time. Note also, that the differential of temperature as a function of radius is again approximated by use of a finite-difference approximation.

The analog block diagram for the solution of these equations is shown in Figure 6. It can be seen that heat-in is provided, as a function of time and bore temperature, by means of a function generator. For each radial increment, the derivative of temperature with respect to time, T, is continuously integrated to give radial temperatures.

Error functions for both the analog and the digital solutions are presented in Figure 7. For both solutions, error is defined as the difference between heat into the bore and heat stored in the radial increment, minus heat dissipated by the surroundings. Percentage of error is defined as error divided by heat into the bore. For the analog solution, these quantities are continuously integrated; whereas, for the digital solution, these quantities are summed for all $\Delta\theta$ time intervals.

RESULTS AND CONCLUSIONS. Results in the form of radial temperature distributions for various thermal contact resistances, after 100 rounds fired, are shown in Figures 8 and 9. Maximum percentage of error for the four solutions presented are 5 and 10 percent, respectively, for the digital and the analog techniques. It can be seen from these figures that the correlation for the analog and the digital solutions is well within ordinarily acceptable limits of engineering accuracy. Typical interface conditions that would correspond to contact resistances used in these calculations are shown in Figure 10.

Transient temperatures (bore and outside wall), for the minimum and the maximum thermal contact resistances under consideration, are presented in Figures 11 and 12.

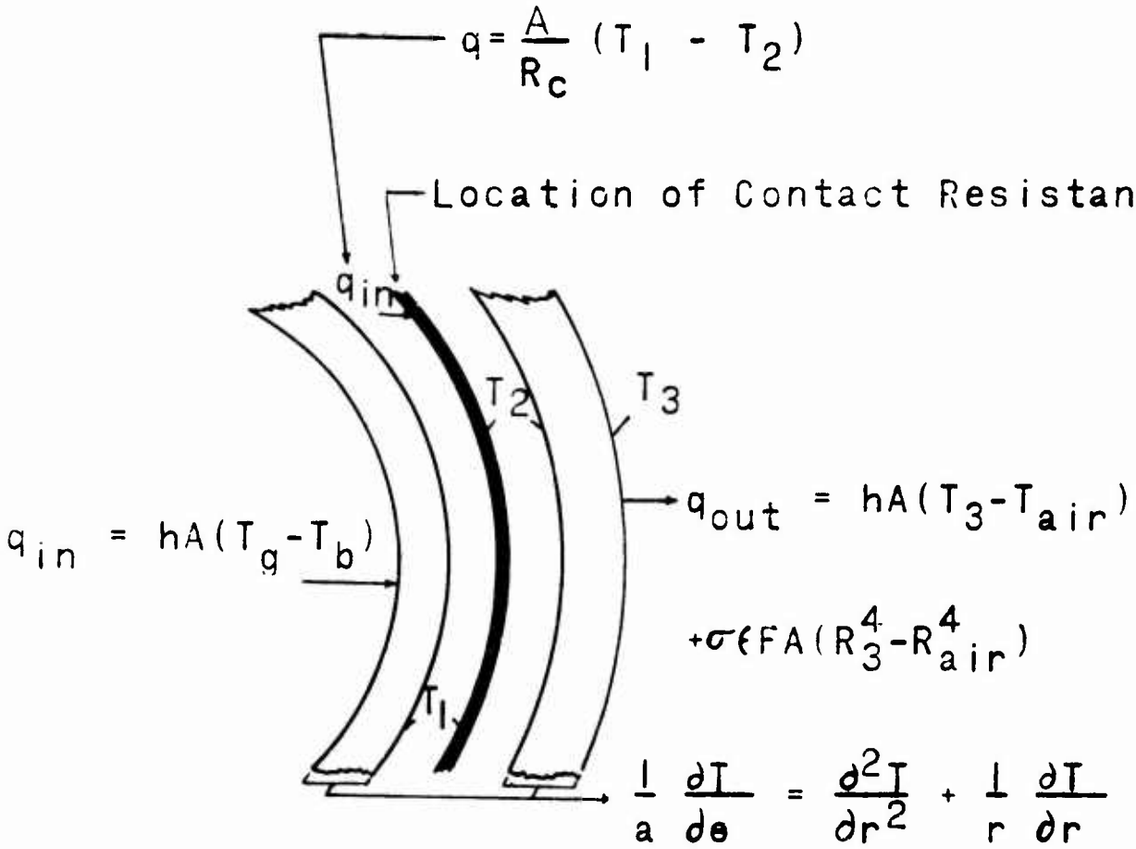
Again, the good correlation between the analog and the digital solutions can be seen. Here, as for the previous results, the differences between the digital and the analog solutions can be attributed to the following differences in solution techniques:

1. Number of radial increments. A significantly larger number of radial increments (approximately 30 for the digital and 12 for the analog) are calculated for the digital solution.

2. Thermal conductivity and effective exterior heat-transfer coefficients are not direct functions of temperature for the analog solution. It is believed that, in the future, these parameters can be input with the use of a function generator similar to the heat-input function generator.

A salient result of this analysis is the excellent correlation between the analog and the digital solutions. It is apparent that the analog solution affords a fast and inexpensive solution which is a good tool for parametric studies in which iterative calculations are involved.

HEAT-TRANSFER EQUATIONS



$$q = \frac{T_i - T_n}{\text{Ln}\,(r_n/r_i)/2\pi k\ell} \quad \text{(Radial conduction equation)}$$

Figure 1

NOMENCLATURE

h_g - propellant gas convection coefficient

ρ - density

c_p - specific heat

k - thermal conductivity

T_g^θ - gas temperature at time θ

T_b^θ - bore temperature at time θ

T_{cr}^θ - temperature of radial increment on the bore side of the contact resistance

R_c - thermal contact resistance

θ - time

$h=h_{air}$ - convection coefficient of the air

$T_n^{\theta\,\prime}$ - temperature of outside radial increment at time θ

σ - Stefan - Boltzmann constant

ε - emissivity

a - thermal diffusivity

r - radius

$\bar{h}=k'$ - effective exterior heat-transfer coefficient

Δc - transformation constant

A_b - surface area of bore increment

V_n - volume of outside radial increment

R_n - Rankin temperature of outside radial increment

Figure 2

GENERAL DIFFERENTIAL EQUATIONS

Equation for bore heating:

$$h_g dA\ (T_g^{\Theta} - T_b^{\Theta}) = \frac{\rho c_p\ dr\ dA}{2}\ \frac{dT}{d\Theta} + \frac{k\ dA}{dr}\ (T_b^{\Theta} - T_{b+1}^{\Theta})$$

T_b - represents bore temperature

Fourier equation considering only radial direction:

$$\frac{1}{r}\ \frac{\partial T}{\partial r} + \frac{\partial^2 T}{\partial r^2} = \frac{1}{a}\ \frac{\partial T}{\partial \Theta} \qquad a = \text{diffusivity}$$

Equation for inner increment adjacent to contact resistance:

$$\frac{k(T_{cr-1}^{\Theta} - T_{cr}^{\Theta})}{r_{cr}\ \text{Ln}\ (r_{cr}/r_{cr-1})} - \frac{\rho c_p\ \Delta r}{2}\ \frac{dT}{d\Theta} = \frac{(T_{cr}^{\Theta} - T_{cr+1}^{\Theta})}{R_c}$$

R_c - contact resistance constant

Equation for leaving contact resistance section to outside layer:

$$\frac{r_{cr}\ (T_{cr}^{\Theta} - T_{cr+1}^{\Theta})}{R_c} = \frac{\rho c_p\ r_{cr}\ \Delta r}{2}\ \frac{dT}{d\Theta} + \frac{k(T_{cr+1}^{\Theta} - T_{cr+2}^{\Theta})}{\text{Ln}\ (r_{cr+2}/r_{cr+1})}$$

Equation for external cooling (free convection):

$$h_{air}\ (T_n^{\Theta} - T_{air})\ dA + \sigma \epsilon\ (T_n^{\Theta} + 460)^4\ dA = \frac{k(T_n^{\Theta} - T_{n-1}^{\Theta})\ dA}{dr} - \frac{\rho c_p\ dr\ dA}{2}\ \frac{dT}{d\Theta}$$

T_n - represents external radial temperature

Figure 3

FINITE-DIFFERENCE EQUATIONS FOR HEAT-TRANSFER DIGITAL SOLUTION CONSIDERING THERMAL CONTACT RESISTANCE

At bore:

$$T_b^{\theta} = T_b^{\theta-1} + \frac{2H_g^{\theta-1}\,\Delta\theta}{\rho c_p\,\Delta r_b}\,(T_g^{\theta-1} - T_b^{\theta-1}) + \frac{2\,\Delta\theta\,a}{\Delta r_b^{\,2}}\,(T_{b+1}^{\theta-1} - T_b^{\theta-1})$$

For inner radial increments:

$$T_i^{\theta} = T_i^{\theta-1} + \frac{a\,\Delta\theta}{r^2\,\Delta c^2}\,(T_{i-1}^{\theta-1} - 2T_i^{\theta-1} + T_{i+1}^{\theta-1})$$

For segment inside the contact resistance:

$$T_{cr}^{\theta} = T_{cr}^{\theta-1} + \frac{2k\,(T_{cr-1}^{\theta-1} - T_{cr}^{\theta-1})\,\Delta\theta}{\rho c_p\,\Delta r^2} - \frac{2(T_{cr}^{\theta-1} - T_{cr+1}^{\theta-1})\,\Delta\theta}{R_c\,\rho c_p\,\Delta r}$$

For segment outside the contact resistance:

$$T_{cr+1}^{\theta} = T_{cr+1}^{\theta-1} + \frac{2\,(T_{cr}^{\theta-1} - T_{cr+1}^{\theta-1})\,\Delta\theta}{\rho c_p\,\Delta r\,R_c} - \frac{2k\,(T_{cr+1}^{\theta-1} - T_{cr+2}^{\theta-1})\,\Delta\theta}{\rho c_p\,\Delta r^2}$$

For outer radial increment:

$$T_n^{\theta} = T_n^{\theta-1} - \frac{2\,\Delta\theta\;h_{air}}{\rho c_p\,\Delta r_n}\,(T_n^{\theta-1} - T_{air}) - \frac{2\,\Delta\theta\,\sigma\,\epsilon}{\rho c_p\,\Delta r_n}$$
$$\left[(T_n^{\theta-1} + 460)^4 - (T_{air} + 460)^4\right] - \frac{2\,\Delta\theta\;k}{\rho c_p\,\Delta r_n^{\,2}}\,(T_n^{\theta-1} - T_{n-1}^{\theta-1})$$

Stability criteria for radial increment equations:

$$T_1^{\theta-1}\left[\,1 - \frac{2\,\Delta\theta\,a}{r^2\,\Delta c^2}\right] \geq 0$$

i.e. $\quad 1 \geq \frac{2\,\Delta\theta\;a}{r^2\,\Delta c^2} \qquad$ or $\qquad \Delta\theta \leq \frac{r^2\,\Delta c^2}{2\,a}$

Figure 4

EQUATIONS USED FOR ANALOG STUDY OF CONTACT RESISTANCE

At bore:

$$\frac{\rho c_p \Delta r \dot{T}_b}{2} = h (T_g - T_b) - \frac{k}{\Delta r} (T_b - T_{b+1})$$

For inner radial increments:

$$\frac{1}{a} \dot{T}_i = \frac{T_{i+1} - 2T_i + T_{i-1}}{\Delta r^2}$$

For segment inside the contact resistance:

$$\frac{\rho c_p \Delta r \dot{T}_{cr}}{2} = \frac{k (T_{cr-1} - T_{cr})}{\Delta r} - \frac{1}{R_c} (T_{cr} - T_{cr+1})$$

For segment outside the contact resistance:

$$\frac{\rho c_p \Delta r \dot{T}_{cr+1}}{2} = \frac{1}{R_c} (T_{cr} - T_{cr+1}) - \frac{k(T_{cr+1} - T_{cr+2})}{\Delta r}$$

For outer radial increment:

$$\frac{\rho c_p \Delta r \dot{T}_n}{2} = -k'(T_n - T_{air}) + \frac{k}{\Delta r} (T_{n-1} - T_n)$$

Nomenclature:

$\dot{T} = \frac{dT}{d\theta}$
θ = time
ρ = density
c_p = specific heat
h = convection coefficient
T_g = gas temperature
T_b = bore temperature
k = thermal conductivity
a = thermal diffusivity
r = radius
R_c = contact resistance coefficient
k' = effective heat-transfer coefficient

Figure 5

ANALOG BLOCK DIAGRAM FOR HEAT-TRANSFER SOLUTION

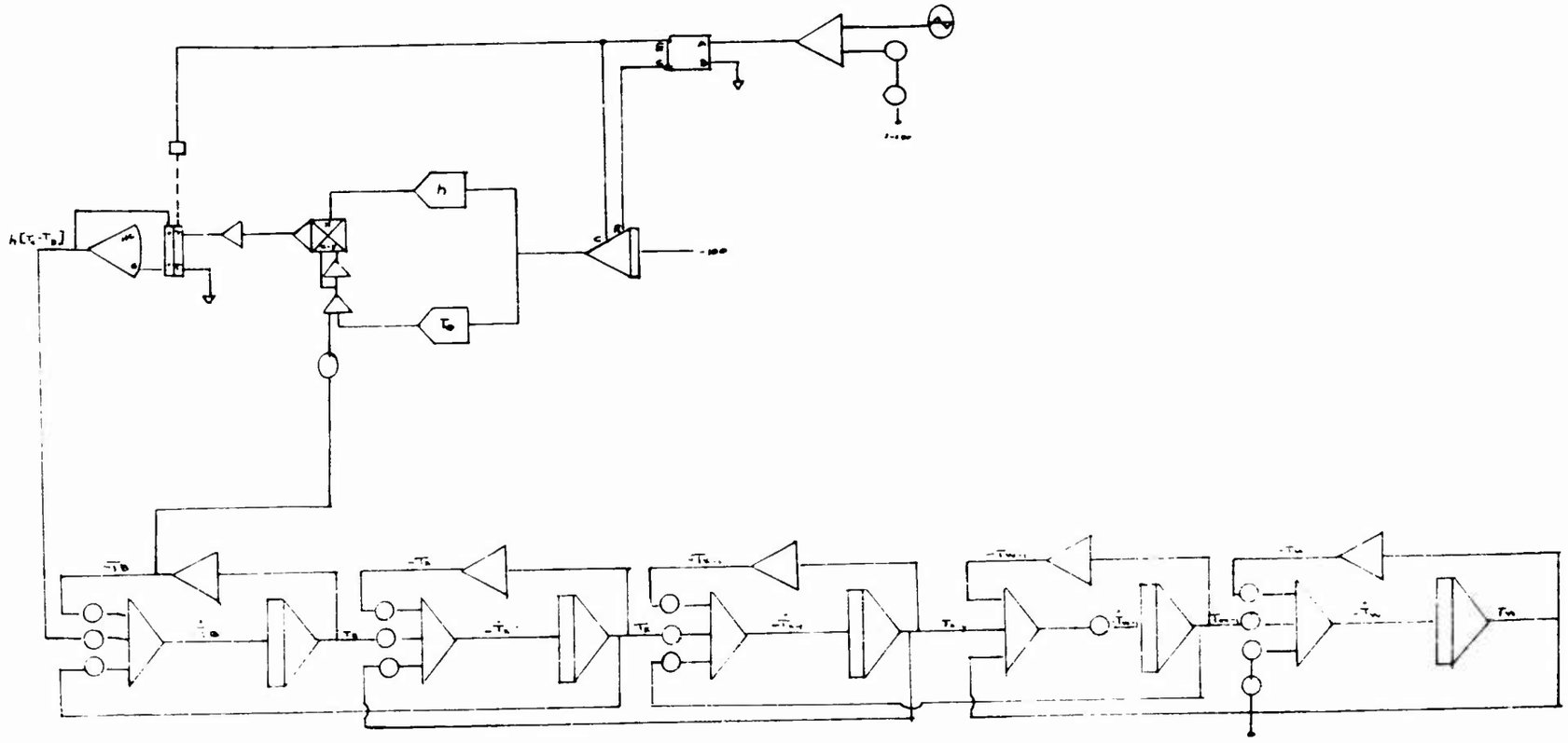


Figure 6

ERROR FUNCTION BASED ON ENERGY BALANCE FOR ANALOG SOLUTION:

$$\text{Error} = \int h_g A_b (T_g - T_b)\, d\theta - 1/2 \int \rho c_p V_1 \dot{T}_1\, d\theta$$

$$- \sum_{i=2}^{i=cr-1} \int \rho c_p V_i \dot{T}_i\, d\theta$$

$$- 1/2 \int \rho c_p V_{cr} \dot{T}_{cr}\, d\theta - 1/2 \int \rho c_p V_{cr+1} \dot{T}_{cr+1}\, d\theta$$

$$- \sum_{i=cr+2}^{i=n-1} \int \rho c_p V_i \dot{T}_i\, d\theta - 1/2 \int \rho c_p V_n \dot{T}_n\, d\theta$$

$$- \int \bar{h} A_n (T_n - T_{air})\, d\theta$$

ERROR FUNCTION BASED ON ENERGY BALANCE FOR DIGITAL SOLUTION:

$$\text{Error} = h_g A_b (T_g^{\theta+1} - T_b^{\theta}) \Delta\theta - 1/2 \rho c_p V_1 (T_1^{\theta+1} - T_1^{\theta})$$

$$- \sum_{i=2}^{i=cr-1} \rho c_p V_i (T_i^{\theta+1} - T_i^{\theta})$$

$$- 1/2\, c_p \rho V_{cr} (T_{cr}^{\theta+1} - T_{cr}^{\theta}) - 1/2\, c_p \rho V_{cr+1} (T_{cr+1}^{\theta+1} - T_{cr+1}^{\theta})$$

$$- \sum_{i=cr+2}^{i=n-1} c_p \rho V_i (T_i^{\theta+1} - T_i^{\theta}) - 1/2\, c_p \rho V_n (T_n^{\theta+1} - T_n^{\theta})$$

$$- h_{air} A_n (T_n^{\theta+1} - T_{air}) \Delta\theta - \sigma \epsilon A_n (R_n^4 - R_{air}^4) \Delta\theta$$

Figure 7

RADIAL TEMPERATURE DISTRIBUTION AFTER 100 ROUNDS FOR VARIOUS CONTACT RESISTANCES

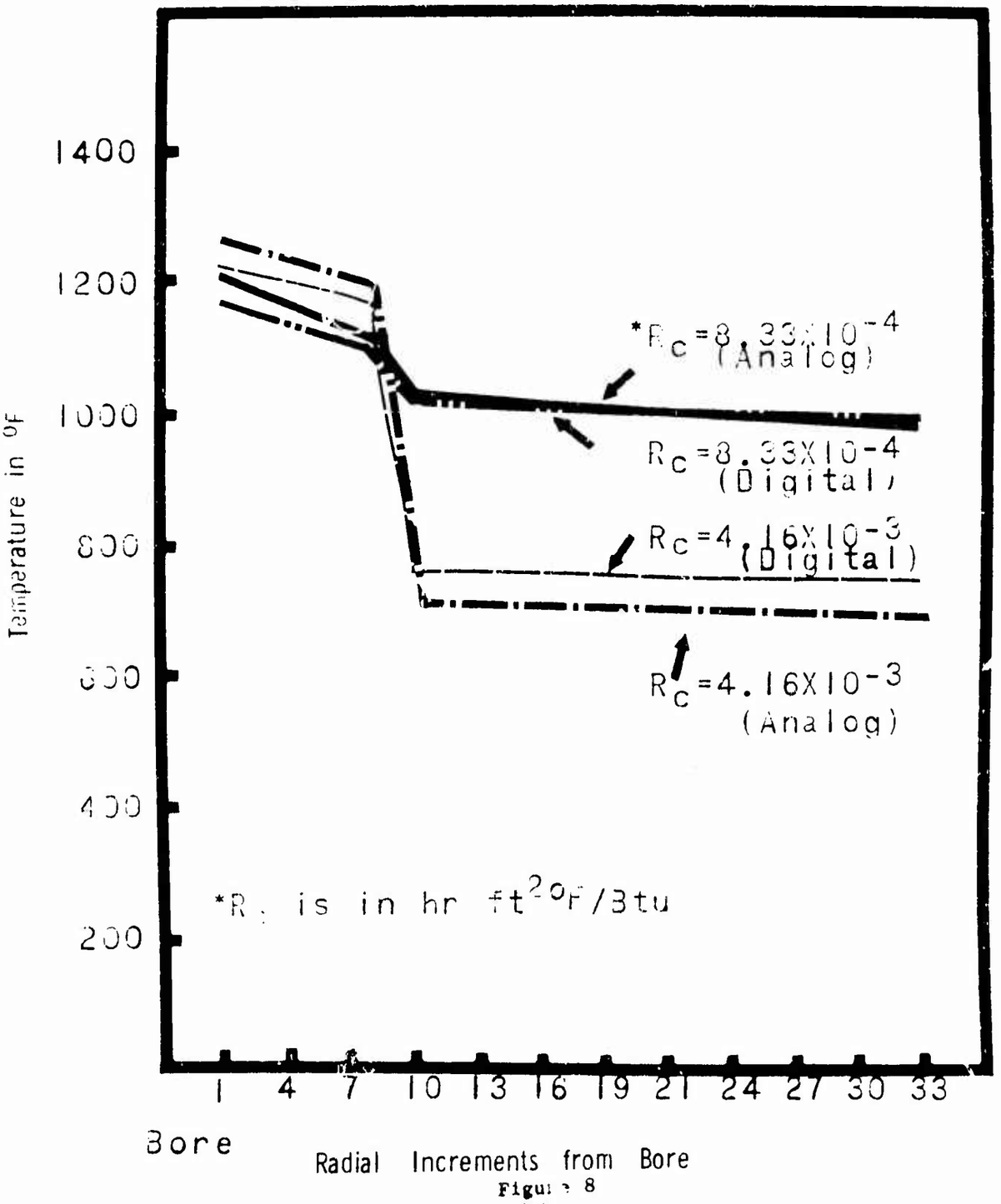


Figure 8

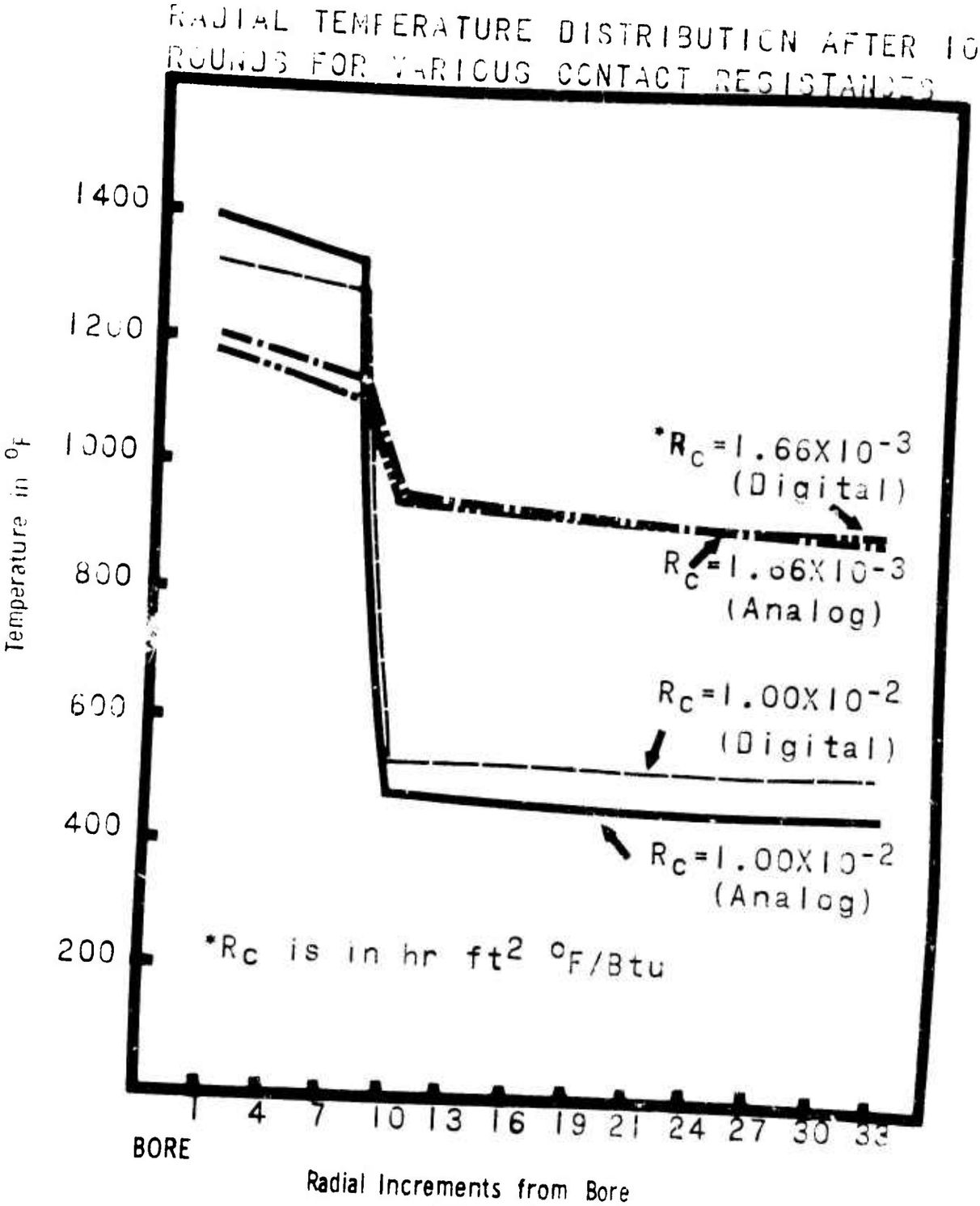

RADIAL TEMPERATURE DISTRIBUTION AFTER 100
ROUNDS FOR VARIOUS CONTACT RESISTANCES
1400
1200
1000
800
600
400
200
Temperature in °F
*Rc=1.66X10-3
(Digital)
Rc=1.66X10-3
(Analog)
Rc=1.00X10-2
(Digital)
Rc=1.00X10-2
(Analog)
*Rc is in hr ft2 °F/Btu
1
4
7
10
13
16
19
21
24
27
30
33
BORE
Radial Increments from Bore

Figure 9

TYPICAL INTERFACE CONDITIONS

Contact Resistance $R_c X10^{-3}$ HR $FT^2 {}^oF/BTU$	Thickness of ZrO_2 Interface (IN.)	Interfacial Material	Interface Pressure (P.S.I.)	Mean Interface Temperature (^oF)
10*	N.A.	Asbestos	5	400
10	.120	ZrO_2	Typical Gun Barrel Pressures	Typical Gun Barrel Temperatures
4.16	.0499	ZrO_2	Typical Gun Barrel Pressures	Typical Gun Barrel Temperatures
1.66	.0199	ZrO_2	Typical Gun Barrel Pressures	Typical Gun Barrel Temperatures
.833	.010	ZrO_2	Typical Gun Barrel Pressures	Typical Gun Barrel Temperatures

*ST Steel to ST Steel, Surface Roughness 100 Microinc ., R.M.S.
Data Taken From: National Advisory Committee for Aeronautics, Technical Note 3295.

Figure 10

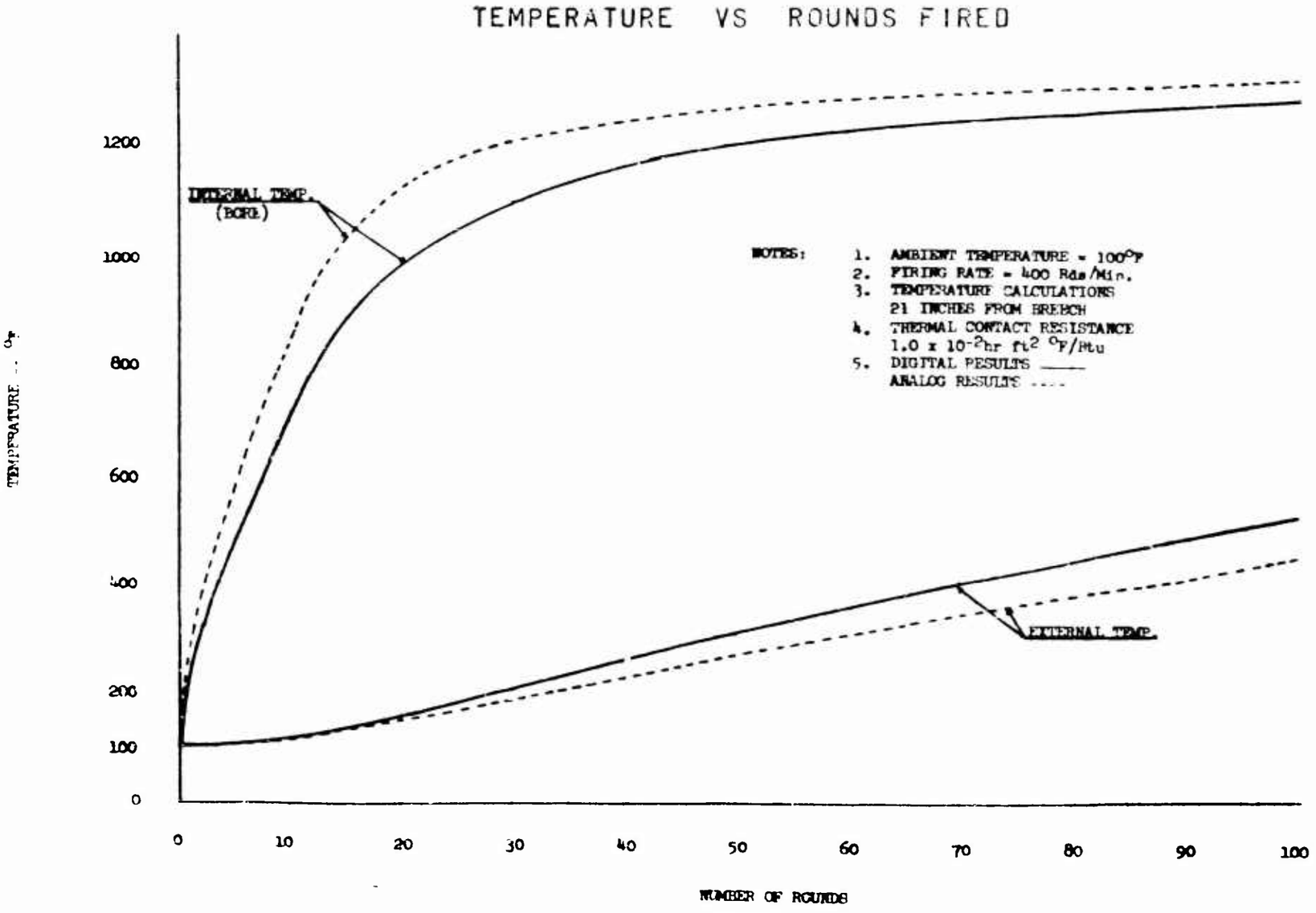

TEMPERATURE VS ROUNDS FIRED
TEMPERATURE - °F
1200
1000
800
600
400
200
100
0
INTERNAL TEMP. (BORE)
EXTERNAL TEMP.
NOTES:
1. AMBIENT TEMPERATURE = 100°F
2. FIRING RATE = 400 Rds/Min.
3. TEMPERATURE CALCULATIONS 21 INCHES FROM BREECH
4. THERMAL CONTACT RESISTANCE 1.0 x 10-2 hr ft2 °F/Btu
5. DIGITAL RESULTS ——
ANALOG RESULTS ----
0
10
20
30
40
50
60
70
80
90
100
NUMBER OF ROUNDS

Figure 11

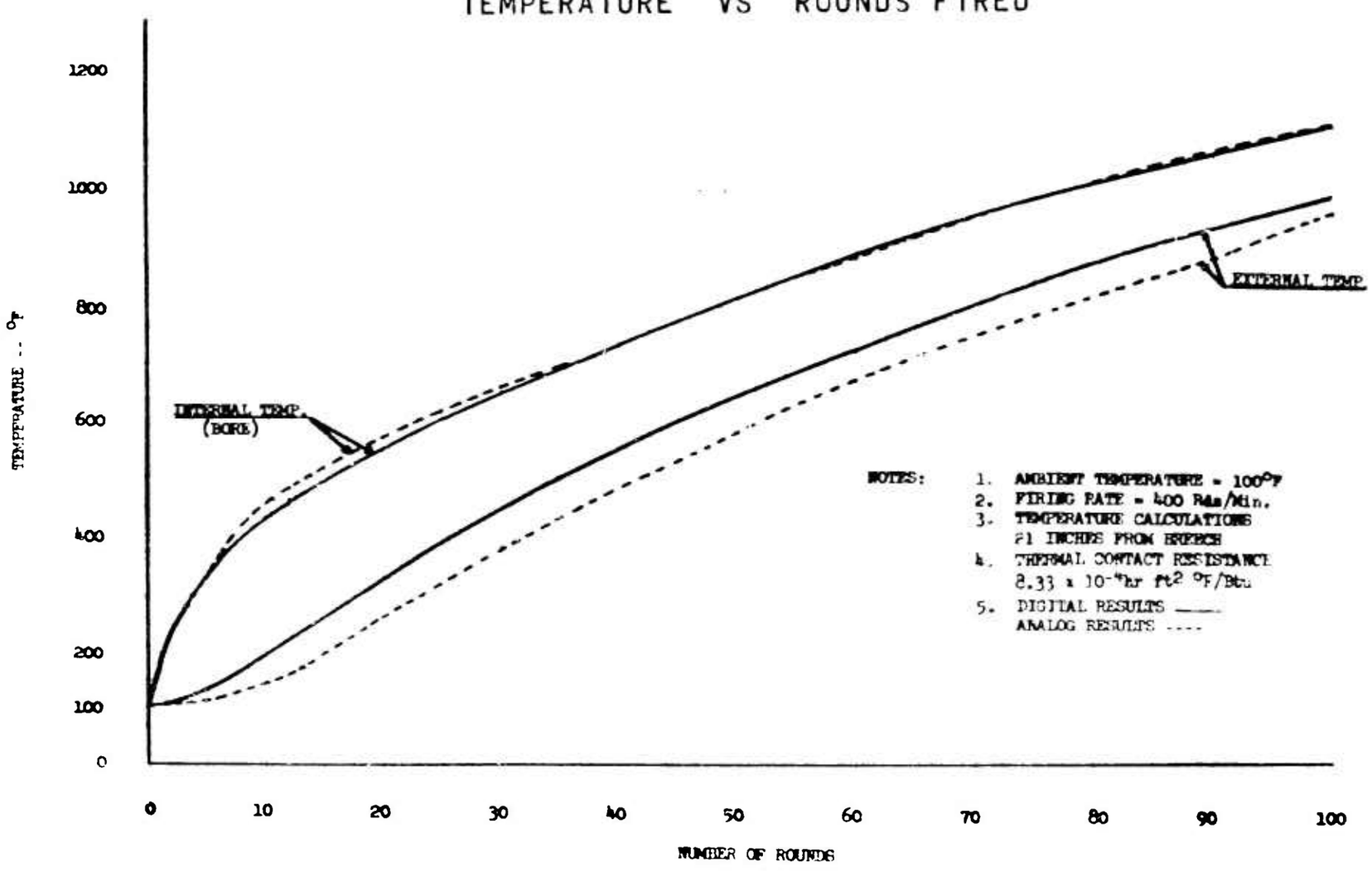

TEMPERATURE VS ROUNDS FIRED
TEMPERATURE -- °F
1200
1000
800
600
400
200
100
0
INTERNAL TEMP. (BORE)
EXTERNAL TEMP.
NOTES:
1. AMBIENT TEMPERATURE = 100°F
2. FIRING RATE = 400 Rds/Min.
3. TEMPERATURE CALCULATIONS @1 INCHES FROM BREECH
4. THERMAL CONTACT RESISTANCE 8.33 x 10⁻⁴ hr ft² °F/Btu
5. DIGITAL RESULTS ——
ANALOG RESULTS ----
0
10
20
30
40
50
60
70
80
90
100
NUMBER OF ROUNDS

Figure 12

A GENERAL SOLUTION TO THE AXISYMMETRIC THERMOELASTICITY PROBLEM IN CYLINDRICAL COORDINATES*

John G. Avery
U. S. Army Missile Command
Redstone Arsenal, Alabama

ABSTRACT. A general solution is developed for the stress and deformation of an isotropic elastic solid subjected to an axisymmetric temperature field. It is presumed that the bounding surfaces of the solid may be conveniently described in cylindrical coordinates r, θ, z. The temperature may be an arbitrary function of the radial and logitudinal coordinates. The solution is obtained by classical techniques within the uncoupled, quasi-static theory of thermoelasticity. Goodier's thermoelastic potential function is used in conjunction with the Boussinesq-Papkovitch functions of three-dimensional elasticity. General forms of the potential function are given. The results are applicable to the determination of thermal stresses due to the axisymmetric heating or cooling of medium length solid or hollow cylinders, including multilayered coaxial cylinders, made of isotropic elastic material.

*This article appeared as Technical Report No. RR-TR-69-5, Redstone Arsenal, Alabama.
**The remainder of this article has been reproduced photographically from the author's manuscript.

SYMBOLS

a, b	Characteristic radial dimensions
A_n, B_n, C_n, D_n	Expansion coefficients
A_{pn}, B_{pn}	Expansion coefficients
B_1, B_2	Components of the Boussinesq-Papkovitch harmonic solution vector
C_1, C_2...	Constants
e	Volume dilatation
E	Modulus of elasticity
$g_n(r)$, $f_n(r)$	Functions of r
$H[\lambda(r)]$	Finite Hankel transform of $\lambda(r)$
k	Thermal conductivity
I, J, K, Y	Bessel functions
L	Characteristic axial dimension
$P_n(r)$, $P_n^*(r)$	Functions of r
r, θ, z	Cylindrical coordinates
s	Variable of integration
S	Bounding surface
S_z	Resultant axial force
t	Time
T	Temperature, relative to a stress free reference temperature
u, v, w	Displacements in r, θ, z directions
$\bar{u}$, $\bar{w}$	Displacements obtained from thermoelastic potential function
$\bar{\bar{u}}$, $\bar{\bar{w}}$	Displacements obtained from homogeneous equilibrium equation
$W(P_1, P_2)$	Wronskian
α	Linear coefficient of thermal expansion

SYMBOLS (Concluded)

β_n	Characteristic value in Fourier series expansion
ϵ_{rr}, $\epsilon_{\theta\theta}$, ϵ_{zz}	Normal strains
$\zeta_n(r; t)$	Coefficient of sine series
$\overline{\zeta}_n(\mu_m)$	Finite Hankel transform of ζ_n
η	Radial location of interface between concentric cylinders
θ	Cylindrical coordinate
$\theta_n(r; t)$	Coefficient of cosine series
$\overline{\theta}_n(\mu_m)$	Finite Hankel transform of θ_n
κ	Thermal diffusivity
μ_m, μ_p	Positive roots of $J_0(\mu b) = 0$
ν	Poisson's ratio
σ_{rr}, $\sigma_{\theta\theta}$, σ_{zz}	Normal stresses
σ_{rz}	Shear stress
ϕ	Thermoelastic potential function
ψ	Points on the boundary surface
∇^2	$\nabla^2 = \frac{\partial^2}{\partial r^2} + \frac{1}{r}\frac{\partial}{\partial r} + \frac{\partial^2}{\partial z^2}$

Section I. INTRODUCTION

The continuing development of ceramics and high temperature metals has increased the engineering applications in which thermally induced stresses play a primary role. Case bonded cylinders used in solid propellant rocket motors, missile structures exposed to aerodynamic heating, laser rods, nuclear fuel elements, cryogenic storage vessels, and transport lines are but several of numerous design problems requiring careful analysis of thermal stresses.

The calculation of thermal stresses resulting from plane temperature distributions in polar coordinates has become routine, and there has been much published work in this area. However, there are few classical solutions available for cases of simultaneous radial and longitudinal temperature variation even though these circumstances are common in practice. The reason for this nonavailability of results is, of course, the additional complexity of solving a problem in three-dimensional thermoelasticity as opposed to a problem of plane stress or plane strain.

This report presents an analytic solution for the thermal stresses and deformations in a finite elastic body whose bounding surfaces are expressed in cylindrical coordinates r, θ, z. The temperature is allowed to vary in both the radial and longitudinal directions, but remains symmetric about the longitudinal axis. Thus, the resulting state of stress and deformation is axisymmetric and is three-dimensional.

The temperature distribution is assumed to be representable in the general form:

$$T(r,z) = \sum_n{}' \theta_n(r) \cos \beta_n z + \sum_n{}' \zeta_n(r) \sin \beta_n z \ .$$

This form is sufficiently general to include a considerable number of applications involving axisymmetric heating of finite cylinders.

The deformations resulting from this temperature distribution are found by solving the displacement equilibrium equations using the two part technique developed by J. N. Goodier [1]. This technique employs a thermoelastic potential function as a particular solution of the nonhomogeneous equilibrium equations. When the thermoelastic potential function has been found, the thermoelasticity problem is reduced to the classic three-dimensional, axisymmetric problem of isothermal elasticity. This is solved by determining the two harmonic functions of Boussinesq-Papkovitch.

The form of the solution facilitates the exact satisfaction of arbitrary stress or displacement boundary conditions on the curved surfaces. The conditions at the flat end surfaces are satisfied only by annulling the resultant forces, i.e., by applying the principle of St. Venant. Consequently, the results presented here will, in general, not accurately represent the actual stresses very near the ends of the cylinder. For problems requiring an exact solution near the end surfaces, several solutions have been presented [2,3].

An effort has been made to keep the analysis as general as possible so that the results may be applied to a wide variety of problems. The most direct applications concern the axisymmetric heating or cooling of medium length solid or hollow cylinders, including multilayer coaxial cylinders, made of isotropic elastic material.

Section II. THE AXISYMMETRIC THERMOELASTICITY PROBLEM IN CYLINDRICAL COORDINATES

This analysis assumes a homogeneous continuum which is isotropic with respect to both its thermal and mechanical properties. Variation of material properties with temperature is neglected. It is further assumed that the deformations obey the restrictions imposed by the linear theory of elasticity. The continuum is initially in a stress free state at some uniform temperature which may be taken to be zero, without any loss of generality. The temperature, T, represents the increment of temperature from this initial stress free condition. Points within the continuum will be located by the cylindrical coordinates (r, θ, z). Consideration will be restricted to the case of temperature and stress fields which are symmetric about the z-axis. Thus, there is no variation with respect to the azimuth angle θ. As a consequence of this symmetry, v, the displacement in the θ direction must vanish, and the strain-displacement relations are:

$$\epsilon_{rr} = u_{,r} \tag{1}$$

$$\epsilon_{\theta\theta} = \frac{u}{r} \tag{2}$$

$$\epsilon_{zz} = w_{,z} \tag{3}$$

$$\epsilon_{rz} = \frac{1}{2}\left(u_{,z} + w_{,r}\right) , \tag{4}$$

where a comma denotes partial differentiation with respect to the subscripted variable.

The constitutive relations for the case considered are:

$$\frac{(1+\nu)(1-2\nu)}{E}\,\sigma_{rr} = (1-2\nu)u_{,r} + \nu e - \alpha(1+\nu)T \tag{5}$$

$$\frac{(1+\nu)(1-2\nu)}{E}\,\sigma_{\theta\theta} = (1-2\nu)\frac{u}{r} + \nu e - \alpha(1+\nu)T \tag{6}$$

$$\frac{(1+\nu)(1-2\nu)}{E}\,\sigma_{zz} = (1-2\nu)w_{,z} + \nu e - \alpha(1+\nu)T \tag{7}$$

$$\frac{(1+\nu)(1-2\nu)}{E}\,\sigma_{rz} = \frac{(1-2\nu)}{2}\left(u_{,z} + w_{,r}\right) \tag{8}$$

$$\sigma_{\theta z} = \sigma_{\theta r} = 0 \ , \tag{9}$$

where the volume dilatation is given by

$$e = \epsilon_{rr} + \epsilon_{\theta\theta} + \epsilon_{zz} = u_{,r} + \frac{u}{r} + w_{,z} \ . \tag{10}$$

Finally, the equations of equilibrium are, for zero body forces:

$$\nabla^2 u - \frac{1}{r^2} u + \frac{1}{1 - 2\nu} e_{,r} = \frac{2(1 + \nu)}{1 - 2\nu} \alpha T_{,r} \tag{11}$$

$$\nabla^2 w + \frac{1}{1 - 2\nu} e_{,z} = \frac{2(1 + \nu)}{1 - 2\nu} \alpha T_{,z} \ . \tag{12}$$

To complete the problem statement, it is necessary to specify the displacements and state of stress on the bounding surfaces S. These boundary conditions may be specified by relations of the form,

$$\sigma_{rr} = \sigma_1(\psi) \text{ on S}$$

$$\sigma_{zz} = \sigma_2(\psi)$$

$$\sigma_{rz} = \sigma_3(\psi) \tag{13}$$

or

$$u = u_1(\psi) \text{ on S.}$$

$$w = w_1(\psi) \tag{14}$$

The final solution of the axisymmetric thermoelastic problem must satisfy the equations of equilibrium (11) and (12) and the boundary conditions (13) and (14).

The reader will recognize that the preceding assumptions and equations are those of the uncoupled, quasi-static theory of thermoelasticity. Neglecting the interaction between thermal and mechanical energy allows the temperature and deformation to be "uncoupled." Consequently, the temperature may be obtained separately, using heat transfer considerations alone, and may then be used as input for the solution of the deformation boundary-value problem. The neglect of mechanical inertia removes the time derivatives from the thermoelastic field equations. Under the additional assumption that the mechanical

boundary conditions do not contain time derivatives, it follows that time may be regarded as a parameter and a transient temperature distribution may be treated as a family of steady-state distributions depending upon the parameter t.

Section III. METHOD OF SOLUTION

1. General

Solutions of equations (11) and (12) will be found by use of the method developed by J. N. Goodier [1]. The solution will be of the form:

$$u = \bar{u} + \bar{\bar{u}}$$

$$w = \bar{w} + \bar{\bar{w}} \ , \tag{15}$$

where $\bar{u}$, $\bar{w}$ are particular solutions of equations (11) and (12), and $\bar{\bar{u}}$, $\bar{\bar{w}}$ are the complementary solutions. The particular solutions are obtained by introducing a thermoelastic potential function, ϕ, such that

$$\bar{u} = \phi_{,r}$$

$$\bar{w} = \phi_{,z} \ . \tag{16}$$

If equation (16) is substituted into the equilibrium equations, subsequent integration yields:

$$\nabla^2\phi = \frac{1 + \nu}{1 - \nu} \alpha T \ . \tag{17}$$

This latter relation is Poisson's equation, for which there are several methods of solution.

2. The Isothermal Elasticity Problem

It remains to solve the homogeneous portion of equations (11) and (12) for the displacements $\bar{\bar{u}}$ and $\bar{\bar{w}}$. It is clear, however, that this constitutes a problem in the classical theory of isothermal elasticity and may be solved by the several techniques associated with that discipline. Following Iuré [4], for example, it may be shown that the displacements can be written in terms of two Boussinesq-Papkovitch functions, $B_1(r,z)$ and $B_2(r,z)$, according to the relations:

$$\bar{\bar{u}}(r,z) = 4(1 - \nu) B_2 - \frac{\partial}{\partial r} (rB_2 + B_1) \tag{18}$$

$$\bar{\bar{w}}(r,z) = - \frac{\partial}{\partial z} (rB_2 + B_1) \ , \tag{19}$$

where B_1 and B_2 are solutions of:

$$B_{1,rr} + \frac{1}{r} B_{1,r} + B_{1,zz} = 0 \tag{20}$$

$$B_{2,rr} + \frac{1}{r} B_{2,r} - \frac{1}{r^2} B_2 + B_{2,zz} = 0 \ . \tag{21}$$

Particular solutions of the following form will be sought:

$$B_1 = \sum_n{}' g_n(r) \cos \beta_n z \ ; \tag{22}$$

$$B_2 = \sum_n{}' f_n(r) \cos \beta_n z \ . \tag{23}$$

Substituting these into equations (20) and (21), the defining relations for f and g are found to be:

$$g_n''(r) + \frac{g_n'(r)}{r} - \beta_n^2 g_n(r) = 0 \tag{24}$$

$$f_n''(r) + \frac{f_n'(r)}{r} - \left(\beta_n^2 + \frac{1}{r^2}\right) f_n(r) = 0 \ , \tag{25}$$

where the primes denote differentiation with respect to r. It is elementary to show that these solutions are:

$$f_n(r) = C_1 I_1\left(\beta_n r\right) + C_2 K_1\left(\beta_n r\right) \tag{26}$$

$$\beta_n \neq 0$$

$$g_n(r) = C_3 I_0\left(\beta_n r\right) + C_4 K_0\left(\beta_n r\right) \ , \tag{27}$$

where $I\left(\beta_n r\right)$ and $K\left(\beta_n r\right)$ are the modified Bessel functions of the first and second kind, respectively. The C's are arbitrary constants to be determined by the specified boundary conditions. The special case $\beta_n = 0$ represents a solution which is independent of the axial coordinate z, i.e., the elementary

case of plane stress or strain. This is discussed in Section VI. Thus, there have been no restrictions placed on f_n at this point. After determination of B_1 and B_2, the displacements are:

$$\bar{\bar{u}} = \sum_n' \left[(3 - 4\nu) f_n(r) - r f_n'(r) - g_n'(r)\right] \cos \beta_n z \qquad (28)$$

$$\bar{\bar{w}} = \sum_n' \left[r f_n(r) + g_n(r)\right] \beta_n \sin \beta_n z \ . \qquad (29)$$

The relations (26) through (29) complete the solution of the associated isothermal elasticity problem, i.e., the solution of the homogeneous portion of equations (11) and (12).

3. The Thermoelastic Potential

The continuum is to be heated in such a manner that the temperature distribution may be represented in the form:

$$T(r, z; t) = \sum_n' \theta_n(r;t) \cos \beta_n z + \sum_n' \zeta_n(r;t) \sin \beta_n z \ . \qquad (30)$$

The time t is considered to be a parameter included within the function θ and ζ and will not be written explicitly in the following expressions. The thermoelastic potential ϕ is found by solving equation (17) with use of the temperature field, equation (30). Considering first the cosine series portion of the temperature expression, the Poisson's equation (17) becomes:

$$\phi_{,rr} + \frac{1}{r}\phi_{,r} + \phi_{,zz} = \frac{1 + \nu}{1 - \nu} \alpha \sum_n' \theta_n(r) \cos \beta_n z \ . \qquad (31)$$

The solution will be taken in the form:

$$\phi = \sum_n' P_n(r) \cos \beta_n z \ . \qquad (32)$$

Substitution of equation (32) into equation (31) indicates that the unknown functions, $P_n(r)$, must be particular solutions of a nonhomogeneous equation of the Bessel type:

$$P_n''(r) + \frac{1}{r} P_n'(r) - \beta_n^2 P_n(r) = \frac{1+\nu}{1-\nu} \alpha \theta_n(r) \quad . \tag{33}$$

Solutions of this equation for several important cases are presented in Section V. Once $P_n(r)$ is determined, the corresponding displacements are obtained directly from equation (16), i.e.,

$$\bar{w} = - \sum_n \beta_n P_n(r) \sin \beta_n z \tag{34}$$

$$\bar{u} = \sum_n P_n'(r) \cos \beta_n z \quad . \tag{35}$$

As mentioned, these are the displacements due to the cosine series portion of equation (30). For the special case when $\beta_n = 0$, there are no additional displacements resulting from the sine series portion. For the general case $\beta_n \neq 0$, however, expressions analogous to equations (31) and (35) may be written for displacements arising from the sine series contribution. It is convenient to think of the functions φ^* and P_n^* such that

$$\varphi^* = \sum_n P_n^*(r) \sin \beta_n z \quad , \tag{36}$$

where $P_n^*(r)$ is the solution of equation (33) when $\theta_n(r)$ is replaced by $\zeta_n(r)$.

Section IV. THE GENERAL SOLUTION

The general solution of the axisymmetric thermoelasticity problem corresponding to the cosine series portion of the temperature distribution is obtained, according to equation (15), as the sum of equations (28), (35), and (29) and (34). The results are:

$$u(r,z) = \sum_n \left\{ \left[-\beta_n r I_0(\beta_n r) + 4(1-\nu) I_1(\beta_n r) \right] C_1 \right.$$
$$+ \left[\beta_n r K_0(\beta_n r) + 4(1-\nu) K_1(\beta_n r) \right] C_2 - \beta_n r I_1(\beta_n r) \frac{C_3}{r}$$
$$\left. + \beta_n r K_1(\beta_n r) \frac{C_4}{r} + P_n'(r) \right\} \cos \beta_n z \qquad (37)$$

$$w(r,z) = \sum_n \left\{ \beta_n r I_1(\beta_n r) C_1 + \beta_n r K_1(\beta_n r) C_2 + \beta_n r I_0(\beta_n r) \frac{C_3}{r} \right.$$
$$\left. + \beta_n r K_0(\beta_n r) \frac{C_4}{r} - \beta_n P_n(r) \right\} \sin \beta_n z \qquad (38)$$

$$\sigma_{rr} \frac{1+\nu}{E} = \sum_n \left\{ \left\{ (3-2\nu)\beta_n I_0(\beta_n r) - \left[\beta_n r + \frac{4(1-\nu)}{\beta_n r} \right] \beta_n I_1(\beta_n r) \right\} C_1 \right.$$
$$- \left\{ (3-2\nu)\beta_n K_0(\beta_n r) + \left[\beta_n r + \frac{4(1-\nu)}{\beta_n r} \right] \beta_n K_1(\beta_n r) \right\} C_2$$
$$+ \beta_n^2 \left[\frac{I_1(\beta_n r)}{\beta_n r} - I_0(\beta_n r) \right] C_3 - \beta_n^2 \left[\frac{K_1(\beta_n r)}{\beta_n r} + K_0(\beta_n r) \right] C_4$$
$$\left. + \beta_n^2 P_n(r) - \frac{1}{r} P_n'(r) \right\} \cos \beta_n z \qquad (39)$$

$$\sigma_{\theta\theta}\,\frac{1+\nu}{E} = \sum_n \left\{ \left[4(1-\nu) I_1(\beta_n r) - (1-2\nu)\beta_n r I_0(\beta_n r) \right] \frac{C_1}{r} \right.$$

$$+ \left[4(1-\nu) K_1(\beta_n r) + (1-2\nu)\beta_n r K_0(\beta_n r) \right] \frac{C_2}{r}$$

$$- \beta_n r I_1(\beta_n r)\,\frac{C_3}{r^2} + \beta_n r K_1(\beta_n r)\,\frac{C_4}{r^2}$$

$$\left. + \frac{P_n'(r)}{r} - \alpha\,\frac{1+\nu}{1-\nu}\,\theta_n(r) \right\} \cos \beta_n z \qquad (40)$$

$$\sigma_{zz}\,\frac{1+\nu}{E} = \sum_n \left\{ \beta_n \left[2\nu I_0(\beta_n r) + \beta_n r I_1(\beta_n r) \right] C_1 \right.$$

$$+ \beta_n \left[-2\nu K_0(\beta_n r) + \beta_n r K_1(\beta_n r) \right] C_2$$

$$+ \beta_n^2 r^2 I_0(\beta_n r)\,\frac{C_3}{r^2} + \beta_n^2 r^2 K_0(\beta_n r)\,\frac{C_4}{r^2}$$

$$\left. - \beta_n^2 P_n(r) - \alpha\,\frac{1+\nu}{1-\nu}\,\theta_n(r) \right\} \cos \beta_n z \qquad (41)$$

$$\sigma_{rz}\,\frac{1+\nu}{E} = \sum_n \left\{ \left[\beta_n r I_0(\beta_n r) - 2(1-\nu) I_1(\beta_n r) \right] C_1 \right.$$

$$- \left[\beta_n r K_0(\beta_n r) + 2(1-\nu) K_1(\beta_n r) \right] C_2$$

$$+ \beta_n r I_1(\beta_n r)\,\frac{C_3}{r} - \beta_n r K_1(\beta_n r)\,\frac{C_4}{r}$$

$$\left. - P_n'(r) \right\} \beta_n \sin \beta_n z \ . \qquad (42)$$

The displacements and stresses resulting from the sine series of the temperature distribution are also given by expressions (37) through (42), provided the following transformation is made:

$$\theta_n(r) \rightarrow \zeta_n(r) \qquad (43)$$

$$\sin \beta_n z \rightarrow -\cos \beta_n z \tag{44}$$

$$\cos \beta_n z \rightarrow \sin \beta_n z \tag{45}$$

$$P_n(r) \rightarrow P_n^*(r) \quad . \tag{46}$$

The relations (37) through (42) and their counterparts resulting from the transformations (43) through (46) constitute the general solution of the axisymmetric thermoelasticity problem in cylindrical coordinates, for the temperature field given by equation (30).

This general solution contains four arbitrary constants which may be used to satisfy prescribed boundary conditions. The solution is given in a form which is effective in satisfying arbitrary displacement or stress conditions on the curved surfaces r = constant. It is generally unable, however, to simultaneously satisfy arbitrary conditions on the plane surfaces z = constant. Consequently, the constants are to be used to satisfy exactly the curved surface boundary conditions; the flat surface conditions may then be satisfied in terms of their resultants, i.e., by appeal to St. Venant's principle.

No restrictions have been placed on the parameter β_n. It is noted, however, that it is specified by the temperature distribution. For a large number of practical applications, β_n will have the value $n\pi/L$, where n is an integer. The following observations relate to β_n of this value; analogous observations may be made for β_n of different form.

The cosine portion of the temperature distribution corresponds to a solution having a distribution of normal stress, σ_{zz}, over the flat ends of the cylinder. This normal stress prevents any longitudinal displacement. At the ends of the cylinder, the resultant of this longitudinal stress is:

$$S_z = 2\pi \int_a^b \sigma_{zz}(r, L)\, r\, dr \quad , \tag{47}$$

where a, b are the inner and outer radii, respectively. Performing this integration on (41) results in:

$$\frac{1+\nu}{2\pi E} S_z = \sum_n \left\{ \left[2\nu r I_1(\beta_n r) \Big|_a^b + \beta_n r^2 I_2(\beta_n r) \Big|_a^b \right] C_1 \right.$$

$$+ \left[2\nu r K_1(\beta_n r) \Big|_a^b - \beta_n r^2 K_2(\beta_n r) \Big|_a^b \right] C_2$$

$$+ C_3 \beta_n r I_1(\beta_n r) \Big|_a^b - C_4 \beta_n r K_1(\beta_n r) \Big|_a^b$$

$$\left. - \beta_n^2 \int_a^b r P_n(r)\, dr - \alpha \frac{1+\nu}{1-\nu} \int_a^b r \theta_n(r)\, dr \right\} \cos \beta_n L \quad . \tag{48}$$

If the ends of the cylinder are free, the above resultant must be annulled. This may be done by applying to the ends a uniform stress of magnitude:

$$\sigma^\circ = \frac{S_z}{\pi(b^2 - a^2)} \quad . \tag{49}$$

The state of stress and displacement resulting from this uniform end stress is:

$$\sigma^\circ_{rr} = \sigma^\circ_{\varphi\varphi} = \sigma^\circ_{rz} = 0 \tag{50}$$

$$\sigma^\circ_{zz} = \frac{S_z}{\pi(b^2 - a^2)} \tag{51}$$

$$w^\circ = \frac{S_z}{E\pi(b^2 - a^2)} z \tag{52}$$

$$u^\circ = -\frac{\nu}{E} \frac{S_z}{\pi(b^2 - a^2)} r \quad . \tag{53}$$

Thus, for the case of free-ends, the stresses and displacements given by equations (50) through (53) must be added to equations (37) through (42). In particular, it must be noted that these displacements must be included in the consideration of free-ended cylinders with displacement boundary conditions.

A similar consideration indicates that the sine portion of the temperature distribution corresponds to a solution having a distribution of radially directed shear stress on the end faces. This system is self-equilibrating, i.e., the resultant is zero. According to the principle of St. Venant, the influence of these stresses will vanish at a short distance from the ends, and they need be given no further consideration.

Section V. SOLUTIONS FOR THE THERMOELASTIC POTENTIAL

The ultimate solution of the problem hinges upon the determination of the thermoelastic potential function for the temperature distribution considered. It is recalled from Section III that a potential function of the following form has been assumed:

$$\varphi\ (r,z) = \sum_n P_n(r) \cos \beta_n z \ . \tag{54}$$

The resulting requirement on $P_n(r)$ is that it be a particular solution of:

$$P_n''(r) + \frac{1}{r} P_n'(r) - \beta_n{}^2 P_n(r) = \frac{1+\nu}{1-\nu} \alpha \theta_n(r) \ . \tag{55}$$

It must be noted that equation (55), and the following evaluations, are valid only when the temperature distribution can be expressed in the form of equation (30). In the sense that equation (30) may represent a double Fourier series in r and z, virtually any temperature distribution $T(r,z)$ may be written in this form. Further, there is no requirement that the temperature distribution be a solution of the Fourier heat conduction equation.

This section will consider the problem of determining P_n for several cases of practical interest. In the following, $P_n(r)$ refers to the solution obtained from the cosine series portion of the temperature distribution. The solution obtained from the sine series portion, $P_n{}^*(r)$, is defined by the same relations if $\theta_n(r)$ is replaced by $\zeta_n(r)$.

1. A Particular Solution Finite at the Origin

A particular solution of equation (55) must remain finite as $r \to 0$ if it is to be used in solutions for the solid cylinder. Although this property is not required for applications involving hollow cylinders, a single solution valid for both cases seems desirable. A particular solution which is finite at the origin, and valid in the region $o < r < b$, $-L < z < L$, may be found by the application of finite Hankel transforms. This transform is defined [5] by:

$$H[f(r)] = \bar{f}(\mu_m) = \int_o^b r f(r) J_0(\mu_m r)\, dr \ , \tag{56}$$

where the μ_m are the roots of the equation:

$$J_0(\mu_m b) = 0 \quad . \tag{57}$$

The inversion theorem is:

$$f(r) = \frac{2}{b^2} \sum_m{}' \bar{f}(\mu_m) \frac{J_0(\mu_m r)}{J_1^2(\mu_m b)} \quad . \tag{58}$$

Taking the transform of 55) and noting that

$$H\left[P_{,rr} + \frac{1}{r} P_{,r}\right] = -\mu_m{}^2 \bar{P}(\mu_m) \quad , \tag{59}$$

if P(r) tends to zero as r tends to b,

$$\mu_m{}^2 \bar{P}_n(\mu_m) + \beta_n{}^2 \bar{P}_n(\mu_m) = -\frac{1+\nu}{1-\nu} \alpha \bar{\theta}_n(\mu_m) \quad . \tag{60}$$

Solving for $\bar{P}(\mu_m)$:

$$\bar{P}_n(\mu_m) = -\frac{1+\nu}{1-\nu} \alpha \frac{\bar{\theta}_n(\mu_m)}{\mu_m{}^2 + \beta_n{}^2} \quad . \tag{61}$$

Applying the inversion formula,

$$P_n(r) = -\frac{2}{b^2} \frac{1+\nu}{1-\nu} \alpha \sum_m{}' \frac{\bar{\theta}_n(\mu_m)}{\mu_m{}^2 + \beta_n{}^2} \frac{J_0(\mu_m r)}{J_1^2(\mu_m b)} \quad , \tag{62}$$

where

$$\bar{\theta}_n(\mu_m) = \int_0^b r \theta_n(r) J_0(\mu_m r)\, dr \quad . \tag{63}$$

Equations (62) and (63) constitute the desired particular solution. The solution corresponding to the sine series portion of the temperature distribution is found by replacing θ_n, $\bar{\theta}_n$, with ζ_n, $\bar{\zeta}_n$ in the above equations.

2. Evaluation for Arbitrary Temperature Distribution in Series Form

Any reasonable temperature distribution may be formally written in the form of equation (30) by the use of a double Fourier series, valid in the interval $o < r < b$, $-L < z < L$. Thus,

$$T(r,z) = \sum_{p,n}{}' A_{pn} J_0\left(\mu_p r\right) \sin \beta_n z + \sum_{p,n}{}' B_{pn} J_0\left(\mu_p r\right) \cos \beta_n z \quad , \tag{64}$$

where μ_p are the positive roots of

$$J_0\left(\mu_p b\right) = 0 \quad , \tag{65}$$

and

$$\beta_n = \frac{n\pi}{L} \quad . \tag{66}$$

Also,

$$A_{pn} = \frac{2}{b^2 L J_1^2\left(\mu_p b\right)} \int_o^b r J_0\left(\mu_p r\right) \int_{-L}^{L} T(r,z) \sin \frac{n\pi z}{L} \, dz dr \tag{68}$$

$$B_{pn} = \frac{2}{b^2 L J_1^2\left(\mu_p b\right)} \int_o^b r J_0\left(\mu_p r\right) \int_{-L}^{L} T(r,z) \cos \frac{n\pi z}{L} \, dz dr \quad . \tag{68}$$

The functions $\theta_n(r)$, $\zeta_n(r)$ are seen to be :

$$\theta_n(r) = \sum_{p}{}' B_{pn} J_0\left(\mu_p r\right) \tag{69}$$

$$\zeta_n(r) = \sum_{p}{}' A_{pn} J_0\left(\mu_p r\right) . \tag{70}$$

Evaluating equation (63) for this case,

$$\overline{\theta}_n\left(\mu_m\right) = \sum_{p}{}' B_{pn} \int_o^b r J_0\left(\mu_p r\right) J_0\left(\mu_m r\right) dr = \frac{b^2}{2} \sum_{m}{}' B_{mn} J_1^2\left(\mu_m b\right) . \tag{71}$$

Inserting equation (71) into equation (62), $P_n(r)$ is found to be:

$$P_n(r) = - \frac{1 + \nu}{1 - \nu} \alpha \sum_m \frac{B_{mn} J_0(\mu_m r)}{\mu_m^2 + \beta_n^2} . \tag{72}$$

This expression, along with the analogous relation for P_n^*, constitutes a solution which is formally valid for any temperature distribution $T(r,z)$. Its use, in practice, will depend upon the complexity of the given function $T(r,z)$.

3. Evaluation for Steady-State Temperature Distribution

It will now be shown that the particular solution, equations (62) and (63), may be easily evaluated for any case of steady-state temperature distribution which satisfies the Fourier heat conduction equation:

$$\nabla^2 T(r,z) = 0 . \tag{73}$$

The solutions of equation (73) which are of the form of equation (30) are:

$$T(r,z) = \sum_n \left[A_n I_0(\beta_n r) + B_n K_0(\beta_n r) \right] \sin \beta_n z + \sum_n \left[C_n I_0(\beta_n r) + D_n K_0(\beta_n r) \right] \cos \beta_n z . \tag{74}$$

Therefore,

$$\theta_n(r) = C_n I_0(\beta_n r) + D_n K_0(\beta_n r) . \tag{75}$$

Evaluating $\bar{\theta}_n(\mu_m)$:

$$\bar{\theta}_n(\mu_m) = C_n \int_0^b r I_0(\beta_n r) J_0(\mu_m r)\, dr + D_n \int_0^b r K_0(\beta_n r) J_0(\mu_m r)\, dr . \tag{76}$$

These integrals are found in several of the standard references on Bessel functions [6]. The results are:

$$\bar{\theta}_n(\mu_m) = \frac{\beta_n b}{\mu_m^2 + \beta_n^2} \left\{ C_n \left[J_0(\mu_m b) I_1(\beta_n b) + \frac{\mu_m}{\beta_n} I_0(\beta_n b) J_1(\mu_m b) \right] \right.$$

$$\left. - D_n \left[J_0(\mu_m b) K_1(\beta_n b) - \frac{\mu_m}{\beta_n} K_0(\beta_n b) J_1(\mu_m b) - \frac{1}{\beta_n b} \right] \right\} \quad . (77)$$

The term $\bar{\zeta}_n(\mu_m)$ is found by replacing C_n, D_n with A_n, B_n in the expression above. These relations, in conjunction with equation (62), provide the solution for the thermoelastic potential corresponding to solutions of the steady-state heat conduction equation.

4. Evaluation for Temperature Distribution Independent of Radial Coordinate

For the special case of θ_n independent of the radial coordinate r, simple algebra applied to equation (33) gives the result:

$$P_n(r) = - \frac{1 + \nu}{1 - \nu} \alpha \frac{\theta_n}{\beta_n^2} , \quad (\beta_n \neq 0) \quad . \tag{78}$$

5. Evaluation for Temperature Distribution Independent of Longitudinal Coordinate

The special case of temperature distribution dependent upon the radial coordinate only corresponds to the special case $\beta_n = 0$ in equation (33), i.e.,

$$P_n''(r) + \frac{1}{r} P_n'(r) = \frac{1 + \nu}{1 - \nu} \alpha \theta_n(r) \quad . \tag{79}$$

This is no longer an equation of the Bessel form; however, the solution given by equations (62) and (63) is still valid, taking $\beta_n = 0$. An alternate solution is easily obtained from equation (79) by the method of variation of parameters. In noting the two linearly independent solutions of the homogeneous equation,

$$P_1(r) = \ln r \quad ; \tag{80}$$

$$P_2(r) = 1 \quad . \tag{81}$$

Forming the Wronskian,

$$W(P_1, P_2) = \begin{vmatrix} \ln r & 1 \\ \frac{1}{r} & 0 \end{vmatrix} = -\frac{1}{r} . \tag{82}$$

The solution is:

$$P_n(r) = -\frac{1+\nu}{1-\nu}\,\alpha \int^{r} s\theta_n(s) \ln\frac{s}{r}\, ds , \tag{83}$$

where s is a dummy variable of integration.

6. Applications

In order to illustrate the use of the equations developed in this section, several examples will be given. The first two involve temperature distributions which are solutions of the Fourier heat conduction equation. These distributions were taken directly from Carslaw and Jaeger [7], Chapter 8, and are typical of solutions of the heat conduction equation in cylindrical coordinates. The third example is very elementary, but represents the procedure to be followed when the temperature distribution is obtained from experimental measurement or is completely arbitrary.

a. Example 1

Finite solid cylinder, $0 < r < b$, $-L < z < L$, is used, initially at unit temperature. At time $t = 0$, all surfaces are suddenly brought to zero temperature.

The temperature distribution is given by:

$$T(r,z) = \frac{8}{\pi b} \sum_{n}{}' \sum_{m}{}' \frac{(-1)^n}{(2n+1)} \frac{J_0(\mu_m r)}{\mu_m J_1(\mu_m b)}\, e^{-\kappa t\left(\mu_m^2 + \beta_n^2\right)} \cos\beta_n z , \tag{84}$$

where

$$\beta_n = \frac{(2n+1)\pi}{2L} . \tag{85}$$

This distribution is already in the form of equation (64). By inspection it is clear that

$$B_{mn} = \frac{8}{\pi b} \frac{(-1)^n}{(2n+1)} \frac{e^{-\kappa t\left(\mu_m^2+\beta_n^2\right)}}{\mu_m J_1\left(\mu_m b\right)} . \tag{86}$$

It follows from equation (72) that

$$P_n(r) = -\frac{8\alpha}{\pi b} \frac{1+\nu}{1-\nu} \frac{(-1)^n}{(2n+1)} \sum_m \frac{e^{-\kappa t\left(\mu_m^2+\beta_n^2\right)}}{\mu_m\left(\mu_m^2+\beta_n^2\right)} \frac{J_0\left(\mu_m r\right)}{J_1\left(\mu_m b\right)} . \tag{87}$$

Boley and Weiner [8], Chapter 3, give an alternate method of obtaining ϕ for transient temperature distributions of this sort.

b. Example 2

Finite hollow cylinder $a < r < b$, $0 < z < L$ is used. Flux of heat into the solid at $r = a$ is a prescribed function $h(z)$. The remaining surfaces are kept at constant temperature taken to be zero.

The steady-state temperature distribution is:

$$T(r,z) = -\frac{2}{k\pi} \sum_n \frac{I_0\left(\beta_n r\right) K_0\left(\beta_n b\right) - K_0\left(\beta_n r\right) I_0\left(\beta_n b\right)}{n\left[I_1\left(\beta_n a\right) K_0\left(\beta_n b\right) + K_1\left(\beta_n a\right) I_0\left(\beta_n b\right)\right]} \sin \beta_n z \int_0^L h(z') \sin \beta_n z' dz', \tag{88}$$

where $\beta_n = n\pi/L$.

From equation (74), it is apparent that

$$A_n = -\frac{2}{k\pi} \frac{K_0\left(\beta_n b\right) \int_0^L h(z') \sin \beta_n z' dz'}{n\left[I_1\left(\beta_n a\right) K_0\left(\beta_n b\right) + K_1\left(\beta_n a\right) I_0\left(\beta_n b\right)\right]} \tag{89}$$

$$B_n = -\frac{I_0\left(\beta_n b\right)}{K_0\left(\beta_n b\right)} A_n . \tag{90}$$

After determination of A_n and B_n, $\bar{\zeta}_n$ is found from equation (77). The solution for $P_n^*(r)$ is then completed by employing equation (62).

c. Example 3

Finite hollow cylinder, $a < r < b$, $-L < z < L$ is used with temperature uniform through the wall and with axial temperature variation which is approximately parabolic; i.e.,

$$T(r,z) = T_0 - T_0 \frac{x^2}{L^2} . \tag{91}$$

The given temperature distribution is not in the form of equation (30). It is easily converted to the assumed form, however, by expansion in a Fourier cosine series:

$$T(r,z) = \frac{2}{3} T_0 + \frac{4T_0}{\pi^2} \sum_{n=1}^{\infty} \frac{(-1)^{n+1}}{n^2} \cos \frac{n\pi}{L} z . \tag{92}$$

It is clear that two θ_n's may be identified:

$$\theta_n(r) = \frac{2}{3} T_0 , \qquad \beta_n = 0 , \qquad (n = 0) \tag{93}$$

$$\theta_n(r) = \frac{4T_0}{\pi^2} \frac{(-1)^{n+1}}{n^2} , \qquad \beta_n \neq 0 , \qquad (n \neq 0) . \tag{94}$$

The first is an example of the special case $\beta_n = 0$, and $P_0(r)$ may be computed directly from equation (83). The second may be computed directly from equation (78).

Section VI. DISCUSSION

The relations (37) through (42) are a general solution of the axisymmetric thermoelasticity problem in cylindrical coordinates. The evaluation of these relations depends upon the determination of the function $P_n(r)$. Some general methods for finding $P_n(r)$ were given in Section V.

The form of the solution is suitable for satisfying exactly the stress or displacement boundary conditions on the curved surfaces; conditions at the end surfaces, z = constant, may be satisfied only in terms of the resultant. Consequently, the solution is not suitable for computations very near the end surface.

A particular form of solution has been selected for both the isothermal portion of the problem [equations (22) and (23)], the temperature distribution [equation (30)], and the thermoelastic potential function [equation (32)]. This form is sufficiently general to be of use for a fairly broad range of applications. However, it must be recognized that an alternate formulation may be of greater value for a particular problem.

1. Plane Stress and Plane Strain

When $\beta_n = 0$, the temperature distribution becomes a function of r only, and the thermoelasticity problem is reduced to one of plane strain or plane stress. Such problems may be solved with g(r) taken as zero. For this case, equations (37) through (42) become:

$$u(r) = C_1 r + \frac{C_2}{r} + \frac{1+\nu}{1-\nu}\frac{\alpha}{r}\int r\theta_n(r)\,dr \tag{95}$$

$$w(r) = 0 \tag{96}$$

$$\sigma_{rr}\,\frac{1+\nu}{E} = \frac{C_1}{1-2\nu} - \frac{C_2}{r^2} - \frac{1+\nu}{1-\nu}\frac{\alpha}{r^2}\int r\theta_n(r)\,dr \tag{97}$$

$$\sigma_{\theta\theta}\,\frac{1+\nu}{E} = \frac{C_1}{1-2\nu} + \frac{C_2}{r^2} + \frac{1+\nu}{1-\nu}\frac{\alpha}{r^2}\int r\theta_n(r)\,dr - \alpha\,\frac{(1+\nu)}{1-\nu}\,\theta_n(r) \tag{98}$$

$$\sigma_{zz}\,\frac{1+\nu}{E} = \frac{2\nu C_1}{1-2\nu} - \alpha\,\frac{1+\nu}{1-\nu}\,\theta_n(r) \tag{99}$$

$$\sigma_{rz} = 0\ . \tag{100}$$

The above results are for the case of plane strain. For plane stress:

$$u(r) = C_1 r + \frac{C_2}{r} + (1+\nu)\,\frac{\alpha}{r}\int r\theta_n(r)\,dr \tag{101}$$

$$\sigma_{rr}\,\frac{1+\nu}{E} = \frac{1+\nu}{1-\nu}\,C_1 - \frac{C_2}{r^2} - (1+\nu)\,\frac{\alpha}{r^2}\int r\theta_n(r)\,dr \tag{102}$$

$$\sigma_{\theta\theta}\,\frac{1+\nu}{E} = \frac{1+\nu}{1-\nu}\,C_1 + \frac{C_2}{r^2} + (1+\nu)\,\frac{\alpha}{r^2}\int r\theta_n(r)\,dr - \alpha(1+\nu)\theta_n(r) \tag{103}$$

$$\sigma_{zz} = \sigma_{rz} = 0\ . \tag{104}$$

2. The Solid Cylinder

For this case the point $r = 0$ is within the continuum and constitutes a singularity unless the constants C_2, C_4 in equations (37) through (42) and C_2 in equations (95) through (104) are taken to be zero.

3. The Multilayered Cylinder

The solutions presented are applicable to multilayered cylinders. For example, the case of two cylinders requires the evaluation of eight constants, in general. Four equations may be obtained from conditions at the interface, and the remaining equations found in the usual manner for a single cylinder. If the interface is located at $r = \eta$, interface boundary conditions may be of the following type:

Bonded Cylinders	Nonbonded Cylinders
$u^1(\eta) = u^2(\eta)$	$u^1(\eta) = u^2(\eta)$
$w^1(\eta) = w^2(\eta)$	$\sigma^1_{rr}(\eta) = \sigma^2_{rr}(\eta)$
$\sigma^1_{rz}(\eta) = \sigma^2_{rz}(\eta)$	$\sigma^1_{rz}(\eta) = 0$
$\sigma^1_{rr}(\eta) = \sigma^2_{rr}(\eta)$	$\sigma^2_{rz}(\eta) = 0$

The superscripts 1 and 2 designate the inner and outer cylinders, respectively.

REFERENCES

1. Goodier, J. N., "On the Integration of the Thermoelastic Equations," Phil Mag VII, 23, 1937, p. 1017.

2. Iyengar, K., Chandrashekhara, K., "Thermal Stresses in a Finite Hollow Cylinder due to an Axisymmetric Temperature Field at the End Surface," Nuclear Engineering and Design, 3, 1966, pp. 382-393.

3. Iyengar, K., and Chandrashekhara, K., "Thermal Stresses in a Finite Solid Cylinder due to an Axisymmetric Temperature Field at the End Surface," Nuclear Engineering and Design, 3, 1966, pp. 21-31.

4. Lure, A. I., Three-Dimensional Problems of the Theory of Elasticity, Chapter 7, Interscience Publishers, 1964.

5. Sneddon, Ian N., Fourier Transforms, Chapter 3, McGraw-Hill Book Company, 1951.

6. McLachlan, N. W., Bessel Functions for Engineers, second edition, Oxford University Press, 1955.

7. Carslaw, H. S., and Jaeger, J. C., Conduction of Heat in Solids, second edition, Oxford University Press, 1959.

8. Boley, B. A., and Weiner, J. H., Theory of Thermal Stresses, John Wiley and Sons, 1962.

BIBLIOGRAPHY

Nowacki, W., Thermoelasticity, Addison-Wesley, 1962.

APPROXIMATE ANALYSIS OF A FLAT, CIRCULAR PARACHUTE IN STEADY DESCENT*

Edward W. Ross, Jr.
U. S. Army Natick Laboratories
Natick, Massachusetts

ABSTRACT. A theory is presented for the stress analysis of a flat, circular parachute in steady, vertical descent. Unlike previous treatments of the problem, this theory does not assume that the shape is known. Instead, the theory presents relations between the pressure distribution in the opened condition and the shape, drag and stresses in lines and fabric. The theory results in a non-linear third order system of ordinary differential equations with boundary conditions at both vent and skirt. This system was solved by a computer program based on the Runge-Kutta method of numerical integration. The results are in fairly good agreement with measurements on parachutes. The computer program can be used for studies of effects of design changes on shape, drag and stress, and the results of a small study of this sort are included.

*This article has appeared as Technical Report No. 69-51-OSD, Office of the Scientific Director, U. S. Army Natick Laboratories, Natick, Massachusetts.
**The remainder of this article has been reproduced photographically from the author's manuscript.

1. INTRODUCTION

In recent years repeated attempts have been made to analyze the behavior of parachutes and devise formulas suitable for their design. Much progress has been made, but the state of knowledge is still not wholly satisfactory. The best analyses currently available, Heinrich and Jamison[1] and Topping, Marketos and Costakos[2] rely on knowing the deformed shape as well as the pressure distribution before the stresses are analyzed even in steady descent. Present knowledge about large deflections of structures suggests that it should be possible to calculate the stresses and deformed shape concurrently, although some assumptions must still be made about the pressure distribution in the deformed state. We shall undertake to do this in the present paper.

To be specific, we analyze a flat circular parachute in steady, vertical descent by an approximate theory for large elastic deflections. This theory is like (but goes beyond) that of Heinrich and Jamison[1]. The parachute is regarded as a completely flexible structure, i. e., none of its elements (cloth, cords, reinforcing tape, etc) have any bending stiffness. The resulting analysis resembles the large-deflection (non-linear) membrane version of thin shell theory but differs from it because of the important part played by the cords. A number of assumptions are made, of which the most important are listed below:

(i) The strains in the fabric and cords are small even though the deflections are large.

(ii) The fabric is supposed to possess no resistance to stresses in the meridional (radial) direction, all forces in this direction being resisted solely by the cords.

(iii) Corresponding points on each gore experience identical stresses and deformations, and the same is true for each cord, i. e., the deformation is, loosely speaking, axially-axisymmetric.

(iv) The circumferential radius of curvature of the gores is everywhere much smaller than the meridional radius of curvature.

(v) For each gore points on a circular arc about the axis of the undeformed parachute lie in a plane perpendicular to the cords after deformation.

The analysis, which is described in the next Section, leads to a non-linear third-order system of ordinary differential equations, which cannot be integrated in closed form. Therefore a computer program was written for the solution of the system, based on the Runge-Kutta method of numerical integration. The program is automatic enough so that it is convenient to study the effect on the deformations, stresses, drag and parachute weight of any two, arbitrarily chosen, design parameters, such as the vertical velocity, number of gores or elastic moduli of various structural elements. A description

of the program is given in Section 3 , and examples of the results obtained are displayed in Section 4. Section 5 contains a discussion of the analysis and results.

2. ANALYSIS

In analyzing the parachute we first treat a generic one of the gores, which is assumed to be a flat sector of a circle in the undeformed state. If G is the number of gores, then the sectorial angle in both the undeformed and deformed states is

$$\alpha = 2\pi/G \tag{1}$$

We examine first the kinematics, then the statics and finally the material behavior of the fabric.

Kinematics: Let A and B denote the material points where a generic circular arc in the undeformed state meets the cords that border the gore. In the undeformed state this arc, $\overline{AB}$, has length, $R\alpha$; see Figure 1. We assume that after deformation the arc $\overline{AB}$ forms a plane circular arc, the plane of the arc being perpendicular to the deformed cords, Figure 2. The points A and B are now at a distance r from the axis and are separated by a distance r_α. If r_{AB} is the radius of this circular arc and 2β is the sectorial angle, then we see from Figure 3 that, provided $0 \leq \beta \leq \pi/2$,

$$r_{AB} \sin\beta = (1/2) r_\alpha \tag{2}$$

$$2\beta r_{AB} = \text{Deformed length of arc } \overline{AB} \tag{3}$$

If $\beta = \pi/2$, we may have a situation where adjacent gores are

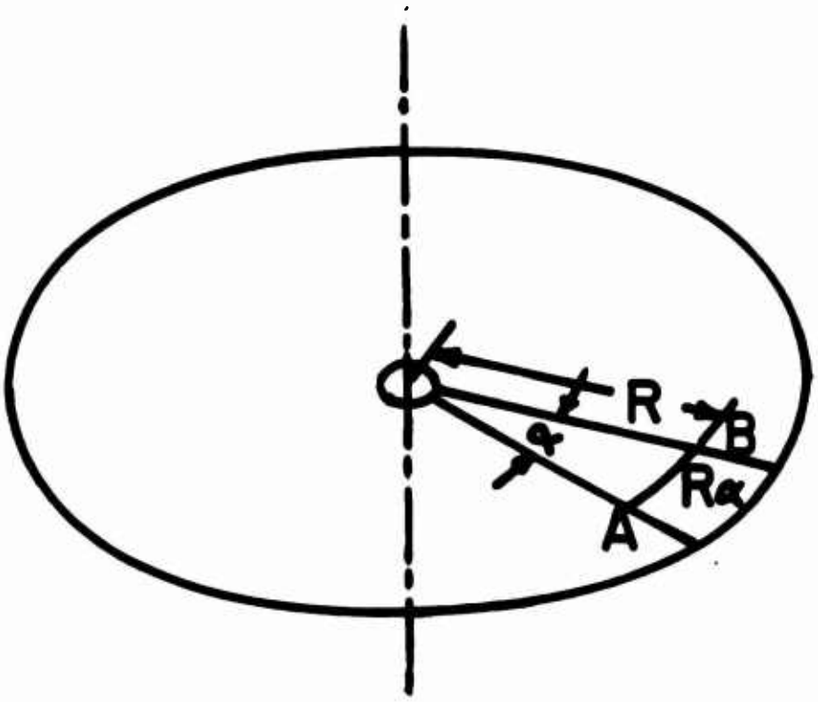


Figure 1: Undeformed parachute gore

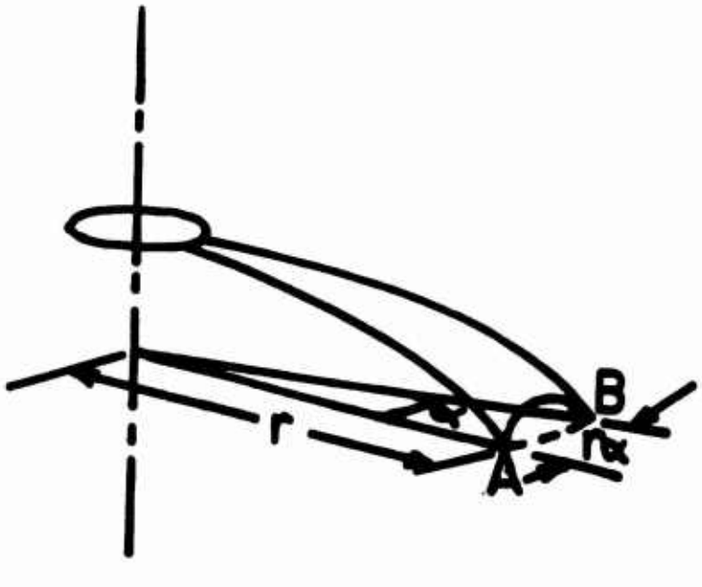


Figure 2: Deformed parachute gore

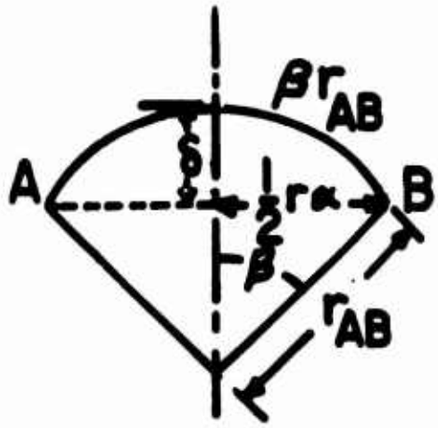


Figure 3: Section of deformed gore normal to cords, $\sigma' = 0$

pressed against each other with a contact length σ' as shown in Figure 4.

In this case

$$r_{AB} = (1/2)r\alpha \tag{4}$$

$$\text{Deformed length of } \overline{AB} = 2\sigma' + \pi r_{AB}$$

$$= 2\sigma' + (\pi/2)r\alpha \tag{5}$$

The undeformed length of $\overline{AB}$ is $R\alpha$, so we may write formulas for the circumferential fabric strain, γ_f, which is assumed small,

γ_f = change in length/original length

$$\gamma_f = (2\beta r_{AB}/R\alpha) - 1 \quad \text{if } \beta < \pi/2 \tag{6}$$

$$\gamma_f = \{[2\sigma' + (\pi/2)r\alpha]/R\alpha\} - 1 \quad \text{if } \beta = \pi/2 \tag{7}$$

Statics: If N_f is the circumferential tension in the gore fabric, with dimensions (lbs/ft) and p is the pressure difference between the inside and outside of the surface, then equilibrium requires

$$N_f = pr_{AB} \tag{8}$$

The forces exerted by the fabric on the cords, per unit length of cord are shown in Figure 5. The forces in the circumferential and normal directions, N_θ and N_n, are found from conditions of equilibrium,

$$N_\theta = N_f \cos\beta \tag{9}$$

$$N_n = 2N_f \sin\beta \tag{10}$$

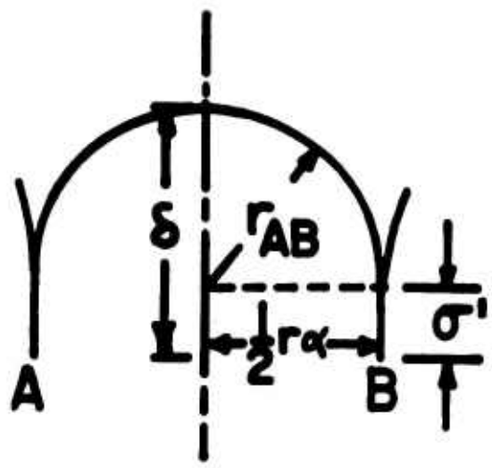


Figure 4: Section of deformed gore normal to cords, $\sigma' \neq 0$

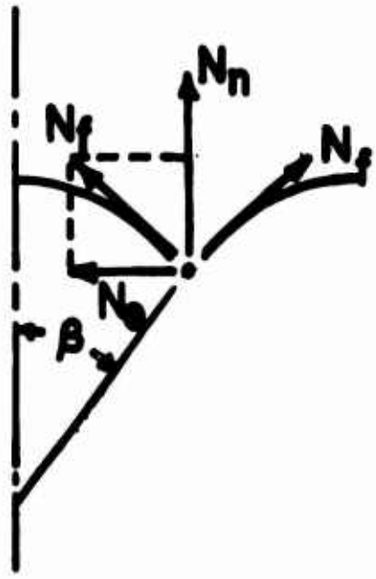


Figure 5: Forces transmitted from gore fabric to cords

If we use (2) and (8), we obtain for $\beta \neq 0$

$$N_\theta = (1/2)pr\alpha \cot \beta \tag{11}$$

$$N_n = pr\alpha \tag{12}$$

These formulas are valid both for $\beta<\pi/2$ and $\beta = \pi/2$, and in the latter case they imply

$$N_\theta = 0.$$

Material Behavior: We assume that the fabric obeys a linear elastic law,

$$N_f = E_f \gamma_f \tag{13}$$

where E_f is the elastic constant of the fabric when stressed in the circumferential direction. If $\beta<\pi/2$, we may use (2), (6) and (8) to rewrite this relation in the form

$$r/R = \beta^{-1}\{\sin\beta+(1/2)(p/E_f)r\alpha\} \tag{14}$$

This can also be written, with the aid of (11) as

$$r/R = \beta^{-1}\sin\beta\{1+(N_\theta/E_f)\sec\beta\},$$

or

$$N_\theta/E_f = \cos\beta\{\beta \csc\beta\,(r/R) -1\} \tag{15}$$

We see from (15) that in the limit as $\beta \to 0$ we obtain

$$N_\theta/E_f \to (r/R) -1.$$

This can be interpreted to mean that, when the fabric is stretched flat between the cords, i. e., when there is negligible bulging of the gores, we recover the linear elastic relation between circumferential stress resultant and circumferential strain.

In the calculations we shall adopt (15) together with formulas equivalent to (14) and (13)

$$\sin\beta - \beta(r/R)+(1/2)(p/E_f)r\alpha = 0 \tag{16}$$

$$N_f = E_f\{\beta\csc\beta(r/R) - 1\} \tag{17}$$

as expressing the material behavior of the fabric when $\beta<\pi/2$.

When $\beta = \pi/2$, the elastic law (13) implies

$$(1/2)(p/E_f)r\alpha = \{[2\sigma'+(\pi/2)r\alpha]/R\alpha\} - 1$$

or

$$\sigma' = (1/2)R\alpha\{1 - (\pi/2)(r/R)+(1/2)(p/E_f)r\alpha\} \tag{18}$$

together with

$$N_\theta = 0 \tag{19}$$

$$N_f = (1/2)pr\alpha \tag{20}$$

We have now completed the portion of the analysis that deals with the fabric.

In analyzing the fabric we have neglected the meridional stresses on the assumption that stresses of this type are borne entirely by the cords. We must now, therefore, analyze the statics and material behavior of the cords.

Statics of Cords: If N_c is the tension force in the cords, measured in lbs, then we can write down the two equations of force equilibrium in the direction tangential and normal to the cords with the aid of Figures 6 and 7. These are

$$dN_c/ds = 2N_\theta\sin(\alpha/2)\cos\phi \tag{21}$$

$$\begin{aligned} N_c d\phi/ds &= N_n - 2N_\theta\sin(\alpha/2)\sin\phi \\ &= pr\alpha - 2N_\theta\sin(\alpha/2)\sin\phi \end{aligned} \tag{22}$$

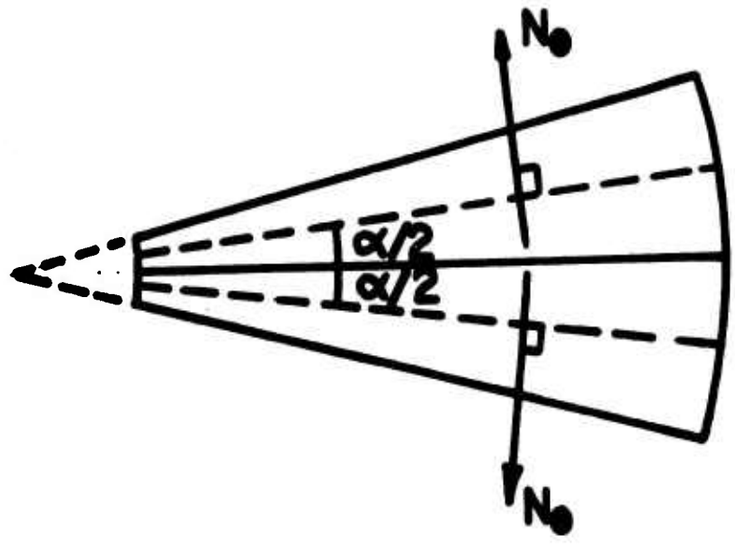


Figure 6: Sketch showing that the resultant of the N_θ forces on a cord is a radial inward force, $2N_\theta \sin(\alpha/2)$ per unit of cord length

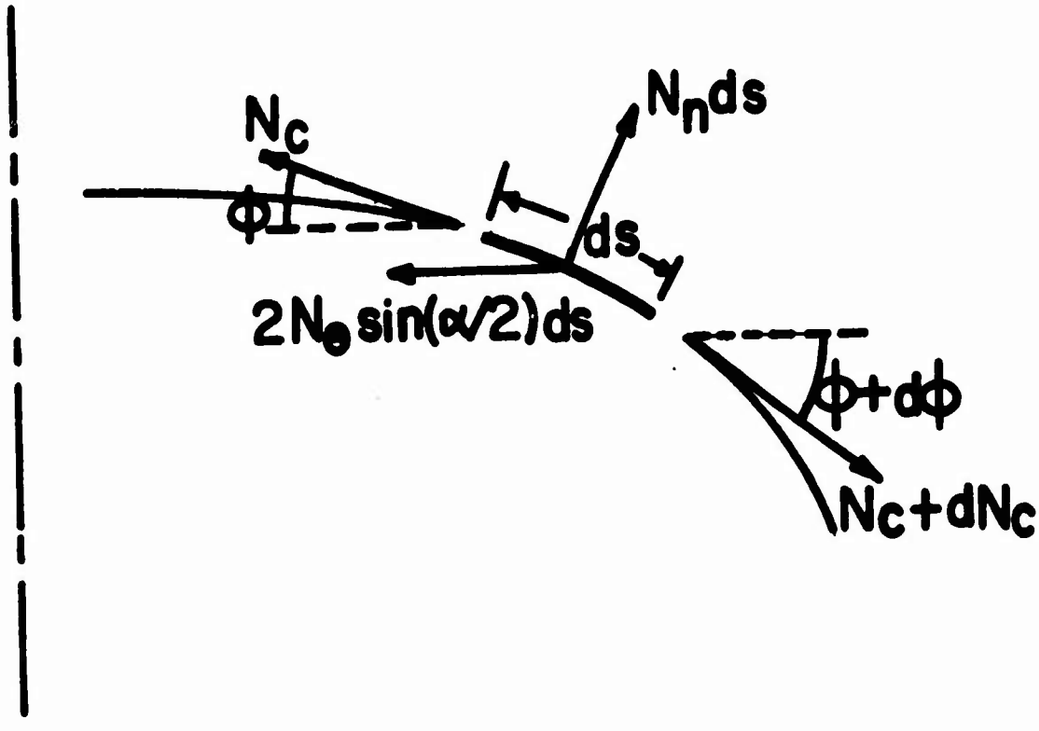


Figure 7: Forces acting on an element of cord with length ds

A partial check on the validity of these equations is provided by studying their behavior as $\alpha \to 0$. If we set $N_c = \pi N_s$, these should reduce to the equations of equilibrium of membrane shell theory,

$$d(rN_s)/dr = N_\theta \tag{23}$$

$$N_s\, d(\sin\phi)/dr + N_\theta(\sin\phi/r) = p. \tag{24}$$

If we use the fact that (see Figure 8)

$$dr = ds \cos\phi, \tag{25}$$

and observe that

$$(2/\alpha)\sin(\alpha/2) \to 1$$

as $\alpha \to 0$, we see that equations (21) and (22) reduce to the proper limit as $\alpha \to 0$.

Material Behavior of Cords: The strain in the cords, γ_s, is assumed to be small and we infer from Figure 9 that

$$\gamma_s = (ds-dR)/dR = (dr/dR)\sec\phi - 1$$

The cords are assumed to obey a linear elastic relation

$$N_c = E_c\gamma_s = E_c\{(dr/dR)\sec\phi - 1\}. \tag{26}$$

This completes the analysis of the cords.

To put these equations into systematic form we observe that

$$dr/dR = \{1+(N_c/E_c)\}\cos\phi = f\cos\phi \tag{27}$$

where

$$f = 1+(N_c/E_c).$$

Since

$$d/ds = (dr/ds)(d/dr) = (dr/ds)(dR/dr)(d/dR)$$

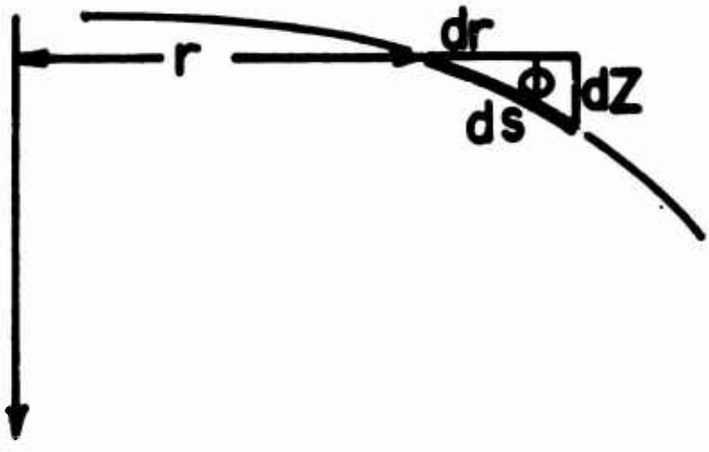


Figure 8: Geometry of deformed cord

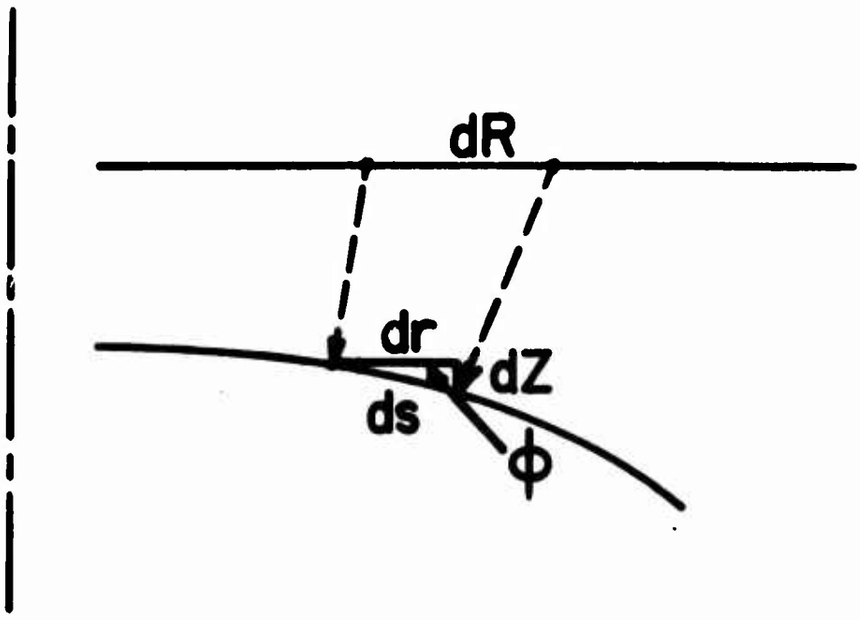


Figure 9: Derivation of formula for strain in cord

we find from (25) and (27) that

$$d/ds = (1/f)\,(d/dR).$$

Thus the equations of equilibrium and elasticity for the cords form the system

$$dr/dR = f\cos\phi \tag{28}$$

$$d\phi/dR = (f/N_c)\{pr\alpha - 2N_\theta \sin(\alpha/2)\sin\phi\} \tag{29}$$

$$dN_c/dR = 2fN_\theta \sin(\alpha/2)\cos\phi \tag{30}$$

where

$$f = 1+(N_c/E_c) \tag{31}$$

and N_θ is determined as follows. If

$$1+(r/2)\{(p\alpha/E_f)-(\pi/R)\} \leq 0$$

then

$$N_\theta = E_f\cos\beta\{(r/R)\beta\csc\beta - 1\} \tag{32}$$

where β is found by solving the transcendental equation

$$\sin\beta - \beta(r/R)+(pr\alpha/2E_f) = 0 \tag{33}$$

If

$$1+(r/2)\{(p\alpha/E_f) - (\pi/R)\} > 0$$

then

$$N_\theta = 0 \tag{34}$$

$$\sigma' = (R\alpha/2)\{1+(pr\alpha/2E_f) - (\pi r/2R)\}$$

This is a third order, non-linear differential equation system in the three unknowns r, ϕ and N_c, and therefore we shall need three edge conditions in order to have a unique solution. At the vent, $r = r_i$ or $R = R_i$,

the cords continue across to the opposite side of the vent through the axis of symmetry (see Figure 10). The elastic law for the cords implies that

$$r_i = R_i + \{(N_c(R_i)/E_c\} \tag{35}$$

We shall take for another condition at the vent

$$\phi = 0. \tag{36}$$

These conditions are satisfied with good accuracy in a flat circular canopy although in other kinds of parachutes, notably those with the pull-down vent, more complicated conditions must be imposed.

The third condition is at the skirt, $r = r_o$ or $R = R_o$. From the geometry, see Figure 11, we obtain

$$r_o - L \cos(\pi - \phi_o) = r_o + L \cos\phi_o = 0 \tag{37}$$

where L is the deformed length of the suspension lines between the skirt and the load (or confluence point). If L_o is the undeformed length of the suspension lines, and γ_L is the strain in the suspension lines (which we do not assume small), then

$$L = L_o(1+2\gamma_L)^{1/2}$$

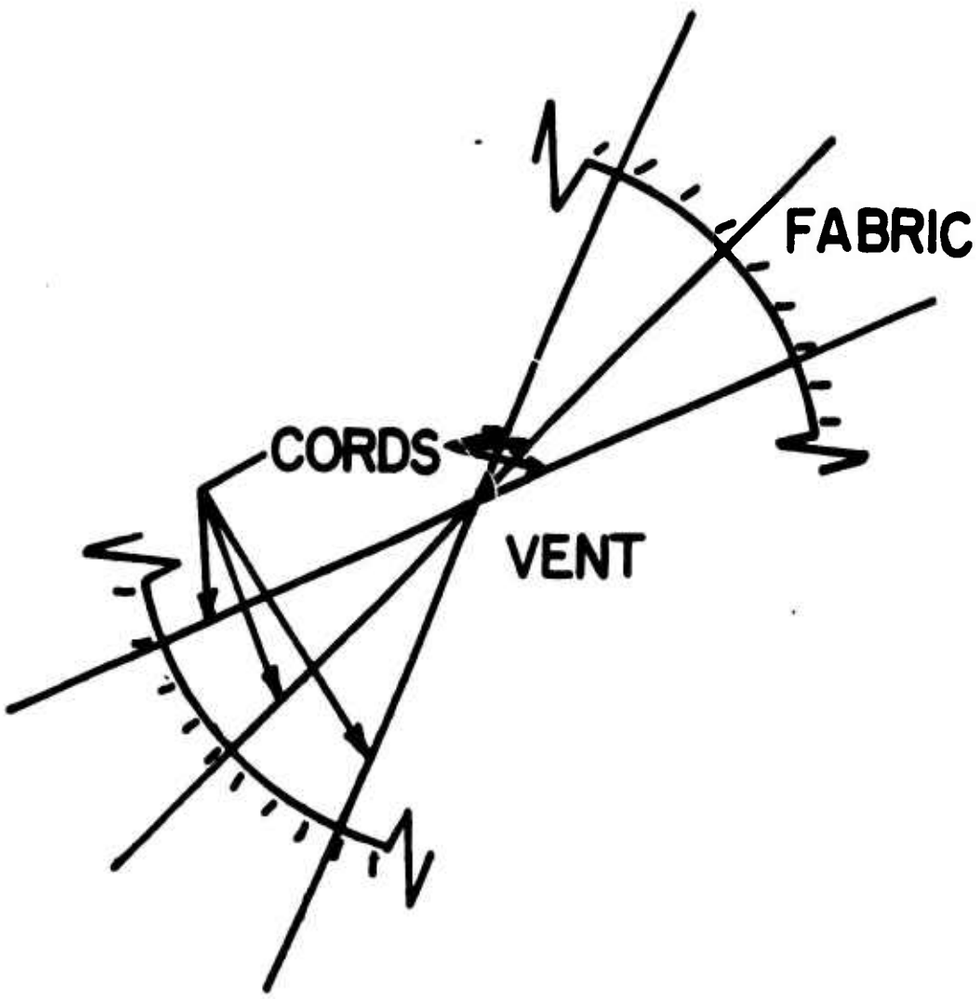


Figure 10: Sketch of the vent

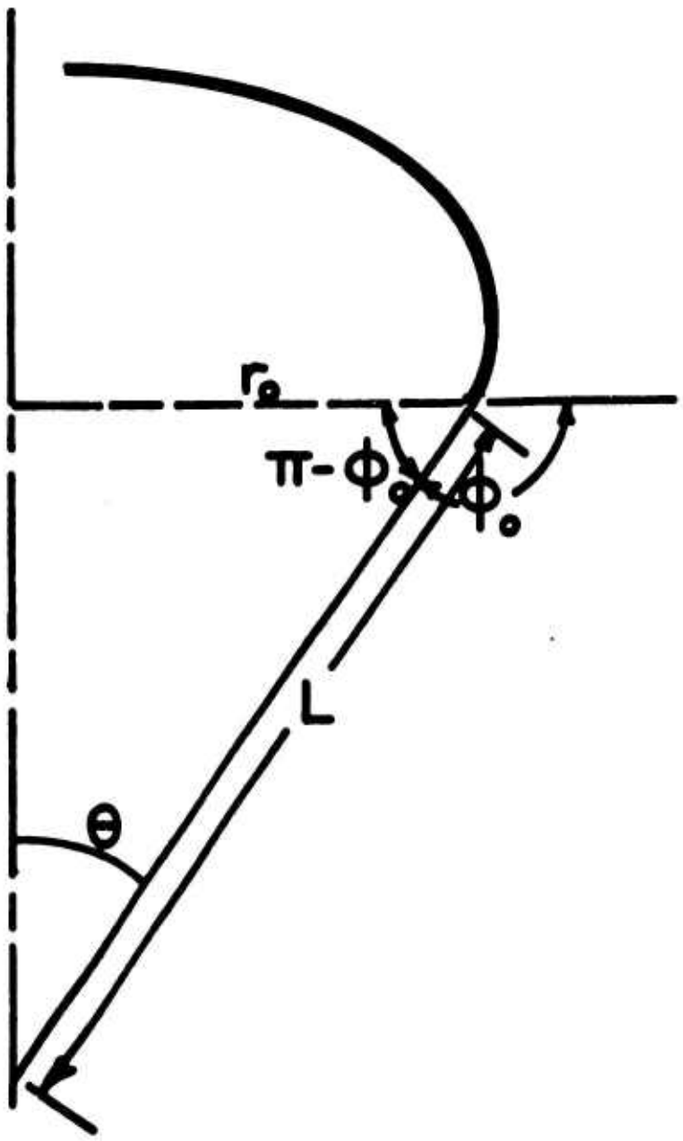


Figure 11: Geometry of skirt and load lines

The tension force in the lines is simply $N_c(R_o)$, the tension force in the cords at the skirt, hence, if E_L is the elastic modulus (lbs) of the lines,

$$\gamma_L = N_c(R_o)/E_L$$

$$L = L_o\left[1+\{2N_c(R_o)/E_L\}\right]^{1/2}$$

Then from (37) we find the condition which has to be satisfied at the skirt,

$$r(R_o)+L_o\{1+[2N_c(R_o)/E_L]\}^{1/2}\cos\phi(R_o) = 0 \qquad (38)$$

We have therefore reduced the problem of finding the deformed shape and stresses in the parachute to that of s lving the system of three, non-linear, ordinary differential equations (28) - (30) for r(R) and ϕ(R) and N_c(R). The quantities f and N_θ, which occur in the right sides of (28) - (30), are determined as functions of N_c, r and R by means of (31) - (34). The edge conditions on the differential equation system are (35), (36) and (38).

When this system has been solved, the drag, or weight of the load, can be found from

$$D = GN_c(R_o)\sin\phi(R_o) \qquad (39)$$

Also the deformed shape is found by calculating the cord profile, r(R) and Z(R), and the gore centerline profile, r_g(R) and Z_g(R), see Figure 12. In this calculation r(R) is of course known directly from the differential equation solution, but Z(R) must be found by integrating

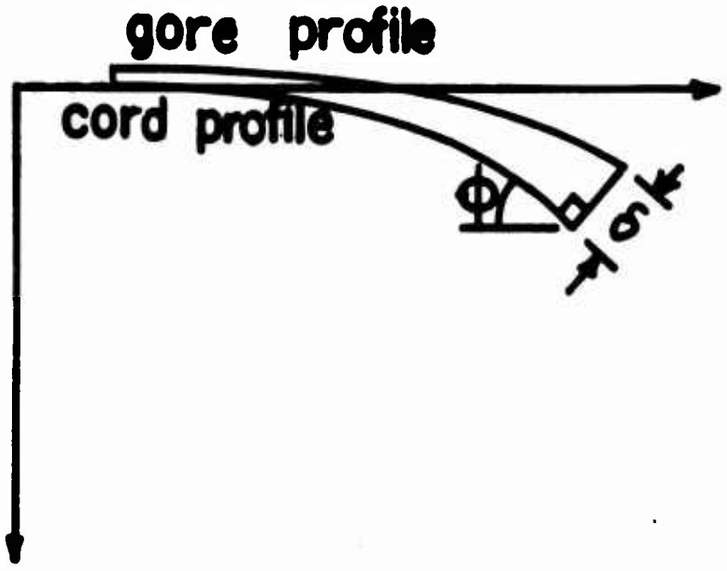


Figure 12: Profiles of deformed cord and gore centerline

$$dZ = dr \tan\phi = (dr/dR)\, dR \tan\phi$$

and so we find with the aid of (28)

$$Z = \int_{R'=0}^{R} f(R')\sin\phi(R')dR'$$

$$Z = \int_{R'=0}^{R} \{1+(N_c(R')/E_c\}\sin\phi(R')dR'. \qquad (40)$$

The gore centerline profile is then found, as in Figure 12,

$$r_g = r+\delta\sin\phi \qquad (41)$$

$$Z_g = Z-\delta\cos\phi \qquad (42)$$

where δ, the depth of centerline bulging, is given by different formulas for $\sigma' = 0$ and $\sigma'>0$. If $\sigma' = 0$, $\beta<\pi/2$ and (see Figure 3)

$$\delta = r_{AB}(1-\cos\beta) = (1/2)\, r\alpha(1-\cos\beta)/\sin\beta$$

$$= (1/2)r\alpha\tan(\beta/2) \qquad (43)$$

If $\sigma'>0$, $\beta = \pi/2$, we find from Figure 4

$$\delta = (1/2)\, r\alpha+\sigma'. \qquad (44)$$

We shall now re-phrase this entire system of equations in dimensionless form by introducing the new definitions

$$\begin{array}{llll} R = xR_i, & r = yR_i & L_o = JR_i, & R_o = x_oR_i, \\ N_c = E_cn_s, & N_\theta = E_fn_c, & N_f = E_fn_f, & Z_g = z_gR_i, \\ p = q\cdot 2E_f/R_i, & U_f = E_fR_i/E_c, & U_L = E_L/E_c, & r_g = y_gR_i, \\ D = E_cW, & \sigma' = \sigma R_i, & Z = zR_i, & \delta = \Delta R_i \end{array} \qquad (45)$$

The equations become

$$dy/dx = f\cos\phi \tag{46}$$

$$d\phi/dx = (2U_f f/n_s)\{q\alpha y - n_c \sin(\alpha/2)\sin\phi\} \tag{47}$$

$$dn_s/dx = 2fU_f n_c \sin(\alpha/2)\cos\phi \tag{48}$$

$$f = 1+n_s \tag{49}$$

If

$$1+q\alpha y-[\pi y/(2x)]<0$$

then

$$n_c = \cos\beta\{\beta(y/x)\csc\beta - 1\} \tag{50}$$

where β satisfies

$$\sin\beta - \beta y/x - q\alpha y = 0 \tag{51}$$

and if

$$1+q\alpha y-(\pi y/2x)\geq 0$$

then

$$n_c = 0, \quad \beta=\pi/2 \tag{52}$$

$$\sigma = (1/2)x\alpha\{1+q\alpha y-(\pi y/2x)\} \tag{53}$$

the edge conditions are

$$n_s(1) = y(1)-1 \tag{54}$$

$$\phi(1) = 0 \tag{55}$$

$$y(x_o)+J\{1+[2n_s(x_o)/U_L]\}^{1/2}\cos\phi(x_o) = 0 \tag{56}$$

The dimensionless load or drag is

$$W = Gn_s(x_o)\sin\phi(x_o), \tag{57}$$

$$z(x) = \int_0^x \{1+n_s(x')\}\sin\phi(x')\,dx' \qquad (58)$$

$$y_g = y+\Delta\sin\phi \qquad (59)$$

$$z_g = z-\Delta\cos\phi \qquad (60)$$

and

$$\Delta = (1/2)y\alpha\tan(\beta/2) \quad \text{if } \beta<\pi/2 \qquad (61)$$

$$\Delta = \sigma+(1/2)y\alpha \quad \text{if } \beta = \pi/2 \qquad (62)$$

In discussing the pressure and stress distributions it is also convenient to define dimensionless stress, drag and pressure coefficients in a manner different from the dimensionless quantities previously defined*. We shall take

$C_p = p/\{(1/2)\rho V^2\}$ = pressure coefficient

$C_{Do} = D/\{(1/2)\rho V^2\pi R_o^2\}$ = drag coefficient

$C_c = N_c/\{(1/2)\rho V^2\pi R_o^2\}$ = cord stress coefficient

$C_f = N_f R_o/\{(1/2)\rho V^2\pi R_o^2\}$ = fabric stress coefficient

If the foregoing analysis is correct, we must satisfy the 3rd order differential equation system (46) - (49) together with the auxiliary equation (50) - (53) and the edge condition (54) - (56). This system was taken as the basis for the computer program. The numerical analysis underlying the computer program is described in the next Section.

---

*Notice that because of (13), (26) and (35) the dimensionless stresses n_f and n_s, defined in (45), are also respectively just the strains γ_f, γ_s.

3. NUMERICAL ANALYSIS OF THE PROBLEM

The numerical analysis of this problem consists primarily of solving the differential equation system (46) - (48) by numerical means and secondarily satisfying the edge conditions. We shall deal below with these two aspects of the problem and then describe other aspects of the computer program.

The treatment of the differential equation system is based on the well-known Runge-Kutta method for numerical integration. The procedure is not quite routine because of the need to evaluate n_c and insert it in the right side of (47) and (48) at each step n_c being determined by (50) - (52). In particular, if

$$1+q\alpha y-\{\pi y/(2x)\}<0,$$

we must determine β by solving (51) and then evaluating t_c from (50). The solution of (51) was accomplished by using the Newton - Raphson iteration defined by

$$\beta_{k+1} = \beta_k - \left\{\frac{q\alpha y+\sin\beta-\beta(y/x)}{\cos\beta - (y/x)}\right\} \qquad (66)$$

As usual with this procedure convergence is uncertain. However, it became clear after a little study that convergence occurred when the initial β was chosen well above the value of β for which

$$\cos\beta = y/x.$$

This condition was satisfied by choosing as starting values

$$\beta = .4 \text{ if } \varepsilon \geq 0$$

$$\beta = .4+(-2\varepsilon)^{1/2} \text{ if } \varepsilon<0.$$

$$\varepsilon = (y/x)-1.$$

In order to avoid difficulties for small values of β in (50), explicit polynomial approximations were used for the trigonometric function, i. e.,

$$\cos \beta \approx 1-C_1\beta^2+C_2\beta^4$$

$$\sin \beta \approx \beta\{1-S_1\beta^2+S_2\beta^4\}$$

C_1, C_2, S_1, S_2 constants

With these approximations we may write (66) and (50) as

$$\beta_{k+1} \approx \beta_k + \left\{ \frac{q\alpha y-\beta[\varepsilon+\beta^2(S_1-S_2\beta^2)]}{\varepsilon+\beta^2(C_1-C_2\beta^2)} \right\} \equiv \beta_k - H_k \quad (67)$$

$$n_c \approx \frac{\{\varepsilon+\beta^2(S_1-S_2\beta^2)\}}{\{1-\beta^2(S_1-S_2\beta^2)\}} \{1-C_1\beta^2+C_2\beta^4\} \quad (68)$$

These formulas are sufficiently accurate for practical purposes and are well-behaved for $0 \leq \beta \leq \pi/2$.

Because the edge conditions (54) - (56) are not all applied at the same point, it is necessary to adopt a trial-and-error scheme in order to satisfy them. This is begun by assuming a value for the deformed vent radius, y(1). Next the values of $n_s(1)$ and $\phi(1)$ are found from (54) and (55), n_c (1) is evaluated as in the preceding paragraph and we can then begin the Runge-Kutta procedure for integrating the differential equation system. With this procedure the solution is built out in the x-direction until the values at the skirt, $y(x_c)$, $\phi(x_o)$ and $n_s(x_o)$ are obtained.

These values should satisfy (56). Usually, of course, they will not, and we must change the assumed value of y(1) and start again. In the program this process is made automatic by including a subroutine that applies the Rule of False Position when a sign change is found in the left side of (56).

In the program a general pressure distribution is assumed, given by

$$C_p = A_o + A_1\phi + A_2\phi^2 + A_3\phi^3 \qquad (69)$$

The constants A_o, A_1, A_2 and A_3 are read in and permit a fairly wide choice of pressure distributions. The scarcity of reliable information on pressure distributions makes this procedure necessary. It is worth noticing that C_p is assumed to be a function of ϕ (the deformed cord angle) and so depends to a certain extent on the deformed shape.

After finding the complete solution, satisfying all the edge conditions, the program carries out the numerical integration of (58), using Simpson's Rule, and calculates the cylindrical coordinates of the cord and gore centerlines by means of (59) - (62).

In order to make the program useful for design purposes, provision is made for the computation of certain information beyond merely the shape and stresses. This extra information includes an analysis of the parachute weight, i. e.,the distribution of the total weight among the different structural elements (fabric, cords, fixtures etc). Also the maximum

cord and fabric stresses, as well as the vent and load line stresses, are calculated and compared with the respective breaking stresses to find safety factors for each structural element. Warning messages are printed if the safety factors fall below unity.

The program is arranged so that in one pass the user may choose any two of the input quantities and vary these independently by chosen numbers of chosen increments, so that the effect on the solutions of changes in these quantities may be studied. For instance, the drop velocity, V, and fabric modulus, E_f, may be varied, or the effect of changing two constants in the hypothetical pressure distribution (69) may be found.

4. EXAMPLES OF RESULTS

This program was used to study the effects of different variables on the shape, drag and stresses. For this purpose a basic set of parameter values was chosen, typical of the C-9 canopy.

Vent radius = 1.4 ft

Ratio of skirt to vent radii = 10

No. of gores = 28

Suspension Line Length = 28 ft

Elastic Modulus of Cords = 2×10^3 lbs

Elastic Modulus of Fabric = 2×10^3 lbs/ft

Elastic Modulus of Load Lines = 2×10^3 lbs

The mass density of air was taken as

$$\rho = 2 \times 10^{-3} \text{ lb-sec/ft}^4.$$

and the drop velocity as

$$V = 20 \text{ ft/sec}$$

The basic pressure distribution was taken as a constant function $C_p = 1.5$, defined by

$$A_o = 1.5, \; A_1 = A_2 = A_3 = 0$$

For this basic configuration the following results were found:

C_{D_o} = Drag coefficient = .626

D_p = max. diameter = .671 D_o

ϕ_o = cord angle at skirt = 109°

or

$\theta = \phi_o - (\pi/2) = 19^\circ$

where $D_o = 2R_o$ is the flat circular diameter and θ is the angle between the suspension lines and the canopy axis. The deformed shape is shown in Figure 13, and the cord and fabric stress coefficients are depicted in Figure 14.

The theory was further tested by investigating the influence of various parameters on the shape, drag and stresses. A large number of results was obtained, the most important of which are displayed in Tables 1 and 2. We may summarize the main features as follows:

(i) Table 1 shows that D_p/D_o, and hence the shape, is not greatly affected by any of the parameter changes. The suspension line length ratio, Λ, has the greatest effect on D_p/D_o, but its effect is not especially large.

(ii) According to Table 1, Λ is the only canopy parameter that affects the drag coefficient significantly. The effects of G and V are small, and the elastic constants have negligible influence.

(iii) The angle, Θ, of the load lines, which is the same as the angle of the cords at the skirt, is seen in Table 1 to be significantly affected only by changes in Λ.

(iv) We conclude from Table 1 that G is the only variable that greatly influences $C_{c\ max}$ although Λ has some effect. In contrast $C_{f\ max}$ is perceptibly affected by changes in all the canopy parameters.

(v) The cord stress is least at the vent and increases to a maximum at the maximum diameter, which is usually at $x = 9$, i. e. near the skirt. Hence the familiar formula

$$C_c = C_{D_o}/G \cos \Theta,$$

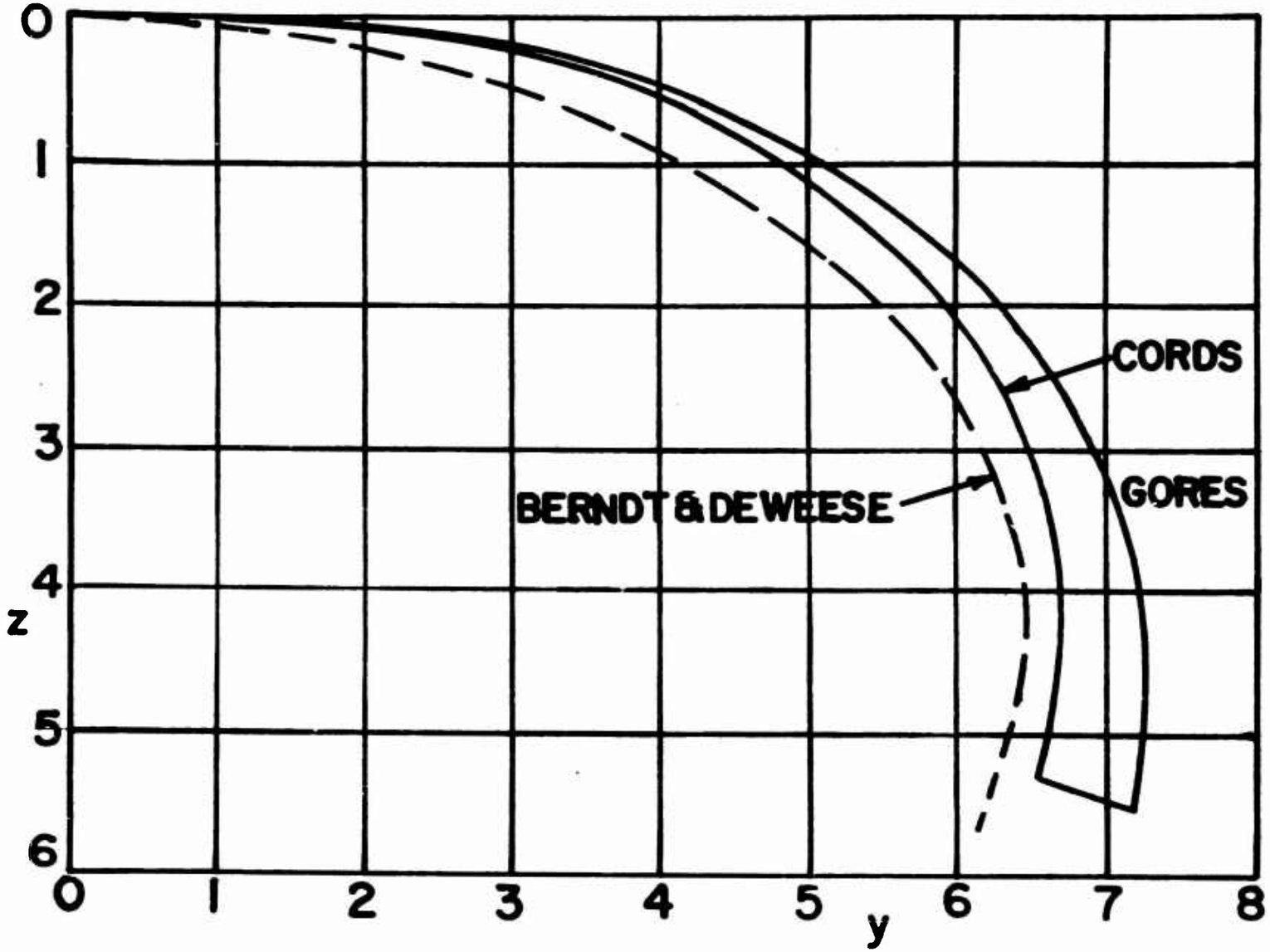


Figure 13: Deformed shape for basic configuration

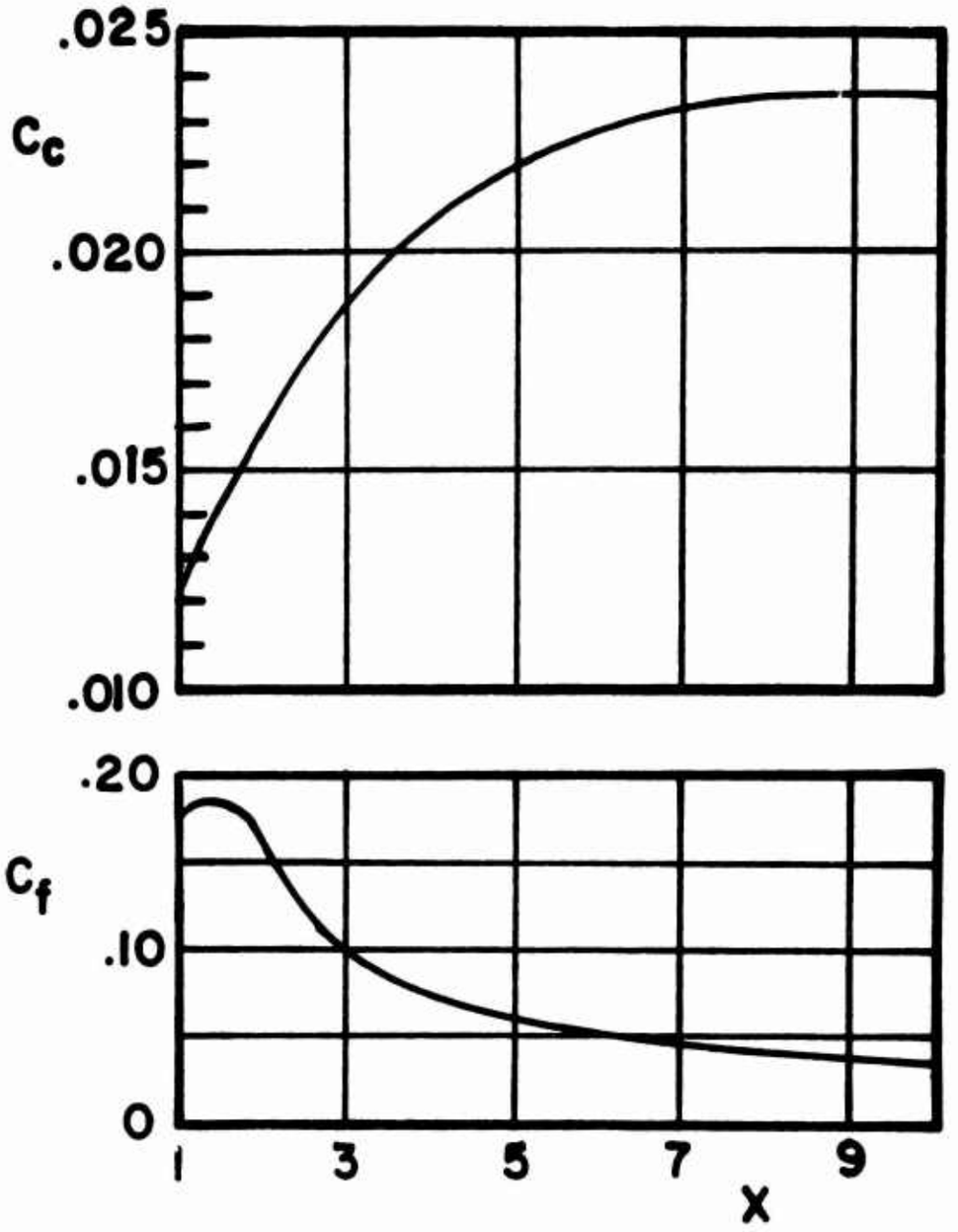


Figure 14: Cord and fabric stress coefficients for basic configuration

TABLE 1

Parameter	D_p/D_o	C_{D_o}	Max C_c	Max C_f	$\theta = \phi_o - (\pi/2)$
E_c					
1000	.673	.627	.0237	.264	19°
2000*	.671	.626	.0237	.185	19°
3000	.671	.625	.0236	.155	19°
E_f					
400	.672	.626	.0237	.087	19°
1200	.672	.626	.0237	.140	19°
2000*	.671	.626	.0237	.185	19°
G					
16	.665	.614	.0406	.219	19°
28*	.671	.626	.0237	.185	19°
40	.674	.630	.0167	.155	19°
Λ					
.7	.645	.549	.0218	.175	26°
1.0*	.671	.626	.0237	.185	19°
1.3	.687	.671	.0248	.191	15°
V					
10	.670	.623	.0236	.210	19°
20*	.671	.626	.0237	.185	19°
30	.673	.629	.0238	.176	19°

*Denotes value of variable for the basic configuration.

TABLE 2

Constant C_p	D max/D_o	C_{D_o}	Max C_c	Max C_f	θ
1.2	.671	.500	.0189	.150	19°
1.5*	.671	.626	.0237	.185	19°
1.8	.672	.751	.0284	.220	19°
Linearly Varying C_p[1]					
$C_p(x_o)$					
1.500	.671	.626	.0237	.185	19°
1.882	.689	.707	.0268	.202	20°
2.268	.702	.785	.0299	.218	20°

[1] In the case labelled "Linearly varying C_p", C_p varies linearly in ϕ between $C_p(1) = 1.5$ (at vent) and $C_p(x_o)$ at the skirt.

which is exactly true only for $C_c(x_o)$, is also approximately true for the maximum value of C_c.

(vi) The fabric stress is greatest at or near the vent and decreases as we go toward the skirt. The exact location of the maximum fabric stress depends on E_f as well as the pressure distribution.

(vii) From Table 2 we see that for constant pressure distributions, changing the pressure scarcely affects the shape and causes merely proportional changes in the stresses. If the pressure increases linearly in ϕ from the vent to the skirt, all quantities are affected.

We shall comment on these results in the following Section.

5. DISCUSSION

The theory developed in this paper is apparently the first in which the shape and stresses are calculated simultaneously. To judge the theory we must of course compare it with experimental results. In making this comparison it is first necessary to understand clearly what the theory does.

If we are given a flat, circular canopy with known geometrical and physical properties (respectively embodied in R_1, R_o, L_c, G and E_f, E_c, and E_L), dropping vertically at known velocity V through air with known mass density, ρ, the analysis furnishes us with the relations between the pressure distribution on one hand and the shape, stresses and drag on the other. If the pressure distribution is known, we can solve these relations (by means of the computer program) to find the quantities of engineering interest. These quantities will depend in general upon the pressure distribution.

An ideal experimental check on the theory would require that simultaneous measurements of pressure distribution, stresses, shape and drag be made on a canopy that is dropping vertically. Conditions for such a test may be difficult or impossible to realize in practice, and it appears that no experiments yet made will permit such a complete check on the theory.

However, many experiments have been made that, while incomplete in some respect, give us the information for a partial check on the theory. For example, Berndt and Deweese[3] made measurements on a C-9 canopy in towed flight. Their results compare with the present calculation for the basic configuration as follows:

Measured	Calculated
$C_{D_o} = .65$	$C_{D_o} = .626$
$D_p/D_o = .648$	$D_p/D_o = .671$
$\theta = 17^o$	$\theta = 19^o$

Their measured shape is plotted in Figure 13. The general agreement is good although the theoretical shape is slightly wider and shallower than the experimental shape. We may conclude from this that the present theory is not grossly in error. However, it is necessary to remark that, if we had assumed a different pressure distribution in the calculations, we could have arrived at quite different values for C_{D_o}, as is evident from Table 2.

The Parachute Handbook[4] gives the general estimate

$$D_p/D_o \approx .7,$$

which compares reasonably well with the present calculations,

$D_p/D_o = .67$ for the cords

$= .73$ for the gore centerlines.

Moreover, the observed generality of this estimate tends to confirm the theory, which predicts that the shape is insensitive to changes in most of the parameters.

The Parachute Handbook[4] shows many experimental results in which C_D is seen to decrease with an increase in V. This does not agree, at first sight, with our results, Table 1, which show that C_{D_o} increases very slowly with an increase in V. The discrepancy is probably due to one or both of two causes:

(a) The canopy may not be descending vertically in the tests. The theory assumes vertical descent and may give inaccurate results if the canopy oscillates or glides laterally.

(b) The pressure distribution may change as the velocity changes. In particular, increasing velocity will cause increase of the tensile stresses and strains in the fabric, and this will lead to greater porosity of the fabric. The increasing porosity will permit increasing air flow from the high-pressure to the low-pressure side of the fabric. Thus the pressure difference will not increase as fast as the impact pressure, or, in other words, the pressure-difference coefficient, C_p, will decrease. This will cause C_{D_o} to decrease.

In general we may say that the present theory represents a first, admittedly somewhat crude, attempt to analyze parachutes without assuming the deformed shape. Clearly, several of the assumptions described in the Introduction are not very accurate, notably (ii), and (v), while (iv) is probably inaccurate near the maximum diameter. Nevertheless the results are good enough to suggest that the general procedure is a workable one which can be a starting point for future efforts.

It is perhaps also useful to point out that this theory represents a step in the direction of calculating the opening behavior of parachutes. For a major part of the difficulty in the opening problem consists of estimating the shape and forces of the inflated part of the canopy. The not-yet-inflated part of the canopy is relatively easily dealt with. The estimate of the shape and forces of the

inflated part of the canopy is much like that of a (smaller) completely open canopy. We may anticipate, therefore, that the present analysis, or one like it, will be an integral part of an analysis of opening behavior.

ACKNOWLEDGMENT

The author is indebted to the members of the Research and Advanced Projects Division in the Airdrop Engineering Laboratory at the U. S. Army Natick Laboratories, particularly Mr. E. J. Glebutowski, for both help and instruction during the course of this work.

REFERENCES

1. Heinrich, H. G. and Jamison, L. R., "Parachute Stress Analysis during Inflation and at Steady State," J. of Aircraft, Vol. 3, (1966), pp. 52-58.

2. Topping, A. D., Marketos, J. D. and Costakos, N. C., "A Study of Canopy Shapes and Stresses for Parachutes in Steady Descent," Wright Air Development Center TR 55-294, Goodyear Aircraft Corp. October 1955.

3. Berndt, R. J. and De Weese, J. H., "Filling Time Prediction Approach for Solid Cloth Type Parachute Canopies," AIAA Aerodynamic Deceleration Systems Conference, Houston, Texas 1966.

4. "Performance of and Design Criteria for Deployable Aerodynamic Decelerators," Air Force Systems Command Report No. ASD-TR-61-579, December 1963.

NOMENCLATURE

A_o, A_1, A_2, A_3	Constants in canopy pressure distribution
C_1, C_2	Constants in formulas for cosine function
C_{D_o}	Drag coefficient based on flat circular area
C_p	Coefficient of net pressure
C_c, C_f	Stress coefficients in cords, fabric
D_p, D_o	Diameters in opened and flat circular states
E_c, E_f, E_L	Elastic moduli of cords, fabric, load lines
f	$1+(N_c/E_c)$
G	Number of gores
J	Dimensionless load line length
L_o, L	Length of load lines in undeformed and deformed states
N_c, N_f	Tension force in cords, fabric
N_θ, N_n	Force resultants on cords in circumferential and normal directions
n_s, n_f,	Dimensionless force in cord, fabric
n_c	Dimensionless circumferential force resultant on cords
p	Net outward pressure on gore fabric
q	Dimensionless pressure
R	Radius of particle in flat circular state
R_i, R_o	Vent and skirt radii in flat circular state
r	Radius of cord in opened state
r_i, r_o	Vent and skirt radii in opened state
r_{AB}	Circumferential radius of curvature of gore

NOMENCLATURE (Cont'd)

s	Arc length of cord
S_1, S_2	Constants in formulas for sine function
U_f, U_l, U_L	Dimensionless elastic constants
V	Vertical velocity
D	Drag force
W	Dimensionless drag
x	Dimensionless radius in flat, circular state
x_o	Dimensionless skirt radius in flat circular state
y	Dimensionless radius in opened state
Z, Z_g	Axial cylindrical coordinate of cords and gore centerline
z, z_g	Dimensionless axial coordinate of cords and gore centerline
α	Included angle of gore
β	Edge angle of gore bulge
γ_s, γ_f, γ_L	Strains in cord, fabric, and load lines
δ	Depth in bulge
Δ	Dimensionless depth of bulge
θ	Angle between load line and axis
Λ	Load line length ratio = $L_o/D_o = JR_l/(2R_o)$
ρ	Mass density of air
σ'	Contact length between adjacent gores
σ	Dimensionless contact length between adjacent gores
ϕ	Angle between cord direction and horizontal
ϕ_o	ϕ at the skirt

BOND STRETCH IN DIATOMIC MOLECULES AND THE FUES POTENTIAL

John D. Stettler and Romas A. Shatas
Solid State Physics Branch, Physical Sciences Laboratory
U. S. Army Missile Command, Redstone Arsenal, Alabama

I. INTRODUCTION. We have previously derived a variational method[1,2] for calculating the bond stretch induced in a diatomic molecule which arises from coupling between vibrational and rotational motion. The previous development was in the context of a weakly anharmonic oscillator for which an expansion of the potential energy about the static equilibrium point was expected to converge rapidly. However, for many diatomic molecules the Fues potential function[3] closely describes the interatomic potential V(r) which governs the vibrational motion. This function is

$$V(r) = \gamma^2(r^{-2} - 2r^{-1}) = -\gamma^2(1 - 2q^2 + 6q^3 - 24q^4 \ldots) \qquad (1)$$

where $q = r - 1$, with $r = 1$ being the equilibrium point. This potential is obviously strongly anharmonic. The applicability of our method to such a case is demonstrated in Section II. Because of the general usefulness of the Fues potential, in Section III we derive in detail the eignfunctions and eigenvalues of the Schrödinger equation for this potential and also evaluate expectation values of various powers of the interatomic distance. Finally, in Section III we use our procedure to evaluate the bond stretch for the Fues potential induced by vibration-rotation coupling.

II. VARIATIONAL METHOD. In spherical coordinates, the Schrödinger partial differential equation for the motion of a diatomic molecule about its center of mass is written as follows

$$\left\{-\frac{\hbar^2}{2\mu}\frac{1}{R^2}\frac{\partial}{\partial R}R^2\frac{\partial}{\partial R} + \frac{\mathcal{L}^2}{2\mu R^2} + U(R)\right\}\Psi(R,\theta,\phi) = E\Psi(R,\theta,\phi)$$

where μ is the reduced mass and $\hbar$ is the Planck's constant divided by 2π. Because $U(R)$ is spherically symmetric, $\Psi(R,\theta,\phi)$ can be written as

$$\Psi(R,\theta,\phi) = R^{-1}\cdot\psi(R)\cdot\Phi(\theta,\phi)$$

where

$$\mathcal{L}^2\Phi(\theta,\phi) = -\hbar^2\sin^{-1}\theta\left\{\frac{\partial}{\partial\theta}\sin\theta\frac{\partial}{\partial\theta} + \sin^{-1}\theta\frac{\partial^2}{\partial\phi^2}\right\}\Phi(\theta,\phi)$$
$$= \hbar^2\,\ell(\ell+1)\,\Phi(\theta,\phi)$$

and

$$H(r) \cdot \psi(r) = [H_{an}(r) + T(r)] \cdot \psi(r) = A\ \psi(r), \tag{2a}$$

with the operator

$$H_{an}(r) = -\frac{d^2}{dr^2} + V(r) \tag{2b}$$

being the anharmonic oscillator Hamiltonian and the operator

$$T(r) = \frac{\Delta}{r^2} \tag{2c}$$

expressing the perturbation term associated with the rotational motion where

$$\Delta = \ell(\ell + 1).$$

Here we have introduced the reduced quantities $r = RR_o^{-1}$, $A = 2\mu\hbar^{-2}R_o^{2}\ E$, $V(r) = 2\mu\hbar^{-2}\ R_o^{2}\ U(R)$, and $\psi(r)$ is the radial eigenfunction $\psi(R)$. The energy E and eigenfunction $\Psi(R,\theta,\phi)$ are characterized by the vibrational and rotational quantum numbers n and ℓ, respectively. The value of R_o is picked so that the equilibrium point for V(r) occurs at r = 1.

In order to introduce the bond stretch ρ arising from coupling between rotation and vibration, we note that Eq. (2a) can be formally transformed to

$$H(r + \rho)\ \ \psi(r + \rho) = A\ \ \psi(r + \rho) \tag{3}$$

and that $H_{an}(r)$ has eigenfunctions $\phi(r)$ and eigenvalues $\mathcal{E}$ such that

$$H_{an}(r)\ \ \phi(r) = \mathcal{E}\ \phi(r) \tag{4}$$

The difference between the Hamiltonians in Eq. (3) and Eq. (4) is the rotational term Eq. (2c) which is repulsive for all values of r. We, therefore, make the ansatz that the effects of T(r) can be represented by an effective bond stretch. In mathematical terms, we assume that there exists a value for ρ such that

$$\psi(r + \rho) \simeq \phi(r)$$

where both functions correspond to the same vibrational quantum number n. Thus we suppose that

$$A = \int_0^\infty dr \; \phi^*(r) \; H(r + \rho) \; \phi(r) \tag{5}$$

and, from our previous development, the best value for ρ is given by the condition

$$0 = \int_0^\infty dr \; \phi(r)^* \; \frac{\partial}{\partial \rho} H(r + \rho) \; \phi(r). \tag{6}$$

Thus the expressions that we have derived for the bond stretch arising from coupling of rotational and vibrational motions are independent of the degree of anharmonicity of the vibrational potential.

III. FUES POTENTIAL. With the choice of the equilibrium point at r = 1, the Fues potential has the form given in Eq. (1). Therefore, Eq. (2a) becomes

$$\left(\frac{d^2}{dr^2} + A + 2\gamma^2 r^{-1} - (\Delta + \gamma^2) r^{-2} \right) \cdot \psi(r) = 0. \tag{7}$$

Because we are interested only in the bound states of the diatomic molecule, the quantity A in Eq. (7) is necessarily nonpositive. We can define $k = (-A)^{\frac{1}{2}}$, $B = \Delta + \gamma^2$, $g = k^{-1} \gamma^2$, and make the change of variables $x = 2kr$ to transform Eq. (7) into

$$\left(\frac{d^2}{dx^2} + gx^{-1} - Bx^{-2} - \frac{1}{4} \right) \psi(x) = 0. \tag{8}$$

We now let

$$\psi(x) = Nx^s L(x) e^{-\frac{1}{2}x} \tag{9}$$

where s is picked such that L(x) is bounded and non-zero at x = 0. This gives a value for s of

$$s = \tfrac{1}{2} + (\tfrac{1}{4} + B)^{\frac{1}{2}}$$

and the differential equation to be satisfied by L(x) becomes

$$x\{-\frac{d^2}{dx^2} + (2s - x)\frac{d}{dx} - s + g\}\ L(x) = 0. \qquad (10)$$

Solutions to Eq. (10) are the confluent hypergeometric functions.[4] In order that $\psi(x)$ of Eq. (9) remains finite as x approaches infinity only those values of A in Eq. (7) are allowed for which

$$s - g = - n$$

where n is a non-negative integer. With this restriction Eq. (10) becomes the defining equation for Laguerre polynomials

$$\{x\frac{d^2}{dx^2} + (a + 1 - x)\frac{d}{dx} + n\}\ L_n^a(x) = 0 \qquad (11)$$

which are chosen such that they have the normalization integral[5]

$$\int_0^\infty x^{a+1}[L_n^a(x)]^2 e^{-x}dx = \Gamma(n + a + 1)^3\frac{2n + a + 1}{n!}\ . \qquad (12)$$

The normalization constant N in $\psi(x)$ of Eq. (9) is determined by the condition that

$$\int_0^\infty \psi^*(r)\ \psi(r)\ dr = 1.$$

Therefore we obtain for the Fues potential the eigenvalues

$$A_n = - \gamma^4(n + s)^{-2} \qquad n = 0,1,2\ .\ .\ . \qquad (13a)$$

and eigenfunctions

$$\psi_n(r) = [\Gamma(n + 2s)^3\frac{(n+s)}{n!\ k}]^{-\frac{1}{2}}\ (2kr)^s\ L_n^{2s-1}(2kr)e^{-kr} \qquad (13b)$$

with

$$s = \tfrac{1}{2} + (\gamma^2 + (\ell + \tfrac{1}{2})^2)^{\frac{1}{2}} \quad , \quad k = \gamma^2 (s + n)^{-1} \quad , \tag{13c}$$

where ℓ is the rotational quantum number. We note that for s an integer $L_n^{2s-1}(x)$ is the associated Laguerre polynomial for which the condition $n \geq 2s - 1 \geq 0$ must hold. Such functions appear in the hydrogen atom eigenfunctions.[6] In our case, however, s is not an integer and, for the cases of interest, s is much larger than n.

In the calculation of the bond stretch ρ and the evaluation of our method, we need to expand Eq. (5) and Eq. (6) in a Taylor series in ρ. Consequently, we have to calculate quantities of the form

$$\left\langle r^m \right\rangle = \int_0^\infty dr \; \psi^*(r) \, r^m \, \psi(r), \tag{14}$$

where $\psi(r)$ is given in Eq. (13b) and m is an integer, generally negative. In order that the integrand of Eq. (14) not be unbounded at the origin, we require that $2s + m \geq 0$. With this restriction Eq. (14) can be evaluated by relating the Laguerre polynomials to the confluent hypergeometric functions, and then using the integral representation of the latter to integrate by parts.[4] This yields

$$\left\langle r^m \right\rangle = \frac{(2k)^{-m}}{2(n + s)} \frac{\Gamma(2s + 1 + m)}{\Gamma(2s)} \tag{15}$$

$$\left\{1 + \frac{n(m + 2)\,(m + 1)}{1^2\,(2s)} + \frac{n(n-1)(m + 3)(m + 2)(m + 1)m}{1^2\,2^2\,(2s)(2s + 1)}\right.$$

$$+ \; . \; . \; . \; +$$

$$\left. + \frac{n!\,(m + n + 1)(m + n) \; . \; . \; . \; (m + 2 - n)}{1^2\,2^2 \; . \; . \; . \; n^2\,(2s)(2s + 1) \; . \; . \; . \; (2s + n - 1)}\right\}.$$

Evaluating the above expression for some values of m, we find that

$$\langle r \rangle = \frac{s(2s+1) + 3n(2s+n)}{2k\,(n+s)}$$

$$\langle r^0 \rangle = 1$$

$$\langle r^{-1} \rangle = \frac{k}{n+s} \qquad (16)$$

$$\langle r^{-2} \rangle = \frac{2k^2}{(n+s)\,(2s-1)}$$

$$\langle r^{-3} \rangle = \frac{2k^3}{s(2s-1)\,(s-1)}$$

These expressions reduce to those for the hydrogen atom when the transformations $k \to (a_o\, n)^{-1}$, $n \to n - \ell - 1$, $s \to \ell + 1$ are made.[6]

IV. BOND STRETCH. In order to calculate the bond stretch attributable to rotation-vibration coupling, we expand Eq. (6) in a Taylor series to obtain

$$0 = \left\langle \frac{\partial}{\partial r} \mathcal{H}(r) \right\rangle + \rho \left\langle \frac{\partial^2}{\partial r^2} \mathcal{H}(r) \right\rangle + \tfrac{1}{2}\rho^2 \left\langle \frac{\partial^3}{\partial r^3} \mathcal{H}(r) \right\rangle + \ldots . \qquad (17)$$

From the form of $\mathcal{H}(r)$ given in Eq. (2a) and the expression Eq. (1) for the Fues potential we find that Eq. (17) becomes

$$\begin{aligned} 0 = {} & -2\gamma^2 \left(\langle r^{-3} \rangle - \langle r^{-2} \rangle \right) - 2\Delta \langle r^{-3} \rangle \\ & + \rho \{ 2\gamma^2 (3 \langle r^{-4} \rangle - 2 \langle r^{-3} \rangle) + 6\Delta \langle r^{-4} \rangle \} \qquad (18) \\ & + \tfrac{1}{2}\rho^2 \{ -12\gamma^2 (2 \langle r^{-5} \rangle - \langle r^{-4} \rangle) - 24\Delta \langle r^{-5} \rangle \} + \ldots . \end{aligned}$$

Because the expectation values in Eq. (18) are with respect to solutions of Eq. (4), we use the expressions in Eq. (13a) and Eq. (16) with Δ equal zero. Solving Eq. (18) under these conditions on ρ, we find that

$$\rho = \frac{\Delta}{\gamma^2} \left(1 - 3 \frac{n + \frac{1}{2}}{\gamma} \right) - \frac{9}{2} \frac{\Delta^2}{\gamma^4} \qquad (19)$$

where we have assumed that the rotational energy is much less than the vibrational energy and the vibrational energy is much less than the disassociation energy. In order to assess the accuracy of Eq. (19), we compare $\langle \mathcal{H}(r + \rho) \rangle - \langle \mathcal{H}(r) \rangle$ to what it should be if our procedure were exact; namely, $A_n(\Delta) - A_n(0)$. We find that

$$\frac{\langle \mathcal{H}(r + \rho) \rangle - \mathcal{H}\langle (r) \rangle}{A_n(\Delta) - A_n(0)} = 1 - \frac{\Delta}{\gamma^2}\left(\frac{9}{4}\frac{(n + \frac{1}{2})}{\gamma} - \frac{\Delta}{\gamma^2}\right) \qquad (20)$$

where $A_n(\Delta)$ is given by Eq. (13a). Equation (20) indicates the accuracy of our method.

REFERENCES

1. R. A. Shatas, "Perturbation Theoretic Calculation of Eigenfunctions and Energy Eigenstates of the Symmetric Linear Diatomic Anharmonic Non-Rigid Vibrator-Rotator," in Trans. 13th Conf. Army Math., ARO-D Report 68-1, Feb. 1968.

2. John D. Stettler and Romas A. Shatas, "Bond Stretch in Diatomic Vibrators Induced by Rotational-Vibrational Interaction, Int. J. Quant. Chem., Vol. 3S, (1969).

3. E. Fues, Ann. Physik 80, 367 (1926).

4. L. D. Landau and E. M. Lifshitz, Quantum Mechanics (Pergamon Press, London, 1958).

5. P. M. Morse and H. Feshbach, Methods of Theoretical Physics (McGraw Hill Book Company, New York 1953).

6. H. A. Bethe and E. E. Salpeter, Quantum Mechanics of One- and Two-Electron Atoms (Academic Press, New York 1957).

NUMERICAL STUDY OF A BEST INTERVAL APPROXIMATION OF THE SQUARE ROOT OF A POSITIVE NUMBER

Fred Frishman
Army Research Office, OCRD
Washington, D. C.

and

William L. Shepherd
Instrumentation Development Directorate
White Sands Missile Range, New Mexico

1. INTRODUCTION

In [1], which was presented at the Fourteenth Conference of Army Mathematicians, we discussed the iterative computation of $\sqrt{N}$:

$$0 < x_0 \leq \sqrt{N} ,$$

$$x_{j+1} = x_j + \frac{N - x_j^2}{2x_j + \frac{N - x_j^2}{2x_j}} , \qquad j = 0, 1, 2,... \tag{1.1}$$

or

$$x_{j+1} = x_j + \frac{N - x_j^2}{2x_j + \delta_j} ,$$

where

$$\delta_j = \frac{N - x_j^2}{2x_j}$$

is a bound on the error in approximating $\sqrt{N}$ by x_j.

Here we want to point out its association with the elementary theory of continued fractions and exhibit some results of numerical experience with it.

2. CONTINUED FRACTIONS

Consider

$$f^{(1)}(x,N) = x + \frac{N - x^2}{2x}$$

Subsequent to the Conference, certain additional statements and corrections were included in Section 3. This paper has been reproduced photographically from the author's copy.

$$f^{(2)}(x,N) = x + \cfrac{N - x^2}{2x + \cfrac{N - x^2}{2x}}$$

$$f^{(3)}(x,N) = x + \cfrac{N - x^2}{2x + \cfrac{N - x^2}{2x + \cfrac{N - x^2}{2x}}}$$

... ...

Problem 3, page 367 of Hall and Knight [2] shows that, for $x > 0$, $N > 0$,

$$\lim_{n \to \infty} [f^{(n)}(x,N)] = \sqrt{N} \tag{2.1}$$

Newton's iteration is

$$x_{j+1} = f^{(1)}(x_j,N) .$$

Our iteration is

$$x_{j+1} = f^{(2)}(x_j,N) .$$

It is intuitively plausible that for

$$x_{j+1} = f^{(n)}(x_j,N) \tag{2.2}$$

$$\lim_{j \to \infty} \{x_j\} = \sqrt{N} ,$$

though we have not proved it.

Now, it is known that Newton's iteration converges "quadratically" to $\sqrt{N}$. It can be shown that our method converges "cubically" to $\sqrt{N}$.

It is conjectured that the order of convergence of (2.2) increases monotonely as n increases. If this is so, an investigation might be made of the trade-off between core storage requirements and computing speed for various values of n. It is likely that the trade-off decisions would depend on the particular machine being used.

3. NUMERICAL RESULTS

The table in the appendix is completely illustrative of the speed with which (1.1) converges. The computations were done on a Hewlett-Packard 9100A desk calculator. This machine does 12 decimal digit floating point calculations. The table below was obtained from an examination of the appendix and similar tables. The table is to be read:

> For N in the interval X, convergence to within less than 5 in the Yth significant digit is obtained in Z or less iterations, and there is at least one N in X for which convergence to within less than 5 in the Yth significant digit cannot be obtained in less than Z iterations.

X	Y	Z
[1, 100]	2	3
[1, 100]	7	4
[1, 100]	12	5
[.01, 1]	2	3
[.01, 1]	7	4
[.01, 1]	12	5
[.25, 1]	4	2
[.25, 1]	12	3
[1, 4]	5	2
[1, 4]	12	3

Reference to the appendix shows that, though δ is no less than 0, it sometimes happens that the computed value of δ is less than 0. This is caused by round-off error; continued iterations indicate that in this case the process is stable.

4. DISCUSSION AND CONCLUSIONS

Since the convergence of (1.1) does not depend on $x_o \leq \sqrt{N}$, it would appear to be a suitable scheme to improve an approximate $\sqrt{N}$ obtained by Tschebychev or other functions [3]; we have not investigated this.

The method as exhibited is fast and stable, and might be very fast for a special purpose fixed subroutine in a binary arithmetic computer.

5. PLANS FOR FUTURE WORK

We also propose comparing the numerical results obtained in this paper with the results from the following iterative scheme which is also suggested in [1]:

$$x_{j+1} = x_j + \frac{N - x_j^2}{2x_j + 1 + \dfrac{N - x_j^2}{2x_j + 1}}$$

Our procedure suggests methods for obtaining cube and higher roots; these are under study at present.

APPENDIX

The table illustrates the numerical experience with the iteration

$$0 < x_0 \leq \sqrt{N}$$

$$x_{j+1} = x_j + \frac{N - x_j^2}{2x_j + \delta_j} \quad ,$$

$$j = 0, 1, 2, \ldots$$

Since

$$x_j \leq \sqrt{N} \leq x_j + \delta_j \quad ,$$

$|\delta_j|$ is a bound on the absolute error in approximating $\sqrt{N}$ by x_j, except for round-off error.

REFERENCES

[1] W. L. Shepherd and F. Frishman, "Best Interval Approximations of the Square Root of a Positive Number," 1968, presented at 14th Conference of Army Mathematicians, Rock Island, Illinois.

[2] H. S. Hall and S. R. Knight, "Higher Algebra," Fourth Edition, 1891, 1950 Printing.

[3] David G. Moursund, "Optimal Starting Values for Newton-Raphson Calculation of $\sqrt{x}$," Communications of the ACM, Vol. 10, No.7, pp 430-432, July, 1967.

TABLE A.1

$x_c = 1,\ 1 \leq N \leq 100$

N	δ_1	δ_2	δ_3	δ_4	δ_5
1.00	0				
1.01	3.1×10^{-8}	-2.5×10^{-11}	-5.0×10^{-12}	-5.0×10^{-12}	-5.0×10^{-12}
1.02	2.5×10^{-7}	-5.0×10^{-12}	-5.0×10^{-12}	-5.0×10^{-12}	-5.0×10^{-12}
1.03	8.2×10^{-7}	-4.0×10^{-11}	0	0	0
1.04	2.0×10^{-6}	3.5×10^{-11}	5.0×10^{-12}	5.0×10^{-12}	5.0×10^{-12}
1.05	3.8×10^{-6}	-3.0×10^{-11}	0	0	0
1.06	6.4×10^{-6}	7.3×10^{-11}	4.9×10^{-12}	4.9×10^{-12}	4.9×10^{-12}
1.07	1.1×10^{-5}	0	0	0	0
1.08	1.5×10^{-5}	5.3×10^{-11}	4.9×10^{-12}	4.9×10^{-12}	4.9×10^{-12}
1.09	2.1×10^{-5}	-1.5×10^{-11}	-4.8×10^{-12}	-4.8×10^{-12}	-4.8×10^{-12}
1.1	2.9×10^{-5}	9.6×10^{-12}	9.6×10^{-12}	9.6×10^{-12}	9.6×10^{-12}
1.5	2.6×10^{-3}	2.7×10^{-9}	-8.2×10^{-12}	-8.2×10^{-12}	-8.2×10^{-12}
2.0	1.5×10^{-2}	3.7×10^{-7}	-1.1×10^{-11}	$+1.1 \times 10^{-11}$	-1.1×10^{-11}
2.5	3.7×10^{-2}	4.8×10^{-6}	9.5×10^{-12}	9.5×10^{-12}	9.5×10^{-12}
3.0	6.7×10^{-2}	2.5×10^{-5}	-3.2×10^{-11}	-5.8×10^{-12}	-5.8×10^{-12}
3.5	1.1×10^{-1}	8.2×10^{-5}	0	0	0
3.90	1.4×10^{-1}	1.8×10^{-4}	1.8×10^{-11}	2.6×10^{-12}	2.6×10^{-12}
3.91	1.5×10^{-1}	1.8×10^{-4}	1.6×10^{-11}	-2.3×10^{-11}	1.6×10^{-11}
3.92	1.5×10^{-1}	1.8×10^{-4}	5.1×10^{-12}	5.1×10^{-12}	5.1×10^{-12}
3.93	1.5×10^{-1}	1.9×10^{-4}	-1.6×10^{-11}	0	0
3.94	1.5×10^{-1}	1.9×10^{-4}	2.3×10^{-11}	-1.5×10^{-11}	2.3×10^{-11}
3.95	1.5×10^{-1}	1.9×10^{-4}	2.1×10^{-11}	-1.8×10^{-11}	2.1×10^{-11}
3.96	1.5×10^{-1}	2.0×10^{-4}	2.6×10^{-11}	2.6×10^{-11}	2.6×10^{-11}
3.97	1.5×10^{-1}	2.0×10^{-4}	-7.6×10^{-12}	-7.6×10^{-12}	-7.6×10^{-12}
3.98	1.5×10^{-1}	2.0×10^{-4}	1.6×10^{-11}	-2.3×10^{-11}	1.6×10^{-11}
3.99	1.5×10^{-1}	2.0×10^{-4}	1.3×10^{-11}	5.1×10^{-12}	5.1×10^{-12}
4	1.5×10^{-1}	2.1×10^{-4}	1.5×10^{-11}	0	0
5	2.5×10^{-1}	7.8×10^{-4}	1.2×10^{-11}	2.3×10^{-12}	2.3×10^{-12}
6	3.7×10^{-1}	2.1×10^{-3}	3.5×10^{-10}	-4.1×10^{-12}	-4.1×10^{-12}
7	5.0×10^{-1}	5.0×10^{-3}	2.5×10^{-9}	7.6×10^{-12}	7.6×10^{-12}
8	6.3×10^{-1}	7.4×10^{-3}	1.3×10^{-8}	-3.6×10^{-12}	-3.5×10^{-12}

TABLE A.1 (Cont'd)

N	δ_1	δ_2	δ_3	δ_4	δ_5
9	7.7×10^{-1}	1.2×10^{-2}	4.5×10^{-8}	8.4×10^{-12}	8.4×10^{-12}
10	9.1×10^{-1}	1.8×10^{-2}	1.4×10^{-7}	1.6×10^{-11}	0
20	2.5	1.5×10^{-1}	4.2×10^{-5}	0	0
30	4.1	4.0×10^{-1}	5.2×10^{-4}	0	0
40	5.8	7.2×10^{-1}	2.4×10^{-3}	7.2×10^{-11}	0
50	7.4	1.1	6.5×10^{-3}	1.4×10^{-9}	0
60	9.1	1.6	1.4×10^{-2}	1.2×10^{-8}	-6.5×10^{-12}
70	1.1×10	2.0	2.6×10^{-2}	6.0×10^{-8}	0
80	1.3×10	2.5	4.2×10^{-2}	2.3×10^{-7}	0
90	1.4×10	2.9	6.3×10^{-2}	6.9×10^{-7}	5.3×10^{-12}
91	1.5×10	3.0	6.6×10^{-2}	7.6×10^{-7}	0
92	1.5×10	3.0	6.8×10^{-2}	8.4×10^{-7}	5.3×10^{-12}
93	1.5×10	3.1	7.0×10^{-2}	9.2×10^{-7}	-1.1×10^{-11}
94	1.5×10	3.1	7.3×10^{-2}	1.1×10^{-6}	5.2×10^{-12}
95	1.5×10	3.2	7.6×10^{-2}	1.2×10^{-6}	0
96	1.5×10	3.2	7.8×10^{-2}	1.3×10^{-6}	5.2×10^{-12}
97	1.6×10	3.3	8.1×10^{-2}	1.4×10^{-6}	5.1×10^{-12}
98	1.6×10	3.3	8.4×10^{-2}	1.5×10^{-6}	-5.1×10^{-12}
99	1.6×10	3.4	8.6×10^{-2}	1.6×10^{-6}	0
99.1	1.6×10	3.4	8.7×10^{-2}	1.7×10^{-6}	-5.1×10^{-12}
99.2	1.6×10	3.4	8.7×10^{-2}	1.7×10^{-6}	0
99.3	1.6×10	3.4	8.7×10^{-2}	1.7×10^{-6}	-5.1×10^{-12}
99.4	1.6×10	3.4	8.8×10^{-2}	1.7×10^{-6}	5.1×10^{-12}
99.5	1.6×10	3.4	8.8×10^{-2}	1.7×10^{-6}	0
99.6	1.6×10	3.4	8.8×10^{-2}	1.7×10^{-6}	0
99.7	1.6×10	3.4	8.8×10^{-2}	1.8×10^{-6}	5.1×10^{-12}
99.8	1.6×10	3.4	8.9×10^{-2}	1.8×10^{-6}	-5.1×10^{-12}
99.9	1.6×10	3.4	8.9×10^{-2}	1.8×10^{-6}	0
100	1.6×10	3.4	8.9×10^{-2}	1.8×10^{-6}	0

A DYNAMIC MODEL OF VEHICLE SYSTEM AVAILABILITY*

Martin Wachs
Mobility, Communication & Electronics Division
Aberdeen Proving Ground, Maryland

ABSTRACT. A mathematical model is presented which is of value in comparing alternative systems of tactical logistic vehicles. As a hypothetical combat mission advances, the requirements for tactical logistic vehicles are computed, and failure and repair rates are used to compute the probabilities of having various numbers of vehicles down for maintenance. These probabilities are used to compute system availability as a function of time during the mission. A computer program is presented, by which the model may be put into operation, and several suggestions are included as to possible uses of the model.

*This paper appeared as Technical Memorandum No. 36 of the Army Materiel Systems Analysis Agency, RDT&E Project No. 1S765801M61302. The remainder of this article has been reproduced photographically from the author's copy.

PRECEDING PAGE BLANK

I. INTRODUCTION

AMSAA Technical Memorandum No. 12, entitled "Conceptual Framework for a Tactical Logistic Vehicle Evaluation Methodology", describes a general approach to modelling the effectiveness of tactical logistic vehicle systems. In that paper the concept of a dynamic model of vehicle system availability was introduced,[1] but the mathematical details of such a model were not presented. This report is a more comprehensive treatment of the dynamic availability model. It includes the background against which such a model was developed, the mathematical formulation of the model, and a computer program by which the model may be put into operation.

II. BACKGROUND FOR THE MODEL

The role of the logistics system is to permit combat commanders as wide a freedom of choice in strategy and tactics as the enemy situation and combat environment will permit. Stated somewhat differently, the effectiveness of the logistics system is its ability to reduce the number of logistical constraints placed upon the tactical units. Some examples of constraints placed upon a tactical combat organization by an inefficient logistics organization are limited maneuverability due to fuel shortages or late deliveries, and limited firepower due to lateness or absence of ammunition deliveries. The effectiveness of the tactical logistic vehicle system may be viewed as the extent to which it prevents these constraints from occurring under a variety of anticipated combat conditions.[2]

The effectiveness of an organization of tactical logistic vehicles (TLV's) is dependent upon the inherent performance of its vehicles in various combat environments, and also upon the ability of the TLV organization to manage and schedule its human and mechanical resources in order to maintain and effectively utilize its vehicles.[3] In a cost-effectiveness comparison of alternative vehicle systems, changes in the number of repair crews or in the stockage of spare parts might

have as significant an effect upon organizational performance as would changes in the type or number of vehicles assigned to the organization. Models are required by which alternative organizational structures and policies may be compared in addition to comparisons of possible alternative vehicles. Such models are most useful if they permit evaluations of effectiveness under a variety of combat conditions and in a wide range of physical environments. The model presented here represents a compromise between these goals and the limitations imposed by computational feasibility.

The model, as presented in the following section, is quite general and may be applied equally well to tracked or wheeled vehicles. With only minor modification it could also be used for the evaluation of tactical logistic aircraft.

III. DESCRIPTION OF THE MODEL

Consider an organization of tactical logistic vehicles whose mission consists of moving a required tonnage of supplies per unit time from some fixed supply point forward to a combat unit which is advancing during the course of a battle. This situation is illustrated in Figure 1, where the rear supply point is located at A, the combat unit is moving forward with a velocity of advance of V_A, and is "currently" located at point B. The distance D(t) represents the distance, at time t, between the supply point and the combat organization, and D_S was the distance at the start of the advance of the combat unit.

Let us suppose that the advancing combat organization requires Q tons/hr of supplies on a regularly scheduled basis. The TLV organization possesses vehicles which have a capacity of C tons and average speeds (over the relevant terrain) of V_F miles per hour when full and V_E miles per hour when empty. In addition a time of t_p hours is required per round trip to load, unload, and process the supplies. At a given time during the mission the number of vehicles which must be operating in order to maintain the required flow of supplies, $N_O^R(t)$, is given by:

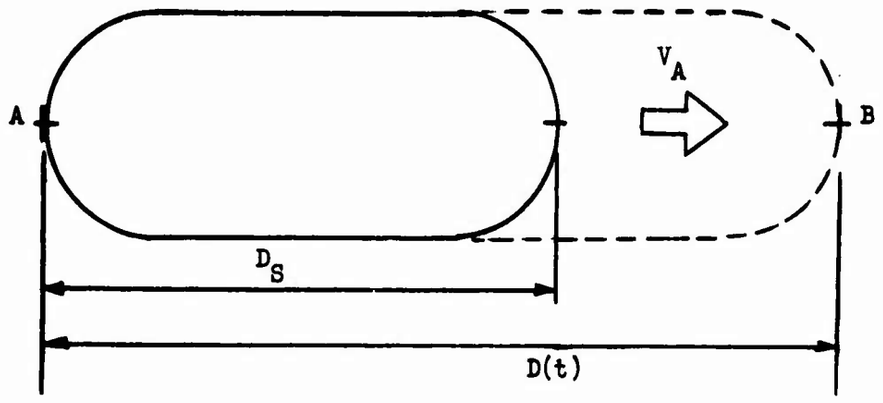


Figure 1. Example of a Logistics Loop

$$N_O^R(t) = \frac{Q}{C}\left[\frac{D(t)}{V_F} + \frac{D(t)}{V_E} + t_P\right]. \qquad (1)$$

The distance D(t) can be determined from the starting distance D_S and the velocity of advance of the combat organization, V_A, as follows:

$$D(t) = D_S + V_A \cdot t \cdot \qquad (2)$$

Using (1) above we may calculate the number of vehicles which must be operating at any time during the mission in order to maintain scheduled deliveries. If the tactical logistic vehicle organization has a total of N_{TOT} vehicles, they will generally be divided into a number which are operating at time t, indicated by $N_O(t)$; those which are down for maintenance at time t, indicated by $N_D(t)$, and those which are operable but not in use at time t, or spares, indicated by $N_S(t)$. At any time during the mission we have:

$$N_{TOT} = N_O(t) + N_D(t) + N_S(t). \qquad (3)$$

It was stated earlier that the effectiveness of the tactical logistic vehicle organization could be visualized in terms of that organization's ability to minimize the logistical constraints upon the tactical commander. At a particular time, if the number of operating vehicles and vehicles down for maintenance is small enough to allow

the number of spares to be greater than zero, the TLV organization has the flexibility to respond to unexpected logistical demands. As the mission proceeds $N_0^R(t)$ increases with time, and $N_0(t)$ increases to meet this requirement. In addition, vehicle failures take place, resulting in nonzero values of $N_D(t)$. A point will be reached at which the number of spares becomes zero. At this point, a logistic constraint exists which affects the tactical organization. At a later point during the mission, $N_0(t)$ will become smaller than $N_0^R(t)$ and required delivery schedules will no longer be met. This places additional and critical constraints upon the tactical organization. The parts of the model described below utilize vehicle requirements determined as above and failure and repair rates in order to express vehicle availability as a function of time during the progress of a mission.

If a vehicle experiences failures which are distributed in time according to a Poisson distribution with a mean failure rate of λ, and if there are C exponential repair channels available with repair rate μ, a set of $N_{TOT} + 1$ differential-difference equations may be written for the probabilities of having 0,1,2, ... i ... N_{TOT} vehicles inoperable at any time during the mission. These equations embody all of the assumptions typical in birth-death processes or queuing theory. Table 1 shows the form of the differential-difference equation for $\frac{dP_{N_D}(t)}{dt}$ for all of the possible conditions which may govern the problem situation. In addition, the table shows the initial condition that at time zero all of the vehicles are operable. Finally, the last line of the table presents the additional condition that at any time the probabilities that the system is in each of the possible states must sum to unity.

The steady state solutions to the set of equations shown in Table 1 are relatively well known and may be found analytically.[4] Because $N_0^R(t)$ changes relatively rapidly with time as the mission advances, however, it is likely that the equations governing the system of vehicles must change in form before the system reaches the steady state.

Conditions	Equations
$N_D(t)=0$	$\frac{dP_0(t)}{dt} = -\lambda N_0^R(t)P_0(t) + \mu P_1(t)$
$N_S(t)>0; N_D(t)<C$	$\frac{dP_{N_D}(t)}{dt} = -[\lambda N_0^R(t)+\mu N_D(t)]P_{N_D}(t)+\lambda N_0^R(t)P_{N_D-1}(t) + \mu[N_D(t)+1]P_{N_D+1}(t)$
$N_S(t)>0; N_D(t)\geq C$	$\frac{dP_{N_D}(t)}{dt} = -[\lambda N_0^R(t)+C\mu]P_{N_D}(t)+\lambda N_0^R(t)P_{N_D-1}(t)+C\mu P_{N_D+1}(t)$
$N_S(t)=0; N_D(t)<C; N_{TOT}-N_D(t)+1<N_0^R(t)$	$\frac{dP_{N_D}(t)}{dt} = -\{\lambda[N_{TOT}-N_D(t)]+\mu N_D(t)\}P_{N_D}(t) + \lambda[N_{TOT}-N_D(t)+1]P_{N_D-1}+\mu[N_D(t)+1]P_{N_D+1}(t)$
$N_S(t)=0; N_D<C; N_{TOT}-N_D(t)+1\geq N_0^R(t)$	$\frac{dP_{N_D}(t)}{dt} = -\{\lambda[N_{TOT}-N_D(t)]+\mu N_D(t)\}P_{N_D}(t)+\lambda N_0^R(t)P_{N_D-1}(t) + \mu[N_D(t)+1]P_{N_D+1}(t)$

TABLE 1. DIFFERENTIAL-DIFFERENCE EQUATIONS FOR PROBABILITY OF $N_D(t)$ VEHICLES BEING DOWN AT TIME t

TABLE 1 CONTINUED

Conditions	Equations
$N_S(t)=0; N_D \geq C; N_{TOT}-N_D(t)+1<N_O^R(t)$	$\frac{dP_{N_D}(t)}{dt} = -\{\lambda[N_{TOT}-N_D(t)]+C\mu\}P_{N_D}(t)+\lambda[N_{TOT}-N_D(t)+1]P_{N_D-1}(t)$ $+C\mu P_{N_D+1}(t)$
$N_S(t)=0; N_D \geq C; N_{TOT}-N_D(t)+1 \geq N_O^R(t)$	$\frac{dP_{N_D}(t)}{dt} = -\{\lambda[N_{TOT}-N_D(t)]+C\mu\}P_{N_D}(t)+\lambda N_O^R(t)P_{N_D-1}(t)+C\mu P_{N_D+1}(t)$
$N_D(t)=N_{TOT}; N_D \geq C$	$\frac{dP_{N_{TOT}}(t)}{dt} = -C\mu P_{N_{TOT}}(t)+\lambda P_{N_{TOT}-1}(t)$
Initial Condition	$P_{N_D}(0) = \begin{cases} 1 & N_D=0 \\ 0 & N_D=1,2,\ldots,N_{TOT} \end{cases}$
Additional Condition	$\sum_{N_D(t)=0}^{N_{TOT}} P_{N_D}(t)=1$

Transient solutions are required, therefore, and the author was unable to find such solutions analytically. A FORTRAN subroutine was therefore employed which utilizes the Kutta Merson Integration Technique in order to find the solution to the set of differential-difference equations during the transient period.[5] The program was written to print the solutions at one-tenth of an hour time increments during the mission. Appendix C contains a user-oriented description of the integration subroutine.

Since the model can compute, at any time during the mission, the probabilities that there are 0,1,2,...,i..., N_{TOT} vehicles down for maintenance, it is also possible to compute the "availability" of the system of vehicles. Availability, at any moment during the mission, is the expected proportion of the total vehicles which are operational (both operating and spares). Availability at time t is given by:

$$A(t) = \frac{N_{TOT} - \sum_{N_D=0}^{N_{TOT}} N_D \cdot P_{N_D}(t)}{N_{TOT}} \quad . \qquad (4)$$

In summary, the inputs to the model describe a simplified mission of a TLV system, and the characteristics of the system itself. The outputs of the model are the time-dependent requirements for the employment of the vehicles which belong to the TLV organization, and time-dependent probabilities that various numbers of vehicles are down for maintenance, as well as the time-dependent availability of the vehicle system. Appendix A describes in more detailed terms the inputs and outputs with which the user of the computer model must become familiar. The final section of this report describes the uses to which the model may be put in the future.

IV. USES OF THE MODEL: RECOMMENDATIONS FOR FUTURE STUDY

In the cost-effectiveness analysis of tactical logistic vehicle systems, comparisons must often be made between many alternative

investments, and the effect of each alternative upon system effectiveness in combat. The model described above is one technique which appears to be useful in making such comparisons.

If two or more vehicles are being considered for a particular combat role, and each has particular speeds, capacities, failure rates, etc. a model such as the one presented here can be used to estimate how long fleets of particular numbers of each vehicle could sustain an advance by a typical combat unit. Expected failures are generated and availability for each fleet may be compared. Comparisons of the costs of each fleet with the outputs of this model could be used to make some comments about the cost-effectiveness of the alternatives.

Parametric analysis using this model could allow an analyst to compare the effects upon availability and mission effectiveness of such alternative investment policies as 1) increasing the fleet size, 2) adding maintenance channels, 3) performing vehicle modifications which might change speeds or failure rates. Tables could be generated which would show the effects of such parametric alterations. These could be used to estimate sensitivity of vehicle system effectiveness to alternative investments.

The model, as it is presented here, is very simple compared to realistic combat situations. Modifications of this model which could be fruitful in terms of making it more realistic might include permitting a change in position of the rear supply point during the progress of the combat mission. The current model only permits a single supply point and a single delivery point. Extensions to more general missions which may require multiple pick-ups and deliveries may be quite useful. Only a single level of maintenance is included in the model as presented here, and modifications which would permit multiple echelons and movement of vehicles between echelons would be computationally feasible, and would add realism to the simulation of a combat environment.

Although extensions of the model in the directions noted would tend to make it more nearly simulate the real combat environment, it

should be emphasized that it is not often necessary to simulate the real world in great detail in order to make meaningful choices. The model in its current form may be sufficient to permit the comparison of alternative vehicles, or to evaluate changes in maintenance policies.

REFERENCES

1. Michael G. Kolifrath, Russell E. Purvis, and Martin Wachs, "Conceptual Framework for a Tactical Logistic Vehicle Evaluation Methodology", Army Materiel Systems Analysis Agency Technical Memorandum No. 12, July 1968, Aberdeen Proving Ground, Maryland, pp. 20-25.

2. Ibid., p. 9.

3. Ibid.

4. H. R. Barton, R. E. Purvis, J. E. Stuart, and W. R. Mallory, "Queuing Model for Determining System Manning and Related Support Requirements", Radio Corporation of America, Camden, New Jersey, January 1964 (AD 434 803). See Appendix I.

5. Glenn A. Beck, "Fortran Kutta Merson Integration Subroutine", Ballistic Research Laboratories, Aberdeen Proving Ground, August 1968, Mimeographed.

APPENDIX A. SUMMARY OF INPUTS AND OUTPUTS

I. Inputs

Following the program deck, which appears as Appendix B, the following data cards are required in order to operate the program:

1) Problem Card

A single data card indicating, in column one, the number of problems to be run. The upper limit of nine problems may be modified by changing the FORMAT statement on card number 4C in the program deck.

2) One additional data card for each problem to be solved. As many cards must be included as problems have been indicated on the "problem" card. Each such data card must be punched with the information and FORMAT as shown below:

COLUMNS	VARIABLE NAME	DEFINITION	FIELD SPECIFICATION
1-6	QREQ	Tonnage to be moved by TLV organization to combat unit, tons/hr.	F6.2
7-12	CAP	Tonnage capacity of each vehicle, tons.	F6.2
13-18	DISTS	Distance from rear supply point to combat unit at start of mission, miles.	F6.2
19-24	VFUL	Speed of each vehicle when loaded to capacity, mph.	F6.2
25-30	VEMP	Speed of each vehicle when empty, mph.	F6.2
31-36	TPROSS	Processing time required per round trip in addition to travel time, hrs.	F6.2
37-42	VADV	Speed at which combat unit is to advance, mph.	F6.2
43-44	NTOT	Total number of vehicles in TLV organization (upper limit is 48).	I2
45-49	FRAT	Failure rate λ for each vehicle, failures/hr.	F5.3

COLUMNS	VARIABLE NAME	DEFINITION	FIELD SPECIFICATION
50-54	RRAT	Repair rate μ per service channel, repairs/hr.	F5.3
55-56	M	Number of repair channels.	I2

II. Outputs

For each problem the computer will print out:

1) The problem number

2) The times, in hours from the start of the mission, that $N_{REQ}(t)$ changes, and the value of $N_{REQ}(t)$ for each time increment.

3) For every tenth of an hour from the time that the mission starts, the time, the current value of $N_{REQ}(t)$, availability, and the probability that 0,1,2..., N_{TOT} vehicles are down at this time. Also shown are the derivatives of each probability, and the sum of the probabilities (as a check). This will continue in increments of 1/10 hour until five hours after $N_{REQ}(t) = N_{TOT}$.

APPENDIX B. COMPUTER PROGRAM

```
* SA227A H WACHS,EXT 3030 LOGISTICS LOOP PROB.                          1
$       MAXO(7000)LINES
        LIST
        DIMENSION T(50),Y(50),YP(50),TC(1)                             2
        EXTERNAL DERIV,TERM,PRIN                                       3
        COMMON NREQ,FRAT,RRAT,NTOT,M,TMAX, NTERM                       4
C.      READ IN THE NUMBER OF PROBLEMS TO BE SOLVED                    4A
        READ 1, NPROB                                                  4B
1       FORMAT  (1I1)                                                  4C
        DO  20   IPROB = 1, NPROB                                      4D
        PRINT  2,  IPROB                                               4E
2       FORMAT(1H ,/////,1H ,15HPROBLEM NUMBER ,I1,/////)              4F
C       GENERATION OF VEH. REQUIREMENTS AND TRANSITION TIMES           5
        READ 10,QREQ,CAP,DISTS,VFUL,VEMP,TPROSS,VADV,NTOT,FRAT,        6
       1RRAT,M                                                         7
10      FORMAT(7F6.2,I2,2F5.3,I2)                                      8
        DIST=0.0$ TIME=0.0$ VEHREQ=0.0                                 9
        NREQ=0$ NREQPR=0$ NSTART=0                                     10
11      DIST = DISTS + VADV * TIME                                     11
        VEHREQ=QREQ/CAP*(DIST/VFUL+DIST/VEMP+TPROSS)                   12
        NREQ=VEHREQ+0.999999                                           13
        IF(NREQPR)110,110,111                                          14
110     NSTART=NREQ                                                    15
111     IF(NREQ-NREQPR)12,12,13                                        16
12      TIME=TIME+0.1$ GOTO 11                                         17
13      T(NREQ)=TIME                                                   18
        PRINT 14,NREQ,T(NREQ)                                          19
14      FORMAT(1H ,5HNREQ=,I2,3X,8HT(NREQ)=,F10.2//)                   20
        IF(NTOT-NREQ)16,16,15                                          21
15      NREQPR=NREQ                                                    22
        TIME=TIME+0.1$ GOTO 11                                         23
C       INITIALIZE VALUES FOR INTEGRATION SUBROUTINE.                  24
C       Y(I) MEANS PROBABILITY OF (I-1) VEHICLES DOWN                  25
16      Y(1)=1.0 $ YP(NTOT+2)=1.0 $ NTERM = NTOT+1                     26
        DO 17  J=2,NTERM                                               27
17      Y(J)=0.0                                                       28
C       DO-LOOP TO CALL KUTMER FOR EACH VALUE OF NREQ                  29
        DO 20 NREQ=NSTART,NTOT                                         30
        IF(NREQ-NTOT)18,19,19                                          31
18      TMAX=T(NREQ+1)$ GOTO 191                                       32
19      TMAX=T(NTOT)+5.0                                               33
```

```
C      PROBLEM ENDS 5 HRS AFTER NREQ=NTOT.                                    34


191    DNXT=0.00001  $  ER=0.0000001  $  PS=0.1  $  NX=NTOT+2                 35
       CALL KUTMER(DNXT,DPST,0.1,NX  ,Y,YP,DERIV,ER,2,W,0,                    36
      1PS,PV,PRIN,TC,1,NTS,TERM)                                              37
20     CONTINUE                                                               37A
       STOP                                                                   38
       END                                                                    39
       SUBROUTINE DERIV(Y,YP)                                                 40
       DIMENSION Y(50),YP(50)                                                 41
       COMMON(USE MAIN)                                                       42
       REQ=NREQ    $   Z=M                                                    43
       DO 50  I=1,NTERM  $  IF (I-1) 10,10,11                                 44
10     YP(1)=-REQ*FRAT*Y(1)+RRAT*Y(2)  $  GO TO 50                            45
11     IF (NTOT-I+1) 50,12,20                                                 46
12     YP(I)=-Z*RRAT*Y(I)+FRAT*Y(I-1)                                         47
       GOTO 50                                                                48
20     IF (NTOT-NREQ-I+1) 40,40,30                                            49
   30  IF (I-1-M) 31,32,32                                                    50
31     ZZ = I-1                                                               51
       YP(I)=-                                                                52
      1       (REQ*FRAT+ZZ*RRAT)*Y(I)+REQ*FRAT*Y(I-1)+RRAT*(ZZ+1.)*Y(I+1)     53
       GOTO 50                                                                55
32     YP(I)=-( REQ*FRAT+Z*RRAT)*Y(I)+ REQ*FRAT*Y(I-1)+Z*RRAT*Y(I+1)          56
       GOTO 50                                                                57
40     IF (I-1-M) 41,42,42                                                    58
41     TOT = NTOT    $   ZZ= I-1                                              59
       IF (NTOT-I+2-NREQ)411, 411, 412                                        60
  411  YP(I)=-((TOT-ZZ)*FRAT+ZZ*RRAT)*Y(I)+(TOT-ZZ+1.)*Y(I-1)*FRAT+(ZZ+      61
     1 1.)*RRAT*Y(I+1)     $ GO TO 50                                        62
  412  YP(I)=-((TOT-ZZ)*FRAT+ZZ*RRAT)*Y(I)+ REQ*FRAT*Y(I-1)+(ZZ+1.)*RRAT      63
     1*Y(I+1)     $ GO TO 50                                                 63A
   42  TOT = NTOT    $ ZZ = I-1                                               63B
       IF(NTOT-I+2-NREQ)421, 421, 422                                         63C
  421  YP(I)=-((TOT-ZZ)*FRAT+Z*RRAT)*Y(I)+(TOT-ZZ+1.)*FRAT*Y(I-1)+Z*          63D
     1RRAT*Y(I+1) $ GO TO 50                                                  63E
  422  YP(I)=-((TOT-ZZ)*FRAT+Z*RRAT)*Y(I)+ REQ*FRAT*Y(I-1)+Z*RRAT*Y(I+1)     63F
50     CONTINUE                                                               64
       RETURN                                                                 65
       END                                                                    66
       SUBROUTINE TERM(Y,YP,TC,PV)                                            67
       DIMENSION Y(50),YP(50),TC(1)                                           68
       COMMON(USE MAIN)                                                       69
       PV = Y(NTOT+2)                                                         70
       TC(1) = Y(NTOT+2) - TMAX                                               71
       RETURN                                                                 72
       END                                                                    73
       SUBROUTINE PRIN(Y,YP)                                                  74
       DIMENSION Y(50),YP(50)                                                 75
       COMMON(USE MAIN)                                                       76
       X=0.0$ AVAIL=0.0                                                       77
       DO 10  I=1,NTERM $  B=I-1                                              78
10     X=X+B*Y(I)                                                             80
       DUM = NTOT    $   AVAIL = (DUM-X)/DUM                                  81
       PRINT 20,Y(NTOT+2),NREQ,AVAIL                                          82
20     FORMAT(1H ,5HTIME=,F5.2,2X,5HNREQ=,I5,2X,13HAVAILABILITY=,F7.3)        83
       PRINT 30                                                               84
30     FORMAT(1H ,9HNO. DOWN,5X,17HPROB. OF NO. DOWN,5X,16H DERIV. OF PRO     85
      1B.//)                                                                  85A
       DO 50  I=1,NTERM  $  J=I-1                                             86
       PRINT 40, J,Y(I), YP(I)                                                87
40     FORMAT(1H ,5X,I2,15X,F7.3,10X,F10.3)                                   88
```

```
50      CONTINUE                                                          89
        SUMP = 0.0                                                        90
        DO 60  K=1,NTERM                                                  91
60      SUMP = SUMP + Y(K)                                                92
        PRINT 70, SUMP                                                    93
70      FORMAT(1H , 23HSUM OF PROBABILITIES = , F5.3,///)                 94
        RETURN                                                            95
        END                                                               96
        SUBROUTINE KUTMER(DNXT,DPST,DMAX,N,Y,YP,DERIV,ER,ME,W,ITYP,PS,  ****   1
       1PV,PRIN,TC,NTC,NTS,TERM) $ DIMENSION Y(50),YP(50),W(100),TC(25)  KUTMER 2
        DIMENSION Q(50),Q1(50),Q2(50),FA(25),FB(25)                       KUTMER 3
        INDD=0 $ IF(ITYP.GT.1)GOTO 70 $ ERM=5.*ER $ ER1=.1*ERM            KUTMER 4
        DPST=DNXT $ I=1 $ ER2=ER1 $ IF(ER2.EQ.0.)ER2=.000001*PS           KUTMER 5
10      CALL DERIV(Y,YP) $ GOTO (20,90,110,130,150,70,250),I              KUTMER 6
20      IF(ITYP.EQ.1)RETURN                                               KUTMER 7
25      CALL TERM(Y,YP,TC,PV) $ GOTO (30,270),I                           KUTMER 8
30      CALL PRIN(Y,YP) $ GOTO (40,360,390),I                             KUTMER 9
40      DO 50 I=1,NTC $ FA(I)=0.                                          KUTMER10
50      FB(I)=0. $ FC=0. $ PV2=AINT(PV/PS+ER2)*PS $ PV1=PV2+PS            KUTMER11
        IF(ABS(PV2-PV).LT.ER2)PV2=PV2-PS                                  KUTMER12
70      H6=DNXT/6. $ H3=H6+H6 $ H8=.125*DNXT $ H2=.5*DNXT $ DO 80 I=1,N   KUTMER13
        Q(I)=Y(I) $ Q1(I)=YP(I)                                           KUTMER14
80      Y(I)=Q(I)+H3*Q1(I) $ I=2 $ GOTO 10                                KUTMER15
90      DO 100 I=1,N                                                      KUTMER16
100     Y(I)=Q(I)+H6*(Q1(I)+YP(I)) $ I=3 $ GOTO 10                        KUTMER17
110     DO 120 I=1,N $ Q2(I)=3.*YP(I)                                     KUTMER18
120     Y(I)=Q(I)+H8*(Q2(I)+Q1(I)) $ I=4 $ GOTO 10                        KUTMER19
130     DO 140 I=1,N $ T1=Q1(I)-Q2(I) $ Q2(I)=4.*YP(I)                    KUTMER20
140     Y(I)=Q(I)+H2*(T1+Q2(I)) $ I=5 $ GOTO 10                           KUTMER21
150     ERMAX=0. $ DO 190 I=1,N $ T1=Q(I)+H6*(Q1(I)+Q2(I)+YP(I))          KUTMER22
        T2=ABS(T1-Y(I)) $ Y(I)=T1 $ IF(ERM.EQ.0.)GOTO 190                 KUTMER23
        GOTO(170,160,180),ME                                              KUTMER24
160     IF(ABS(T1).GE.1.)T2=T2/ABS(T1)                                    KUTMER25
170     IF(T2.GT.ERMAX)ERMAX=T2 $ GOTO 190                                KUTMER26
180     IF(T1.EQ.0.)GOTO 170 $ T1=T2/ABS(T1) $ J=I+I $ T2=W(J-1)*T2       KUTMER27
        T1=W(J)*T1 $ IF(T2.GT.T1)T2=T1 $ GOTO 170                         KUTMER28
190     CONTINUE $ DPST=DNXT $ IF(ERM.EQ.0.)GOTO 240                      KUTMER29
        IF(ERMAX.EQ.0.)GOTO 210 $ T1=ER1/ERMAX                            KUTMER30
        IF(T1.GE.1..AND.INDD.GT.0)GOTO 192 $ IF(ABS(T1-1.).LT..5)GOTO 195 KUTMER31
        DNXT=DPST*T1**.2 $ GOTO 200                                       KUTMER32
  192   INDD=INDD-1 $ GOTO 220                                            KUTMER33
195     DNXT=DPST*(1.+.2*(T1-1.))                                         KUTMER34
200     IF(ABS(DNXT).LT.DMAX)GOTO 220                                     KUTMER35
210     IF(INDD.GT.0)GOTO 192 $ DNXT=DMAX $ IF(DPST.LT.0.)DNXT=-DMAX      KUTMER36
220     IF(ERMAX.LT.ERM)GOTO 240 $ DO 230 I=1,N                           KUTMER37
230     Y(I)=Q(I) $ INDD=3 $ I=6 $ GOTO 10                                KUTMER38
240     I=7 $ GOTO 10                                                     KUTMER39
250     IF(ITYP.GT.1)RETURN $ TPV=PV $ DO 260 I=1,NTC                     KUTMER40
260     Q1(I)=TC(I) $ I=2 $ GOTO 25                                       KUTMER41
270     DO 300 I=1,NTC $ IF(TC(I).GT.0.)GOTO 280 $ FB(I)=1. $ GOTO 290    KUTMER42
280     FA(I)=1.                                                          KUTMER43
290     IF(FA(I).EQ.FB(I))GOTO 370                                        KUTMER44
300     CONTINUE $ IF(ABS(PV-PV1).LT.ER2)GOTO 350                         KUTMER45
        IF(ABS(PV-PV2).LT.ER2)GOTO 350 $ IF(FC.NE.0.)GOTO 340             KUTMER46
305     IF(PV.GT.PV1)GOTO 330 $ IF(PV.GT.PV2)GOTO 70 $ PV3=PV2            KUTMER47
310     FC=1. $ SH=DNXT                                                   KUTMER48
320     DNXT=DPST*(PV3-PV)/(PV-TPV) $ GOTO 70                             KUTMER49
330     PV3=PV1 $ GOTO 310                                                KUTMER50
340     IF(FC.GT.4.)GOTO 350 $ FC=FC+1. $ GOTO 320                        KUTMER51
350     I=2 $ GOTO 30                                                     KUTMER52
```

```
360   PV1=PV+PS $ PV2=PV-PS $ IF(FC.EQ.0.)GOTO 305 $ FC=0. $ DNXT=SH     KUTMER53
      GOTO 305                                                           KUTMER54
370   IF(ABS(TC(I)).LT.ER2)GOTO 380 $ DNXT=DPST*TC(I)/(Q1(I)-TC(I))      KUTMER55
      GOTO 70                                                            KUTMER56
380   NTS=I $ I=3 $ GOTO 30                                              KUTMER57
390   RETURN $ END                                                       KUTMER58
END                                                                      KUTMER58
```

APPENDIX C. DESCRIPTION OF KUTTA MERSON INTEGRATION SUBROUTINE

Glenn A. Beck

This subroutine computes the solution of a system of first order ordinary differential equations with automatic step-size adjustment.

I. SUBROUTINE KUTMER (dnxt,dpst,dmax,n,y,yp,deriv,er,me,w,ityp,ps,pv,prin, tc,ntc,nts,term)

dnxt — Step-size to be used for next step. dnxt must be set to a reasonable value before KUTMER is referenced. The sign of dnxt will determine the direction of integration.

dpst — Actual step-size used on the step just completed. dpst is not used (but must be specified) if ityp = 0. If ityp ≠ 0 and it is desired to hit a particular point, dnxt should be saved, then dpst used to compute a new step-size and after the particular point is hit dnxt should be reset.

dmax — Absolute value of the maximum step-size to be used.

n — Number of equations to be integrated. n must include the independent variable. n must be less than or equal to 50, To allow n to be greater than 50 change the dimensions of Q,Q1 and Q2 to be greater than or equal to n.

y — One-dimensional array of length n which contains the integrals. The elements of y must be defined as the initial condition before KUTMER is referenced. One of the elements of y must be the independent variable.

yp — One-dimensional array of length n for storing the derivatives by routine deriv. The elements of yp must be the derivative of the corresponding elements of y. The element of yp which corresponds to the independent variable in y must have a value of 1.

deriv — A subroutine which computes the derivatives and stores them in yp. The first statement of the subroutine must be SUBROUTINE deriv (y,yp). The actual name of deriv must appear in an EXTERNAL statement in the program which references KUTMER. Any variables other than y and yp required to compute the derivatives must be passed through COMMON. y and yp must be declared as one-dimensional arrays in deriv.

er — If er = 0 do not adjust the step-size.
If er ≠ 0 adjust the step-size so that the maximum error will be approximately er.

me — If me = 1 use absolute error to compute the new step-size.

If me = 2 a) use absolute error to compute the new step-size if the integrals are ≤ 1.
b) use relative error to compute the new step-size if the integrals are > 1.

If me = 3 use the weights stored in array w along with the absolute and relative errors to compute the new step-size.

w — One-dimensional array of length 2n to use when me = 3. w is not used (but must be specified) if me = 1 or 2.

ityp — If ityp = 0 Do not return from KUTMER until some tc has changed sign.

If ityp > 0 The variables following ityp on the dummy variable list are not used (but must be specified in the CALL).

If ityp = 1 RETURN from KUTMER immediately after the initial derivatives have been computed, no integration is done.

If ityp > 1 RETURN from KUTMER after each step. At the RETURN the derivatives have been evaluated using the values of the integrals at the end of the step.

ps — Print step. ps must be greater than 0. ps determines the frequency of references of routine prin (see prin).

pv — Print variable. Must be defined in subroutine term. pv determines the frequency of references of routine prin (see prin).

prin — Print (or store) routine. prin will be referenced as follows:
1) After initial derivatives have been computed.
2) When pv is an integer multiple of ps with a tolerance of

$\pm$ er/2 when er ≠ 0 or $\pm 10^{-6}$ times ps when er = 0.
Additional integration steps are taken if required to meet the tolerance.

3) When some tc = 0 with a tolerance of $\pm$ er/2 when er $\neq$ 0 or $\pm$ 10^{-6} times ps when er = 0 after the tc has changed sign. The routine will take additional integration steps to meet the tolerance. In this case, immediately after prin RETURN s to KUTMER KUTMER will RETURN to the program which referenced it. The first statement of the subroutine must be SUBROUTINE prin (y,yp). The actual name of prin must appear in an EXTERNAL statement in the program which references KUTMER. Any required variables other than y and yp must be passed through COMMON. y and up must be declared as one-dimensional arrays in prin.

tc — A one-dimensional array of length ntc. The elements of tc must be completed in subroutine term. KUTMER will RETURN to the routine which referenced it when tc(nts) has changed sign.

ntc — The number of tc's computed in subroutine term. ntc must be less than 26. To allow ntc to be more than 25, change the dimensions of FA and FB in KUTMER to be greater than or equal to ntc.

nts — The subscript of the tc which changed sign and caused termination of integration.

term — Termination routine. It is referenced at the end of each integration step. It must define pv and the tc's. The first statement of the subroutine must be SUBROUTINE term (y,yp,tc, pv). The actual name of term must appear in an EXTERNAL statement in the program which references KUTMER. Any variables other than y,yp,tc and pv must be passed through COMMON. y,yp, and tc must be declared as one-dimensional arrays in term.

II. DESCRIPTION OF THE METHOD

A. The integration formulas.

To solve the following system of differential equations

$$y_i(t_m + h) = y_i(t_m) + \int_{t_m}^{t_m + h} y_i' \, dt \quad i = 1 \ldots m$$

the computation required is as follows:

$$y_{i,0} = y_i(t_m)$$

$$y_{i,1} = y_{i,0} + \frac{1}{3} h\, y'_{i,0}$$

$$y_{i,2} = y_{i,0} + \frac{1}{6} h\, y'_{i,0} + \frac{1}{6} h\, y'_{i,1}$$

$$y_{i,3} = y_{i,0} + \frac{1}{8} h\, y'_{i,0} + \frac{3}{8} h\, y'_{i,2}$$

$$y_{i,4} = y_{i,0} + \frac{1}{2} h\, y'_{i,0} - \frac{3}{2} h\, y'_{i,2} + 2h\, y'_{i,3}$$

$$y_{i,5} = y_{i,0} + \frac{1}{6} h\, y'_{i,0} + \frac{2}{3} h\, y'_{i,3} + \frac{1}{6} h\, y'_{i,4}$$

$$y_i(t_m + h) = y_{i,5}$$

This requires 5 evaluations of y' for each integration step.

B. Error estimates and step-size computation.

When the differential equations fulfill certain conditions an estimate of the truncation error $EA_{m,1}$ of the ith integral y_i at integration step m is

$$EA_{m,1} = \frac{1}{720}|h^5 y_i^v| = \frac{1}{5}|y_{i,5} - y_{i,4}|$$

and an estimate of the relative truncation error $ER_{m,i}$ is

$$ER_{m,1} = \frac{1}{5}|(y_{i,5} - y_{i,4})|y_{i,5}| \ .$$

E_m, which is used to compute the step-size to be used for the next step, is computed by one of 3 methods specified by me, the 9th variable in the KUTMER reference.

Method 1). Used when me = 1 when KUTMER is referenced.

$$E_m = \max_i [EA_{m,i}]$$

Method 2). Used when me = 2 when KUTMER is referenced.

$$E_m = \max_i [\min(EA_{m,i} ER_{m,i})]$$

This method uses absolute error when $|y_i| \leq 1$ and

relative error when $|y_i| > 1$.

Method 3). Used when me = 3 when KUTMER is referenced.

$$E_m = \max_i [\min(WA_i * EA_{m,i}, WR_i * ER_{m,i})]$$

where the WA_i and WR_i must be stored in the array w

before KUTMER is referenced with

$w(2i-1) = WA_i$ and $w(2i) = WR_i$

This method will use $WA_i * EA_{m,i}$ when $|y_i| \leq \frac{WR_i}{WA_i}$

and $WR_i * ER_{m,i}$ when $|y_i| > \frac{WR_i}{WA_i}$

Method 3 is used only when one is very familiar with the system being integrated and many runs of the same nature are required. The values for WA_i and WR_i are determined only by common sense and trial and error.

After computing E_m by one of the above methods the program computes a new step-size h_{m+1} such that, hopefully, E_{m+1} will be near er/10 where er is the 8th variable in the KUTMER reference. If it is assumed that y_i^v is constant over the interval then the ratio of the equations

$$E_{m+1} = er/10. = \frac{1}{720} h_{m+1}^5 y^v$$

$$E_m = \frac{1}{720} h_m^5 y^v$$

yields $h_{m+1} = h_m \sqrt[5]{\frac{er/10}{E_m}}$

Generally h_{m+1} will be nearly equal to h_m, i.e. $\sqrt[5]{\frac{er/10}{E_m}}$ will be near one. When $\frac{1}{2} \leq \frac{er/10}{E_m} \leq \frac{3}{2}$ the fifth root is computed by the

following approximation

$$\sqrt[5]{\frac{er/10}{E_m}} = 1 + \frac{1}{5}\left(\frac{er/10}{E_m} - 1\right)$$

Otherwise $\left(\frac{er/10}{E_m}\right)^{.2}$ is computed which is much slower.

The routine will attempt to yield an error of er/10 and will redo the step with a smaller interval if the error is greater than er. When a step is redone because the error is greater than er the step-size will not be increased for the next three steps. This feature should aid in integrating over discontinuities.

III. SUGGESTIONS FOR INCREASING EFFICIENCY

All actual variables in the references to deriv, term and prin are the corresponding dummy variables in the KUTMER SUBROUTINE statement. Hence the variables can be passed to these routines through COMMON if the appropriate number of dummy variables are placed in the SUBROUTINE statement of these subroutines. This is most important in routine deriv because it is referenced 5 times for each integration step.

Example showing important statements only

```
EXTERNAL DERIV
COMMON Y(10),YP(10)

CALL KUTMER (DN,DP,1.,10,Y,YP,DERIV------


END
SUBROUTINE DERIV(DUM,DUM)
COMMON Y(10),YP(10)
DIMENSION DUM(1)

YP(I) = ------------------


RETURN
```

If the variables are passed through COMMON then the dummy variables could be deleted from the SUBROUTINE DERIV statement if the actual variables are removed from the CALL in statement 10 of KUTMER.

ANALOG/HYBRID SOLUTIONS TO ALGEBRAIC EQUATIONS AND BOUNDARY-VALUE PROBLEMS

Arthur Hausner
Harry Diamond Laboratories
Washington, D. C.

ABSTRACT. An experimental method is outlined for achieving the simplest possible stable feedback connections in a direct nulling solution of algebraic equations on an analog computer. Although the proof of stability is given for linear equations, it is inferred that the method works also for most nonlinear equations. Both situations are successfully demonstrated. In essence, the method requires a sensitivity test near the root, with the computer nulling previously connected residual errors. Once the feedback structure is obtained, the circuit automatically tracks solutions for wide variations of parameters.

The technique is extended to analog/hybrid solutions of boundary-value problems, where stable feedback connections producing discrete changes in solution estimates are determined experimentally. A five-parameter optimal control problem is solved automatically by this method.

1. INTRODUCTION. In the first part of this paper, we consider solving a system of n algebraic (or transcendental) equations

$$f_k \equiv f_k(x_1, x_2, \ldots, x_n, a_1, a_2, \ldots, a_m) = 0 \qquad (1)$$

in n variables x_i, i, k = 1, 2, ..., n, and m parameters a_j, j = 1, 2, ..., m, on an analog computer. Two situations arise in practice:

1. The a_j are time varying and the solutions are needed instantly for feedback in differential equations to be solved by the computer.

2. The a_j are stationary, but solutions to many runs are required.

A simple but frequent example containing time-varying parameters occurs when obtaining a quotient $x_1 = a_1/a_2$ on the computer. There is no satisfactory analog component to perform division directly; the computer is actually set up to solve

$$a_2x_1 - a_1 = 0 \qquad (2)$$

PRECEDING PAGE BLANK

As a_1 and a_2 vary with time, a constructed circuit must "track" the solution of (2) with small error.

Another more complicated example involving time-varying parameters occurs in the solution of Lagrange's equations on an analog computer [1]. The x_i are accelerations and the a_j are velocity and position coordinates and other functions of time.

An analog computer integrates differential equations continuously and simultaneously, necessitating an instantaneous generation of all functions required with small error. This is completely different, in principle, from a digital computer that can temporarily halt its solution process to generate all required functions. Thus, when the parameters a_j are time varying, a constructed circuit to solve (1) must track the solutions x_i with as small dynamic error as possible.

On the other hand, stationary-parameter problems present less stringent requirements. If a solution is obtained for one set of parameters, a reasonably small delay in obtaining a solution for another set is quite tolerable, so that a broader class of techniques can be used for solution. The principal emphasis in this paper is in a discussion of a technique developed for stationary-parameter problems with a direct extension to solutions of boundary-value problems containing stationary parameters.

2. CONVERSION TO DIFFERENTIAL EQUATIONS. Since the main strength of analog computers lies in the ability to solve differential equations rapidly, it is quite natural to attempt solutions of (1) by converting to an equivalent formulation involving differential equations. The basic method of solving (1) involves synthesizing a stable set of differential equations which has the x_i as asymptotic solutions. Suppose we construct a set of functions $\phi_i(f_1, f_2, \ldots, f_n)$ with the property that all $\phi_i = 0$ implies that all $f_k = 0$. Further, suppose that the solution

$$\dot{x}_i + \phi_i(f_1, f_2, \ldots, f_n) = 0 \qquad (3)$$

approaches a constant set of x_i for stationary parameters. Fundamental considerations [2] permit us to conclude that the ϕ_i approach 0 and that the x_i approach solutions to (1). We modify (3) to include gain constants g_i:

$$\dot{x}_i + g_i\phi_i(f_1, f_2, \ldots, f_n) = 0 \qquad (4)$$

where $g_i >> 0$, which has the effect of increasing the convergence rate. If the system (4) is stable about a solution x_i of (1), little dynamic error can be expected even when the a_j are time varying. We emphasize that a computer solution can be time scaled to reduce rates of changes of the a_j to any desired level. The g_i can be made as large as 10^9 and as close to zero as desired. Since functions are amplitude scaled to be less than 1 in magnitude and cannot be read with more than four decimal places, gains of the order of magnitude of 10^4 are usually sufficient to track solutions with dynamic errors less than 0.0001 in magnitude. In fact, dynamic errors can usually be made much less than other computing errors. Thus, the considerations usually involved in a construction of system (4) are its stability and its simplicity.

3. THE CONTINUOUS GRADIENT METHOD. In the continuous gradient method we construct a positive definite function ρ of the f_k and select the ϕ_i to move along the negative gradient of ρ. For example, if

$$\rho = \frac{1}{2} \sum_{k=1}^{n} f_k^2 \tag{5}$$

then

$$\dot{\rho} = \sum_{k=1}^{n} f_k \left(\sum_{i=1}^{n} \frac{\partial f_k}{\partial x_i} \dot{x}_i \right) = \sum_{i=1}^{n} \dot{x}_i \left(\sum_{k=1}^{n} f_k \frac{\partial f_k}{\partial x_i} \right) \tag{6}$$

The choice

$$\dot{x}_i + g_i \sum_{k=1}^{n} f_k \frac{\partial f_k}{\partial x_i} = 0 \tag{7}$$

results in

$$\dot{\rho} = - \sum_{i=1}^{n} g_i \left(\sum_{k=1}^{n} f_k \frac{\partial f_k}{\partial x_i} \right)^2 \leq 0 \tag{8}$$

for any set of $g_i > 0$. Naturally, we choose as large a set of g_i as possible (usually all equal) to maximize the convergence rate. Unfortunately, system (7) may be quite complicated for analog computer use, requiring as many as n^2 multiplications of two variables and the generation of as many as n^2 additional functions $\partial f_k/\partial x_i$. While attractive from stability considerations, the method suffers in its need of much equipment. Multiplication of two variables requires one multiplier, usually an expensive piece of equipment. Most installations, therefore, have a limited number of multipliers, which may limit the size of a problem that can be attacked by this method. (It must be remembered that all operations must be performed simultaneously in analog computers for the most efficient use.) On the other hand, multiplication of a variable by a constant (say g_i) requires only inexpensive and usually plentiful potentiometers. Thus, unless some of the f_k are linear in some of the x_i, this method may not be realizable on an available computer.

If we take

$$\rho = \sum_{k=1}^{n} |f_k| \tag{9}$$

the choice

$$\dot{x}_i + g_i \sum_{k=1}^{n} \frac{\partial f_k}{\partial x_i} \operatorname{sign} f_k = 0 \tag{10}$$

approaches the solution to (1). Signum functions are obtained approximately on analog computers by the use of electromechanical relays or electronic switches, which are also in short supply.

4. THE DIRECT METHOD. Application of (7) to (2) shows that the solution to

$$\dot{x}_1 + g_1 a_2 (a_2 x_1 - a_1) = 0 \tag{11}$$

converges rapidly to the quotient a_1/a_2 for large g_1, for all values of a_1 and $a_2 \neq 0$. (It is called a four-quadrant division mechanization.) From simple considerations, we also know that the solution to

$$\dot{x}_1 + g_1(a_2x_1 - a_1) = 0 \tag{12}$$

converges to a_1/a_2 if $a_2 > 0$ and

$$\dot{x}_1 - g_1(a_2x_1 - a_1) = 0 \tag{13}$$

converges to a_1/a_2 if $a_2 < 0$. Either system is simpler than (11) and is preferred when applicable. These are called <u>direct</u> systems; i.e., the residual error functions f_k (or their negative) of (1) are used directly in integrators, thus eliminating the additional multipliers, switches, and possibly needed partial derivatives.

The direct method in n dimensions requires solving

$$\dot{x}_i + g_i f_k = 0 \text{ or } \dot{x}_i + g_i(-f_k) = 0, \quad i,k = 1,2,\ldots,n \tag{14}$$

with constants $g_i >> 0$. Both i and k (not necessarily equal) are exhaustively used in writing down the n equations contained in (14). In effect, each residual error f_k is "assigned" as feedback to one of the x_i integrators.

In vector-matrix notation, we write system (14) as

$$\dot{\vec{x}} + \vec{G}\vec{f} = \vec{0}, \qquad \vec{x}_0 = \vec{x}(0) \tag{15}$$

where the vector $\vec{x}$ contains elements x_i, the vector $\vec{f}$ contains elements f_k or $-f_k$, and the <u>gain</u> matrix $\vec{G}$ is diagonal with $g_{i,i} = g_i >> 0$. An initial condition vector $\vec{x}_0$ is the initial $\vec{x}$ at the start of computation, when computer time $\tau = 0$.

There are three distinct difficulties in synthesizing direct nulling systems:

1. Such a system may not exist.

2. If a system exists, we must determine the $\vec{G}$ matrix, and an ordering of the elements of $\vec{f}$ (including the signs to be used), so that (15) is stable near a root of (1). Further, it is desirable to arrange a system that is stable for wide variations of parameters.

3. Because the a_j are time varying or may be changed, a system stable for one set of a_j may not be stable for another set. It is then necessary to reorder the elements of $\vec{f}$, redetermine their signs and the gain matrix $\vec{\vec{G}}$ to achieve stability once again.

To see that a system may not exist, consider the trivial one-dimensional case $f \equiv x^2 = 0$. Both cases

$$\dot{x} + gx^2 = 0 \text{ and } \dot{x} - gx^2 = 0 \tag{16}$$

are not stable about a neighborhood of the root $x = 0$. Slight disturbances such as noise (inevitable on analog computers) will produce instability.

Difficulty number 2 is the subject of attack in this paper. Under suitable assumptions, we shall present an experimental method for constructing such a stable system.

Difficulty number 3 primarily tends to discourage programmers from using a direct method for time-varying a_j unless stability can be guaranteed for all cases. In the division mechanization [(12) or (13)], for example, it is often known that a_2 does not change sign during a problem solution. The direct method is then applicable. It is too inconvenient to seek out a new stable system when instabilities occur during the solution of a complicated problem involving time-varying parameters. (An exception, perhaps, is a method described by Rybashov [3], who fixed an ordering of the f_k and a gain matrix and just tried to determine the signs of the f_k. His method, however, can fail even for linear equations.) A most important case for which stability can be guaranteed occurs for linear equations

$$\vec{f} \equiv \vec{\vec{A}}\vec{x} + \vec{b} = \vec{0} \tag{17}$$

when it is known that the characteristic roots of $\vec{\vec{A}}$ have positive real parts. The system

$$\dot{\vec{x}} + g(\vec{\vec{A}}\vec{x} + \vec{b}) = 0, \qquad g >> 0 \tag{18}$$

is asymptotically stable at the roots of (17), and further, approaches the roots from any set of initial conditions. This fact has been used in the matrix inversion needed for solving Lagrange's equations of motion [1]; the matrix there is positive definite although time varying. Thus, the direct method can be very powerful for conserving equipment when applicable.

For stationary-parameter problems, the direct method is quite important, since a delay in determining a stable system can be tolerated. Also, we shall see that the proposed construction procedure for continuous stable systems is easily extended to boundary-value problems containing stationary parameters.

5. CONSTRUCTION OF A STABLE SYSTEM FOR LINEAR EQUATIONS. We assume a set of linear equations that produces the system (17) with $|\vec{A}| \neq 0$ for one ordering of rows. The vector $\vec{b}$ does not enter into stability considerations and can be ignored in the construction procedure. A programmer is the operator of an analog computer, and he may test partial systems quickly for stability during construction. The key to this procedure is that he do so, with the results of the computer determining the feedback and gain connections. We start with the system

$$\dot{\vec{x}} = \vec{0}, \qquad \vec{x}_0 = \vec{c} \tag{19}$$

for any convenient $\vec{c}$ and construct circuits to generate the f_k from

$$\vec{f} \equiv \vec{\vec{A}}\vec{x} \tag{20}$$

Now,

1. Systematically perturb each $(x_i)_0$ by a fixed amount Δx and record the change Δf_k in each f_k (a sensitivity test) to find $\partial f_k/\partial(x_i)_0$. Find the maximum of $|\partial f_k/\partial(x_i)_0|$, obvious by inspection the first time this is done. If f_s is most sensitive to variations in x_r use f_s as the feedback error to x_r. In case of ties, the choice is arbitrary. Connect f_s or $-f_s$ (whichever is stable) to the integrator producing x_r through a gain potentiometer g_r set to an arbitrary upper limit, say 10. The computer is now mechanized to solve

$$\begin{aligned} \dot{x}_i &= 0, \qquad i \neq r, \qquad (x_i)_0 = c_i \\ \dot{x}_r &+ 10(\pm f_s) = 0, \qquad (x_r)_0 = c_r \end{aligned} \tag{21}$$

That one of the signs will be stable is obvious, since if $a_{s,r} = 0$, a perturbation in $(x_r)_0$ could not affect f_s. If $a_{s,r} > 0$, the system

$$\dot{x}_r + 10a_{s,r}x_r + \text{constants} = 0 \qquad (22)$$

is stable, and if $a_{s,r} < 0$, the system

$$\dot{x}_r - 10a_{s,r}x_r + \text{constants} = 0 \qquad (23)$$

is stable.

2. Repeat step (1) for unused f_k and for only those x_i to which no feedback is connected. Allow system (21) to integrate until $f_s = 0$, and determine the maximum of $|\partial f_k / \partial (x_i)_0|$. We shall show that if a perturbation in $(x_i)_0$ produces a change in f_k, there exists a gain g_i such that when either $\dot{x}_i + g_i f_k = 0$ or $\dot{x}_i - g_i f_k = 0$ is replaced in the system, the new subsystem is stable. All previously "used" $\vec{f}$ components and $f_k \to 0$ when the computer is placed in operate. In practice, the maximum of $|\partial f_k / \partial (x_i)_0|$ is selected for choosing the x_i and f_k components in an attempt to select eigenvectors as nearly orthogonal as possible. The actual value of g_i and the sign of f_k are selected by trial: we examine stability characteristics for a small value of g_i first to select the proper sign. The value of g_i is then increased to obtain the fastest possible convergence. All gains are relative so that we arbitrarily limit any one to a maximum of 10.

3. The process is continued until all x_i and f_k are exhausted. One by one, we use one of the f_k (or $-f_k$) as an input to one of the integrators producing x_i.

The process of adding feedback loops in this way changes characteristic root locations of previous connections. After the feedback structure is obtained, the effect of each g_i on the convergence rate can be determined experimentally, if desired, and relative final gains can be chosen to maximize the convergence rate. Finally, the gains can be multiplied by any large positive constant for extremely rapid convergence.

6. PROOF OF STABILITY OF THE CONSTRUCTED SYSTEM. This proof is by induction on the m^{th} feedback connection, $m \leq n$. Given the matrix $\vec{A}$, where $|\vec{A}| \neq 0$, we wish to show that the constructed system produces a matrix $\vec{B}$ consisting of a reordering of the rows of $\vec{A}$ (including possible sign changes of all elements in each row) and a gain matrix $\vec{G}$ such that

$$\dot{\vec{x}} + \vec{G}\vec{B}\vec{x} = \vec{0} \tag{24}$$

is stable. The first feedback loop is obviously stable. Assume at the $m-1^{st}$ stage of construction, the subsystem

$$\begin{pmatrix} \dot{z}_1 \\ \dot{z}_2 \\ \cdot \\ \cdot \\ \cdot \\ \dot{z}_{m-1} \end{pmatrix} + \begin{pmatrix} g_1 & & & 0 \\ & g_2 & & \\ & & \cdot & \\ & & & \cdot \\ 0 & & & g_{m-1} \end{pmatrix} \begin{pmatrix} b_{1,1} & b_{1,2} & \cdots & b_{1,m-1} \\ b_{2,1} & b_{2,2} & \cdots & b_{2,m-1} \\ \cdot & \cdot & & \cdot \\ \cdot & \cdot & & \cdot \\ \cdot & \cdot & & \cdot \\ b_{m-1,1} & b_{m-1,2} & \cdots & b_{m-1,m-1} \end{pmatrix} \begin{pmatrix} z_1 \\ z_2 \\ \cdot \\ \cdot \\ \cdot \\ z_{m-1} \end{pmatrix} = \begin{pmatrix} 0 \\ 0 \\ \cdot \\ \cdot \\ \cdot \\ 0 \end{pmatrix} \tag{25}$$

is stable, where each z_i is the x_i in order of selection. We call the partial gain matrix $\vec{G}_{m-1}$, the partial coefficient matrix $\vec{B}_{m-1}$, and the partial vector system $\vec{z}_{m-1}$. Clearly $|\vec{B}_{m-1}| \neq 0$ and, therefore $|\vec{G}_{m-1}\vec{B}_{m-1}| \neq 0$. Each eigenvalue of $\vec{G}_{m-1}\vec{B}_{m-1}$ has positive real parts.

Let a new row with subscript m be added with extremely small gain g_m, together with the corresponding m^{th} column. From an expansion of the new determinantal equation we find that the old eigenvalues λ_1, λ_2, ..., λ_{m-1} are continuous with respect to g_m at $g_m = 0$; for sufficiently small g_m, they will have positive real parts. Also $\lambda_m = 0$ when $g_m = 0$. Hence, we concentrate on the value of the new eigenvalue λ_m introduced by the new row. The determinantal expansion of the new matrix product $\vec{G}_m\vec{B}_m$ yields [4]

$$0 = |\vec{G}_m\vec{B}_m - \lambda_m\vec{I}| = |\vec{G}_m\vec{B}_m| - a\lambda_m + 0(\lambda_m^2) \tag{26}$$

where a is the sum of the product of all combinations of m-1 eigenvalues. The principal term of this sum as $g_m \to 0$ and $\lambda_m \to 0$ comes from

$$a \simeq \prod_{j=1}^{m-1} \lambda_j = |\vec{G}_{m-1}\vec{B}_{m-1}| \tag{27}$$

Hence, for sufficiently small g_m

$$\lambda_m \simeq \frac{|\vec{C}_m \vec{B}_m|}{|\vec{C}_{m-1} \vec{B}_{m-1}|} \tag{28}$$

and is real. Now, λ_m is directly proportional to a small g_m if $|\vec{B}_m| \neq 0$. We control its sign by inverting the signs of the terms in row m if $|\vec{B}_m| < 0$ as part of the construction procedure.

Suppose $|\vec{B}_m| = 0$. Then the last column added to $\vec{B}_{m-1}$ must be expressible as a linear combination of the previous columns; i.e., there exists a vector $\vec{z}_m$ such that $\vec{B}_m \vec{z}_m = \vec{0}$. In the operate mode, we selected f_k as row m because

$$f_k = \sum_{j=1}^{m-1} b_{k,j} \; z_j + b_{k,m}(z_m)_0 + \text{other constant terms}$$

changed greatly when $(z_m)_0$ was changed, after all previously chosen

$$f_i = \sum_{j=1}^{m-1} b_{i,j} \; z_j + b_{i,m}(z_m)_0 + \text{other constant terms}$$

were forced to zero. Because the last row of $\vec{B}_m \vec{z}_m$ cannot change when the m^{th} component $(z_m)_0$ is changed ($\vec{B}_m \vec{z}_m = \vec{0}$), f_k is constant for all $(z_m)_0$. Since the choice was based on maximum sensitivity, we see that no other row would have done either. Hence, n - m + 1 rows of the original $\vec{A}$ matrix were linearly dependent on m - 1 rows; the rank of $\vec{A}$ is m - 1, contradicting the hypothesis that $|\vec{A}| \neq 0$. This method, therefore, provides the rank of the matrix when its determinant is zero.

We note that the final $\vec{B}$ matrix often contains negative or zero diagonal elements, producing complex characteristic roots, but ones with large positive real parts. Because $|\vec{B}_m| > 0$, all the discriminants $|\vec{B}_i|$, i = 1, 2, ..., m-1, are positive.

Example

Consider the equation with nominal matrix coefficients

$$\begin{pmatrix} 4 & 7 & 3 & 7 \\ 0 & 6 & 9 & 9 \\ 1 & 9 & 0 & 9 \\ 5 & 3 & 5 & 5 \end{pmatrix} \begin{pmatrix} x_1 \\ x_2 \\ x_3 \\ x_4 \end{pmatrix} + \begin{pmatrix} b_1 \\ b_2 \\ b_3 \\ b_4 \end{pmatrix} = \begin{pmatrix} 0 \\ 0 \\ 0 \\ 0 \end{pmatrix} \tag{29}$$

Ignoring the $\vec{b}$ vector and normalizing the rows of $\vec{A}$, we set

$$\begin{pmatrix} f_1 \\ f_2 \\ f_3 \\ f_4 \end{pmatrix} = \begin{pmatrix} .5714 & 1 & .4286 & 1 \\ 0 & .6667 & 1 & 1 \\ .1111 & 1 & 0 & 1 \\ 1 & .6 & 1 & 1 \end{pmatrix} \begin{pmatrix} x_1 \\ x_2 \\ x_3 \\ x_4 \end{pmatrix} \tag{30}$$

Since a "1" exists in every column, the first feedback loop is arbitrary. We let

$$\dot{x}_4 + 10f_4 = 0 \tag{31}$$

with $z_1 = x_4$. Using $(x_1)_0 = (x_2)_0 = (x_3)_0 = 0.2$, the nominal and perturbed values of all remaining f_k are measured in the operate mode with $f_4 = 0$, as shown in Table 1. We see that a tie exists between variations in f_2 due to perturbations in x_1 and variations in f_3 due to perturbations in x_3. We arbitrarily use $z_2 = x_3$,

$$\dot{x}_3 + g_2(-f_3) = 0 \tag{32}$$

and determine by trial that $g_2 = 10$ produces the most rapid convergence of this second-order subsystem. The system $\dot{x}_3 + g_2 f_3 = 0$ was unstable, necessitating the sign change.

Proceeding, we construct Table 2 and find we need f_2 as feedback to x_1. We determine by trial that

$$\dot{x}_1 + g_3(-f_2) = 0 \tag{33}$$

is stable, with $g_3 = 3$ producing the most rapid convergence. With one equation left, we find that we can use

$$\dot{x}_2 + 10f_1 = 0 \tag{34}$$

for stability and fast convergence. In terms of the original variables, the final system (with the $\vec{B}$ matrix reordered in both columns and rows) is

$$\begin{pmatrix}\dot{x}_1\\ \dot{x}_2\\ \dot{x}_3\\ \dot{x}_4\end{pmatrix} + \begin{pmatrix}3 & 0 & 0 & 0\\ 0 & 10 & 0 & 0\\ 0 & 0 & 10 & 0\\ 0 & 0 & 0 & 10\end{pmatrix}\left[\begin{pmatrix}0 & -.6667 & -1 & -1\\ .5714 & 1 & .4286 & 1\\ -.1111 & -1 & 0 & -1\\ 1 & .6 & 1 & 1\end{pmatrix}\begin{pmatrix}x_1\\ x_2\\ x_3\\ x_4\end{pmatrix} + \begin{pmatrix}-b_2/9\\ b_1/7\\ -b_3/9\\ b_4/5\end{pmatrix}\right] = \begin{pmatrix}0\\ 0\\ 0\\ 0\end{pmatrix} \tag{35}$$

and remains stable for wide variations of the coefficients. (All coefficients represented by potentiometers were individually varied for the full range without instabilities.) The presence of zero main diagonal terms may disturb intuitive feelings that suggest these should be large; but, in fact, such ideas are somewhat fanciful, applying only when all characteristic roots are real. We may rest assured that this underdamped system is "strongly" stable.

7. EXTENSION TO NONLINEAR EQUATIONS. The construction procedure for nonlinear equations remains the same as for linear equations. But, since the Jacobian matrix $\vec{J}(\vec{f},\vec{x})$ at a root is parameter dependent, any given stable structure may not be stable for new sets of parameters. If the characteristic roots of the Jacobian matrix are sensitive near the root, we must, in effect, be at the root for the sensitivity tests. It might seem that this requirement defeats the purpose; i.e., a solution to (1) must first be obtained before the construction can be achieved. This is not always so. First, many situations arise where solutions are known for one set of parameters. When a stable direct system can be constructed for this set, it aids immeasurably in obtaining solutions to a new set of a_j. Each a_j is changed one at a time from its old to its new value. If any instability is encountered, a new feedback

structure can be obtained by sensitivity testing at the then existing set of a_j. Second, since the procedure requires generation of all f_k, some relaxation method can be used to obtain an approximate first solution, or it may be possible to perform sensitivity tests to find it. Suppose $(f_k)_0$ are values of the f_k for the initial guesses $(x_i)_0$. Define

$$f_k' = f_k - (f_k)_0 \tag{36}$$

The f_k' are now zero, while the $(f_k)_0$ may be considered as n additional parameters. By obtaining a stable feedback structure that drives the f_k' to zero, the $(f_k)_0$ may slowly be reduced to zero to obtain the solution to the original case. Feedback structures will have to be changed during the process if instabilities result, as is true with other parameters.

If the Jacobian elements are not too sensitive near the solution, sensitivity testing enables construction of a stable system near the root.

The conditions for which this procedure works for nonlinear equations are derivable from fundamental stability theorems [2]. Writing

$$\vec{f} = J\vec{x} + \vec{w} \tag{37}$$

we assume $\vec{w}$ continuous in a region about the root and the usual condition concerning the order of the nonlinear term:

$$||\vec{w}||/||\vec{x}|| \to 0 \text{ as } ||\vec{x}|| \to 0 \tag{38}$$

under some suitable metric such as

$$||\vec{w}|| = \sum_{i=1}^{n} |w_i|, \quad \text{and} \quad ||\vec{x}|| = \sum_{i=1}^{n} |x_i| \tag{39}$$

Because of the large magnitude of the diagonal elements of $\vec{G}$ and the possible time scaling, both $\vec{J}$ and $\vec{w}$ may be considered constant in this application. As is well known, it is then necessary that $\vec{G}\vec{J}$ have characteristic roots with non-negative real parts at the root for the system

$$\dot{\vec{x}} + \vec{G}(\vec{J}\vec{x} + \vec{w}) = \vec{0} \tag{40}$$

to be stable at the root. Our construction procedure does not work if $|\vec{J}| = 0$. Also, for $|\vec{J}| \neq 0$, we may construct a system such that

$$\dot{\vec{y}} + \vec{G}\vec{J}\vec{y} = \vec{0} \tag{41}$$

is stable at $\vec{y} = \vec{0}$. By a fundamental stability theorem of nonlinear equations, system (40) is therefore constructable at the root of (1) [or (37)] if

(1) $|\vec{J}| \neq 0$ at the root

(2) $\vec{w}$ is continuous in a region about the root

(3) $||\vec{w}||/||\vec{x}|| \to 0$ as $||\vec{x}|| \to 0$.

Example

We solve the system

$$\begin{aligned} f_1 &\equiv x^2 + y^2 + z^2 - 1 = 0 \\ f_2 &\equiv xy + yz + xz - 0.25 = 0 \\ f_3 &\equiv a_1x + a_2y + a_3z - 0.25 = 0 \end{aligned} \tag{42}$$

for roots near the nominal values of $a_1 = 0.5$, $a_2 = -0.5$, and $a_3 = 0.5$. At the nominal values of parameters, there are four roots, of which $x \simeq 0.93$, $y \simeq 0.36$, and $z \simeq -0.07$ is the one of interest to be tracked with changing parameters.

We quickly find that f_1 is most sensitive to changes in x when compared with other perturbations. Hence, we mechanize

$$\dot{x} + 10f_1 = 0 \tag{43}$$

and determine Table 3 in the operate mode. We then find that

$$\dot{z} + 10f_2 = 0, \quad \dot{y} - 10f_3 = 0 \tag{44}$$

are stable. Since the f_k are near zero, the gain coefficients were determined after magnifying each f_k for convergence characteristics

observations. The equations remained stable even when each coefficient was varied one at a time between the limits $0 \leq a_1 \leq 1$, $-1 \leq a_2 \leq 0$, and $0 \leq a_3 \leq 1$.

8. EXTENSION TO BOUNDARY-VALUE PROBLEMS. Analog/hybrid computers contain the means to change parameters in discrete amounts between solution runs in a repetitive operation mode. This means that, while a system of differential equations is being solved repetitively at a rate as high as 1000 solution/sec independent of the number of equations, each solution may be different because some iteration procedure continually adjusts constants in an attempt to satisfy some needed conditions. An important class of problems amenable to an efficient attack by such computers are boundary-value problems where error functions have the form

$$f_k \equiv f_k[y_1(t_k), y_2(t_k), \ldots, y_s(t_k), x_1, x_2, \ldots, x_n, a_1, a_2, \ldots, a_m] = 0 \qquad (45)$$

and the values $y_p(t_k)$, $p = 1, 2, \ldots, s$, are obtained by solving a system of differential equations

$$\frac{dy_p}{dt} = h_p(t, y_1, y_2, \ldots, y_s, x_1, x_2, \ldots, x_n, a_1, a_2, \ldots, a_m) \qquad (46)$$

In (45), each t_k is a specific value of the independent variable t, the x_i are now adjustable parameters with both $i, k = 1, 2, \ldots, n$, and the a_j are stationary parameters. As the a_j are changed, new values of the x_i must be found to satisfy (45).

A continuous direct nulling system must be replaced by a discrete system:

$$\vec{x}_q - \vec{x}_{q-1} + \vec{G}\vec{f}_q = \vec{0} \qquad (47)$$

After the q^{th} solution of the differential equations (46) using constants $\vec{x}_{q-1}$, the residual errors $\vec{f}_q$ are determined. Discrete changes $\Delta\vec{x}_q = \vec{x}_q - \vec{x}_{q-1}$ are made from (47) and new constants $\vec{x}_q$ are used in the $q+1^{st}$ solution of the differential equations. If system (47) can be constructed to produce stable solutions for one set of parameters a_j, then by reasoning similar to the continuous direct nulling case, we sometimes can expect the system to be stable for wide variations of parameters.

Construction of system (47) is similar to the continuous case; it requires finding a temporary gain matrix $\vec{G}'$ where the characteristic roots of $\vec{G}'\vec{J}$ not only have positive real parts, but also that all variables using

$$\vec{x}_q - \vec{x}_{q-1} + \vec{G}'\vec{f}_q \approx \vec{0} \tag{48}$$

resemble a closely sampled sequence of the variables of an equivalent continuous system mechanization.

In practice, the sensitivities of each f_k to perturbations in $(x_i)_0$ are determined by reading the stored set of f_k in the repetitive operation mode. Again selection of an f_k for use as a discrete feedback for changes in x_i [in the sense of (48)] is made on the basis of maximum sensitivity after all previously "used" f_k are forced to zero. The values of the diagonal elements of $\vec{G}'$ are determined quickly and easily with analog computers by observing graphs of all f_k with time. They should be small enough to present a rather smooth convergence pattern, with their relative values chosen for a near orthogonal condition as in the continuous case. After the feedback structure is obtained, we use

$$\vec{G} = g\vec{G}' \tag{49}$$

with $g > 1$, and maximize the convergence rate by trial. This procedure guarantees that $\vec{G}\vec{J} - \vec{I}$ has characteristic roots within the unit circle, one of the sufficient conditions for stability [5]. The sensitivity tests still cannot find a stable system unless $|\vec{J}| \neq 0$, so that conditions for constructability remain identical with those of the continuous case.

An Optimal Control Example

It was decided to attack a rather involved problem to determine the feasibility of tracking solutions of boundary-value problems containing many adjustable parameters with the method suggested. Accordingly, we selected an optimal control rendezvous problem, reported by Darcy and Hannan [6] and solved by them manually by a relaxation method on an analog computer.

A maneuvering vehicle attempts rendezvous with a target. The target is in circular orbit with angular velocity ω about the origin of an inertial reference frame, and both vehicle and target are confined to the plane of orbit. The vehicle contains a thruster capable of producing accelerations up to a_{max} ft/sec^2. It can be rotated to accelerate the vehicle in any direction in the plane. This system is described by the equations

$$d^2x/dt^2 - 2\omega\, dy/dt = c_1 \cos c_2$$

$$d^2y/dt^2 + 2\omega\, dx/dt - 3\omega^2 y = c_1 \sin c_2 \tag{50}$$

where the thrust c_1 is subject to $0 \leq c_1 \leq a_{max}$, c_2 is the "steering" angle of the thruster, and x and y are rotating rectilinear coordinates in the plane, with origin at the target. Initial coordinates and their velocities are given. The problem is how to select $c_1(t)$ and $c_2(t)$ so that the integral

$$\rho = \int_0^{t_f} (1 + \lambda c_1)\, dt \tag{51}$$

is minimized, while the vehicle is transported to the origin, arriving there with zero velocity. If $\lambda = 0$, this is a time optimal problem. If $\lambda > 0$, some restriction is placed on the amount of fuel expended.

A state variable set of equations for the system is

$$dy_1/dt = y_2, \qquad dy_2/dt = 2\omega y_4 + c_1 \cos c_2$$

$$dy_3/dt = y_4, \qquad dy_4/dt = -2\omega y_2 + 3\omega^2 y_3 + c_1 \sin c_2 \tag{52}$$

with $y_1 = x$, $y_2 = dx/dt$, $y_3 = y$, and $y_4 = dy/dt$.

By means of the maximum principle [7], the equation

$$dy_0/dt = 1 + \lambda c_1 \tag{53}$$

is added to the system, and the Hamiltonian H is formed:

$$H = p_0(1 + \lambda c_1) + p_1 y_2 + p_2(2\omega y_4 + c_1 \cos c_2)$$

$$+ p_3 y_4 + p_4(-2\omega y_2 + 3\omega^2 y_3 + c_1 \sin c_2) \tag{54}$$

where the p_j satisfy the adjoint system

$$dp_0/dt = 0, \qquad dp_1/dt = 0, \quad dp_2/dt = -p_1 + 2\omega p_4$$

$$dp_3/dt = -3\omega^2 p_4, \qquad dp_4/dt = -2\omega p_2 - p_3 \tag{55}$$

Optimal controls are chosen and are continuously mechanized on the computer. According to the maximum principle, it is necessary that

$$c_1 = a_{max}\, U(\lambda p_0 + p_2 \cos c_2 + p_4 \sin c_2) \tag{56}$$

where U is the unit step function, and

$$\tan c_2 = p_4/p_2 \tag{57}$$

for optimality. Equation (57) reduces to

$$\sin c_2 = p_4/(p_2^2 + p_4^2)^{1/2}, \quad \cos c_2 = p_2/(p_2^2 + p_4^2)^{1/2} \tag{58}$$

with (56) transforming to

$$c_1 = a_{max} U[(p_2^2 + p_4^2)^{1/2} + \lambda p_0] \tag{59}$$

We may take $p_0 = -1$; it remains to find p_1, also constant, and $(p_2)_0$, $(p_3)_0$, and $(p_4)_0$ which transport the y_j of (52) to the origin at some time t_f. For optimality, it is also necessary that $H = 0$ throughout the trajectory and in particular at $t = t_f$. We see from (54) that

$$H(t_f) = -1 - \lambda c_1 + p_2 c_1 \cos c_2 + p_4 c_1 \sin c_2 \tag{60}$$

when each $y_j = 0$. This fifth condition reduces to

$$H(t_f) = -1 + c_1 \{[p_2^2(t_f) + p_4^2(t_f)]^{1/2} - \lambda\} = 0 \tag{61}$$

Since the thrust c_1 is off or on full blast from (59), we finally get

$$a_{max}\{[p_2^2(t_f) + p_4^2(t_f)]^{1/2} - \lambda\} - 1 = 0 \tag{62}$$

because, from (61), c_1 cannot equal zero at $t = t_f$. The five residual error functions are

$$f_1 = y_1(t_f),\ f_2 = y_2(t_f),\ f_3 = y_3(t_f),\ f_4 = y_4(t_f)$$

$$f_5 = a_{max}\{[p_2^2(t_f) + p_4^2(t_f)]^{1/2} - \lambda\} - 1 \tag{63}$$

and the five adjustable constants are p_1, $(p_2)_0$, $(p_3)_0$, $(p_4)_0$, and t_f. A circuit was mechanized to solve system (52) and its adjoint (55) while continuously mechanizing the optimal controls. The first set of stationary parameters investigated was

$$\lambda = 0, \quad \omega = 1.175 \times 10^{-3} \text{ rad/sec}, \quad a_{max} = 1 \text{ ft/sec}^2$$

$$(y_1)_0 = -100{,}000 \text{ ft}, \quad (y_2)_0 = 200 \text{ ft/sec} \tag{64}$$

$$(y_3)_0 = 50{,}000 \text{ ft}, \quad (y_4)_0 = 80 \text{ ft/sec}$$

It took about 20 min of oscilloscope observations to adjust the constants to give a near first solution. The value of each $f_k(t_f)$ was within 20 percent of the maximum absolute value of $f_k(t)$. It became clear that the adjustable constants were near their needed values. Fortunately, the Jacobian matrix, although not explicityly known in this problem, was fairly insensitive at the solution, so that sensitivity testing produced a stable circuit that converged to the proper solutions. Figure 1 shows the optimal trajectories obtained for this case. Each variable y_1 -- y_4 is graphed with scale factors omitted but calculable from the initial values in (64). Figure 2 shows typical real-time convergence graphs of normalized values of each f_k, from initial values that are quite large. Although the convergence time was about 3 sec, it was also reduced to 0.5 sec by solving the equations more rapidly.

With one solution obtained, it becomes an easy matter to vary any parameter and obtain new solutions very quickly. Figure 3 illustrates new solutions obtained when λ was increased from 0 to 4. At $\lambda = 4$, it was noticed that the $f_k(t_f)$ oscillated with small damping, indicating that the feedback structure, although still stable, could be improved. New sensitivity tests were performed manually (taking about 30 min), and the feedback loops, restructured. The new structure was stable for $0 \leq \lambda \leq 9$, which represented the interval of interest.

Other parameters were similarly varied with solutions successfully tracked in most cases.

9. CONCLUSIONS. The procedures described for tracking solutions to algebraic equations on analog computers and boundary-value problems on analog/hybrid computers are extremely efficient in terms of equipment. But there are distinct disadvantages in terms of getting a first solution and maintaining stability as parameters are changed. First solutions are often available through insight or previous work. Also, because the f_k are generated on the computer, a relaxation process can often be used (as in the optimal control example given) to obtain first solutions; or it may be possible to perform manual sensitivity tests to find them. We have not investigated automating the sensitivity testing for this purpose, a distinct possibility. Thus, the disadvantages of the procedure are not nearly so difficult to combat as one might initially fear.

REFERENCES

1. Hausner, A., "The Solution of Lagrange's Equations by Analog Computation," IEEE Trans on Elect Comp, Vol. 14, Feb 1965.

2. Bellman, R., Stability Theory of Differential Equations, McGraw-Hill Book Co., New York, N. Y., 1953, p. 75 ff.

3. Rybashov, M. V., "Finding the Roots of Systems of Finite Equations by Means of an Electronic Simulator, Using Differential Equations with Variable Structure," Automatika i Telemekhanika, Vol. 22, Dec. 1961.

4. Bellman, R., Introduction to Matrix Analysis, McGraw-Hill Book Co., New York, N. Y., 1960, pp. 94-95.

5. Bellman, R., "On the Boundedness of Solutions of Nonlinear and Difference Equations," Trans of the Amer Math Soc, Vol., 62, 1947, p. 357 ff.

6. Darcy, V. J., and R. A. Hanne, "An Application of an Analog Computer to Solve the Two-Point Boundary-Value Problem for a Fourth-Order Optimal Control System," IEEE Trans on Auto-Control, Feb. 1967.

7. Pontryagin, L. S., et al, The Mathematical Theory of Optimal Processes, trans by K. N. Trirgoff, John Wiley and Sons, New York, N. Y., 1962.

TABLE 1

for $f_4 = 0$	nominal values $x_1 = x_2 = x_3 = 0.2$	$x_1 = 0.21$ $x_2 = x_3 = 0.2$	$x_2 = 0.21$ $x_1 = x_3 = 0.2$	$x_3 = 0.21$ $x_1 = x_2 = 0.2$
f_1	.1204	.1245	.1163	.1262
$\|\Delta f_1\|$		.0041	.0041	.0058
f_2	.1870	.1970	.1861	.1870
$\|\Delta f_2\|$		.0100	.0009	0
f_3	.2978	.3069	.2938	.3078
$\|\Delta f_3\|$		.0091	.0040	.0100

TABLE 2

for f_3 $=f_4 = 0$	nominal values $x_1 = x_2 = 0.2$	$x_1 = 0.21$ $x_2 = 0.2$	$x_2 = 0.21$ $x_1 = 0.2$
f_1	.0503	.0511	.0520
$\|\Delta f_1\|$		.0008	.0017
f_2	.1870	.1970	.1861
$\|\Delta f_2\|$		.0100	.0009

TABLE 3

for $f_1 = 0$	nominal values $y = 0.36$ $z = -0.07$	$y = 0.37$ $z = -0.07$	$y = 0.36$ $z = -0.06$
f_2	-.0055	+.0022	+.0075
$\lvert\Delta f_2\rvert$		.0077	.0130
f_3	+.0002	-.0067	+.0054
$\lvert\Delta f_3\rvert$		.0069	.0052

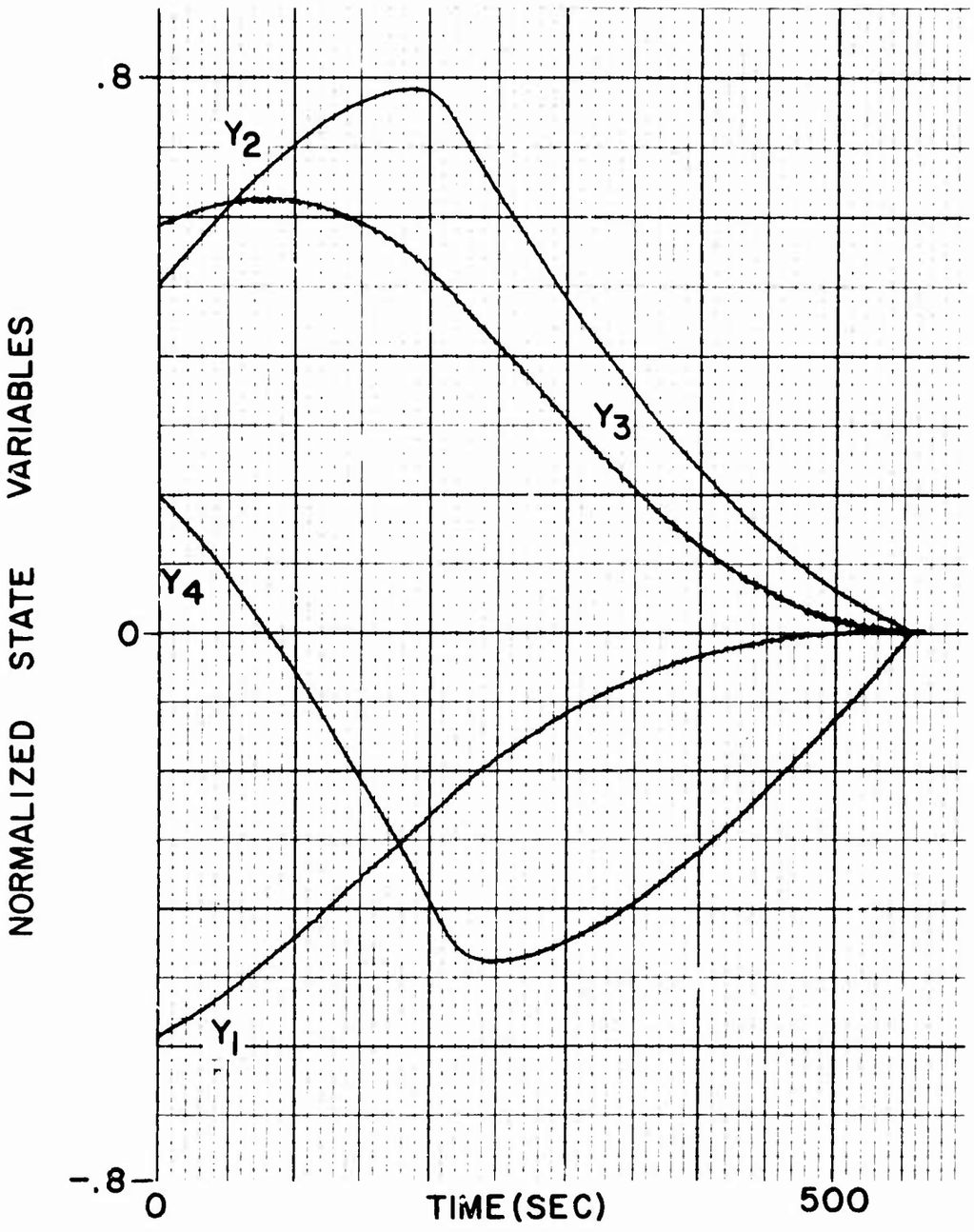
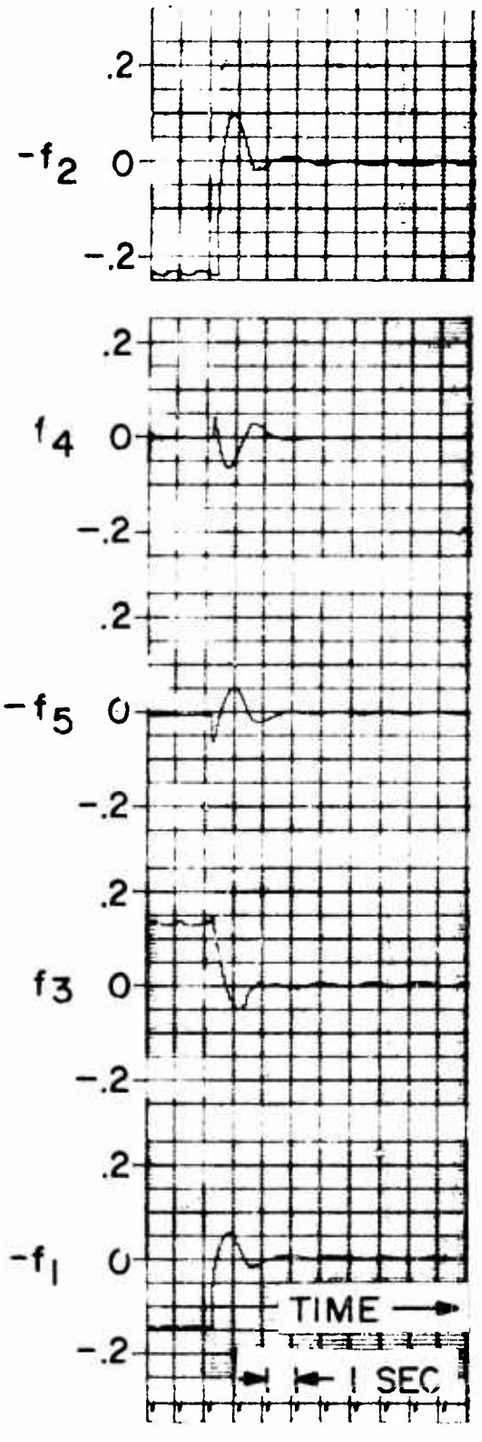


Figure 1

OPTIMAL TRAJECTORIES FOR NOMINAL PARAMETERS



Figure

TYPICAL STABILITY GRAPHS OF ILS FIVE ERROR FUNCTIONS

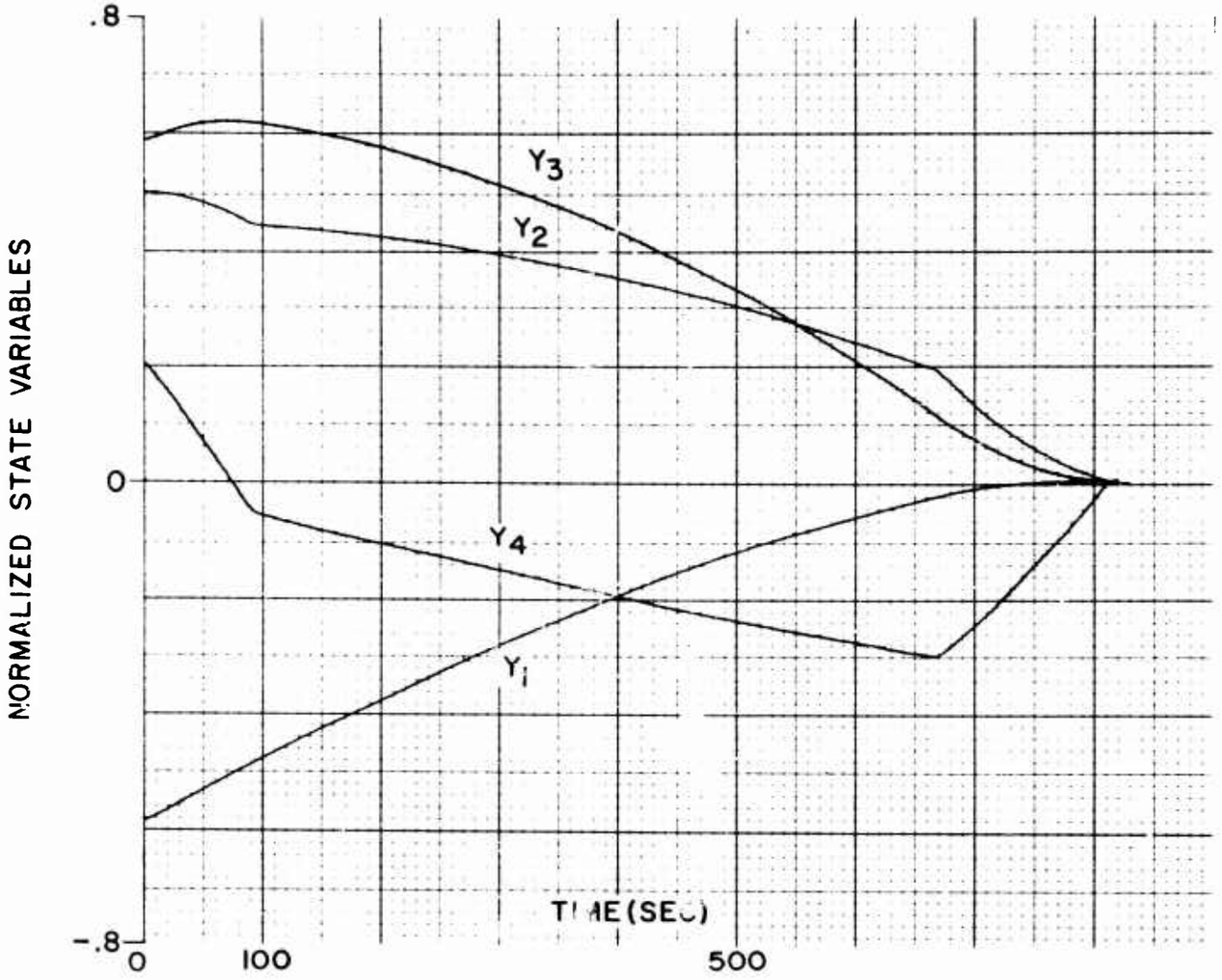


Figure 3

OPTIMAL TRAJECTORIES FOR $\lambda = 4$.

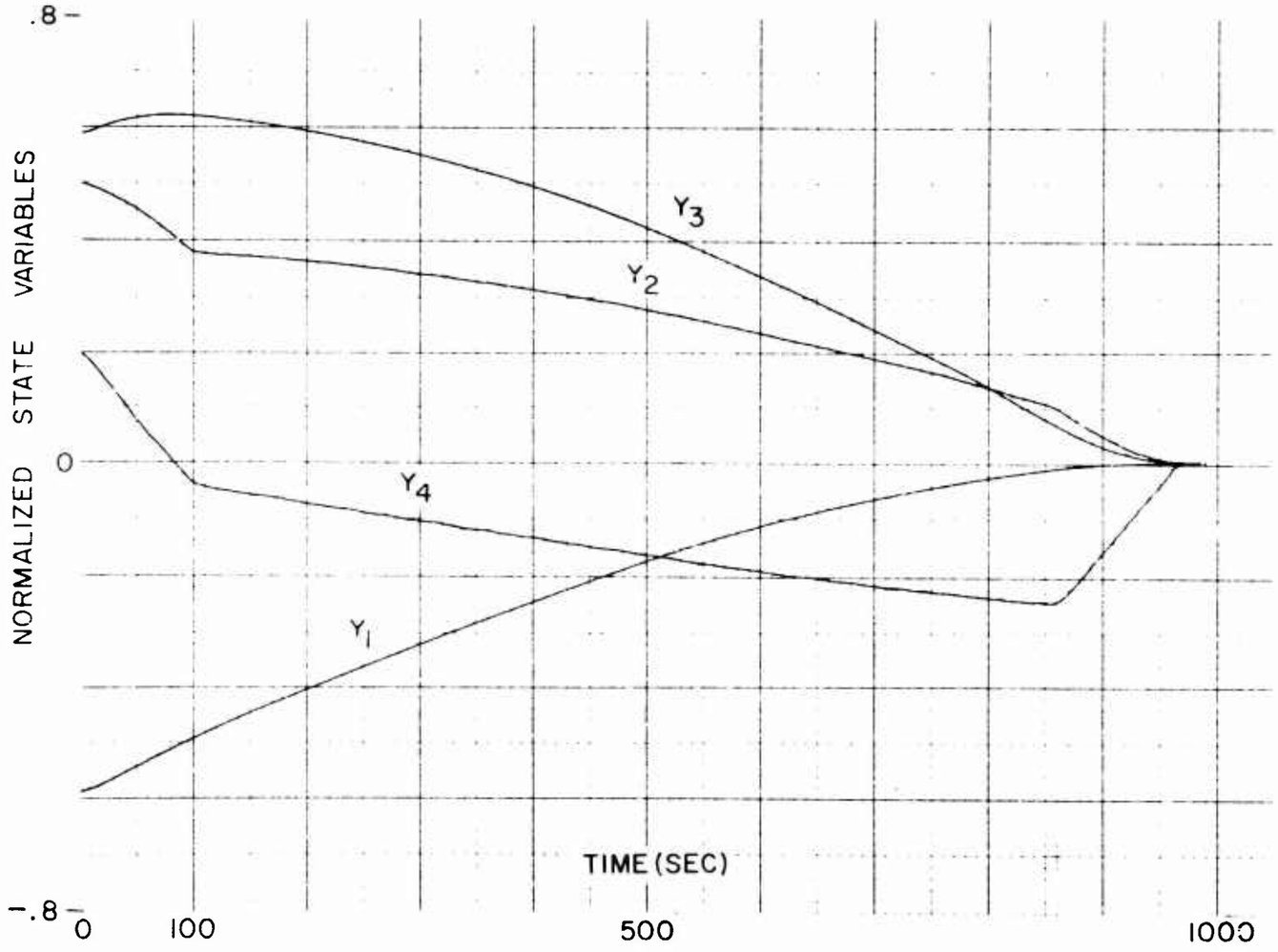


Figure 4

OPTIMAL TRAJECTORIES FOR $\lambda = 9$

A RAPIDLY CONVERGING ITERATIVE TECHNIQUE FOR COMPUTING WIND COMPENSATION LAUNCHER SETTINGS FOR UNGUIDED ROCKETS

Louis D. Duncan and Bernard F. Engebos
U. S. Army Electronics Command
White Sands Missile Range, New Mexico

ABSTRACT. This paper presents the development and evaluation of two algorithms for the determination of wind compensating launcher settings for unguided rockets. The algorithms are designed for use in an iterative trajectory simulation process and can be used to determine launch angles which will yield one of many possible trajectory objectives. One algorithm provides the first estimate as a function of the ballistic wind; the other controls the iteration.

Four test cases are presented to evaluate the technique. Sixteen different wind profiles were applied to four separate unguided rockets. Two different trajectory objectives were considered - nominal burnout attitude and nominal impact. The tests show that the process converges rapidly, usually requiring only one or two iterations.

INTRODUCTION. The trajectory of an unguided rocket or projectile will be affected by the wind encountered during flight. This pertubation of the trajectory is commonly called wind effect. If one desires to obtain a predetermined value of a given trajectory objective (such as impact of a given booster, orientation of the velocity vector at burnout, etc.), it is necessary to determine a launcher setting which will compensate for the wind effect. The sophistication of the algorithms to determine these launcher settings depends not only on the specified trajectory objective, but also on the rocket configuration and the nominal trajectory.

A first-order approximation of the wind effect may be obtained by a technique called "wind weighting." This technique is discussed in Apprndix A. Several procedures [Lewis (1949, James and Harris (1960), Hennigh (1964), Duncan and Engebos (1966a, 1966b)] based on the wind weighting technique have been developed which give first-order approximations for the launcher settings required to compensate for the wind effect.

In the previous developments, the model was usually restricted to considering either a specific trajectory objective or a specific type of trajectory or both. This paper presents a procedure which allows for a much wider range of applicability.

The model presented herein has a twofold capability. An approximation for launcher settings based upon the wind weighting technique is developed. For missile projects which require more accurate computations, an iterative

 PRECEDING PAGE BLANK

procedure is developed. The algorithms for the iteration converge rapidly; the wind-weighting-based model is used as a first approximation. The iterative procedure can also be used to refine the numerical values for the wind-weighting-based model. The use of the complete model as an operational tool requires a real-time computational capability (Duncan and Rachele, 1967).

COORDINATE SYSTEMS AND TRANSFORMATIONS. In this development, it is assumed that the rocket trajectory is specified in a right-hand topocentric coordinate system (x,y,z). The positive x-axis points east, and the positive y-axis points north. The azimuth angle, α, and the elevation angle, β, are defined in Figure 1.

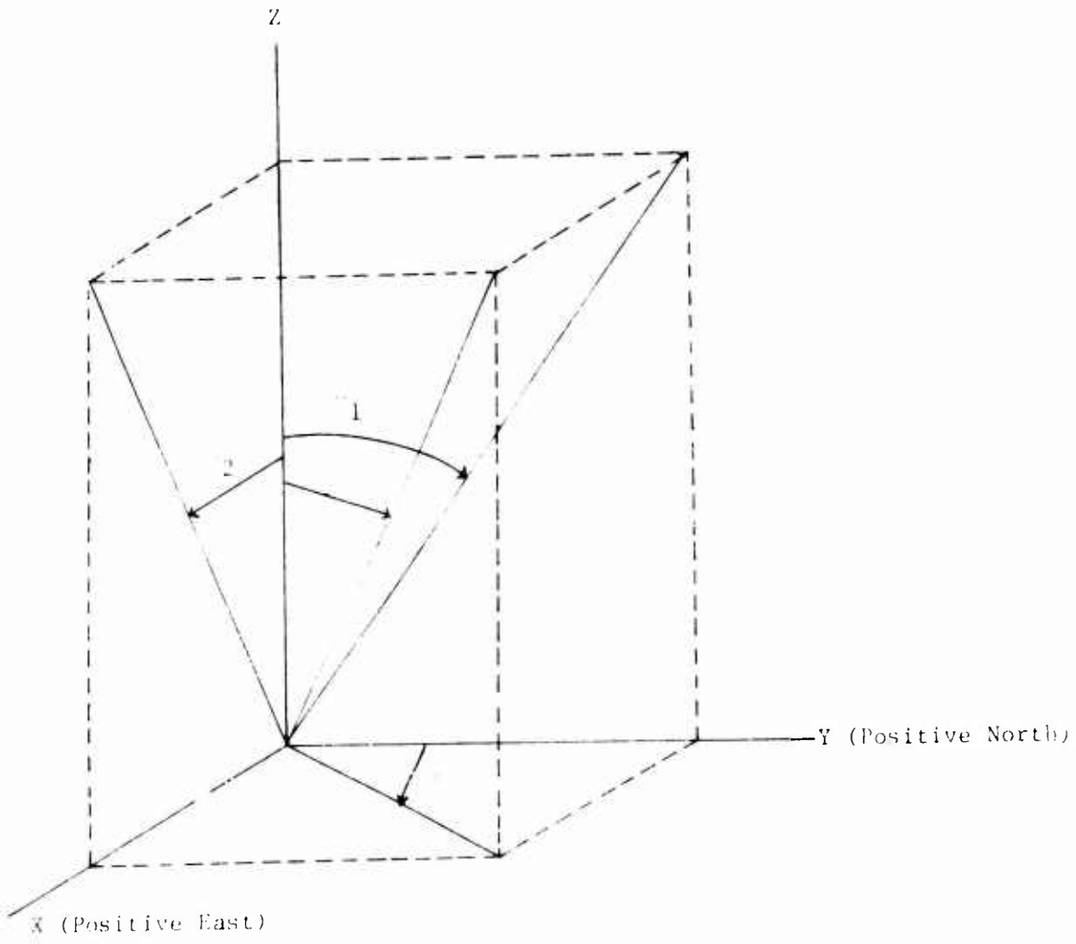


Figure 1

The equations developed herein are based upon the angles θ_1 and θ_2 which are the components of the elevation angle in the y-z and x-z planes, respectively. There is, of course, a one-to-one correspondence between the pair (θ,α) and the pair (θ_1,θ_2). The transformation equations are

$$\theta_1 = \tan^{-1} (\tan \theta \cos \alpha) \tag{1}$$

$$\theta_2 = \tan^{-1} (\tan \theta \sin \alpha)$$

and

$$\alpha = \tan^{-1} (\tan \theta_2 \cot \theta_1)$$

$$\theta = \tan^{-1} [\tan \theta_1 \cot^{-1} (\tan \theta_2 \cot \theta_1)] \tag{2}$$

$$= \tan^{-1} (\tan \theta_1 / \cos \alpha).$$

DISCUSSION. The launch angles required to compensate for wind effect depend upon the desired trajectory objective. These angles are determined by an iterative process of trajectory simulation. The first estimate is determined from the ballistic wind. A trajectory is computed using these angles. If the simulated objective is not within tolerance of nominal, a correction for launcher angles is determined from the error vector and a new trajectory is simulated. The iteration is continued until the tolerance is achieved. This procedure requires two algorithms, one for the first estimate and another for the iteration step.

The first estimate is based upon the ballistic wind. The algorithm for this estimate can be expressed in functional form by

$$\Delta\theta_1 = f_1(W_x, W_y)$$

$$\Delta\theta_2 = f_2(W_x, W_y) \tag{3}$$

where W_x and W_y are the East-West, North-South ballistic winds, respectively, and $\Delta\theta_1$ and $\Delta\theta_2$ are required changes from nominal settings*

*When the procedure is used in a real-time meteorological system where launcher settings are computed for consecutive (timewise) wind profiles, W_x and W_y are replaced by the changes in the ballistic winds from the last profile and $\Delta\theta_1$ and $\Delta\theta_2$ become changes from the settings obtained for that profile.

The functional form for the iteration step is similar,

$$\Delta\theta_1 = g_1(\alpha, \beta)$$
$$\Delta\theta_2 = g_2(\alpha, \beta) \tag{4}$$

where α and β are the component deviations from the nominal objective and $\Delta\theta_1$ and $\Delta\theta_2$ are the changes in the launcher settings required for the next iteration. Although the development presented herein is directed toward either of the following trajectory objectives:

1. Orientation of velocity vector at burnout; and
2. The x,y coordinates of the impact of either the afterbody or a prescribed booster, it is apparent that the procedure is applicable to many other constraints.

EXPRESSIONS FOR THE ALGORITHM FUNCTIONS. The development of the algorithms requires the determination of suitable expressions for f_1, f_2, g_1, and g_2. Since there is little or no theoretical indication of these expressions, an empirical approach is indicated. Various types of expressions may be determined by a curve fitting procedure and then tested for accuracy and suitability. The empirical approach may, of course, yield entirely different functional forms for different missile configurations. The general procedure is, however, invariant. It consists of determining expressions for g_1 and g_2, using these expressions in the determination of expressions for f_1 and f_2, and finally, testing the algorithms.

The following paragraphs will discuss the expressions for f_1, f_2, g_1, and g_2 for the Athena missile. Other missile systems will be discussed in later sections.

To determine approximating expressions for g_1 and g_2, several trajectory simulations were performed. Each of the trajectories was computed for no-wind conditions; various changes in the launch angles were used for the simulations. The pertinent information (for the determination of g_1 and g_2) was extracted from these simulations and is presented in Table I. An inspection of these results suggests that each of $\Delta\theta_{1b}$, Δv_{2b}, ΔX, and ΔY is approximately linear in each of the independent variables and that the contributions of the independent variables are approximately additive.

TABLE I. CHANGE IN BURNOUT ATTITUDE AND IMPACT FOR SPECIFIC CHANGES IN LAUNCH ANGLES (REGULAR ATHENA)

		Burnout		Impact	
$\Delta\theta_1$	$\Delta\theta_2$	$\Delta\theta_{1b}$	$\Delta\theta_{2b}$	ΔX	ΔY
(rad)		(rad)		(km)	
.02	0	.057063	-.006082	14.48	34.85
-.02	0	.055821	.007035	-15.07	-27.98
0	-.02	.004602	-.066587	-54.77	-11.28
0	.02	-.005573	.065389	51.36	13.94
.01	.01	.028378	-.003154	7.32	16.63
-.01	0	-.028068	.003392	- 7.46	-14.82
0	.01	-.002662	.032854	26.14	6.69
0	-.01	.002420	-.033154	-27.00	- 5.93
-.01	-.01	-.025603	-.030040	-33.84	-20.98
-.01	.01	-.030780	.036510	18.08	- 8.01
.01	-.01	.030747	-.036046	-20.28	10.82
.01	.01	.025773	.029452	34.04	23.06

This observation suggests a least-squares fit of the generic form

$$g(\varepsilon_1, \varepsilon_2) = \alpha\varepsilon_1 + \beta\varepsilon_2 \qquad (5)$$

where $(\varepsilon_1, \varepsilon_2)$ represents either $(\Delta\theta_{1b}, \Delta\theta_{2b})$ or $(\Delta X, \Delta Y)$ as appropriate.

The departures from linearity and additivity may be investigated by fitting the form

$$g(\varepsilon_1, \varepsilon_2) = a\varepsilon_1^2 + b\varepsilon_1 + c\varepsilon_2^2 + d\varepsilon_2 + e\varepsilon_1\varepsilon_2. \qquad (6)$$

Equation (5) will be referred to as the bilinear fit while (6) will be called quadratic. Each expression provides a good fit to the data in the sense that the residuals are small. The residuals for Eq. (6) are, as would be expected, somewhat smaller. Tests revealed that either of these forms provides a suitable algorithm for the iteration. These tests will be discussed in detail in a later section.

A similar procedure was used to determine expressions for f_1 and f_2. Trajectory simulations were made with various values of ballistic winds

introduced into the calculations. The iterative procedure was used to determine the launcher angles required to compensate for the effect of winds. The results of these simulations are shown in Table II. As before, the quadratic and bilinear forms were fit to the data. The independent variables in this case were the components of ballistic wind, (W_x, W_y). An examination of the residuals indicated that both forms provided a good fit to the data.

EVALUATION OF THE PROCEDURE. Since the equations developed in the preceding section cannot be verified by theoretical techniques, an empirical test of their accuracy is dictated. This section describes the tests and presents the results therefrom.

Sixteen different wind profiles were used in the evaluation. Some of these profiles were measured during missile support operations at White Sands Missile Range, while the others are hypothetical. These wind data are shown in Figures 2, 3, 4, and 5. It should be observed that there is considerable variation among the profiles; hence, it is believed that, collectively, they provide a good test for the evaluation of the algorithms.

To show that the algorithms are not restricted to a given missile configuration and to investigate the possibility of using a missile-invariant form for the algorithm expressions, four different rockets were used in the evaluation. These were: two configurations of the Athena which have quite different nominal trajectories; the Aerobee-350; and the Ballistic Missile Target System (BMTS). A short description of each will be given in the following paragraphs.

Two independent iterations were performed. The first was to match nominal impact; the second, was to match nominal burnout angles. A convergence tolerance of 1500 meters was selected for the impact iteration except for one case, the "regular" Athena where a tolerance of 300 meters was used. This smaller tolerance was used to show the speed with which the iteration converges. Compatible tolerances, which differed for each rocket, were used for the iterations to burnout angles.

The first and most exhaustive test was performed on the "regular" Athena. This is a typical configuration of several slightly different Athena missiles fired from Green River, Utah, to impact on White Sands Missile Range. The Athena is a two-stage (for the ascent trajectory) unguided rocket which is fired at a nominal elevation angle of approximately 13.5 degrees and achieves an apogee of approximately 250 kilometers and a range of 725 kilometers.

Both the quadratic and bilinear equations were used to perform the iterations; these were performed as independent cases. The results are shown in Tables III and IV. Two things should be observed from these results. First, both expressions provide rapid convergence. Second, there is no significant difference in the results obtained from the two expressions. This suggests the use of the simpler bilinear equations.

TABLE II. CHANGE IN LAUNCH ANGLE REQUIRED TO COMPENSATE FOR SPECIFIED BALLISTIC WIND TO MATCH EITHER NOMINAL IMPACT OR BURNOUT ATTITUDE (REGULAR ATHENA)

		Burnout		Impact	
W_x	W_y	$\Delta\theta_1$	$\Delta\theta_2$	$\Delta\theta_1$	$\Delta\theta_2$
(mps)		(rad)		(rad)	
5	0	-.000210	-.034690	-.000702	-.034263
- 5	0	.000287	.034524	.000404	.034279
0	5	-.033055	-.000243	-.032452	.000455
0	- 5	.033326	.000198	.032233	.000621
5	5	-.033193	-.035085	-.032940	-.034928
5	- 5	.033038	-.034346	.031432	-.033492
- 5	5	-.032857	.034437	-.031932	.033869
- 5	- 5	.033098	.034580	.032871	.034731
10	0	-.000350	-.069466	-.001356	-.068608
-10	0	.000642	.068824	.001039	.068255
0	10	-.065791	-.000527	-.064460	-.001021
0	-10	.066858	.000354	.064703	.001243

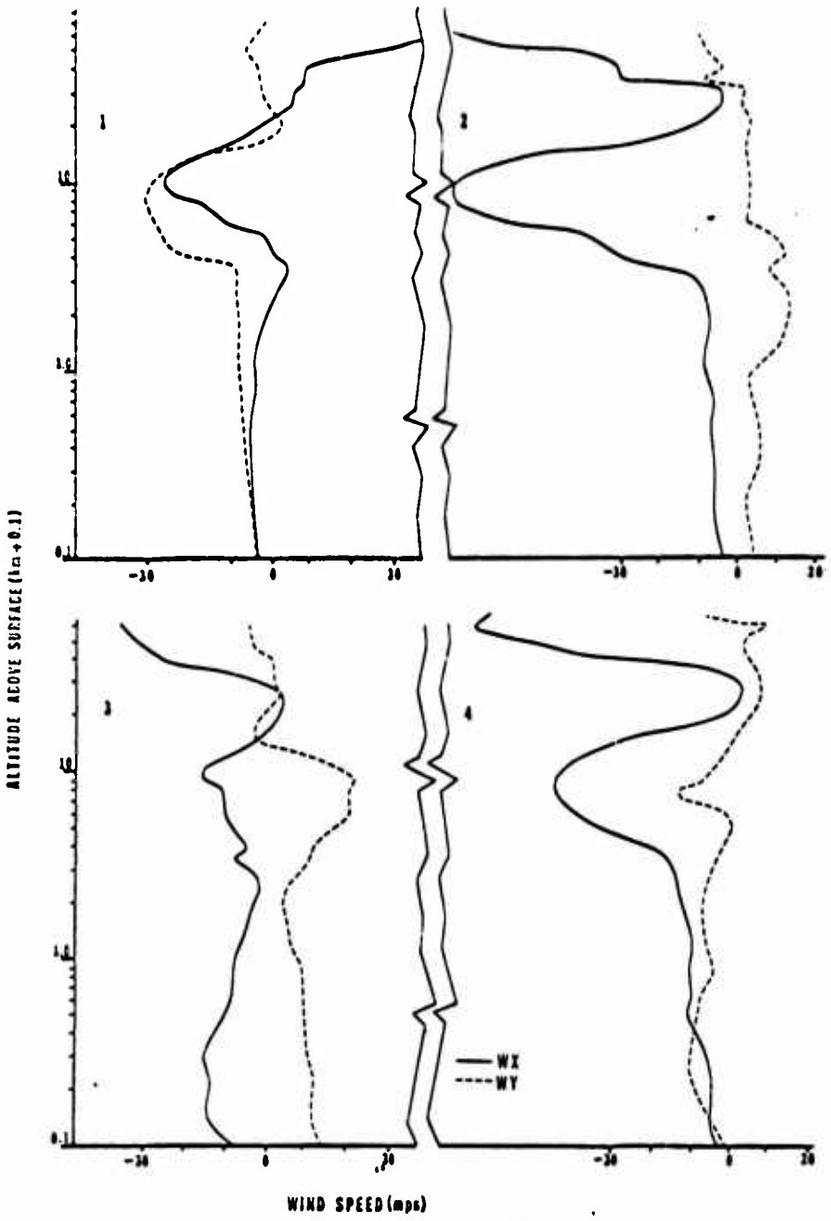


FIGURE 2. Wind Profiles Used in the Evaluation.

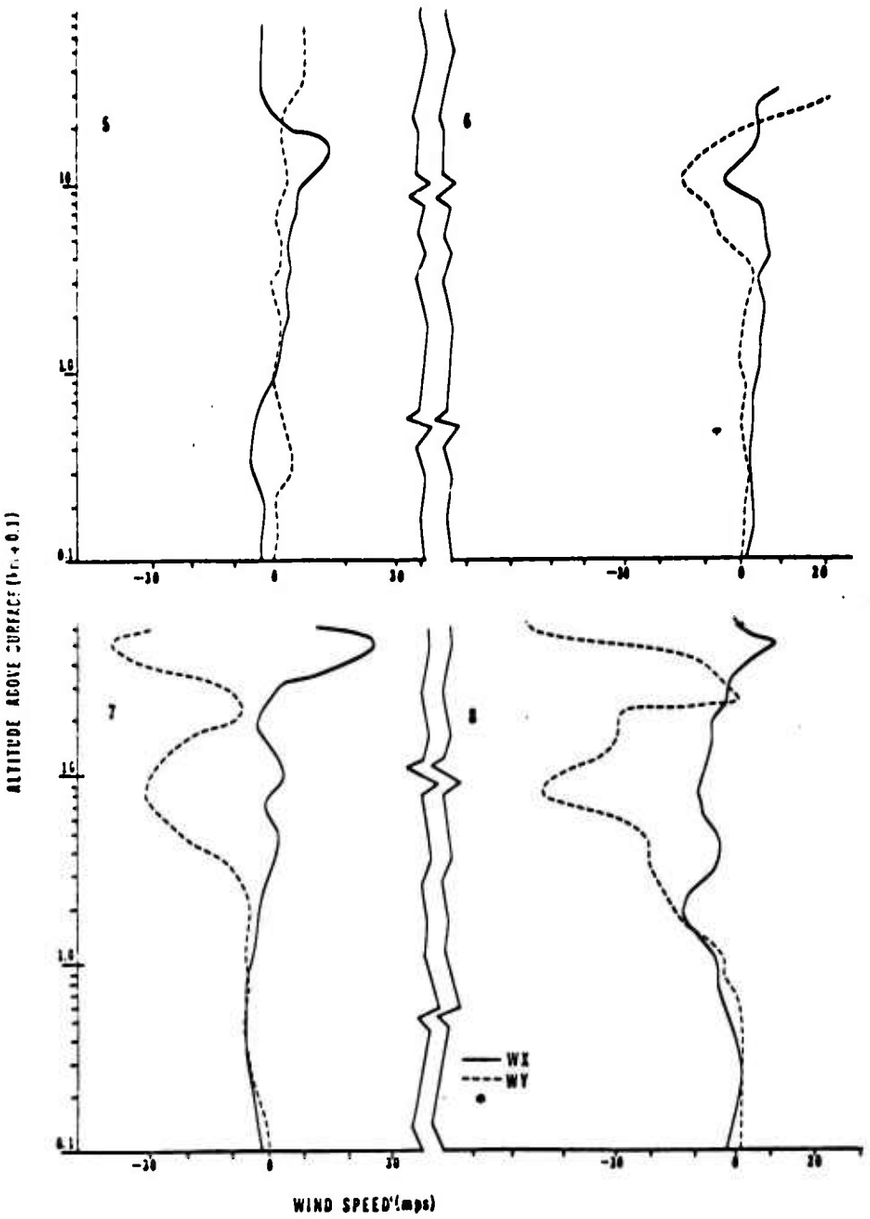


FIGURE 3. Wind Profiles Used in the Evaluation.

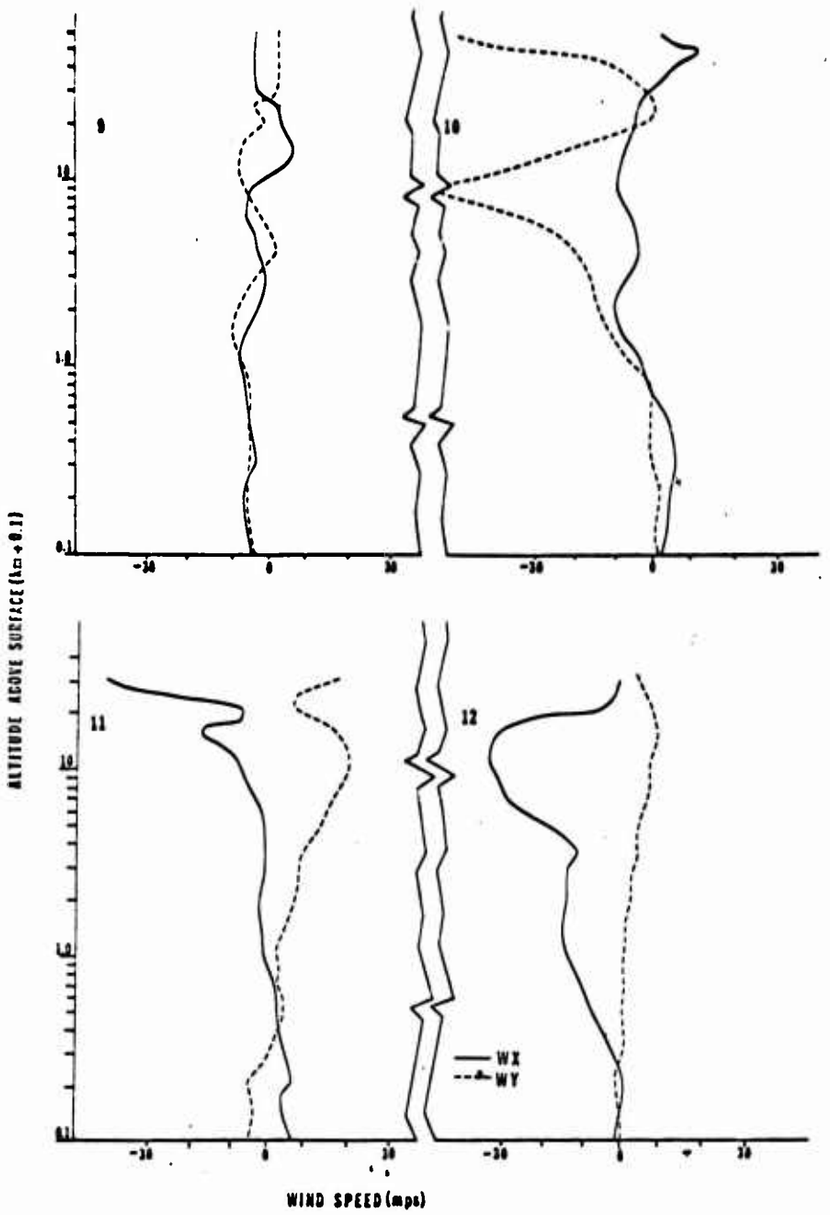


FIGURE 4. Wind Profiles Used in the Evaluation.

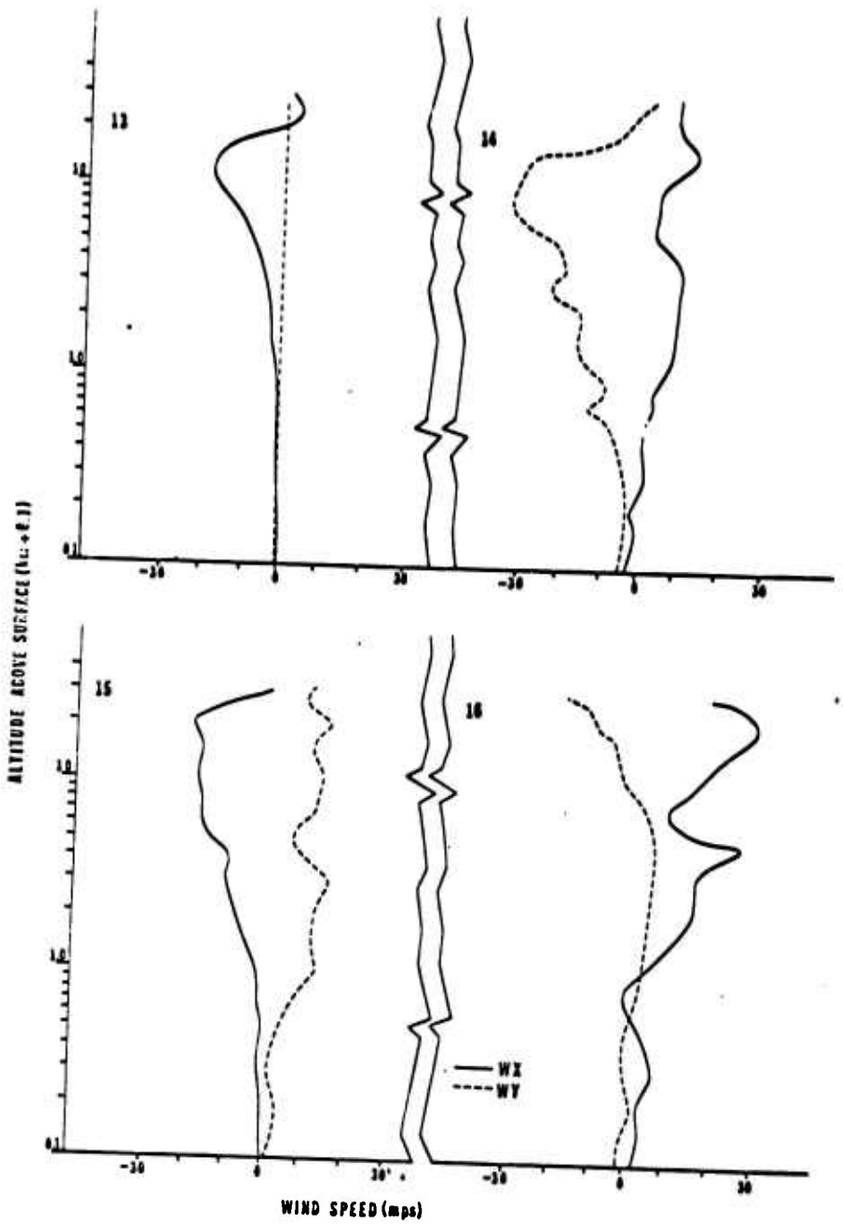


FIGURE 5. Wind Profiles Used in the Evaluation.

TABLE III. TEST CASE I, REGULAR ATHENA ITERATION TO IMPACT

Run	B.W.	Quadratic Equations				Bilinear Equations			
		θ_{1L}	θ_{2L}	X	Y	θ_{1L}	θ_{2L}	X	Y
	(mps)	(rad)		(km)		(rad)		(km)	
Nominal		-.2121	.1151	306.2	-643.7	-.2121	.1151	306.2	-643.7
1	- 4.15	-.1468	.1479	304.6	-643.5	-.1470	.1480	304.8	-643.7
	- 8.93	-.1473	.1473	306.2	-643.7	-.1472	.1486	306.1	-643.7
2	-12.91	-.2481	.2135	299.9	-647.1	-.2473	.2133	299.9	-646.0
	5.11	-.2467	.2155	306.6	-643.8	-.2467	.2155	306.6	-643.7
		-.2466	.2153	306.1	-643.7	-.2466	.2153	306.1	-643.7
3	-11.29	-.2881	.2011	305.2	-644.1	-.2871	.2002	303.6	-643.1
	10.59	-.2879	.2014	306.2	-643.7	-.2879	.2014	306.2	-643.7
4	-12.14	-.1602	.2082	300.9	-648.2	-.1602	.2090	303.0	-647.8
	- 6.95	-.1578	.2095	306.2	-643.8	-.1578	.2095	306.2	-643.8
5	- 1.29	-.2274	.1248	307.3	-642.5	-.2274	.1247	307.3	-642.5
	2.14	-.2281	.1245	306.2	-643.7	-.2281	.1245	306.2	-643.7
6	2.22	-.2075	.0982	306.0	-643.4	-.2075	.0982	306.0	-643.4
	- 0.68								
7	- 2.48	-.1731	.1349	299.7	-643.3	-.1732	.1342	299.8	-643.4
	- 5.34	-.1746	.1378	306.3	-643.7	-.1745	.1377	306.1	-643.5
8	- 3.28	-.1569	.1411	304.4	-641.7	-.1571	.1412	304.5	-641.7
	- 7.55	-.1587	.1423	306.1	-643.6	-.1587	.1423	306.1	-643.6
9	- 5.40	-.1703	.1570	306.1	-643.7	-.1704	.1572	306.6	-643.7
	- 5.67					-.1703	.1570	306.2	-643.7
10	- 0.13	-.1672	.1170	299.5	-644.4	-.1672	.1169	299.3	-644.5
	- 6.21	-.1678	.1197	306.1	-643.5	-.1677	.1196	306.0	-643.4
11	0.44	-.2272	.1115	306.6	-644.7	-.2272	.1115	306.6	-644.7
	2.09	-.2264	.1111	306.2	-643.6	-.2265	.1111	306.2	-643.7
12	-10.13	-.2091	.1925	301.5	-646.6	-.2088	.1927	302.3	-646.0
	- 0.26	-.2078	.1939	306.3	-643.7	-.2078	.1939	306.3	-643.7
13	- 1.69	-.2119	.1281	304.3	-644.5	-.2119	.1281	304.3	-644.5
	0.01	-.2116	.1287	306.2	-643.7	-.2116	.1287	306.2	-643.7
14	2.55	-.1377	.0972	305.6	-642.9	-.1376	.0969	304.7	-643.1
	-10.36	-.1384	.0976	306.1	-643.6	-.1383	.0976	306.2	-643.7
15	- 3.66	-.2602	.1425	305.8	-644.3	-.2600	.1423	305.3	-644.2
	6.71	-.2598	.1426	306.2	-643.6	-.2598	.1426	306.2	-643.7
16	8.10	-.2312	.0525	306.5	-641.8	-.2311	.0528	307.6	-641.5
	2.48	-.2325	.0528	306.2	-643.7	-.2325	.0527	306.2	-643.6

TABLE IV. TEST CASE I, REGULAR ATHENA ITERATION TO BURNOUT ANGLES (RADIANS)

Run	B.W. (mps)	Quadratic Equations				Bilinear Equations			
		θ_{1L}	θ_{2L}	θ_{1b}	θ_{2b}	θ_{1L}	θ_{2L}	θ_{1b}	θ_{2b}
	Nominal	-.2121	.1151	-.6597	.3753	-.2121	.1151	-.6597	.3753
1	- 4.15	-.1449	.1472	-.6620	.3745	-.1456	.1477	-.6640	.3762
	- 8.93	-.1441	.1476	-.6598	.3753	-.1441	.1476	-.6599	.3754
2	-12.91	-.2490	.2145	-.6635	.3657	-.2493	.2147	-.6642	.3666
	5.11	-.2475	.2176	-.6598	.3758	-.2474	.2175	-.6598	.3758
3	-11.29	-.2896	.2022	-.6617	.3755	-.2901	.2019	-.6631	.3748
	10.59	-.2889	.2022	-.6597	.3753	-.2889	.2022	-.6596	.3753
4	-12.14	-.1589	.2081	-.6632	.3674	-.1598	.2094	.6663	.3723
	- 6.95	-.1574	.2106	-.6600	.3757	-.1574	.2105	.6599	.3754
5	- 1.29	-.2279	.1250	-.6589	.3733	-.2279	.1250	-.6589	.3772
	2.14	-.2283	.1244	-.6598	.3753	-.2283	.1244	-.6598	.3753
6	2.22	-.2064	.0976	-.6597	.3753	-.2064	.0976	-.6597	.3753
	- 0.68								
7	- 2.48	-.1721	.1346	-.6663	.3712	-.1723	.1347	-.6670	.3718
	- 5.34	-.1696	.1361	-.6601	.3754	-.1696	.1361	-.6602	.3754
8	- 3.28	-.1553	.1406	-.6625	.3761	-.1558	.1409	-.6639	.3772
	- 7.55	-.1544	.1404	-.6599	.3754	-.1544	.1404	-.6599	.3754
9	- 5.40	-.1693	.1568	-.6608	.3764	-.1697	.1572	-.6619	.3778
	- 5.67	-.1690	.1565	-.6597	.3753	-.1690	.1565	-.6598	.3753
10	- 0.13	-.1657	.1164	-.6666	.3705	-.1660	.1164	-.6673	.3707
	- 6.21	-.1632	.1181	-.6600	.3753	-.1632	.1181	-.6601	.3753
11	0.44	-.2276	.1116	-.6576	.3732	-.2276	.1116	-.6577	.3733
	2.09	-.2283	.1121	-.6598	.3754	-.2283	.1121	-.6598	.3754
12	-10.13	-.2094	.1931	-.6604	.3682	-.2096	.1935	-.6611	.3698
	- 0.26	-.2089	.1953	-.6598	.3756	-.2089	.1952	-.6598	.3755
13	- 1.69	-.2120	.1282	-.6602	.3724	-.2120	.1282	-.6602	.3724
	0.01	-.2188	.1291	-.6598	.3753	-.2118	.1291	-.6598	.3753
14	2.55	-.1347	.0959	-.6641	.3779	-.1354	.0959	-.6658	.3779
	-10.36	-.1332	.0953	-.6599	.3754	-.1333	.0953	-.6600	.3754
15	3.66	-.2614	.1432	-.6595	.3723	-.2616	.1431	-.6580	.3720
	6.71	-.2622	.1440	-.6598	.3753	-.2622	.1441	-.6598	.3753
16	8.10	-.2307	.0519	-.6590	.3770	-.2310	.0523	-.6599	.3786
	2.48	-.2310	.0513	-.6598	.3753	-.2310	.0513	-.6597	.3752

Only the results from the use of the bilinear equations are presented for each of the other three test cases. In every instance, the iteration converged rapidly - frequently converging on the first estimate.

The Aerobee-350, used for the second test case, is a two-stage unguided high-altitude probe which is fired nearly vertical (elevation angles between 2 and 3 degrees). The nominal range and altitude vary between 100 and 150 km and 320 and 400 km, respectively. The results for this test are presented in Table V.

A special Athena trajectory requirement was the subject of the third test case. The nominal elevation angle for this trajectory is 18.534 degrees. This is near, but below, the critical angle of 17.6 degrees. (The critical angle is defined to be the elevation angle which results in maximum horizontal range under no-wind conditions.) The nominal range for this trajectory is 718.6 kilometers while the maximum (no-wind) range is 721.2 kilometers. The nominal impact could not be obtained for wind profiles 7, 8, 10, and 14. It was determined that the maximum range for these profiles was 715.6, 716.4, 715.6, and 713.1 kilometers, respectively. This decrease in maximum range is caused primarily by the increased drag and lift due to a head wind. The results of this test are presented in Table VI.

The final test case was for the BMTS vehicle. This is a two-stage unguided rocket fired at a nominal elevation angle of 30.2 degrees (for the case considered here), resulting in nominal range and altitude of 293 kilometers and 89.4 kilometers, respectively. The nominal elevation angle is considerably below critical angle. The results of this test are presented in Table VII.

CONCLUSIONS. A rapidly converging iterative technique to compute wind-compensated launcher settings for unguided rockets was developed and discussed. This technique is applicable to a wide range of possible trajectory objectives-specified attitude at a given time, space point, specified booster impact, etc.

The procedure consists of two algorithms. The first provides an initial estimate for the launcher setting as a function of the ballistic wind, and as such, it is easily adaptable to field operations. The second algorithm, the iterative step, converges rapidly (one or two passes) to the desired objective.

Sixteen wind profiles were used in four separate test cases to provide an evaluation of the procedure. Two different functional forms for the algorithms were investigated - a quadratic form and a bilinear form. Two specific trajectory objectives were considered in each test case - nominal burnout attitude and nominal impact. In each test, the iteration converged rapidly to the desired objective. There appeared to be no significant difference between the results obtained from the quadratic and bilinear equations.

TABLE V. APPLICATION OF BILINEAR EQUATIONS TO AEROBEE 350

Run	BW_x	BW_y	To Burnout θ_{1L}	To Burnout θ_{2L}	To Burnout θ_{1b}	To Burnout θ_{2b}	To Impact θ_{1L}	To Impact θ_{2L}	To Impact X	To Impact Y
	(mps)		(rad)		(rad)		(rad)		(km)	
	Nominal		.0348	.0065	.0845	.0081	.0348	.0065	- .1	102.0
1	- 4.96	- 9.13	.1108	.0478	.0850	.0078	.1107	.0478	- .5	102.7
2	-14.23	4.86	-.0055	.1251	.0849	.0081	-.0055	.1250	.6	102.3
3	-11.58	10.85	-.0554	.1031	.0837	.0100	-.0553	.1030	2.1	101.0
			-.0551	.1023	.0845	.0081	-.0549	.1022	- .1	102.0
4	-11.99	- 7.49	.0972	.1064	.0855	.0078	.0971	.1063	- .1	102.9
5	- 0.60	1.97	.0184	.0115	.0856	.0082	.0185	.0115	-0.0	103.3
6	2.33	- 0.91	.0424	-.0129	.0841	.0078	.0424	-.0129	- .4	101.7
7	- 2.36	- 6.25	.0868	.0262	.0836	.0073	.0868	.0262	-1.0	101.3
8	- 3.47	- 7.55	.0977	.0354	.0850	.0082	.0976	.0353	- .1	102.9
9	- 5.35	- 5.86	.0837	.0511	.0853	.0085	.0836	.0510	.3	102.9
10	- 0.22	- 6.59	.0997	.0083	.0837	.0075	.0896	.0083	- .7	101.4
11	0.61	1.40	.0232	.0013	.0851	.0075	.0233	.0014	- .6	102.5
12	- 9.78	- 0.23	.0368	.0880	.0849	.0074	.0368	.0879	- .7	102.3
13	- 2.11	- 0.01	.0349	.0241	.0845	.0077	.0349	.0241	- .4	102.0
14	2.15	-10.68	.1237	-.0115	.0845	.0085	.1236	-.0114	.4	102.1
15	- 4.36	- 7.20	-.0250	.0429	.0842	.0075	-.0250	.0428	- .6	101.4
16	9.50	2.75	.0119	-.0726	.0847	.0076	.0119	-.0725	- .9	102.2

TABLE VI. TEST CASE 3, APPLICATION OF BILINEAR EQUATIONS TO LOW ANGLE ATHENA

		To Burnout				To Impact			
Run	B.W.	θ_{1L}	θ_{2L}	θ_{1b}	θ_{2b}	θ_{1L}	θ_{2L}	X	Y
	(mps)	(rad)		(rad)		(rad)		(km)	
	Nominal	-.2871	.1577	-.8818	.5732	-.2871	.1151	325.1	-640.4
1	- 4.23	-.2190	.1912	-.8901	.5723	-.2063	.1844	320.8	-640.7
	- 8.56	-.2158	.1923	-.8823	.5735	-.1985	.1822	324.1	-639.4
2	-11.79	-.3194	.2574	-.8812	.5646	-.3238	.2586	325.5	-643.4
	5.04	-.3193	.2600	-.8820	.5741	-.3309	.2628	325.8	-639.4
3	-11.29	-.3639	.2542	-.8901	.5739	-.3650	.2549	323.9	-643.1
	10.77	-.3607	.2548	-.8815	.5733	-.3693	.2583	325.2	-640.2
4	-11.14	-.2268	.2495	-.8858	.5738	-.2179	.2432	324.2	-644.4
	- 7.05	-.2253	.2497	-.8819	.5733	-.2254	.2485	326.9	-640.9
						-.2283	.2492	325.5	-640.7
5	- 1.52	-.3024	.1705	-.8852	.5759	-.3044	.1716	324.5	-639.9
	2.08								
6	2.17	-.2852	.1385	-.8844	.5716	-.2835	.1377	323.4	-640.7
	- .43					-.2805	.1370	324.9	-640.5
7	- 2.26	-.2527	.1754	-.8842	.5532	Solution does not exist			
	- 4.31	-.2508	.1818	-.8820	.5735				
8	- 3.54	-.2317	.1856	-.8868	.5717	Solution does not exist			
	- 6.96	-.2297	.1865	-.8822	.5734				
9	- 5.49	-.2403	.2023	-.8877	.5801	-.2343	.1986	326.0	-640.1
	- 5.69	-.2384	.2008	-.8821	.5731				
10	.16	-.2470	.1549	-.8840	.5519				
	- 5.23	-.2451	.1617	-.8820	.5733	Solution does not exist			
11	.63	-.2999	.1523	-.8779	.5755	-.3006	.1527	331.3	-641.5
	1.60	-.3015	.1512	-.8820	.5732	-.3109	.1555	324.4	-640.4
12	- 9.37	-.2791	.2359	-.8760	.5640	-.2811	.2358	325.2	-644.7
	- .38	-.2809	.2382	-.8820	.5736	-.2902	.2416	325.5	-640.1
13	- 1.42	-.2865	.1692	-.8806	.5674	-.2872	.1695	324.5	-642.5
	.01	-.2867	.1709	-.8819	.5733	-.2908	.1721	325.2	-640.2
14	2.25	-.2138	.1365	-.8954	.5711	Solution does not exist			
	- 9.71	-.2084	.1385	-.8827	.5733				
15	- 3.36	-.3354	.1868	-.8779	.5707	-.3384	.1887	329.7	-643.3
	6.50	-.3368	.1872	-.8820	.5732	-.3501	.1933	324.4	-639.7
16	8.01	-.3099	.0904	-.8843	.5707	-.3052	.0879	324.9	-640.1
	2.37								

TABLE VII. TEST CASE IV, APPLICATION OF BILINEAR EQUATIONS TO BMTS

Run	B.W.	To Burnout				To Impact			
		θ_{1L}	θ_{2L}	θ_{1b}	θ_{2b}	θ_{1L}	θ_{2L}	X	Y
	(mps)	(rad)		(rad)		(rad)		(km)	
	Nominal	-.3965	.3842	-.6056	.5837	-.3965	.3842	199.2	-215.1
1	- 6.37	-.3580	.4286	-.6153	.5859	-.3543	.4292	198.3	-214.1
	- 6.37	-.3513	.4279	-.6056	.5843				
2	-11.12	-.4301	.4613	-.6231	.5808	-.4371	.4759	198.6	-217.2
	3.56	-.4177	.4650	-.6054	.5858	-.4418	.4845	199.0	-215.1
3	-12.43	-.4900	.4701	-.6293	.5885	-.5052	.4939	197.3	-214.5
	12.12	-.4738	.4688	-.6054	.5854	-.4931	.4848	199.4	-215.4
4	- 8.11	-.3660	.4407	-.6184	.5863	-.3638	.4439	200.1	-216.3
	- 5.41	-.3572	.4399	-.6058	.5846				
5	- 1.88	-.4051	.3972	-.6067	.5853	-.4066	.4001	199.7	-214.9
	1.02								
6	0.56	-.3854	.3804	-.6047	.5831	-.3939	.3784	199.2	-215.2
	- 1.54								
7	- 0.62	-.3894	.3886	-.6031	.5826	-.3886	.3882	199.2	-213.1
	- 1.11					-.3810	.3779	198.7	-214.5
8	- 3.53	-.3688	.4089	-.6095	.5818	-.3659	.4083	198.0	-214.5
	- 4.46								
9	- 4.81	-.3594	.4178	-.6129	.5879	-.3556	.4172	200.0	-215.4
	- 5.97	-.3547	.4154	-.6058	.5839				
10	2.17	-.3819	.3692	-.5968	.5827	-.3795	.3652	200.3	-212.8
	- 1.86	-.3880	.3690	-.6058	.5833	-.3762	.3566	198.5	-214.2
11	2.13	-.3851	.3694	-.6035	.5837	-.3831	.3660	200.5	-216.7
	- 1.40								
12	- 6.63	-.3974	.4303	-.6159	.5813	-.3990	.4364	199.2	-214.0
	- 0.67	-.3900	.4300	-.6057	.5845	-.4061	.4462	199.3	-215.2
13	- 1.69	-.3965	.3959	-.6088	.5821	-.3988	.3977	199.1	-216.1
	0.05								
14	- 0.25	-.3474	.3862	-.6053	.5836	-.3410	.3798	198.1	-213.6
	- 7.18					-.3296	.3686	198.4	-214.1
15	- 1.84	-.4267	.3969	-.6088	.5838	-.4311	.4026	200.7	-216.9
	4.18					-.4453	.4161	199.2	-215.2
16	6.20	-.3931	.3411	-.5975	.5847	-.3913	.3350	199.4	-214.6
	0.25	-.3988	.3396	-.6056	.5834				

BIBLIOGRAPHY

Duncan, Louis D., and Bernard F. Engebos, "Techniques for Computing Launcher Settings for Unguided Rockets," ECOM-5077, Atmospheric Sciences Laboratory, White Sands Missile Range, New Mexico, 1966.

Engebos, Bernard F., and Louis D. Duncan, "A Nomogram for Field Determination of Launcher Angles for Unguided Rockets," ECOM-5088, Atmospheric Sciences Laboratory, White Sands Missile Range, New Mexico, 1966.

Hennigh, Keith E., "Field Wind Weighting and Impact Prediction for Unguided Rockets," NASA, Washington, D. C., 1964.

James, Robert L., Jr., and Ronald J. Harris, "Calculation of Wind Compensation for Launching of Unguided Rockets," Langley Research Center, Langley Field, Virginia, 1960.

Lewis, J. V., "The Effect of Wind and Rotation of the Earth on Unguided Rockets," Ballistic Research Laboratory, Aberdeen Proving Ground, Maryland, 1949.

Walter, Dr. Everett L., "Six-Variable Ballistic Model for a Rocket," MM-445, Missile Meteorology Division, U. S. Army Signal Missile Support Agency, White Sands Missile Range, New Mexico, 1962.

Wilson, G. G., "A Technique for Predicting Nonlinear Wind Compensation of Ballistic Rocket Systems," Sandia Laboratories, Albuquerque, New Mexico, 1967.

APPENDIX A

BALLISTIC WIND WEIGHTING

The technique of wind weighting is the usual method of determining first-order effects of the wind on the trajectory of an unguided rocket. One of the earliest discussions of this procedure was given by Lewis (1949) who also presented a procedure for calculating the information required by the weighting technique. Since Lewis' original paper, many improvements have been made in the trajectory simulation algorithms required to calculate the constants for the wind weighting. A discussion of the algorithms for simulation would require a lengthy discourse of flight dynamics and aerodynamics and will, therefore, be omitted. A partial bibliographical listing of the theoretical development of these algorithms is presented in the references.

This appendix will discuss the techniques, assumptions, and limitations of wind weighting and present the basic procedure for computing the required constants. The availability of a computer simulation program capable of determining the trajectory for a given set of conditions is assumed.

Wind velocity is ordinarily a function of altitude. A wind profile is defined to be the triple $(W_x(z), W_y(z), z)$ where z is altitude and $W_x(z)$, $W_y(z)$ are the x and y components of wind at height z.

Wind weighting is based upon two fundamental concepts - the ballistic wind and the unit wind effect. The ballistic wind is that constant wind (as a function of altitude) which has the same first-order effect on the rocket (trajectory) as the actual wind profile. The unit wind effect is the wind effect of a constant unit wind. A concept closely associated with, and required for the computation of, the ballistic wind is the wind weighting curve. Let f(z) be the wind effect for a wind profile consisting of a uniform unit wind up to altitude z and a zero wind above z. The wind weighting function, g(z), is f(z) divided by the unit wind effect; the graph of g(z) is the wind weighting curve. The derivative $g'(z) = dg(z)/dz$ is the wind weighting factor function.

The ballistic wind is determined from the wind profile by the integrals

$$BW_x = \int W_x(z)g'(z)dz$$

$$BW_y = \int W_y(z)g'(z)dz.$$

In practice the integrals are usually replaced by finite sums. The atmosphere is divided into horizontal strata (wind layers) wherein the wind is assumed constant; the average value over the layer is usually used. If the boundaries of the strata are $z_1 < z_2 < \ldots < z_n$, then the ballistic wind is approximated by

$$BW_x = \sum_{i=1}^{n-1} W_x[g(z_{i+1}) - g(z_i)]$$

$$BW_y = \sum_{i=1}^{n-1} W_y[g(z_{i+1}) - g(z_i)]$$

The value $g(z_{i+1}) - g(z_i)$ is often called the weighting factor or the ballistic factor for the ith layer.

The wind effect is calculated by multiplying the ballistic wind by the unit wind effect. These calculations inately assume

1. The effect of the wind in any particular stratum is directly proportional to the wind in that stratum.

2. The effects of the wind in the various strata are independent.

It is easy to take issue with these assumptions; in fact, one can produce results of trajectory simulations which contradict the assumptions. However, for determining first-order effects, which is the aim of the wind weighting technique, the assumptions are reasonable.

DETERMINATION OF THE WIND WEIGHTING CURVE. In the preceding section, a definition of wind effect was omitted. Such a definition is unnecessary unless one is interested in quantitative results. If one considers the trajectory to be defined by a family of parameters, then wind effect can be broadly defined as the change in these parameters due to the wind encountered along the trajectory. Typical parameters are: first-stage impact, orientation of velocity vector at burnout of a particular stage, etc.

The calculation of the wind weighting function requires the computation of a number of trajectories. Each trajectory simulation is based upon the same set of initial conditions; however, different wind profiles are used for each simulation. These calculations yield a series of values for the trajectory parameters from which one determines the wind weighting function.

There are numerous procedures which can be followed in performing the calculations. The following procedure is somewhat typical and serves as a more precise explanation of the general procedure given above. For simplicity of explanation it will be assumed that one is interested in wind effect on impact (either afterbody or a given booster). Consider altitudes $0 = z_o < z_1 < z_2 < \ldots < z_n$ and, for each $0 \leq i \leq n$, wind profiles P_i where each P_i consists of a zero wind above altitude z_i and a uniform wind (of constant nonzero magnitude, say C, and constant direction) below z_i. (The same value of the wind velocity is used in the nonzero portion of each profile.) Note that P_o is the zero profile; the corresponding trajectory is usually called the no-wind (nominal) trajectory. Let R_i be the range, from launcher to impact, for the simulated trajectory which uses the ith profile. The unit wind effect is

$$\sigma = (R_n - R_o)/C.$$

Specific values for the wind weighting function, g(z), at the points z_i are

$$g(z_i) = (R_i - R_o)/C.$$

Observe that $g(z_o) = 0$ and $g(z_n) = 1$.

The wind weighting curve may be plotted from the values of g(z). Of course, one must choose the z_i's sufficiently dense to describe the graph. The choice of z_n sometimes presents problems. This altitude must be such that any wind effect above z_n can be ignored. Apogee altitude will clearly satisfy this requirement.

TWO-DIMENSIONAL REFINEMENTS. In the general discussion of wind weighting, it was assumed that the weighting factor curve and the unit wind effect were one-dimensional in the sense that the magnitude of the wind effect for the uniform profiles was assumed to be independent of wind direction. This assumption is quite good for near-vertical firings; however, for other cases, the results can sometimes be improved by extending the technique and using separate wind weighting curves and unit wind effects for the x and y wind components. The definitions are similar to those given earlier. The x-unit wind effect, σ_x, is the x-component of the wind effect for a profile with components $W_x = 1$, $W_y = 0$ throughout. For a given altitude, z, let P(z) be the wind profile with components $W_x = 1$, $W_y = 0$ below z and $W_x = W_y = 0$ above z. The wind weighting

function for the x-component, $g_x(z)$, is the wind effect for P(z) divided by σ_x. The functions $g_y(z)$ and σ_y are defined analogously.

The component wind effects and wind weighting curves are calculated similarly to those for the one-dimensional case and will not be explicitly outlined.

ON THE VORTEX SOLUTION FOR THE TURBINE BLADE-FLOW-FIELD, AND CORRELATION WITH OBSERVED PERFORMANCE

F. Edward McDonald and Jacqueline A. Benton
U. S. Army Mobility Equipment Research & Development Center
Fort Belvoir, Virginia

ABSTRACT. Within the present paper, an analytical procedure is developed wherein the classic free vortex flow-theory is applied to prediction of the turbine blade-flow field.... Simultaneously, all required loss factors are developed and correlated with known blade limit-loading parameters, such that turbine stage performance may be predicted with unusual accuracy.

The method, in general, has been experimentally confirmed.

INTRODUCTION. While the present paper primarily deals with a little known application of the free vortex theory to solution of the turbine blade-flow-field, and evaluation of pressure loss therein..., it is also felt that the problems encountered in establishing the end points of a curved orthogonal in the presence of two somewhat different transcendential curves (blade surfaces), may be of some considerable interest..., particularly to those working within the field of internal aerothermodynamics.

Likewise, while several solutions are presently known wherein a numerical value for X_{s1} is determined, for a selected value of X_{p2} (see Figures 4 and 8*)..., thus defining a curved orthogonal simultaneously normal to both blade surfaces..., equation (22) employs a particular solution as derived within Appendix A.

Other solutions may be derived by those interested in the apparently simple, though rather complex simultaneous requirements.

The major advantages of the present analytical procedures, however, are found in the facts that...

1. The free vortex theory is successfully translated into the blade channel flow-plane, in such manner that both the maximum and minimum blade-surface velocities are readily determined, along with the associated diffusion parameters,

2. That pressure loss, associated with the diffusion concept, is successfully correlated with actual pressure loss across a blade row,

3. And that turbine stage efficiency is analytically predicted with unusual accuracy.

*Figures and Nomenclature can be found at the end of this article. The remainder of this paper has been reproduced photographically from the author's copy.

I TURBINE BLADE FLOW-FIELD CONSIDERATIONS:

Much has been written on the nature of the turbine blade-flow-field, and probable velocity distribution within blade flow-channels, however, an exact correlation of actual flow distribution with theory has been very difficult, if not impossible. While the flow-field can be readily determined with a static blade cascade, instrumentation physically small enough to make the desired measurements in actual turbine rotors, with little or no flow disturbance, can not tolerate the very high dynamic forces nor the high stream velocities at which these measurements would be desired. Therefore, of necessity, several analytical methods were devised, some of which afforded excellent prediction in terms of the flow-field effect on pressure loss across a blade row.

Those analytical methods of particular value may be identified as the stream filament method of reference (1), the constant curvature and vortex methods of reference (2), and the vortex method of reference (3) through (5).

The stream filament method of reference (1) assumes a blade mean camber line, super-imposes a blade foil section thereon, computes velocity and flow along streamlines and across orthogonals, and modifies the blade section until desired flow and local critical velocity ratios are achieved.....The two methods of reference (2) assumes the suction surface, computes the streamline and orthogonal flow, and defines the required adjacent pressure surface, iterating until the desired critical velocity ratio patterns are achieved.

On the other hand, the vortex method of reference (3) through (5) uniquely employs the free vortex concept, recognizes Euler's postulations regarding

behavior of the fluid particle in free rotational motion, and either analyzes an existing blade or predicts performance of a new design.

II FREE VORTEX THEORY TRANSLATED INTO BLADE CHANNEL FLOW:

Figure 1 is now considered in order to discuss the internal aerothermodynamics of rotational flow within the annuli.

Within Figure 1 a turbine stator is utilized for demonstration purposes. In view (a) we are looking upstream, therefore the flow is coming up out of the paper. Let it also be agreed that the axial velocity component V_z is numerically constant from root to tip.

It will also be noted that, since both the circles defining blade height (i.e., root and tip) are truly concentric, then a flow orthogonal l_o will be a straight line as shown.

Now classic free vortex theory states that when fluid rotation is simultaneously present, and when the flow is "left to its own devices" so to speak, it will of its own accord assume a tangential velocity distribution from root to tip, such that a static pressure gradient will be established between the inner and outer boundaries. This static pressure gradient will obey the law

$$\frac{dP}{dr} = \frac{\rho}{g} \cdot \frac{V_{tan}^2}{r} \qquad (1)$$

with the net result that the centrifugal force of a particle mass dm, will

everywhere be balanced by an equal and opposite centripetal force generated by the static pressure gradient dP, such that the fluid particle will essentially remain at a constant radii dr as it passes through the machine.

Referring now to Figure 2 (a).....The velocity diagram associated with Figure 1 is shown for a particular axial velocity component V_z.

Upon considering Figure 2 (a) one can theorize that, should the axial component V_z be reduced to zero, while the whirl or tangential components are still present, then the tangential components will again so arrange themselves that the requirements of equation (1) will again be satisfied, thus producing Figure 2 (b).

This is indeed the case, and is readily observed by the classic "barnyard" experiment of setting water into free rotational motion in the kitchen sink..... Upon allowing time for flow stabilization, and upon dropping small bits of cork into the water at various radii, it will be observed that the requirements of equation (1) are essentially satisfied. That is to say, considerably higher tangential velocity will be observed at small radii, as compared with reduced tangential velocity at larger radii.....Thus the arrangement of the tangential velocity components of Figure 2 (b) is easily confirmed. (It should be observed, however, that a flow must also exist.....i.e., the sink plug must be removed..... as otherwise a "wheel" type rotation will ultimately result.)

Referring now to Figure 3.....The outer circle or tip boundary of the annulus has now been enlarged and offset in such manner that the origin of r_2 no longer coincides with that of r_1. It will also be noted that a curved orthogonal is now generated, which orthogonal is simultaneously exactly normal to both the inner and outer boundaries at, respectively, r_1 and r_2.....Here, again, we can theorize that if the free vortex concept also holds over the

length of a curved orthogonal, then a velocity distribution must also exist such that the static pressure gradient will tend to satisfy the requirements of equation (1).

Again, a simple experiment with water flowing in a curved channel, has demonstrated the validity of the foregoing concept.

III DETERMINATION OF BLADE SURFACE VELOCITIES:

When we consider a segment of Figure 3, between limits A-A and B-B, we simultaneously generate one passage of the turbine blade row of Figure 4 in all its essential details.

Now from classic free vortex theory, exemplified by equation (1) repeated here,

$$\frac{dP}{dr} = \frac{\rho}{g} \frac{V_{tan}^2}{r} \qquad (1)$$

from which we may write,

$$\frac{dP}{\rho} = \frac{V_{tan}^2}{g} \frac{dr}{r} \qquad (2)$$

Also, from Euler's relations governing motion of a fluid particle in free rotation, we can write

$$\frac{dP}{\rho} + \frac{V\,dV}{g} = 0 \qquad (3)$$

From consideration of (2) and (3), we can arrive at

$$\frac{dV}{V} = -\frac{dr}{r} \qquad (4)$$

Now since the boundary surfaces will always be known (i.e., equations defining the blade surfaces and spacing), we can write and solve the definite integrals

$$\int_{r_1}^{r_2} \frac{dV}{V} = -\int_{r_1}^{r_2} \frac{dr}{r} \qquad (5)$$

from which it is obvious that

$$\log_e V_2 + \log_e r_2 = \log_e V_1 + \log_e r_1 \qquad (6)$$

therefore

$$V_2\, r_2 = V_1\, r_1 = C = \text{a constant} \qquad (7)$$

which, upon inserting numerical values and complying with the continuity equation (9), exactly satisfies the ultimate intentions of equation (1).

Now the mean channel velocity V_m will always be known for any orthogonal within the blade channel, at any particular wheel radius, since it is obvious that

$$V_m = \left\{ \left[1 - \left(\frac{l_o - l_2}{l_o' - l_2} \right) \right] (V_2 - V_o) \right\} + V_o \qquad (8)$$

when the blade row is treated as a nozzle.

This is true for any particular wheel radius, since relative inlet velocity V_o and upstream pseudo-orthogonal length l_o', flow, temperature, pressure, and exit orthogonal length l_2 and velocity V_2.....are completely known upon first establishing a design.

Therefore any change in orthogonal length dl, at constant wheel radius dr, has the same effect as an area change within a nozzle dA.....where the requirements of continuity are simultaneously satisfied.....i.e., where

$$\frac{W}{A} \equiv \rho V \qquad (9)$$

From (6) and (7) the mean channel velocity at the mid point of any given orthogonal, at any wheel radius, can be written as

$$V_m = \frac{1}{(r_2 - r_1)} \int_{r_1}^{r_2} V \, dr \qquad (10)$$

or, in terms of channel radii or radius ratio,

$$V_m = \frac{1}{(r_2 - r_1)} \int_{r_1}^{r_2} C \frac{dr}{r} \qquad (11)$$

which, upon integration, yields

$$V_m = \frac{C \log_e \frac{r_2}{r_1}}{r_2 - r_1} \qquad (12)$$

Now for the <u>suction surface velocity</u> at that point where a given orthogonal is normal to the suction surface, and utilizing equation (12)

$$V_m = \frac{V_1 r_1 \log_e \frac{r_2}{r_1}}{r_2 - r_1} \qquad (13)$$

and dividing through by r_1

$$V_m = \frac{V_1 \log_e \frac{r_2}{r_1}}{\frac{r_2}{r_1} - 1} \qquad (14)$$

$$\therefore V_1 = V_m \frac{\frac{r_2}{r_1} - 1}{\log_e \frac{r_2}{r_1}} \qquad (15)$$

Likewise, for the pressure surface velocity at that point where the same orthogonal is normal to the pressure surface, again from (12),

$$V_m = \frac{V_2 \, r_2 \, \log_e \frac{r_2}{r_1}}{r_2 - r_1} \tag{16}$$

and dividing through this time by r_2

$$V_m = \frac{V_2 \, \log_e \frac{r_2}{r_1}}{1 - \frac{r_1}{r_2}} \tag{17}$$

$$\therefore \; V_2 = V_m \frac{1 - \frac{r_1}{r_2}}{\log_e \frac{r_2}{r_1}} \tag{18}$$

Referring now to Figure 4.....In order to solve equations (15) and (18), however, it is obvious that two prior solutions must be available.....i.e., a solution for the radii r_1 and r_2.....and a solution for mean channel velocity Vm.

Now at the time a given design is established, two equations defining the blade snape are also determined in terms of

$$Y_{s...p} = f(X)_{s...p} \tag{19}$$

Also, since blade spacing S is assigned at design time, then location of a point P_2 on the adjacent blade is found by

$$Y_{p2} = f(X)_{p1} + S \tag{20}$$

and for point S_1 on the first blade

$$Y_{s1} = f(X)_{s1} \tag{21}$$

therefore the absolute location of both points can be established.

It will be observed, however, that for a particular numerical value for X_{p_2}.....there is one and only one numerical value for X_{s_1} which, considered simultaneously, will define those points on both blade surfaces where the smallest possible circle will be exactly tangent thereto.

Thus with a given numerical value for X_{p_2}, the required X_{s_1} value is found by setting

$$F(\hat{X}) = 0 \tag{22}$$

and instructing the computer to iterate on X_{s_1} until equation (22) is satisfied .....See Appendix A for a particular derivation of F(X).

Thereafter, since both functions of equation (19) are known, the two required radii are simply

$$r_{1\ldots2} = \frac{\left\{ 1 + \left[f'(X) \right]^2_{s\ldots p} \right\}^{3/2}}{f''(X)_{s\ldots p}} \qquad (23)$$

For the mean channel velocity V_m, however, a solution for the orthogonal length l_o must first be found for the two compatible points P_2 and S_1.

Referring now to Figure 8.....It will be noted that upon solution of equation (22), radius r_o (or r_o') of the inscribed circle can be found by the methods given in Appendix A. Thereafter, again with simple trigonometry, the cosin of 1/2 angle Z is readily found.

Then by the Huygenian solution, the required orthogonal length is found by

$$l_o = \frac{1}{3} \left\{ \left[8 \sqrt{2\ r_o \left(r_o \cos \frac{Z}{2} \right)} \right] - C_h \right\} \qquad (24)$$

With l_o known (and with V_o, V_2, l_o' and l_2 determined at design time) V_m is determined by equation (8), and the local surface velocities by solution of equations (15) and (18).

It follows, therefore, that free vortex flow-theory has now been translated into the coordinate system of the turbine blade flow-channel, such that any local velocity may be determined for any streamline, or on either blade surface, and at the location of any desired orthogonal..... as required.

Particular attention is directed to the fact, however, that in subsequent correlation of blade loss with overall stage efficiency.....it is only necessary to determine the minimum pressure surface and maximum suction surface velocities .....for subsequent evaluation of the required diffusion parameters.

Thus the computer is instructed to determine and readout $V_{s\ max}$ and $V_{p\ min}$.

IV INTRODUCING THE NACA DIFFUSION PARAMETER:

A very considerable amount of highly satisfactory basic turbomachine research was carried out by NACA (circa 1948-58), a small portion of which resulted in development of a limiting blade-loading parameter known as the diffusion factor.

Originally, their diffusion factor was applicable only to compressor blade elements and was defined by equation (13), of reference (6), repeated here in reference (6) terminology,

$$D = \left(1 - \frac{V_2}{V_1}\right) + \frac{\Delta V_\theta}{2\sigma V_1} \qquad (25)$$

where V_1, V_2, ΔV_θ and σ are, respectively, inlet and exit velocity, tangential velocity change, and blade solidity defined by blade chord over spacing at mean blade height.

Later, the diffusion factor concept was extended to turbine design and, while application was restricted to the blade suction surface alone.....experimental results and correlation with actual stage loss were highly satisfactory. For instance, see Figure 10 of reference (10). Reference (7) is also representative of a portion of this work.

For turbines, considering the blade suction surfaces only, NACA defined this parameter by

$$D_s = \frac{V_{s\ max} - V_2}{V_{s\ max}} \tag{26}$$

Still later, as shown for instance in references (4), (5) and (8), application of the diffusion factor concept was extended to include the effect of <u>both</u> blade surfaces.....i.e., both the suction and pressure surfaces.

Thus the final diffusion parameter is defined as the sum of both the suction and pressure surface factors where.....for the suction surface

$$D_s = \frac{V_{s\ max} - V_2}{V_{s\ max}} \tag{27}$$

$$= 1 - \frac{V_2}{V_{s\ max}} \tag{28}$$

and for the pressure surface

$$D_p = \frac{V_1 - V_{p\,min}}{V_1} \tag{29}$$

$$= 1 - \frac{V_{p\,min}}{V_1} \tag{30}$$

and finally

$$D = \sum D_s + D_p \tag{31}$$

Upon referring to Figure 5, the inter-relation of these diffusion factors with blade surface velocities will be observed.

V INTRODUCING THE PRESSURE LOSS PARAMETER:

While it apparently is not widely known, examination of large quantities of good two dimensional cascade test data will confirm the fact that total pressure loss across a cascade can be exactly defined by

$$\Delta P'_{loss} = L' \left[\frac{2(\bar{\gamma} - 1)}{\bar{\gamma}} \right] \left(\frac{1}{2} \rho V^2 \right) \tag{32}$$

for a given operating condition.....where the term ($\rho V^2/2$) defines the average dynamic head across a given cascade.....expecially so where the inlet incidence angle approaches zero (equivalent design point operating conditions), and where L' is a constant, the numerical value of which experimentally satisfies equation (32).

Reference (9), working with the known validity of equation (32), derived the "a-b" functions based on the local fluid static-to-total pressure ratios, where the "a" function considers the effect of blade inlet velocity while the "b" function considers the effect of blade exit velocity.

Thus as derived in reference (9) (in nomenclature of the present paper),

$$a = 1 - L'\left\{\left(\frac{P}{P'}\right)^{1/\bar{\gamma}}\left[1 - \left(\frac{P}{P'}\right)^{(\bar{\gamma}-1)/\bar{\gamma}}\right]\right\}_{\text{inlet}} \qquad (33)$$

and

$$b = 1 + L'\left\{\left(\frac{P}{P'}\right)^{1/\bar{\gamma}}\left[1 - \left(\frac{P}{P'}\right)^{(\bar{\gamma}-1)/\bar{\gamma}}\right]\right\}_{\text{exit}} \qquad (34)$$

Now reference (4), among other considerations, suggested that the "a-b" functions could be employed within a nozzle flow function, such that the rather vague discharge coefficient could be eliminated.....Thereafter any blade row could then be treated as a nozzle, and mass flow determined by

$$W = \frac{D_c \; K \; A_{th} \; f(\delta^*) \; P_1' \; a}{\sqrt{T_1'} \; b} \qquad (35)$$

wherein W, D_c, A_{th}, $f(\delta^*)$, P_1' and T_1' are, respectively; mass flow rate, a dimensional constant converting pressure to psfa, total blade throat area, throat area correction due to displacement boundary layer thickness, total inlet pressure, and total inlet temperature.....a and b as before.....while K is a restriction factor (incorporating the ψ function) defined by

$$K = \sqrt{\frac{2g}{R}\left(\frac{\bar{\gamma}}{\bar{\gamma}-1}\right)\left[\left(\frac{P_2}{P_1'}\right)^{2/\bar{\gamma}} - \left(\frac{P_2}{P_1'}\right)^{(\bar{\gamma}+1)/\bar{\gamma}}\right]} \qquad (36)$$

for <u>subsonic</u> throat velocity which, for <u>sonic</u> throat velocity, reduces to

$$K_{max} = \sqrt{\frac{2g}{R}\left(\frac{\bar{\gamma}}{\bar{\gamma}+1}\right)\left(\frac{2}{\bar{\gamma}+1}\right)^{2/(\bar{\gamma}-1)}} \qquad (37)$$

Likewise, reference (4) also suggested that if the "a-b" functions were valid (equations 33 and 34), in consideration of the known validity of equation (32), then the term L' (in equations 33 and 34) could probably be

correlated with the NACA diffusion factors D_s, D_p.....and that a correlation might be established between these factors and overall stage efficiency.

This subsequently proved to be the case since, upon inspection of equations (32), (33) and (34).....it will be noted that

$$P'_1 \; a = P'_2 \; b \tag{38}$$

$$\therefore \quad P'_2 = P'_1 \; \frac{a}{b} \tag{39}$$

from which it is also observed that

$$\Delta P'_{loss} = P'_1 \left(1 - \frac{a}{b} \right) \tag{40}$$

which exactly satisfies equation (32).

Thereafter the computer could be instructed to select various numerical values of L' for insertion into the "a-b" functions, to determine the diffusion factors from blade channel analysis, and to finally arrive at a correlation of the pressure losses with L' (see next section).....then to iterate on L' selection until <u>computed</u> values equalled <u>selected</u> values.....thus defining pressure loss and stage efficiency.

In general, pressure loss is usually computed and reported in terms of $\bar{\omega}$ where, for two dimensional loss

$$\bar{\omega}_{2d} = \frac{P_1' - P_2'}{P_1' - P_2} \tag{41}$$

and for three dimensional effects

$$\bar{\omega}_{3d} = \bar{\omega}_{2d} \left[1 + \left(\frac{\cos \varphi}{\sigma_m \, AR} \right) \right] \tag{42}$$

The reference (5) work experimentally confirmed the reference (4) postulations, and provided test results from which apparently accurate numerical correlations were derived.

The various correlation procedures may now be demonstrated.

VI THE VARIOUS CORRELATIONS:

During the earlier NACA research work with the blade diffusion parameter, and considering only the blade suction-surface diffusion factor D_s (see equation (26)),it was found that a remarkably close and completely reproducible correlation existed between D_s, overall stage efficiency η_t, and mean blade solidity σ_m .....where

$$L = f(D_s) = \frac{(1 - \eta_t)}{\sigma_m} \qquad (43)$$

(See, for instance, Figure 10 in reference (10).)

The function $f(D_s)$ in equation (43) is not given here, since more useful correlations were subsequently found.

Further NACA research work, with six different transonic turbine designs, also developed the fact that the <u>total</u> diffusion factor (see equation (31) this paper) could also be correlated with stage efficiency, etc., in accordance with

$$L = f(D) = \frac{(1 - \eta_t)}{\sigma_m} \qquad (44)$$

(See Figure 11 in reference (10).)

Here again, the function f(D) in (44) is not given for the following reasons.....

While the NACA work was carried out with six different transonic turbines, the variations between designs were apparently such as to get several answers in addition to diffusion effects.

The work of reference (4) and (5), on the other hand, was carried out with four transonic turbine variations, which variations were so arranged

that these correlations would be either confirmed or denied with greater assurance.

This work, i.e., reference (4) and (5), very definitely confirmed the NACA work, and extended the scope of these correlations to the point that

$$L_{NACA} = \left(\frac{D}{10}\right)^{.905} = \frac{(1 - \eta_t)}{\sigma_m} \qquad (45)$$

It was also found that these correlations were equally applicable to both stators and rotors and.....significantly.....that the loss factors L' in the "a-b" functions (see equations 33 and 34) would also correlate with diffusion factor, overall stage efficiency, and mean radius blade solidity .....for both stators and rotors.....Thus, for rotors

$$L' = \sqrt[n]{\left(\frac{D}{10}\right)^{.905}} \qquad (46)$$

$$= \sqrt[n]{\frac{(1 - \eta_{stage})}{\sigma_{m\ rotor}}} \qquad (47)$$

and for stators

$$L' = \sqrt[n']{\left(\frac{D}{10}\right)^{.905}} \tag{48}$$

$$= \sqrt[n']{\frac{(1 - \eta_{\text{stage}})}{\sigma_m \text{ stator}}} \tag{49}$$

where for rotors

$$n = 2 = \text{constant} \tag{50}$$

and for stators

$$n' = 3/2 = \text{constant} \tag{51}$$

This correlation is shown in Figure 6 of the present paper.

Note that while the slope of this curve (Figure 6) is slightly greater than that of Figure 11 in reference (10), it will be recalled that blade design variations of the reference (4) and (5) turbines were such as to specifically confirm or deny the validity of this design approach.

The question as to why the numerical value of n and n' remains approximately constant from one basic turbine design to another, is not presently known with certainty.....However, it is conceivable that the effect of blade tip leakage and increased "corner" loss from boundary layer interference, within rotors, may generate the larger n value.

It is apparent, however, that with the foregoing correlations experimentally determined from ten different transonic turbines, and as further

confirmed by additional high-subsonic machines not referenced here.....it follows that overall turbine stage design point efficiency can be predicted within one percent, or less. Thus performance of true state-of-the-art machines can be predicted with greater assurance.

VII SOME EXPERIMENTAL RESULTS AND CONCLUSIONS:

To discuss the exceedingly high performance or work output achieved by these advanced turbines, it will first be necessary to define a turbine work parameter.

One of the most useful turbine work parameters, first proposed we believe by NACA, may be defined as

$$\frac{\Delta H_t}{\theta_{cr}^2} \tag{52}$$

where ΔH_t equals actual total-to-total turbine work in BTU/lb flow, and θcr^2 is equal to a critical velocity ratio squared. Thus,

$$\theta_{cr}^2 = \left(\frac{V_{cr}}{V_{cr}^*}\right)^2 \tag{53}$$

where V_{cr} is taken with instantaneous values of γ and T at true turbine inlet

temperature, while V_{cr}^* is taken with similar instantaneous values at some base or reference temperature, usually at 518.4°R.

Thus, defining

$$V_{cr} = \sqrt{\frac{2\gamma}{\gamma+1} g R T_1'} \tag{54}$$

and

$$V_{cr}^* = \sqrt{\frac{2\gamma}{\gamma+1} g R 518.4} \tag{55}$$

(Note that the critical velocity V_{cr} can not be attained in actual practice.....It is a reference velocity widely employed in turbine aerothermodynamics.)

Particular attention is directed to the fact that, in terms of the work output parameter defined by equation (52), the six NACA turbines provided numerical design point work outputs ranging from a phenomenal 20 to 23 +.

This work,in general, is covered by references (7), (8), and (10) through (14).

The reference (4) and (5) work with four super-performance turbines, carried out by the senior author of this paper, provided similar and yet higher work outputs.....One of these machines, at a tip speed of 1300ft/sec, turbine inlet temperature of 1960°R, with a rotor root relative inlet Mach Number slightly greater than 1.0, an absolute root gas turning angle of 108

degrees, a total-to-total efficiency of .875 where 100% is taken as 1.0; achieved the phenomenal work output of 25 +.

This work is summarized in reference (4)[1] and (5)[1].

It may also be of some considerable interest to note that the entirely reproducible work output from these ten different super-performance turbines, at their normal long-life design points.....achieved between 11 and 20 years ago.....is still approximately twice that (100% greater) of any presently available commercial machines known to the writers.

In regards to the validity of the four analytical methods discussed herein, as compared with a widely employed relaxation method for determination of blade loss, particular attention is now directed to Figure 7.

In Figure 7, predicted turbine blade loss for a particular stage, of a 32,000 HP closed Brayton cycle machine, is shown in terms of $\bar{\omega}$ versus percent blade height.....where mass-averaged two dimensional pressure loss is taken as

$$\bar{\omega}_{2d} = \frac{P_1' - P_2'}{P_1' - P_2} \qquad (41)$$

The upper solid line is the computer readout of blade loss as predicted by the present method.....the hatched area indicates loss prediction of the three NACA methods, reference (1) and (2) (note the close agreement).....while the dashed line is the computer readout blade loss as determined by the relaxation method.....

---

(1) at Fairchild Engine Division (formally Ranger Aircraft Engine)

Subsequently, scale models of the first two stages were built from this design, and rigorously tested.....Both stages, it may be observed, ran almost exactly in accordance with the heavy solid line (slightly within the hatched area), wherein total-to-total efficiency was predicted within less then 1%.

From the foregoing, as now considered from eleven different turbine designs, it can only be concluded that:

(1) Turbine blade loss apparently tends to confirm predictions made by the vortex approach, and

(2) Turbine designs can now be evolved, wherein the design point can be established much closer to true state-of-the-art performance, with solid assurance.

NOMENCLATURE

Symbol:	Entity:	Units:
A	Area in general	ft^2
AP	Blade aspect ratio	height/chord
a	Loss function, see equation (33)	
b	Loss function, see equation (34)	
C	A constant	
C_h	Chord length	inches
D	Total diffusion factor	
D_c	Dimensional constant	
D_p	Diffusion factor, pressure surface	
D_s	Diffusion factor, suction surface	
d	Derivative	
$f(\delta^*)$	Displacement boundary layer thickness	ft
g	Gravitational acceleration constant	32.174 ft/sec^2
ΔH_t	Total-to-total turbine work	BTU/lb
K	A flow function, see equation (36)	
K_{max}	Maximum possible value for K	
L	Loss factor in general, see equations (43)	
L_{NACA}	NACA loss factor, see equation (45)	
L'	Loss factor, present paper, see equation (46)	
l_o	Orthogonal length in general	inches
l_o'	Upstream pseudo-orthogonal length	inches
n	A constant, see equation (46)	
n'	A constant, see equation (48)	
P	Pressure	psfa

NOMENCLATURE

Symbol:	Entity:	Units:
R	Gas constant	ft-lbs/lb°R
r	Radius in general	inches
r_o	Radius, see Figure 8	
r'_o	Radius, see Figure 8	
S	Blade spacing	inches
T	Temperature	°R
V	Velocity	ft/sec
W	Working fluid flow rate	lbs/sec
X	Dimension from base ordinate	inches
Y	Dimension from base abscissa	inches
Z	Orthogonal included angle	degrees
	Greek:	
γ	Angle	degrees
γ	Specific heat ratio	cp/cv
η	Efficiency	percent x 10^{-2}
ρ	Density	lbs/ft^3
σ	Blade solidity	chord/spacing
φ	Blade stagger angle	degrees
ω	Pressure loss coefficient	

NOMENCLATURE

Symbol:	Primes:	Units:
'	Prime = total conditions	
*	Star = base or reference condition	
‾	Bar = mean integrated or mass averaged value	
	Subs:	
1	First effect or station or blade suction surface	
2	Second effect or station or blade pressure surface	
2d	Two dimensional	
3d	Three dimensional	
cr	Critical value	
m	Mean	
max	Maximum	
min	Minimum	
o	Orthogonal	
p	Pressure surface	
s	Suction surface	
t	Turbine	
tan	Tangential direction	
z	Relative to orthogonal angle, see Figure 8	

REFERENCE

(1) Hupert, M. C., and MacGregor, C:
Comparison between predicted and observed performance of gas turbine stator blades designed for free vortex flow.
NACA, TN-1810, 1949

(2) Alpert, S:
Design methods for two dimensional channels.....for high solidity cascades.
NACA, TN-1931, 1949.

(3) McDonald, F. Edward:
Probable vortex flow-fields within bladed turbomachines.
Lloyd-Rogers Co., USNTS report R-4, 1943.

(4) McDonald, F. Edward:
Analytical definition of the blade flow-field by the vortex approach.
Fairchild Engine Division, R&D E-461, July 1954

(5) McDonald, F. Edward:
Performance evaluation of a high work output transonic turbine incorporating blades designed in accordance with the vortex flow-field.
Fairchild Engine Division, R&D E-600, May 1956.

(6) Lieblein, S., Schwenk, F. C., and Broderick, R. L:
Diffusion factor for estimating losses and limiting blade loadings in axial-flow-compressor blade elements.
NACA, RM E53D01, 8 June 1953.

(7) Whitney, W. J., Monroe, D. E., and Wong, R. Y:
Investigation of transonic turbine designed for zero diffusion on suction-surface velocity.
NACA, RM E54F23, 24 August 1954.

(8) Hauser, C. H., and Nusbaum, W. J:
Experimental investigation of a high subsonic Mach number turbine having low rotor suction-surface diffusion.
NACA, RM E56G25, 10 October 1956.

(9) Kochendorfer, F. D., and Nettles, J. C:
An analytical method of estimating turbine performance.
NACA TR-930, 1949.

REFERENCE

(10) Miser, J. W., Stewart, W. L., and Monroe, D. E:
Effect of high rotor pressure-surface diffusion on performance of a transonic turbine.
NACA, RM E55H29a, 3 November 1955.

(11) Stewart, W. L., Wong, R. Y., and Evans, D. G:
Design and experimental investigation of a transonic turbine with slight negative reaction across rotor hub.
NACA, RM E53L29a, 12 March 1954.

(12) Wong, R. Y., Monroe, D. E., and Wintucky, W. T:
Investigation of effect of increased diffusion of rotor-blade suction-surface velocity on performance of transonic turbine.
NACA, RM E54F03, 24 August 1954.

(13) Whitney, W. J., Wong, R. Y., and Monroe, D. E:
Investigation of a transonic turbine designed for a maximum rotor-blade suction-surface relative Mach number of 1.57.
NACA, RM E54G27, 11 October 1954.

(14) Whitney, W. J., Stewart, W. L., and Wong, R. Y:
Effect of reduced stator-blade trailing-edge thickness on overall performance of a transonic turbine.
NACA, RM E55H17, 1955.

APPENDIX A

by: Mrs. Jacqueline A. Benton

DERIVATION OF F(X) = 0:

In deriving equation (22) where it is required that F(X) = 0, reference is now made to Figure 8. Note that the blade surface curves have been distorted to some considerable extent, particularly for the suction surface, in order to more clearly demonstrate orthogonal geometry.

It will also be observed that for a particular numerical value of X_{p2}, there is one and only one X_{s_1} value which, simultaneously, will define those points where the smallest possible circle is exactly tangent to both blade surfaces, at P_2 and S_1.....This requirement for the smallest possible circle is absolute since then, and then only, the points of tangency will also define the end points of an orthogonal simultaneously normal to both blade surfaces.

Under these conditions r_o will exactly equal r_o', and the center of this circle will occur at the intersection of both r_1 (extended) and r_2.....Also, the tangents of P_2 and S_1 will always intersect, since the turbine blade passage is always converging within the area of interest, thus defining $r_{z1...2}$ and the angle Z.

Upon bisecting the angle Z, the line of bisection will simultaneously pass through the intersection of $r_{z1...2}$, $r_{1...2}$, and the center of the inscribed circle when, and only when, point S_1 is correctly located in relation to a given point P_2.

As is the case with complex geometric problems, several possible solutions can usually be found.

In the present case for instance, a particular solution may now be deduced without laying pencil to paper.....

Now with the knowledge that any tangent to either blade surface is taken in relation to a horizontal base line, rotate a line about S_1 (from the horizontal) in an amount equal to the angle γ .....thus producing a line passing through S_1 and parallel to the line bisecting angle Z.

The radius r_{z1} is then one diagonal of a rectangle.....Then with the geometric law of complimentary or mirror image angles, one can immediately write

$$\tan\ (S_1 - \gamma) \equiv \tan \frac{1}{2} Z \qquad (A - 1)$$

when, and only when, point S_1 is correctly located in relation to P_2.....in accordance with the foregoing requirements.

GEOMETRIC PROOF:

Referring to Figure 8.....Let $Y_s = f(X)_s$ and $Y_p = f(X)_p$ represent the equations of the blade suction and pressure surfaces, respectively.....Also,

let S equal the dimensional spacing between two adjacent blades.

Now choose a point P_2 (X_{p2}, Y_{p2}) on the pressure surface of the adjacent blade, where

$$X_{p2} = X_{p1} \qquad (A - 2)$$

$$Y_{p2} = Y_{p1} + S \qquad (A - 3)$$

$$\tan P_2 = f'(X)_p \qquad (A - 4)$$

Let S_1 (X_{s1}, g) be the desired point on the suction surface of the first blade, where

$$g = f(X)_s \qquad (A - 5)$$

$$g' = f'(X)_s \qquad (A - 6)$$

Now with the first derivatives of the known equations defining the suction and pressure surfaces either or both tangents (i.e., radii $r_{z1...2}$) and their point of intersection can be readily found. Also, since

$$\tan Z = \frac{g' - \tan P_2}{1 + g' \cdot \tan P_2} \qquad (A - 7)$$

then

$$\cos Z = \frac{1}{\sqrt{1 + \tan^2 Z}} \qquad (A - 8)$$

$$\tan \frac{Z}{2} = \sqrt{\frac{(1 - \cos Z)}{(1 + \cos Z)}} \qquad (A - 9)$$

If we now drop a vertical from P_2 to a horizontal line containing S_1, the tangent of angle γ between this vertical and chord C_h is then

$$\tan \gamma = \frac{(X_{s1} - X_{p2})}{(Y_{p2} - Y_{s1})} \qquad (A - 10)$$

Now since tan S_1 equals g', then

$$\tan (S_1 - \gamma) = \frac{g' (Y_{p2} - Y_{s1}) - (X_{s1} - X_{p2})}{(Y_{p2} - Y_{s1}) + g' (X_{s1} - X_{p2})} \qquad (A - 11)$$

Therefore, when point S_1 is correctly chosen in relation to P_2,

$$\tan (S_1 - \gamma) \equiv \tan \frac{Z}{2} \qquad (A - 12)$$

Thus an expression has been derived such that equation (22) can be satisfied by setting

$$F(X) = 0 = \tan \frac{Z}{2} - \tan (S_1 - \gamma) \qquad (A - 13)$$

Thereafter, in numerical computation, any point S_1 can be found relative to any point P_2, by iterating on X_{s1} until $F(X) = 0$.

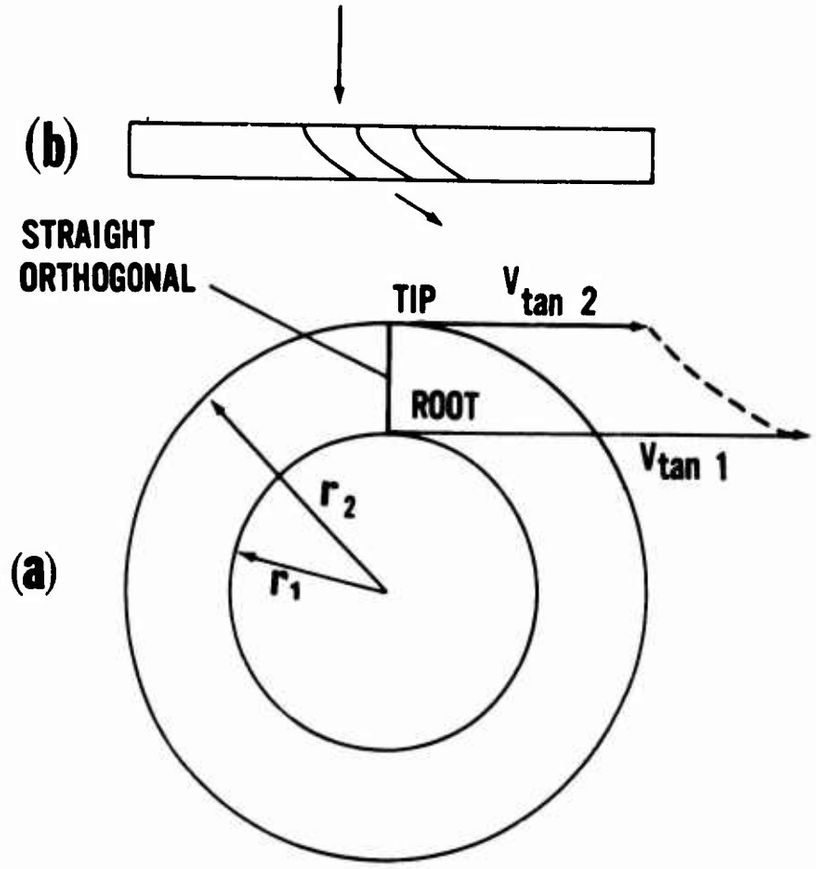


FIG. 1 STATOR EXIT VORTEX FLOW

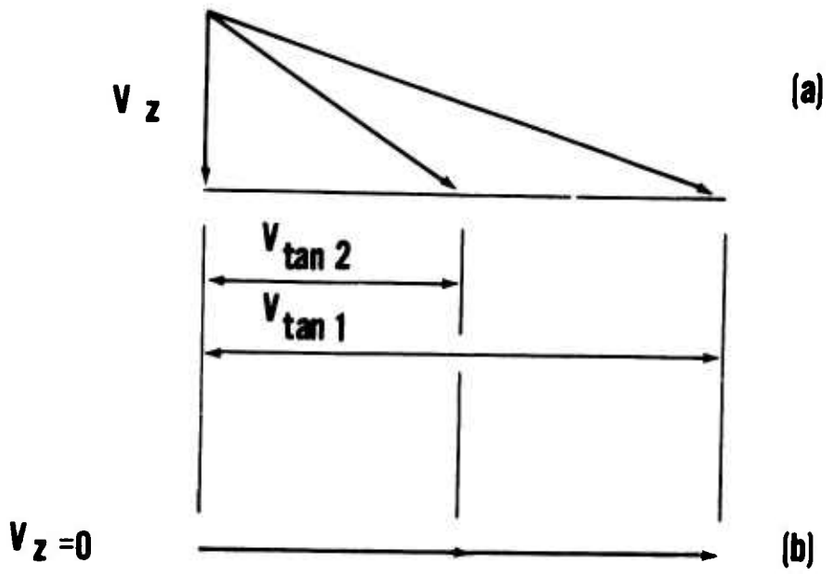


FIG. 2 EQUIVALENT VELOCITY DIAGRAMS

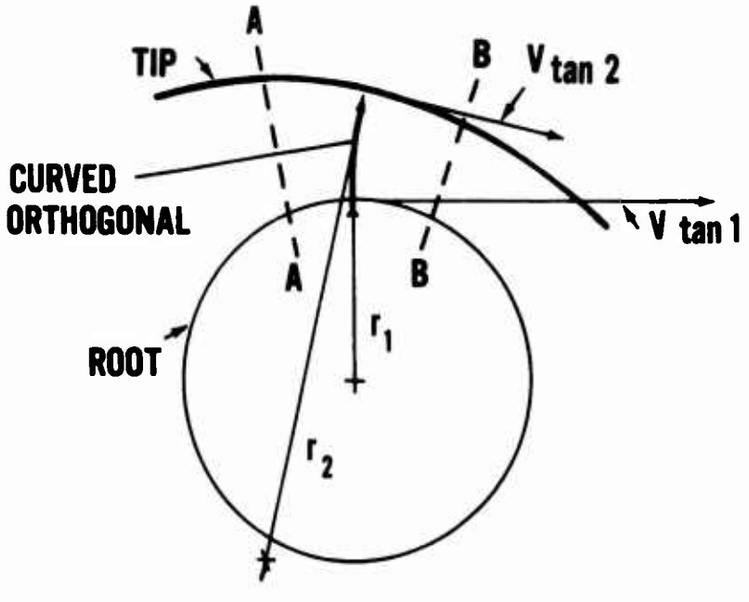


FIG. 3 CURVED ORTHOGONAL IN CONVERGING CHANNEL

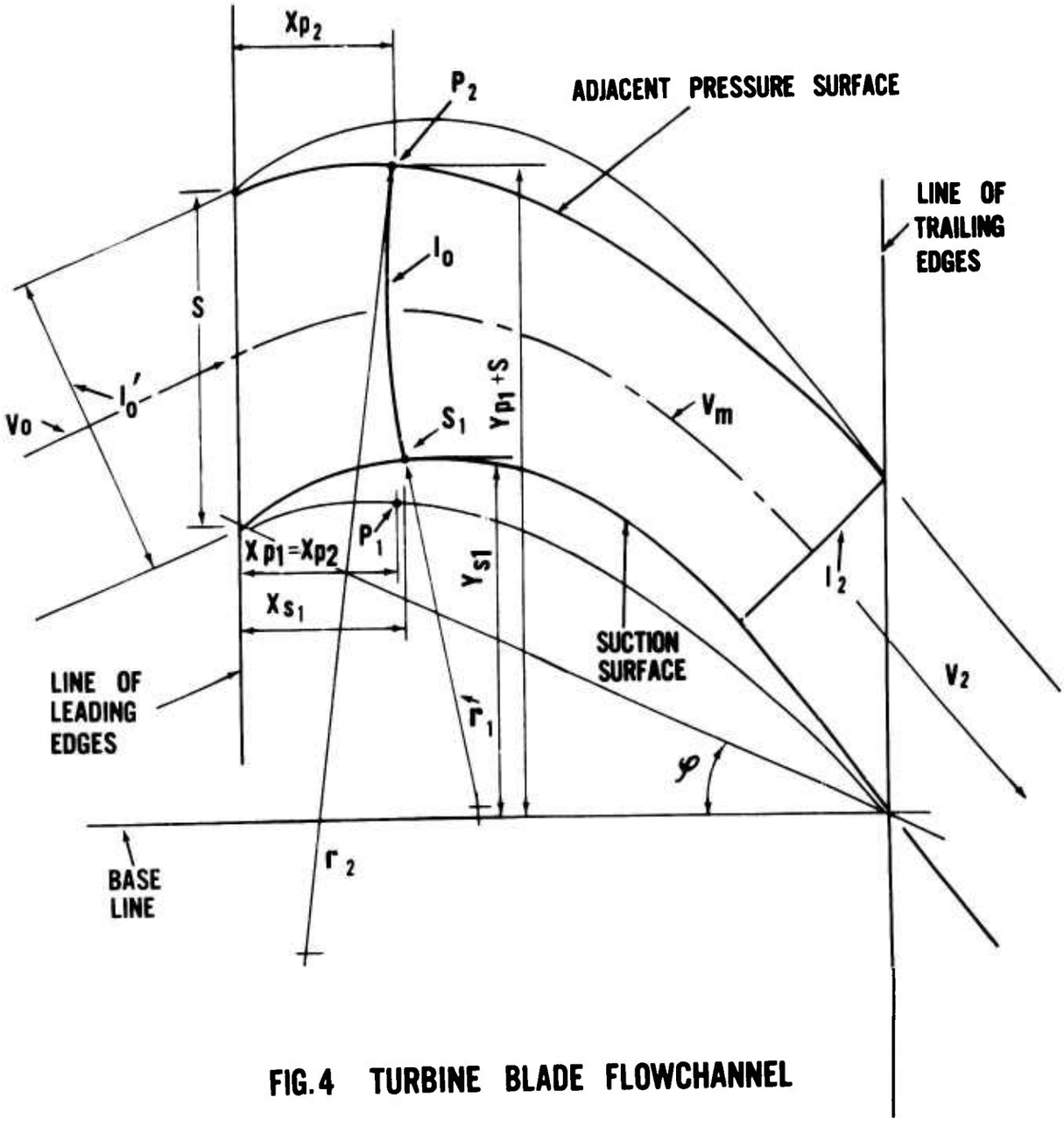


FIG. 4 TURBINE BLADE FLOWCHANNEL

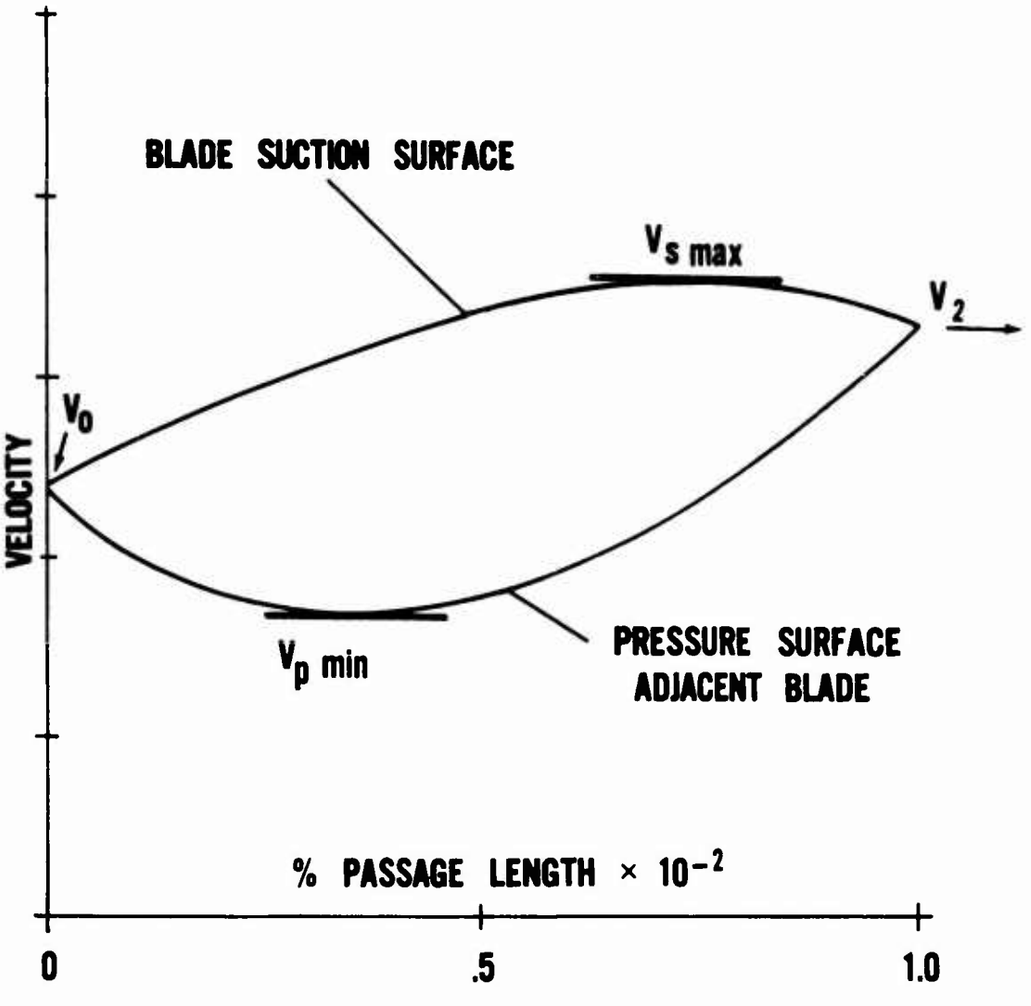


FIG. 5 IDEALIZED BLADE SURFACE VELOCITIES VERSUS % PASSAGE LENGTH

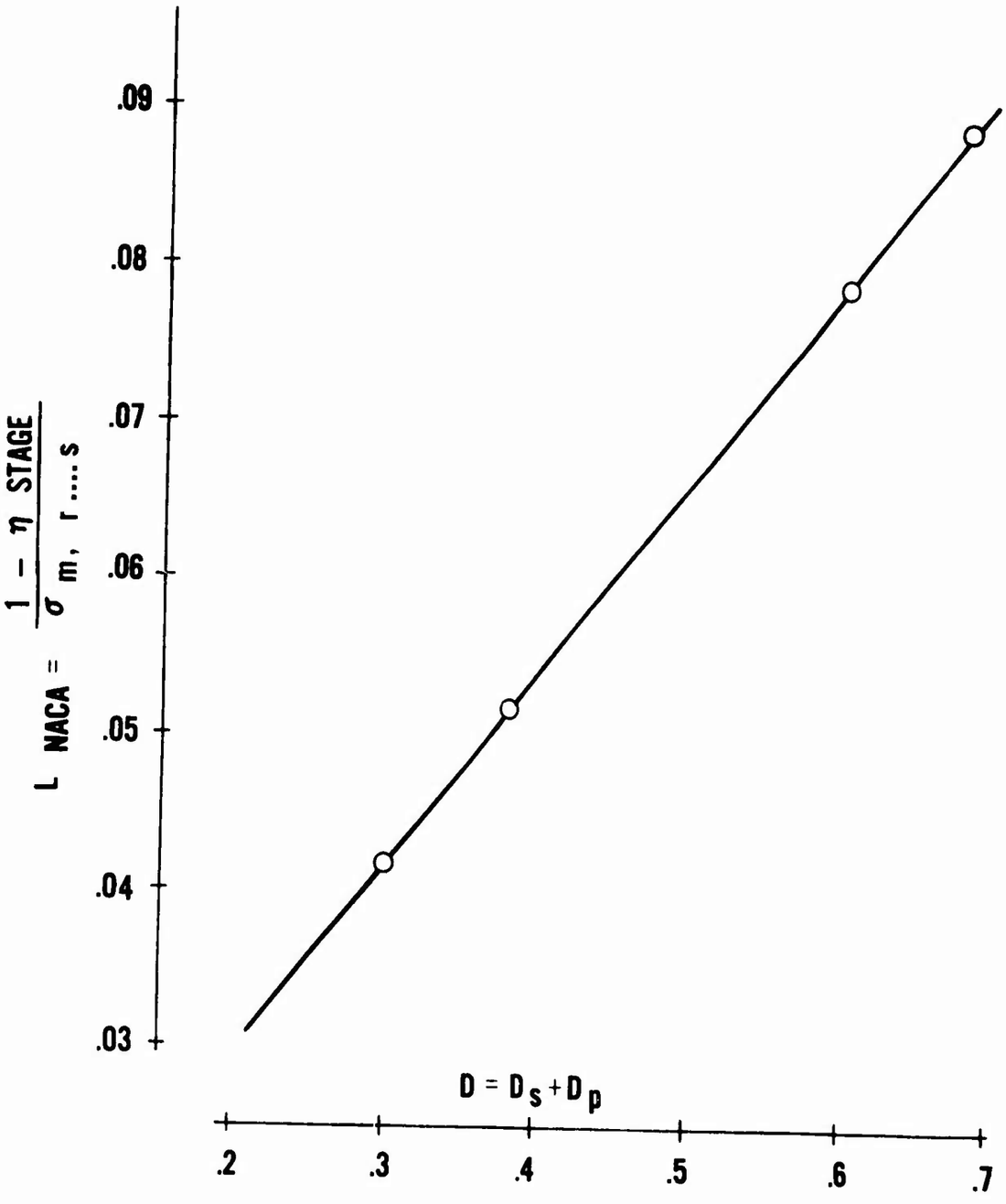


FIG. 6 NACA PRESSURE LOSS PARAMETER VERSUS TOTAL DIFFUSION FACTOR.....TEST POINTS FROM 4 REFERENCE (5) TURBINE ROTORS

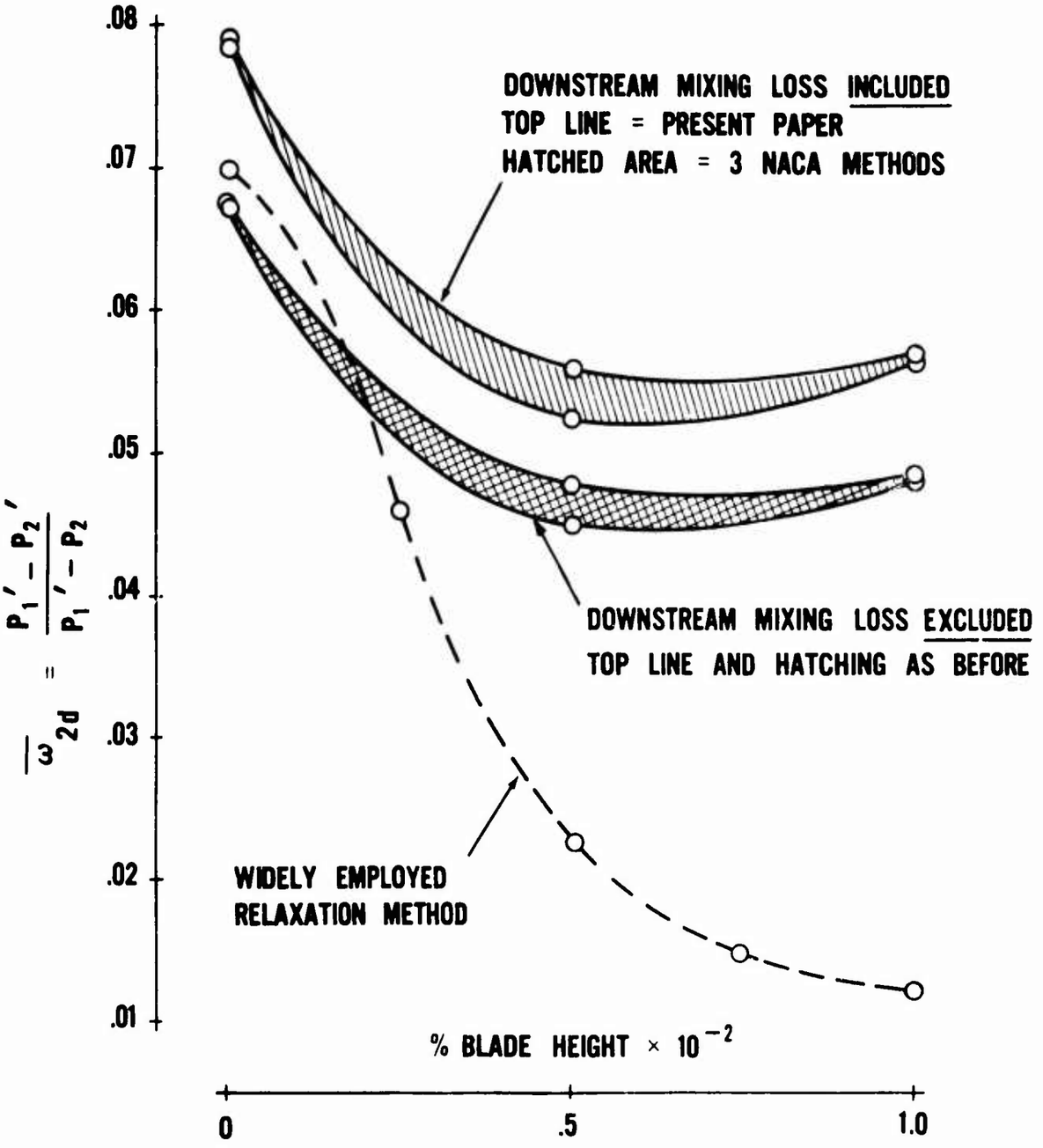


FIG.7 PREDICTED TWO DIMENSIONAL BLADE TOTAL PRESSURE LOSS VERSUS BLADE HEIGHT....FOR TURBINE TEST MODEL, ROTOR II (OF A 32,000 HP MACHINE)

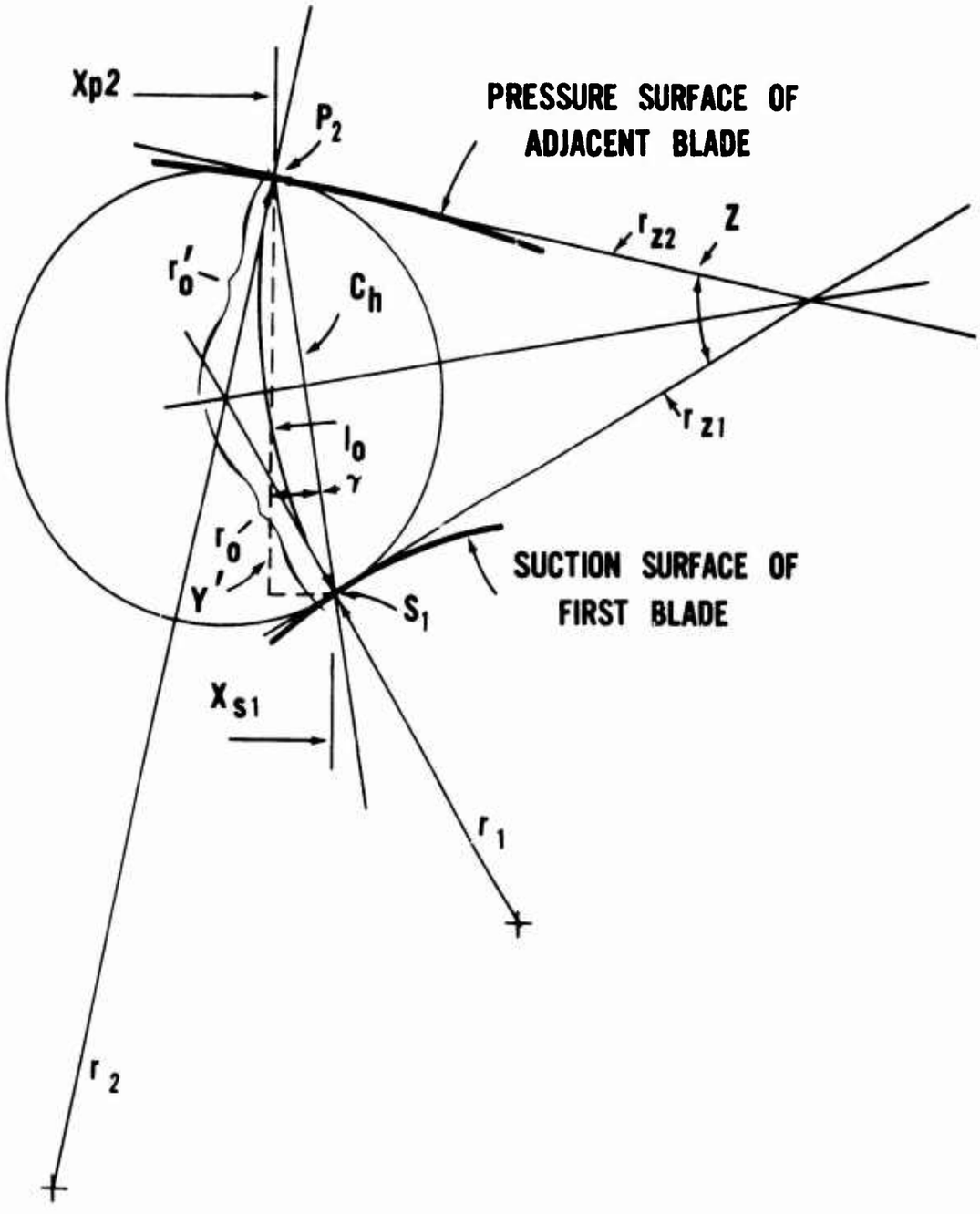


FIG. 8 DEVELOPMENT OF F(X) = 0
SEE APPENDIX A

FORCED OSCILLATIONS IN SECOND ORDER SYSTEMS WITH UNBOUNDED NONLINEARITIES

Jagdish Chandra*
Maggs Research Center
Watervliet, New York

and

B. A. Fleishman**
Rensselaer Polytechnic Institute
Troy, New York

1. INTRODUCTION. In this paper, we investigate periodic solutions and related boundary value problems for a family of nonlinear differential equations in which the nonlinearity may be discontinuous (and/or unbounded). Specifically, we establish the existence of harmonic solutions for equations of the type

$$\frac{d^2x}{dt^2} + x + f(x) = a\cos\omega t \qquad (DE,f)$$

where the function $f(x)$ is odd, satisfies $xf(x) \geq 0$ for all x and has a jump discontinuity. All quantities are real-valued, and the constants a and ω are assumed always to satisfy $a \neq 0$ and $\omega > 1$.

What we ordinarily mean by a harmonic (periodic) solution of (DE,f) is a solution with period $2\pi/\omega$ which is exactly out of phase (in phase when $0 < \omega < 1$) with the forcing function $a\cos\omega t$. Now it is easily verified (See [4]) that a solution of the boundary value problem consisting of (DE,f) and the boundary conditions

$$\dot{x}(0) = 0, \quad x(\tau) = 0 \qquad (1)$$

where $\tau = \pi/2\omega$), when extended for all t, yields such a harmonic (periodic) solution of (DE,f). Because it is the boundary value problem, denoted henceforth by BVP(f), which is treated directly below, and because of

*Research supported by the Department of Army under Project No. 1T061101A91A.
**Research supported by Contract AF49(638)-1661 between the Office of Scientific Research of the U. S. Air Force and Rensselaer Polytechnic Institute.

PRECEDING PAGE BLANK

the relationship between BVP(f) and the periodicity problem, in this paper by a harmonic solution we shall mean a solution of BVP(f) which is positive for $0 \leq t < \tau$.

When f(x) is uniformly bounded and smooth (except perhaps for a jump at x = 0), (DE,f) is known [3] to possess a harmonic solution. The restriction that f(x) experience a jump only at the origin is crucial in [3]; in this case a new (unsymmetric) smooth nonlinearity is constructed which coincides with f(x) for $x > 0$. This technique does not work, however, when f(x) has a jump discontinuity at points other than at x = 0. Our principal purpose here is to consider this problem. Further, it is shown that the restriction that f(x) be uniformly bounded may be relaxed considerably: in Section 4, we consider a class of unbounded nonlinearities which satisfy suitable growth conditions.

The existence of a solution of BVP(f) is established below by use of the well known point-mapping method; to employ this method, we need to know that, for each value of the real parameter α in a certain interval, the initial value problem (DE,f), $x(0) = \alpha$, $\dot{x}(0) = 0$ possesses a unique solution on $[0,t]$ which depends continuously on α. This initial value problem is treated in Section 5.

For ease of exposition, we have restricted ourselves to functions f(x) with a single discontinuity. Similar results can be obtained for a broader class of problems, involving nonlinearities with multiple discontinuities. Such problems will be discussed elsewhere. A particular case of multiple discontinuities, in which the nonlinearity is piecewise constant is treated in [5] by a special technique.

2. PRELIMINARY RESULTS. Let F denote the class of functions f(x) with the following properties: f(x) is odd, $f(x) \geq 0$ when $x > 0$, and f(x) is continuous for $x \geq 0$ except perhaps at $x = \sigma$ $(0 < \sigma < b)$, where f(x) has a jump discontinuity.

In Sections 3, 4, and 5, we introduce subsets of F denoted, respectively, by F_M (f(x) uniformly bounded by a positive constant M), F_g (f(x) unbounded but subject to a growth restriction), and F_L ($f \in F_M \cup F_g$ but in addition satisfying a Lipschitz condition in each interval of continuity).

When f(x) is piecewise continuous, we mean by a solution of (DE,f) on an interval I a function x(t) which is continuously differentiable on this interval, possesses a piecewise continuous second derivative and satisfies (DE,f) wherever the second derivative exists. In case f(x) is continuous a solution is to have a continuous second derivative and satisfy (DE,f) at all points of I.

Let IVP(α,f) denote the initial value problem of solving (DE,f) subject to the initial conditions

$$x(0) = \alpha, \quad \dot{x}(0) = 0. \tag{2}$$

By use of the method of variation of parameters, a solution of IVP(α,f) on an interval I containing the origin is easily seen to satisfy

$$x(t) = (\alpha-b)\cos t + b\cos\omega t - \int_0^t \sin(t-s)\, f(x(s))\, ds \quad (t\in I) \tag{3}$$

where

$$b = \frac{a}{1-\omega^2}.$$

Conversely, a continuous solution of (3) on I is a solution of IVP(α,f) on I.

Let $x(t;\alpha,f)$ denote a solution of IVP(α,f) which is known to exist and be unique on $[0,\tau]$. (When f(x) is Lipschitzian, such a unique solution is known to exist (See, for instance, [6]); however, this becomes less evident when f(x) is piecewise continuous. We establish in Section 5 the existence, uniqueness and continuous dependence on initial data of solutions of IVP(α,f) when f belongs to a subset of our class F of piecewise continuous nonlinearities.)

Let A be a set of values of α for which (unique) $x(t;\alpha,f)$ exists. We define on A a mapping T by the formula

$$T(\alpha) = x(\tau;\alpha,f).$$

Clearly $x(t;\alpha,f)$ will be a harmonic solution of (DE,f) for those values of α for which $T(\alpha) = 0$ and $x(t;\alpha,f) > 0$ for $0 < t < \tau$. Any such value of α will henceforth be called a <u>harmonic point</u>.

The following theorem is a restatement, under weaker assumptions, of one appearing originally in [2] and [3].

<u>Comparison Theorem</u>: Suppose that $f_1(x)$ and $f_2(x)$ are piecewise continuous functions and that $f_1(r) \geq f_2(s)$ for all $r > 0$, $s > 0$. Let α_1 be a harmonic point of (DE,f_1) and α_2 a harmonic point of (DE,f_2). Then

$$\alpha_1 \geq \alpha_2.$$

Proof: Let $x_i(t;\alpha_i,f_i)$ be a harmonic solution of (DE,f_i) $(i=1,2)$. Then, using (3), the harmonic points α_i $(i=1,2)$ are given by

$$\alpha_i = b + \sec\tau \int_0^\tau \sin(\tau-s)\, f_i(x_i)\, ds.$$

So

$$\alpha_1 - \alpha_2 = \sec\tau \int_0^\tau \sin(\tau-s)\, \{f_1(x_1) - f_2(x_2)\}\, ds \geq 0.$$

Here we have used the facts that $0 \leq \tau-s \leq \pi/2$ and $x_i(s;\alpha_i,f_i) > 0$ $(i=1,2)$ for $s\in(0,\tau)$.

In the linear case, $f(x) \equiv 0$, the equation $(DE,0)$ has a unique harmonic point $b = a/(1-\omega^2)$. The ideal relay equation

$$\frac{d^2x}{dt^2} + x + M \operatorname{sgn} x = a\cos\omega t \qquad (DE,M\ \operatorname{sgn})$$

where M is a positive constant and sgn x = signum x = x/(x) $(x\neq 0)$, is known [7] to have a harmonic point, which we denote by d_M:

$$d_M = b + M(\sec\tau - 1). \tag{4}$$

According to the Comparison Theorem, d_M is the unique harmonic point of (DE, M sgn).

3. EXISTENCE OF A HARMONIC SOLUTION: f UNIFORMLY BOUNDED. In this section we assume always that f is contained in the subset of F consisting of those $f\in F$ which satisfy $|f(x)| \leq M$ for all x, where M is a given positive constant.

When $f\in F_M$, it is not hard to see that there is a subinterval of $(0,d_M)$ on which $f(x) > 0$, and there is also a subinterval of $(0,d_M)$ on which $f(x) < M$. These facts are needed in Lemma 2 and Corollary 1 of Lemma 3.

From the Comparison Theorem follows immediately

Lemma 1: If α is a harmonic point of (DE,f),

$$b \leq \alpha \leq d_M.$$

Thus, for $f \in F_M$ we know that we must look for a harmonic point (if any exists) in the interval $[b,d_M]$. To show that one does exist (that is, that there exists at least one harmonic solution) we use the well-known point-mapping method [1]; namely, we demonstrate that T is a continuous mapping and carries the interval $[b,d_M]$ into an interval which contains zero in its interior (so that at least one point in $[b,d_M]$ is mapped into zero under T).

We show below, first of all, that $T(d_M) > 0$, $T(b) < 0$ and $\dot{x}(t;\alpha,f) < 0$ on $0 < t \leq \tau$ for any $\alpha \in [b,d_M]$. The continuity of $T(\alpha)$ in α follows from the continuous dependence on the initial datum α, which is known to hold when $f(x)$ satisfies a uniform Lipschitz condition. But in our case, where $f(x)$ is discontinuous, the continuous dependence of $x(t;\alpha,f)$ on α cannot be taken for granted; it is established in Section 5.

In Lemma 2 and Lemma 3, below, we assume that for each $\alpha \in [b,d_M]$ there exists a solution of IVP(α,f) which is defined for all $t \in [0,\tau]$. In Section 5, we demonstrate that this is not an empty assumption.

Lemma 2: $T(d_M) = x(\tau;d_M, f) > 0$.

Proof: Since $|f(x)| \leq M$,

$$\int_0^\tau \sin(\tau-s)\, f(x(s))ds \geq M \int_0^\tau \sin(\tau-s)ds = M(1-\cos\tau).$$

But

$$x(\tau;d_M,f) = (d_M-b)\cos\tau - \int_0^\tau \sin(\tau-s)\, f(x(s))ds$$

$$\geq (d_M-b)\cos\tau - M(1-\cos\tau)$$

$$= [d_M - b - M(\sec\tau-1)]\cos\tau = 0.$$

Thus, $x(\tau;d_M,f) \geq 0$. Now, suppose $x(\tau;d_M,f) = 0$. Then $x(t;d_M,f)$ takes all values in $o \leq x \leq d_M$, on a subinterval of which $f(x) < M$. Therefore, retracing the steps above,

$$\int_0^\tau \sin(\tau-s)\, f(x(s))\, ds < M(1-\cos\tau)$$

and

$$x(\tau,d_M,f) > 0.$$

Corollary: If α is a harmonic point of (DE,f) then $\alpha < d_M$.

Proof: From Lemma 1, $\alpha \leq d_M$. But if $\alpha = d_M$, $x(\tau;d_M,f) = 0$, contradicting Lemma 2.

Lemma 3: Suppose $b\omega \geq M$. Then for $\alpha\epsilon[b,d_M]$, $\dot{x}(t;\alpha,f) < 0$ on $0 < t \leq \tau$.

Proof:

$$\dot{x}(t;\alpha,f) = (b-\alpha)\sin t - b\omega\sin t - \int_0^t \cos(t-s)\, f(x(s))ds$$

$$\leq (b-\alpha)\sin t - b\omega\sin t + M\int_0^t \cos(t-s)ds$$

$$\leq (b-\alpha)\sin t - b\omega(\sin\omega t - \sin t)$$

$$\leq -\eta(t) < 0$$

where $\eta(t) = b\omega(\sin\omega t - \sin t)$.

Corollary 1: $T(b) = x(\tau;b,f) < 0$.

Proof: On the contrary, assume that $x(\tau;b,f) \geq 0$. Then, since $\dot{x}(t;b,f) < 0$, $x(t;b,f) > 0$ for $0 \leq t < \tau$. This implies $f(x(t)) > 0$, so that from (3)

$$x(\tau;b,f) = -\int_0^\tau \sin(\tau-s)\, f(x(s))\, dx < 0.$$

This contradiction completes the proof.

Corollary 2: If α is a harmonic point of (DE,f), then $\alpha > b$.

On the basis of the preceding lemmas, which establish the fact that the mapping T carries $[b,d_M]$ into an interval containing zero in its interior, and in view of continuity of the solution $x(t;\alpha,f)$ in α (which will be demonstrated in Section 5), we have proved

Theorem 1: Suppose $f \in F_M$. Then there exists an $\alpha, \alpha \in (b,d_M)$, which is a harmonic point of (DE,f), provided

$$b\omega \geq M.$$

4. EXISTENCE OF HARMONIC SOLUTION: f UNBOUNDED: Now we extend the results of the preceding section to a class of unbounded nonlinearities. In this section, it is assumed always that f belongs to F_g, the subset of F consisting of functions f(x) which obey the following growth condition: There exists a positive number $\overline{x}$ (where $\overline{x} > b > \sigma > 0$) such that for $x > 0$

$$f(x) \leq f(\overline{x}) = \frac{\overline{x} - b}{\sec \tau - 1} \qquad (x \leq \overline{x}) \qquad (4)$$

$$f(x) < \frac{x - b}{\sec \tau - 1} \qquad (x > \overline{x}).$$

To motivate this extension, let us consider an arbitrary $f \in F$. For a given $\alpha > b$, suppose $x(t;\alpha,f)$ is a harmonic solution of (DE,f). Since $f(x(t)) \geq 0$ for $0 \leq t \leq \tau$, it follows from $\dot{x}(t;\alpha,f) < 0$ on $(0,\tau]$ (modifying slightly the proof of Lemma 3) that $x(t;\alpha,f) < \alpha$ on $(0,\tau)$. Define the odd truncated function $f_0(x)$ by

$$f_0(x) = \begin{cases} f(x), & 0 \leq x \leq \alpha \\ f(\alpha), & x > \alpha. \end{cases}$$

Since $x(t;\alpha,f)$ takes values only in $-\alpha \leq x \leq \alpha$, where $f(x)$ and $f_0(x)$ are identical, $x(t;\alpha,f)$ is a harmonic solution of

$$\frac{d^2x}{dt^2} + x + f_0(x) = a\cos\omega t \qquad (DE,f_0)$$

as well as of (DE,f). Since $|f_0(x)| \leq f(\alpha)$, we find, from the Comparison Theorem of Section 2 (using $M = f(\alpha)$, that

$$b \leq \alpha \leq b + f(\alpha)[\sec \tau - 1]. \tag{6}$$

Inequality (6) imposes a necessary condition to be satisfied by the amplitude α of a harmonic solution (if any exists) of (DE,f). Thus, if for all x greater than some $\overline{x} > 0$, $x > b + f(x)[\sec \tau - 1]$, there cannot exist a harmonic solution with amplitude greater than $\overline{x}$. This motivates the definition of the set F_g.

On the basis of the preceding discussion, we have

Lemma 6: Suppose $f \in F_g$. If α is a harmonic point of (DE,f), then

$$b \leq \alpha \leq \overline{x}. \tag{7}$$

Thus, in order to investigate harmonic solutions of (DE,f), for $f \in F_g$, it is sufficient to consider solutions of IVP(α,f) where $b \leq \alpha \leq \overline{x}$.

Define the truncated function $\overline{f}(x)$ by

$$\overline{f}(x) = \begin{cases} f(x), & 0 \leq x \leq \overline{x} \\ \dfrac{\overline{x} - b}{\sec \tau - 1}, & x > \overline{x}. \end{cases} \tag{8}$$

clearly, $|\overline{f}(x)| \leq (\overline{x} - b)/(\sec \tau - 1)$ and Lemmas 2 and 3 can be restated in terms of $\overline{f}$, and thus in terms of f. We have, for instance,

Lemma 2: Let $x(t;\bar{x},f)$ be a solution of IVP$(\bar{x};f)$. Then $x(\tau;\bar{x},f) > 0$. If α is a harmonic point of (DE,f), $\alpha < \bar{x}$.

We shall merely state the existence result.

Theorem 2: Let $f \in F_g$. Then, there exists an $\alpha \in (b,\bar{x})$ which is a harmonic point of (DE,f) provided

$$b\omega \geq \frac{\bar{x} - b}{\sec \tau - 1}.$$

5. EXISTENCE, UNIQUENESS AND CONTINUOUS DEPENDENCE OF A SOLUTION OF IVP(α,f). Let F_L be the subset of F consisting of those elements in F_M or F_g which, except at $x = \pm\alpha$ are Lipschitzian: for $x \geq 0$

$$f(x) = \begin{cases} f_1(x), & x \leq \sigma \\ f_2(x), & x \geq \sigma \end{cases}$$

where $f_1(x)$ and $f_2(x)$ are Lipschitz continuous on their respective domains of definition. Obviously, $F_L \subset (F_M \cup F_g)$.

Throughout this section, it is assumed that $\alpha \in [b,\bar{x}]$, $\bar{x} > b > \alpha > 0$ and that $f \in F_L$. Calculations and results are stated explicitly for members f of F_g (which satisfy the growth restriction (5)). They are easily modified for members f of F_M (uniformly bounded).

We work with the trajectories of solutions in $t,x,\dot{x}$ - space (phase space). Given the constant $N > 0$ (which for the moment is arbitrary), let

$$D = D_1 \cup D_2 \cup D_3$$

where

$$D_1 = \{(t,x,\dot{x}) \mid 0 \leq t \leq \tau,\ \sigma \leq x \leq \bar{x},\ |\dot{x}| \leq N\}$$

$$D_2 = \{(t,x,\dot{x}) \quad 0 \leq t \leq \tau,\ -\sigma \leq x \leq \sigma,\ |\dot{x}| \leq N\}$$

$$D_3 = \{(t,x,\dot{x}) \mid 0 \leq t \leq \tau,\ -\bar{x} \leq x \leq -\sigma,\ |\dot{x}| \leq N\}.$$

We shall prove that for each $\alpha \in [b,\bar{x}]$ the solution $x(t;\alpha,f)$ can be continued uniquely up to $t = \tau$ and that this solution depends continuously on the initial datum α.

Since in D_1 $f(x)$ is Lipschitz continuous, there exists a t_1 $(0 < t_1 \leq \tau)$ such that for $0 \leq t < t_1$, IVP(α,f) has a unique solution whose trajectory is in D_1. This trajectory approaches the boundary of D_1 as $t \to t_1$. Let us denote this solution by $x(t;\alpha,f)$. Then $x(t;\alpha,f)$ satisfies the integral equation (3) (with f replaced by f_2) on $[0,t_1)$ For $0 < t < t_1$

$$\dot{x}(t;\alpha f) = -(\alpha-b) \sin t - b\omega \sin t - \int_0^t \cos(t-s)\, f_2(x(s))ds$$

$$\leq -(\alpha-b) \sin t - b\omega \sin\omega t + \frac{\bar{x} - b}{\sec \tau - 1} \sin t$$

$$\leq -\eta(t) < 0$$

where $\eta(t) = b\omega(\sin\omega t - \sin t)$, provided

$$b\omega \geq \frac{\bar{x} - b}{\sec \tau - 1}. \tag{9}$$

(For the remainder of this section we assume that (9) holds.) Further,

$$-\dot{x}(t;\alpha,f) \leq (\alpha-b) \sin t + b\omega \sin\omega t + \frac{\bar{x} - b}{\sec \tau - 1} \int_0^t \cos(t-s)ds$$

$$\leq (\bar{x} - b) \sin \tau + b\omega + \frac{\bar{x} - b}{1 - \cos\tau} \sin\tau \cdot \cos\tau$$

$$= b\omega + \frac{\bar{x} - b}{1 - \cos\tau} \sin \tau.$$

Therefore, if we choose

$$N > b\omega + \frac{\bar{x} - b}{1 - \cos\tau} \sin\tau,$$

$$0 > \dot{x}(t;\alpha,f) > -N.$$

Thus, the trajectory of solution $x(t;\alpha,f)$, for $0 \leq t < t_1$, is bounded away from the boundaries $\dot{x} = \pm N$ and remains below the plane $x = \bar{x}$. Hence, as $t \to t_1$, the trajectory either approaches the boundary $t = \tau$ (in which case $t_1 = \tau$) or the boundary $x = \sigma$. Now if $t_1 = \tau$, we have a well defined solution of (DE,f) on $0 \leq t \leq \tau$ which depends continuously on α. When $t_1 < \tau$ define

$$v_1(t_1,\alpha) = \lim_{t \to t_1 - 0} \dot{x}(t;\alpha,f) < 0.$$

Thus, $x(t,\alpha,f)$ is not tangent to the plane $x = \sigma$ at $t = t_1$. Clearly, v_1 is a continuous function of (t_1,α). Now t_1 is obtained by solving the functional equation

$$x(t_1;\alpha,f) = \sigma.$$

Since $x(t;\alpha,f)$ is a strictly decreasing function of t, there exists a unique solution $t_1 = \mu_1(\alpha,\sigma)$ where $\mu_1(\alpha,\sigma)$ is a continuous function of α.

We now continue this solution for $t > t_1$ as the unique solution of the initial value problem

$$\frac{d^2x}{dt^2} + x + f_1(x) = a \cos \omega t$$

$$x(t_1) = \sigma, \quad \dot{x}(t_1) = v_1 < 0$$

in D_2. Since $f_1(x)$ is Lipschitz continuous in D_2, there exists a

$t_2 (t_1 < t_2 \leq \tau)$ such that the unique continuation remains in D_2 for $t_1 < t < t_2 \leq \tau$ and depends continuously on the "initial" data t_1, v_1. Since these "initial" data themselves are continuous functions of α, we are assured of continuous dependence on α of the extended solution on $0 \leq t < t_2 \leq \tau$.

In order to gain insight into subsequent continuation of this solution, let us consider the comparison problem

$$\frac{d^2x}{dt^2} + x + \frac{\bar{x} - b}{\sec \tau - 1} = a \cos\omega t$$

satisfying $x(0) = b$, $\dot{x}(0) = 0$. The unique solution of this problem is given by

$$x_\ell(t) = \frac{\bar{x} - b}{\sec \tau - 1} (\cos t - 1) + b \cos\omega t.$$

On their common interval of existence, $x_\ell(t)$ provides a lower bound for $x(t;\alpha,f)$:

$$x(t;\alpha,f) - x_\ell(t) = (\alpha - b) \cos t - \frac{\bar{x} - b}{\sec \tau - 1} (\cos t - 1) - \int_0^t \sin(t-s) f(x(s)) ds$$

$$\geq (-b) \cos t - \frac{\bar{x} - b}{\sec \tau - 1} (\cos t - 1) + \frac{\bar{x} - b}{\sec \tau - 1} (\cos t - 1)$$

$$= (\alpha - b) \cos t$$

$$\geq 0.$$

Since $x_\ell(t)$ is a strictly decreasing function of t on $[0,\tau]$, $x(t;\alpha,f)$ remains above the boundary $x = -\sigma$ for $0 \leq t \leq \tau$ (and therefore $t_2 = \tau$) if

$$x_\ell(t) = \frac{\bar{x} - b}{\sec\tau - 1}\,(\cos t - 1) = -(\bar{x} - b)\cos\tau > -\sigma$$

or

$$\sigma > (\bar{x} - b)\cos\tau. \tag{10}$$

Remark: If we assume that

$$b > \sigma > b\omega\,(1-\cos\tau)$$

then (9) implies (10); for from (9)

$$\bar{x} - b \leq b\omega\,(\sec\tau - 1) < \sigma\sec\tau.$$

If (10) does not hold, the trajectory for $x(t;\alpha,f)$ may approach the boundary $x = -\sigma$ as $t \to t_2$. It is easily verified that

$$\nu_2(t_2,\omega) = \lim_{t \to t_2 - 0} \dot{x}(t;\alpha,f) < 0.$$

We now continue the solution for $t > t_2$ as the unique solution of the initial value problem

$$\frac{d^2x}{dt^2} + x + f_2(x) = a\cos\omega t$$

satisfying $x(t_2) = -\sigma$, $\dot{x}(t_2) = \nu_2 < 0$. The trajectory thus obtained remains above the plane $x = -\bar{x}$ (and therefore reaches the plane $t = \tau$); for, from the comparison problem,

$$x(t;\alpha,f) \geq x_\ell(\tau) = -(\bar{x} - b)\cos\tau > -\bar{x}.$$

The above discussion is summarized in

Theorem 3: Suppose $f \in F_L \cap F_g$, where $0 < \sigma < b < \bar{x}$. Then for each $\alpha \in [b,\bar{x}]$ there exists a unique solution $x(t;\alpha,f)$ of the initial value problem IVP(α,f) on $0 \leq t \leq \tau$ which depends continuously on α, provided

$$b\omega \geq \frac{\bar{x} - b}{\sec \tau - 1} .$$

In phase space the trajectory of this solution crosses each plane of discontinuity $x = \pm \sigma$ at most once.

If further $\sigma > b\omega(1 - \cos \tau)$ the unique solution of IVP(α,f) remains above the plane $x = -\sigma$ for $0 \leq t \leq \tau$; that is, the trajectory intersects at most one plane of discontinuity of f.

(If $f \in F_L \cap F_M$, replace $\bar{x}$ above by d_M.)

REFERENCES

1. A. A. Andronov, A. A. Vitt, and S. E. Khaikin. Theory of Oscillators. Pergamon Press, New York, 1966. (Translated from the Russian.)

2. O. Benediktsson. Forced Oscillations in Second Order Systems with Bounded Nonlinearities. Doctoral Dissertation, Rensselaer Polytechnic Institute, 1965.

3. O. Benediktsson and B. A. Fleishman. Forced Oscillations in Second Order Systems with Bounded Nonlinearities. Proc. Internal. Symposium on Differential Equations and Dynamical Systems, pp. 497-503, Academic Press, New York, 1967.

4. J. Chandra and B. A. Fleishman. Positivity and Comparison results for nonlinear boundary value problems and related periodic solution. Jour. Math. Anal. Appl., 24, pp. 545-554, 1968.

5. J. Chandra and B. A. Fleishman. A Canonical Representation for Solutions of a Class of Nonlinear Problems. Internat. J. Nonlinear Mechanics, 4, 1969. (To appear.)

6. E. A. Coddington and N. Levinson. Ordinary Differential Equations. McGraw Hill, New York, 1955.

7. B. A. Fleishman. Harmonic and Subharmonic Responses of an On-Off Control System to Sinusoidal Inputs. J. Franklin Inst., 270, pp. 99-113, 1960.

AN EVALUATION OF THE CONSTANTS IN THE INTEGRALS OF SCHWARZ-CHRISTOFFEL TRANSFORMATION

Kanu R. Gandhi
Army Materials and Mechanics Research Center
Watertown, Massachusetts

ABSTRACT. An iterative method is proposed here by which the singularities in the Schwarz-Christoffel transformation are evaluated numerically. The numerical integration near singularities are performed by the Gaussian quadrature. Finally, a set of non-linear integral type relations are obtained in terms of the unknown singularity locations. The system is solved by a linear perturbation method, and the singularities are determined iteratively. The method is applied to the problem of a circular hole with radial cracks.

INTRODUCTION. Frequently, two-dimensional problems of mechanics are formulated in terms of complex variable theory. Sometimes, it is convenient to transform a boundary value problem by introducing a set of curvilinear coordinates or equivalently by carrying out conformal transformation. If the physical domain in which the problem is formulated happens to have sharp discontinuities like corners or cusp-like cracks the Schwarz-Christoffel Transformation is pertinent. Although the expression for the Schwarz-Christoffel Transformation is not complicated, the fact remains that the large majority of the image points of the corners on the unit circle have to be determined before the mapping function can be determined completely. This frequently is a problem when the number of sharp corners are numerous.

The image points are related to the actual shape in the physical plan by a non-linear relation of the type.

$$\phi(Z_i) - \phi(Z_{i-1}) = \int_{A_{i-1}}^{A_i} f(\theta, A_1 - - - -A_M)\, d\theta \qquad (1)$$

Where $A_1 - - - - A_M$ are the image points of the sharp discontinuities on the unit circle.

θ is a variable in the parameter plane.

ϕ is some function of Z, unique to a particular geometry.

It will be noted in Eq. (1) that the unknowns $A_1 - - - - A_M$ appear not only in the integrand, but also in the limits of the integral.

Furthermore, the manner in which A's appear in the function f is usually non-linear. An iterative method proposed here aims at determining the accurate values of A's. The basic philosophy of this method is quite general, however, we shall consider the specific geometry of circular hole with numerous unsymmetrical radial cracks.

PROBLEM OF CIRCULAR HOLE AND RADIAL CRACKS. Let us consider a circular hole with radial cracks in an infinite region located in the complex A-plane. We wish to determine a conformal transformation between the Z-plane and an auxiliary ζ-plane such that the unit circle in the latter plane maps into the circular cutout with radial cracks (region τ). The region external to the unit circle will be considered to map into region outside of τ. (Figure 1).

The appropriate Schwarz-Christoffel Transformation can be written down as below:

$$\frac{dZ}{d\zeta} = \frac{Z(\zeta - e^{i\alpha_{s1}})\ (\zeta - e^{i\alpha_{s2}})\ - - - - - - - (\zeta - e^{i\alpha_{sK}})}{\zeta\sqrt{(\zeta - e^{i\alpha_1})\ (\zeta - e^{i\alpha_2})\ - - - - - - - - - (\zeta - e^{i\alpha_{2K}})}} \quad (2)$$

whence, K = number of radial cracks; $\alpha_{s1} - - - \alpha_{sK}$ = images of crack tips on the unit circle.

$\alpha_1 - - - \alpha_{2K}$ = images of junctions of cracks and the circle.

R = radius of the circular cutout.

Without compromising the generality of the problem, for simplicity, let us assume a symmetry about the real axis.

On the unit circle, $\zeta = e^{i\theta}$ Eq. (2) simplifies into:

$$\frac{dZ}{Z} = - \frac{\sin\theta\ (\cos\theta - \cos\alpha_{s1})\ - - - - - - (\cos\theta - \cos\alpha_{sK})d\theta}{\sqrt{(\cos\theta - \cos\alpha_1)\ (\cos\theta - \cos\alpha_2)\ - - (\cos\theta - \cos\alpha_{2K})}} \quad (3)$$

Integrating both sides from 0 to θ, we have:

$$\log Z \Big]_0^Z = - \int_0^\theta \frac{\sin\theta \prod_{i=1}^{i = K/2 - 1} (\cos\theta - \cos\alpha_{si})\ d\theta}{\prod_{i=1}^{i=K} \cdot\ (\cos\theta - \cos\alpha_i)^{\frac{1}{2}}} \quad (4)$$

If K number of cracks are of equal length L and are separated by an angle of $2\pi/K$, we can express all α_{si} and all α_i in terms of only one parameter called 'TH'. Using K-fold symmetry we have:

$\alpha_1 = TH$

$\alpha_2 = 2\pi/K - TH$

$\alpha_{s1} = 2\pi/K$

$\alpha_3 = 2\pi/K + TH$

- - - - - - - -

- - - - - - - -

- - - - - -

$\alpha_{2K-1} = 2(K-1)\pi/K - TH$

$\alpha_{sK} = 2(K-1)\pi/K$

$\alpha_{2K} = 2(K-1)\pi/K + TH$

Using these values of α_{si} and α_i in Eq. (4) and simplifying we can show that:

$$\text{Log } Z \Big|_0^Z = -\int_0^\theta \sqrt{2}\, \sin K\theta/2 \cdot (\cos K\theta + \cos K'TH')^{-1/2} d\theta \quad (5)$$

From Eq. (5) one can also derive the following relation:

$$\left(\frac{L}{R} + 1\right)^K = \left(\sqrt{2} + \sqrt{1 - \cos 'TH'}\right)(1 + \cos K'TH')^{-1} \quad (6)$$

R = radius in Z-plane

TH = angular parameter

Eq. (6) enables us to determine 'TH' for any particular crack configuration involving the polar symmetry. Once 'TH' is determined we can easily find the locations of all singularities on the unit circle.

This is best illustrated by the example in Figure 2, where K = 4. As we see the tips of four cracks map symmetrically on the unit circle while the junctions of crack and the circle map symmetrically on each side of the image of crack tip at an angle 'TH'. So knowning the symmetrical solution we shall solve for any unsymmetrical situation when crack lengths are arbitrary and they are separated by almost any angle.

ITERATIVE SCHEME. In order to develop an iterative scheme, let us refer to Figure 3 and adopt the numbering scheme shown for the sharp corners in Z-plane and corresponding singularities in ζ-plane. Let $Z_o, Z_1, - - - - -, Z_{3K/2}$ be the complex values of sharp corners in the physical or Z-plane. Their corresponding images on the unit circle are located at θ respectively = $0, A_1, - - - - -, \pi$. Here, we can arbitrarily assume that the point on the unit circle $\theta = 0$ maps into point Z_o in Z-plane. We also see that by symmetry the point $Z_{3K/2}$ corresponds to the point given by π on the unit circle.

We see that the Eq. (3) implies also the following set of equations:

$$\text{Log } Z_i - \text{Log } Z_{i-1} = -\int_{A_{i-1}}^{A_i} \frac{\text{Sin}^{\alpha} \prod_{i=1}^{i=\frac{K}{2}-1} (\cos\theta - \cos \alpha_{si})\, d\theta}{\prod_{i=1}^{i=K} (\cos\theta - \cos \alpha_i)^{1/2}} \qquad (7)$$

Let $\Delta Z_i = \log Z_i - \log Z_{i-1}$.

Eq. (5) can be written in an abbreviated form as:

$$\Delta Z_i = F_i(A_1, A_2, - - - - - A_{3K/2-1}) \qquad (i = 1, 3K/2) \qquad (8)$$

The above equation states that the relation between Z and the unknown singularities on the unit circle is connected through an integral operator F.

The relations given by Eq. (8) are obviously non-linear and the unknown A_i's appear as the limits of the integral. Besides the structure of the integrand (see Eq. 7) is such that it becomes infinite at one or both limits. This makes the accurate determination of the unknowns A_i challenging.

We shall proceed to describe an iterative method which would converge on unknown A_i's if the starting values are good.

We define:

$\{A^\circ\}$ = vector containing starting values of singularities or image points of corners on the unit circle, where M = 3K/2-1

$\{\Delta A^1\}$ = first order correction applied to $\{A\}$ after i^{th} iteration in an attempt to satisfy Eq. (8).

So after the first iteration better estimate of A is given by:

$$\{A^1\} = \{A^\circ\} + \{\Delta A^1\}$$

Vector $\{\Delta A^1\}$ is determined by using multi-dimensional Taylor's series and retaining only linear terms of ΔA_j. Then,

$$F_i\left[\{A^\circ\} + \{\Delta A^1\}\right] = F_i\left[\{A^\circ\}\right] + \sum_{J=1}^{M}\left(\frac{\partial F_i}{\partial A_J}\right)_0 \Delta A_J + \sum_{J=1}^{M}\left(\frac{\partial^2 F_i}{\partial A_J^2}\right)\frac{\Delta A_J^2}{2!} \tag{9}$$

$$+ \ldots, \quad [i=1, \frac{3K}{2}]$$

Neglecting squares and higher powers of ΔA_j and equating the right side to ΔF_i we get the following set of linear equations in ΔA_J.

$$\Delta Z_i = F_i\left[\{A^\circ\}\right] + \sum_{J=1}^{M}\left(\frac{\partial F_i}{\partial A_J}\right)\cdot \Delta A_J \qquad (i=1,\ 3K/2) \tag{10}$$

As expected, it turns out that one equation is redundant in (10). In a linear system of equations, it is easy to find the redundant equation and then solve for the vector $\{\Delta A\}$.

This process of finding linearized correction to the successive values of $\{A\}$ finally converges to some value $\{A^F\}$; as shown below.

$$\begin{aligned}
\{A^1\} &= \{A^\circ\} + \{\Delta A^1\} \\
\{A^2\} &= \{A^1\} + \{\Delta A^2\} \\
&\cdots\cdots \\
\{A^F\} &= \{A^{F-1}\} + \{0\}
\end{aligned} \tag{11}$$

Superscript gives the result after the particular number of iteration.

EVALUATION OF $F_i(\{A^\circ\})$. In solving the set of equations (9), we see that we need to evaluate $F_i(\{A^\circ\})$, which as defined earlier is the same as evaluating the right hand side integral at the current or the starting values of vector {A}. To evaluate such an integral, the procedure used is known as numerical method of Gaussian quadrature. As we see the integrand goes to infinity at one or both the limits. Integrals are of the following forms:

$$\int_a^b \frac{f(y)dy}{\sqrt{(b-y)}} = \sqrt{b-a} \sum_{i=1}^{n} w_i f(y_i) + R_n \qquad (12)$$

$$\int_a^b \frac{f(y)}{\sqrt{(y-a)(b-y)}}\, dy = \sum_{i=1}^{n} w_i f(y_i) + R_n$$

f(y) is a function of y, well behaved between the limits a and b. R_n is the remainder.

On the right hand side of above integrals is the typical Gaussian quadrature formula. The peculiar character of this method of numerical integration is that the discrete values of y_i at which the function f(y) is evaluated is related to the roots of applicable orthogonal polynomial. Besides each ordinate is weighted by corresponding weights w_i. In this way we obtain a greater accuracy than any other numerical integration scheme like Simpson's rule.

EVALUATION OF $\left(\frac{\partial F_i}{\partial A_J}\right)_0$. The partial derivative of F_i with respect to any A_J is also evaluated at the current or starting value of {A}. It was found to be sufficiently accurate to do this numerically by giving a small perturbation δ to the A_J. Using central difference formula:

$$\frac{\partial F_i}{\partial A_J} = \frac{F_i(A_1 - - - A_J + \delta - - -) - F_i(A_1 - - A_J - \delta - -)}{2\delta}$$

The suitably small value of δ was determined by a few trials.

CONVERGENCE OF ITERATIVE SCHEME. As mentioned earlier this iterative scheme requires a starting solution which should not be too far removed from the final solution sought.

A good starting value is proved out by simply trying it out and finding whether convergence is obtained with a few iterations only. If lack of convergence is obvious, it only means that the problem has to be further broken up in smaller and gentler steps, such that the difference between the starting and the final geometry is sufficiently smooth.

Frequently a convenient starting solution is easily obtained for equal cracks symmetrically spaced about the polar axis. For a particular situation it means solving Eq. (6) for the parameter 'TH' for the right value of K, R, and some assumed value of L. Knowning 'TH' the locations of image points of crack tips and junctions of cracks with the circle are immediately found out by using K-fold symmetry. The example for K = 4 given in Figure 2 is pertinent. Thus, the vector $\{A^\circ\}$ which lists all the singularities on the unit circle in consecutive order is set up, which in fact is our starting solution. This solution can be improved in small steps until the solution for any desired layout of the cracks is obtained.

RESULTS AND DISCUSSION. This paper will be concluded by presenting some results obtained by using this iterative method, after which the mapping function $Z = w(\zeta)$ is obtained by expanding in power series of the form.

$$Z = c[\zeta + \sum_{n=1}^{\infty} A_n \zeta^{1-n}] \qquad (13)$$

The above expansion is obtained by using Eq. (1) with known values of α_{s1}, α_{s2} - - - - - π and α_1, α_2 - - - α_K and remembering that we have assumed symmetry about the real axis. The expansion like Eq. (13) is obtained for Eq. (1) by equating the coefficients of like powers.

In the remaining part of the paper, we shall apply this method to solving three problems each with a separate geometrical layout of cracks. In each case the starting was done by symmetrical solution for eight cracks and a rapid convergence was obtained by our iterative method. The solution for each of the problems is presented in tabular form giving the coordinates x and y (see Figures 4, 6, 8) and the visual forms as the curve plots (Fiugres 5, 7, 9). For the facility of a genuine comparison the true geometry and our series solutions are presented together.

In problem 1, starting with equal cracks, we have rotated one of the cracks and brought it very close to the X-axis at an arbitrary angle of $\pi/24$. (See Figure 4)

The two tables present x and y coordinates of important points (0-12) for their "true values" and those obtained by the iterative technique and series expansion. A visual representation of the same is given in Figure 5.

In problem 2, the crack located on the X-axis is made 10 times longer than the other cracks.

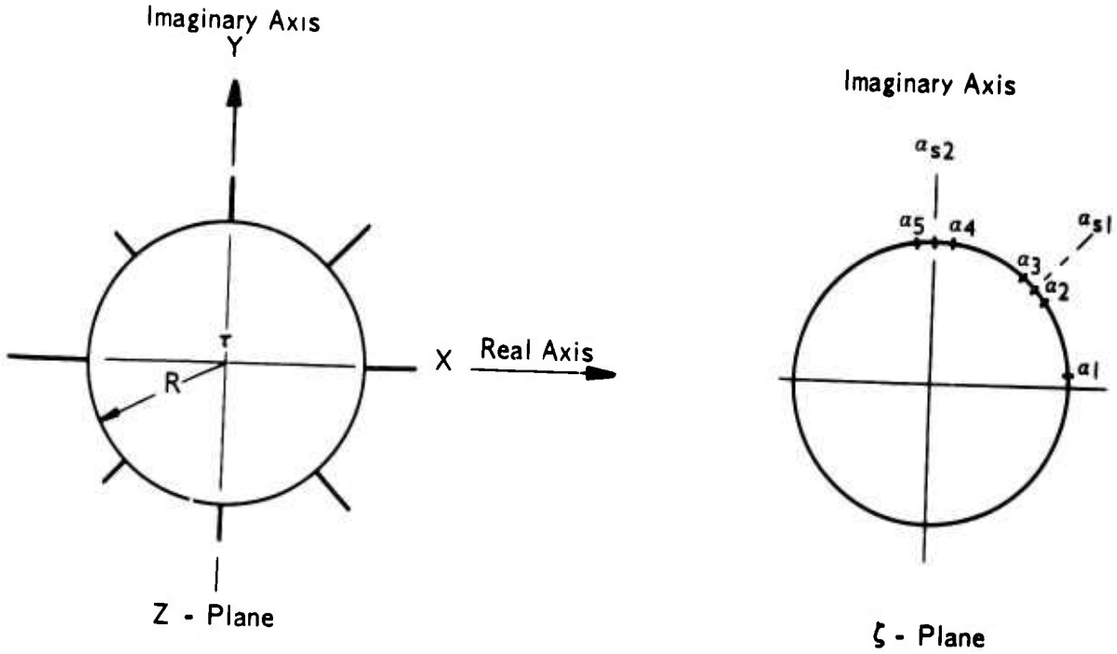
The results are presented in Figures 6, 7 in the same way as for problem 1.

In problem 3, two of the cracks are made 10 times longer than the remaining cracks.

The results are presented in Figures 8, 9 in the same way as for problem 1.

ACKNOWLEDGEMENT

The writer is grateful to Mr. J. I. Bluhm and Mr. O. L. Bowie for general encouragement and criticism.



R = Radius of the hole

$\alpha_1, \alpha_2, \ldots\ldots$ } = Image points of sharp corners,
$\alpha_{s1}, \alpha_{s2}, \ldots\ldots$ } equivalently the singularities.

Figure 1. MAPPING OF CIRCULAR HOLE WITH RADIAL CRACKS

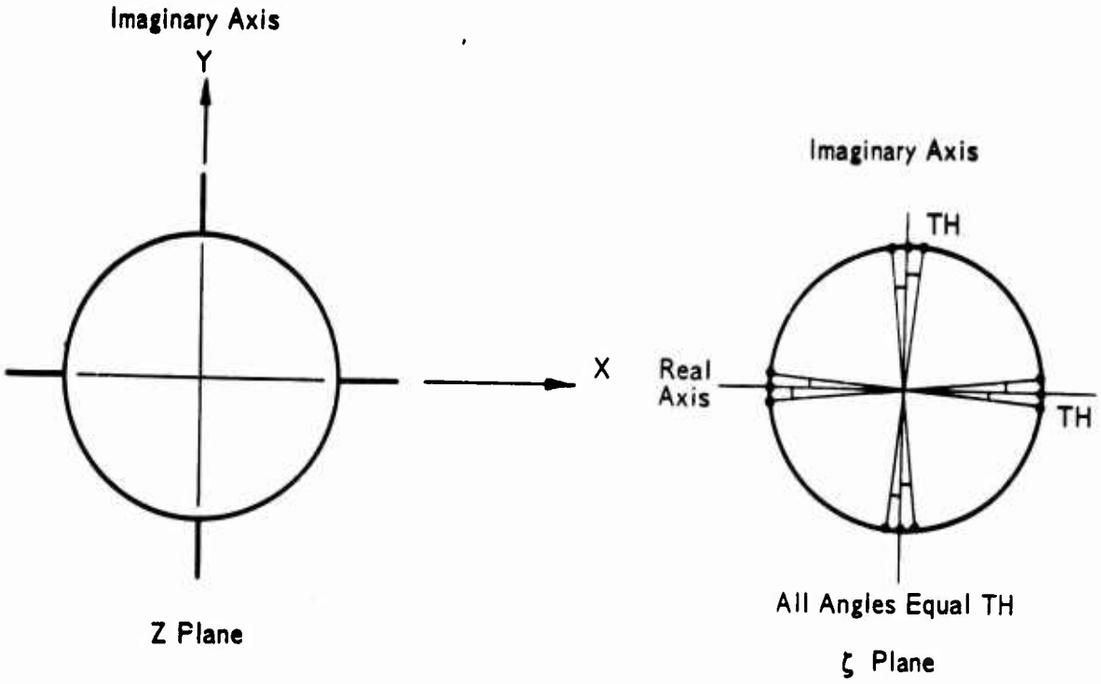
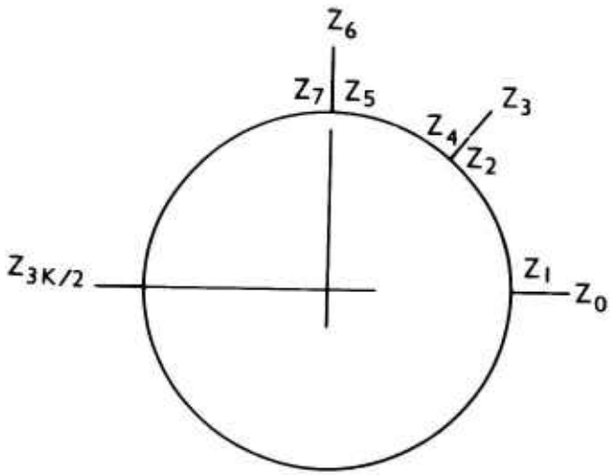


Figure 2. MAPPING OF FOUR EQUAL CRACKS SYMMETRICALLY LOCATED

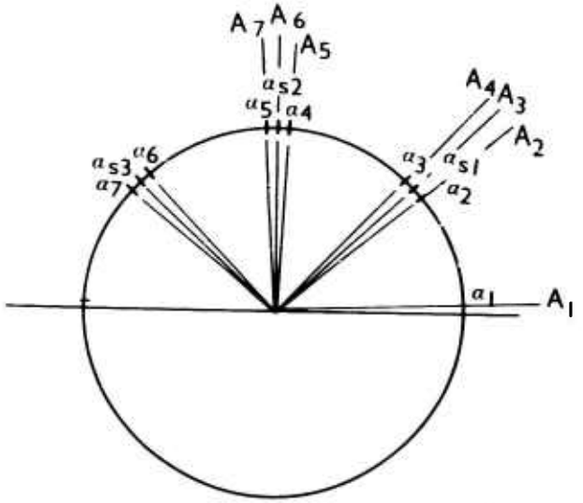


Z - Plane

Continuous Numbering of Stations

Z - Vector

$$\begin{Bmatrix} Z_1 \\ Z_2 \\ \cdot \\ \cdot \\ \cdot \\ Z_{3K/2} \end{Bmatrix}$$



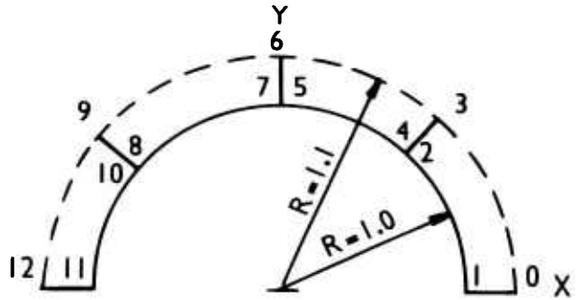
ζ - Plane

Continuous Numbering of Singularities

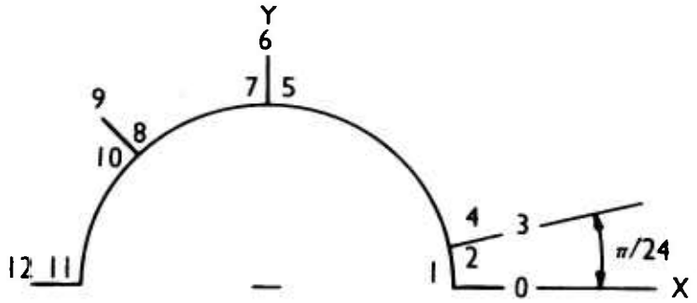
A - Vector

$$\begin{Bmatrix} A_1 \\ A_2 \\ \cdot \\ \cdot \\ A_{3K/2-1} \\ \pi \end{Bmatrix}$$

Figure 3. ITERATIVE SCHEME



Starting Geometry



Solution Sought

True Values at Points

Points	X	Y
0	1.1	0.0
1	1.0	0.0
2	0.99	0.1300
3	1.089	0.1430
4	0.99	0.1300
5	0.0	1.0
6	0.0	1.1
7	0.0	1.0
8	-0.707	0.707
9	-0.7777	0.7777
10	-0.707	0.707
11	-1.0	0.0
12	-1.1	0.0

Results of Series Solution

Points	X	Y
0	1.09989	0.0
1	1.01563	0.01447
2	1.00631	0.11779
3	1.08911	0.14154
4	1.00271	0.14692
5	0.02155	1.01342
6	0.00838	1.10036
7	-0.00550	1.01382
8	-0.70170	0.73210
9	-0.77168	0.78398
10	-0.72113	0.71284
11	-1.01386	0.01367
12	-1.10010	0.000

Figure 4. PROBLEM I - ROTATION OF EQUAL CRACKS

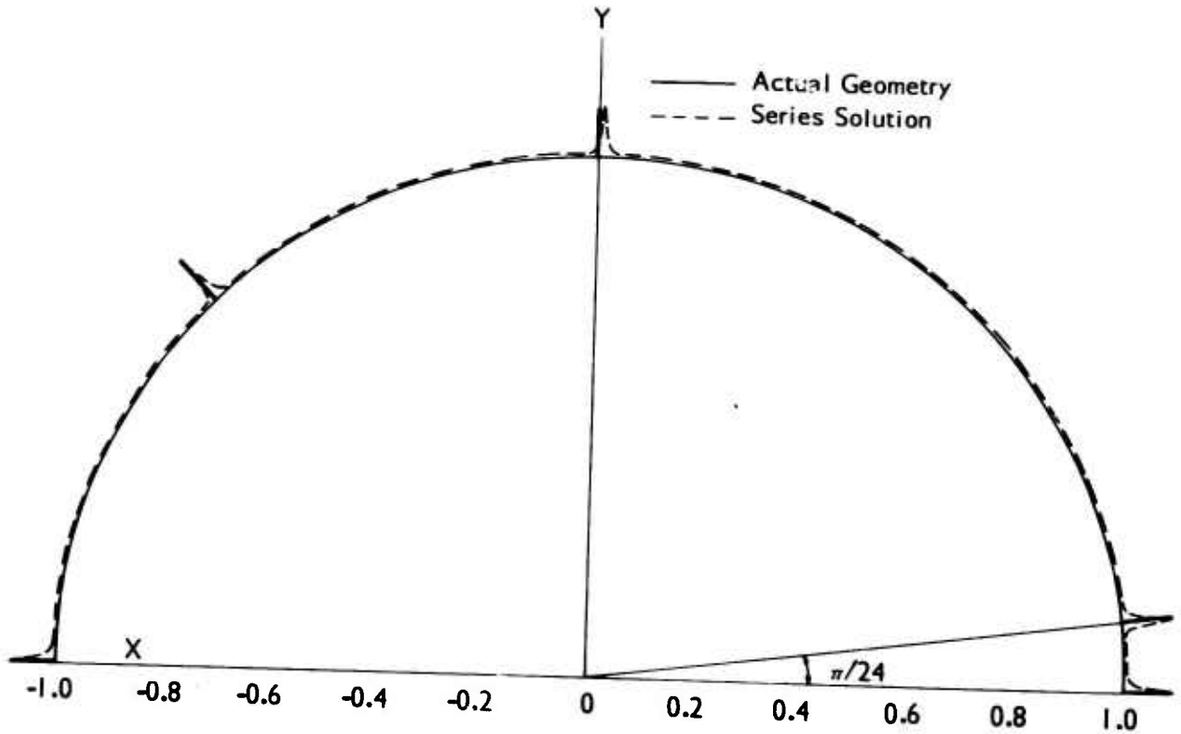
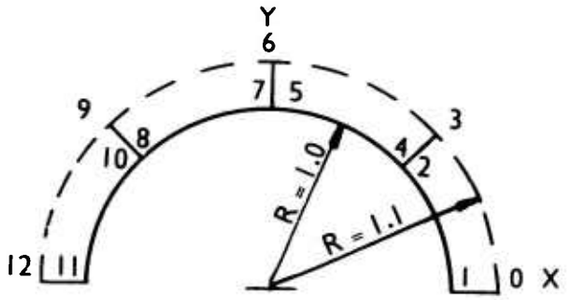
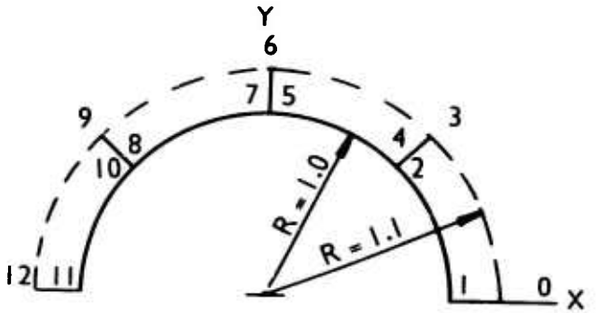


Figure 5. PROBLEM I - ROTATION OF EQUAL CRACKS



Starting Geometry



Solution Sought

True Values at Points

Points	X	Y
0	2.0	0.0
1	1.0	0.707
2	0.707	0.707
3	0.7777	0.7777
4	0.707	0.707
5	0.0	1.0
6	0.0	1.1
7	0.0	1.0
8	-0.707	0.707
9	-0.7777	0.7777
10	-0.707	0.707
11	-1.0	0.0
12	-1.1	0.0

Results of Series Solution

Points	X	Y
0	1.99957	0.0
1	1.03758	0.03800
2	0.73048	0.70626
3	0.77894	0.77862
4	0.70734	0.73015
5	0.01567	1.01451
6	0.00047	1.09815
7	-0.01514	1.01375
8	-0.70709	0.72774
9	-0.77698	0.77731
10	-0.72736	0.70695
11	-1.01438	0.01447
12	-1.09906	0.0

Figure 6. PROBLEM 2 - MAKING ONE CRACK VERY LONG

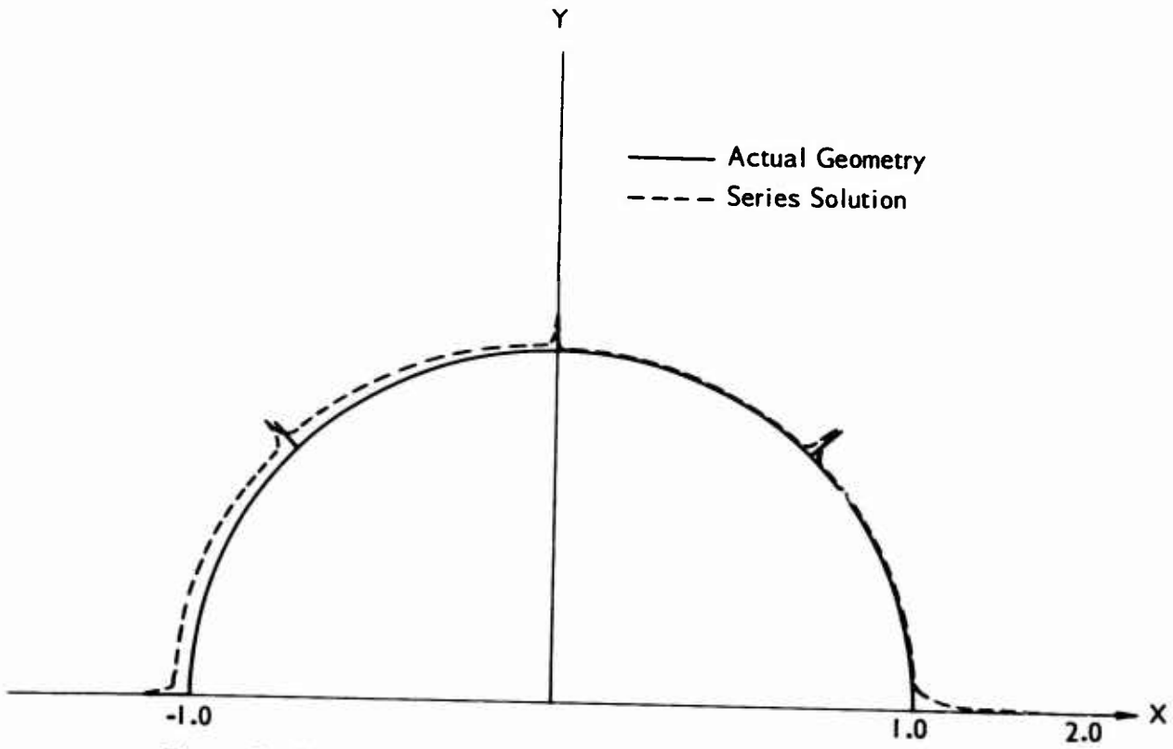
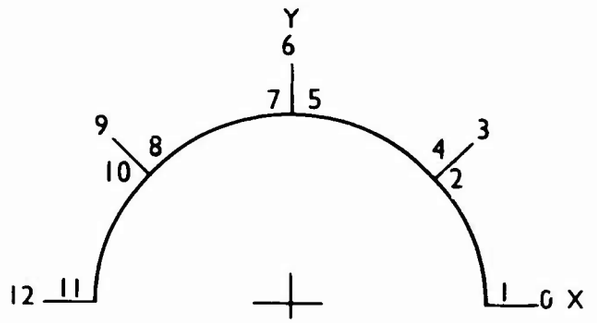
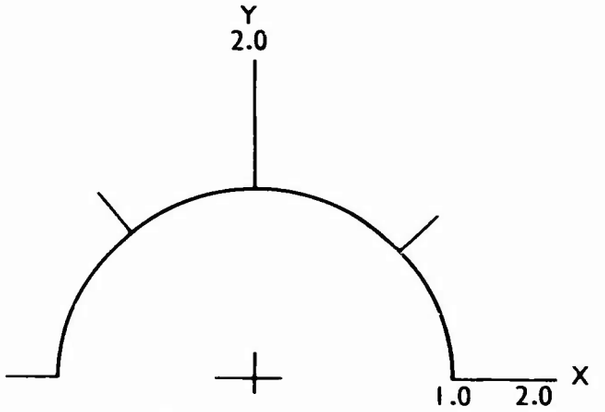


Figure 7. PROBLEM 2 - MAKING ONE CRACK VERY LONG



Starting Geometry



Solution Sought

True Values at Points

Points	X	Y
1	2.0	0.0
2	1.0	0.0
3	0.707	0.707
4	0.7777	0.7777
5	0.707	0.707
6	0.0	1.0
7	0.0	2.0
8	0.0	1.0
9	-0.707	0.707
10	-0.7777	0.7777
11	-0.707	0.707
12	-1.0	0.0
13	-1.1	0.0

Results of Series Solution

Points	X	Y
1	2.0003	0.0
2	1.04204	0.04175
3	0.73465	0.70732
4	0.77644	0.77651
5	0.70737	0.73473
6	0.04165	1.04199
7	0.00031	2.00003
8	-0.03964	1.03981
9	-0.70689	0.73102
10	-0.77904	0.77902
11	-0.73077	0.70670
12	-1.01560	0.01532
13	-1.09982	0.0

Figure 8. PROBLEM 3 - MAKING TWO CRACKS VERY LONG

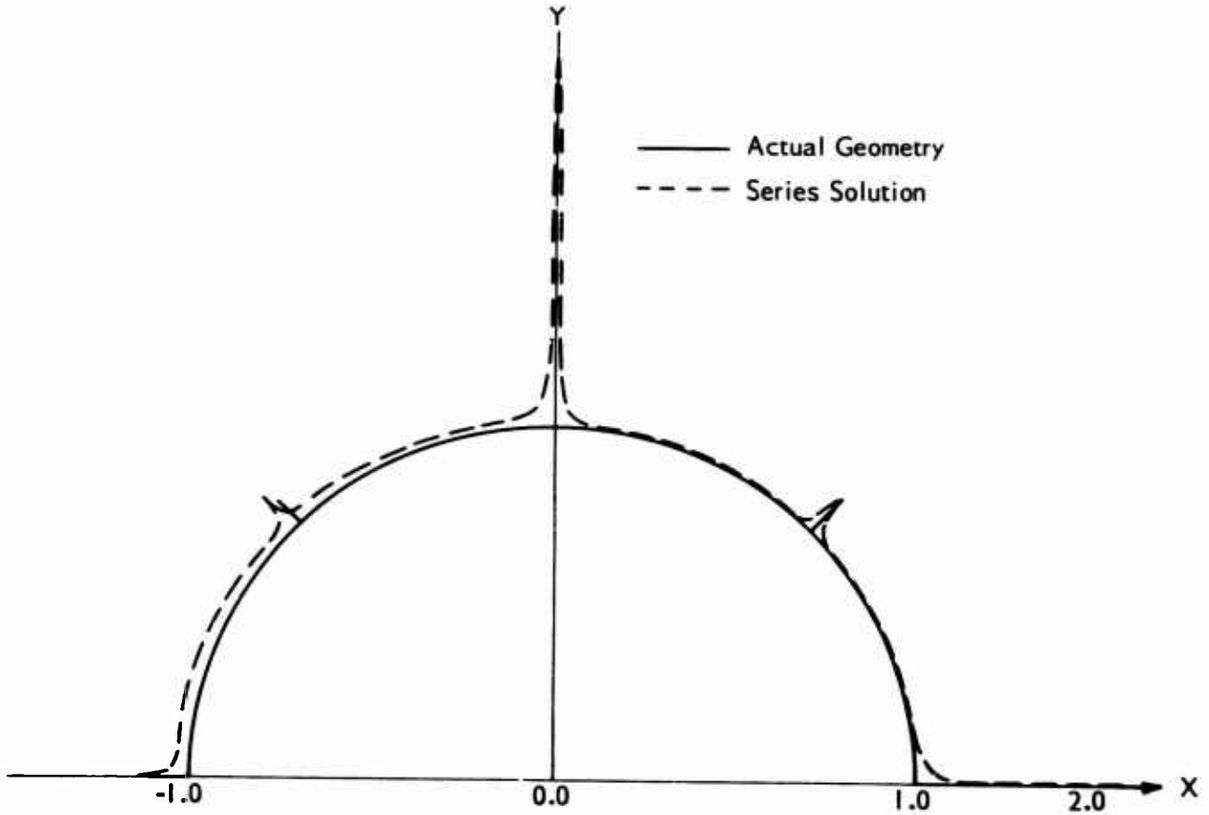


Figure 9. PROBLEM 3 - MAKING TWO CRACKS VERY LONG

A NUMERICAL TECHNIQUE FOR THE GENERATION OF CONTOURS

Merle J. Biggin
U. S. Army Topographic Command, Corps of Engineers
Washington, D. C.

With the advent of the electronic digital computer, processes in many fields have been scrutinized for the possibility of automation, The mapping industry is no stranger to the field of automation. Work has been done and much more will undoubtedly be done on developing methods and procedures for automating the production of maps. Since much work in the production of a map requires a great amount of time and labor, successful application of automated techniques in map production can result in substantial returns.

This paper will address the production of contours, a process of map making which has benefitted from automation. I will begin by describing the process as it has been done in the past and then proceed through the conceptual and mathematical development of the technique for automating this process. Finally, I will discuss the use of this technique at the United States Army Topographic Command, hereafter denoted as TOPOCOM.

I am sure that everyone here is familiar with a map in one form or another. The most common map is probably the road map found in any service station. The purpose of the road map is to represent, in a graphic form, the network of roads and cities in an area. This enables you, the user, to decide upon the most desirable route, for example, from Washington, D. C., to St. Louis, Missouri.

Another map which may be less familiar to you is the topographic map. As its name implies, this map represents the topography of an area. Topography is a term used to describe a map which depicts in graphic form the relief or shape of the earth, man-made and natural features, and their relationship to one another. These maps, for example can be used by civil engineers for determining the best place to build a road. They are also used by many others, including the largest user, the military engineer.

One of the most important features of a topographic map is the contour. A contour is a line on a map that represents an imaginary line on the surface of the earth along which all points lie at the same elevation. The simplest example of this imaginary line is the shoreline of a lake. Raising the level of the lake by a certain interval will result in another imaginary line. Graphically representing these imaginary lines on a map is one of the problems faced by a map maker.

PRECEDING PAGE BLANK

Until sixty years ago contours were drawn by men out in the field. Since then, the use of aerial photography has revolutionized the production of contours. Aerial photographs give one the ability to reconstruct the features of the earth at a reduced scale in the laboratory. Using precision instruments, elevations can be measured and contours can be very accurately constructed in much less time than by going into the field. Very simply described, this phase of map production is accomplished by stereoscopically viewing the photographs and tracing lines which are of constant elevation. The production of contours is still a manual operation which requires a large amount of time in view of the need for quickly producing maps today.

As a result of the need to produce maps quickly, an automated method of compiling map information was developed by the Army. This method features an electronic correlation of corresponding images on two photographs to arrive at a gridded network of elevations covering the area of interest. These data are the input to the automated contouring process.

Our input data were derived from a measurement process. Therefore, at best our only cause for worry is random measurement error. I have found through experience and analysis of the data acquisition system that the only additional errors of significance are occasional blunders, which are of sufficient magnitude and distribution that they may easily be located and corrected. Random errors in the data result in non-smooth and sometimes discontinuous contours. Therefore, the data must be smoothed or adjusted to eliminate these undesirable effects.

There are many methods of smoothing which can be applied to this problem. One method is to divide the surface to be contoured into many small surfaces which can be adjusted by fitting planes or higher-order surfaces to the data. The difficulty with this method is that there usually aren't enough data points available to adequately define a surface which contains the desired degree of detail and continuity between adjacent surfaces for topographic mapping. A second method is to smooth the data one profile at a time - a profile being a series of points which have equal x or y values. The disadvantage of this approach is the difficulty in finding a simple function which will exhibit the detail required over the complete profile. A modification of the last method was the approach to smoothing that was developed.

By smoothing only short segments of profiles one can use polynomials of low degree and still retain an adequate amount of detail. In order to enforce sufficient continuity between segments, the smoothing is accomplished on overlapping intervals.

In our case, a typical area or model to be contoured contains an average of 250,000 points; with smoothing done on 12 to 14 points per profile segment. Since this represents more than 30,000 data adjustments,

the only remaining serious problem is to develop an efficient smoothing algorithm.

The following discussion describes the development of the smoothing algorithm. Using a polynomial of degree r with n observation equations we have observations of the form:

$$Z_i = a_o + a_1 X_i + a_2 X_i^2 + \ldots + a_r X_i^r \, , \; i = 1,2,\ldots,n \, , \; r<n$$

where: Z_i are the observed elevations on a profile segment

X_i are their corresponding horizontal positions and

a_j are the coefficients of the rth degree polynomial

using matrix notation we can write the observation equations as

$Xa = z$ where X is a Vandermonde matrix formed from the horizontal positions,

a is the vector of polynomial coefficients, and

z is the vector of observed elevation values.

Since we want to perform a smoothing operation, it is preferable to have a highly overdetermined system. This is accomplished sufficiently well when n the number of observation equations, is two to five times r, the degree of the smoothing polynomial to be determined. A least squares adjustment is performed with the result that the estimated values of the polynomial coefficients are elements of the vector

$$\bar{a} = (X^T X)^{-1} \quad X^T z$$

substituting the estimated values of the polynomial coefficients into the observation equations gives us the smoothed values of the elevations.

$$\bar{z} = X\bar{a} = X(X^T X)^{-1} \quad X^T z \quad = Bz$$

Ordinarily these series of computations, to obtain the smoothed values of the elevations, would be performed for each interval which is adjusted. As noted previously, this may amount to a great many adjustments and hence a large amount of computing time.

The amount of computing time can be reduced as follows: we first assume the number of data points, in a profile segment over which we are smoothing, is constant for the entire model. On a profile, the horizontal positions of the elevations are equally spaced and of a constant interval, therefore the adjustment matrix B is constant. Once it is computed, it

need not be computed again and a data adjustment is performed by the multiplication of one vector by one matrix. This is where the savings of computation time is realized, but a work of caution is given. Realizing that the matrix B is of dimension nxn, the saving of computation time is decreased and actually becomes a loss when the number of observation equations becomes large compared to the degree of the polynomial used in the adjustment.

After the adjustment has been performed, the maximum difference between the observed and the computed elevations is determined. If this maximum difference is greater than an arbitrary tolerance, the corresponding observation is replaced by the computed value. This allows one to use the same adjustment matrix B in readjusting the data which has been corrected for erratic observations, resulting in an iterative adjustment process. Since our data contains only random errors and occasional blunders, it usually requires only one or two iterations to converge to a satisfactory solution.

After the elevation data has been smoothed, the next step is to determine the points which define a contour. That is, X, Y values of points which have an elevation value that is a multiple of the contour interval. These are determined by examining two adjacent points of the grid. If the elevation of one point is above and the other below a contour level, then the horizontal position of the contour point is determined by a linear interpolation between the two data points. This process continues until all points of the grid are examined in this manner. The final step in the contouring process is arranging these contour points in a sequence such that, an X, Y plotter, when commanded to proceed to successive points in the sequence, will describe the contour.

The process of arranging these points into a contour sequence is as follows: considering only those points of one contour level, a starting point is selected. We then examine all points in the immediate vicinity of the start point. That point which is nearest to the starting point is considered to be the next point in the sequence of contour points. This new point is now considered as the starting point and the process continues in an identical manner until there are no unused points remaining in the immediate vicinity of the last point to be considered. The two possibilities which result are that the contour closes upon itself or that it goes to the edge of our model. In either case, if an unused contour point of that elevation remains, the process of arranging the points into a contour sequence is initiated again. The next contour elevation is processed in the same manner after all contour points of a particular elevation have been ordered into contour sequences. This process continues until the area has been completely contoured, at which time the contour sequences are used to command an X, Y plotter to draw the contours.

This contouring technique was developed on an IBM computer at TOPOCOM. A model consisting of a grid network of 120,000 points can be processed in a little less than ten minutes. With this large amount of data it is necessary to use intermediate data storage devices. At our installation we are presently limited to magnetic tape storage. I anticipate a significant decrease in processing time when the program is modified for a computer with larger memory and/or faster access storage devices.

This automated contouring technique has not been completely implemented into the present map production procedures at TOPOCOM. Of course, all new developments require time for implementation into a production environment. And, an automated component of a system cannot be fully utilized until all other components of the system are made compatible through modifications which may include the automation of those components.

I have described how the automated contouring process of map production has been developed at TOPOCOM. The development of the efficient data adjustment scheme allows large amounts of data to be used in the automatic contouring process to produce the required detail for topographic mapping. The short time necessary for processing on a computer will make this technique a feasible component of an automated map production system.

In conclusion, this technique shows that the production of contours can be automated. The large amounts of data which will become available, as automated methods of data acquisition are developed, will make such a technique a necessary part of an automated system for map production.

THE STRESSES PRODUCED IN A SEMI-INFINITE LINEAR COSSERAT CONTINUUM BY A MOVING SURFACE FORCE

George Eason
Mathematics Research Center, U. S. Army
Madison, Wisconsin

ABSTRACT. The problem considered here is that of a semi-infinite homogeneous isotropic solid, to the surface of which is applied a line load moving with uniform velocity for all time. In an attempt to assess the effects of couple stresses in such problems, the solid is assumed to be of linear Cosserat (or micropolar) type. Plane strain conditions are assumed, and a solution is obtained by means of integral transforms which is valid when the speed of the applied load is below that of Rayleigh waves for the solid. The stress components are expressed in terms of single integrals which may be evaluated numerically. As an example, the value of one of the stress components is calculated at the surface of the half-space.

1. INTRODUCTION. In recent years, there has been considerable interest in continuum models which incorporate couple-stress terms into the equations of elasticity. Couple-stress effects were considered by the Cosserats [1], but much of the recent work is based on the papers of Mindlin [2,3,4] and Eringen [5,6,7]. This literature has been reviewed in [8] and it will not be examined again here. Of particular relevance to the present work are references [4] and [7] in which the basic equations for the type of material considered here are established. It should be noted that somewhat similar basic equations have been encountered in the theory of composite elastic solids (see [11]) and in the theory of plates [12, 13].

Almost all the problems solved in the context of couple stress theory have been for statical situations and comparitively little attention has been given to problems involving wave propagation. The basic equations for a linear Cosserat (or micro-polar) continuum were examined in [8] and the significance of the various elastic wave speeds established. Solutions corresponding to plane waves and surface waves were obtained. By using a somewhat different approach from that used in [8] Suhubi [14] and Parfitt and Eringen [15] have also considered plane wave propagation. The form of the basic equations developed in [8] is adopted here to consider the quasi-static problem of a semi-infinite homogeneous isotropic solid, to the surface of which is applied a line load moving with uniform velocity for all time. Plane strain conditions are envisaged. This is likely to be the simplest problem in which both wave propagation and couple stress effects play a part. Problems of this type have been considered in the context of classical elasticity by Sneddon [9], Cole and Huth [10] and other authors. The method of solution adopted here is similar to that used in [9] and [10] and is by means of integral transforms.

This paper has been issued as an MRC Technical Summary Report No. 994.

PRECEDING PAGE BLANK

The basic equations of the problem are stated in section 2 and a solution is obtained by means of Fourier transforms corresponding to an applied force which is in a direction normal to the surface of the solid. This solution is in the form of an integral with an infinite range. It should be possible to evaluate this integral numerically away from the surface of the solid. On the surface of the solid, this is not likely to be possible and in section 3 an alternative form for the integral is obtained by means of contour integration. Some numerical results are presented in graphical form for the non-zero surface stress. It is found that the presence of couple stress terms in the equations leads to additional terms in the expressions for the stress components which are of significance near the point of application of the force.

The remainder of this paper has been reproduced photographically from the author's manuscript.

2. The solution of the basic equations.

The basic equations for a linear Cosserat continuum have been established in [4, 7]. The notation to be adopted here is essentially that of Mindlin [4]. In terms of a cartesian tensor notation the equations of motion, in the absence of body force and body couple terms, are

$$\tau_{ij,\,i} + \sigma_{ij,\,i} = \rho \ddot{u}_j \,, \tag{2.1}$$

$$\mu_{\ell ij,\,\ell} + \sigma_{ij} = \rho k^2 \ddot{\psi}_{ij} \,, \tag{2.2}$$

where a dot denotes differentiation with respect to time, τ_{ij} and σ_{ij} are respectively the symmetric and antisymmetric parts of the stress tensor, u_i is a component of the displacement vector, $\mu_{\ell ij}$ is the couple stress, ψ_{ij} is the rotation of the micro-structure, ρ is the density of the macro-structure and k is related to the size of the micro-structure (see [3]). For a homogeneous isotropic solid of this type the stress-strain relations take the forms

$$\tau_{ij} = \lambda\, \delta_{ij}\, u_{k,\,k} + \mu\,(u_{j,\,i} + u_{i,\,j}) \,, \tag{2.3}$$

$$\sigma_{ij} = 2\beta\,(\omega_{ij} - \psi_{ij}), \tag{2.4}$$

$$\mu_{ijk} = \alpha_1(\delta_{ik}\,\psi_{\ell j,\,\ell} + \delta_{ij}\,\psi_{k\ell,\,\ell}) + 2\alpha_2\,\psi_{jk,\,i} + \alpha_3\,(\psi_{ij,\,k} + \psi_{ki,\,j}) \,, \tag{2.5}$$

where α_1, α_2, α_3, β, λ and μ are constants and δ_{ij} is the Kronecker delta. The quantity ω_{ij} is the rotation of the macro-structure given by

$$\omega_{ij} = \frac{1}{2}\,(u_{j,\,i} - u_{i,\,j}) \,. \tag{2.6}$$

In [8] it was shown that by taking suitable combinations of (2.1)-

(2.6) it is possible to express these equations in terms of certain basic wave speeds. In particular it was found that the basic equations may be combined to give

$$c_1^2 \epsilon_{,ii} = \ddot{\epsilon} , \tag{2.7}$$

$$c_3^2 \omega_{ki,jj} + (c_3^2 - c_5^2)(\zeta_{k,i} - \zeta_{i,k}) = \ddot{\omega}_{ki} , \tag{2.8}$$

$$c_4^2 \zeta_{j,kk} - \nu^2 \zeta_j + \nu^2 \omega_{ij,i} = \ddot{\zeta}_j , \tag{2.9}$$

where

$$\epsilon = u_{i,i} , \tag{2.10}$$

$$\zeta_j = \psi_{ij,i} , \tag{2.11}$$

and

$$c_1^2 = (\lambda + 2\mu)/\rho , \tag{2.12}$$

$$c_3^2 = (\mu + \beta)/\rho , \tag{2.13}$$

$$c_4^2 = (2\alpha_2 - \alpha_1 - \alpha_3)/\rho k^2 , \tag{2.14}$$

$$c_5^2 = \mu / \rho , \tag{2.15}$$

$$\nu^2 = 2\beta/\rho k^2 . \tag{2.16}$$

Equations (2.8) and (2.9) may be combined to give one single equation if this is desired.

Let $x = x_1$, $y = x_2$ be cartesian coordinates and let t denote the time. The problem to be considered here is that of a half-space, $y > 0$, to the surface of which is applied a line load moving with uniform velocity w in the positive x-direction for all time. The case of normal loading is

considered and plane strain conditions are assumed. Equations (2.7), (2.8) and (2.9) then result in the equations

$$\{c_1^2 \left(\frac{\partial^2}{\partial x^2} + \frac{\partial^2}{\partial y^2}\right) - \frac{\partial^2}{\partial t^2}\} \epsilon = 0 , \tag{2.17}$$

$$\{c_3^2 \left(\frac{\partial^2}{\partial x^2} + \frac{\partial^2}{\partial y^2}\right) - \frac{\partial^2}{\partial t^2}\} \omega_{12} - (c_3^2 - c_5^2)\left(\frac{\partial^2}{\partial x^2} + \frac{\partial^2}{\partial y^2}\right) \psi_{12} = 0, \tag{2.18}$$

$$\{c_4^2 \left(\frac{\partial^2}{\partial x^2} + \frac{\partial^2}{\partial y^2}\right) - \frac{\partial^2}{\partial t^2} - \nu^2\} \psi_{12} + \nu^2 \omega_{12} = 0 , \tag{2.19}$$

where now

$$\epsilon = \frac{\partial u}{\partial x} + \frac{\partial v}{\partial y} , \tag{2.20}$$

$$\omega_{12} = \frac{1}{2}\left(\frac{\partial v}{\partial x} - \frac{\partial u}{\partial y}\right) , \tag{2.21}$$

and $u = u_1$, $v = u_2$ are the displacement components. The problem under consideration here is quasi-static, and it is to be expected that all quantities will depend on y and z alone, where

$$z = x - wt . \tag{2.22}$$

Equations (2.17), (2.18) and (2.19) now take the forms

$$\{(c_1^2 - w^2) \frac{\partial^2}{\partial z^2} + c_1^2 \frac{\partial^2}{\partial y^2}\} \epsilon = 0 , \tag{2.23}$$

$$\{(c_3^2 - w^2) \frac{\partial^2}{\partial z^2} + c_3^2 \frac{\partial^2}{\partial y^2}\} \omega_{12} - (c_3^2 - c_5^2)\left(\frac{\partial^2}{\partial z^2} + \frac{\partial^2}{\partial y^2}\right)\psi_{12} = 0, \tag{2.24}$$

$$\{(c_4^2 - w^2) \frac{\partial^2}{\partial z^2} + c_4^2 \frac{\partial^2}{\partial y^2} - \nu^2\} \psi_{12} + \nu^2 \omega_{12} = 0 . \tag{2.25}$$

Equations (2.24) and (2.25) combine to give the single equation

$$\left[\left\{\left(c_3^2 - w^2\right)\frac{\partial^2}{\partial z^2} + \frac{\partial^2}{\partial y^2}\right\}\left\{\left(c_4^2 - w^2\right)\frac{\partial^2}{\partial z^2} + c_4^2\frac{\partial^2}{\partial y^2}\right\}\right.$$

$$\left. - \nu^2\left\{\left(c_5^2 - w^2\right)\frac{\partial^2}{\partial z^2} + c_5^2\frac{\partial^2}{\partial y^2}\right\}\right]\left(\omega_{12}, \psi_{12}\right) = 0 . \qquad (2.26)$$

To obtain solutions of (2.23) and (2.26) it is convenient to introduce an infinite Fourier transform in z defined by

$$\bar{f}(\zeta, y) = \int_{-\infty}^{\infty} f(z, y)\, e^{i\zeta z}\, dz . \qquad (2.27)$$

When (2.23) and (2.26) are multiplied by $\exp(i\zeta z)$ and an integration performed with respect to z over the range $-\infty$ to $+\infty$ it is found that

$$\left\{c_1^2\frac{\partial^2}{\partial y^2} - \zeta^2\left(c_1^2 - w^2\right)\right\}\bar{\epsilon} = 0 , \qquad (2.28)$$

$$\left[\left\{c_3^2\frac{\partial^2}{\partial y^2} - \zeta^2\left(c_3^2 - w^2\right)\right\}\left\{c_4^2\frac{\partial^2}{\partial y^2} - \zeta^2\left(c_4^2 - w^2\right)\right\}\right.$$

$$\left. - \nu^2\left\{c_5^2\frac{\partial^2}{\partial y^2} - \zeta^2\left(c_5^2 - w^2\right)\right\}\right]\left[\bar{\omega}_{12}, \bar{\psi}_{12}\right] = 0 . \qquad (2.29)$$

Solutions of these equations which are valid when w is less than the least of c_1, c_3, c_4 or c_5 may now be written down. The solutions which remain finite as $y \to \infty$ are given by

$$\bar{\epsilon} = A\left(n_1^2 - \zeta^2\right) e^{-n_1 y} , \qquad (2.30)$$

$$\bar{\omega}_{12} = \left(n_2^2 - \zeta^2\right) B_1\, e^{-n_2 y} + \left(n_3^2 - \zeta^2\right) C_1\, e^{-n_3 y} , \qquad (2.31)$$

$$\bar{\psi}_{12} = \left(n_2^2 - \zeta^2\right) B_2\, e^{-n_2 y} + \left(n_3^2 - \zeta^2\right) C_2\, e^{-n_3 y} , \qquad (2.32)$$

where A, B_1, B_2, C_1 and C_2 are independent of y. In (2.30)

$$n_1 = \left| \frac{\zeta}{c_1} (c_1^2 - w^2)^{1/2} \right| , \tag{2.33}$$

and in (2.31) and (2.32)

$$n_{2,3} = \frac{1}{c_3 c_4 \sqrt{2}} \Bigg(\{c_5^2 \nu^2 + \zeta^2 [c_3^2 (c_4^2 - w^2) + c_4^2 (c_3^2 - w^2)]\}$$

$$\pm \Big\langle \{c_5^2 \nu^2 + \zeta^2 [c_3^2 (c_4^2 - w^2) + c_4^2 (c_3^2 - w^2)]\}^2 - 4 c_3^2 c_4^2 [\zeta^4 (c_3^2 - w^2)(c_4^2 - w^2) +$$

$$+ \nu^2 \zeta^2 (c_5^2 - w^2)] \Big\rangle^{1/2} \Bigg)^{1/2}$$

$$= \frac{1}{c_3 c_4 \sqrt{2}} \Bigg(\{c_5^2 \nu^2 + \zeta^2 [c_3^2 (c_4^2 - w^2) + c_4^2 (c_3^2 - w^2)]\}$$

$$\pm \Big\langle \{\zeta^2 w^2 (c_3^2 - c_4^2) + \frac{\nu^2}{c_3^2 - c_4^2} (2 c_3^2 c_4^2 - c_5^2 c_3^2 - c_5^2 c_4^2)\}^2$$

$$+ \frac{4 \nu^4 c_3^2 c_4^2 (c_5^2 - c_4^2)(c_3^2 - c_5^2)}{(c_3^2 - c_4^2)^2} \Big\rangle^{1/2} \Bigg)^{1/2} , \tag{2.34}$$

where n_2 corresponds to the upper sign and n_3 to the lower sign. Using arguments similar to those used in [8] it is not difficult to show that, for the range of values of w being considered here, n_1, n_2 and n_3 are always real regardless of the ordering of the wave speeds c_3, c_4 and c_5. Once w assumes values greater than the lowest wave speed in the solid the solution presented here may require modification and treatment of the various cases which can occur becomes extremely complicated.

The quantities B_1, B_2 and C_1, C_2 are not independent but are linked through either (2.24) or (2.25). When (2.31) and (2.32) are substituted into

(2.25) it is found that

$$\nu^2 B_1 = -B_2 \{c_4^2 n_2^2 - \zeta^2(c_4^2 - w^2) - \nu^2\}, \tag{2.35}$$

$$\nu^2 C_1 = -C_2 \{c_4^2 n_3^2 - \zeta^2(c_4^2 - w^2) - \nu^2\}. \tag{2.36}$$

The remaining conditions which determine the unknown coefficients A, B_1, B_2, C_1 and C_2 are provided by the conditions assumed on the boundary $y = 0$.

Equations (2.30) and (2.31) may be solved for the transformed displacement components to give expressions of the forms

$$\bar{u} = -i\zeta A e^{-n_1 y} + 2 B_1 n_2 e^{-n_2 y} + 2 C_1 n_3 e^{-n_3 y}, \tag{2.37}$$

$$\bar{v} = -A n_1 e^{-n_1 y} - 2 i B_1 \zeta e^{-n_2 y} - 2 i C_1 \zeta e^{-n_3 y}. \tag{2.38}$$

By taking the appropriate forms of (2.3), (2.4) and (2.5) and transforming with respect to z expressions may be obtained for the stress components which give

$$\bar{\tau}_{11} + \bar{\tau}_{22} = \bar{\tau}_{xx} + \bar{\tau}_{yy} = 2(\lambda + \mu)\bar{\epsilon}, \tag{2.39}$$

$$\bar{\tau}_{11} - \bar{\tau}_{22} = \bar{\tau}_{xx} - \bar{\tau}_{yy} = 2\mu\left(-i\zeta\bar{u} - \frac{d\bar{v}}{dy}\right)$$

$$= -2\mu\{A(n_1^2 + \zeta^2) e^{-n_1 y} + 4 i B_1 \zeta n_2 e^{-n_2 y} + 4 i C_1 \zeta n_3 e^{-n_3 y}\}, \tag{2.40}$$

$$\bar{\tau}_{12} = \bar{\tau}_{xy} = \mu\left(\frac{d\bar{u}}{dy} - i\zeta\bar{v}\right)$$

$$= 2\mu\{i\zeta n_1 A e^{-n_1 y} - (n_2^2 + \zeta^2) B_1 e^{-n_2 y} - (n_3^2 + \zeta^2) C_1 e^{-n_3 y}\}, \tag{2.41}$$

$$\bar{\sigma}_{12} = \bar{\sigma}_{xy} = 2\beta(\bar{\omega}_{12} - \bar{\psi}_{12}), \tag{2.42}$$

$$\bar{\mu}_{112} = \bar{\mu}_{xxy} = -i\zeta(2\alpha_2 - \alpha_1 - \alpha_3)\bar{\psi}_{12}, \tag{2.43}$$

$$\bar{\mu}_{212} = \bar{\mu}_{yxy} = (2\alpha_2 - \alpha_1 - \alpha_3)\frac{d\bar{\psi}_{12}}{dy} \quad . \tag{2.44}$$

The problem being considered here is that of a point force of magnitude P which moves with velocity w and which is applied in a direction normal to the boundary. Such an applied force is represented by the boundary conditions

$$\tau_{22} = - P\, \delta(x - w t) = - P\, \delta(z) , \tag{2.45}$$

$$\tau_{21} + \sigma_{21} = 0 , \tag{2.46}$$

$$\mu_{212} = 0 , \tag{2.47}$$

where $\delta(x)$ is the Dirac delta function. These expressions result in the conditions on $y = 0$

$$\bar{\tau}_{22} = - P , \tag{2.48}$$

$$\bar{\tau}_{21} + \bar{\sigma}_{21} = 0 , \tag{2.49}$$

$$\bar{\mu}_{212} = 0 , \tag{2.50}$$

so that

$$A\zeta^2 (2c_5^2 - w^2) + 4i\zeta B_1 n_2 c_5^2 + 4i\zeta C_1 n_3 c_5^2 = -P/\rho , \tag{2.51}$$

$$i\zeta n_1 c_5^2 A - [c_3^2 n_2^2 + \zeta^2(2c_5^2 - c_3^2)]B_1 - [c_3^2 n_3^2 + \zeta^2(2c_5^2 - c_3^2)]C_1$$

$$+ (c_3^2 - c_5^2)(n_2^2 - \zeta^2)B_2 + (c_3^2 - c_5^2)(n_3^2 - \zeta^2)C_2 = 0, \tag{2.52}$$

$$n_2(n_2^2 - \zeta^2)B_2 + n_3(n_3^2 - \zeta^2) C_2 = 0 . \tag{2.53}$$

Equations (2.35), (2.36), (2.51), (2.52) and (2.53) may now be solved to give

$$A = -P\, \xi / \rho\Delta , \tag{2.54}$$

$$B_1 = - \frac{i P \phi_2 n_3 n_1 c_5^2 (n_3^2 - \zeta^2)}{\rho\zeta \Delta} , \tag{2.55}$$

$$C_1 = \frac{i P \phi_3 n_2 n_1 c_5^2 (n_2^2 - \zeta^2)}{\rho \zeta \Delta} , \tag{2.56}$$

where

$$\phi_1 = (c_3^2 - c_5^2)(2 c_5^2 - w^2) , \tag{2.57}$$

$$\phi_2 = (c_4^2 - w^2) \zeta^2 + \nu^2 - c_4^2 n_2^2 , \tag{2.58}$$

$$\phi_3 = (c_4^2 - w^2) \zeta^2 + \nu^2 - c_4^2 n_3^2 , \tag{2.59}$$

$$\eta_2 = (2 c_5^2 - w^2) [c_3^2 n_2^2 + \zeta^2 (2c_5^2 - c_3^2)] - 4 n_1 n_2 c_5^4 , \tag{2.60}$$

$$\eta_3 = (2 c_5^2 - w^2) [c_3^2 n_3^2 + \zeta^2 (2c_5^2 - c_3^2)] - 4 n_1 n_3 c_5^4 , \tag{2.61}$$

$$\xi = (2 c_5^2 - w^2) \{ c_4^2 (n_2^2 - \zeta^2)(n_3^2 - \zeta^2)(n_2 - n_3) + (\zeta^2 w^2 - \nu^2)[n_2 (n_2^2 - \zeta^2) - n_3 (n_3^2 - \zeta^2)] \} , \tag{2.62}$$

$$\Delta = \phi_1 \nu^2 (n_3^2 - \zeta^2)(n_2^2 - \zeta^2)(n_2 - n_3) - \phi_3 \eta_3 n_2 (n_2^2 - \zeta^2) + \phi_2 \eta_2 n_3 (n_3^2 - \zeta^2) . \tag{2.63}$$

By substituting from (2.54) into (2.30) and then into (2.39) it is found that

$$\bar{\tau}_{11} + \bar{\tau}_{22} = \frac{2 P w^2 (c_1^2 - c_5^2) \xi \zeta^2 e^{-n_1 y}}{c_1^2 \Delta} , \tag{2.64}$$

and the Fourier transform inversion theorem then gives

$$\tau_{11} + \tau_{22} = \frac{P w^2 (c_1^2 - c_5^2)}{\pi c_1^2} \int_{-\infty}^{\infty} \frac{\xi \zeta^2 e^{-n_1 y} e^{-i \zeta z}}{\Delta} d\zeta$$

$$= \frac{2 P w^2 (c_1^2 - c_5^2)}{\pi c_1^2} \int_0^{\infty} \frac{\xi \zeta^2 \cos(\zeta z)}{\Delta} e^{-n_1 y} d\zeta . \tag{2.65}$$

By following a similar procedure to that just used for the sum of the normal stress components it is found that

$$\tau_{11} - \tau_{22} = \frac{2 P c_5^2}{c_1^2 \pi} \int_0^\infty \frac{\cos(\zeta z)}{\Delta} \{(2c_1^2 - w^2)\, \xi \zeta^2 \, e^{-n_1 y}$$

$$- 4 n_1 n_2 n_3 c_1^2 c_5^2 [\, \phi_2 (n_3^2 - \zeta^2) e^{-n_2 y} - \phi_3 (n_2^2 - \zeta^2) e^{-n_3 y} \,] \} d\zeta, \quad (2.66)$$

$$\tau_{12} = \frac{2 P c_5^2}{\pi} \int_0^\infty \frac{n_1 \sin(\zeta z)}{\zeta \Delta} \{ - \xi \zeta^2 \, e^{-n_1 y}$$

$$+ c_5^2 n_3 \phi_2 (n_3^2 - \zeta^2)(n_2^2 + \zeta^2) e^{-n_2 y} - c_5^2 n_2 \phi_3 (n_2^2 - \zeta^2)(n_3^2 + \zeta^2) e^{-n_3 y} \} d\zeta, \quad (2.67)$$

$$\sigma_{12} = - \frac{2 P c_5^2 (c_3^2 - c_5^2)}{\pi} \int_0^\infty \frac{n_1 \sin(\zeta z)}{\zeta \Delta} (n_2^2 - \zeta^2)(n_3^2 - \zeta^2) [\, n_3 (\phi_2 - \nu^2) e^{-n_2 y}$$

$$- n_2 (\phi_3 - \nu^2) \, e^{-n_3 y} \,] d\zeta \, . \quad (2.68)$$

It is unlikely that these integrals can be evaluated analytically so that it will be necessary to use numerical methods. The quantity Δ has zeros at $\zeta = 0$ and at $\zeta\, w = \nu$, but for both values of ζ the numerators also vanish so that the integrands do not possess singularities. In addition, for a given combination of elastic wave speeds, there is a value of w, say w_R, such that for $w < w_R$ the quantity Δ has no additional zeros, but for $w > w_R$ there is another positive real zero in the range of integration. The value w_R corresponds to the Rayleigh wave speed in a classical elastic solid and places an additional restriction on the range of validity of the present solution. In practice this is not a serious additional restriction since w_R is usually close

to the smallest wave speed. In the following it is assumed that $w < w_R$. For this range of w the integrands have no singularities and it should be possible to evaluate the integrals as they stand for $y > 0$ since there is an exponential decay with ζ. However major interest in these results is likely to be for points near the surface of the solid in which case the integrals cannot be evaluated as they stand. In the next section some consideration will be given to their evaluation by transforming the path of integration so that it lies along the positive imaginary axis in the ζ-plane.

3. Transformation of the integrals.

In order to discuss the integrals obtained in the previous section more fully it is necessary to consider the singularities of their integrands which lie in the first quadrant of the complex ζ-plane. Due to the zeros of n_2 and n_3 there may be singularities when

$$\zeta = 0 , \tag{3.1}$$

$$\zeta = i\,a , \tag{3.2}$$

where

$$a = \frac{\nu(c_5^2 - w^2)^{1/2}}{(c_3^2-w^2)^{1/2}(c_4^2-w^2)^{1/2}} . \tag{3.3}$$

Near the origin n_3 behaves like $\zeta(c_5^2-w^2)^{1/2}/c_5$ so that $\zeta = 0$ is not a branch point. In addition, there are branch points due to the zeros of the inner square root of n_2 and n_3 at the points

$$\zeta = i|b_1 \pm b_2| \quad \text{if } c_3,\ c_4,\ > c_5 , \tag{3.4}$$

$$\zeta = R\,e^{i(\frac{\pi}{2} - \psi)} = R(\sin\psi + i\cos\psi) \quad \text{if } c_3 > c_5 > c_4 , \tag{3.5}$$

where

$$b_1 = \frac{\nu c_3 (c_4^2 - c_5^2)^{1/2}}{w|c_4^2 - c_3^2|} , \tag{3.6}$$

$$b_2 = \frac{\nu c_4 (c_3^2 - c_5^2)^{1/2}}{w|c_4^2 - c_3^2|} , \tag{3.7}$$

$$R = \frac{\nu c_5}{w(c_3^2 - c_4^2)^{1/2}} , \tag{3.8}$$

$$\psi = \tan^{-1}\left\{ \frac{c_3(c_5^2 - c_4^2)^{1/2}}{c_4(c_3^2 - c_5^2)^{1/2}} \right\} . \tag{3.9}$$

It is of interest to note that the angle ψ is independent of w. Due to the difference in the nature of the singularities the cases $c_3, c_4 > c_5$ and $c_3 > c_5 > c_4$ must be considered separately. The possible cases in which $c_5 = c_3$ or c_4 will not be considered here.

In addition to these branch points it is possible that there may be poles in the first quadrant due to the zeros of Δ. It is not possible to determine such poles analytically and in any particular case their existance must be investigated numerically. In the numerical examples considered here this was done, and the only poles found were those which lie on the real axis when $w > w_R$, and which have already been mentioned in section 2. This completes the discussion of the singularities of the integrand.

On the surface of the solid $\tau_{22} = -P\,\delta(z)$ and $\tau_{21} + \sigma_{21} = 0$ are assumed boundary conditions so that the remaining normal stress and shear

stress components are known once $\tau_{11} + \tau_{22}$ and σ_{12} are known. The evaluation of these quantities in the two cases which occur will now be considered. The other integrals of section 2 may be discussed by using the same methods. It is convenient at this stage to write

$$\tau_{11} + \tau_{22} = \frac{2 P w^2 (c_1^2 - c_5^2)}{c_1^2 \pi} \Re (I_1), \tag{3.10}$$

$$\sigma_{12} = - \frac{2 (c_3^2 - c_5^2) P c_5^2}{\pi} \Im (I_2), \tag{3.11}$$

where

$$I_1 = \int_0^\infty \frac{\xi \zeta^2}{\Delta} e^{i\zeta z} e^{-\zeta m_1 y} d\zeta, \tag{3.12}$$

$$I_2 = \int_0^\infty \frac{n_1 e^{i\zeta z}}{\zeta \Delta} (n_2^2 - \zeta^2)(n_3^2 - \zeta^2)[n_3(\phi_2 - \nu^2) e^{-n_2 y} - n_2(\phi_3 - \nu^2) e^{-n_3 y}] d\zeta, \tag{3.13}$$

$$m_1 = (c_1^2 - w^2)^{1/2} / c_1 . \tag{3.14}$$

(i) $c_4 , c_3 > c_5$.

In this case there are branch points given by (3.2) and (3.4). It may be shown that $|b_1 - b_2| > a$ and that the branch point at $\zeta = i a$ is a zero of n_2 if $w < d$, and is a zero of n_3 if $d < w < c_5$, where

$$d = \left\{ \frac{c_4^2 c_3^2 - c_4 c_3 (c_4^2 - c_5^2)^{1/2} (c_3^2 - c_5^2)^{1/2}}{c_4^2 + c_3^2 - c_5^2} \right\}^{1/2} . \tag{3.15}$$

Two subcases must be considered corresponding to $w < d$ and $w > d$. In order to make all quantities single valued cuts are introduced along the positive

imaginary axis of the ζ-plane.

We now wish to consider the integrals I_1 and I_2 taken around the contour in the first quadrant of the ζ-plane and which is shown in Fig. 1. The contour consists of a segment of the real axis OA from O to R^*; an arc of a circle of (large) radius R^* connecting A to B, the point $\delta + i R^*$; and a path from B to O which lies just to the right of the imaginary axis and is indented by semi-circles of (small) radius δ at each of the branch points C, D and E. For both I_1 and I_2 there is no contribution from the arcs around C, D and E as $\delta \to 0$ and there is no contribution from the arc AB as $R^* \to \infty$. For both integrals it is found that the integral from O to A may be replaced by the sum of the integrals from O to E, E to D, D to C and C to B.

In order to carry out the transformation it is useful to list the values of n_2 and n_3 on the imaginary ζ-axis. It is found that, writing $\zeta = i s$ and

$$H = w^2 c_5^2 - s^2 (2 c_3^2 c_4^2 - c_3^2 w^2 - c_4^2 w^2) ; \qquad (3.16)$$

On OE,

$$\left.\begin{aligned} n_2 &= \frac{1}{c_3 c_4 \sqrt{2}} \{ w^2 | c_3^2 - c_4^2 | [(b_1+b_2)^2 - s^2]^{1/2} [(b_1-b_2)^2 - s^2]^{1/2} + H \}^{1/2} = \gamma_2 , \\ n_3 &= \frac{i}{c_3 c_4 \sqrt{2}} \{ w^2 | c_3^2 - c_4^2 | [(b_1+b_2)^2 - s^2]^{1/2} [(b_1-b_2)^2 - s^2]^{1/2} - H \}^{1/2} = i\gamma_3 ; \end{aligned}\right\} \qquad (3.17)$$

On ED, $w < d$,

$$\left.\begin{aligned} n_2 &= \frac{i}{c_3 c_4 \sqrt{2}} \{ -H - w^2 | c_3^2 - c_4^2 | [(b_1+b_2)^2 - s^2]^{1/2} [(b_1-b_2)^2 - s^2]^{1/2} \}^{1/2} = i\gamma_4 , \\ n_3 &= i \gamma_3 ; \end{aligned}\right\} \qquad (3.18)$$

On ED, $d < w < c_5$,

$$\left.\begin{aligned} n_2 &= \gamma_2 , \\ n_3 &= -\frac{1}{c_3 c_4 \sqrt{2}} \{H - w^2 | c_3^2 - c_4^2 | [(b_1+b_2)^2 - s^2]^{1/2} [(b_1-b_2)^2 - s^2]^{1/2}\}^{1/2} = -\gamma_1 ; \end{aligned}\right\} \quad (3.19)$$

On DC,

$$\left.\begin{aligned} n_2 &= r(\sin\Phi + i\cos\Phi) = E_1 + i E_2 , \\ n_3 &= r(-\sin\Phi + i\cos\Phi) = -E_1 + i E_2 , \end{aligned}\right\} \quad (3.20)$$

where

$$r = \frac{1}{c_3 c_4 \sqrt{2}} \{H^2 + w^4 (c_3^2 - c_4^2)^2 [s^2 - (b_1 - b_2)^2][(b_1+b_2)^2 - s^2]\}^{1/4} , \quad (3.21)$$

$$\Phi = \tan^{-1} \left\{ \frac{2 c_3^2 c_4^2 r^2 + H}{2 c_3^2 c_4^2 r^2 - H} \right\} ; \quad (3.22)$$

On BC,

$$\left.\begin{aligned} n_2 &= \frac{i}{c_3 c_4 \sqrt{2}} \{-H + w^2 | c_3^2 - c_4^2 | [s^2 - (b_1+b_2)^2]^{1/2} [s^2 - (b_1-b_2)^2]^{1/2}\}^{1/2} = i\gamma_6 , \\ n_3 &= \frac{i}{c_3 c_4 \sqrt{2}} \{-H - w^2 | c_3^2 - c_4^2 | [s^2 - (b_1+b_2)^2]^{1/2} [s^2 - (b_1-b_2)^2]^{1/2}\}^{1/2} = i\gamma_7 , \end{aligned}\right\} \quad (3.23)$$

Now that the values of n_2 and n_3 are known the integrals I_1 and I_2 may be expressed in terms of integrals taken along the imaginary axis in the ζ-plane. The procedure is straightforward and results in

$$I_1 = -i\int_0^a \frac{s^2(A_8 + iA_9)}{A_6 + iA_7} e^{-sz} e^{-ism_1y}\,ds$$

$$-i\int_a^{|b_1-b_2|} \frac{s^2 B_3}{B_2} e^{-sz} e^{-ism_1y}\,ds$$

$$-i\int_{|b_1-b_2|}^{b_1+b_2} \frac{s^2 E_8}{E_7} e^{-sz} e^{-ism_1y}\,ds$$

$$-i\int_{b_1+b_2}^{\infty} \frac{s^2 F_4}{F_3} e^{-sz} e^{-ism_1y}\,ds, \qquad (3.24)$$

$$I_2 = i\int_0^a \frac{m_1 e^{-sz}}{A_6 + iA_7}(s^2+\gamma_2^2)(s^2-\gamma_3^2)\{i\gamma_3(A_1-\nu^2)e^{-\gamma_2 y} - \gamma_2(A_2-\nu^2)e^{-i\gamma_3 y}\}ds$$

$$+i\int_a^{|b_1-b_2|} \frac{m_1}{B_2} e^{-sz}(s^2-\gamma_4^2)(s^2-\gamma_3^2)\{\gamma_3(A_1-\nu^2)e^{-i\gamma_4 y} - \gamma_4(A_2-\nu^2)e^{-i\gamma_3 y}\}ds$$

$$-i\int_{|b_1-b_2|}^{b_1+b_2} \frac{m_1}{E_7} e^{-sz}[(s^2+E_1^2-E_2^2)^2+4E_1^2E_2^2]\{[E_1(E_3-\nu^2)+E_2E_4-iE_2(E_3-\nu^2)$$

$$+iE_1E_4]e^{-(E_1+iE_2)y} + [E_1(E_3-\nu^2)+E_2E_4+iE_2(E_3-\nu^2)-iE_1E_4]e^{(E_1-iE_2)y}\}ds$$

$$+i\int_{b_1+b_2}^{\infty} \frac{m_1 e^{-sz}}{F_3}(s^2-\gamma_6^2)(s^2-\gamma_5^2)[\gamma_5(A_1-\nu^2)e^{-i\gamma_6 y} - \gamma_6(A_2-\nu^2)e^{-i\gamma_5 y}]ds, \qquad (3.25)$$

when $w < d$. When $d < w < c_5$ the results for I_1 and I_2 remain unaltered except that the integrals with range a to $|b_1 - b_2|$ in (3.24) and (3.25) are replaced by

$$-i\int_a^{|b_1-b_2|} \frac{s^2 D_5\, e^{-sz}\, e^{-ism_1 y}}{D_3 + i D_4}\, ds \quad , \tag{3.26}$$

and

$$-i\int_a^{|b_1-b_2|} \frac{m_1 e^{-sz}}{D_3+iD_4}(s^2+\gamma_2^2)(s^2+\gamma_1^2)\{\gamma_1(A_1-\nu^2)e^{-\gamma_2 y}+\gamma_2(A_2-\nu^2)e^{-\gamma_1 y}\}ds, \tag{3.27}$$

respectively. In (3.24)-(3.27)

$$A_1 = \nu^2 - s^2(c_4^2 - w^2) - c_4^2\gamma_2^2 , \tag{3.28}$$

$$A_2 = \nu^2 - s^2(c_4^2 - w^2) + c_4^2\gamma_3^2 , \tag{3.29}$$

$$A_3 = (2c_5^2 - w^2)[c_3^2\gamma_2^2 - s^2(2c_5^2 - c_3^2)] , \tag{3.30}$$

$$A_4 = -4 s m_1 \gamma_2 c_5^4 , \tag{3.31}$$

$$A_5 = -(2c_5^2 - w^2)[c_3^2\gamma_3^2+s^2(2c_5^2 - c_3^2)] + 4 s m_1 \gamma_3 c_5^4 , \tag{3.32}$$

$$A_6 = \phi_1 \nu^2(s^2 - \gamma_3^2)(s^2+\gamma_2^2)\gamma_2 - A_2A_5\gamma_2(\gamma_2^2+s^2) - A_1A_4\gamma_3(s^2-\gamma_3^2), \tag{3.33}$$

$$A_7 = -\phi_1 \nu^2(s^2-\gamma_3^2)(s^2+\gamma_2^2)\gamma_3 + A_1A_3\gamma_3(s^2 - \gamma_3^2) , \tag{3.34}$$

$$A_8 = (2 c_5^2-w^2)\gamma_2(\gamma_2^2+s^2)[c_4^2(s^2-\gamma_3^2) - (s^2w^2 + \nu^2)], \tag{3.35}$$

$$A_9 = (2 c_5^2 - w^2)\gamma_3(s^2-\gamma_3^2)[c_4^2(s^2 + \gamma_2^2) - (s^2 w^2 + \nu^2)], \tag{3.36}$$

$$B_1 = -(2c_5^2 - w^2)[c_3^2\gamma_4^2 + s^2(2c_5^2-c_3^2)] + 4 s m_1 \gamma_4 c_5^4 , \tag{3.37}$$

$$B_2 = \phi_1\nu^2(s^2-\gamma_3^2)(s^2-\gamma_4^2)(\gamma_4-\gamma_3) - A_2A_5\gamma_1(s^2-\gamma_4^2) + A_1B_1\gamma_3(s^2-\gamma_3^2), \tag{3.38}$$

$$B_3 = (2c_5^2-w^2)\{c_4^2(s^2-\gamma_4^2)(s^2-\gamma_3^2)(\gamma_4-\gamma_3) - (s^2w^2+\nu^2)[\gamma_4(s^2-\gamma_4^2) - \gamma_3(s^2-\gamma_3^2)]\}, \tag{3.39}$$

$$D_1 = (2c_5^2 - w^2)[c_3^2\gamma_1^2 - s^2(2c_5^2 - c_3^2)] , \tag{3.40}$$

$$D_2 = 4\, s\, m_1\, \gamma_1\, c_5^4 \,, \tag{3.41}$$

$$D_3 = \varphi_1\, \nu^2 (\gamma_1^2 + s^2)(\gamma_2^2 + s^2)(\gamma_1 + \gamma_2) - A_2 D_1 \gamma_2 (\gamma_2^2 + s^2) - A_1 A_3 \gamma_1 (\gamma_1^2 + s^2), \tag{3.42}$$

$$D_4 = -4\, s\, m_1\, c_5^4\, \gamma_1\, \gamma_2\, (\nu^2 + s^2\, w^2)(\gamma_2^2 - \gamma_1^2) \,, \tag{3.43}$$

$$E_3 = \nu^2 - s^2 (c_4^2 - w^2) - c_4^2 (E_1^2 - E_2^2) \,, \tag{3.44}$$

$$E_4 = -2\, c_4^2\, E_1\, E_2 \,, \tag{3.45}$$

$$E_5 = (2\, c_5^2 - w^2)[c_3^2 (E_1^2 - E_2^2) - s^2 (2c_5^2 - c_3^2)] + 4\, s\, m_1\, E_2\, c_5^4 \,, \tag{3.46}$$

$$E_6 = 2\, E_1\, [(2\, c_5^2 - w^2)\, c_3^2\, E_2 - 2\, s\, m_1\, c_5^4 \,], \tag{3.47}$$

$$E_7 = 2\, \phi_1\, \nu^2\, E_1 [(s^2 + E_1^2 - E_2^2)^2 + 4\, E_1^2 E_2^2] - 2 E_1 (E_3 E_5 - E_4 E_6)(s^2 + E_1^2 - 3E_2^2)$$
$$-2\, E_2 (E_4 E_5 + E_3 E_6)(s^2 + 3E_1^2 - E_2^2) \,, \tag{3.48}$$

$$E_8 = 2\, E_1 (2c_5^2 - w^2) \{c_4^2 [(s^2 + E_1^2 - E_2^2)^2 + 4\, E_1^2 E_2^2] - (s^2 w^2 + \nu^2)(s^2 + E_1^2 - 3E_2^2)\}, \tag{3.49}$$

$$F_1 = -(2c_5^2 - w^2)[c_3^2 \gamma_6^2 + s^2 (2c_5^2 - c_3^2)] + 4\, s\, m_1\, \gamma_6\, c_5^4 \,, \tag{3.50}$$

$$F_2 = -(2\, c_5^2 - w^2)[c_3^2 \gamma_5^2 + s^2 (2c_5^2 - c_3^2)] + 4\, s\, m_1\, \gamma_5\, c_5^4 \,, \tag{3.51}$$

$$F_3 = \phi_1 \nu^2 (s^2 - \gamma_5^2)(s^2 - \gamma_6^2)(\gamma_6 - \gamma_5) - F_2 F_4 \gamma_6 (s^2 - \gamma_6^2) + F_1 F_3 \gamma_5 (s^2 - \gamma_5^2), \tag{3.52}$$

$$F_4 = (2c_5^2 - w^2)\{c_4^2 (s^2 - \gamma_6^2)(s^2 - \gamma_5^2)(\gamma_6 - \gamma_5) - (s^2 w^2 + \nu^2)[\gamma_6 (s^2 - \gamma_6^2) - \gamma_5 (s^2 - \gamma_5^2)]\}, \tag{3.53}$$

and E_1 and E_2 are given by (3.20).

The quantity σ_{12} is given by the imaginary part of I_2, and when $y = 0$ (3.25) gives contributions from all the ranges of integration. The quantity $\tau_{11} + \tau_{22}$ is given by the real part of I_1, and when $y = 0$ the result for this quantity simplifies considerably to give

$$\tau_{11} + \tau_{22} = \frac{2 P w^2 (c_1^2 - c_5^2)}{c_1^2 \pi} \int_0^a \frac{s^2 (A_9 A_6 - A_8 A_7) e^{-sz} ds}{A_6^2 + A_7^2}, \qquad (3.54)$$

if $w < d$, and if $d < w < c_5$, we must add to (3.54) the term

$$- \frac{2 P w^2 (c_1^2 - c_5^2)}{c_1^2 \pi} \int_a^{|b_1 - b_2|} \frac{s^2 D_9 D_8 e^{-sz} ds}{D_7^2 + D_8^2} . \qquad (3.55)$$

These expressions for $\tau_{11} + \tau_{22}$ are now in a form which is suitable for numerical evaluation. Further discussion of these results will be left until after consideration of the next case.

(ii) $c_3 > c_5 > c_4$

In this case there are branch points given by (3.2) and (3.5). The quantity a may be greater than, or less than, R so that these two subcases will be considered individually. The branch point at $s = i a$ is always a zero of n_2. In order to make all quantities single valued cuts are introduced along the positive imaginary axis in the ζ-plane and also along an arc of a circle of radius R between $\zeta = iR$ and $\zeta = r \exp i(\frac{i}{2}\pi - \psi)$.

We now consider the integrals I_1 and I_2 taken around a contour in the first quadrant of the ζ-plane and which consists of a segment of the real axis OA from O to R^* (see Fig. 2): an arc of a circle of radius $R^* > R$ connecting A to B, the point $\delta + iR^*$; a path from B to C and from E to O which lies just to the right of the imaginary axis and is indented by a semi-circle of radius δ at the branch point F; and a path from C to E around the cut connecting the branch point D to the imaginary axis. Fig. 2 shows the

resulting contour when $a < R$. When $a > R$ the only change is that the branch point F lies above C on the imaginary axis. There is no contribution to either I_1 or I_2 from the arcs around F and D as $\delta \to 0$, nor is there a contribution from the arc AB as $R^* \to \infty$. For $w < w_R$ there are no poles in the first quadrant so that the integral from O to A is replaced by the sum of the integrals from O to E, E to C and C to B.

As in case (i), it is useful to tabulate the values of n_2 and n_3 on the various sections of the contour before considering the integrals. Writing $\zeta = i s$ on the imaginary axis, $\zeta = R \exp i(\frac{1}{2}\pi - \theta)$ on E D and D C, introducing H defined by (3.16), and a quantity K, where

$$K = w^2(c_3^2 - c_4^2)[(R^2 - s^2)^2 + 4 s^2 R^2 \sin^2 \psi]^{1/2}, \tag{3.56}$$

it is found that, for $a < R$:

On OF

$$\left.\begin{aligned} n_2 &= \frac{1}{c_3 c_4 \sqrt{2}}(K + H)^{1/2} = \gamma_2, \\ n_3 &= \frac{i}{c_3 c_4 \sqrt{2}}(K - H)^{1/2} = i\gamma_3, \end{aligned}\right\} \tag{3.57}$$

where γ_2 and γ_3 are also given by (3.17);

On F E

$$\left.\begin{aligned} n_2 &= \frac{1}{c_3 c_4 \sqrt{2}}(-H - K)^{1/2} = i\gamma_4, \\ n_3 &= i\gamma_3, \end{aligned}\right\} \tag{3.58}$$

where γ_4 is also given by (3.18);

On B C

$$\left.\begin{aligned} n_2 &= i\gamma_3 \ , \\ n_3 &= i\gamma_4 \ . \end{aligned}\right\} \tag{3.59}$$

The values of n_2 and n_3 on E D are respectively equal to the values of n_3 and n_2 on C D, so that with the particular forms (3.12) and (3.13) for I_1 and I_2 it is found that the integral along the path E D C gives no contribution to I_1 or I_2. This result also holds for the case $a > R$. When $a > R$ the branch point F lies above C so that on O E n_2 and n_3 are given by (3.57), on F B they are given by (3.59), and on C F by

$$\left.\begin{aligned} n_2 &= i\gamma_3 , \\ n_3 &= \gamma_2 \ . \end{aligned}\right\} \tag{3.60}$$

The integrals I_1 and I_2 may now be expressed in terms of integrals along the imaginary axis. This process is straightforward and will not be carried out here in the general case. When $y = 0$ the quantity $\tau_{11} + \tau_{22}$ is still given by (3.54) however, so that this result holds regardless of the ordering of the elastic constants provided that $w < d$.

With the stress component τ_{22} given by (2.45), (3.54) essentially determines the stress component τ_{11} on the surface of the solid. In the classical elastic solution τ_{11} is zero everywhere on the surface except at the point of application of the force, so that (3.54) gives a measure of the influence of the couple stress effects. After making the change of variable defined by

$$s = \nu q / c_5$$

in the integral in (3.54), the quantity ν enters into the expression as a

multiplicative constant and through the quantity Z alone, where

$$Z = \nu z / c_5 .$$

Figures 3 and 4 show the variation of $\tau_{11} + \tau_{22}$ with Z for four combinations of the elastic wave speeds, including examples of the three different orderings which are possible. Figure 3 is for $w^2/c_5^2 = 0.1$, a relatively small value of w, and Figure 4 is for $w^2/c_5^2 = 0.7$, a relatively large value of w. In Figure 3 the curves remain close together, although curve B decays more rapidly than the others. For the larger value of w (see Fig. 4) curves A, C and D are still close together but curve B takes a much larger value at the origin and also decays more rapidly than the other curves. For all the curves the effects due to the inclusion of the couple stress terms are greatest near the point of application of the force and they fall off quite rapidly away from the origin. These effects are most noticable for large values of w in the case $c_3 > c_5 > c_4$, although this may be due to the selected value of w being close to the value of c_4.

Acknowledgment. The author would like to thank Mr. J. Al-Abdulla for carrying out the numerical work involved in this paper.

REFERENCES

1. E. Cosserat and F. Cosserat, Théorie des Corps Déformables, Hermann and Fils, Paris (1909).
2. R. D. Mindlin and H. F. Tiersten, Arch. Rat. Mech. Anal., 11, 415(1962).
3. R. D. Mindlin, Arch. Rat. Mech. Anal., 16, 51(1964).
4. R. D. Mindlin, Int. J. Solids Structs., 1, 265 (1965).
5. A. C. Eringen and E. S. Suhubi, Int. J. Eng. Sci., 2, 189(1964).
6. E. S. Suhubi and A. C. Eringen, Int. J. Eng. Sci., 2, 389(1964).
7. A. C. Eringen, J. of Math. Mech., 15, 909(1966).
8. G. Eason, M. R. C. Technical Summary Report No. 985 .
9. I. N. Sneddon, Rend. Circ. Math. Palermo (ii), 1, 57(1952).
10. J. D. Cole and J. H. Huth, J. Appl. Mech., 25, 433(1958).
11. G. Herrmann and J. D. Achenbach, Mechanics of Generalized Continua, I. U. T. A. M. Symposium, editor E. Kröner, Springer-Verlag, Berlin (1968).
12. T. R. Kane and R. D. Mindlin, J. Appl. Mech., 23, 277(1956).
13. R. D. Mindlin and M. A. Medick, J. Appl. Mech. 26, 561(1959).
14. E. S. Suhubi, Bull. Istanbul Tek. Univ. 19, 138(1969).
15. V. R. Parfitt and A. C. Eringen, J. Acoust. Soc. Amer. 45, 1258 (1969).

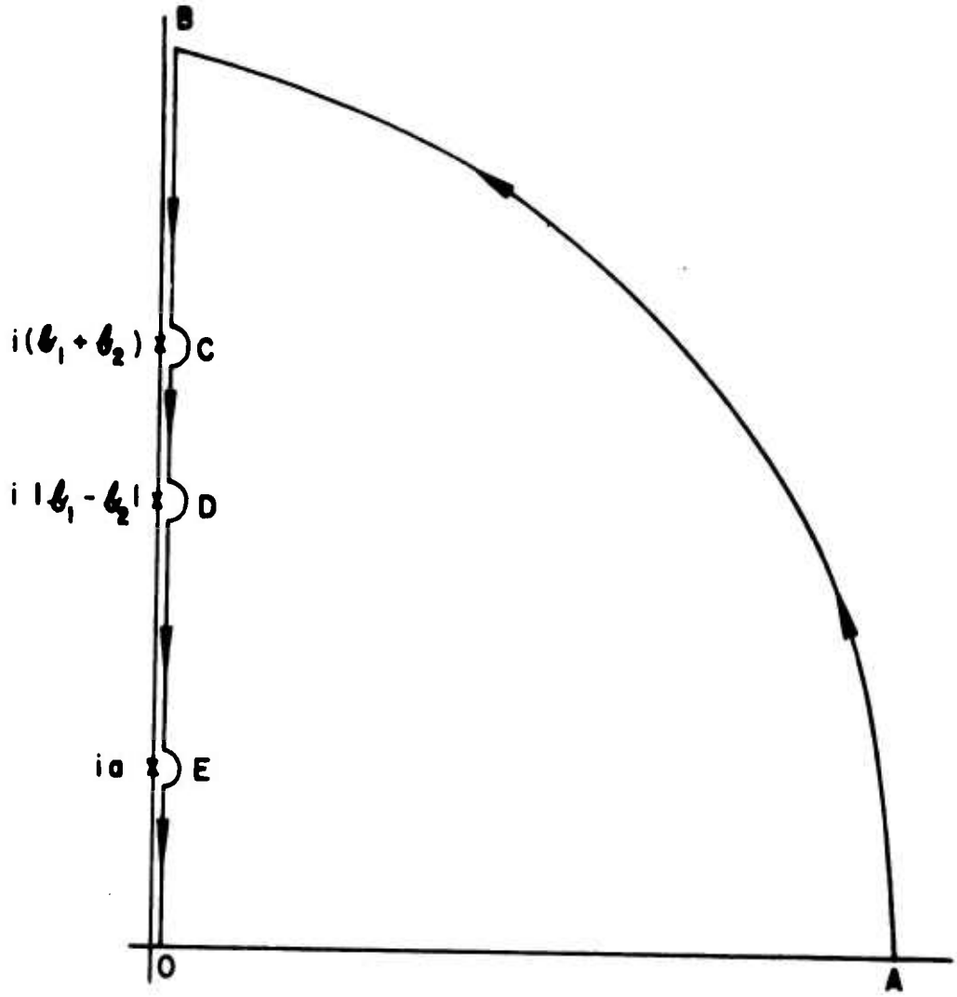


Fig. 1

Contour in the ζ-plane, c_3, $c_4 > c_5$, × branch points

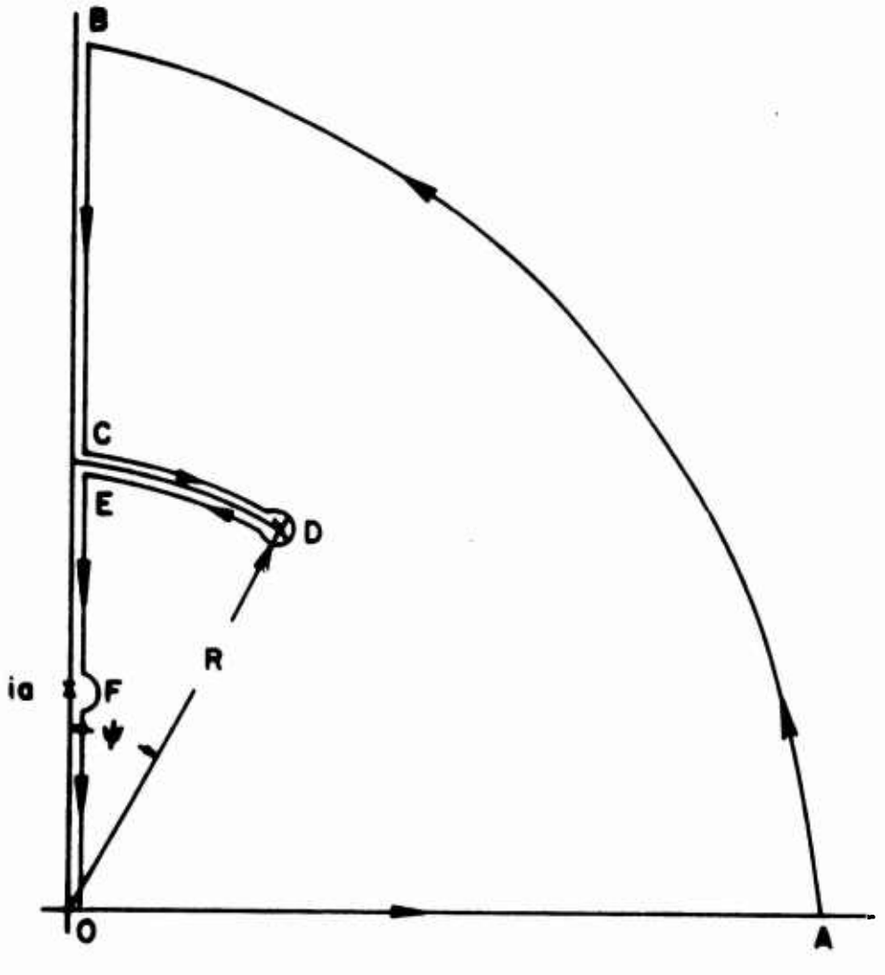


Fig. 2

Contour in the ζ-plane, $c_3 > c_5 > c_4$, $a < R$, $\times$ branch points

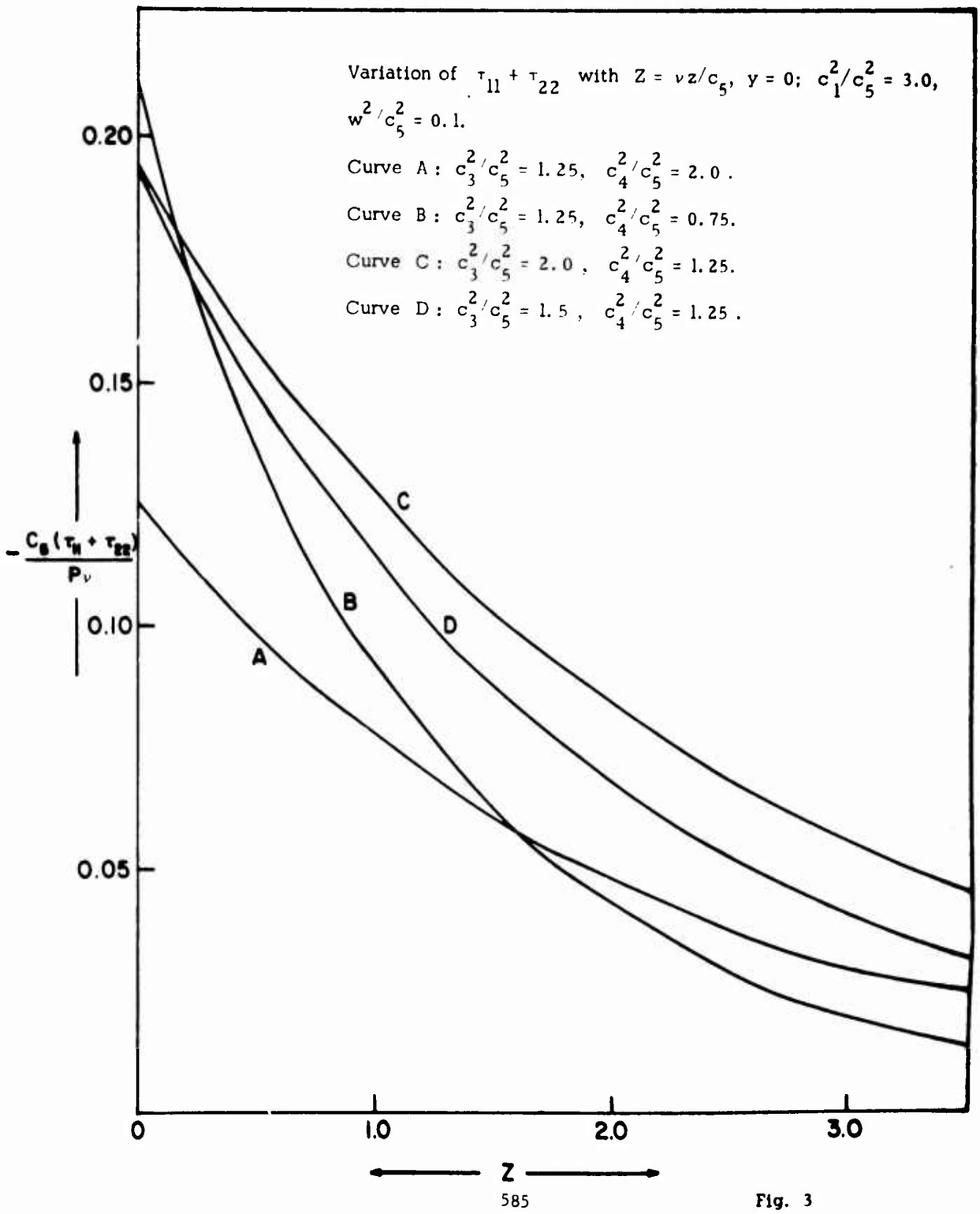

Variation of $\tau_{11} + \tau_{22}$ with $Z = \nu z/c_5$, $y = 0$; $c_1^2/c_5^2 = 3.0$, $w^2/c_5^2 = 0.1$.
Curve A : $c_3^2/c_5^2 = 1.25$, $c_4^2/c_5^2 = 2.0$.
Curve B : $c_3^2/c_5^2 = 1.25$, $c_4^2/c_5^2 = 0.75$.
Curve C : $c_3^2/c_5^2 = 2.0$, $c_4^2/c_5^2 = 1.25$.
Curve D : $c_3^2/c_5^2 = 1.5$, $c_4^2/c_5^2 = 1.25$.
0.20
0.15
0.10
0.05
$-\frac{C_s(\tau_{11} + \tau_{22})}{P_\nu}$
A
B
C
D
0
1.0
2.0
3.0
Z

Fig. 3

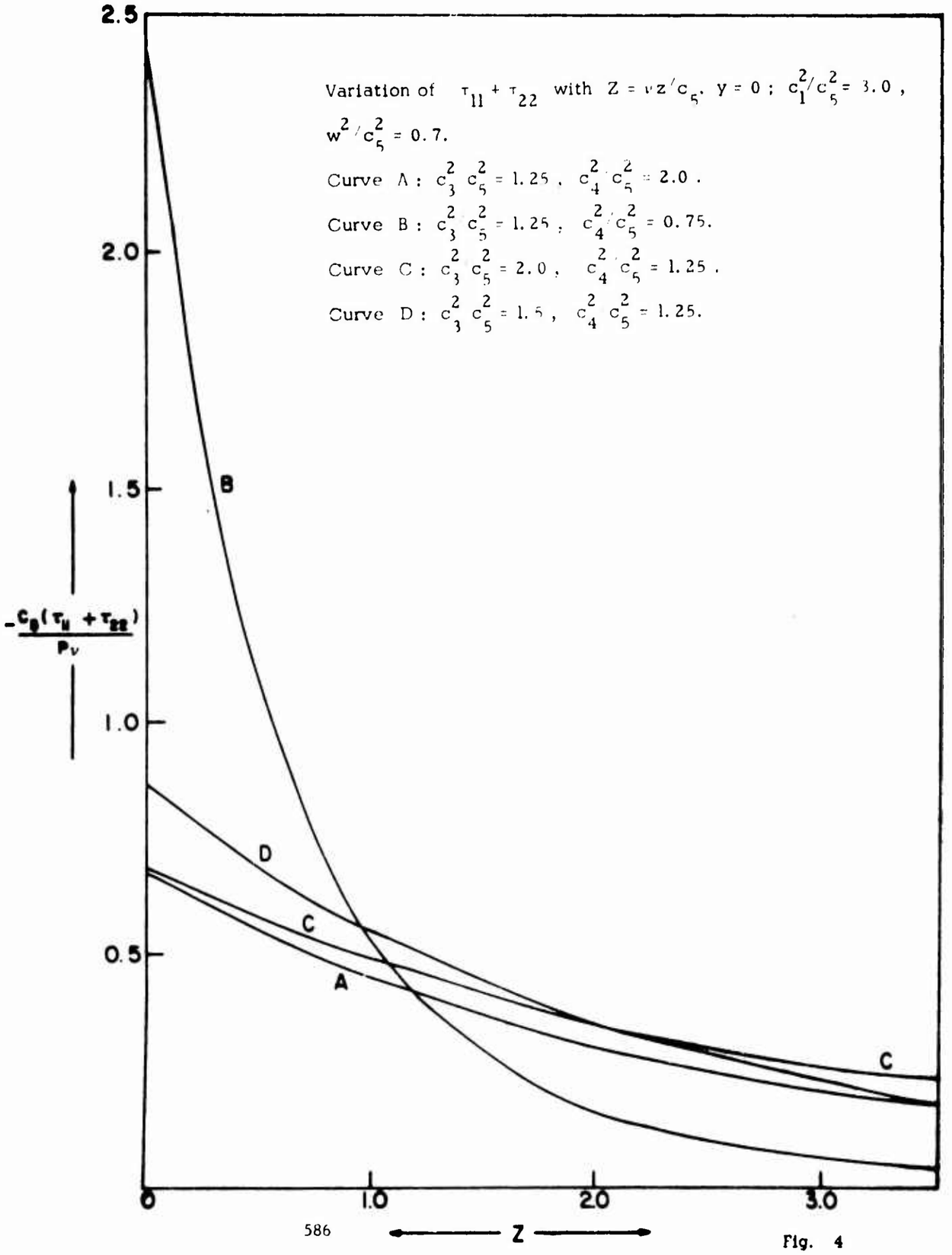

Variation of $\tau_{11} + \tau_{22}$ with $Z = wz/c_5$, $y = 0$; $c_1^2/c_5^2 = 3.0$, $w^2/c_5^2 = 0.7$.
Curve A : $c_3^2\ c_5^2 = 1.25$, $c_4^2\ c_5^2 = 2.0$.
Curve B : $c_3^2\ c_5^2 = 1.25$, $c_4^2\ c_5^2 = 0.75$.
Curve C : $c_3^2\ c_5^2 = 2.0$, $c_4^2\ c_5^2 = 1.25$.
Curve D : $c_3^2\ c_5^2 = 1.5$, $c_4^2\ c_5^2 = 1.25$.
$-\frac{c_5(\tau_{11} + \tau_{22})}{p_v}$
2.5
2.0
1.5
1.0
0.5
0
1.0
2.0
3.0
Z
A
B
C
D
C

Fig. 4

SURF*

R. E. Meyer
Mathematics Research Center, U. S. Army
The University of Wisconsin
Madison, Wisconsin

ABSTRACT. The following is a review of some phases of research, over the last decade, on water waves strongly influenced by the seabed. The first sections discuss progress made in the understanding of the transformation of waves into run-up and back-wash on a beach. This phenomenon is closely related to the theory of singular partial differential equations. Section VIII summarizes results on the resonance of unbounded water bodies adjacent to shores.

I. INTRODUCTION. Research on water waves has a long history, but until recently, little was known about waves on which the seabed has an important influence. This review reports on some phases of recent work on such waves which are relevant to many shore processes, especially beach erosion. However, the main stimulus for the work came from tsunamis, the earth-quake generated waves which travel over long distances. In the open ocean, their wave length is of the order of 50 miles and their height is usually less than 1 foot. But when they strike a coast, they can reach up to 60 feet and can drown whole harbors and cities.

The process by which they wreak such havoc is a very familiar one. When a wave rolls up a beach, there comes a moment at which the wave converts itself into a swoosh and sheet of water surging up the beach, and then draining back to sea. This transformation of wave into run-up sheet is a familiar sight. But the mechanism which causes this transformation remained completely unknown until the last decade.

The classical, linear theory of small-amplitude surface waves turned out to be defeated by this problem, because it has a singularity at the shore [1]. That singularity stems directly from the linearization and sets severe limits to the use of the theory for the study of shore processes.

II. THE BEACH EQUATIONS. The key to a new approach was a realization that beach slopes are small. There are exceptions to that, but the general rule is that ocean bed slopes are very small [2], typically of the order of 1/1000. Steep slope, in marine geology, tends to mean about 1/100.

*This article has appeared as Technical Summary Report #978 of the Mathematics Research Center. Sponsored by the Mathematics Research Center under Contract No. DA-31-124-ARO-D-462.

Being non-dimensional, however, a slope fails to provide a scale. On the other hand, observation indicates that waves rolling up a beach have a fairly well-defined propagation velocity, u_0. That suggests the following scales.

u_0	for velocities
u_0^2/g	for vertical lengths
$u_0^2/(\varepsilon g)$	for horizontal lengths
$u_0/(\varepsilon g)$	for times
ρu_0^2	for pressures.

In these units, the equations of hydrodynamics for two-dimensional motion are as follows. The kinematical equations, i.e., mass conservation and kinematic boundary conditions at the seabed and free surface (Figure 1) are respectively

$$\partial u/\partial x + \partial v/\partial y = 0$$

$$u dh_0/dx + v = 0 \qquad \text{at } y = -h_0(x)$$

$$\partial \eta/\partial t + u\partial \eta/\partial x = v \qquad \text{at } y = \eta(x,t).$$

Vertical integration from seabed to free surface then gives

$$\partial h/\partial t + \partial(h\,\bar{u})/\partial x = 0, \tag{1}$$

where

$$h(x,t) = h_0(x) + \eta(x,t), \quad \bar{u}(x,t) = \frac{1}{h}\int_{-h_o}^{\eta} u\,dy$$

represent respectively the local, total water depth and the average horizontal velocity.

The dynamical equations express conservation of momentum under the influence of gravity,

$$\frac{\partial u}{\partial t} + u\frac{\partial u}{\partial x} + v\frac{\partial u}{\partial y} = -\frac{\partial p}{\partial x}$$

$$\varepsilon^2\left(\frac{\partial v}{\partial t} + u\frac{\partial v}{\partial x} + v\frac{\partial v}{\partial y}\right) = -\frac{\partial p}{\partial y} - 1 ,$$

and the assumption,

$$p = 0 \quad \text{at} \quad y = \eta(x,t) ,$$

that the air pressure has negligible influence on the water motion. Viscosity is neglected on the ground that, a decade ago, too little was understood even about the inviscid processes of water waves. Vertical integration of the first momentum equation from seabed to free surface gives [3]

$$\partial\bar{u}/\partial t + \bar{u}\ \partial\bar{u}/\partial x + \partial\eta/\partial x = \frac{1}{h}\frac{\partial}{\partial x}\int_{-h_0}^{\eta}(u-\bar{u})^2 dy - \frac{1}{h}\int_{-h_0}^{\eta}\frac{\partial}{\partial x}(p - p_{stat})\,dy .$$

Now, as the seabed slope $\varepsilon \to 0$, the second momentum equation shows, under suitable assumptions on the velocity field, that the pressure approaches the hydrostatic pressure $p_{stat} = \eta - y$. The last integral above therefore tends to zero with ε. The vorticity is

$$\zeta = \partial u/\partial y - \varepsilon^2\ \partial v/\partial x,$$

and thus $\partial u/\partial y \to 0$ with ε, if the motion is irrotational, e.g., because the waves invade water initially at rest. The other integral in the last equation then also tends to zero with ε. This remains true, even for a viscous fluid, as long as the boundary layer thickness remains negligible compared with the total water depth. The dynamical equations then reduce to [3]

$$\partial\bar{u}/\partial t + \bar{u}\partial\bar{u}/\partial x + \partial(h-h_0)/\partial x = 0. \qquad (2)$$

Equations (1) and (2) are known in hydraulics (where they are a valid approximation for rather different reasons [4]) as the shallow-water equations of flow in channels of variable depth. They are nonlinear,

hyperbolic equations and are known [1] to predict that the fronts of waves will steepen gradually until their steepness becomes inconsistent with the assumptions on which the equations are based. This is called bore formation.

More precisely, a bore is a narrow region (Figure 2) in which the velocity gradient and surface slope are too steep to be consistent with the large horizontal scale of the rest of the motion. What happens in that narrow region is not yet understood clearly, but one can try to ignore it and just postulate that mass and momentum are conserved and energy is not increased. Then further progress is usually possible [1], provided no information on the bore is sought beyond its position $x = x_b(t)$, velocity $V = dx_b/dt$, and strength $M = \Delta h/h$ (Figure 2).

It should be emphasized that bores are not synonymous with breakers. Wave breaking is observed to occur in a number of different ways under different circumstances, including short waves on the open sea, and the model just described is known not to account for all forms of wave breaking even on beaches. Conversely, bores need not involve wave breaking.

The shallow-water equations were first used by Carrier and Greenspan [5] to study waves on a plane beach - before the argument supporting their application was known - because they do not prescribe a fixed shore position. They found the standing wave solutions (the bar over u will be omitted from here on)

$$u = \sigma^{-1} A\omega J_1(\omega\sigma) \cos(\omega\lambda - \psi)$$

$$\eta = \frac{1}{4} A\omega J_0(\omega\sigma) \sin(\omega\lambda - \psi) - \frac{1}{2} u^2$$

$$x = \eta - \sigma^2/16,$$

where

$$\lambda = 2(u + t), \quad \sigma = 4h^{1/2},$$

A, ω, ψ are arbitrary constants, except that $|A| < 1$, and J denotes Bessel's function. They are a generalization of the standing wave solutions of tidal theory [6], which they approach with increasing distance from shore, where

$$\eta \sim \frac{1}{4} A\omega J_0 (4\omega|x|^{1/2}) \sin(2\omega t - \psi).$$

In contrast to tidal theory, however, they predict a moving shore line $h(x,t) = 0$ with maximum landward penetration $x_{max} = |A\omega|/4$.

These standing waves are bore-free; the run-up is not of the thin-sheet type observed with larger waves and breakers, and Greenspan [7] emphasized the question whether pregressive waves incident on a beach could ever remain bore-free.

III. BORE CLIMB PROBLEM. Whitham then began a study [8] of how a bore would move into water at rest on a plane beach (Figure 3). This is best considered at the hand of an x,t-diagram (Figure 3) where the successive bore positions can be plotted as a bore path, $x = x_b(t)$. Given the initial bore position and strength, and the water wave behind the bore at that time, can the future bore positions be predicted from (1) and (2)? Conservation of mass and momentum across the bore can then be expressed [1] by

$$u_b/V = 1 - h_0/h_b, \quad 2V^2 = h_b(1 + h_b/h_0) \tag{3}$$

where $V = dx_b/dt$ is the bore velocity, h_0 stands for the water depth, $h_0 = -x_b$, on the landward side of the bore (where the water is at rest), and u_b, h_b denote respectively the horizontal velocity and total water depth on the seaward side of the bore. Unless the bore has zero strength ($u_b = 0$, $h_b = h_0$), energy cannot be conserved as well, and the postulate of non-increasing energy is found to imply [1]

$$h_b \geq h_0 = -x_b \text{ for } V > 0, \tag{4}$$

which determines the appropriate root of the quadratic system (3). The description of the bore by (3) and (4) represents a floating boundary condition for the system (1), (2) in the bore climb problem.

It is relevant that all the work on this problem predates the understanding [3] why (1), (2) apply to waves on beaches of small slope sufficiently close to shore. That issue appeared irrelevant in view of the fact that the bore climb problem was the simplest known analog of an important class of nonlinear problems in gas dynamics. Keller, et al., [8] wished to check on an hypothesis concerning shock propagation [9], and Ho and Meyer [10] then used the problem for a study of a phenomenon of forgetfulness of which hints could be detected in some results of explosion theory [11, 12].

The question here arising is best explained at the instance of the similarity solutions of gas dynamics [e.g., 13]. Envisage an explosion problem with axial or spherical symmetry, so that pressure, density, etc. depend on a distance r and time t. The problem is then described by nonlinear, hyperbolic differential equations with awkward, floating, nonlinear boundary conditions representing shocks. Solutions may exist, however, for which the pressure (referred to a scale $p_0(t)$) depends only on one combination $r/t^n = \xi$, say, of the independent variables, and similarly for the density, etc. The differential equation then reduce to ordinary differential equations with respect to ξ. Such similarity solutions are, of course, <u>particular</u> solutions of the gas dynamical equations with shock conditions, and they satisfy initial conditions of a particular type. None the less, it has been often proposed [13] that these solutions, despite the uniqueness theorem, be used to describe physical gas motions with quite different types of initial conditions. Such use of the similarity solutions can be justified only on a hypothesis that these nonlinear problems have whole classes of solutions which forget their initial conditions! Such a phenomenon is not without precedent, electrical transients are a classical example. What is unprecedented is that many proposed applications of gas dynamical similarity solutions require a hypothesis that classes of solutions forget their initial conditions <u>in a finite time</u>. Can this be consistent with the established uniqueness of the solutions?

IV. <u>THEORY OF BORE COLLAPSE</u>. Ho and Me[illegible] conjectured that the bore climb problem involves such a phenomenon [illegible] forgetfulness and that it stems from a singularity of the differential equations. In the field of ordinary differential equations, it is well-known that there is a distinction between a singularity of a solution and a singu[illegible]rity of the differential equation itself, and that the second concept is of fundamental importance. In the field of partial differential equations, however, the second concept is still quite unexplored.

It is not obvious why (1), (2) should be singular equations. But a transformation of independent variables from x,t to Riemann invariants [14]

$$\alpha = u + t + 2h^{\frac{1}{2}} - 1, \quad \beta = 2h^{\frac{1}{2}} - u - t + 1 \qquad (5)$$

transforms them into

$$\frac{\partial x}{\partial \beta} = (u+c)\frac{\partial t}{\partial \beta}, \quad \frac{\partial x}{\partial \alpha} = (u-c)\frac{\partial t}{\partial \alpha}, \qquad (6)$$

$$c = h^{\frac{1}{2}} \geq 0, \qquad (7)$$

whence

$$\frac{\partial^2 t}{\partial\alpha\partial\beta} + \frac{3/2}{\alpha+\beta}\left(\frac{\partial t}{\partial\alpha} + \frac{\partial t}{\partial\beta}\right) = 0 , \qquad (8)$$

and this is clearly singular at $\alpha + \beta = 4h = 0$, i.e., at the shore line $h(x,t) = 0$.

To explain the nature of the bore climb problem, it is necessary to mention the characteristics of (1), (2). There are two families (Figure 4), viz. the advancing characteristic lines $dx/dt = u + c$, on which α = const., by (6), and the receding characteristic lines $dx/dt = u - c$, on which β = const.

Initially, both families of characteristics issue from the x-axis (Figure 4), and the initial data determine the solution in a characteristic triangle [15], quite independently of the bore. This part of the problem is classical, so the relevant analysis of the bore climb problem starts with data on the receding characteristic line C shown in Figure 5. For uniqueness, it is necessary, by (6), to prescribe (i) the initial bore position $x_B(0)$ and bore velocity $V(0)$ and (ii) the Riemann invariant $\alpha = u + t + 2c - 1$ as a function $\alpha = \alpha_c(t)$ on C (which then becomes a known curve [16]). These will be referred to as the seaward data.

Uniqueness, however, is not required for an analysis aiming to demonstrate asymptotic properties, as $c = h^{\frac{1}{2}} \to 0$, common to a class of solutions. Ho and Meyer [10] therefore refrained pointedly from specifying $\alpha_c(t)$. Instead, they specified only [16] that

$$\alpha_c(t) \text{ is strictly increasing, and} \qquad (9)$$

$$4c^{3/2}\frac{dt}{d\alpha_c} + \int_0^t c^{1/2}\,dt' \text{ is piecewise} \qquad (10)$$

continuous and non-increasing on C' .

These will be referred to as the Monotoneity Condition.

$$\alpha_c(t) \text{ is continuous} \qquad (11)$$

can be assumed without loss of physical generality, since it can always be obtained [10] by a postponement of the initial time. Apart from (9) to (11), Ho and Meyer [10] regarded the seaward data $\alpha_c(t)$ as unknown.

The numerical samples [8] show that the problem class so formulated has a sub-class with the property [16]

If $x_b(t') < 0$ for $0 \leq t' \leq t$, then

$$u_b(t) > 0 \text{ and } \alpha(x_b(t),t) < \alpha_c(\tau) \tag{12}$$

for some τ independent of t. (That $u_b(t) > 0$ means the bore does not peter out before reading the initial shore position $x = 0$ (Figure 4), and the rest of (12) means only that the function class $\alpha_c(t)$ is defined by (9) to (11) for a sufficient time interval $[0,\tau]$ to determine (in principle) the bore development as long as the bore position remains short of $x = 0$.) The assumptions (1) to (4) and (9) to (12) imply [16].

Theorem 1. The bore reaches the initial shore position $x = 0$ in a finite time (say, T).

The specification of the bore climb problem may now be completed as follows. Let D' denote the closed set in the x,t-diagram (Figure 6) bounded by the bore path, the seaward characteristic line C and the line $t = T$. It is to be anticipated that a singularity of the differential equations may occur at (0,T), and no assumptions should therefore be made about the solution at that point. Accordingly, delete (0,T) from D' and call the resulting set D (Figure 6). The numerical samples [8] show that our problem class has a nonempty subclass satisfying the final assumption

$$\begin{aligned} &\alpha(x,t) \text{ and } \beta(x,t) \text{ possess piecewise continuous} \\ &\text{bounded first derivatives on every closed} \\ &\text{subset of D.} \end{aligned} \tag{13}$$

The assumptions (9) to (13) have been presented here in detail because it is a relevant feature of the bore collapse theory [10, 16, 17] that it is based on the specification of the bore climb problem by (1) to (4) and (9) to (13) only and proceeds from this specification without any further assumption or approximation. Since these data are insufficient for uniqueness, the analysis [10, 16] employes methods similar to those of the theory of differential inequalities. Indeed, the Monotoneity Condition is clearly an inequality, and so is (4), and even (1), (2) can be turned into inequalities [16]. Among the results [8, 10, 16] obtained by their help, the following are here relevant.

Theorem 2. As the bore approaches the shore, the bore velocity V tends to a limit.

Theorem 3. That limit is positive.
Accordingly, lim V may be identified with the scale u_0.

Corollary. The bore height h_b then tends to zero, and the bore strength grows beyond bounds; but the total water depth h does not vanish in D (Figure 6).

Theorem 4. The family of characteristic lines catching the bore (Figure 4) has a limiting member, L, which catches the bore just as the bore reaches the shore (Figure 7).

The existence of such a limiting characteristic [11] is an important feature of the gas dynamical problems in which indications of forgetfulness have been detected. It also has implications regarding uniqueness; the bore development is determined already by the part of the motion represented by the subregion R (Figure 8) of D, and the Monotoneity Condition (9), (10) on C is not needed beyond L.

Corollary. The water velocity u and total water depth h are continuous on the closure of R.

The solutions of our problem class therefore have no obvious singularity at the singular point (0,T) of the differential equations. The question thus becomes whether this uniform continuity extends also the derivatives of u and h. The first derivatives can be expressed [10] in terms of

$$a = 8h^{3/2}\,\partial t/\partial\alpha, \qquad b = 8h^{3/2}\,\partial t/\partial\beta\ . \tag{14}$$

Theorem 5. As the limiting characteristic L approaches the bore (Figure 8), the values of a on the R-side of L approach a limit, say a_0.

Theorem 6. $a_0 \neq 0$.

Corollary. The asymptotic relation between the bore position x_b and bore height h_b, as the bore approaches the shore, is

$$x_b \sim \frac{-1}{2}\, h_b^2 \left[1 + 4h_b^{1/2} + \frac{23}{2} h_b + 28\, h_b^{3/2} + 59\, h_b^2 + \frac{502}{5} h_b^{5/2} + \frac{32}{11a_0} h_b^{11/4} + O(h_b^3)\right]$$

$$\text{as } h_b \to 0\ .$$

Observe that the coefficients of the first six terms are pure numbers and hence, are independent of the seaward data! Only the seventh-order asymptotic approximation is, through a_0, dependent on the seaward data. The solutions of the bore climb problem thus display a remarkably selective memory. Their asymptotic behavior, close to shore, is decisively controlled by a purely qualitative feature of the seaward data; viz., the Monotoneity Condition. But they forget all quantitative properties of those data up to the sixth-order asymptotic approximation.

Figure 9 shows the bore velocity vs. the bore position for three quite different values of a_0 [10]. Observe that the limiting value of the bore velocity, in these units, is actually unity (Figure 9). The rapid rise of V is associated with a rapid fall of the bore height. The bore thus 'collapses' at the shore in a process converting potential into kinetic energy.

Of course, by the time the bore comes this close to shore, the argument (Section II) supporting the beach equations (1), (2) and bore conditions (3), (4) has failed. The dominant horizontal scale is then $|x_b(t)|$, compared with which the bore thickness δ (Figure 2) cannot remain negligible.

V. RUN-UP THEORY. None the less, it is natural to ask whether the mathematical analysis can be extended beyond the bore arrival time (now taken to be $t = 0$) and what it might predict - even though it be impossible to tell a priori whether such predictions could be relevant to water motion. Shen [17] succeeded in obtaining such an extension based on the single assumption that the Monotoneity Condition (9), (10) on C (Figure 8) and also (11), extend beyond L for an arbitrarily short time. That leaves the solutions not only indeterminate, but with (12) and (13) abandoned, existence of solutions of (1), (2) is also in question.

The analysis is carried out in the plane of the Riemann invariants (5), where the shore line $h = (\alpha + \beta)^2/16 = 0$ is fixed and the bore path, seaward characteristic C, and limiting characteristic L are as shown in Figure 10. Theorem 6 and the extension of monotoneity on C determine certain properties of the solutions in the narrow strip to the right of L in Figure 10. The most relevant results [17] are

Theorem 7. The solutions exist up to, and only up to, the x,t-image of a singular line of the fluid acceleration through $\alpha = \beta = 0$ in the first quadrant (Figure 11).

Theorem 8. The x,t-image of the origin $\alpha = \beta = 0$ is, not a point, but a curve $x_s(t) = t - t^2/2$. The x,t-image of the singular line of the fluid acceleration asymptotes to the parabola $x_s(t)$.

Since $\alpha = \beta = 0$ implies $h = (\alpha + \beta)^2/16 = 0$, $x_s(t)$ represents the path of a shore line swinging up the beach and down to sea again (Figure 12). In fact, it moves just like a particle under gravity on a smooth inclined plane, kicked off initially at $x = 0$ with velocity u_0 [18]. The maximum penetration is therefore $x_{max} = u_0^2/(2\varepsilon g)$. As a Corollary [17], the water depth close to the moving shore line is found to be much smaller than for the standing waves of Section II.

However, the physical significance of the theory is placed in jeopardy by the singularity of the fluid acceleration, which limits the existence of any solution of (1), (2), - unless this singularity can be interpreted in terms of bore formation [1]. Theorem 6 implies [17] that an interpretation in terms of a reflected bore is impossible; it could only be a bore across which the water depth increases from the landward to the seaward side, just as in Figure 3. The specifications of the problem do not determine the x,t-path of the singularity in any detail, but in view of Theorem 8, it must be roughly as shown by the cross-hatched curve in Figure 13. Any interpretation in terms of bore formation must therefore involve a secondary bore in the back-wash, which faces landward, like the original bore, but moves seaward (Figure 13). The prediction of such an anomalous bore was most unexpected to the investigators. But in view of the rigorous logical cohesion of the theory, it is impossible to ignore some of its predictions, while accepting others. The mathematical run-up analysis therefore appeared quite academic to its authors - until they found evidence of the anomalous, back-wash bore in a television commercial [18].

Of course, the theory describes a grossly idealized model of fluid motion (Section II), and its predictions must be interpreted accordingly. For instance, the discontinuity of the shore line velocity at the bore arrival time (Figure 12) can only imply a prediction of shore line accelerations of the order of the fluid acceleration within the bore. Again, the thin run-up sheet must, particularly at its tip, be dominated by friction [19].

None the less, it is an indication of the remarkable promises hidden in the fledgling theory of singular partial differential equations that a qualitative description of, not only a breaker collapse, but also a whole run-up, and even back-wash, structure is contained in that one, magnificent singularity of the beach equations.

VI. RUN-UP EXPERIMENT. An experiment designed to test the theory quantitatively was undertaken by Miller [20]. To this end, a plate was pushed into water at rest in a channel to generate a bore traveling towards a plane beach (Figure 14). Except for small, and for very large, bore strengths, the water motion behind the bore is then uniform as long as the bore travels over the flat part of the channel bed. This arrangement was chosen because the predicted run-up height is $r_{th} = u_0^2/(2g)$, and u_0 is a known function [8] of the bore strength for this classical type of bore.

The main experimental results [20] of relevance here were measurements of the run-up height

$$r_{exp} = h_1 f(M,\varepsilon)$$

as function of bore strength $M = (h_2 - h_1)/h_1$ and beach angle ε (Figure 14). The results for $\varepsilon = 10°$ are shown in Figure 15 together with the theoretical curve reduced by a factor 0.63. The dependence of run-up on bore strength is seen to be adequately approximated, and the reduction factor is not entirely unreasonable, because an overestimate is to be expected from the inviscid theory, and because it is an asymptotic theory predicting only $r_{th} = h_1 \lim_{\varepsilon \to 0} f(M,\varepsilon)$. The approximation of run-up dependence on bore strength is similarly adequate [21] for the other beach slopes tested, provided a suitable reduction factor is applied for each slope. The test of the theory is therefore whether the necessary reduction factors approach, as $\varepsilon \to 0$, a value just short of unity. But that does not happen at all (Figure 16) [21], and the theory therefore fails grossly to predict the quantitative dependence of run-up on beach slope.

This may indicate [20] a need for a re-examination of the applicability of the theory, but the view may also be taken that closer quantitative agreement with observation may be more than should be asked of a theory of this type. As more and more complicated and sophisticated physical phenomena come under scrutiny, it should perhaps be expected that close quantitative agreement between theory and experiment will become the exception, rather than the rule. To obtain very close agreement, the investigator tends to be driven towards theories closely tailored to experiment, theories of an ad-hoc character, which tend to be a disappointing basis for further advances. Alternatively, he tends to be driven toward heavily computational theories, which tend to become intransparent. As increasingly sophisticated phenomena come under study, we may find more and more often that the most fruitful relation between theory and observation is one in which they illuminate each other, even if they do so over a distance.

If the theory is not rejected outright, then the most plausible cause of its failure to predict observation is the neglect of dissipation, except within the bore. Freeman and Le Méhauté [22] have reported a computation of run-up from the beach equations with a hydraulic friction term. From these, the friction correction to the inviscid run-up implied by Méhauté's model may be roughly estimated [21]. The run-up so estimated depends markedly on beach slope [22], and adequate agreement with the experimental dependence of run-up on both bore strength and beach slope is obtained [21], at small beach slopes (Figure 17) if two undetermined parameters are chosen suitably. Of course, this agreement results from manipulation of ad-hoc elements of the theory, and thus implies no more than that the role of dissipation should be studied more closely. The further discoveries of Miller [20] about the finer structure of bores, and their relation to run-up, also deserve attention.

VII. THE TSUNAMI AMPLIFICATION PROBLEM. An attempt had been made meanwhile to extend the beach theory from the description of one wave to that of any number of successive waves. The valididty of the beach equations (Section II) is probably restricted to quite a narrow zone near the shore [3], and the connection to equations valid further out is not yet clear. The problem was therefore formulated [23] by specifying (i) water at rest initially and (ii) the surface elevation at a fixed distance from the initial shore position (Figure 18).

This led immediately to the need to face the basic, singular boundary value problem of the Euler-Poisson-Darboux equation (8), and Taylor [24] succeeded in establishing the existence and uniqueness theorem for it.

Further, he used the Laplace transform to obtain the solution for a particular case in which the surface elevation, at a fixed distance from the initial shore position, is approximately simple harmonic [23]. He was able to show that the motion then remains bore-free forever, if the amplitude is below a bound $A(\omega)$ dependent on the frequency ω . He also showed that $A(\omega) > 0$, except for a countable set of exceptional frequencies [23], which suggests a resonance phenomenon.

Carrier [25] has pointed out that the proper physical formulation is to specify only the incident wave, not the surface elevation resulting from both incident and reflected wave. In the notation (14), this amounts to specifying a, rather than a + b as in [23]. But the basic theorems are unaltered, and the resonance indication led to developments in another direction.

It had become clear that considerable progress had been made in understanding the damage mechanism of tsunamis, which is run-up. Similarly, their motion in the open ocean was understood to a reasonable degree. To connect the two required an understanding of tsunami amplification above continental and island slopes. Tidal theory [6] and classical, small-amplitude wave theory [26] both predict amplification of two-dimensional wave motion by a factor $\varepsilon^{-1/2}$, where ε is the small slope. Carrier [25] combined the latter theory with the standing-wave theory of the nonlinear beach equations and obtained the same amplification factor, modified slightly by dispersive effects in the open ocean. However, an amplification dependent only on off-shore slope fails to explain the extraordinary selectivity in the local incidence of tsunami damage. Thus, while there is strong support for the factor $\varepsilon^{-1/2}$, it can describe only part of the actual tsunami amplification.

Carrier [25] studied the wave-guide effect which an under-water mountain chain would have o. tsunami propagation. Taylor's [23] resonance indication on the other hand, drew attention to evidence suggesting a frequency-sensitivity of tsunami amplification; tide gauges respond to different tsunamis with a frequency dependent on the guage location,

rather than on the tsunami event [27]. However, Shen [28] showed that Taylor's resonance indication arose directly from his specification of the problem and did not indicate actual resonance. In fact, by means of the stability corollary of Taylor's existence theorem, Shen [28] proved that two-dimensional, bore-free motion on a plane beach governed by (1), (2) admits no resonance.

Since bores are dissipative, they do not provide a plausible mechanism for the generation of resonance, and it became likely that any resonance must involve three-dimensional motion.

VIII. RESONANCE OF UNBOUNDED WATER BODIES. Ursell had first discovered that an infinite water body can resonate. He proved [29], on the classical, small-amplitude theory, that water under gravity in a channel bounded only by vertical side walls and a plane beach has discrete eigenvalues. The eigenfunctions are three-dimensional motions generalizing Stokes' edge wave, i.e., they decay exponentially with distance from shore. That implies a finite energy - effectively, only a finite part of the infinite water body resonates. It implies also that there are no discrete eigenfunctions approaching progressive waves far from shore, so that the resonance cannot be excited by waves from the sea. Ursell had to wiggle the channel in order to demonstrate the resonance experimentally, and he thereby discovered [29] that the cut-off frequency of the continuous spectrum is also resonant. (Galvin [30] has since shown that the resonance can be excited subharmonically by progressive waves.)

Ursell's discovery was greatly extended by two independent studies using different approaches. Longuet-Higgins [31] used tidal theory, mostly for steep seabed slopes, while Shen [32] used the classical theory, like Ursell, but for small seabed slopes. Ursell's discrete spectrum then has a large parameter $M = \omega L^{1/2}(\varepsilon g)^{-1/2}$, dependent on the frequency ω and an intrinsic length scale L representing the 'finite' extent of the resonating water body. Introduction of this parameter casts the classical, small-amplitude theory of surface waves into a form analogous to the short-wave limit of electromagnetic theory, and Shen therefore applied Keller's [33] geometrical optics approximation.

The two approaches thus start from the opposite ends of the spectrum, but the long-wave limit ($M \to 1$) of the geometrical optics approximation [32] does, in fact, yield the results of the long-wave approximation [31] for small seabed slope. The geometrical optics approximation [32] also gives the small-slope approximation to Ursell's [29] exact spectrum for all M. Moreover, it is not a short-wave theory in the oceanographical sense, since the influence of the seabed on the waves remains important.

Indeed, this influence is the cause of resonance. The local phase velocity is an increasing function of the local water depth and therefore, if a wave crest lies obliquely across the depth contours, then the variation of phase velocity turns the crest gradually toward the shallows,

during propagation. A wave which initially propagated obliquely towards the sea may thus be turned around gradually to propagate shoreward, without being able to reach the open ocean. And if it be then reflected from the shore or from other boundaries, it may end up facing in the same direction in which it faced initially. It is then plausible that resonance may result, if the phase relationships are just right.

The theory [32] bypasses such phase relationships to arrive at spectral relations much more directly by topological calculations. They are simple enough to bring quite realistic topographies within practical reach. Shen began with a study of channels of infinite length with vertical side walls and arbitrary, monotone depth variation. He found a contably infinite number of the spectra discovered by Ursell. Each such component has a continuous spectrum with cut-off below which it has a finite (though possibly large) number of discrete, resonant eigenfrequencies. The cut-offs of different components are at different frequencies, so that the total spectrum is mixed, with discrete eigenvalues embedded in the continuous spectrum. The continuous spectrum corresponds to modes of progressive character far from shore, while the discrete spectrum corresponds to edge waves trapped over part of the slope.

All this depends on the side walls. For a continental slope without any lateral boundary, the whole spectrum is continuous. There are still modes trapped over part of the slope, often called shelf waves, but there is no resonance.

An infinitely long channel with a submerged mountain range across it (Figure 19) has the same type of mixed spectrum. The resonant modes are trapped above the crest, with exponential damping on both sides (Figure 19).

Quite different results are obtained [32] when, not only the motion, but also the topography, is three-dimensional. For a submerged, axially symmetrical seamount in an unbounded basin (Figure 19 may serve again), the spectrum is wholly continuous, and the waves are trapped, not over the seamount, but outside a disc of damping centered over the seamount.

But just let the sea-level drop until the mount emerges as a round island (Figure 20) and everything changes again. Now resonant modes exist [32] and they consist of edge waves between the shore and an annulus of damping (Figure 20) outside of which there are again waves. The situation is thus the opposite of what Ursell discovered - all <u>but</u> a finite part of the water body now resonates. These modes, moreover, have progressive character, far from the island, and are therefore not immune to direct harmonic excitation from the ocean.

An even more startling result is that resonance now becomes a matter of degree, rather than the clear-cut, classical phenomenon. The wave

motions separated by the damping annulus (Figure 20) are not independent, and any such mode therefore involves leakage of energy by radiation to infinity [31]. The leakage is negligible, and the mode therefore fully resonant, if the damping annulus is wide compared with the exponential decay length. But if it is narrow by comparison, then the resonance is weak and unlikely to be observed.

Apart from the leakage, the spectrum of a round island [32] is of the same, mixed type as that of a channel. But the spectral components corresponding to the longest modes fail to have discrete eigenvalues below their cutoffs. And those components corresponding to the next-longest modes have only weakly resonant discrete eigenvalues. The question arises whether this result is related to the observation [27] that tsunamis are not amplified at isolated, small islands?

Further complications may arise from a shelf around an island, A sufficiently pronounced shelf causes gaps in the continuous part of some spectral components, and further resonant eigenvalues may occur in some of those gaps [32]. The corresponding modes have additional damping and wave annuli (Figure 21).

One of the most remarkable results was obtained from the long-wave approximation for a circular sill with steep sides (Figure 22), for which Longuet-Higgins [31] calculated the detailed, complex spectrum - resonance frequencies and leakage damping coefficients - and the response to existation by plane progressive waves incident from the open sea. The long-wave approximation also yielded estimates of the effect of the earths rotation - a splitting of the eigenfrequencies - and of slight departures from axial symmetry - a splitting of frequencies and coupling between pairs [31].

Part of the purpose of this review is a plea for more experiments. Those on run-up were seen in Section VI to have greatly illuminated the subject. But those on resonance around islands are still outstanding. The phenomena discussed in this section are likely to be significant for shore processes, even if the edge waves do not obtrude to the naked eye. Waves resembling trapped waves around a reef were observed from a Texas tower in the Atlantic during a storm [34]; the wave height appears to have exceeded 100 feet.

ACKNOWLEDGEMENT. Nearly all the work reviewed was supported by the U. S. Army, U. S. Navy or National Science Foundation. The author is indebted to the Army Research Office, Durham, for the invitation that prompted this review, and to the National Science Foundation (Grant GP-11319) and the Army Mathematics Research Center, for partial support of its preparation.

REFERENCES

1. J. J. Stoker, Water Waves, Interscience Pdblishers, New York, 1957, 567 pp.

2. F. P. Shepard, Submarine Geology, 2nd ed., Harper & Row, New York, 1963.

3. R. E. Meyer and A. D. Taylor, On the equations of surf, J. Geophys. Res. 68, 1963, 6443-6445.

4. K. O. Friedrichs, On the derivation of the shallow water theory, Commun. Pure Appl. Math. 1, 1948, 81-85.

5. G. F. Carrier and H. P. Greenspan, Water waves of finite amplitude on a sloping beach, J. Fluid Mech. 4, 1958, 97-109.

6. Sir. H. Lamb, Hydrodynamics 6th ed., Dover Publications, New York, 1945, 738 pp.

7. H. P. Greenspan, On the breaking of water waves of finite amplitude on a beach, J. Fluid Mech. 4, 1958, 330-334.

8. H. B. Keller, D. A. Levine and G. B. Whitham, M.tion of a bore over a sloping beach, J. Fluid Mech. 7, 1960, 302-316.

9. G. B. Whitham, On the propagation of shock waves through regions of non-uniform area or flow, J. Fluid Mech. 4, 1958, 337-360.

10. D. V. Ho and R. E. Meyer, Climb of a bore on a beach, Psrt 1, Uniform beach slope, J. Fluid Mech, 14, 1962, 305-318.

11. H. Guderley, Luftfahrtforschung 19, 1942, 302.

12. R. B. Payne, A numerical method for a converging cylindrical shock, J. Fluid Mech. 2, 1957, 185-200.

13. W. D. Hayes and R. F. Probstein, Hypersonic Flow Theory, Academic Press, New York, 1959, 464 pp.

14. R. E. Meyer, Theory of characteristics of inviscid gas dynamics, Encyclopedia of Physics, Vol. IX, Springer-Verlag, BTrlin, 1960, 815 pp.

15. R. Conrant and D. Hilbert, Methods of Mathematical Physics, Vol. 2, 2nd ed., Interscience Publishers, New York, 1967, 830 pp.

16. R. E. Meyer, An asymptotic method for a singular hyperbolic equation, Arch. Rat. Mech. Anal. 22, 1966, 185-200.

17. M. C. Shen and R. E. Meyer, Climb of a bore on a beach, Part 3, Run-up, J. Fluid Mech. 16, 1963, 113-125.

18. D. V. Ho, R. E. Meyer and M. C. Shen, Long surf, J. Marine Res. 21, 1963, 219-232.

19. R. F. Dressler, Hydraulic resistance effects upon the dam break functions, J. Res. Natl. Bureau Standards 49, 1952, 217-225.

20. R. L. Miller, Experimental determination of run-up of undular and fully developed bores, J. Geophys. Res. 73, 1968, 4497-4510.

21. R. E. Meyer, Nste on wave run-up, to appear in J. Geophys. Res.

22. J. C. Freeman and B. Le Mehaute, Wave breakers on a beach and surges on a dry bed, J. Hydraulic Div. Am. Soc. Civil Engrs. 90, 1964, 187-216.

23. A. D. Taylor, Water waves at the shoreline, Univ. Wisconsin, Dept. Math., ONR Tech. Rep. 1202 (27)/3, 1965, 47 pp.

24. A. D. Taylor, On singular boundary value problems for the EPD equation, Univ, Wisconsin, Dept. Math., ONR Tech. Rep. 1202 (27)/4, 1965, 104 pp.

25. G. F. Carrier, Gravity waves on water of variable depth, J. Fluid Mech. 24, 1966, 641-659.

26. J. J. Stoker, Surface waves in water of variable depth, Quart. Appl. Math. 5, 1947, 1-54.

27. G. Van Dorn, Scripps Inst. Oceanography, private communciation.

28. M. C. Shen, Math. Dept., University of Wisconsin, private communication.

29. F. Ursell, Edge waves on a sloping beach, Proc. Roy. Soc. A214, 1952, 79-97.

30. C. J. Galvin, Subharmonic resonance of edge waves, U. S. Army Coastal Engin. Res. Center Memo. 28 July 1967, Washington, D. C.

31. M. S. Longuet-Higgins, On the trapping of wave energy round islands, J. Fluid Mech. 29, 1967, 781-821.

32. M. C. Shen, R. E. Meyer and J. B. Keller, Spectra of water waves in channels and around islands, Phys. Fluids 11, 1968, 2289-2304.

33. J. B. Keller, Surface waves on water of non-uniform depth, J. Fluid Mech. 4, 1958, 607-614.

34. R. L. Miller, Geophys, Sci. Dept., Univ. Chicago, private communication.

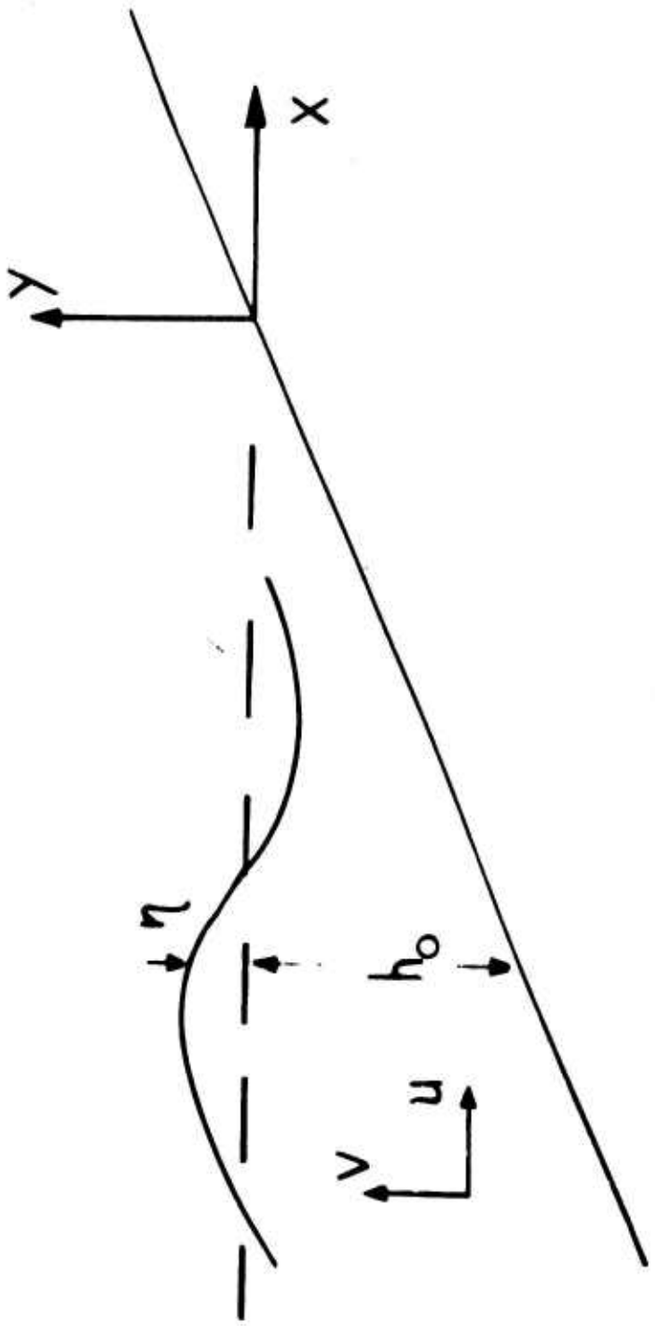


Figure 1

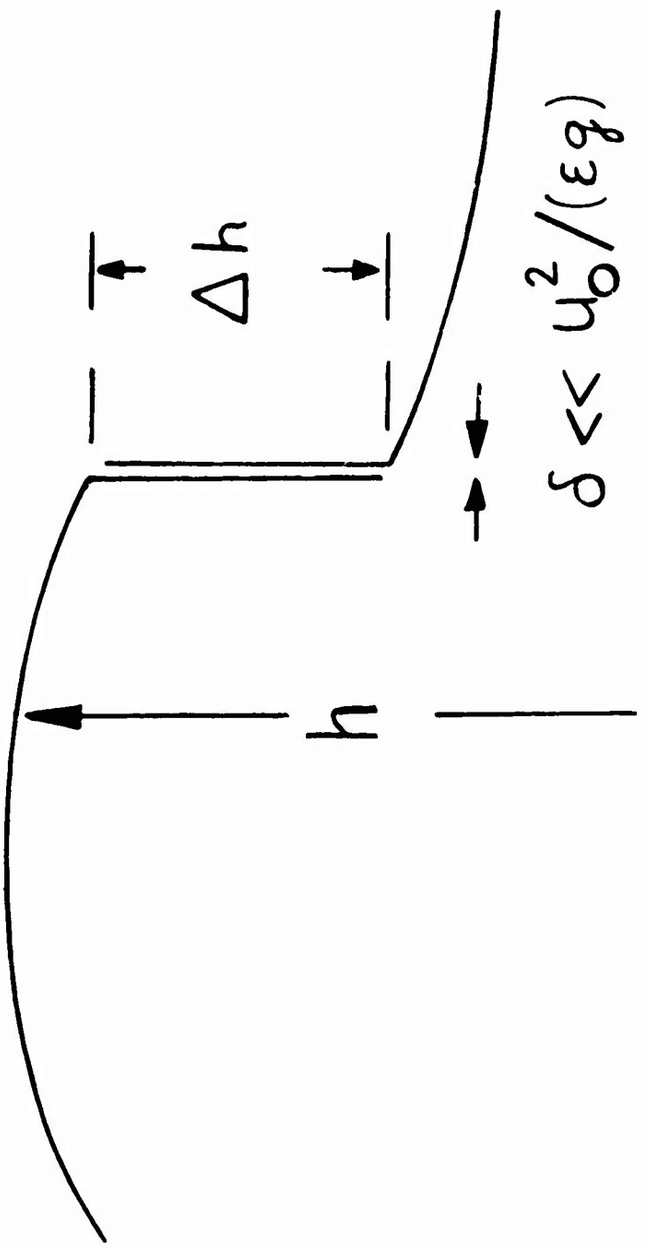


Figure 2

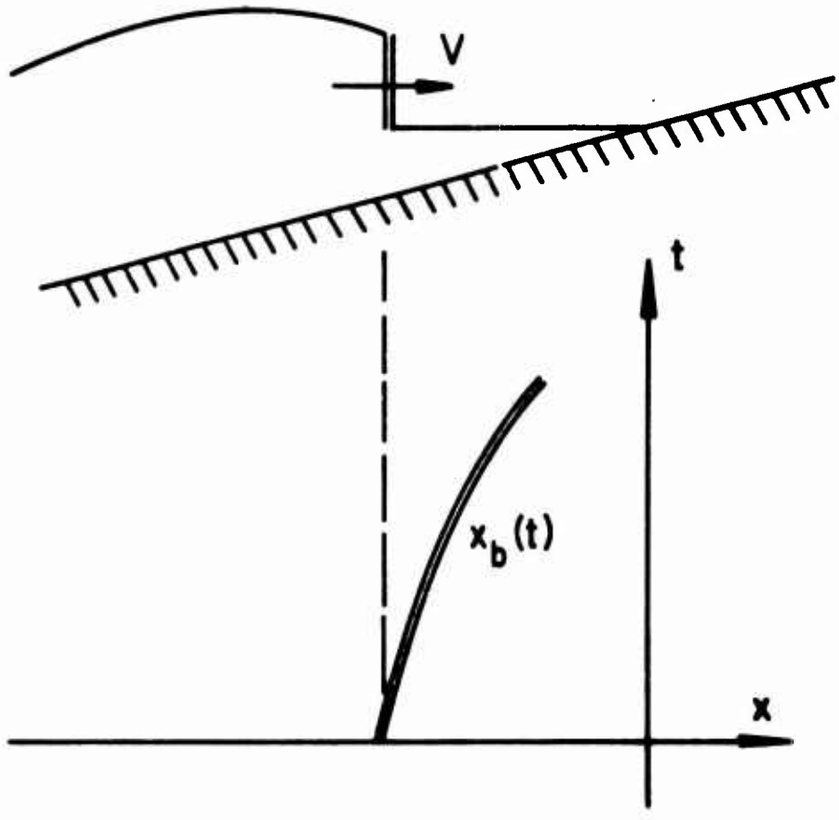


Figure 3

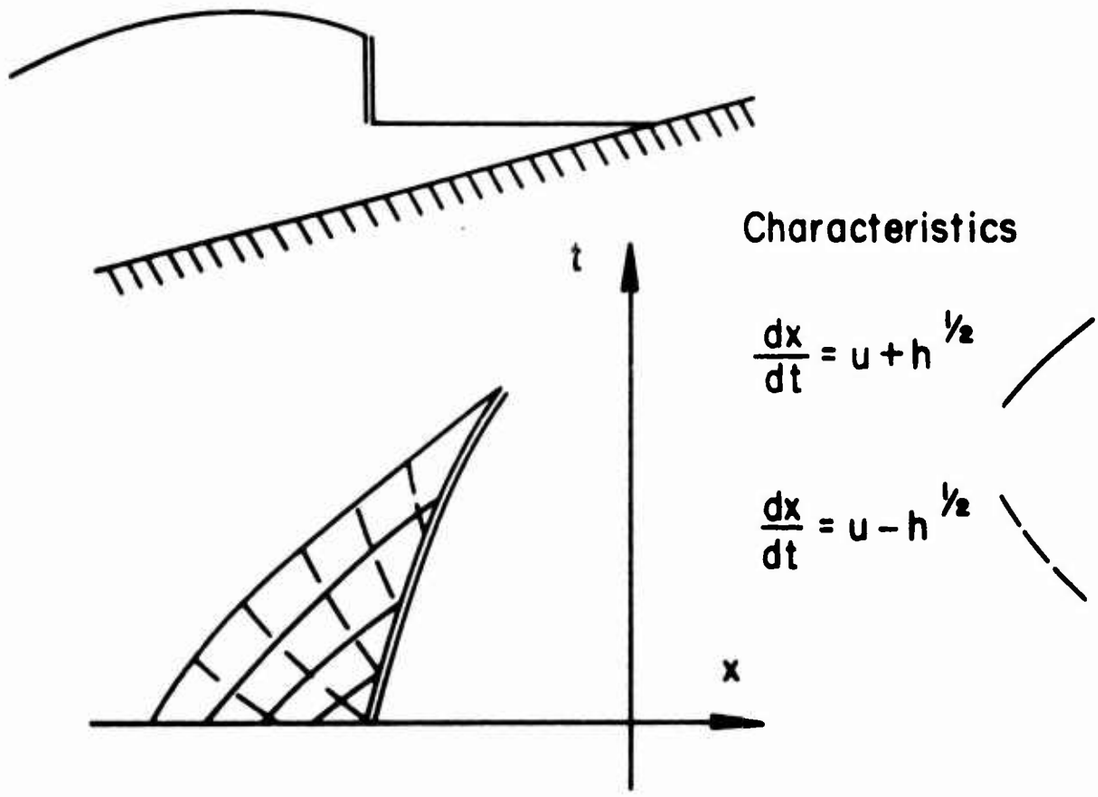


Figure 4

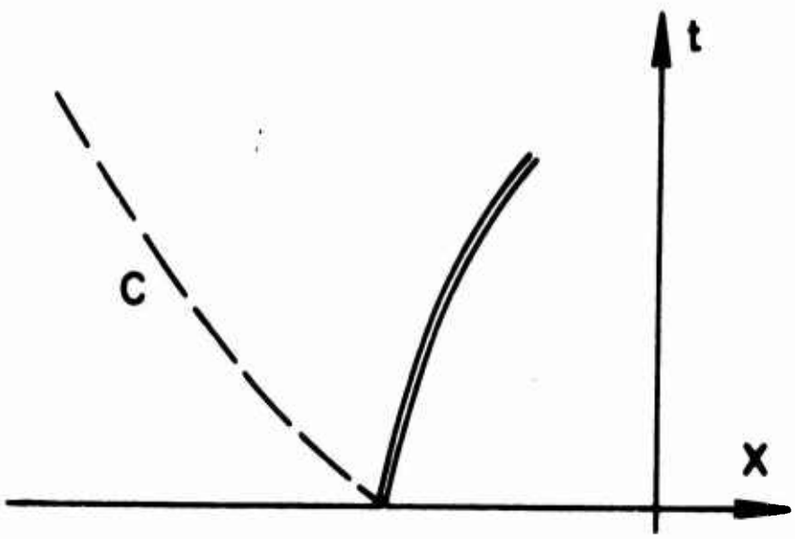


Figure 5

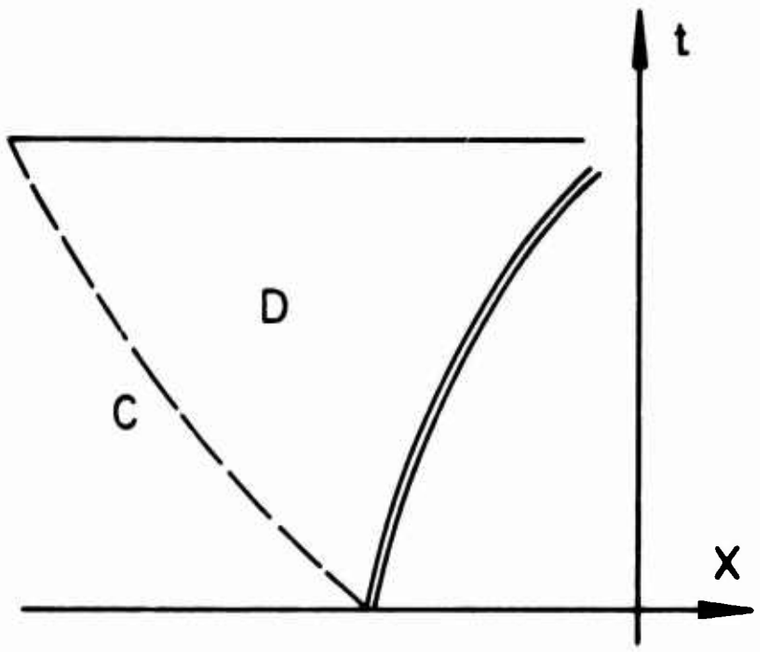


Figure 6

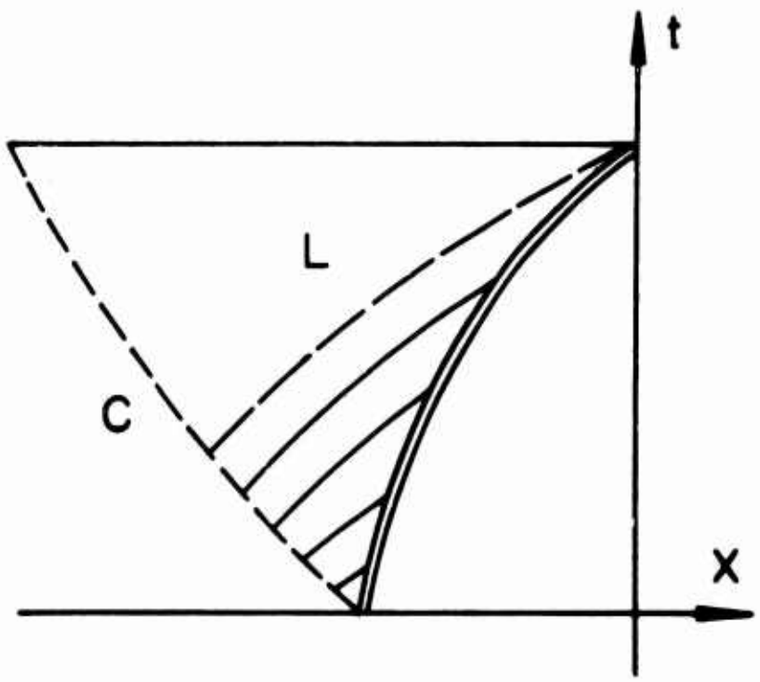


Figure 7

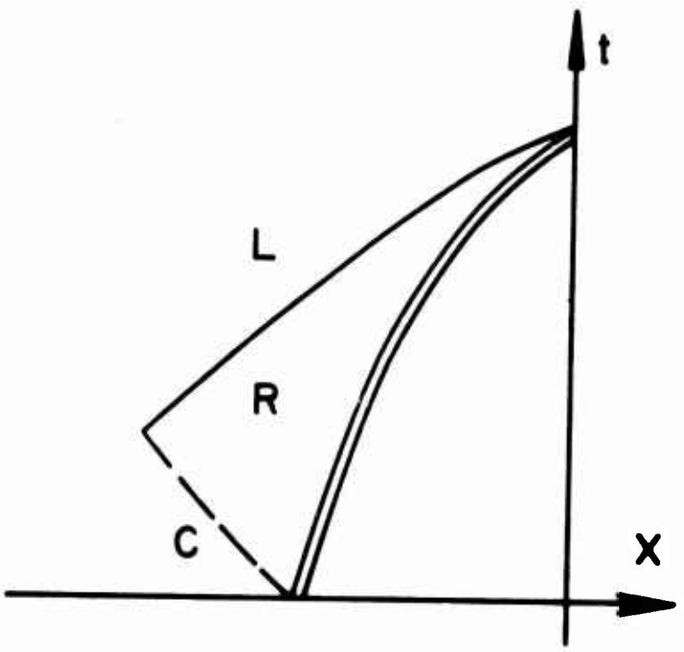


Figure 8

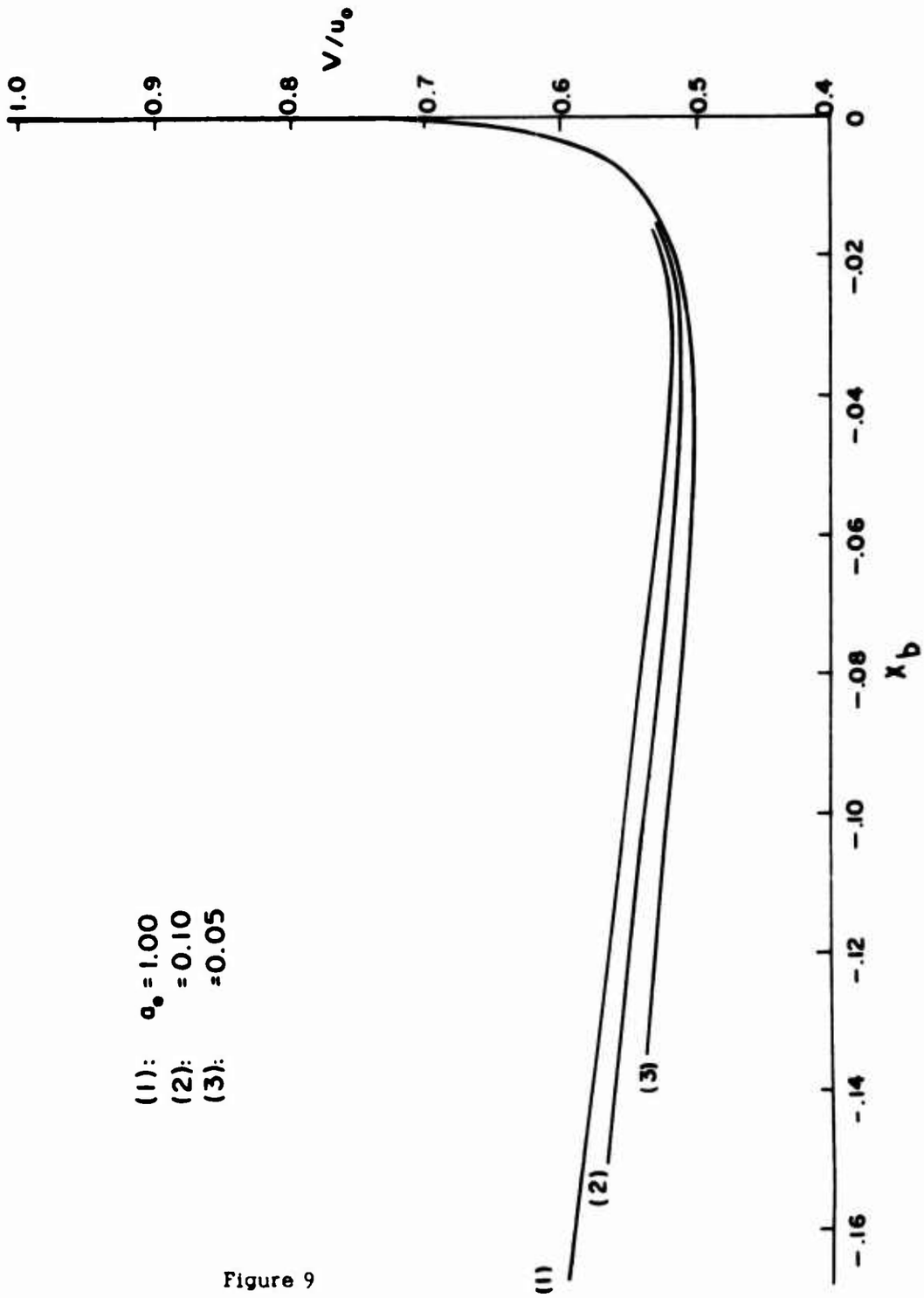

V/u_o
1.0
0.9
0.8
0.7
0.6
0.5
0.4
0
-.02
-.04
-.06
-.08
-.10
-.12
-.14
-.16
x_b
(1)
(2)
(3)
(1): a_o = 1.00
(2): = 0.10
(3): = 0.05

Figure 9

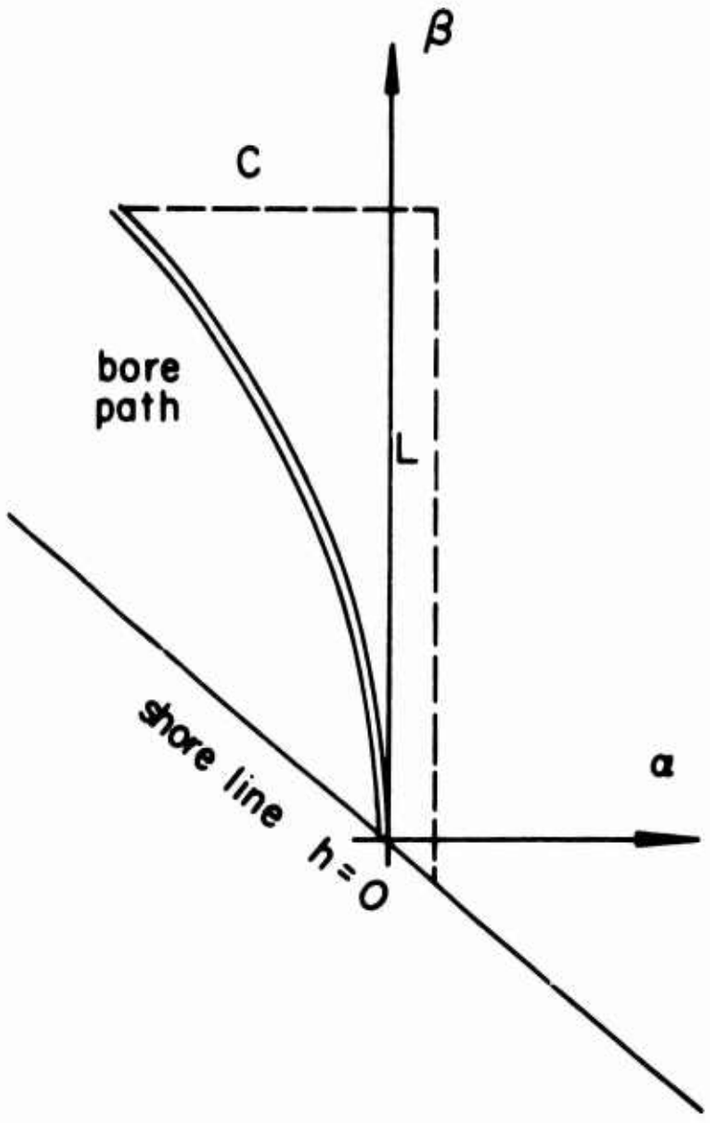


Figure 10

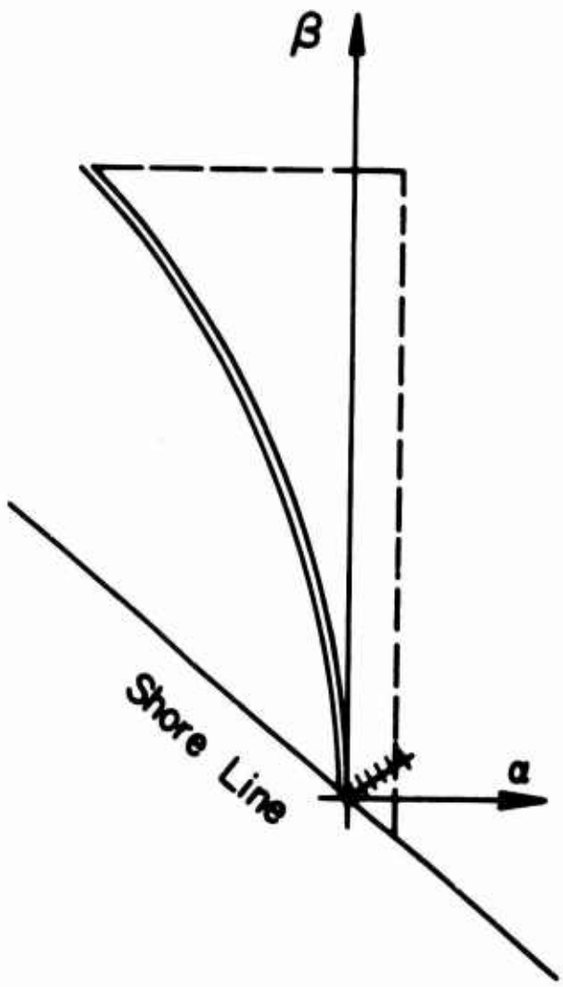


Figure 11

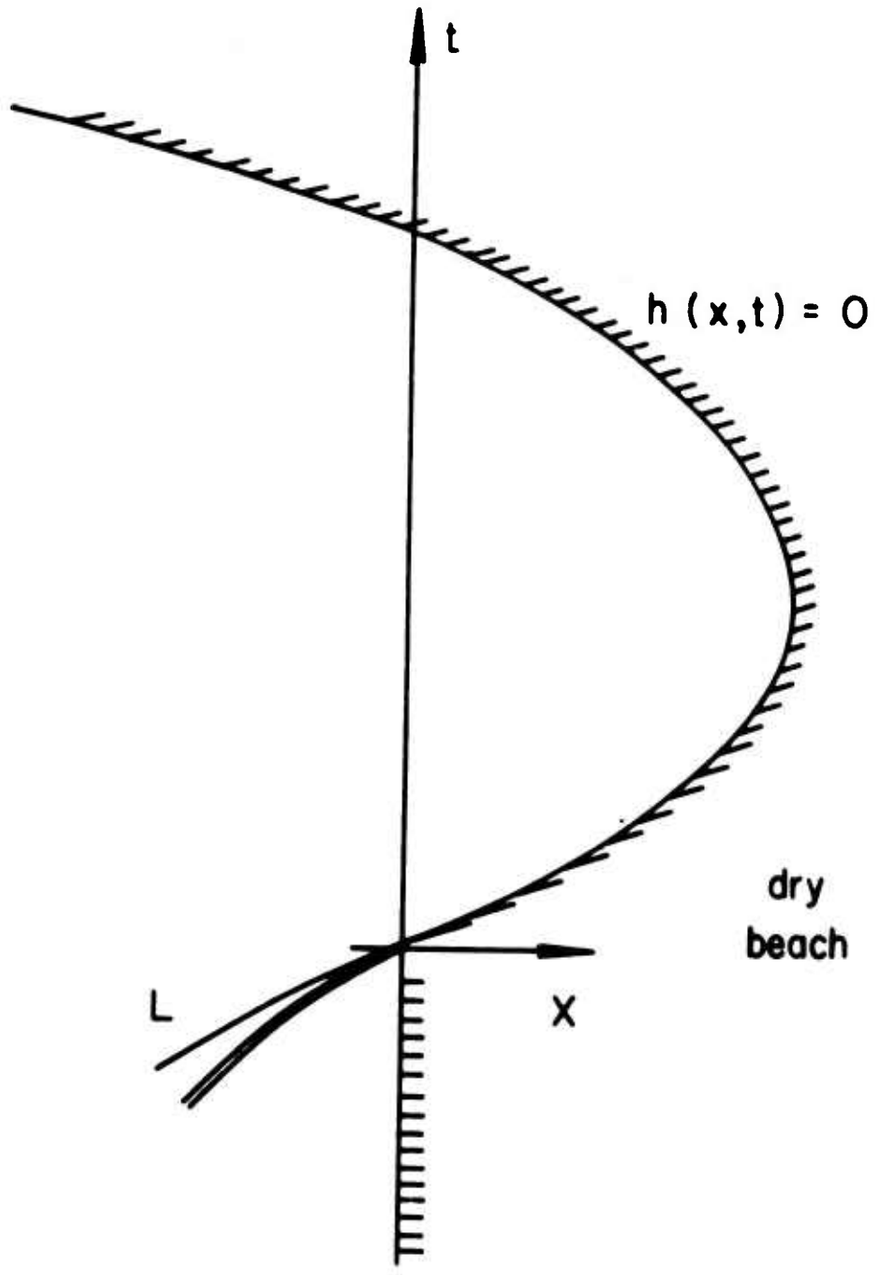


Figure 12

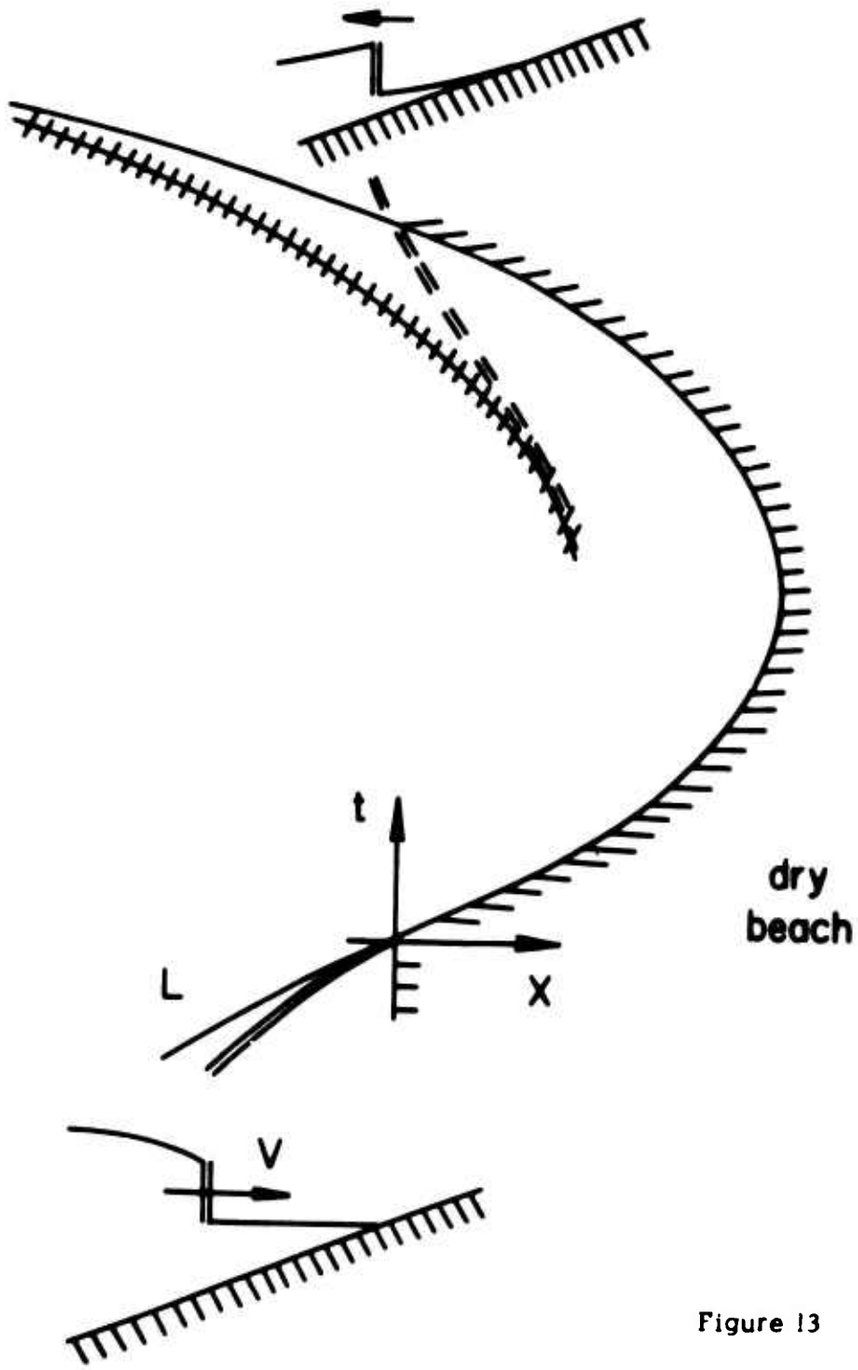


Figure 13

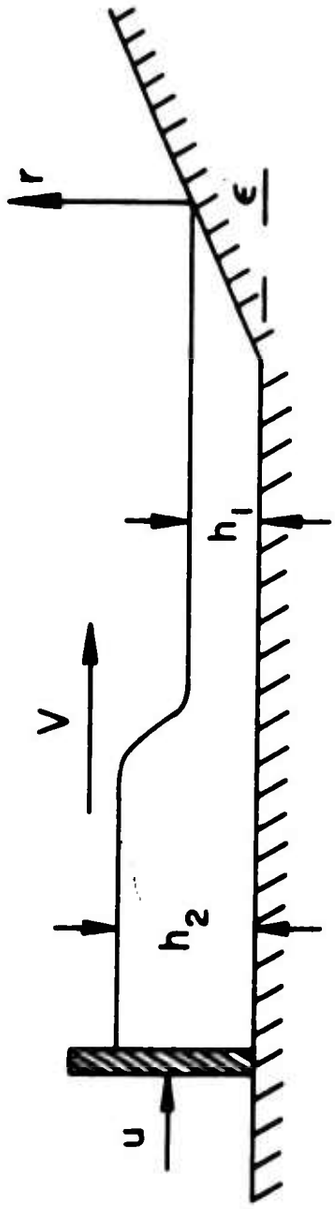


Figure 14

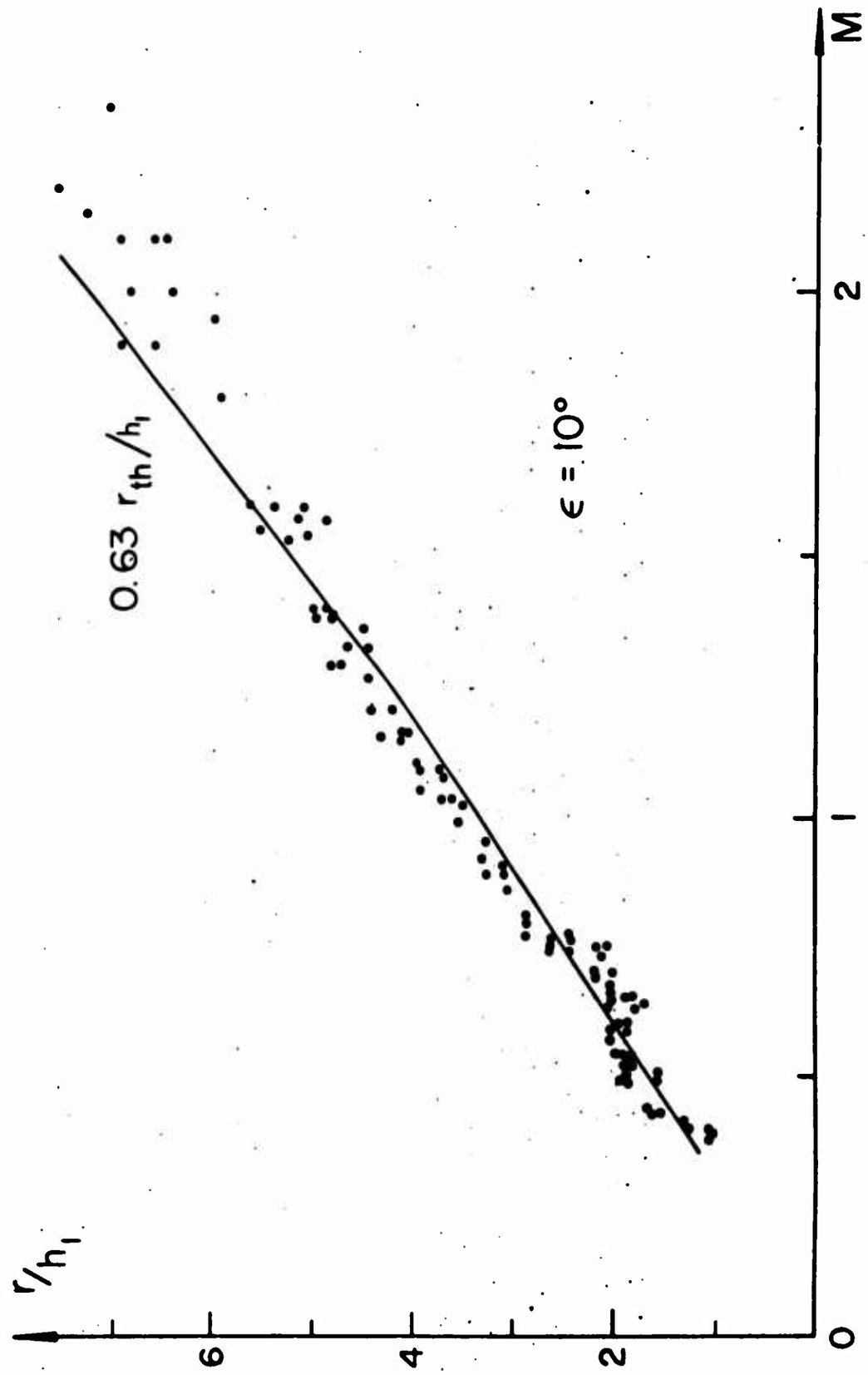
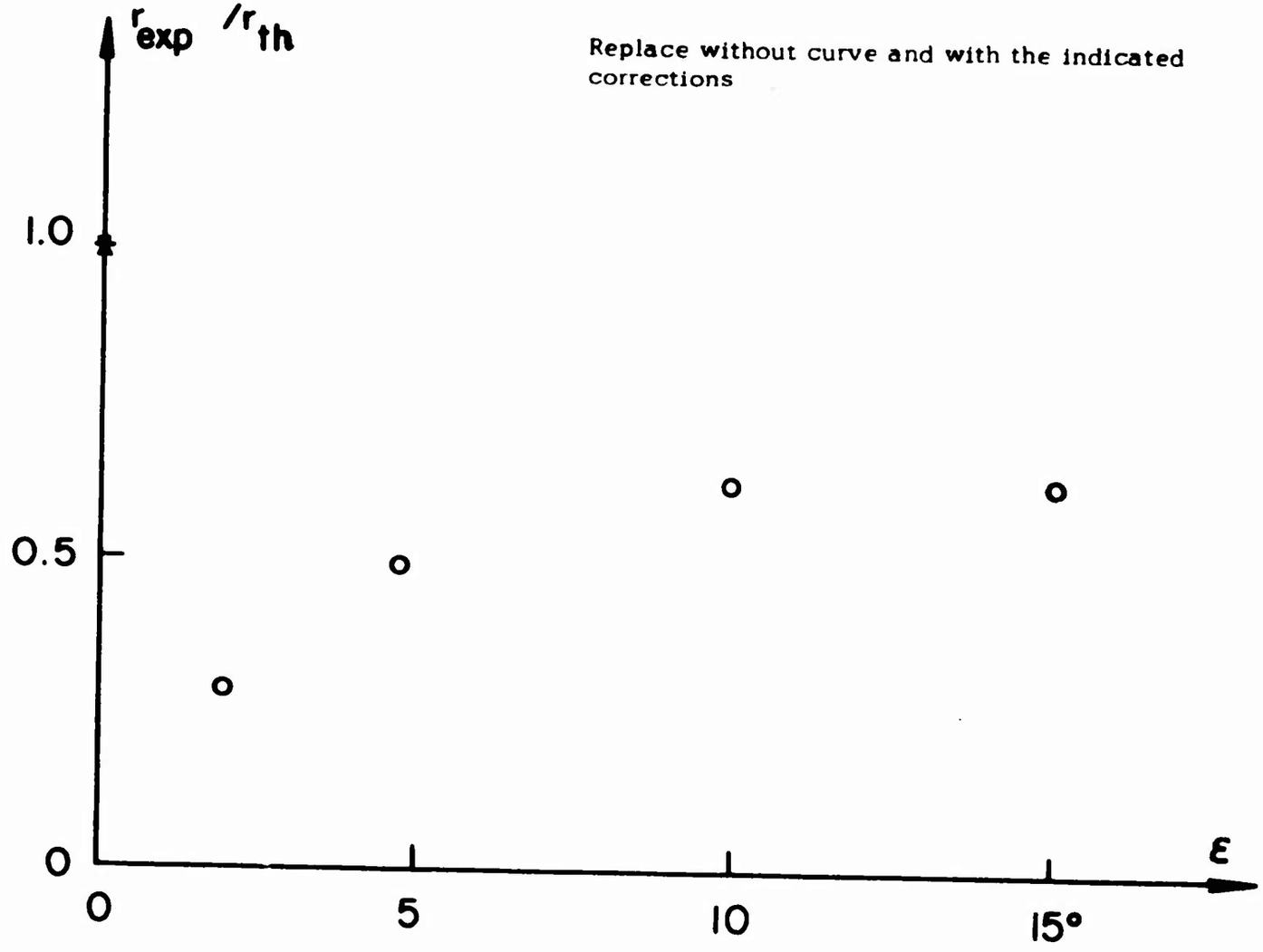


Figure 15



Replace without curve and with the indicated corrections

Figure 16

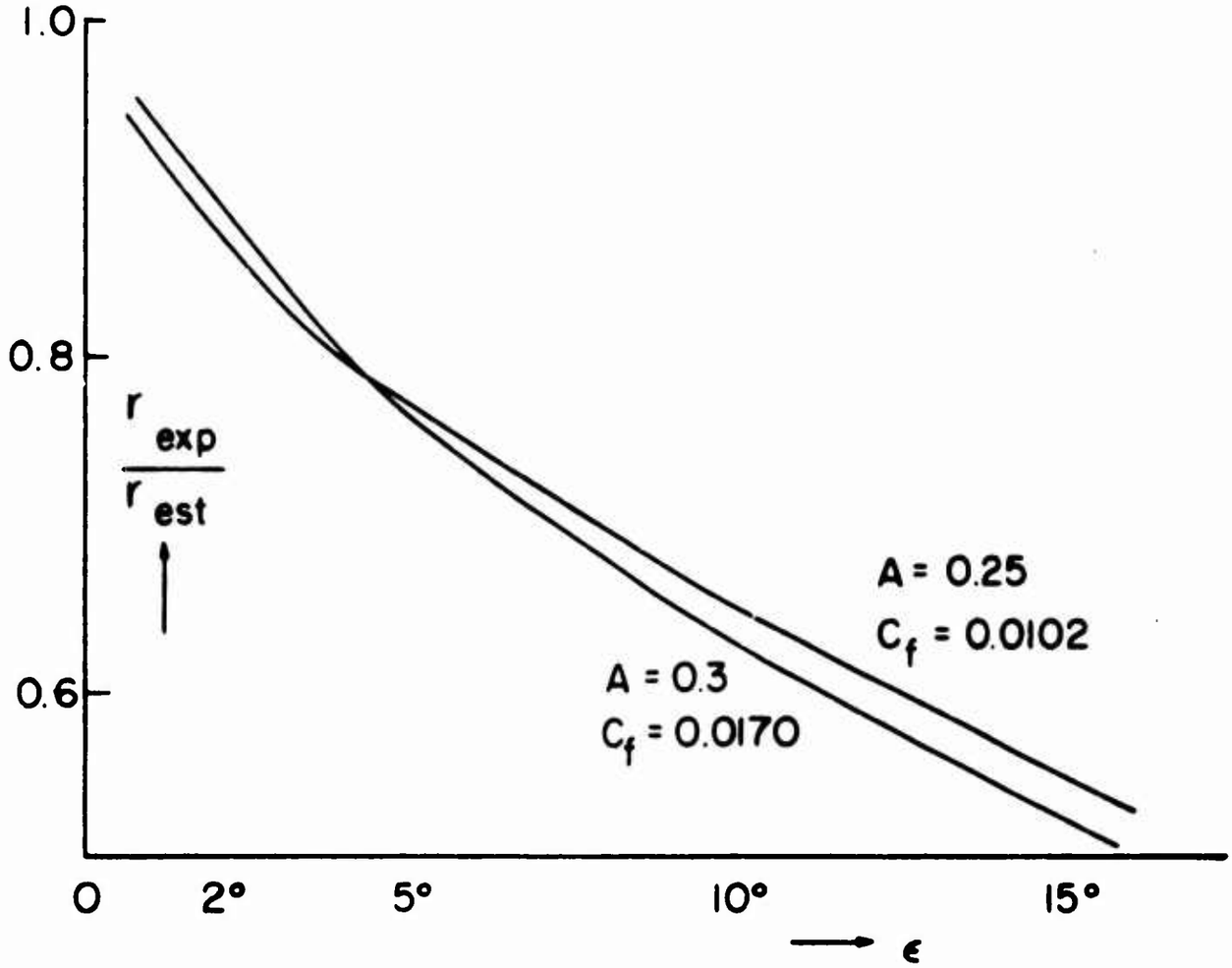


Figure 17

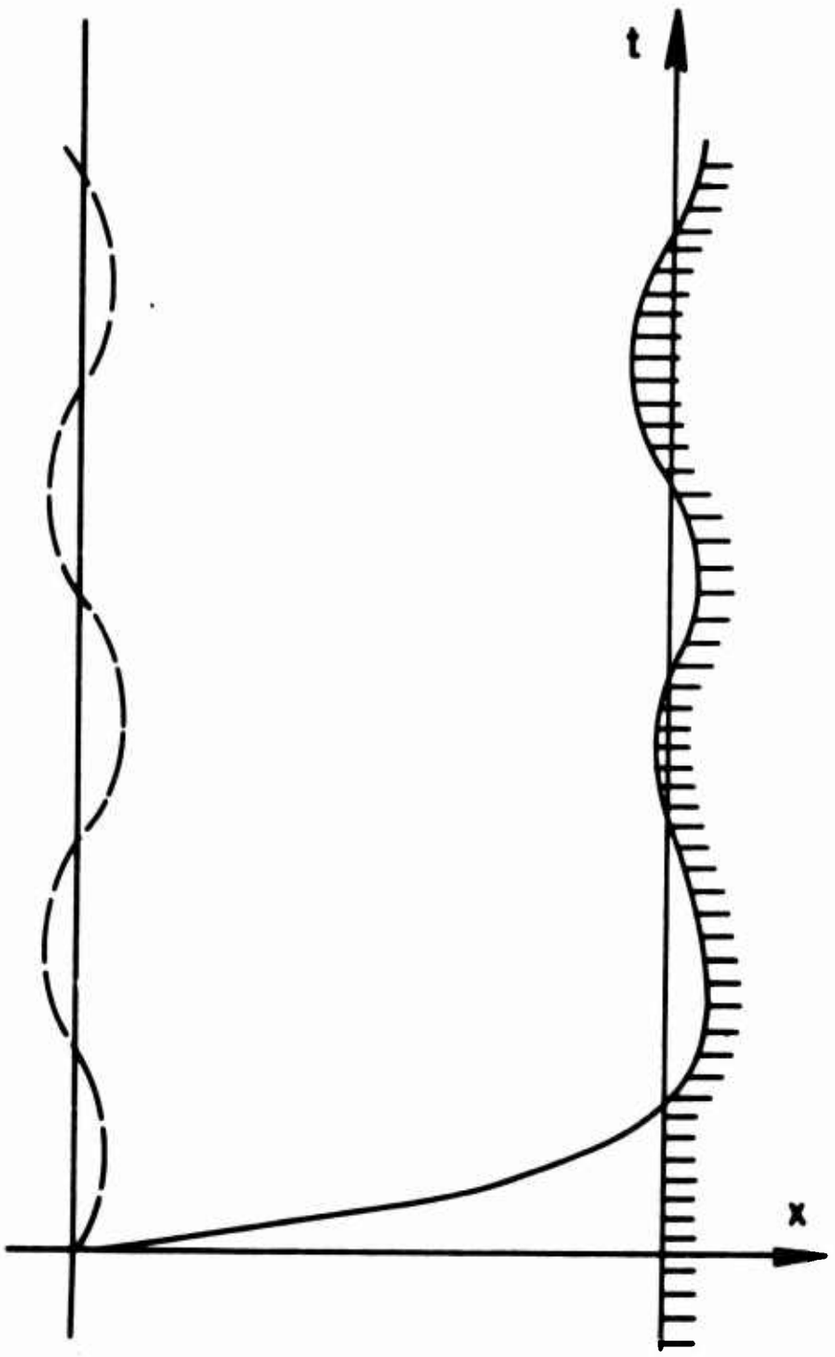


Figure 18

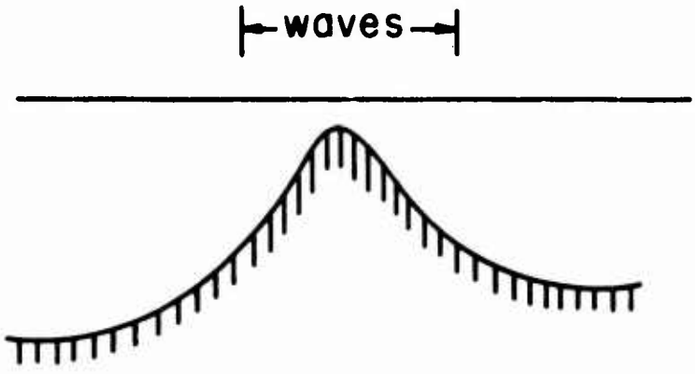


Figure 19

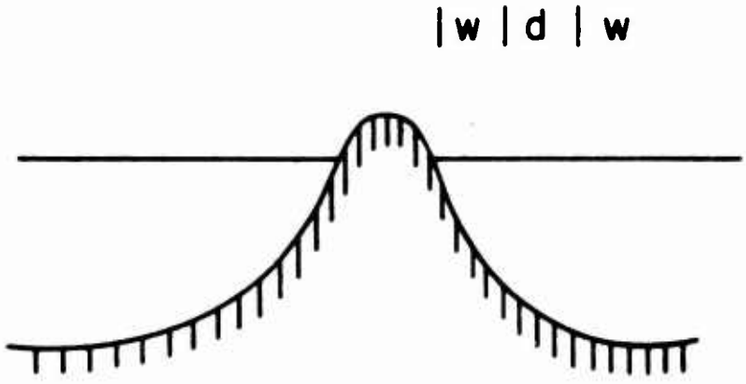


Figure 20

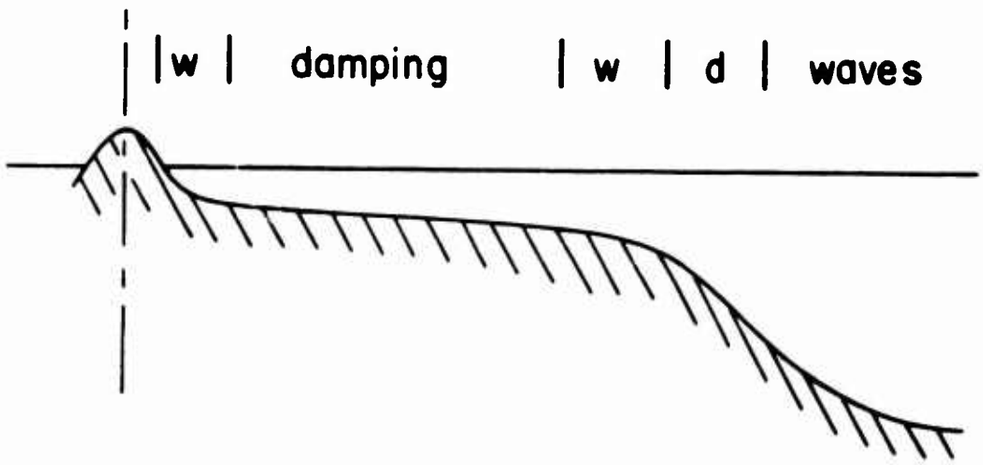


Figure 21

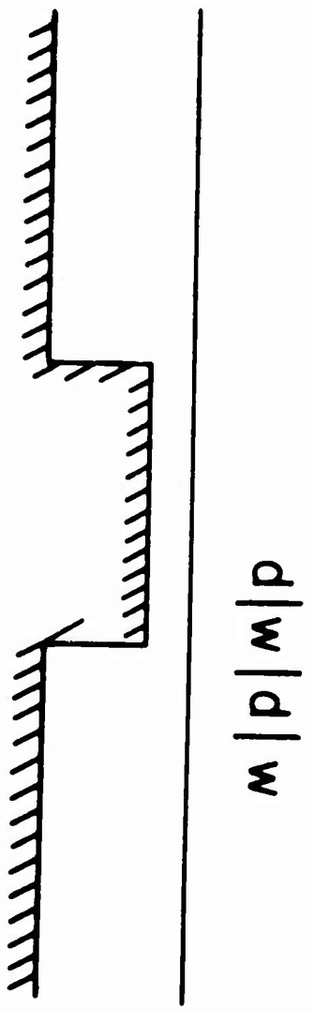


Figure 22

ATTENDANCE LIST

William S. Agee, White Sands Missile Range
Gary Anderson, Watervliet Arsenal
Velma M. Archer, Aviation Systems Command
John G. Avery, Army Missile Command
Elwood D. Baas, White Sands Missile Range
Mark E. Barkley, Aviation Systems Command
Havard M. Bauer, Aviation Systems Command
Dominic P. Biagioli, Aeronautical Chart & Information Center, St. Louis
Merle J. Biggin, U. S. Army Topographic Command
Erwin Biser, Fort Monmouth
Frank A. Blackshear, Aviation Systems Command
Oscar Bowie, Materials and Mechanics Research Center
James L. Boyd, Aeronautical Chart & Information Center
E. J. Brunelle, Watervliet Arsenal and Rensselaer Polytechnic Institute
Michael B. Bryant, Aviation Systems Command
Nicholas P. Callas, Air Force Office of Scientific Research
G. Catron, Aviation Systems Command
Jagdish Chandra, Watervliet Arsenal
S. Charmonman, University of Missouri
Choon Yun Cho, Advanced Materiel Concepts Agency
Shun-chin Chou, Materiels and Mechanical Research Center
Yu-Tang Chou, Waterways Experimentation Station
Horace M. Clevenger, Aviation Systems Command
Patsy R. Courtney, Aviation Systems Command
Louis P. Crnarich, Picatinny Arsenal
Julian L. Davis, Picatinny Arsenal
Francis G. Dressel, Army Research Office-Durham
W. B. Driver, Aviation Systems Command
Wendell A. Dwyer, Scott Air Force Base
George Eason, Mathematics Research Center
Gilbert G. Elchinger, Aviation Systems Command
Bernard F. Engebos, White Sands Missile Range
Martin W. Foster, Aviation Systems Command
Joel C. Frazer, Aeronautical Chart & Information Center
Culin Freese, Materials and Mechanics Research Center
Fred Frishman, Office, Chief of Research and Development
Alan S. Galbraith, Army Research Office-Durham
K. R. Gandhi, Army Materials and Mechanics Research Center
Alfred G. Gilbert, Aeronautical Chart & Information Center
Howard M. Gilby, Aviation Systems Command
B. C. Gray, Fort Detrick
Arthur Hausner, Harry Diamond Laboratories
Roger H. Heidenreich, Aviation Systems Command
John W. Hollis, Aviation Systems Command
Walter Howard, Frankford Arsenal
R. R. Huilgol, Mathematics Research Center
Connie Hume, Aeronautical Chart & Information Center
Moayyed Hussain, Watervliet Arsenal
Edmund N. Inselmann, Army Materiel Command

Herman F. Karreman, Mathematics Research Center
Carl J. Kemmer, Aviation Systems Command
Lawrence A. Kiefer, Aviation Systems Command
Badrig M. Kurkjian, Army Materiel Command
Leon Kotin, Fort Monmouth
Charles W. Kullmann, Aviation Systems Command
George V. Johnson, Army Mobility Equipment Command
George Larry, Jr., Aeronautical Chart & Information Center
Kenneth E. Lavoie, Rock Island Arsenal
Robert P. Lee, White Sands Missile Range
Eric L. Leese, Canadian Defense Research Board, Ottawa, Ontario
Siegfried H. Lehnigk, Redstone Arsenal
Robert W. Lewis, Aviation Systems Command
Barbara H. Lyles, Aviation Systems Command
Homer T. Malone, Aeronautical Chart & Information Center
Mark J. Malone, Scott Air Force Base
C. Masaitis, Aberdeen Proving Ground
James Medlin, Data Central, Inc., St. Louis
R. E. Meyer, University of Wisconsin
Lothrop Mittenthal, Office, Director of Defense Research & Engineering
Margaret Mulligan, Aviation Systems Command
John Mundy, Aviation Systems Command
Louis Nardizzi, Southern Methodist University
Michael C. Nerdahl, Rock Island Arsenal
Arthur J. Ostdiek, Harry Diamond Laboratories
Casey K. C. Pan, Rock Island Arsenal
Pasqual Perrino, Walter Reed Army Institute of Research
Cecelia F. Planthold, Aviation Systems Command
Henry J. Porter, Aviation Systems Command
Louis B. Rall, Mathematics Research Center
Struan R. Robertson, Watervliet Arsenal
Catherine M. Robinder, Rock Island Arsenal
Dwayne A. Rollier, Scott Air Force Base
Edward W. Ross, Jr., Natick Laboratories
Robert L. Ryan, Watervliet Arsenal
Miss Scharn, Fort Belvoir
Gerald A. Shanholt, Fort Belvoir
Arthur L. Smith, Materiel Systems Analysis Agency
Norman H. Smith, Army Mobility Equipment Command
Friedrich K. Soechting, Picatinny Arsenal
James E. Spear, Jr., Aeronautical Chart & Information Center
G. Norman Stanard, Aviation Systems Command
John D. Stettler, Redstone Arsenal
Shunsuke Takagi, CRREL, Hanover, N. H.
Darrel M. Thomsen, Rock Island Arsenal
John M. Toler, Army Mobility Equipment Command
Joseph Weinstein, Fort Monmouth
L. C. Young, Mathematics Research Center
Martin Wachs, University of Illinois

Unclassified
Security Classification

DOCUMENT CONTROL DATA - R & D

(Security classification of title, body of abstract and indexing annotation must be entered when the overall report is classified)

1. ORIGINATING ACTIVITY *(Corporate author)*
U. S. Army Research Office - Durham
Box CM, Duke Station
Durham, North Carolina 27706

2a. REPORT SECURITY CLASSIFICATION
Unclassified

2b. GROUP
NA

3. REPORT TITLE
TRANSACTIONS OF THE FIFTEENTH CONFERENCE OF ARMY MATHEMATICIANS

4. DESCRIPTIVE NOTES *(Type of report and inclusive dates)*
Interim Technical Report

5. AUTHOR(S) *(First name, middle initial, last name)*

6. REPORT DATE
January 1970

7a. TOTAL NO. OF PAGES
642

7b. NO. OF REFS

8a. CONTRACT OR GRANT NO.

b. PROJECT NO.

c.

d.

9a. ORIGINATOR'S REPORT NUMBER(S)
ARO-D Report 70-1

9b. OTHER REPORT NO(S) *(Any other numbers that may be assigned this report)*

10. DISTRIBUTION STATEMENT
This document is subject to special export controls and each transmittal to foreign governments or foreign nationals may be made only with prior approval of the U. S. Army Research Office - Durham.

11. SUPPLEMENTARY NOTES
None

12. SPONSORING MILITARY ACTIVITY
Army Mathematics Steering Committee on behalf of the Chief of Research and Development

13. ABSTRACT
This is the technical report resulting from the Fifteenth Conference of Army Mathematicians. It contains 27 of the papers presented at that meeting. These treat various Army applied mathematical problems.

14. Key Words:

Elastic spherical cavity
Torsional motion
Information systems
Tensors
Elastic and viscoelastic layered systems
Kinetics of viscoelastic plates
Cyclic systems of differential equations
Functional differential systems
Stress analysis
High frequency vibrations
Forced oscillations
Hurwitz and Hermite matrices
Kalman filter
Analogue and digital algorithms
Circular parachutes
Variational methods
Approximations to roots of positive numbers
Dynamic models
Vortex rate sensor
Analog/hybrid solutions
Wind compensation launcher settings
Turbine blade-flow-field
Forced oscillations
Schwarz-Christoffel transformations
Numerical techniques
Cosserat continuum
Surf

DD FORM 1 NOV 68 1473 REPLACES DD FORM 1473, 1 JAN 64, WHICH IS OBSOLETE FOR ARMY USE.

Security Classification